EVOLUTION & DIVERSITY DYNAMICS LAB

fnrs LA LIBERTÉ DE CHERCHER

LIÈGE université

Re-assessment of the impact of the Late Triassic extinction events on the diversification of raptorial marine reptiles

Antoine Laboury

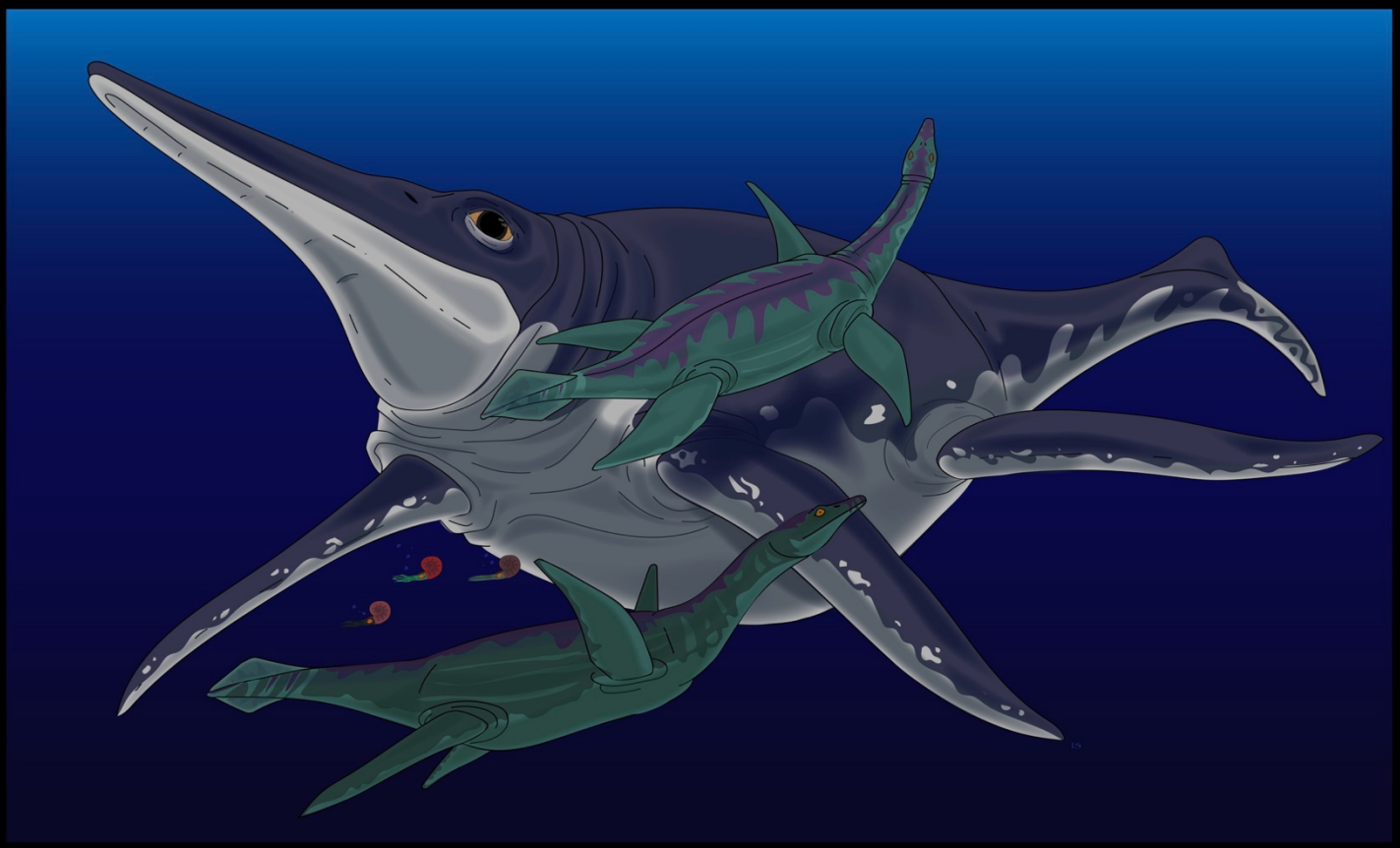

Ph.D. advisor:
Prof. Valentin Fischer

University of Liège
Faculty of Sciences

Academic year 2024 – 2025

EVOLUTION & DIVERSITY DYNAMICS LAB

fnrs LA LIBERTÉ DE CHERCHER

LIÈGE université

Re-assessment of the impact of the Late Triassic extinction events on the diversification of raptorial marine reptiles

Antoine Laboury

Ph.D. dissertation submitted in partial fulfilment of the requirements for the degree of Doctor of Sciences from the University of Liège

Ph.D. advisor: Prof. FISCHER Valentin

Jury:

Dr. **Loïc Michel**	University of Liège, Belgium	President
Prof. **Valentin Fischer**	University of Liège, Belgium	Thesis advisor
Dr. **Bruno Frederich**	University of Liège, Belgium	Internal examiner, Secretary
Prof. **Torsten M. Scheyer**	University of Zurich, Switzerland	Internal examiner
Dr. **Thomas L. Stubbs**	Open University, United Kingdom	Internal examiner
Dr. **Davide Foffa**	University of Birmingham, United Kingdom	External examiner
Dr. **Erin Maxwell**	Natural History Museum of Stuttgart, Germany	External examiner

Academic year: 2024 – 2025

ABSTRACT

The Triassic (259.1–201.3 million years ago) represents a pivotal period in Earth's history, marking the establishment of complex marine trophic networks that still persist nowadays. The recovery of marine life following the largest-ever biodiversity crash at the Permian–Triassic transition occurred during the Early to Middle Triassic and was notably characterized by the rapid radiation of multiple reptile lineages that invaded aquatic ecosystems. These reptiles diversified in nearshore and oceanic habitats, resulting in a wide variety of body sizes, feeding strategies, and locomotion styles. However, the Early Jurassic fossil record is much less diversified and indicates that nearly all 'typically Middle Triassic' faunas adapted to coastal environments disappeared, in addition to gigantic forms. Only a fraction of ichthyosaurians (the 'fish-shaped' reptiles) and plesiosaurians (initially long-necked eosauropterygians) successfully crossed the Triassic–Jurassic (T/J) transition. This strong reduction in marine reptile disparity has been associated to the end-Triassic mass extinction event (ETME), that forced, under this paradigm, a macroevolutionary bottleneck, in which only pelagic raptorial predatory forms survived. However, studies supporting this hypothesis used, in addition of phylogenetic data to reconstruct the evolution of disparity, coarse temporal intervals, thus potentially confounding multiple temporally-isolated events.

The aim of this Ph.D. project is therefore to quantitatively re-assess the influence of Late Triassic events on the evolutionary history of both ichthyosaurians and eosauropterygians. This project involves a comprehensive examination of their morphological evolution from the Middle Triassic to the end of the Early Jurassic, alongside the quantification of the phylogenetic signal in their extinction patterns and the influence of body size in extinction susceptibility. Furthermore, to perform disparity analyses, I compiled extensive morphological datasets that incorporate a great number of 3D models of specimens digitised for the first time during this project.

The overall findings of this project strongly challenge the hypothesis of a sudden and severe evolutionary bottleneck affecting the diversity and the disparity of raptorial marine reptiles at or close to the T/J transition. Instead, the loss of 'Triassic' forms appears to be the result of a more gradual pattern of selective extinctions throughout the Late Triassic, most of which were unrelated from the ETME. A major faunistic turnover, likely driven by marine regression, is thought to have occurred during the early Late Triassic, leading to

the extinction of coastal faunas and facilitating the diversification of taxa adapted to life in the open-ocean. While both ichthyosaurians and eosauropterygians were impacted by the reduction of flooded continental shelves, the latter appeared more severely affected. Eosauropterygians indeed experienced a significant drop in disparity, associated with the disappearance of 'typical Middle Triassic' lineages that had previously undergone a remarkable ecomorphological diversification, reflecting the occupation of multiple ecological niches. Among ichthyosaurians, the T/J transition has traditionally been associated with a notable decrease in disparity and a substantial shift in morphospace occupation. However, our morphological analyses reveal a high diversity of craniodental phenotypes during the Early Jurassic, as shown by the occupation of previously unexplored regions in morphospace and a substantial overlap with those of their Triassic predecessors. Even if this pattern suggests a minor effect of the end-Triassic events on the morphological evolution of ichthyosaurians, these events coincided with the final demise of the whale-sized shastasaurids, suggesting a certain degree of phylogenetic clustering in extinctions and potentially a greater susceptibility among large-bodied taxa during the ETME.

RÉSUMÉ

Le Trias (259.1–201.3 millions d'années) représente un période charnière dans l'histoire de la Terre, marquée notamment par la mise en place de chaines trophiques marines complexes qui persistent encore de nos jours. Le rétablissement des écosystèmes marins suite au plus grand effondrement de la biodiversité jamais enregistré, à la limite entre le Permien et le Trias, est caractérisé par la radiation rapides de reptiles ayant récemment colonisé le milieu aquatique. Ces reptiles se sont massivement diversifiés dans les milieux littoraux et océaniques, résultant ainsi en une grande variété de tailles corporelles, de stratégies alimentaires mais également de types de nage. Cependant, le registre fossile du Jurassique inférieur est beaucoup moins diversifié et indique que toutes les faunes 'typiques du Trias Moyen' adaptées aux environnements côtiers ont disparu, en plus des formes gigantesques. Seule une fraction des ichthyosaures (les reptiles dits 'thunniformes') et les plésiosaures (initialement des eosauroptérygiens à long cou) ont franchi avec succès la transition Trias–Jurassique. Cette forte réduction de la disparité morphologique des reptiles marins a été communément associée à l'extinction de masse de la fin du Trias (ETME), qui a provoqué, selon ce paradigme, un goulot d'étranglement macroévolutif au travers duquel seuls les prédateurs pélagiques ont survécu. Cependant, les études soutenant cette hypothèse ont utilisé, en plus de données phylogénétiques pour retracer l'évolution de la disparité morphologique, des intervalles de temps relativement larges, confondant ainsi plusieurs événements temporellement isolés en un seul.

L'objectif de ce projet de thèse est donc de réévaluer de manière quantitative l'influence des événements du Trias supérieur sur l'histoire évolutive des ichthyosaures et des eosauroptérygiens. Ce projet implique un examen approfondi de leur évolution morphologique, du Trias moyen à la fin du Jurassique inférieur, parallèlement à la quantification du signal phylogénétique dans leurs patterns d'extinction, ainsi que l'influence de la taille sur leur risque d'extinction. De plus, pour réaliser les analyses de disparité, j'ai compilé de larges ensembles de données morphologiques, comprenant un grand nombre de modèles 3D de spécimens numérisés pour la première fois.

L'ensemble des résultats de ce projet remettent fortement en question l'hypothèse d'un goulot d'étranglement évolutif soudain et sévère affectant la diversité et la disparité des reptiles marins au moment de la transition Trias–Jurassique (T/J). Au

contraire, la disparition des formes ‘typiques du Trias’ semble résulter d'un schéma plus graduel d'extinctions sélectives tout au long du Trias supérieur, dont la plupart furent indépendantes de l'ETME. Un important renouvellement faunistique, probablement induit par une importante régression marine, semble survenir dès le début du Trias supérieur, provoquant l'extinction des faunes côtières et facilitant la diversification des taxons adaptés à une vie pélagique. Bien que les ichthyosaures et les eosauroptérygiens aient tous deux été impactés par la réduction des habitats de plus faible profondeur, ces derniers semblent avoir été plus sévèrement affectés. En effet, les eosauroptérygiens ont connu une chute importante de leur disparité, associée à la disparition de lignées dites ‘typiques du Trias moyen’ ayant précédemment subi une diversification morphologique remarquable, reflétant l'occupation d’une multitude de niches écologiques. Chez les ichthyosaures, la transition T/J a traditionnellement été associée à une diminution notable de la disparité et à un changement drastique dans l'occupation de leur morpho-espace. Cependant, nos analyses morphologiques multivariées révèlent une grande diversité de phénotypes cranio-dentaires au Jurassique Inférieur, illustrée par l’occupation de régions inexplorées du morpho-espace et une forte superposition avec celles des espèces du Trias. Même si ces analyses suggèrent un effet mineur des événements de la fin du Trias sur l'évolution morphologique des ichthyosaures, ils coïncident néanmoins avec la disparition finale des gigantesques shastasauridés, suggérant un certain degré de regroupement phylogénétique dans les extinctions et potentiellement une plus grande susceptibilité d’extinction chez les espèces de très grande taille lors de l'ETME.

REMERCIEMENTS — ACKNOWLEDGMENTS

Cette thèse de doctorat représente pour moi l'accomplissement d'un travail intense (voire très intense). Même si l'on peut supposer qu'un tel projet est le fruit d'un effort individuel, ce dernier n'aurait jamais pu voir le jour sans l'aide, tant professionnelle que morale, dont j'ai eu la chance de bénéficier au cours de ces quelques années.

Mes premiers remerciements vont à mon promoteur, Valentin Fischer, à qui je dois cette opportunité unique. Je tiens à particulièrement souligner la qualité de son encadrement, sa disponibilité et sa patience pour répondre à mes nombreuses questions ainsi que son soutien tout au long de la thèse. Valentin a toujours réussi à me recadrer lorsque j'avais tendance à m'éparpiller et à vouloir partir dans de nombreuses directions en même temps. Sans ses précieux conseils, la thèse n'aurait jamais pu être celle que vous vous apprêtez à lire (si vous en avez le courage et la patience). Nos nombreuses conversations sur les reptiles marins et sa passion pour le café vont indéniablement me manquer. Travailler à ses côtés a été un honneur pour moi.

Speaking of supervision, how could I not express my immense gratitude to Prof. Torsten Scheyer and Dr. Tom Stubbs? Their unwavering support, along with their enthusiasm and kindness throughout the entire duration of my PhD, have been invaluable to me. I have learned so much from them, and if I have become the scientist writing these words, it is also largely thanks to them I am truly honoured to have had the chance to collaborate with them. A special thanks goes to Torsten for his thoughtful supervision and the warm hospitality he extended during my research visits to Zurich.

Merci énormément au Prof. Baurain pour avoir fait partie de mon comité, pour son intérêt envers ce projet, pourtant éloigné de sa discipline, et pour l'ensemble des conseils fournis durant nos réunions. Je voudrais également remercier tous les curateurs et responsables de collections pour m'avoir autorisé à scanner ou étudier leur matériel mais également tous les chercheurs que j'ai eu le plaisir de côtoyer et qui ont fait évoluer mon regard sur ce sujet de thèse ou bien tout simplement sur la paléontologie, lors de nos conversations passionnantes, le plus souvent autour d'une, voire plusieurs bières.

Comment parler de cette thèse sans mentionner, l'EDDy Lab ? De nombreuses personnes ont transité par le laboratoire au cours de ces dernières années. Cependant, j'ai pu tisser des liens forts avec certaines d'entre elles que je n'oublierai jamais.

Narimane, Isaure (merci pour cette magnifique illustration), Léa, Raphaël, Romain, Christophe, Francesco, Guillaume et Melvin, merci du fond du cœur pour tous les bons moments passés en votre compagnie. Bien entendu, je remercie également les autres membres du labo que j'ai eu le plaisir de côtoyer tels que Julien, Cyrille, Léonard, Jamie, Rebecca ou encore Roland. Les bâtiments du B18– B20 à l'Université de Liège et les personnes y travaillant resteront aussi gravés dans ma mémoire. Mention spéciale pour Joëlle, Mariella, Valentine, Martin, Hadrien ou encore Bernard pour l'accueil au sein du département de Géologie et pour tout ce que vous m'avez apporté. J'ai passé avec vous des super moments.

Comme je l'ai mentionné au début de cette section, ce travail n'aurait pas pu se faire sans un énorme soutien moral. Et pour cela, quoi de mieux que d'être entouré par sa famille et ses amis ? Alors, un tout grand merci à mes parents pour m'avoir accompagné durant mes coups de mou et mes angoisses mais surtout pour avoir réussi à me rebooster lorsque j'en avais besoin. Je tiens également à remercier les autres membres de ma famille et ma belle-famille ainsi que tous mes amis pour avoir cru en moi et fait l'effort d'essayer de comprendre le sujet de ma thèse. Bien entendu, je me dois de remercier comme il se doit ma merveilleuse compagne, Alex, pour tout le soutien apporté, dans les bons comme dans les mauvais moments. L'avoir eu à mes côtés lors de cette épreuve a été une véritable force et m'a permis de surmonter de nombreux obstacles.

Finally, I would like to sincerely thank Dr. Bruno Frederich, Dr. Davide Foffa and Dr. Erin Maxwell for agreeing to be the examiners of this work as well as Dr. Loïc Michel for acting as president of the thesis jury.

'Don't adventures ever have an end? I suppose not. Someone else always has to carry on the story.'

J.R.R Tolkien, The Lord of the Rings

PUBLICATIONS DURING ENROLMENT

Laboury, A., R. F. Bennion, B. Thuy, R. Weis, and V. Fischer. 2022. Anatomy and phylogenetic relationships of *Temnodontosaurus zetlandicus* (Reptilia: Ichthyosauria). *Zoological Journal of the Linnean Society* 195:172–194.

MSc thesis work, **Appendix I**

Fischer, V., **A. Laboury**, K. Bernacki, L. Garbay, Y. Gillen, C. Rollinger, A. Thill, R. Weis, and B. Thuy. 2022. A fragmentary leptonectid ichthyosaurian from the lower Pliensbachian of Luxembourg. *Palaeontologia Electronica* 25.

Side project, **Appendix II**

Laboury, A., T. M. Scheyer, N. Klein, T. L. Stubbs, and V. Fischer. 2023. High phenotypic plasticity at the dawn of the eosauropterygian radiation. *PeerJ* 11:e15776.

Thesis **Chapter 1**

Laboury, A., T. L. Stubbs, A. S. Wolniewicz, J. Liu, T. M. Scheyer, M. E. H. Jones, and V. Fischer. 2024. Contrasting macroevolutionary patterns in pelagic tetrapods across the Triassic–Jurassic transition. *Evolution* qpae138.

Thesis **Chapter 2**

TABLE OF CONTENTS

INSTITUTIONAL ABBREVIATIONS

AGC, Alfred Gillett Collection, cared for by the Alfred Gillett Trust, C & J Clark Ltd, Street, Somerset, UK; **AGM**, Anhui Geological Museum, Hefei, Anhui, China; **BESC**, Material including this abbreviation in the label are located in the MSNM; **BGS**, The British Geological Survey, Keyworth, Nottingham, UK; **BRLSI**, Bath Royal Literary and Scientific Institution, Bath, UK; **BRSMG**, City of Bristol Museum and Art Gallery, Bristol, UK; **BRSUG**, University of Bristol, Bristol, UK; **BT**, Urwelt-Museum Oberfranken, Bayreuth, Germany, **CAMSM**, Sedgwick Museum of Earth Sciences, Cambridge University, Cambridge, UK; **CMC**, Cincinnati Museum Center, Museum of Natural History and Science, Cincinnati, Ohio, USA; **CMNH**, Chongqing Museum of Natural History, Chongqing, China; **DONMG**, Doncaster Museum and Art Gallery, Doncaster, UK; **FMNH**, Field Museum of Natural History, Chicago, USA; **FWD**, Werkforum, Dotternhausen- Dormettingen, Baden-Württemberg, Germany; **FZVE**, Material including this abbreviation in the label are located in the Museum of Natural History, University of Nevada, Las Vegas, USA; **GMPKU**, Geological Museum of Peking University, Beijing, China; **GMR,** Geological Survey of Guizhou Province, Guiyang, People's Republic of China ; **GNG**, Guanling National Geopark of Fossil Biota; **GPIT**, Palaeontological Collection of Tübingen University, Tubingen, Germany; **HAUFF**, Urwelt-Museum Hauff, Holzmaden, Germany; **GSM**, British Geological Survey, Keyworth, UK; **GZG**, Geoscience Centre, Georg-August University Göttingen; **HFUT**, Hefei University of Technology, Hefei, Anhui, China; **IGPS**, Institute of Geology and Paleontology, Tohoku University, Sendai, Japan; **IRSNB**, Royal Belgian Institute of Natural Sciences, Brussels, Belgium; **IVPP**, Institute of Vertebrate Paleontology and Paleoanthropy, Chinese Academy of Sciences, Beijing, China; **JLW**, Private collection Jos Lankamp, Borne, The Netherlands; **LACM**, Natural History Museum of Los Angeles County, Los Angeles, USA; **LEICS**, Leicestershire Museums, Arts and Records Service, Leicester, UK; **LPV**, Luoping Vertebrate Collection, Chengdu Institute of Geology and Mineral Resources, Chengdu, China; **LWL-MFN**, LWL-Museum für Naturkunde, Munster, Germany; **LYMPH**, Lyme Regis Philpot Museum, Lyme Regis, UK; **MACN**, Museo Argentino de Ciencias Naturales Bernardino Rivadavia, Buenos Aires, Argentina; **MAMSPLP**, Musée des Amis de la Mine, Saint-Pierre La Palud, France; **MANCH**, The Manchester Museum, Manchester, UK; **MCZ**, Museum of Comparative Zoology, Harvard University, Cambridge; **MHN**, Museon, The Hague, The Netherlands; **MB**, Naturkundmuseum Berlin, Berlin, Germany; **MFSN**, Museo Friulano di Storia Naturale,Udine, Italy; **MHNTV**, Muséum d'Histoire naturelle de Toulon et du Var, Toulon, France; **MMM**, Musée Municipal de Milleau, Aveyron, France; **MNHL**, National Museum of Natural History (Naturalis), Leiden, The Netherlands; **MNHNL**, Musée national d'histoire naturelle de Luxembourg, Luxembourg; **MUPA-ATZ**, El Atance collection, Museo de Paleontología de Castilla-La Mancha, Cuenca, Spain; **NHMW**, Naturhistorisches Museum, Wien, Austria; **NHMUK**, National History Musem, London, UK; **NMNS**, National Museum of Natural Science, Taichung, Taiwan, China; **NME**, Natuurmuseum Enschede, Enschede, The Netherlands; **NMING**, National Museum of Ireland, Dublin, Ireland; **NMO**, Naturmuseum Olten, Olten, Switzerland; **NMW**, National Museum of Wales, Cardiff, UK; **NSM-LV**, Neveada State Museum, Las Vegas Collections, USA; **OMU**, Urwelt-Museum, Bayreuth, Germany; **OUMNH**, Oxford University Museum of Batural History, Oxford, UK; **PIMUZ**, Paläontologisches Institut der Universität Zürich, Zürich, Switzerland; **PLV**, Palaeontology collections, Katholieke Universiteit Leuven; **PMO**, Natural History Museum, University of Oslo (Palaeontological collection), Oslo, Norway; **ROM**, Royal Ontario Museum, Toronto, Canada; **SGU**, Saratov State University, Saratov, Russia; **SIPG**, Steinmann-Institut, Paläontologie, Universität Bonn, Germany; **SMNS**, Staatliches Museum für Naturkunde, Stuttgart, Germany; **TCD**, Geological Museum, Trinity College Dublin, Dublin, Ireland; **(R)TMP**, Royal Tyrrell Museum of Palaeontology, Drumheller, Canada; **TTNCM**, Somerset County Museum, Taunton, UK; **TWE**, Museum TwentseWelle, Esnchede, The Netherlands; **UCMP**, Museum of Paleontology, University of California, Berkeley, USA; **UMO**, Urwelt-Museum Oberfranken, Bayreuth; Germany; **UNM**, University of Nottingham Museum, Nottingham, UK; **UPM**, Undory Palaeontological museum, Undory, Russia; **USNM**, Smithsonian Institution, Washington, USA; **WGSC**, Wuhan Centre of China Geological Survey, China; **WHGMR**, Wuhan Institute of Geology and Mineral Resources; **WHITM**, Whitby Museum, Whitby, UK; **WGSC**, Wuhan Centre of China Geological Survey, Wuhan, Hubei, China; **WS**, Keichousaurus Museum of Xingyi National Geological Park, Xingyi, Guizhou, China; **XNGM**, Xingyi National Geopark Museum, Xingyi, Guizhou, China; **YGMIR**, Yichang Institute of Geology and Mineral Resources, Yichang, China; **YORYM**, Yorkshire Museum, York, UK; **ZIN PH,** Zoological Institute of the Russian Academy of Sciences, St Petersburg, Russia; **ZMNH**, Zheijiang Museum of Natural History, Hangzhou, China.

GENERAL INTRODUCTION

Marine amniote generalities and the weirdness of Triassic faunas

Over the past roughly 250 million years, the evolution of the biosphere has been continuously influenced by successive land to sea transitions experienced by tetrapods (Kelley and Pyenson 2015; Vermeij and Motani 2018). Although factors facilitating the initial colonization of marine environments remain unclear, ecological disruptions in terrestrial and marine ecosystems after major extinction events presumably played a crucial role in these transitions (Vermeij and Motani 2018). Since the Cenozoic, mammals (*e.g.* cetaceans, pinnipeds and sirenians), along, to a lesser extent, with birds (*e.g.* pinguins), have been regarded as one of the dominant amniotes in the seas (Vermeij and Dudley 2000; Pyenson et al. 2014). During the Mesozoic (251.9–66 Ma), similar ecological niches to those of extant marine mammals were filled by a polyphyletic assemblage termed 'Mesozoic marine reptiles' (Bardet 1994; Motani 2009; Bastiaans 2024). Throughout this era, tens of lineages of terrestrial amniotes independently re-invaded the marine realm and ruled the oceans for millions of years (Motani 2009; Benson 2013; Bardet et al. 2014; Kelley and Pyenson 2015). While some reptiles are still nowadays dependent on marine ecosystems (*e.g.* sea turtles, the saltwater crocodile and squamates such as sea snakes or marine iguana), their taxonomical and ecological diversities are far from those of their predecessors (Motani 2009; Rasmussen et al. 2011; Benson 2013). Marine reptiles indeed underwent a remarkable diversification over the course of the Mesozoic, evolving a wide range of body plans that notably reflect adaptations to different swimming styles, body sizes or feeding strategies (O'Keefe 2002; Stubbs and Benton 2016; Foffa et al. 2018b, 2024; Gutarra and Rahman 2021; Sander et al. 2021; Gutarra et al. 2023).

The evolutionary history of Mesozoic marine reptiles began in the aftermath of the Permian–Triassic mass extinction event (PTME), currently regarded as the most severe biodiversity crisis in Earth's history (Raup and Sepkoski 1982; Sepkoski 1996; Bambach et al. 2004; McGhee et al. 2013; Dal Corso et al. 2022). The intense volcanic activity of the Siberian traps–leading to global warming, acidification and anoxia–profoundly affected the entire biosphere, resulting in the loss of ≥ 90% of the metazoan diversity (Wignall

2001; Knoll et al. 2007; McGhee et al. 2013; Benton and Newell 2014; Song et al. 2014). The Triassic subsequently witnessed the long and delayed recovery of ecosystems in the aftermath of the PTME (Song et al. 2011, 2018; Chen and Benton 2012; Benton et al. 2013; Cheng et al. 2022). The severity of the extinction led to a profound restructuring of ecosystems, and the Triassic is considered as an exceptional period of proliferation and ecological innovation (Stanley 2009; Chen and Benton 2012; Salamon et al. 2012; Benton et al. 2013; Benton 2014; Motani et al. 2015a; Romano et al. 2016; Stubbs and Benton 2016; Qiao et al. 2022). One key aspect of the Triassic biotic recovery in marine ecosystems is the extremely rapid radiation of multiple lineages of reptiles that had recently invaded the marine realm, at the expense of other predators (*e.g.* fishes and temnospondyls) (Chen and Benton 2012; Scheyer et al. 2014; Motani et al. 2017; Kear et al. 2023). Indeed, within the first few million years of the Triassic, marine reptiles underwent an extraordinary morphological diversification in both nearshore and pelagic environments, producing numerous body plans and craniodental architectures reflecting the occupation of an extremely wide array of ecological niches (Dick and Maxwell 2015; Stubbs and Benton 2016; Moon and Stubbs 2020; Reeves et al. 2021; Sander et al. 2021; Wang et al. 2022; Gutarra et al. 2023). This radiation not only saw the emergence of Ichthyopterygia and Eosauropterygia, which account for a sizeable chunk of the total taxonomic diversity of Mesozoic marine reptiles, but also a panoply of less speciose and shorter-lived lineages that were restricted to the Triassic (Carroll and Dong 1991; Motani 2009; Li et al. 2011; Benson 2013; Motani et al. 2015b; Wang et al. 2022; Wolniewicz et al. 2023; Bastiaans 2024). Some of these lineages, such as small hupehsuchians, omphalosaurids, saurosphargids, and thalattosaurs are currently regarded as close-relative of either ichthyopterygians (Motani et al. 2015b; Jiang et al. 2016; Qiao et al. 2022), or eosauropterygians (Neenan et al. 2013; Simões et al. 2020; Wang et al. 2022; Wolniewicz et al. 2023) while the others represent independent invasions of more distantly related taxa, such as *Vancleavea* or the tanysaurian archosauromorphs (Nesbitt et al. 2009; Kelley 2012; Spiekman et al. 2024).

Most notably, Triassic marine reptiles developed numerous unique feeding strategies and prey acquisition methods in the evolutionary history of marine reptiles such as lunge feeding in the edentulous, long-snouted hupehsuchians (Carroll and Dong 1991; Motani et al. 2015a), herbivory in the enigmatic *Atopodentatus* (Cheng et al. 2014; Li et al. 2016), or durophagy among diverse lineages (*e.g.* omphalosaurids, thalattosaurs, mixosaurids ichthyopterygians and placodont sauropterygians) (Rieppel 2002; Kelley et al. 2014; Huang et al. 2020; Qiao et al. 2022) — though some Late Cretaceous

globidensine mosasaurids further developed a durophageous dentition (Bardet et al. 2005; Fischer et al. 2022a; MacLaren et al. 2022). Additionally, Triassic marine reptiles also displayed a wide range of body sizes, with some macropredatory ichthyopterygians rapidly evolving towards gigantism (Moon and Stubbs 2020; Sander et al. 2021; Gutarra et al. 2023). Collectively, the Triassic therefore concentrates a wide range of peculiar morphotypes and an enormous amount of disparity (*i.e.* morphological diversity), making faunas from that period markedly different from those of the Jurassic and the Cretaceous. While 'typically' Triassic marine reptile lineages progressively disappeared over multiple extinction events during this period, only ichthyopterygians and eosauropterygians crossed the Triassic–Jurassic transition (Bardet 1994; Motani 2009; Thorne et al. 2011; Kelley 2012; Renesto and Dalla Vecchia 2018) and will therefore be described in detail in the following sections.

Anatomy and systematics of Ichthyopterygia

Generalities

Ichthyopterygia is a clade of fully aquatic eel- to tuna-shaped reptiles that appeared in the fossil record only ~2 million years after the PTME and that became extinct by the end of the Cenomanian (~94 Ma, early Late Cretaceous) (Bardet 1992; Motani 2005; Fischer et al. 2016; Kear et al. 2023). Spanning 156 million years, Ichthyopterygia was the second longest-lived clade of Mesozoic marine reptiles, only surpassed by sauropterygians (Motani 2009; Bardet et al. 2014). Ichthyopterygians were part of the first wave of Mesozoic reptiles to colonize the marine realm, emerging either prior or shortly after the end of the Permian (Carroll and Dong 1991; Rieppel 2000; McGowan and Motani 2003; Motani et al. 2017; Wang et al. 2022; Kear et al. 2023; Bastiaans 2024). These animals rapidly achieved a broad geographic distribution along the northern coast of the Pangea supercontinent, as their early evolutionary history is relatively well-documented with fossils from Canada, Svalbard archipelago, Japan, China, and eastern Russia (Brinkman et al. 1992; Motani 1998a; Motani et al. 1998; McGowan and Motani 2003; Cuthbertson et al. 2013; Maxwell and Kear 2013; Bardet et al. 2014; Takahashi et al. 2014; Huang et al. 2019; Nakajima et al. 2022; Kear et al. 2023) Early Triassic ichthyopterygians retained a plesiomorphic ('ancestral') morphology of small- to medium-sized 'lizard with flippers' (Motani et al. 1996; Motani 2005; Huang et al. 2019). Indeed, these animals exhibited a typical phenotype of anguilliform swimmers (**Figure 1A**), featuring a relatively small head, a streamlined body shape with an elongated trunk, the absence of a dorsal and caudal fins, and limbs that did not yet evolved into efficient flippers (Massare and Callaway 1990;

Motani et al. 1996; Motani 1997a, 1998a; Motani and You 1998a; Benson 2013; Chen et al. 2013; Huang et al. 2019). Despite their (at the time) recent invasion into marine environments, early-diverging ichthyopterygians rapidly developed key traits associated with a fully aquatic life. These adaptations notably include viviparity — the ability to give birth to live young — (Motani et al. 2014; Miedema and Maxwell 2022), and a reorganization of the inner bone structure in some taxa which are presumed to have a pelagic lifestyle (Nakajima et al. 2022; Kear et al. 2023).

Ichthyosauria, meaning 'fish-lizard', represents the major clade within Ichthyopterygia, comprising all taxa with the exception of early-diverging lineages of the Early Triassic (Motani 1999b; Ji et al. 2016; Huang et al. 2019). Ichthyosaurians were the first marine reptiles that evolved a highly hydrodynamic body profile, adapted for high-speed swimming and resembling to those observed in extant delphinoids, tuna fish or lamnid sharks (Buchholtz 2001; Motani 2002b, 2005, 2009; McGowan and Motani 2003; Lingham-Soliar and Plodowski 2007; Lingham-Soliar 2016; Bonnevier Wallstedt et al. 2024) (**Figure 1B**). Ichthyosaurians were tail-propelled raptorial tetrapods, characterized by a streamlined morphology, limbs modified into compact paddles resulting from hyperphalangy and hyperdactyly, a reduction of the pelvic girdle size, along the presence of a dorsal fin and a crescent-shaped caudal fluke (Motani 2005, 2009; Benson 2013). Furthermore, their cranium is distinguished by an elongated snout, the presence of conical teeth and large orbits filled by sclerotic rings (Motani, 2005), making them efficient predators to capture not only soft-bodied preys and fishes but also larger tetrapods among bigger species (Pollard 1968; Massare 1987a; Böttcher 1989; Kear et al. 2003; Massare and Young 2005; Lomax 2010; Dick et al. 2016; Fischer et al. 2016). The well-known 'fish-shaped' phenotype (**Figure 1B**) however almost exclusively concerns members of Parvipelvia–which appeared in the early Norian (~227–216 Ma) during the Late Triassic–and mainly encompasses all post-Triassic ichthyosaurians (**Figure 2**) (Motani 1999b, 2005; McGowan and Motani 2003). Evidence from the fossil record instead indicates that such a highly hydrodynamic profile was progressively acquired over the course their evolutionary history during the Triassic (Motani et al. 1996; McGowan and Motani 2003; Motani 2005), likely driven by selective extinctions through time (*e.g.* see Kelley et al. 2014).

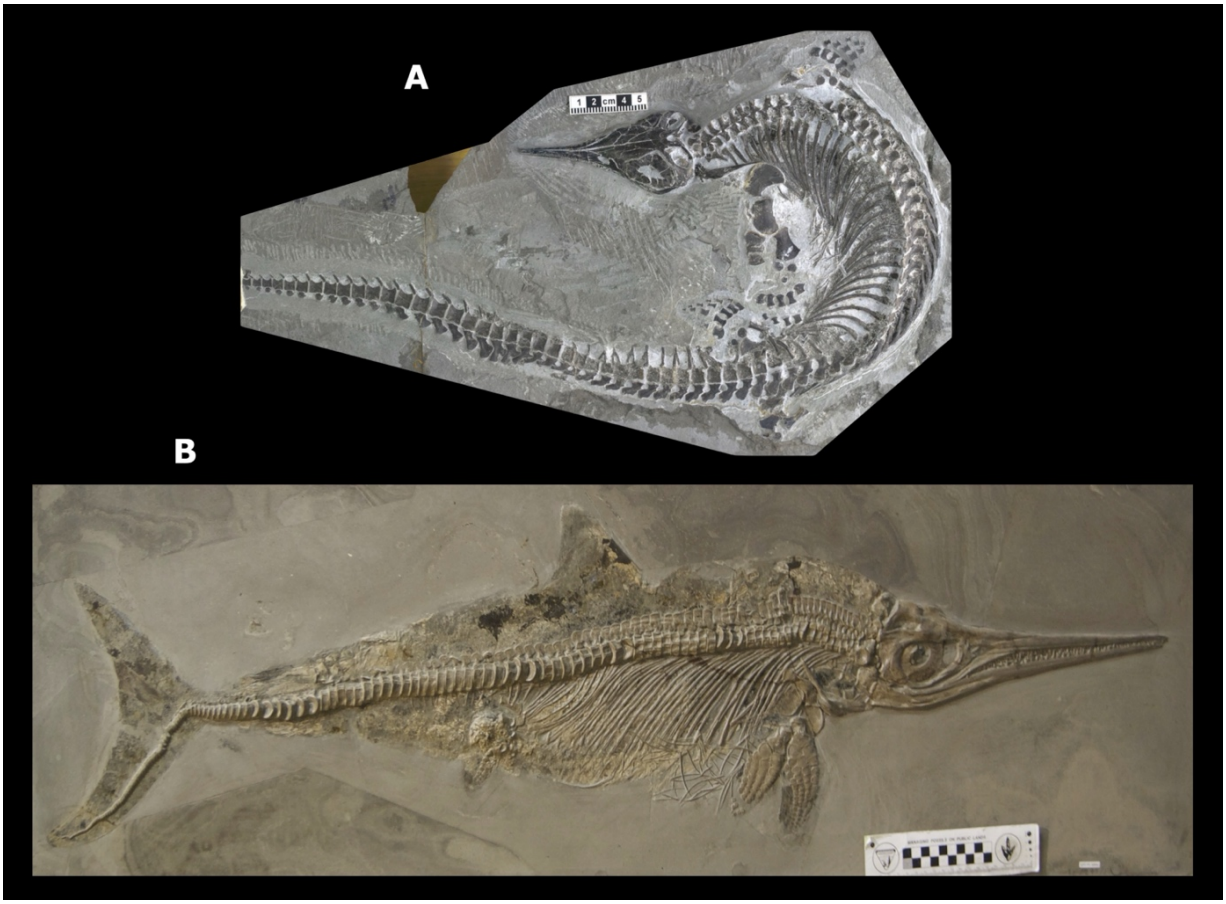

Figure 1. Body plan of (A) an Early Triassic ichthyopterygian and (B) an Early Jurassic 'fish-shaped' ichthyosaurian'. (A) *Chaohusaurus brevifemoralis* (AGM AGB 7401; modified from Huang et al. 2019). (B) *Stenopterygius quadriscissus* (GPIT PV 30042). In (B) each square on the scale bar equals 1 cm.

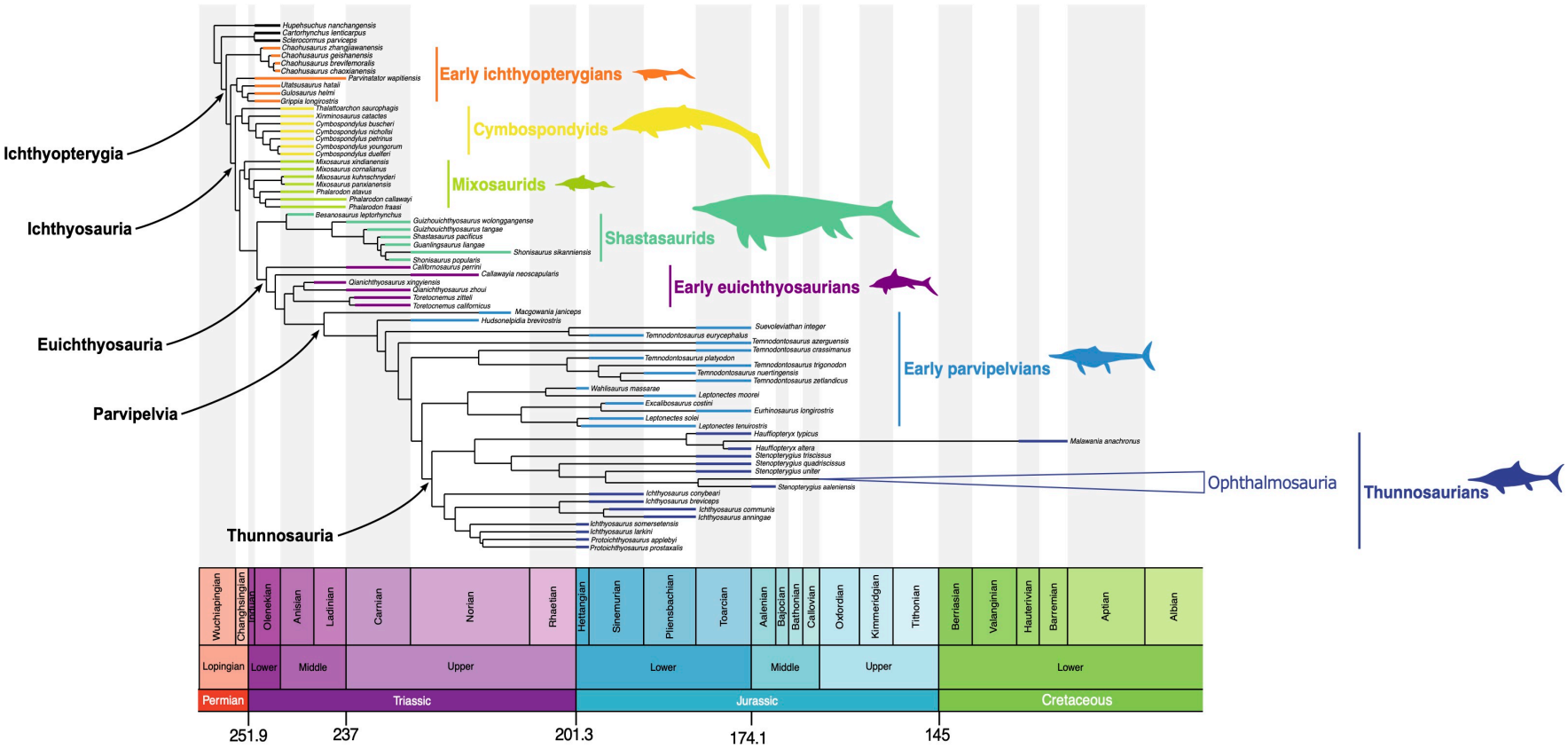

Figure 2. Time-scaled ichthyosaurian phylogenetic composite tree arising from the datasets of Bindellini et al. (2021) and Laboury et al. (2022) for Triassic and post-Triassic taxa respectively. The composite tree has been calibrated by using the Hedman algorithm.

Cymbospondylids and mixosaurids

Middle Triassic ichthyosaurian assemblages were predominantly dominated by two major lineages, cymbospondylids and mixosaurids. Cymbospondylidae is widely regarded as the most primitive ichthyosaurian clade (**Figure 2**) (Motani 1999b; Ji et al. 2016; Motani et al. 2017; Huang et al. 2019; Sander et al. 2021), although some recent phylogenetic analyses have placed this clade as more derived than mixosaurids (Moon 2017). Cymbospondylids and mixosaurids both exhibited a broad distribution across the Tethys and the Panthalassa oceans, with fossils discovered in China, Europe, Svalbard archipelago and North America(Merriam 1908; Sander 1989a, 1992; Nicholls and Brinkman 1995; Fröbisch et al. 2006, 2013; Jiang et al. 2006b, 2008a, 2009; Hurum et al. 2014; Klein et al. 2020; Sander et al. 2021; Fang et al. 2024). Cymbospondylids primarily includes large to gigantic pelagic taxa, ranging from almost 5 to 17m long (Merriam 1908; Fröbisch et al. 2006, 2013; Klein et al. 2020; Sander et al. 2021). The recent discovery of *Cymbospondylus youngorum* (**Figure 3A**), estimating at 17m in length, has revealed that these animals were among the earliest marine reptiles to evolve towards gigantism (Sander et al. 2021). Even though their overall anatomy is incompletely known, cymbospondylids are characterized by an elongated trunk (Merriam 1908; Sander 1989a), which, given to their size, indicates that they were among the largest macropredators during the Anisian (247.2–242 Ma, early Middle Triassic).

Mixosauridae is one of the best-known ichthyosaurian clades, which have been intensively studied in recent years due to the availability of well-preserved material (Brinkman 1996; Maisch and Matzke 1998; Schmitz et al. 2004; Kolb et al. 2011; Renesto et al. 2020; Engelschiøn et al. 2023; Miedema et al. 2023a,b; Fang et al. 2024). Mixosaurids (**Figure 3B and C**) were small-bodied, ranging from 0.5 to 2m long, coastal or semi-pelagic ichthyosaurians (Motani 2005; Roberts et al. 2022). These animals have developed a more compact fusiform body shape, characterized by a large cranium, flippers — though less derived and compact than those of parvipelvians — a dorsal fin, as well as a modified tail adapted for high-speed acceleration (Motani 1998b, 1999a, 2005; Renesto et al. 2020; Roberts et al. 2022; Bindellini et al. 2024). Compared with the coeval cymbospondylids and early-diverging shastasaurids (see below) which lacked a dorsal fin, and retained a more anguilliform swimming style, it has recently been proposed that mixosaurids convergently developed morphological adaptations likely similar to those of the ‘fish-shaped’ parvipelvians (Bindellini et al., 2024). Mixosauridae consists of two genera, primarily differentiated by their dentition. More specifically, *Phalarodon* possesses posterior bulbous crushing teeth, characteristic of durophagous

taxa, whereas *Mixosaurus* exhibits a more uniform dentition, with some posterior teeth that may increase in size (Motani 1997b, 1999d; Liu et al. 2013; Engelschiøn et al. 2023).

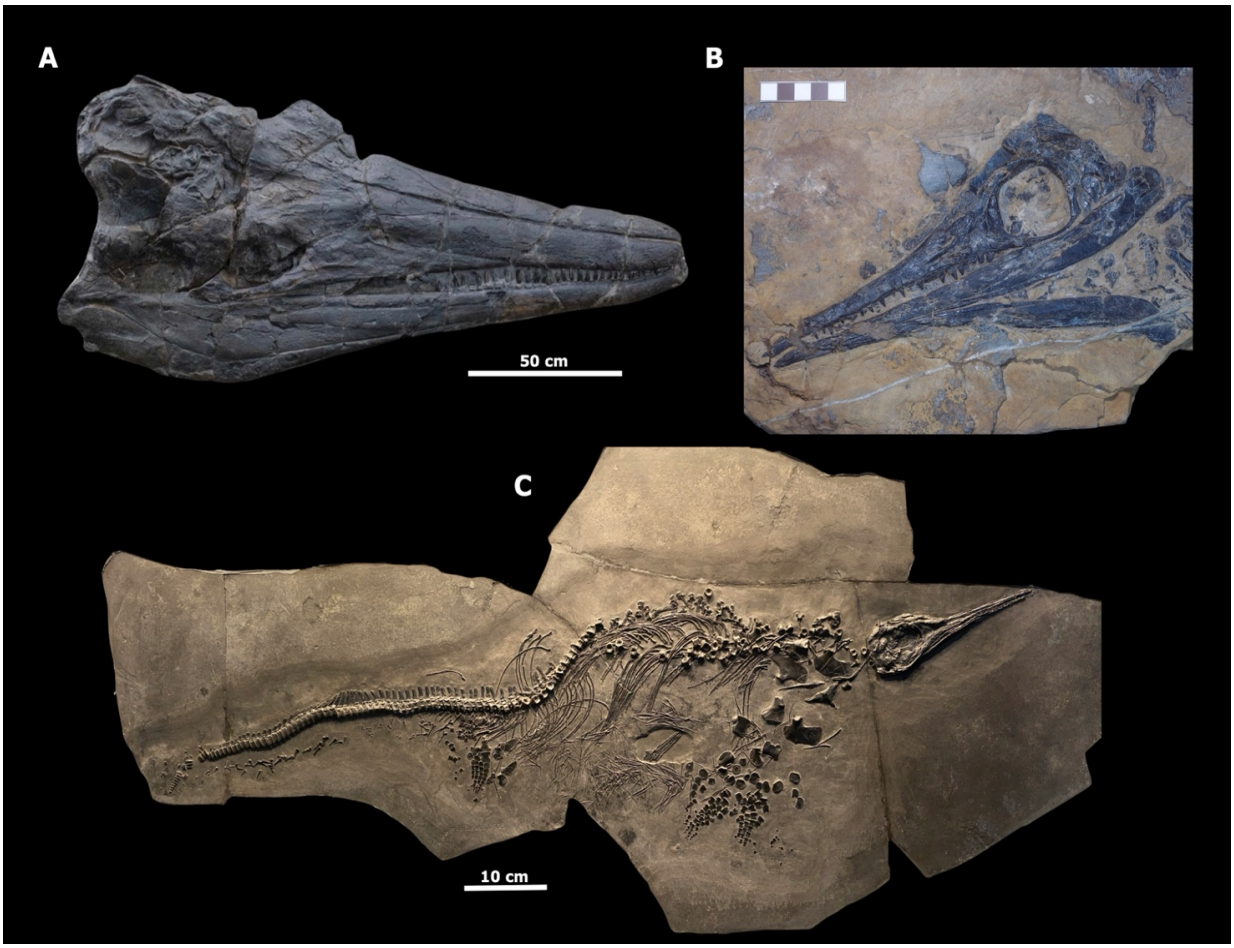

Figure 3. Anatomy of cymbospondylids and mixosaurids. (A) Cranium of *Cymbospondylus youngorum* (LACM DI 157871; modified from Sander et al. 2021). (B) Cranium of *Mixosaurus panxianensis* (GMPKU–P–1033; photo provided by A. S. Wolniewicz). (C) Partially articulated specimen of *Mixosaurus cornalianus* (PIMUZ T 4848; photo provided by F. Miedema). In (B), each square on the scale bar equals 1 cm.

Shastasaurids and early euichthyosaurians

Although they seemingly emerged in the Middle Triassic, the Late Triassic — often regarded as a prolific period for ichthyosaurians, considering the diversity of forms and ecologies — witnessed the diversification of two geographically widespread pelagic lineages: shastasaurids and euichthyosaurians (Merriam 1902; Dong 1972; Callaway and Massare 1989; McGowan 1995, 1996a; Dal Sasso and Pinna 1996; Nicholls and Manabe 2004; Sander et al. 2011; Yang et al. 2013; Fischer et al. 2014b; Motani et al. 2017; Zverkov et al. 2022). These two lineages form together the clade Merriamosauria (see Chapter 2) (Motani, 1999b). Shastasaurids include large to colossal taxa, ranging from 5 to more than 20 m long, with the whale-sized species representing the most gigantic marine tetrapods of the Mesozoic (Dal Sasso and Pinna 1996; Nicholls and Manabe 2004; Sander et al. 2011, 2022; Lomax et al. 2018a, 2024; Bindellini et al. 2021; Kelley et al. 2022). As mentioned by Bindellini et al. (2021), phylogenetic relationships among shastasaurids remain controversial. Indeed, even though some studies recovered the clade as monophyletic (Motani 1999b; Jiang et al. 2016; Ji et al. 2016; Motani et al. 2017; phylogenetic analyses in the Chapter 3), 'Shastasauridae' rather appears polyphyletic (Moon 2017; Maxwell and Cortés 2020; Laboury et al. 2022) or as a grade (Sander 2000; Sander et al. 2011; Bindellini et al. 2021, 2024) in numerous phylogenies. As evidenced by their craniodental architecture, shastasaurids are considered as a disparate group, which has displayed a broad spectrum of feeding strategies such as edentulous ram-feeders (Nicholls and Manabe 2004; Sander et al. 2011; Motani et al. 2013), 'soft-prey specialists' (Bindellini et al., 2021) and macropredators (Motani et al. 1999; Jiang et al. 2020; Kelley et al. 2022 but also see Sander et al. 2022) (Figure 4). While shastasaurids retained an elongated, flexible trunk similar to cymbospondylids, their long tail would feature a pronounced heterocercal caudal fluke, suggesting a more anguilliform or subcarangiform swimming style compared to euichthyosaurians (Motani 2008; Bindellini et al. 2024). Furthermore, in fast raptorial feeders such as *Besanosaurus* and *Guizhouichthyosaurus*, the combination of relatively long forefins and tail morphology likely enhanced their manoeuvrability during hunting (Shang and Li 2009; Bindellini et al. 2024).

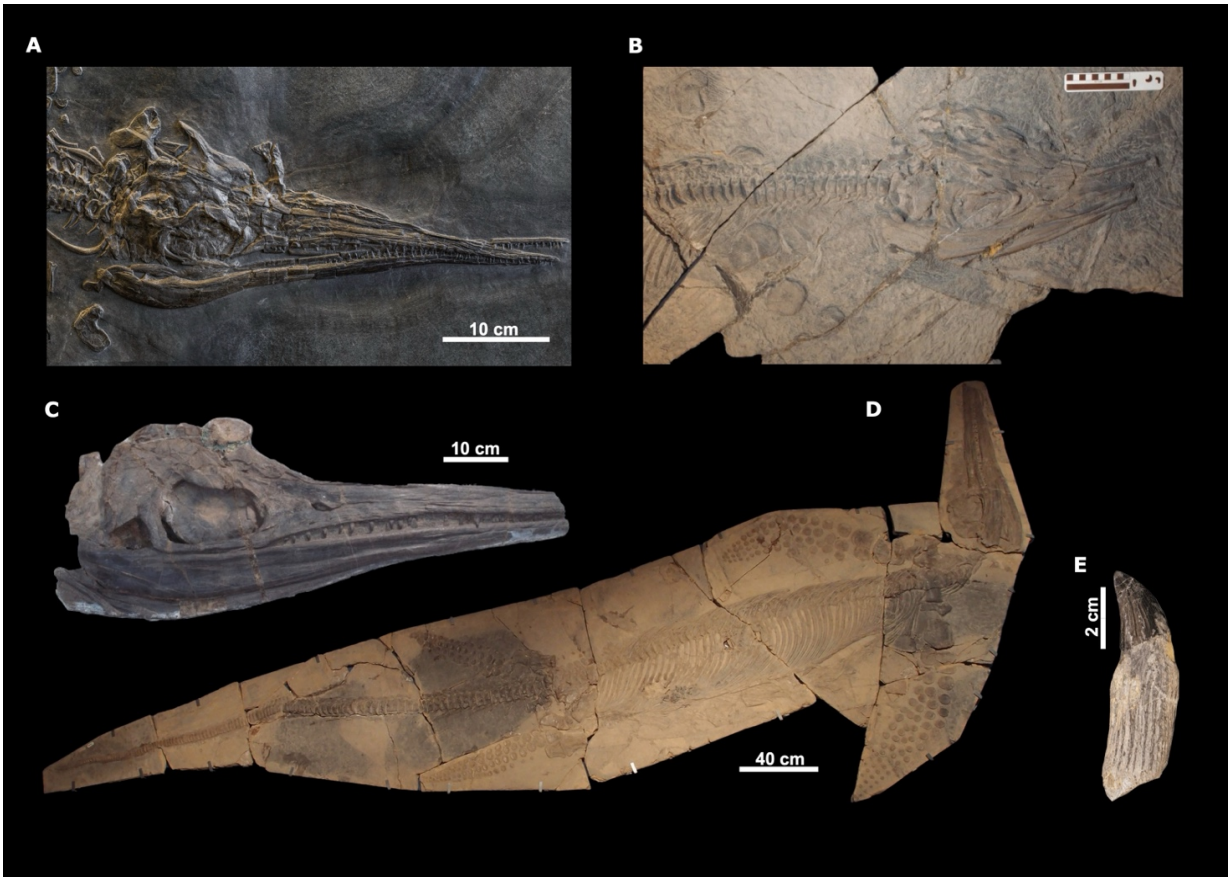

Figure 4. Craniodental and postcranial anatomy of shastasaurids. (A) Cranium of 'soft-prey specialist' *Besanosaurus leptorhynchus* (PIMUZ T 4376; modified from Bindellini et al. 2021). (B) Cranium the short-snouted, edentulous *Guanlingsaurus liangae* (YGMIR SPCV03108; photo provided by A. S. Wolniewicz). (C and D) Cranium (C) and nearly complete skeleton of the macropredatory *Guizhouichthyosaurus tangae* (C: IVPP V 11869 and D: YGMIR TR0001, photos provided by A. S. Wolniewicz). (E) Complete tooth of *Shonisaurus* (UMNH VP 32539; modified from Kelley et al. 2022). In (B), each square on the scale equals 1

Euichthyosauria is the clade that comprises toretocnemids and their sister lineage, the parvipelvians, along more basal species such as *Callawayia neoscapularis* or *Californosaurus perrini* (Motani et al. 2017; Huang et al. 2019; Bindellini et al. 2021). Toretocnemids are Middle to Late Triassic (242–227 Ma; Ladinian–Carnian) ichthyosaurians primarily documented from China and North America (Merriam 1908; Li 1999; Lucas 2002; Yang et al. 2013), though some remains exhibiting a toretocnemid affinity have also been recently discovered in the Russian Arctic (Zverkov et al. 2022). Most of our knowledge of Toretocnemidae primarily comes from examination of *Qianichthyosaurus* specimens from China (Li 1999; Nicholls et al. 2002; Yang et al. 2013).

Toretocnemids are peculiar small-sized ichthyosaurians (1–1.5 m in length) which closely resemble parvipelvians, sharing features such as a short, robust trunk and a caudal fluke (Li 1999; Nicholls et al. 2002; Motani 2008; Yang et al. 2013). However, some differences are still notable between the two lineages. Indeed, the cranium of *Qianichthyosaurus* is characterized by a slenderer and shorter snout, as well as relatively larger orbits, while their zeugopodial bones (*e.g.* radius, ulna, tibia and fibula) are still elongated, retaining a more plesiomorphic condition (**Figure 5A**) (Merriam, 1908; Nicholls et al., 2002; Yang et al., 2013).

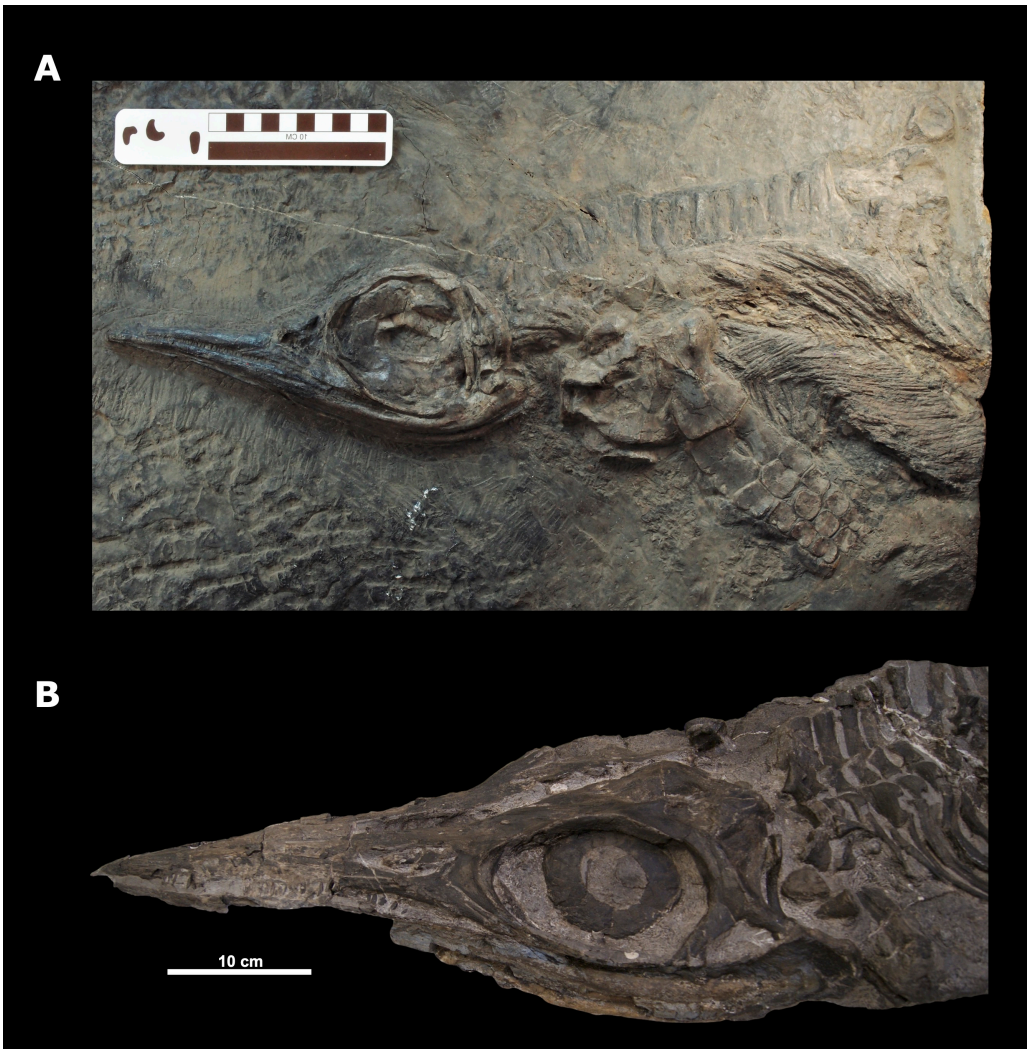

Figure 5. Anatomy of toretocnemids and early diverging parvipelvians. (A) Anterior skeleton of the toretocnemid *Qianichthyosaurus zhoui* (IVPP V 11839; photo provided by A. S. Wolniewicz). (B) Cranium of the Late Triassic parvipelvian *Macgowania janiceps* (TMP 2009.121.0001). In (A), each square on the scale bar equals 1 cm.

Parvipelvia, meaning ‘small pelvic girdle’, is the best known clade of ichthyosaurians, comprising all ‘fish-shaped’ ichthyosaurians (**Figure 1B**) from the Norian to the end of the Cenomanian (McGowan 1995, 1996a; Motani 2005, 2009; Fischer et al. 2016). During the Late Triassic, small- and medium-sized early diverging parvipelvians, such as *Hudsonelpidia brevirostris* and *Macgowania janiceps* (**Figure 5B**), found in the Pardonet Formation (British Columbia, Canada), were the only representatives of this clade (McGowan 1995, 1996a). Parvipelvia became the only surviving lineage in the aftermath of the Triassic–Jurassic (T/J) transition (Motani 2005; Thorne et al. 2011), and exhibited a considerable taxonomic diversity in the Early Jurassic (**Figure 2**), represented by iconic clades such as *Ichthyosaurus*, Leptonectidae, *Temnodontosaurus*, *Hauffiopteryx* or *Stenopterygius*. However, the systematic of Early Jurassic parvipelvians appears poorly constrained (see topologies from Godefroit 1993, Motani 1999b, Maisch and Matzke 2000, Ji et al. 2016, Moon 2017, Maxwell and Cortés 2020, Bindellini et al. 2021, Laboury et al. 2022), though their classification is getting better, thanks to the adoption of an apomorphy-based taxonomy (*e.g.* Maisch 2008; Martin et al. 2012; Lomax 2016; Lomax and Massare 2016; Maxwell and Cortés 2020; Swaby and Lomax 2020; Laboury et al. 2022).

The evolution of parvipelvians during the Early Jurassic is exceptionally well-documented, owing to the presence of Lagerstätten sites which exhibit a remarkable preservation of hundreds of specimens, such as Lyme Regis (Blue Lias Formation; 201.3–190.8 Ma; Hettangian–Sinemurian) or Holzmaden (Posidonienschiefer Formation; ~182.7–180.7 Ma; lower Toarcian) in Western Europe (Owen 1840, 1861; Fraas 1891; von Huene 1922). The first ichthyosaurian material to be scientifically described by Home (1814) — later classified as *Temnodontosaurus platyodon* (specimen NHMUK PV R 1158) — was collected by Joseph and the renowned Mary Anning in 1811 at Lyme Regis, along the southern coast of England (Torrens, 1995). These Lagerstätten have greatly enhanced our understanding of ichthyosaurian aspects such as ontogenetic development (Miedema & Maxwell, 2019, 2022), body shape, skin structure through preserved impressions (Lingham-Soliar 1999, 2001; Lingham-Soliar and Plodowski 2007; Lindgren et al. 2018), as well as gastric content (Pollard 1968; Böttcher 1989; Dick et al. 2016).

In addition to a broad range of body sizes (from 1 to 10 m long), Early Jurassic parvipelvians displayed distinct cranial architectures (**Figure 6**) and dental morphologies, indicating diverse feeding specializations and probable niche partitioning (McGowan 1989b, 2003; McGowan and Motani 2003; Martin et al. 2012; Dick and Maxwell 2015; Maxwell and Cortés 2020; Fischer et al. 2022b; Bennion et al. 2024). This

morphological diversity is mainly exemplified by the presence of apex predators among the large temnodontosaurids (**Figure 6A**) (McGowan 1996b; Bennion et al. 2024), longirostrine forms, such as the swordfish *Eurhinosaurus* (**Figure 6B**) (McGowan 1989a,b, 2003; Martin et al. 2012), alongside small, fast swimmers that were either soft-prey specialists or generalists (Massare 1987; Dick and Maxwell 2015). These fast swimmers among Early Jurassic taxa are represented by thunnosaurians, essentially comprising ichthyosaurids and stenopterygids (**Figure 6C and D**) (Motani 1999b; Fischer et al. 2013a) which evolved towards a more pronounced thunniform body plan (Massare 1988; Motani 1996, 2002a,b, 2005; Buchholtz 2001).

The Early Jurassic is characterized by a turnover between the relatively similar assemblages from the Hettangian to the Pliensbachian and those of the Toarcian — coinciding with the Jenkyns Event, also termed as the early Toarcian Oceanic Event (Jenkyns 1985, 2010; Müller et al. 2016; Reolid et al. 2020, 2024) — marked by the radiation of stenopterygids (McGowan and Motani 2003; Fischer et al. 2022 and references therein; Reolid et al. 2024). Subsequently, the Early–Middle Jurassic transition saw the final demise of non-thunnosaurian parvipelvians, resulting in a significant loss of peculiar ecological adaptations (Lingham-Soliar 2003; Maxwell 2012; Vincent et al. 2013b; Brusatte et al. 2015; Stubbs and Benton 2016; Fischer et al. 2021a; Miedema et al. 2024; Reolid et al. 2024). While some stenopterygids persisted in the Aalenian and Bajocian stages (174.1–168.3 Ma; Middle Jurassic) (Fernández 1994; Maxwell et al. 2012), the Middle Jurassic witnessed the radiation and ensuing dominance of ophthalmosaurids until the end of the ichthyosaurian evolutionary history (Maxwell et al. 2012; Fischer 2013; Fischer et al. 2021a; Miedema et al. 2024).

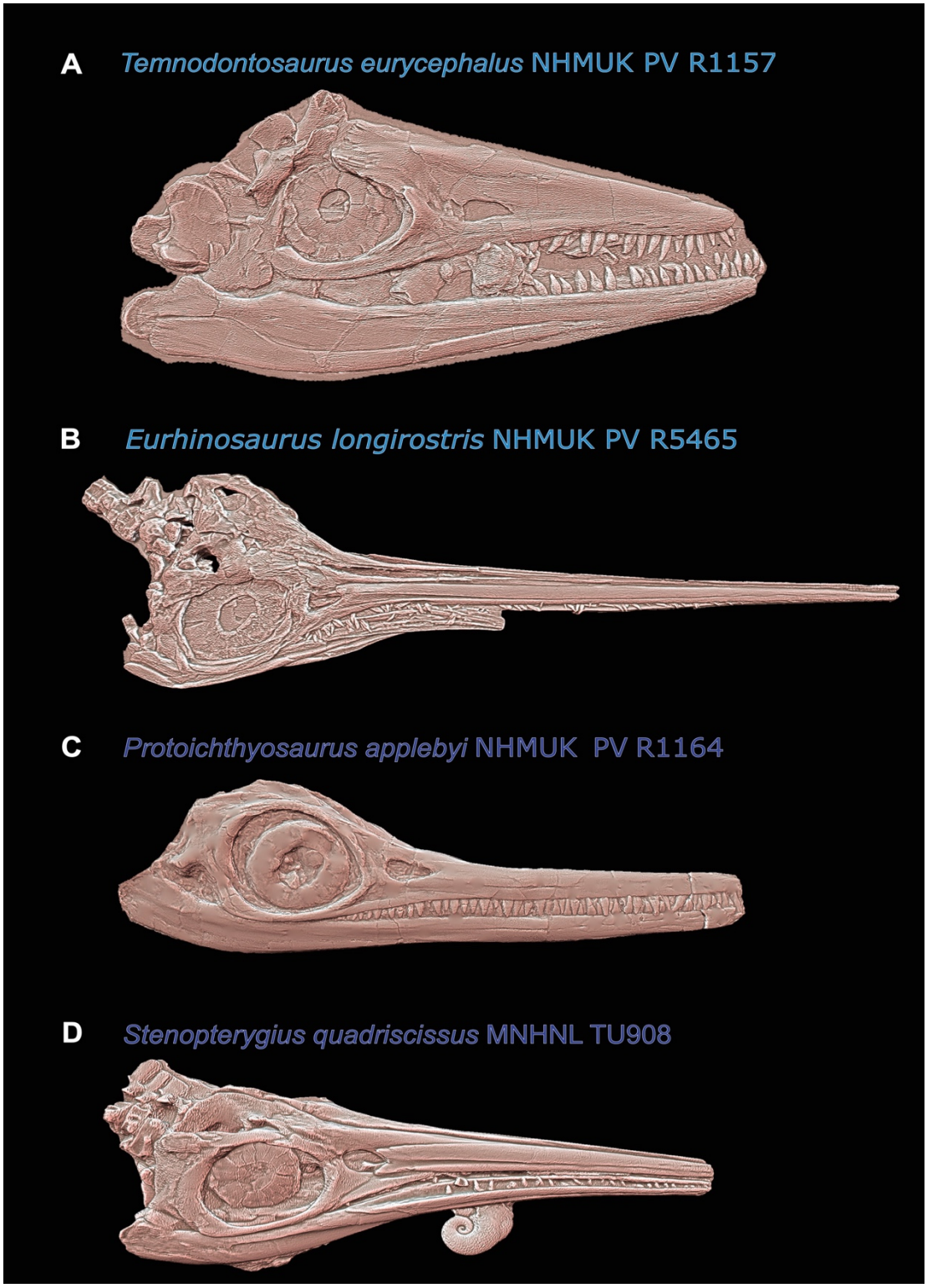

Figure 6. Diversity of craniodental architecture among Early Jurassic parvipelvians. The name of each taxon is coloured with respect to its relative group (light blue: early parvipelvians, dark blue: thunnosaurians,). 3D models were created by (A and B) R. F. Bennion, (C) E. Coombs and (D) V. Fischer.

Anatomy and systematics of Sauropterygia

Generalities

Sauropterygia represents, by far, the longest-lived and the most speciose clade of Mesozoic marine reptiles (Rieppel 2000; Motani 2009; Benson et al. 2010; Bardet et al. 2014). Like ichthyopterygians, sauropterygians rapidly emerged as a fully aquatic clade during the Olenekian (Case 1936; Rieppel 2000; Jiang et al. 2014; Wang et al. 2022), suggesting a Permian to an earliest Triassic origin. These reptiles disappeared at end of the Maastrichtian (66 Ma; end of the Cretaceous), thus lasting for more than 180 million years (Bardet 1994; Rieppel 2000; Motani 2009; Benson et al. 2010; Bardet et al. 2014). Sauropterygia has been primarily divided into two major lineages — placodonts and eosauropterygians — each marked by extremely distinct morphologies, reflecting adaptations to markedly different ecological niches (Rieppel 2000; Motani 2009). However, the recent study of Wolniewicz et al. (2023) also includes the peculiar armoured saurosphargids from the Triassic in Sauropterygia, thereby questioning the conventional composition of this clade.

Placodonts were flat and slow armoured (*e.g.* cyamodontoid placodonts) and unarmored (*e.g.* more basal forms such as *Placodus* and *Paraplacodus*) marine reptiles restricted to the Triassic, which mainly inhabited coastlines and intraplatform basins of Tethys Ocean (outcropping in present-day Europe, Middle East and China) (Hagdorn and Rieppel 1999; Rieppel 2000, 2001b; Jiang et al. 2008b; Scheyer et al. 2012; Wang et al. 2019). These animals are mainly characterized by a short, robust skull, bearing highly specialized crushing dentition with globular or 'plate-shaped' teeth (**Figure 7A–C**), making them as one of the most extreme examples of durophagy in tetrapods (Rieppel 2000, 2001b, 2002; Scheyer et al. 2012; Neenan et al. 2013, 2014; Crofts et al. 2016). With a highly pachyostostic skeleton, coupled with the presence of a carapace in cyamodontoids (**Figure 7D**), placodonts were well-adapted to walk on the seafloor while capturing prey, their heavy bodies serving as ballast (Scheyer et al. 2012; Bardet et al. 2014).

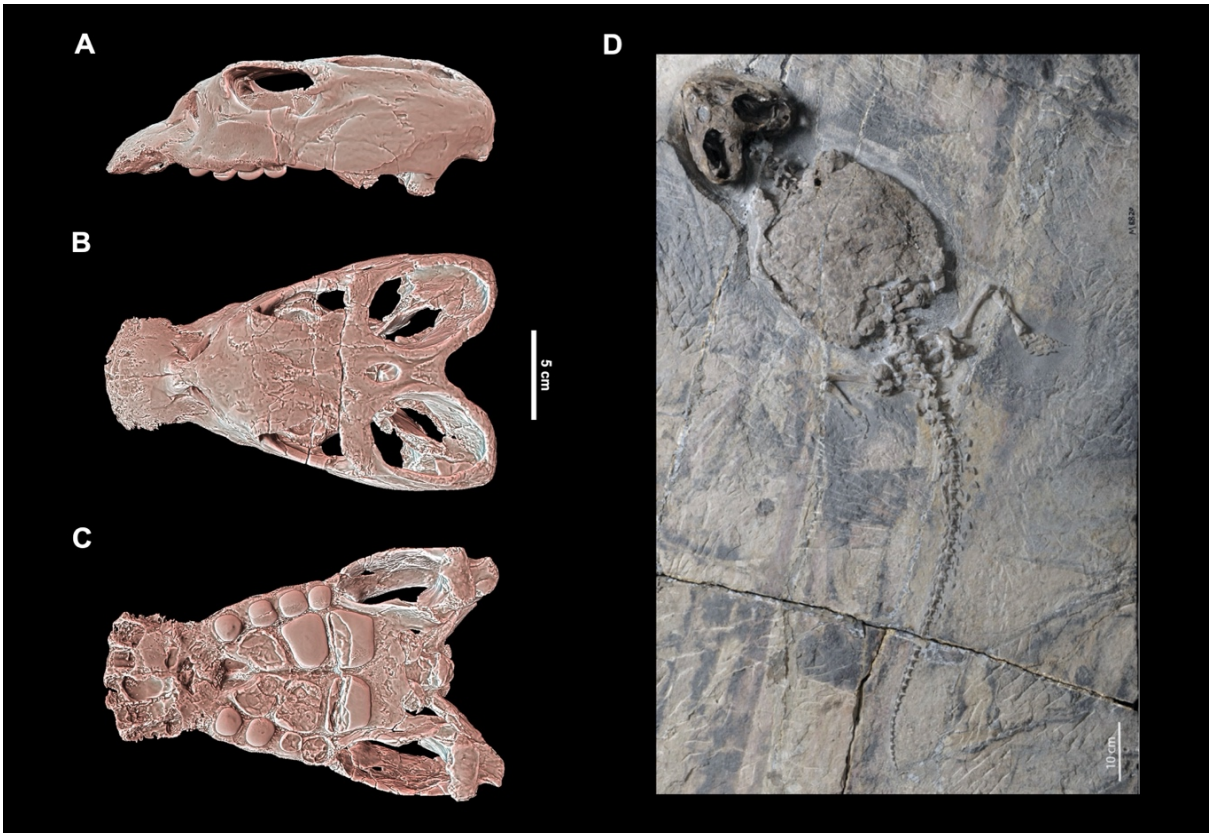

Figure 7. Craniodental and body shape of placodont. (A–C) Cranium of the *Placodus gigas* (3D model of OMU BT 13, provided by T. M. Scheyer) in (A) lateral, (B) dorsal and (C) palatal views. (D) Skeleton of the armoured cyamodontoid *Cyamodus orientalis* (ZMNH M8820; from Wang et al. 2019).

Eosauropterygia constitutes a much larger monophyletic group which englobes distinct lineages such as lizard-like pachypleurosauroids, flat-headed predatory nothosauroids and long-necked pistosauroids, the latter including the well-known plesiosaurians (**Figures 8 and 9**) (Rieppel 2000; Motani 2009). Apart from plesiosaurians, all eosauropterygians exclusively lived during the Triassic and were restricted to western and eastern margins of the Tethys — similarly to placodonts — as well as to the nearshore of eastern Panthalassa oceans (outcropping in present-day North America) (Case 1936; Rieppel 2000; Benton et al. 2013; Bardet et al. 2014; Scheyer et al. 2019; Kear et al. 2024). Observations of the fossil record and recent quantitative studies suggest that the Middle Triassic represents a highly prolific period for eosauropterygians, during which they reached a peak in both taxonomical diversity and morphological disparity (Stubbs and Benton 2016). Middle Triassic species indeed exhibited an extensive range of body sizes, feeding strategies and swimming modes (Rieppel 2002; Liu et al. 2014; Stubbs and

Benton 2016; Reeves et al. 2021). While plesiosaurians were later characterized by an impressive amount of disparity, notably marked by new morphotypes, cranial convergences and variation in neck elongation, they never reached comparable levels to their predecessors (O'Keefe 2002; Stubbs and Benton 2016; Fischer et al. 2017, 2018, 2020b; O'Keefe et al. 2017; Foffa et al. 2018b).

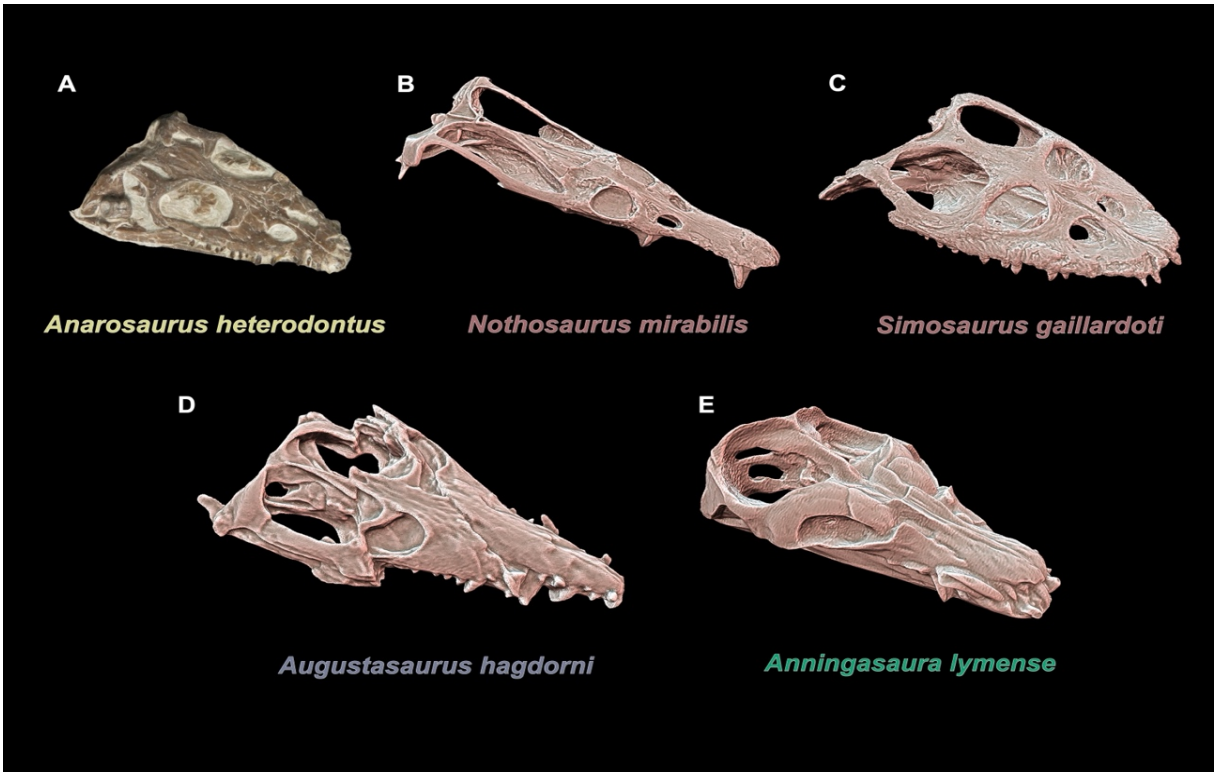

Figure 8. Comparison in eosauropterygian craniodental architecture between (A) a pachypleurosauroid (NMNHL RGM443855; modified from a photo of N. Klein), (B) a nothosaurian (3D model of SMNS 13155), (C) a simosaurid (3D model of GPIT-PV-60638), and (D) a early diverging pistosauroid (3D model of FMNH PR 1974, generated by R. Bennion) and (E) a basal plesiosaurian (3D model of NHMUK PV OR 49202). The name of each taxon is coloured with respect to its relative group (light yellow: pachypleurosauroids, dull red: nothosauroids, dull purple: pistosauroids, green: basal plesiosaurians). Not to scale.

Despite the abundance of well-preserved material, the phylogenetic relationships of Triassic eosauropterygians remain debated. Historically, Pachypleurosauroidea, Nothosauroidea and Pistosauroidea were considered a four monophyletic clades (Rieppel and Lin 1995; Rieppel 2000). However, discoveries of Chinese eosauropterygians, exhibiting a mix of pachypleurosauroidean and nothosauroidean

traits, have challenged this traditional view (Holmes et al. 2008; Klein et al. 2022b). Recent studies have indeed contested the monophyly of Pachypleurosauroidea which rather appeared as a grade of basal eosauropterygians (Liu et al. 2011; Ma et al. 2015; Shang and Li 2015; Jiang et al. 2019; Shang et al. 2020; Wang et al. 2022). While Pachypleurosauroidea is however regarded as monophyletic, the placement of Nothosauroidea varies within eosauropterygians, being recovered as the sister clade of either Pachypleurosauroidea (Neenan et al. 2013; Li and Liu 2020; Hu et al. 2024), or Pistosauroidea (Liu et al. 2011; Xu et al. 2022, 2023). The subsequent description of the different Triassic eosauropterygian lineages will follow traditional classification in which all clades are monophyletic.

Pachypleurosauroids

Pachypleurosauroids are very small to medium-sized Middle Triassic eosauropterygians — the largest measuring 1.2 m long (Carroll & Gaskill, 1985) — retaining a plesiomorphic lizard-like appearance (**Figure 10 A–C**). These animals have been extensively documented from sedimentary deposits of the Germanic Basin (Lower Muschelkalk), Alpine Triassic (primarily Besano Formation) and eastern Tethys (Guanling and Zhuganpo Formations, China). Among well sampled localities, the UNESCO World Heritage site of Monte San Giorgio (Switzerland/Italy border) represents an exceptionally Lagerstätten, yielding hundreds of well-preserved and complete specimens of *Neusticosaurus* and *Serpianosaurus* (Peyer 1932; Carroll and Gaskill 1985; Rieppel 1989; Sander 1989b; Beardmore and Furrer 2016; Klein et al. 2022b; Klug et al. 2024). The abundance of pachypleurosauroid material from Europe and China has offered a detailed understanding of their anatomy, as well as examination of life traits such as viviparity or sexual dimorphism (Sander 1988, 1989b; Rieppel 1989; Lin and Rieppel 1998; Cheng et al. 2004, 2009; Klein and Griebeler 2018; Griebeler and Klein 2019). Pachypleurosauroids usually have a small cranium, characterized by a short, rounded snout, large orbits, and a homodont, and short, pointy teeth in the majority of taxa (**Figure 10**) (Rieppel 2000 but see Liu et al. 2011 and Xu et al. 2023).

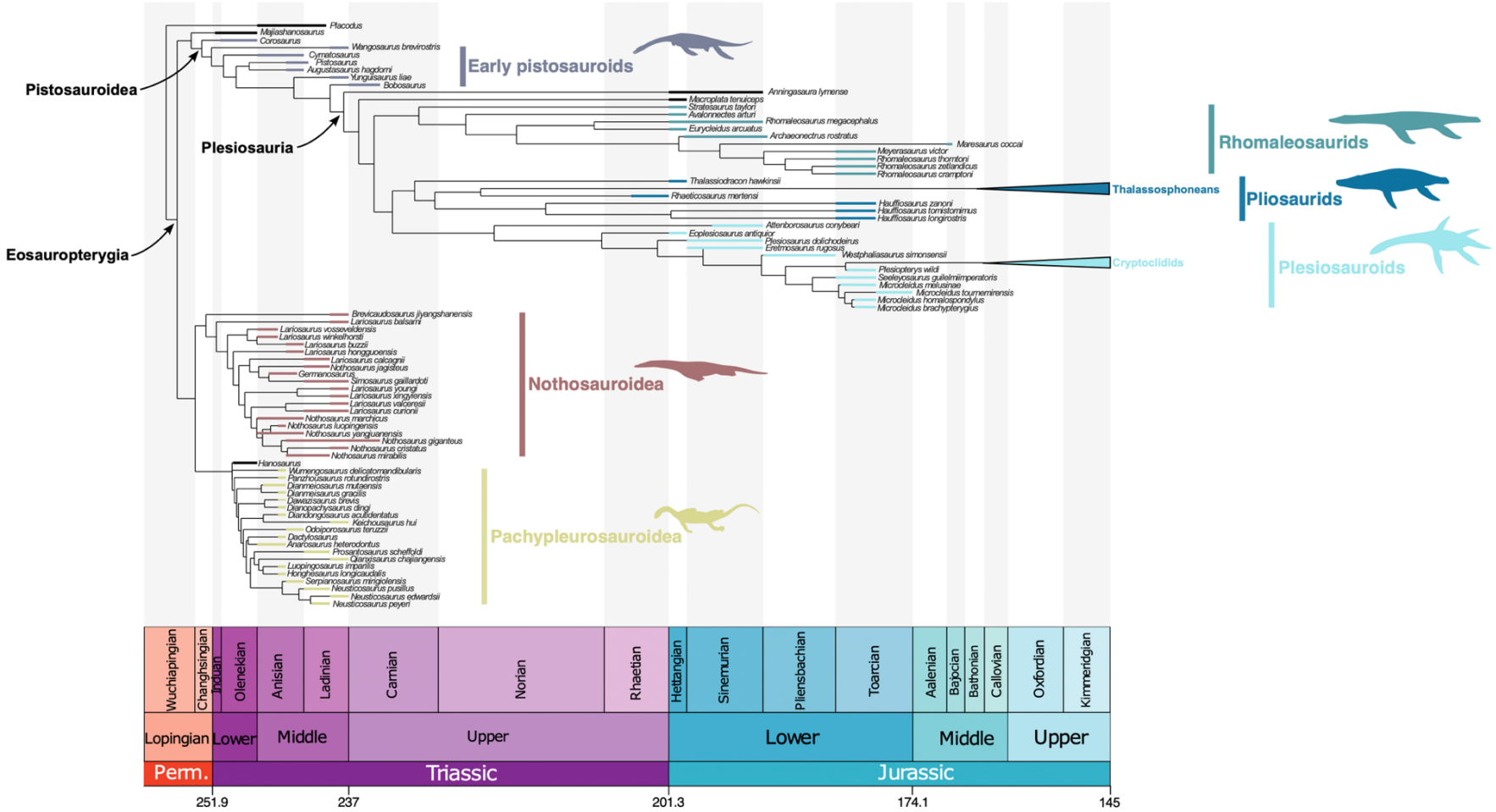

Figure 9. Time-scaled composite eosauropterygian phylogenetic tree arising from the datasets of Huang et al. (2024) and Wintrich et al. (2017) for Triassic and post-Triassic taxa respectively. The composite tree has been calibrated by using the Hedman algorithm.

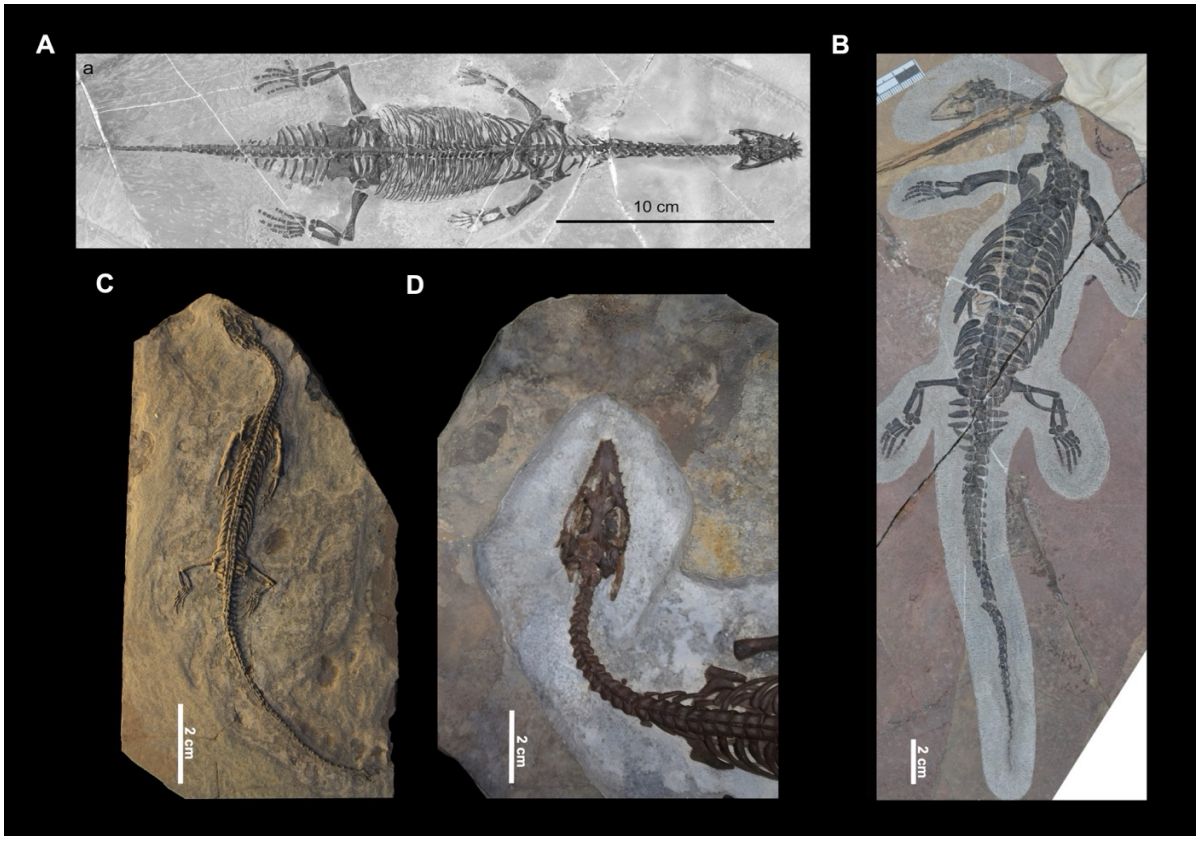

Figure 10. Body shape and cranial anatomy of pachypleurosauroids. (A–C) Skeletons of (A) *Diandongosaurus acutidentatus* (NMNS00093-F034398; from Sato et al. 2014), *Chusaurus xiangensis* (WGSC V 1901; modified from Liu et al. 2023) and *Neusticosaurus pusillus* (PIMUZ T 4829). (D) Cranial anatomy of *Serpianosaurus mirigiolensis* (PIMUZ T 3933).

Examination of the fossil record tends to indicate that pachypleurosauroids from the eastern Tethyan realm (present-day China) displayed broader morphological range, compared to their western counterparts (present-day Europe), with the most significant differences found in their craniodental architecture (see Li et al. 2011; Wu et al. 2011; Cheng et al. 2012; Xu et al. 2023). Postcranially, pachypleurosauroids are distinguished by an elongated body shape, marked by a relatively long neck (**Figure 10**) (but see Cheng et al. 2012), and a varying degree of pachyostosis in their dorsal centra and ribs (Rieppel 2000; Klein 2012; Liu et al. 2023). All pachypleurosauroids possess plesiopedal (terrestrially proportioned) limbs, possibly suggesting return to land, while their robust, flat and curved humeri indicate rowing movements along lateral undulation during swimming,thereby increasing manoeuvrability in aquatic environments (Sues and Carroll 1985; Rieppel and Lin 1995; Rieppel 2000; Gutarra and Rahman 2021).

Nothosauroids

Nothosauroids somewhat resemble to extant crocodilians and inhabited western and eastern coastlines of the Tethys Ocean, mainly during the Middle Triassic (Tintori and Renesto 1990; Rieppel 2000; Rieppel et al. 2003; Jiang et al. 2006a; Klein and Albers 2009; Klein et al. 2016b; Lin et al. 2017; Shang et al. 2020, 2022). The earliest remains have been documented from the Olenekian (Scheyer et al. 2019; Li and Liu 2020), and these reptiles likely disappeared by the end of the early Late Triassic (~237–234 Ma; early Carnian) (Rieppel and Wild 1996; Dalla Vecchia 2008; Liu et al. 2014; de Miguel Chaves et al. 2018b).Nothosauroidea comprises two main groups, nothosaurians and simosaurids, that are primarily distinguished by their craniodental morphology (**Figure 11A and B**), and notable difference in postcranial anatomy.

Nothosaurians exhibit an elongated and dorsoventrally flattened cranium characterized by a relatively long and constricted snout (Rieppel, 2000, 2002). They also possess elongated supratemporal fenestra, providing extensive attachment for the jaw adductor musculature (Rieppel, 2002). This cranial architecture, combined with the presence of an heterodont dentition on their slender 'pincer' jaw, likely indicates a piscivorous diet marked by a rapid snapping bite, in which their enlarged fangs may have functioned as a fish-trap to prevent prey escape (Chatterjee and Small 1989; Rieppel 2002). Nothosaurians have displayed a broad range of body sizes — varying from less than 1m to 5m long, (*e.g.* see Rieppel and Wild 1996 Jiang et al. 2006a, Klein and Albers 2009, Liu et al. 2014 — and large species also preyed on smaller marine reptiles including pachypleurosauroids and placodonts (Sander 1989b; Tschanz 1989a; Rieppel 2002; Liu et al. 2014). The body plan of nothosaurians shares certain similarities with that of pachypleurosauroids, including elongated neck, trunk and tail, though nothosaurians possess a proportionally longer head (Carroll and Gaskill 1985; Storrs 1993; Rieppel 1999, 2000; Klein et al. 2015; Wang et al. 2022). Additionally, nothosaurians still retain a plesiomorphic paddle-like limbs, probably bearing webbed extremities (Krahl, 2021; Rieppel, 1998, 2000; Storrs, 1993). Although their locomotion may have involved lateral undulation, their enlarged humerus (**Figure 11C**) — also characterized by microanatomical specialization (*e.g.* see Krahl et al. 2013; Klein et al. 2016a) — alongside hyperphalangy in some taxa and evidence from swimming tracks, indicate that these animals likely used their forelimbs for propulsion in a form resembling a 'rowing flight' (Carroll and Gaskill 1985; Storrs 1993; Zhang et al. 2014; Klein et al. 2015, 2022a; Krahl 2021).

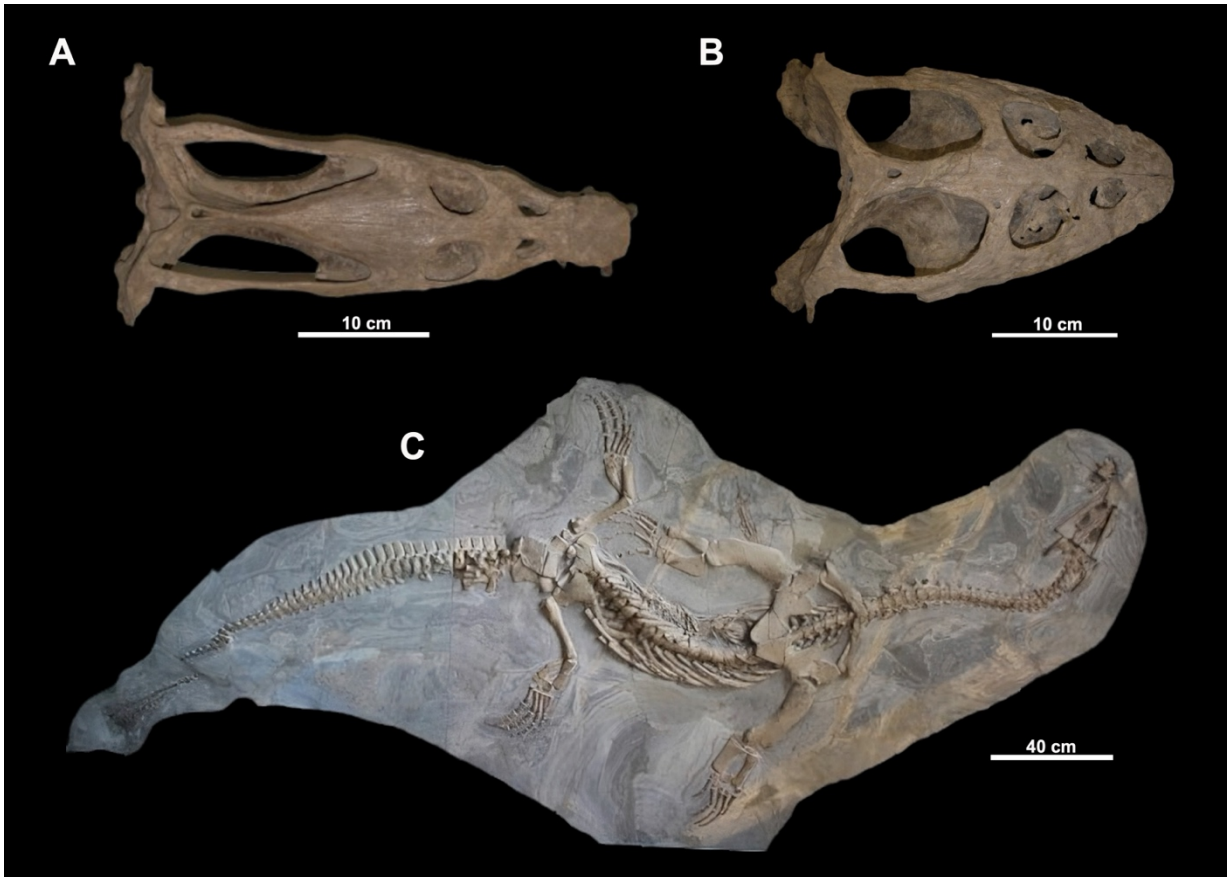

Figure 11. Cranial anatomy and body shape of nothosauroids. (A and B) Cranial architecture of (A) *Nothosaurus mirabilis* (SMNS 16433) and (B) *Simosaurus gaillardoti* (SMNS 10360). (C) Skeleton of *Lariosaurus calcagnii* (PIMUZ T 4836).

Simosaurids are relatively large eosauropterygians (3–4 m long) currently represented by two taxa: *Simosaurus gaillardoti* and *Paludidraco multidentatus*. These two species have displayed distinct morphotypes, highlighting peculiar feeding adaptions among Nothosauroidea (Rieppel 1994, 2002; de Miguel Chaves et al. 2018b). *Simosaurus* is distinguished by a robust mandible and skull, which features a rounded, unconstricted brevirostrine snout (**Figure 11B**) (Rieppel 1994, 2000; de Miguel Chaves et al. 2018a). Its relatively bulbous and blunt teeth suggest some degree of durophagy, reflecting a diet that may have included shelled cephalopods or hard-scaled fishes (Rieppel 1994, 2002; Klein and Griebeler 2016). Even though *Simosaurus* is regarded as an active swimmer, its more robust and compact body shape would have limited its swimming efficiency compared to nothosaurians (Klein & Griebeler, 2016). By contrast to *Simosaurus*, the early Carnian *Paludidraco*, with its gracile skull and mandible gathering

numerous small teeth, has been interpreted as a filter feeder (de Miguel Chaves et al. 2018b). Its postcranial skeleton exhibits extreme pachyostosis, helping in buoyancy control or bottom-walking in shallow waters, and then facilitating foraging at the seafloor, similar to the behaviour observed in sirenians (Houssaye 2009; Houssaye et al. 2016; de Miguel Chaves et al. 2018b).

Early-diverging pistosauroids

Pistosauroidea is mainly known for including the speciose clade Plesiosauria (Rieppel, 2000). Early diverging pistosauroids consist of a small set of Triassic species closely related to plesiosaurians, with the majority living during the Middle Triassic (Meyer 1839; Fritsch 1894; Sander et al. 1997; Rieppel and Werneburg 1998; Rieppel 2000; Cheng et al. 2006; Ma et al. 2015). However, some phylogenies recover Olenekian taxa within Pistosauroidea (*e.g.* see Wang et al. 2022; Hu et al. 2024). Indeed, the phylogenetic affinities of certain taxa has been questioned, most notably, *Wangosaurus brevirostris*. While initially classified as the basal-most pistosauroid, this taxon also shares certain morphological similarities with nothosauroids (**Figure 12A and B**), notably the overall body plan (Ma et al. 2015). Analyses then recovered *Wangosaurus* either as the earliest-branching pistosauroid (Jiang et al. 2019; Lin et al. 2021; Xu et al. 2022, 2023) or as a nothosauroid (Shang et al. 2020; Wang et al. 2022), highlighting uncertainties regarding its classification. Nonetheless, pending future evidence of a nothosauroid affiliation, *Wangosaurus* will be considered as a member of Pistosauroidea in this work, as suggested by its original description (Ma et al. 2015). Additionally, the presumed pistosauroids *Corosaurus* and *Cymatosaurus* have also been recovered as nothosauroids in some tree topologies (Storrs 1991; Neenan et al. 2013; Ma et al. 2015; Jiang et al. 2019), emphasizing the need for further clarification of the phylogenetic relationships within the eosauropterygians.

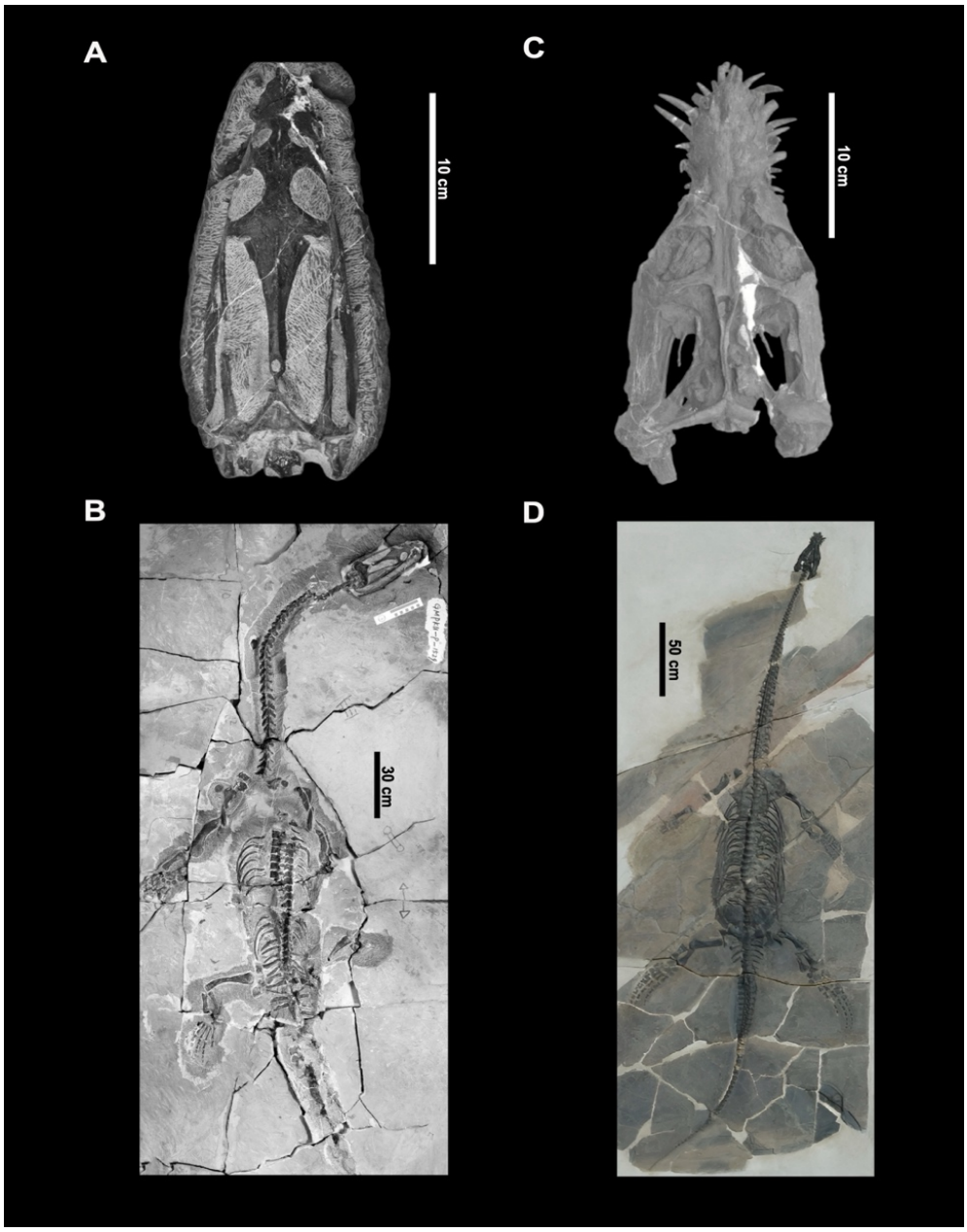

Figure 12. Cranial anatomy and body shape of pistosauroids. Cranial architecture and skeleton of (A and B) *Wangosaurus brevitrostris* (GMPKU-P-1529; modified from Ma et al. 2015) and (C and D) *Yunguisaurus liae* (ZMNH M8738; (C) modified from Sato et al. 2014; (D) photo of the skeleton provided by W. Wang).

Morphologically, early diverging pistosauroids are considered intermediate between other Triassic and post-Triassic eosauropterygians, thereby bridging the gap in the acquisition of the distinctive plesiosaurian body plan (Rieppel et al. 2002; Cheng et al. 2006; Dalla Vecchia 2006; Sato et al. 2014; Gutarra and Rahman 2021). Among early

pistosauroids, *Yunguisaurus liae* is the best-preserved taxon (Sato et al. 2014b; Shang et al. 2017b), and offers substantial insights into their body plan (**Figure 12C and D**). Measuring approximatively 4 m in length, this species exhibits an elongated body shape, characterized primarily by very long neck and tail, while the trunk appears to have been stiffened, as in plesiosaurians (Sato et al. 2014b; Shang et al. 2017b). Less complete taxa, such as *Bobosaurus* or *Augustasaurus*, also display relatively long necks, though not to the same extent as in *Yunguisaurus* (Sander et al. 1997; Rieppel et al. 2002; Dalla Vecchia 2006). Both appendicular girdles in *Yunguisaurus* are well-developed and support limbs that evolved into slender hydropedal paddle-like fins, revealing the premises of underwater flight in eosauropterygians (see below) (Sato et al. 2014b; Gutarra et al. 2023). However, limb bones in pistosauroids still retain a plesiomorphic morphology, closely resembling those of nothosauroids, due to their elongated shape (Storrs 1991; Sander et al. 1997; Cheng et al. 2006; Dalla Vecchia 2006; Sato et al. 2014b). Their enhanced swimming abilities likely facilitated a broader geographic distribution than their other Triassic relatives since taxa have been found not only along the margins of the Tethys but also in those of the Panthalassa Ocean (outcropping present-day North America) (Case 1936; Sander et al. 1997). The nothosauroid-like appendicular skeleton of *Wangosaurus* lacks the development of such fins (**Figure 11B**) (Ma et al., 2015), suggesting that it may have still relied on a rowing motion for swimming. The craniodental morphology of pistosauroids (excepted *Wangosaurus*) appears more similar to that of plesiosaurians than nothosauroids (**Figure 11C**), though it is marked by a more elongated narrow snout (Meyer 1847–1855; Storrs 1991; Rieppel 2000, 2002; Rieppel et al. 2002; Cheng et al. 2006; Sato et al. 2014). Indeed, compared to nothosauroids, their cranium is less flattened and has an elevated skull roof marked by smaller temporal fenestra and by a sagittal crest (Rieppel, 2002). Additionally, the larger 'pincer-jaws' of pistosauroids lacks procumbent fangs typical of nothosauroids, which suggests that these animals rather punctured their preys with a relatively strong bite, therefore reflecting a distinct feeding strategy from that of nothosauroids (Rieppel, 2002).

Plesiosaurians

The cosmopolitan plesiosaurians are the most speciose and longest-lived eosauropterygian lineage, with an evolutionary history spanning over 140 million years, as they thrived from the Late Triassic to the end of the Cretaceous (Taylor and Cruickshank 1993; Motani 2009; Ketchum and Benson 2010; Benson et al. 2012; Bardet et al. 2014; Benson and Druckenmiller 2014; Wintrich et al. 2017). The earliest diagnostic plesiosaurian specimen dates back to the Rhaetian (Wintrich et al., 2017), though some

older remains from the early–middle Norian (227–211.4 Ma; Late Triassic) suggest that they should have appeared earlier (Sennikov & Arkhangelsky, 2010). Plesiosaurians developed a unique morphology and swimming style among marine tetrapods. Their overall body shape, characterized by a stiffened trunk, a shortened tail, and highly developed girdles supporting four large and rigid hydrofoil-like flippers, was highly specialized in quadrupedal underwater flight (Storrs 1993; O'Keefe 2001b; O'Keefe and Carrano 2005; Carpenter et al. 2010; Muscutt et al. 2017; Gutarra et al. 2022; Fukuhara et al. 2024). Even though extant marine tetrapods such as marine turtles, pinguins or sea lions are capable of swimming by using their lateral flapping appendages, they exclusively relied on their forelimbs to propel themselves (Gutarra and Rahman 2021; Krahl and Werneburg 2023), leaving locomotion of plesiosaurians with no extant analogues (Liu et al. 2015; Muscutt et al. 2017; Gutarra et al. 2022).

Plesiosaurians exhibited an impressive diversity of morphologies, mainly influenced by the variation in head size relative to neck elongation, giving rise to two main endpoints: the 'plesiosauromorph' and the 'pliosauromorph' (**Figure 13**) (O'Keefe 2001a, 2002). The 'plesiosauromorph' body architecture primarily refers to small-headed and long-necked plesiosaurians, with elasmosaurids as the most extreme example (*e.g.* see Buchy 2005, Kubo et al. 2012, Soul and Benson 2017, Fischer et al. 2021b and Sachs et al. 2021), while the 'pliosauromorph' morphotype characterizes taxa that displayed a large head along a small-neck (O'Keefe 2002). This latter convergently evolved within phylogenetically and temporally distant groups (pliosaurids and polycotylid plesiosauroids) (Fischer et al. 2017, 2020; Soul and Benson 2017). However, this simple dichotomy obscures a variety of morphologies that are considered as 'intermediate'(Benson et al. 2013; Smith and Benson 2014). Wide differences in tooth shape and positioning, as well as rostrum elongation indicate that plesiosaurians colonized a large variety of feeding guilds throughout their evolution (Chatterjee and Small 1989; Fischer et al. 2017, 2020, 2022a; O'Keefe et al. 2017).

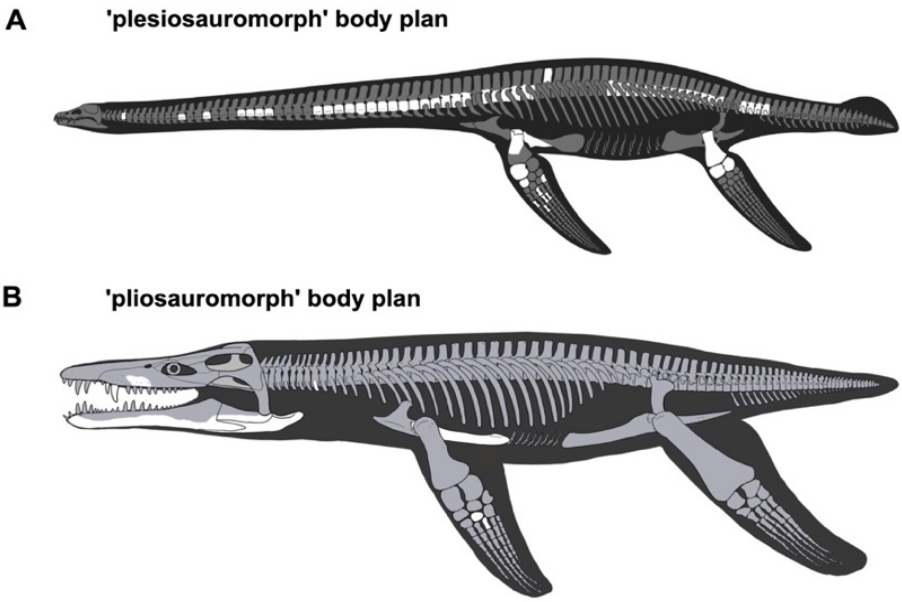

Figure 13. Typical two extreme body plans displayed by plesiosaurians. (A) long-necked and small-headed plesiosauroid *Jucha squalea* (modified from Fischer et al. 2021b). (B) short-necked and large-headed pliosaurid *Lorrainosaurus keileni* (modified from Sachs et al. 2023).

The global systematic and interrelationships among Plesiosauria consistently evolved over the past two centuries (see Ketchum and Benson 2010 for a comprehensive review). Recent phylogenetic analyses have led to the growing consensus that plesiosaurians can be primarily classified into three major clades: Rhomaleosauridae, Pliosauridae, and Plesiosauroidea, with Rhomaleosauridae traditionally viewed as the most basal (Benson et al. 2012; Benson and Druckenmiller 2014; Vincent et al. 2017; Wintrich et al. 2017; Fischer et al. 2021b, 2023; Sachs et al. 2024). According to the timing of branching event implied by time-scaled phylogenies and fossil evidence, all three clades likely emerged during the Late Triassic (Storrs 1994; Wintrich et al. 2017).

Similar to parvipelvians, the early evolutionary history of plesiosaurians during the Early Jurassic is notably well-documented, mainly due to the abundance of fossils discovered in Europe, particularly within the Blue Lias and Posidonienschiefer Formations (*e.g*. Owen 1840, 1865; Benton and Spencer 1995; Großmann 2007; Benson et al. 2012). In the aftermath of the Triassic–Jurassic transition, plesiosaurians were primarily represented by a diverse range of poorly diversified basal species, notably including the earliest rhomaleosaurids, pliosaurids, and plesiosauroids (Owen 1840; Ketchum and Smith 2010; Benson et al. 2012, 2015a; Vincent and Benson 2012). During

the Early Jurassic, medium- to large-sized rhomaleosaurids dominated the ecosystems and were the main macropredators there, alongside large ichthyosaurians like *Temnodontosaurus* (Cruickshank 1994; Smith and Dyke 2008; Ketchum and Smith 2010; Benson et al. 2012; Smith and Benson 2014; Smith and Araújo 2017). These plesiosaurians displayed a peculiar body plan, regarded as intermediate between 'pliosauromorph' and 'plesiosauromorph' morphotypes, notably featuring a large, robust cranium, bearing enlarged caniniform teeth, and a relatively elongated neck (**Figure 14A**) (Cruickshank 1994; Smith and Dyke 2008; Ketchum and Smith 2010; Benson et al. 2012; Smith and Benson 2014; Smith and Araújo 2017). However, the Early Jurassic was not solely defined by the dominance of rhomaleosaurids but also witnessed the initial radiation of the relatively morphologically similar (*i.e.* long-necked) early pliosaurids and plesiosauroids (**Figure 14B and C**) (Carte and Bailey 1863; Owen 1865; Andrews 1922; Huene 1923; White 1940; Sciau et al. 1990; O'Keefe 2001a; Großmann 2006, 2007; Smith and Vincent 2010; Benson et al. 2011b; Vincent 2011; Brown et al. 2013; Vincent et al. 2017). Like other marine reptiles (*e.g.* ichthyosaurians and thalattosuchians) plesiosaurians underwent a pronounced faunal turnover across the Early–Middle Jurassic transition (Vincent et al. 2013b; Fischer et al. 2021a; Reolid et al. 2024; Sachs et al. 2024). This latter marked the extinction of early plesiosaurians — comprising the majority of rhomaleosaurids — and their replacement in favour of the morphologically well-diversified cryptoclidian plesiosauroids and the thalassophonean pliosaurids which subsequently dominated the marine ecosystems for the rest of the Mesozoic (Ketchum and Benson 2011b; Benson and Druckenmiller 2014; Cau and Fanti 2014; Foffa et al. 2018a; Madzia et al. 2019; Fischer et al. 2021a; Reolid et al. 2024; Sachs et al. 2024). The last few rhomaleosaurids disappeared during the Middle Jurassic (Gasparini 1997; Sato and Wu 2008; Benson et al. 2015b), and their vacated ecological niche was rapidly filled by the very large thalassophonean pliosaurids which became the main macropredators from the Middle Jurassic to the early Late Cretaceous (Knutsen et al. 2012a; Foffa et al. 2014, 2018b; Fischer et al. 2015; Zverkov et al. 2018; Zverkov and Pervushov 2020; Martill et al. 2023; Sachs et al. 2023).

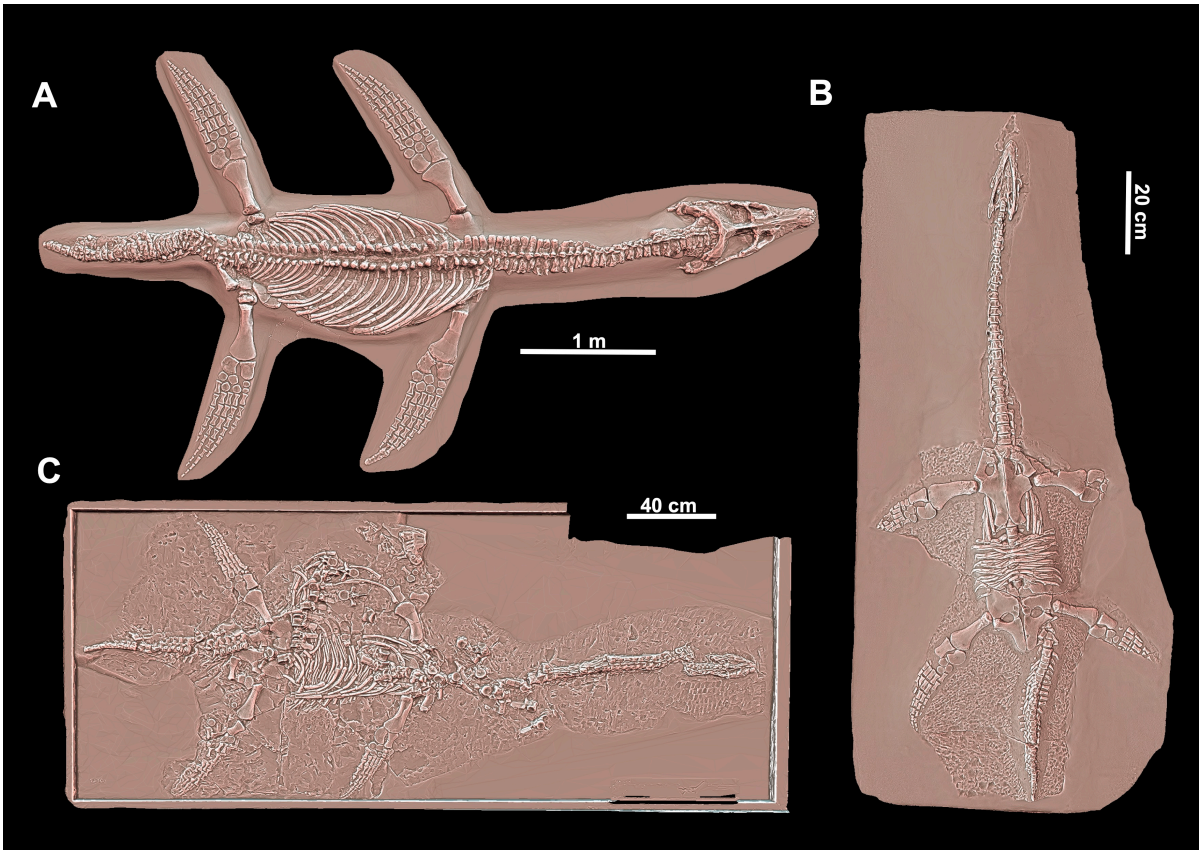

Figure 12. Body shapes exhibited by Early Jurassic plesiosaurians, 3D models. (A) the macropredatory *Rhomaleosaurus cramptoni* (NHMUK PV R 34), (B) the 'plesiosauromorph' early pliosaurid *Thalassiodracon hawkinsi* (NHMUK PV OR 2018) and (C) the plesiosauroid *Plesiosaurus dolichodeirus* (NHMUK PV R 22656).

Evolution of marine reptiles assemblages across the Middle Triassic–Early Jurassic time interval

Middle Triassic assemblages

The Middle Triassic represents, by many standards, the 'Golden Age' of marine reptiles. Their evolution during this period is exceptionally well-documented, due to the extensive number of specimens found in Lagerstätten and highly fossiliferous site across western North America, central Europe and south of China (*e.g.* Fossil Hill Fauna, Monte San Giorgio, Lower Muschelkalk, Luoping and Xingyi biotas) (Merriam 1906, 1908; Peyer 1944; Brinkmann 1998; Furrer 2003; Benton et al. 2013; Klug et al. 2024).

During this period, marine reptiles experienced an intense taxonomic and morphological diversification notably in shallow water environments, probably as the consequence of the novel ecological opportunities provided by the ongoing biotic recovery of ecosystems following the Permian–Triassic mass extinction event (PTME) (Benson et al. 2010; Benson and Butler 2011; Kelley et al. 2014; Stubbs and Benton 2016; Reeves et al. 2021). This diversification indeed coincided with the resurgence of coral and metazoan reefs, along the onset of the 'Mesozoic Marine Revolution' which represents a major period of evolutionary arms race between hard-shelled benthic communities and their predators (Vermeij 1977; Brayard et al. 2011; Chen and Benton 2012; Salamon et al. 2012; Song et al. 2018). The radiation experienced by these animals in the Middle Triassic gave rise to the most disparate marine reptile assemblages of the whole Mesozoic, with numerous coeval linages evolving into a broad range of sizes, morphologies, and trophic specializations, facilitating the establishment of stable and complex trophic networks (Hu et al. 2011; Song et al. 2011, 2018; Chen and Benton 2012; Benton et al. 2013; Fröbisch et al. 2013; Liu et al. 2014; Stubbs and Benton 2016; Sander et al. 2021). Marine reptiles from epicontinental seas and intraplatform basins of the Tethys Ocean displayed a large variety of feeding strategies. These ranged from durophagy across a large panoply of taxa (*e.g.* *Simosaurus*, mixosaurids, thalattosaurs and mostly exacerbated in placodonts) to macropredation (*e.g.* among large nothosaurians and ichthyosaurians), with adaptations in piscivory and teuthophagy in between (*e.g.* among small pachypleurosauroids, medium-sized nothosauroids, pistosauroids, the shastasaurid ichthyosaurian *Besanosaurus*, archosauromorphs and saurosphargids) (Rieppel 2002; Neenan et al. 2013; Liu et al. 2014; Jiang et al. 2020; Spiekman et al. 2020, 2023; Bindellini et al. 2021). In these environments, marine reptile assemblages were mainly dominated (in terms of taxonomic and morphological diversity) by sauropterygians (Stubbs and Benton 2016; Reeves et al. 2021).

The Anisian-aged Fossil Hill Fauna (Augusta Mountains, Nevada, USA) from the eastern Panthalassa Ocean have provided valuable insights on the recovery of open-ocean environments during the Middle Triassic. As in the shallow waters of the Tethys Ocean, pelagic ecosystems seemed to recovered during that stage from the mass extinction event with the setting of stable, multi-level food webs (Fröbisch et al. 2013; Sander et al. 2021). Higher trophic levels of the Fossil Hill Fauna were mainly occupied by the large pelagic raptorial cymbospondylids ichthyosaurians, with the largest species (*e.g.* *Thalattoarchon* and *Cymbospondylus youngorum*) acting as apex predators in these ecosystems (Merriam 1908; Fröbisch et al. 2006, 2013; Klein et al. 2020; Sander et al.

2021). Alongside cymbospondylids, this marine reptile assemblage also contains mixosaurids, the durophagous *Omphalosaurus,* and the sole sauropterygian, the pistosauroid *Augustasaurus* (Merriam 1906; Sander and Bucher 1990; Sander et al. 1997; Rieppel et al. 2002; Schmitz et al. 2004; Schmitz 2005). The stability of these upper levels was largely sustained by the great abundance of smaller preys, including nektonic cephalopods, conodonts, and, to a lesser extent, fishes (Bucher 1988; Monnet and Bucher 2005; Orchard 2007; Fröbisch et al. 2013; Brayard et al. 2017; Sander et al. 2021). This multi-level structure of the Fossil Hill Fauna trophic network and the large supply of preys also facilitated the burst in evolution toward gigantism among cymbospondylids, yielding this fauna as remarkable in terms of body size disparity, with small mixosaurids coexisting alongside the colossal *Cymbospondylus youngorum* — reaching a length of more than 17 meters (Sander et al. 2021).

Late Triassic assemblages

The Late Triassic (237–201.3 Ma), encompassing the Carnian, Norian and Rhaetian stages, stands out as a pivotal interval in the evolution of aquatic ecosystems. During this period, marine reptile faunas underwent significant, yet poorly characterized changes, that collectively resulted in the dominance of pelagic parvipelvian ichthyosaurians and plesiosaurian eosauropterygians by the earliest Jurassic (Bardet 1994; Benson et al. 2010, 2012; Thorne et al. 2011; Dick and Maxwell 2015; Renesto and Dalla Vecchia 2018). However , the fossil record from the Late Triassic, mainly from the Norian and Rhaetian stages is particularly scarce, which hinders a comprehensive understanding of the evolution of marine reptile assemblages in the latest stages of the Triassic (Benson et al. 2010; Benson and Butler 2011; Dunhill et al. 2014b; Fischer et al. 2014b; Wintrich et al. 2017), forcing many studies to bin Late Triassic data in a single interval (Thorne et al. 2011; Dick and Maxwell 2015; Moon and Stubbs 2020)

The Carnian (237–227 Ma; early Late Triassic) corresponds to a phase of global restructuring within marine ecosystems, primarily driven by the setting of a warm-humid climate, likely induced by volcanic activity–and rapid sea-levels fluctuations (Kelley et al. 2014; Lu et al. 2018; Dal Corso et al. 2020; Zhang et al. 2021). Indeed, a substantial marine regression event within the first few million years of the Late Triassic, which significantly reduced the extent of flooded continental shelves, likely drove the extinction of ‘typical Middle Triassic’ forms adapted to nearshore habitats (Haq et al. 1987; Bardet 1994; Motani 2008; Benson and Butler 2011; Kelley et al. 2014; Renesto and Dalla Vecchia 2018). This extinction event resulted in a pronounced decline in global taxonomic

diversity, marked by the loss of unique morphologies, feeding strategies and by a substantial reduction in durophagy (Bardet 1994; Ketchum and Benson 2010; Benson and Butler 2011; Kelley et al. 2014). Among surviving lineages, Sauropterygia was particularly affected and saw the extinction of pachypleurosauroids, nothosauroids, most early pistosauroids, and a sharp decline in placodont diversity (Bardet 1994; Rieppel and Wild 1996; Dalla Vecchia 2006; Benson and Butler 2011; de Miguel Chaves et al. 2018b; Renesto and Dalla Vecchia 2018)

Conversely, marine reptiles that previously adapted to an open-ocean lifestyle — therefore less dependent to shallow water ecosystems — appeared less affected by these early late Triassic sea-levels fluctuations, leading to a predominance of pelagic faunas across the globe (*e.g.* see Zverkov et al. 2022 and references therein). Despite a poorer fossil record, pelagic taxa from the Carnian are well represented in the eastern tethysian (Guanling, China) and panthalassan localities (California and Nevada, USA and Sonora, Mexico). Indeed, these assemblages host a series of small- to medium-sized early ichthyosaurians, such as toretocnemids, as well as large to gigantic shastasaurids (Merriam 1908; Camp 1980; Li 1999; Yin et al. 2000; Shang and Li 2009; Sander et al. 2011; Zverkov et al. 2022), in addition to relatively large proportions of thalattosaurs (Merriam 1904, 1906; Benton et al. 2013; Bastiaans 2024 and references therein). Although their swimming abilities remain poorly understood, evidence indicates that some Late Triassic thalattosaurs, though not fully 'pelagic,' were able to make frequent incursions into open waters (D. Baastians, pers. comm.). The presence of shastasaurids is a marker of the Late Triassic. Some of them acted as apex predators (Dong 1972; Kelley et al. 2022; Sander et al. 2022), while edentulous forms presumably preyed using ram-feeding (Motani et al. 2013). Fossil evidence from the early to middle Norian is scarcer, but localities from the British Columbia (Pardonet Formation, Canada) and the New Siberian Islands (Russian Arctic) suggest a certain similarity in open-water assemblages with those from the Carnian, although small toretocnemids were likely replaced by the earliest parvipelvians (McGowan 1994a, 1995, 1996a, 1997; Nicholls and Manabe 2004; Zverkov et al. 2022). Pelagic eosauropterygians remained absent from these assemblages. However, an undiagnostic eosauropterygian with plesiosaurian affinities have been reported from the Norian deposits in Wilczek Land (Russian Arctic) (Sennikov and Arkhangelsky 2010), though its poor state of preservation precludes any further interpretation (Wintrich et al. 2017).

The latest Triassic extinctions and their impact on the macroevolution of marine reptiles

The Triassic–Jurassic (T/J) transition (201.3 Ma) is traditionally associated with a monumental decline in biodiversity which affected both terrestrial and marine ecosystems (Schoepfer et al. 2022). As a result, the end-Triassic extinction event (ETME) is recognized as one of the 'Big Five' mass extinctions of the Phanerozoic (Raup and Sepkoski 1982, 1984). This list of five statistically distinct events from background extinction rates initially draws from a compilation of the diversity of invertebrate families and are thought to represent sudden and extremely severe crises (Raup and Sepkoski 1982; Sepkoski 1984; Alroy 2010; McGhee et al. 2013). The ETME is widely attributed to extensive volcanism from the Central Atlantic Magmatic Province (CAMP), linked to the breakup of the supercontinent Pangea (Tanner et al. 2004; Whiteside et al. 2010; Blackburn et al. 2013; Ruhl et al. 2020; Bos et al. 2024).While it is undeniable that invertebrate marine communities were heavily impacted by global warming, ocean acidification, and anoxia linked with CAMP volcanism (Raup and Sepkoski 1982; Tanner et al. 2004; Greene et al. 2012; Hodges and Stanley Jr 2015; Jost et al. 2017; He et al. 2020, 2022; Schoepfer et al. 2022; Bond et al. 2023), recent studies suggest that the ecological severity of the ETME may not have been as extreme as previously thought (Dunhill et al. 2018; Lucas and Tanner 2018; Cribb et al. 2023). Furthermore, the traditional vision of a singular, catastrophic extinction event confined to the very end of the Rhaetian has been increasingly challenged, as it may conflate a series of protracted complex biological crises that culminated at the T/J transition (Benton 1986; Hallam 2002; Tanner et al. 2004; Bambach 2006; Lucas and Tanner 2008, 2018). Indeed, the latest Triassic (*i.e.* the late Norian and the Rhaetian) was characterized by successive episodes of environmental upheavals, including rapid sea-level oscillations, bolide impact, and volcanic activity predating to CAMP eruptions (Hodych and Dunning 1992; Tanner et al. 2004; Rigo et al. 2020; Schoepfer et al. 2022). These abiotic factors likely resulted in a gradual, or rather step-wise pattern of extinction among mollusks (*e.g.* ammonites and bivalves) and microvertebrates (*i.e.* conodonts) throughout this period (Hallam and Wignall 1999; McRoberts et al. 2008; Lucas and Tanner 2018 and references therein). Nevertheless, the effect of the ETME on corals and reefs seems clear and abrupt (Greene et al. 2012; Martindale et al. 2012). Consequently, the breadth, the nature, and the tempo of the end-Triassic events are far from clear and might not fit a 'mass extinction' scenario if extinctions were diffuse and selective over the course of the latest Triassic.

The scarcity of fossil data from the Norian and the Rhaetian stages limits our understanding of how extinctions events during the latest Triassic influenced the macroevolution of marine reptiles. Indeed, the fossil record from this period mainly comprises isolated/fragmented and poorly diagnostic specimens (but see Neenan and Scheyer 2014; Wintrich et al. 2017; Lomax et al. 2024).Nevertheless, a handful Rhaetian localities in Europe, including sites in England, southern France, Germany, Switzerland, and Austrai, have yielded marine reptile remains, providing valuable insights on changes in assemblages on either sides of the Triassic–Jurassic transition (Sauvage 1876, 1903; Pinna and Mazin 1993; Storrs 1994; Müller 2007; Karl et al. 2014; Neenan and Scheyer 2014; Mears et al. 2016; Wintrich et al. 2017; Lomax et al. 2018a, 2024; Scheyer et al. 2022; Bastiaans 2024; Cawthorne et al. 2024). From what is known, the Rhaetian concentrates the final demise of the last coastal forms, including thalattosaurs, placodonts and probably saurosphargids which may have survived through the latest Triassic in some shallow water refugia located in the Alpine region (Pinna and Mazin 1993; Renesto and Tintori 1995; Neenan and Scheyer 2014; Scheyer et al. 2022; Bastiaans 2024 and references therein).

Among pelagic taxa, the end of the Rhaetian coincided with the last occurrence of shastasaurids (Fischer et al. 2014b; Lomax et al. 2018a, 2024; Sander et al. 2022). As a result, only two clades of marine reptiles crossed the Triassic–Jurassic transition: the ‘fish-shaped’ parvipelvians among Ichthyosauria and the ‘underwater flier’ plesiosaurians within Eosauropterygia — which were already present in the Rhaetian (Storrs 1994; Fischer et al. 2014b; Wintrich et al. 2017). Both these clades will be found in number at the very start of the Early Jurassic (Motani 2009; Benson et al. 2010, 2012; Thorne et al. 2011; Bardet et al. 2014). Consequently, latest Triassic events are commonly thought to drive a profound turnover between the Late Triassic and the Early Jurassic marine reptile faunas.

Despite the high taxonomic diversities among parvipelvians and plesiosaurians recorded at the base of the Jurassic, it has been widely accepted that Early Jurassic assemblages are significantly less morphologically disparate than those of the Triassic (Thorne et al. 2011; Benson et al. 2012; Stubbs and Benton 2016; Moon and Stubbs 2020; Reeves et al. 2021; Gutarra et al. 2023). Thorne et al. (2011) reported a severe decline in ichthyosaurian disparity at or close to the T/J transition, resulting from a macroevolutionary bottleneck, induced by a massive extinction event at that time. The bottleneck scenario however primarily arose from the use of coarse time interval as the Carnian, Norian and Rhaetian stages were all englobed in the ‘Late Triassic’ bin, spanning

more than 25 Ma. As a result, the massive drop in disparity detected by Thorne et al. (2011) at the very end of the Rhaetian may instead conflate earlier multiple extinction phases into a single event. Furthermore, the T/J bottleneck is thought to have not only reduced the overall amount of disparity, but also to have driven marked changes in morphology between Triassic and post-Triassic ichthyosaurians. These changes have been reflected by a complete shift in morphospace occupation generated by using Principal Coordinate Analysis (PCoA), based on phylogenetic characters (Thorne et al. 2011; Moon and Stubbs 2020). Yet, the use of such characters with ordination methods is not recommended, as cladistic data are not considered as a good proxy of morphological and ecological disparity (Anderson and Friedman 2012). In contrast to the bottleneck scenario, the examination of the fossil record tends to rather indicate more temporally diffuse and phylogenetically clustered extinctions throughout the Late Triassic (Benson et al. 2010, 2012; Benson and Butler 2011; Renesto and Dalla Vecchia 2018), suggesting a weaker impact of the T/J transition on the macroevolution of ichthyosaurians and eosauropterygians.

Goals of the thesis and structure of the chapters

The review attempted above demonstrates the need of clarification concerning the impact of the Late Triassic extinction events on the macroevolution of pelagic raptorial marine reptile clades that crossed the T/J transition. In such a context, the aim of this Ph.D. project is to better understand the disappearance of the Middle–Late Triassic ichthyosaurians and eosauropterygians, and to assess whether their extinction is compatible with a ‘mass extinction’ scenario. To do so, the thesis aimed at answering these two main questions:

- How did ichthyosaurians and eosauropterygians morphologically diversify on both sides of the Triassic–Jurassic transition? Can we detect a permanent shift in their morphospace occupation, and if so, when?

- Were the extinctions concentrated at or close to the Triassic–Jurassic transition, compatible with a mass extinction scenario or were they the result of a more gradual and selective patterns throughout the Late Triassic?

This thesis will address these questions using quantitative palaeobiology, combining 3D surface scanning, computation of disparity, phylogenetic comparative methods, and statistics. The research conducted during this Ph.D. is detailed in Chapters 1, 2, and 3, while additional publications deriving from my master thesis and side projects are included in the appendix.

Both **Chapters 1** and **2** delves into the ecomorphological diversification of eosauropterygians and ichthyosaurians by using multivariate morphometric analyses. For these two chapters, I created extensive morphological datasets containing biomechanical and architecturally informative traits — notably collected on numerous 3D models generated as part of this project — which have been analyzed ordination methods, including principal coordinate analysis (PCoA) and non-metric multidimensional scaling (NMDS).

The **Chapter 1** (published as Laboury et al. 2023, *PeerJ*) thoroughly investigates the phenotypic diversification of Middle Triassic eosauropterygians, by exploring their patterns of morphospace occupation, possible evolutionary convergences, as well as regional patterns of disparity. Although broad macroevolutionary studies of whole Mesozoic marine reptiles evidenced that the highest amount of eosauropterygian disparity was recorded during the Middle Triassic (Stubbs and Benton 2016; Reeves et al. 2021; Gutarra et al. 2023), little is known about diversification dynamics of Eosauropterygia during that period. Results from this chapter highlight a clearly distinct colonization of the ecomorphospace among the small lizard-like pachypleurosauroids, the flat headed nothosauroids, and the long-necked pistosauroids, with no evidence of whole-body convergent evolution. This global pattern is mostly driven by craniodental differences and inferred feeding specializations. Additionally, significant regional differences are identified among nothosauroids and pachypleurosauroids, with the latter likely undergoing notable diversification in the eastern Tethys during the Anisian. Consequently, the chapter 1 indicates that the high phenotypic plasticity characterizing the evolution of the plesiosaurians was already present in their Triassic ancestors.

The **Chapter 2** (published as Laboury et al. 2024, *Evolution*) comprehensively retraces and compares the morphological evolution of both ichthyosaurians and eosauropterygians across the Middle Triassic–Early Jurassic time interval, in order to assess the influence of Late Triassic events on their disparity and morphology. This chapter reveals for the first time the existence of contrasted macroevolutionary patterns

between these two lineages. Indeed, the craniodental ecomorphospace occupation of eosauropterygians retains a deep phylogenetic structure while ichthyosaurians continued to radiate into different the same areas of the morphospace, seemingly regardless of phylogenetic affinity. Furthermore, overall results support the existence of a major extinction event that likely decimated multiple coastal forms during the early Late Triassic and that should be disconnected from the end-Triassic mass extinction. As a result, the latest Triassic extinction appears much less severe than previously thought.

Finally, the **Chapter 3** focuses on the selectivity and the intensity of extinctions affecting ichthyosaurian and eosauropterygians from the Middle Triassic to the end of the Early Jurassic, while also assessing the suitability of body size as a predictor of extinction vulnerability. The phylogenetic clustering (*i.e.* selectivity) in extinctions was evaluated using Fritz and Purvis' *D* statistic, applied to composite supertrees calibrated with multiple time-scaling methods, while the correlation between body size and extinction risk was analyzed through phylogenetic generalized least square regression (PGLS). The Chapter 3 highlights evidence of phylogenetic signal in extinctions through the Middle Triassic–Early Jurassic time interval across our time-dated phylogenies, with no significant influence of body size. Furthermore, the early Late Triassic is characterized by severe and highly selective extinctions, reflecting the loss of 'Middle Triassic' taxa, which is consistent with results of the Chapter 2. While extinction pressures may not have targeted specific body sizes, the end-Triassic events still led to the eradication of gigantic shastasaurids, potentially suggesting greater extinction susceptibility among larger-bodied taxa specifically across the T/J transition.

CHAPTER 1: MORPHOLOGICAL DIVERSIFICATION OF MIDDLE TRIASSIC EOSAUROPTERYGIANS

Laboury, A., T. M. Scheyer, N. Klein, T. L. Stubbs, and V. Fischer. 2023. High phenotypic plasticity at the dawn of the eosauropterygian radiation. *PeerJ* 11:e15776. DOI: 10.7717/peerj.15776.

Abstract

The initial radiation of Eosauropterygia during the Triassic biotic recovery represents a key event in the dominance of reptiles secondarily adapted to marine environments. Recent studies on Mesozoic marine reptile disparity highlighted that eosauropterygians had their greatest morphological diversity during the Middle Triassic, with the co-occurrence of Pachypleurosauroidea, Nothosauroidea and Pistosauroidea, mostly along the margins of the Tethys Ocean. However, these previous studies quantitatively analysed the disparity of Eosauropterygia as a whole without focussing on Triassic taxa, thus limiting our understanding of their diversification and morphospace occupation during the Middle Triassic. Our multivariate morphometric analyses highlight a clearly distinct colonization of the ecomorphospace by the three clades, with no evidence of whole-body convergent evolution with the exception of the peculiar pistosauroid *Wangosaurus brevirostris*, which appears phenotypically much more similar to nothosauroids. This global pattern is mostly driven by craniodental differences and inferred feeding specializations. We also reveal noticeable regional differences among nothosauroids and pachypleurosauroids of which the latter likely experienced a remarkable diversification in the eastern Tethys Ocean during the Pelsonian. Our results demonstrate that the high phenotypic plasticity characterizing the evolution of the pelagic plesiosaurians was already present in their Triassic ancestors, casting eosauropterygians as particularly adaptable animals.

Authors' contributions: AL, VF, TLS, TMS conceived and designed the study. AL and NK collected the data. AL performed the analyses, wrote the code with the inputs from VF, prepared all and wrote the draft of the manuscript, with contribution of all authors.

INTRODUCTION

The Triassic biotic recovery following the Permian–Triassic transition mass extinction (PTME) represents a crucial episode in Earth's history, characterized by the colonization of the oceans by reptiles and the emergence of modern trophic networks in these aquatic ecosystems that are still in place today (Benton et al. 2013; Fröbisch et al. 2013; Liu et al. 2014; Scheyer et al. 2014; Kelley and Pyenson 2015; Foffa et al. 2018b; Vermeij and Motani 2018; Huang et al. 2020; Sander et al. 2021; Dai et al. 2023). Marine reptiles dominated the whole Mesozoic and explored numerous ecological niches as demonstrated by their ecomorphological diversification (Bardet et al. 2014; Stubbs and Benton 2016; Foffa et al. 2018b; Moon and Stubbs 2020; Reeves et al. 2021; Sander et al. 2021; Fischer et al. 2022a; Maclaren et al. 2022). Marine reptiles experienced an unprecedented burst of diversification during the Middle Triassic, likely driven by the novel ecological opportunities provided by the shallow epicontinental seas connected to the Tehtys and Panthalassa oceans (Benson and Butler 2011; Stubbs and Benton 2016; Moon and Stubbs 2020; Reeves et al. 2021). Sauropterygia is the most speciose and the longest-lived (Olenekian–Maastrichtian; *e.g.* Benson et al., 2010; Jiang et al., 2014) clade of marine reptiles and its members were key components of marine trophic chains for the entire Mesozoic. This clade is divided into two major lineages, the durophagous Placodontia and the disparate Eosauropterygia which includes the lizard-like pachypleurosauroids, the flat headed nothosauroids, and the long-necked pistosauroids, in which plesiosaurians are nested (Motani, 2009; Rieppel, 2000). The Triassic representatives of Sauropterygia are essentially restricted to the western and eastern margins of the Tethys Ocean (outcropping in present-day Europe and China, respectively) (Bardet et al., 2014; Rieppel, 2000) althought some taxa such as *Corosaurus* and *Augustasaurus* and remains with nothosauroidean affinity have been found in Eastern Panthalassa as well (outcropping in present-day North America) (Case 1936; Sander et al. 1997; Rieppel 2000; Bardet et al. 2014; Scheyer et al. 2019; Kear et al. 2024).

Recent studies of marine reptile disparity through time have demonstrated that sauropterygians became the most disparate clade by the Anisian (Stubbs and Benton 2016; Reeves et al. 2021) and that morphological diversity was mostly driven by the emergence of the profound durophagous adaptations of placodonts (Stubbs and Benton 2016; Reeves et al. 2021; Fischer et al. 2022a). Concerning eosauropterygians, qualitative observations in the fossil record reveal a diversification of morphologies related to both their feeding strategies (Rieppel, 2002) and swimming modes during the Middle Triassic

(Krahl et al. 2013; Klein et al. 2016a; Xu et al. 2022). Quantitative analyses suggest a burst in skull size and high disparity during that period (Stubbs and Benton 2016; Gutarra et al. 2023), associated with the appearance of small-sized pachypleurosauroids and gigantic nothosaurians(Liu et al. 2014). Post-Triassic sauropterygians (*i.e*. Plesiosauria) would seemingly never again reach such a high disparity even if their evolution was punctuated by periods of high morphological diversification, craniodental convergences and variations in neck elongation (O'Keefe 2002; Fischer et al. 2017, 2018; Soul and Benson 2017; Reeves et al. 2021).

However, studies which have analyzed the disparity of Sauropterygia mostly consider the clade as a whole, or only investigated the morphological evolution of the derived plesiosaurians, leaving thus the Triassic clades relatively understudied. As a consequence, little is known about the diversification dynamics and morphospace occupation of the Triassic eosauropterygian clades, as well as the existence of phenotypical convergence amongst them. Recent analyses of the temporal trends of vertebrate diversity have highlighted the importance of analyzing regional dynamics, as the structure of the fossil record (*i.e*. which niches are sampled and how) fluctuates geographically (Close et al., 2020; MacLaren et al., 2022). Qualitative evidence suggests that Middle Triassic eosauropterygians display geographical differences in their assemblages: pachypleurosauroids found in the Anisian of China (Luoping and Panxian biotas) appear to have greater morphological diversity, especially in the craniodental region (Wu et al. 2011; Cheng et al. 2012, 2016; Xu et al. 2022, 2023; Liu et al. 2023) while some European nothosauroids seemed to have developed unique feeding strategies and anatomy(Rieppel 1994; de Miguel Chaves et al. 2018b,a; Cabezuelo Hernández et al. 2024). In this paper, we investigate the cranial and postcranial morphological diversification of Middle Triassic eosauropterygians and explore their patterns of morphospace occupation and possible evolutionary convergence. We also characterize the spatiotemporal distribution of their disparity along the Tethys Ocean.

MATERIAL AND METHODS

Morphological data

We gathered a set of 35 cranial and postcranial linear measurements (**Figure 13**) on 36 Triassic eosauropterygian species (17 pachypleurosauroids, 16 nothosauroids and 3 pistosauroids; see supplements for chapter 1; **Table S1.1**). We collected data directly

from specimens (by a digital calliper with a precision of 0.01 mm), on high-precisions 3D models using Meshlab v2022.02 (Cignoni et al., 2008), or using ImageJ (v.1.53) on first-hand pictures and pictures from the literature, when no other alternative was found. The 3D models were generated with a Creaform HandySCAN 300 laser scanner at resolution varying from 0.2 to 0.5 mm, depending on the size of the specimen and with an Artec Eva white light scanner at resolution ~0.5 mm. These 3D models are available on MorphoSource: https://www.morphosource.org/projects/000508432?locale=en. These measurements were used to calculate 27 dimensionless quantitative morphofunctional ratios with clear biomechanical and architectural implications (Anderson et al. 2011; MacLaren et al. 2017, 2022; Fischer et al. 2020; Bennion et al. 2022). In addition to these ratios, we also added the absolute height of the dental crown, as it represents an informative ecological signal in marine predators (Fischer et al. 2022a). Finally, we used 4 discrete traits adapted from Stubbs & Benton (2016) to better characterize the morphology of the teeth and the mandible. Twenty-one traits are devoted to craniodental anatomy and 10 sample the postcranial region (see Supplements for the chapter 1 for the definition and the percentage of completeness of each trait). All species have been submitted to a 40% completeness threshold to prevent any distortions in our ordination analyses caused by an excessive amount of missing data. The counterpart of a such threshold is, however, the exclusion of seemingly peculiar phenotypes (notably *Corosaurus, Cymatosaurus, Bobosaurus*, and *Paludidraco*). The initial total amount of missing entries in our dataset before applying the threshold equals 21.01%, with respectively 14.81% and 36.11% for the craniodental and postcranial regions.

Phylogenetic analyses

We generated phylogenetic trees by reanalysing the recently published dataset of Xu et al. (2022), containing 149 characters coded across 50 taxa within maximum parsimony framework, in TNT (v1.5) (Goloboff & Catalano, 2016). In order to minimize the impact of homoplasy, we used the implied weighting method to reduce the weight of each character proportionally to their homoplasy. This method seems to be the most adequate in a maximum parsimony framework as it provides more accurate results than equal weighting (Goloboff et al., 2018; M. R. Smith, 2019). We decided to use different values of the concavity constant *k* (6, 9 and 12) to test the influence of different character weighting; increasing the *k* value reduces the penalty applied to homoplastic characters which thus play a greater role in estimating phylogenetic relationships.

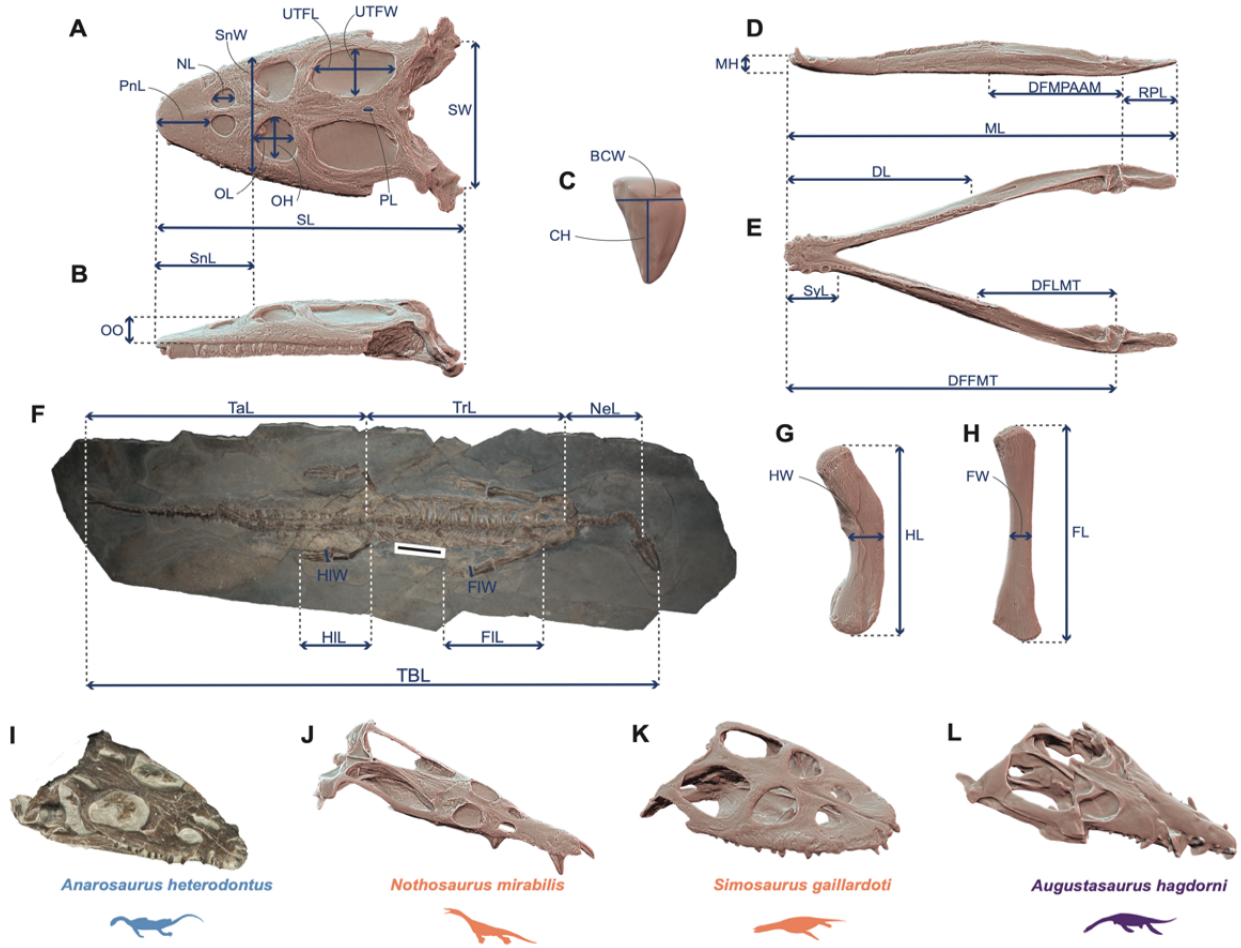

Figure 13. Linear measurements used to calculate ecomorphological traits and example of Middle Triassic eosauropterygian craniodental architectures. (A–H) Linear measurements used to compute the ecomorphological traits used in our disparity analyses: (A and B) cranial measurements shown on the 3D model of *Simosaurus gaillardoti* (SMNS 16363) in (A) dorsal and in (B) lateral views; (C) tooth measurements shown on the 3D tooth model of *Simosaurus gaillardoti* (GPIT-PV-60638) in labial view; (D and E) mandibular measurements shown on the 3D model of *Nothosaurus giganteus* (SMNS 18058) in (D) dorsal and in (E) lateral views; (F) postcranial measurements (excepted on humerus and femur) shown on the complete specimen of *Neusticosaurus edwardsii* (PIMUZ T2810); (G) humerus measurements shown on the 3D model of *Nothosaurus giganteus* (SMNS 81311); (H) femur measurements shown on the 3D model of *Nothosaurus giganteus* (SMNS 1589b). (I–L) Examples of Middle Triassic eosauropterygian cranial architectures (I) *Anarodontus heterodontus* (NMNHL RGM443855); (J) *Nothosaurus mirabilis* (SMNS 13155); (K) *Simosaurus gaillardoti* (GPIT-PV-60638); (L) *Augustasaurus hagdorni* (FMNH PR1974). Colors indicate eosauropterygian clade; blue for Pachypleurosauroidea, orange for Nothosauroidea and purple for Pistosauroidea. Abbreviations: BCW, basal crown width; CH; crown height; DFFMT, distance fulcrum — first mandible tooth; DFMLT, distance fulcrum — last mandible tooth; DFMPAAM, distance fulcrum — mid-point of attachment of the adductor muscles; DL, dentigerous length; FL, femur proximodistal length; FW, femur width; FlL, forelimb length; FlW, forelimb width;

humerus proximodistal length; HW, humerus width; HlL, hindlimb length; HlW, hindlimb width; MH, mandible height; ML, mandible length; NeL; neck length; NL, naris length; OL, orbit length; OH, orbit height; OO, ocular offset; PL, parietal foramen length; RPL, retroarticular process length; PnL, prenarial length; SL, skull length; SW, skull width; SnL, snout length; SnW, snout width; SyL, symphysial length; TBL, total body length; TaL, tail length; Trl, trunk length; UTFL, upper temporal fenestra length; UTFW, upper temporal fenestra width.

We set the maximum number of trees to 100 000 and we used the New Technology Search (ratchet activated: 200 iterations; drift activated: 10 cycles; 10 hits and 10 trees per replication). We applied a tree bisection-reconnection (TBR) algorithm on trees recovered by the ratchet to fully explore islands of most parsimonious trees. Our most parsimonious tree, generated with a *k* value of 12, has a length of 25.520 and can be visualized in the supplements for chapter 1 (**Figure S1.1**). As the phylogenetic dataset of Xu et al. (2022) does not include all the species we sampled in our ecomorphological dataset, we added manually six species using the literature and the *phytools* (v0.7-80) and *paleotree* (v3.3.25) packages (Bapst 2012; Revell 2012): we split the OTU '*Neusticosaurus'* of the dataset of Xu et al. (2022) into its three species, *Neusticosaurus pusillus* as the sister taxa of the clade composed of *Neusticosaurus edwardsii* and *Neusticosaurus peyeri* (Klein et al. 2022b); *Prosantosaurus scheffoldi* as the sister lineage of the clade comprising *Serpianosaurus* and *Neusticosaurus* (Klein et al. 2022b)*; Brevicaudosaurus jiyangshanensis* as the sister lineage of Nothosauridae (Shang et al. 2020); *Nothosaurus luopingensis* as the sister lineage of *Nothosaurus yangjuanensis* (Shang et al. 2022), and *Luopingosaurus imparilis* as the sister lineage of *Honghesaurus longicaudalis* (Xu et al. 2023). We pruned the resulting tree by removing all the taxa which have not been included in our ecomorphological dataset, using the *ape* v5.2 package (Paradis et al., 2004). The final taxon sampling set can be visualized in the Supplements for chapter 1 (**Figure S1.2**). We then time-scaled it using the minimum branch length algorithm, using a minimal value of 0.5 Myr, using the *paleotree* package (v3.3.25) (Bapst, 2012) (**Figure S1.2**). The age range of each species of our dataset is provided in Supplements for chapter 1 (**Table S1.1**).

Ordination methods, phylo-ecomorphospace occupation and disparity

All analyses were performed in the R statistical environment (v. 4.2.1) (R Core Team, 2023) and followed the protocol established by Fischer et al. (2020) which is designed to visualize the density of trait space occupancy and test for the existence of a macroevolutionary landscape. Each continuous trait in the morphological dataset was z-transformed (assigning to all continuous traits a mean of 0 and a variance of 1) prior to

computation of a Gower distance matrix. We used the Gower metric as our dataset contains both continuous and discrete traits (Gower 1971). We submitted our distance matrix to a cluster dendrogram analysis using the Ward clustering criterion in order to visualize the morphological similarities among Triassic eosauropterygians. To evaluate the statistical support of our clustering results, we applied a multiscaled bootstrapping procedure, the 'Approximatively Unbiased P-value' method implemented in the pvclust *package* (v2.2-0) (Suzuki et al. 2019). This method creates subsamples of different sizes from our original distance matrix. We ran it from 0.5 to 10 times the size of our distance matrix, at increments of 0.5 and 1000 bootstraps per increment. We also created tanglegrams (**Figure S1.3**) using the *dendextend* package (v.1.16.0) (Galili 2015) to compare the phylogenetic position and the phenotypic distance of taxa and we tested their correlation by computing Mantel tests (1000 permutations) using the vegan *package* (v2.5-2) (Oksanen et al. 2022). We ran multivariate morphospace analyses via both principal coordinate analysis (PCoA) applying the Caillez correction for negative eigenvalues, using the *ape* package (v5.2) (Paradis et al. 2004) and non-metric multidimensional scaling (NMDS, dimensions=2), using the *vegan* package (v2.5-2) (Oksanen et al. 2022). We computed phylomorphospaces to visualize the ecomorphological trajectories across the evolution of Triassic eosauropterygians. Density of morphospace occupation was computed using a Kernel two-dimensional density estimate on the PCoA phylomorphospace, using the modified *ggphylomorphospace* function provided in Fischer et al. (2020). We also displayed the PCoA morphospace occupation in both eastern and western Tethyan realm extracted from the main analyses comprising all taxa for the following time bins of Middle Triassic: Bithynian, Pelsonian, Illyrian (substages of the Anisian) , as well as Fassanian and Longobardian (substages of the Ladinian) for the Western and Eastern Tethys provinces. The density of taxa generated in the main PCoA analysis has also been displayed on these plots. The distribution of skull lengths and width (the maximum distance between left and right quadrates) are reported in **Figures 14C and D**, respectively.

Convergence analyses

We firstly tested the significance of interclade ecomorphological convergence by applying the convergence metrics Ct1, Ct2, Ct3, and Ct4 (Grossnickle et al. 2024), which derive from the commonly used metrics of Stayton (2015), on selected pairs of taxa based on the results of our ordination analyses. The first two metrics quantify the phenotypic distance of a pair of taxa by comparison to the dissimilarity of their respective ancestral nodes while the metric C3 and C4 include the total amount of evolution (sum of all

phenotypic distances) in the clade defined by the last common ancestor of this pair of taxa. We selected our most parsimonious tree (**Figure S1.2**) to test the significance of these supposed convergences by evaluating the character evolution under 1000 Brownian simulations using respectively the first two and all axes of the PCoA, generated with the whole-body data. These analyses have been computed using the convevol *package* (V2.0.0) (Brightly and Stayton 2023). We also used the method developed by Castiglione et al. (2019), using the *RRphylo* package (2.7.0) (Castiglione et al. 2018). This latter is based on whether or not the phenotypic dissimilarity between species tested for convergence (and measurement via the angle Ø between their phenotypic vectors) is smaller than expected by their phylogenetic distance under a Brownian Motion model of evolution. In this method, the time spent since cladogenetic divergence represents a crucial factor (Castiglione et al. 2019). We also applied this method using the first two and all axes of the PCoA as for the computation of the Ct metrics.

We decided to test possible ecomorphological convergence between the pistosauroid *Wangosaurus brevirostris* and two nothosauroids considering as the closest taxa to this taxon in the dendrogram (**Figure 14A**), *Lariosaurus calcagnii* and *Brevicaudosaurus jiyangshanensis*. Even if *Wangosaurus* is found to be phylogenetically the most basal pistosauroid in many phylogenetic analyses (Ma et al. 2015; Jiang et al. 2019; Lin et al. 2021; Xu et al. 2022, 2023), its craniodental architecture and limbs appear quite similar to that of nothosauroids (Ma et al. 2015). In our dendrogram (**Figure 14A**), the singular nothosauroid *Simosaurus gaillardoti* is found to be morphologically closer to pachypleurosauroids. Therefore, we also decided to investigate the existence of any convergence of *Simosaurus* with the closest pachypleurosauroid in our morphospace, *Qianxisaurus chajiangensis* which also possess a peculiar tooth morphology potentially reflecting a hard-shell prey preference (Cheng et al. 2012; Benton et al. 2013; Stubbs and Benton 2016). As less than 40% of postcranial information is available for *Simosaurus* (**Table S1.2**), we only use the first two and all axes of the PCoA generated only with all craniodental data (**Figure S1.5A**).

Morphofunctional disparity analyses

We used all axes of PCoA to compute a bootstrapped distribution of the total morphofunctional disparity (sum of ranges, 1000 Bootstrap iterations) using the *dispRity* package (v1.2.3) (Guillerme 2018) for both Pachypleurosauroidea and Nothosauroidea in the western and eastern Tethys regions. The significance of difference between the regional disparities for both clades have been calculated with the non-parametric

Wilcoxon test. We also calculated the overall morphofunctional disparity for both clades (Pachypleurosauroidea and Nothosauroidea) independently of the location of the taxa (**Figures S1.6A and B**) and for both regions (western and eastern Tethys) without distinguishing the clades (**Figures S1.6C–E**). Given the small number of pistosauroids in our dataset, we decided to not include them in per-clade analyses, but they are sampled for regional disparities (**Figures S1.6C–E**).

RESULTS

Cluster dendrogram, morphospace occupation and evolutionary convergence

A clear division in the cluster dendrogram separates species of the dataset into two extremely robust groups (**Figure 14 A**). The first one comprises all pistosauroids and all nothosauroids (except for *Simosaurus gaillardoti*). In this section of the dendrogram, the primitive pistosauroid *Wangosaurus brevirostris* clusters with two nothosauroids, *Brevicaudosaurus jiyanshanensis* and *Lariosaurus calcagnii*. The second main group in the dendrogram includes all pachypleurosauroids which form a well-defined cluster and *S. gaillardoti*, occupying the most basal position. In the phylo-ecomorphospace (**Figure 14B**), Triassic eosauropterygians tend to globally occupy distinct regions, with the pistosauroids located closer to nothosauroids than to pachypleurosauroids, thus reflecting broad-scale phylogenetic relationships as evidenced by the significant correlation between phenotypic and phylogenetic distances found by our Mantel test (r= 0.687 and p-value =0.001). The distinction of clades in the morphospace is mainly due to craniodental morphology; the postcranial skeleton appears less plastic and is marked by a large overlap between pachypleurosauroids and nothosauroids, suggesting a different signal (**Figures S1.5A and B**). The density of phenotypes recovers two main regions of occupation in the morphospace; one is located at the negative values along the PCoA axis 1 and represents the pachypleurosauroidean morphospace occupation while the other comprises all pistosauroids and all nothosauroids with the exception of *Simosaurus*. These two peaks are well separated by a trough with no clear 'intermediate' species sampled in our dataset.

Pachypleurosauroids tend to occupy a wider portion of the morphospace than nothosauroids (without *S. gaillardoti*), reflecting a higher degree of morphological

variation (see also **Figure S1.6B**). However, the inclusion of the peculiar *Simosaurus* greatly increases the disparity of nothosauroids (**Figure S1.6A**), as it occupies a unique region of the ecomorphospace. Indeed, *S. gaillardoti* is characterized by a brevirostrine skull with no rostral constriction, the presence of homodont durophagous dentition, and a relatively small upper temporal fenestra (**Figure 13K**) (Rieppel 1994), contrasting with the usually gracile skulls of nothosaurians, characterized by extremely elongated temporal region and specialized heterodont piercing dentition (**Figure 13J**) (Rieppel 2002).

As previously mentioned, the position of *Wangosaurus* in the dendrogram and in the morphospace suggests a greater morphological resemblance with nothosauroids than with the more derived pistosauroids, such as *Augustasaurus hagdorni* and *Yunguisaurus liae*. Our statistical convergence tests using Ct metrics recover *Wangosaurus brevirostris* as convergent with *Brevicaudosaurus jiyangshanensis* and with *Lariosaurus calcagnii,* its closest relatives in the dendrogram, no matter the number of PCoA axes used (**Table 1**). The method developed by Castiglione et al. (2019) also unambiguously identify phenotypic convergence between *Wangosaurus* and *Brevicaudosaurus* but not with *L. calcagnii* in this case (**Table 2**). Nevertheless, the significance of phenotypic convergence between *Wangosaurus* and some nothosauroids could be debated due to persisting uncertainties concerning the phylogenetic affinities of *Wangosaurus*. Indeed, this taxon is often recovered as the most basal pistosauroid (Ma et al. 2015; Jiang et al. 2019; Lin et al. 2021; Xu et al. 2022, 2023, as well as this chapter) but some studies considered it as a basal nothosauroid (Shang et al. 2020; Wang et al. 2022). For this reason, we also tested the morphological convergence of *Wangosaurus* with the two previous taxa by forcing *Wangosaurus* as a nothosauroid (see Material and Methods, section phylogenetic analyses). Even with this phylogenetic constraint, *Wangosaurus* is still found to be statistically convergent with *Brevicaudosaurus* when both using the Ct metrics and the method of Castiglione et al. (2019) (**Tables 1 and 2**). The morphological convergence with *L. calcagnii* is barely noticeable and only recovered by the Ct metrics computed with the first two axes of the PCoA (**Table 1**). Evidence of craniodental convergence between *Simosaurus gaillardoti* and *Qianxisaurus chajiangensis* is almost absent and is only recovered with the method of Castiglione et al. (2019) when using all axes of the PCoA (**Tables 1 and 2**). The results of our analyses thus only unambiguously highlight a phenotypical convergence between *Wangosaurus and Brevicaudosaurus* whereas other case of convergence tested in this paper should be interpreted cautiously.

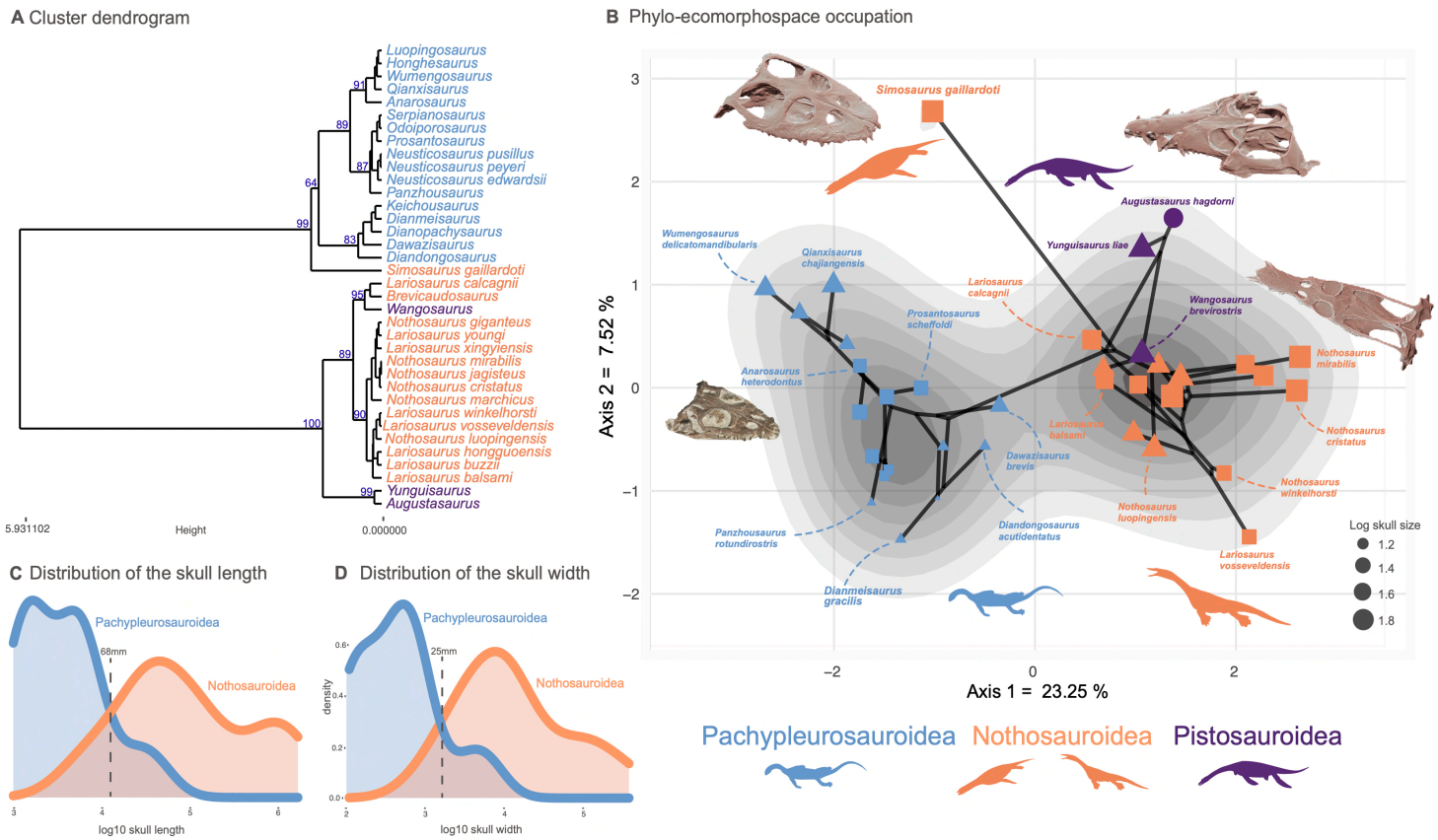

Figure 14. Cluster dendrogram, functional phylo-ecomorphospace occupation and size distribution of Middle Triassic eosauropterygians. (A) Cluster dendrogram using the whole-body dataset. Values of the support of the main nodes (approximate unbiased p-value in percentage) have been indicated at their corresponding nodes. (B) Phylo-ecomorphospace occupation based on the first two axes of our PCoA analysis using the whole-body dataset, superimposed on the density of taxa. Data points are shaped according to the corresponding province (square: western Tethys, triangle: eastern Tethys and circle: eastern Panthalassa) sizes are scaled to the relative skull size (log skull length). (C and D) Size distribution among pachypleurosauroids and nothosauroids: (C) log skull length and (D) log skull width.

Table 1. Results of the convergence tests using the Ct measures derived from the Stayton C-measures for selected pairs of taxa using the first two and all axes of the PCoA analyses using the whole-body dataset and on the craniodental dataset for *Simosaurus gaillardoti* and *Qianxisaurus chajiangensis*.

Taxon pair	PCo axes	Ct1	p-value	Ct2	p-value	Ct3	p-value	Ct4	p-value
Simosaurus gaillardoti* – *Qianxisaurus chajiangensis	PCo 1–2	0.108	0.260	0.030	0.215	0.043	0.269	0.010	0.171
	All axes	-0.093	0.327	-0.033	0.381	-0.035	0.300	-0.006	0.354
Wangosaurus brevirostris*– *Lariosaurus calcagnii	PCo 1–2	0.688	0.024	0.114	0.035	0.218	0.039	0.077	0.033
	All axes	0.106	0.041	0.028	0.049	0.035	0.053	0.009	0.057
Wangosaurus brevirostris*– *Brevicaudosaurus jiyangshanensis	PCo 1–2	0.704	0.013	0.108	0.017	0.308	0.006	0.073	0.013
	All axes	0.106	0.013	0.026	0.013	0.040	0.013	0.008	0.021
Wangosaurus brevirostris* as a basal nothosauroid– *Lariosaurus calcagnii	PCo 1–2	0.565	0.031	0.067	0.031	0.185	0.026	0.052	0.025
	All axes	-0.247	0.922	-0.047	0.724	-0.079	0.699	-0.016	0.532
Wangosaurus brevirostris* as a basal nothosauroid – *Brevicaudosaurus jiyangshanensis	PCo 1–2	-0.229	0.025	-0.008	0.025	-0.066	0.035	-0.007	0.024
	All axes	-3.098	0.182	-0.165	0.121	-0.496	0.268	-0.057	0.025

Table 2. Results convergence tests by using the Castiglione et al. (2019) method for selected pairs of taxa using the first and all axes of the PCoA analyses using the whole-body dataset and the craniodental dataset for *Simosaurus gaillardoti* and *Qianxisaurus chajiangensis*

Taxon pairs	PCo axes	Ang.state	Ang.state.time	p.ang.state	p.ang.state.time
Simosaurus gaillardoti* – *Qianxisaurus chajiangensis	PCo 1–2	46.778	0.410	0.382	0.215
	All axes	75.96	0.666	0.377	0.044
Wangosaurus brevirostris* – *Lariosaurus calcagnii	PCo 1–2	17.768	0.655	0.174	0.082
	All axes	85.296	3.145	0.458	0.118
Wangosaurus brevirostris* – *Brevicaudosaurus jiyangshanensis	PCo 1–2	3.547	0.120	0.049	0.011
	All axes	72.235	2.447	0.303	0.022
Wangosaurus brevirostris* as a basal nothosauroid – *Lariosaurus calcagnii	PCo 1–2	17.768	0.211	0.174	0.092
	All axes	85.296	1.014	0.459	0.149
Wangosaurus brevirostris* as a basal nothosauroid – *Brevicaudosaurus jiyangshanensis	PCo 1–2	3.545	0.041	0.04	0.017
	All axes	72.235	0.835	0.310	0.036

Regional and temporal patterns of disparity

Pachypleurosauroids and nothosauroids each evolved an approximate equal amount of disparity, even if nothosauroids appears to be slightly more disparate (p-value < 0.001) (**Figure S1.6A**). This difference in magnitude is mainly due to the unique craniodental morphology of *Simosaurus gaillardoti*. By removing this taxon and comparing pachypleurosauroids and nothosauroids present in the high-density area located on the positive values along the PCoA axis 1 (**Figure 14B**), pachypleurosauroids appear much more diverse ecomorphologically (p-value < 0.001) (**Figure S1.6B**). The western Tethyan faunal province records a greater amount of disparity than the eastern Tethyan one (p-value < 0.001) (**Figure S1.6C**), but this difference is once again exaggerated by the presence of *Simosaurus* (p-value < 0.001) (**Figure S1.6D**). Our results also show a strong geographical differentiation in the amount of ecomorphological disparity of the two clades. Pachypleurosauroids are clearly more disparate in the eastern Tethyan realm (p-value < 0.001) (**Figure 15B**) whereas nothosauroids have a disparity maximum in the western Tethyan realm (p-value = 0) (**Figure 15C**) even with the absence of *Simosaurus* (p-value = 0) (**Figure S1.5E**). These regional patterns can be visualized in the morphospace occupation of each geographical regions (**Figures 15D and J**). Furthermore, the temporal evolution of disparity seems to also vary within these two regions (**Figures 15D–L**). In the western Tethyan realm, the greatest eosauropterygian ecomorphological diversification likely occurred during the Fassanian (early Ladinian; **Figure 15 H**), while the maximum of disparity in the eastern Tethyan realm is recorded during the Pelsonian (middle Anisian), with the diversification of pachypleurosauroids (**Figure 15K**). All these results thus tend to highlight a strong geographical and temporal decoupling in the ecomorphological diversification of Triassic eosauropterygians.

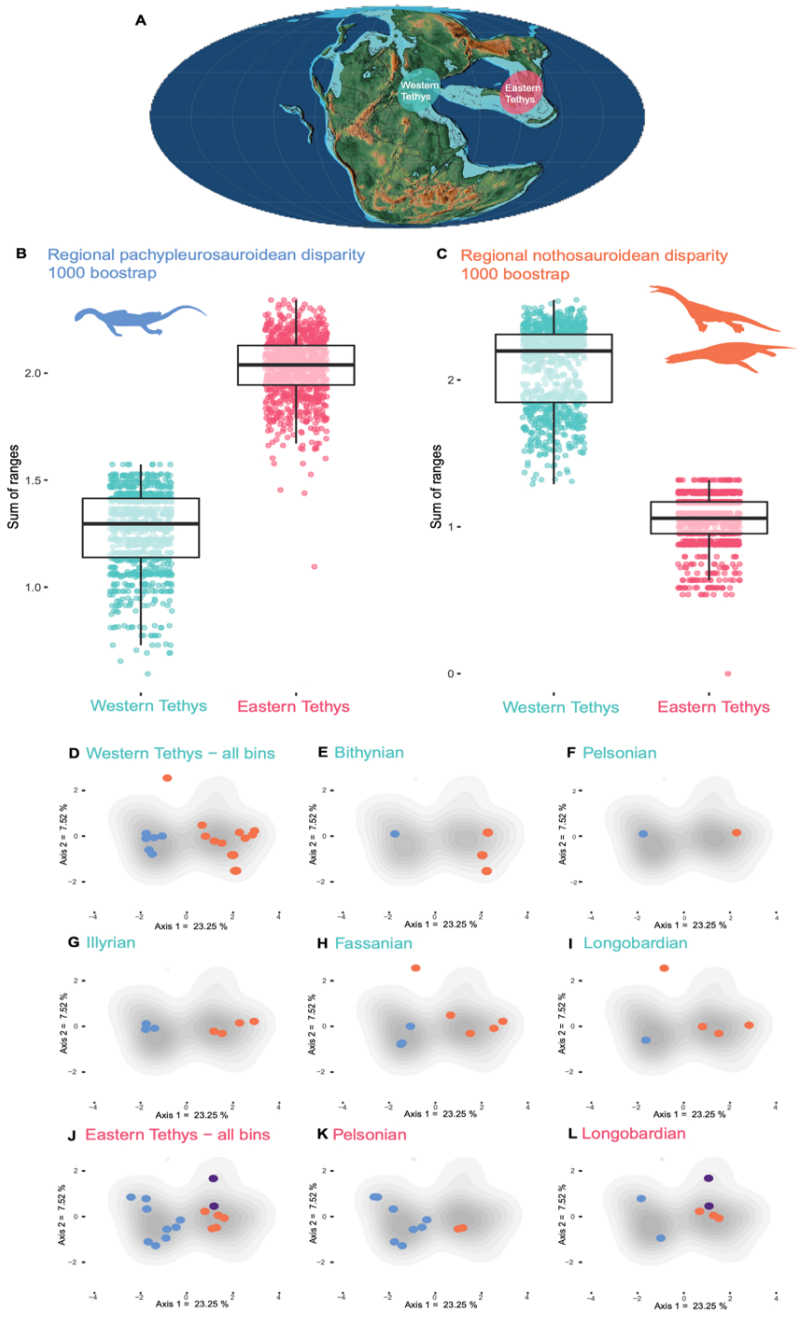

Figure 16. Regional and temporal pachypleurosauroids and nothosauroids pattern of ecomorphological disparity. (A) Paleobiogeography of the Middle Triassic (Ladinian) modified from Scotese (2016). (B and C) Comparison of the total disparity between the western and eastern Tethyan realm (B) for pachypleurosauroids and (C) nothosauroids. (D–L) Eosauropterygian ecomorphospace occupation through time during the Middle Triassic superimposed on the density of taxa (grey shades). (D–I) In the western Tethys and (J–L) in the eastern Tethys. Bithynian, Pelsonian and Illyrian are time bins of the Anisian while Fassanian and Longobardian are time bins of the Ladinian. Eastern Tethys eosauropterygians have only been found in the Pelsonian and Longobardian, in the Luoping, Panxian and Xingyi biotas respectively.

DISCUSSION

The early evolutionary trajectories of Triassic eosauropterygians reflect dietary specialization

Our ordination and convergences analyses provide new insights into the diversification of Triassic eosauropterygians and reveal a global colonization of distinct ecomorphospace regions for each clade (with the exception of *Wangosaurus*). This lack of overlap during their "early burst" radiation (Stubbs and Benton 2016) reflects the influence of developmental constraints among clades and supports the inference of a substantial and rapid trophic specialization in eosauropterygians, mainly reflected in their craniodental architecture and body size (Rieppel 2000, 2002). In a previous study which aimed to investigate the feeding mechanics in Triassic early sauropterygians by reconstructing their jaw adductor musculature, Rieppel (2002) highlighted the near absence of an overlap in the inferred feeding strategies of Triassic eosauropterygians. On one hand, the craniodental architecture of pachypleurosauroids, which are usually small-sized — rarely exceeding 50 cm according to Rieppel (2000) — is indeed characterized by a rounded, short and blunt snout, a very short symphysis and a homodont peg-like dentition, strongly suggesting that they have captured their prey by suction feeding, followed by a rapid snapping bite (Rieppel 2002; Xu et al. 2023). Pachypleurosauroids likely evolved a wider array of feeding strategies through time, however. Xu et al. (2023) reported a progressive reduction in the length of the hyoid apparatus and an increase in snout length, involving a gradual shift away from suction feeding for some derived species mostly in eastern Tethys (Wu et al. 2011; Cheng et al. 2012; Xu et al. 2023). On the other hand, nothosauroids and pistosauroids likely used their narrow and 'pincer jaw', to conduct sideward-directed snapping bites (Rieppel 2002). Their skull morphology and dentition suggest, here also, a range of food procurement strategies (Rieppel 2002). The dentition and the cranial architecture of pistosauroids should be more suitable to puncture prey, while the presence of procumbent and enlarged fangs in nothosauroids might have served as a fish-trap (Chatterjee and Small 1989; Rieppel 2002). Large species such as *L. calcagnii* , *N. giganteus* and *N. zhangi* could have nevertheless occupied the top of the food chain in their ecosystems and preyed on smaller marine reptiles (Sander 1989b; Tschanz 1989; Rieppel 2002; Liu et al. 2014). The isolated position of *S. gaillardoti* with respect to other nothosauroids in the ecomorphospace is mainly explained by its unique feeding strategy as it represents the only eosauropterygian to have developed a more durophagous dentition to crush hard-shelled preys such as ammonoids or hard-scaled fishes (Rieppel

1994, 2002; Klein and Griebeler 2016; Klein et al. 2022a). The magnitude of durophagy in *Simosaurus* is however not comparable to that of placodont sauropterygians which possess a much more robust mandible and teeth highly modified into low bulbs and tooth plates (Rieppel 2000, 2001b, 2002; Scheyer et al. 2012; Neenan et al. 2013, 2014, 2015; Crofts et al. 2016).

The postcranial anatomy of Triassic eosauropterygians appears to be less plastic than their craniodental skeleton, which is also possibly the case in short-necked plesiosaurian, besides relative neck length (O'Keefe 2002; Soul and Benson 2017; Fischer et al. 2020). This homogeneity in the morphological diversification of the postcranial region may reflect a conservative locomotion mode in nearshore habitats, through lateral body oscillation combined with forelimb propulsion by using rowing movements, especially in nothosauroids (Sues and Carroll 1985; Sander 1989b; Rieppel and Lin 1995; Zhang et al. 2014; Klein et al. 2015, 2022a; Gutarra and Rahman 2021; Xu et al. 2022). It is noteworthy to mention that pistosauroids occupied a portion of the ecomorphospace that has not been colonized by any other eosauropterygians, possibly reflecting the transition from the undulating non-pistosauroids to the pelagic paraxial swimming seen in plesiosaurians (Sato et al. 2014b).

The coexistence of many of the species analyzed suggests that their diverse morphologies represent the occupation of multiple ecological niches, potentially indicating niche partitioning. The fairly rapid ecomorphological specialization of eosauropterygians is probably best understood in the context of increasing complexity of marine trophic webs of the shallow marine and coastal environments of the Tethys during the Middle Triassic, following the recovery of the PTME (Chen and Benton 2012; Benton et al. 2013; Liu et al. 2014, 2021; Scheyer et al. 2014; Li and Liu 2020). Indeed, such a diversification pattern is not exclusive of eosauropterygians and have also been detected in ichthyosaurians, tanysaurians, and saurichthyid fishes as well (Benton et al. 2013; Wu et al. 2018; Spiekman et al. 2020, 2024; Bindellini et al. 2021; Sander et al. 2021)

Regional diversification patterns in eosauropterygians

Our results quantitatively reveal a pervasive regional difference in the disparity of the eosauropterygian assemblages along the Tethys margins suggesting a different biogeographical diversification for pachypleurosauroids and nothosauroids. Pachypleurosauroids seemed to undergo a remarkable ecomorphological radiation during the Pelsonian in the eastern Tethyan realm, shortly after their earliest appearance in the fossil record of that region (Jiang et al. 2014). This diversification mostly occurred

in the Luoping, as well as in the Panxian biotas, leading to the coexistence of numerous species with distinct feeding strategies (*e.g.* see the craniodental architecture of *Luopingosaurus*, *Diandongosaurus* or *Wumengosaurus*) or unique swimming capabilities among pachypleurosauroids (*e.g. Honghesaurus*) (Wu et al. 2011; Benton et al. 2013; Sato et al. 2014a; Shang and Li 2015; Cheng et al. 2016; Liu et al. 2021; Xu et al. 2022, 2023). By comparison, European — and more specifically the Alpine — pachypleurosauroids exhibit greater morphological similarity (Sander 1989b; Rieppel 2000; Renesto et al. 2014; Beardmore and Furrer 2016; Klein et al. 2022b), and are thus characterized by lower values of disparity. However, the validity of the taxonomic diversity of Chinese pachypleurosauroids could be questioned. With the exception of the abundant *Keichousaurus hui* for which the ontogenetic series is well known (Lin and Rieppel 1998; Cheng et al. 2009), a series of species are based on a single specimen and are in need of a thorough taxonomic reinvestigation. This possible overestimation of Chinese pachypleurosauroids could also affect regional disparity patterns.

Nothosauroids have been found to be more abundant and disparate in the western Tethys compared to their eastern relatives. The total ecomorphological disparity of European nothosauroids is potentially underestimated in our analyses by the absence of the peculiar but fragmentary simosaurid *Paludidraco multidentatus* from the Upper Triassic of Spain, whose unique anatomy suggest a manatee-like feeding and locomotion mode (de Miguel Chaves et al. 2018b; Cabezuelo Hernández et al. 2024). The unique morphologies of *Paludidraco* and *Simosaurus* would attest to the higher potential of diversification in feeding strategies in primitive European nothosauroids, compared to the more derived nothosaurians which appeared more similar, excepted in their size (Rieppel and Wild 1996; Liu et al. 2014).

Variation in the quality of the fossil record, notably Lagerstätten effects can be a powerful driver of spatiotemporal differences in diversity and can have complex impacts on disparity trends(Benson et al. 2010; Benson and Butler 2011; Flannery Sutherland et al. 2019). In our study, localities from both the eastern and western Tethys have been intensively sampled overtime, especially in Luoping, Panxian, Xingyi (China), and Monte San Giorgio and Winterswijk (Europe), allowing comparisons between these two regions (Rieppel 2000; Furrer 2003; Motani et al. 2008; Benton et al. 2013; Renesto et al. 2014; Beardmore and Furrer 2016; Heijne et al. 2019). Nevertheless, Chinese assemblages which have been characterized as exceptional in terms of faunal communities represent temporally disconnected ‘snapshots’ of the Pelsonian (Luoping and Panxian) and Longobardian (Xingyi) while European localities have produced a rather continuous

Middle Triassic time series (Rieppel 2000; Röhl et al. 2001; Furrer 2003b; Hu et al. 2011; Benton et al. 2013). Thus, if spatial heterogeneities in the fossil record are not the cause, what could have driven the observed differences among eosauropterygian phenotypes across Tethysian provinces? Both regions were likely subtropical shallow platform environments characterized by a rather similar vertebrate assemblages mainly composed of saurichthyid fishes (Wu et al. 2009; Benton et al. 2013; Maxwell et al. 2015, 2016), mixosaurid ichthyosaurians (Brinkmann 1998; Motani 1999c; Jiang et al. 2006b; Maisch et al. 2006; Fang et al. 2024; Klug et al. 2024), placodonts (Hagdorn and Rieppel 1999; Rieppel 2001b; Jiang et al. 2008b; Scheyer et al. 2012; Neenan et al. 2013, 2015; Wang et al. 2019), saurosphargids (Li et al. 2011), thalattosaurs (Müller 2005; Cheng et al. 2010; Bastiaans 2024), and tanysaurians (Rieppel et al. 2008; Spiekman et al. 2020, 2023; Wang et al. 2023), in addition to eosauropterygians. This broad-brush homogeneity in the faunas is expected to result from a dispersal route along coastlines of the Tethys, allowing exchanges between the European and Chinese provinces (Rieppel 1999; Bardet et al. 2014) (Bardet et al., 2014; Rieppel, 1999).

Drivers of this decoupling in disparity among pachypleurosauroids and nothosauroids remains unclear and require a thorough reinvestigation of the differences between ecosystems along the margins of the Tethys Ocean. However, this variation reveals the importance of analysing regional dynamics rather than a summed-up, oversimplified signal when spatial heterogeneities appeared strong, as recently demonstrated by Close et al. (2020) and (MacLaren et al. 2022) .

Eosauropterygia, a plastic clade throughout most of its history

Eosauropterygia and Ichthyosauria were the longest-lived clades of Mesozoic marine reptiles. Patterns of their morphological diversification have been analyzed using skull size, mandible shape, and skeletal characteristics, suggesting an early-burst radiation that gave rise to a variety of morphologies in shallow marine environments during the Middle Triassic (Stubbs and Benton 2016; Moon and Stubbs 2020; Reeves et al. 2021). However, the remodelling of marine ecosystems led by extinction events during the Late Triassic profoundly altered their evolutionary histories, with only pelagic morphotypes surviving across the Triassic–Jurassic boundary (Benson et al. 2010; Benson and Butler 2011; Thorne et al. 2011; Dick and Maxwell 2015; Wintrich et al. 2017). These selective extinctions forced a quantitative drop in the disparity but are coupled with the emergence of parvipelvians and plesiosaurians during the Late Triassic (Motani 2009; Benson et al. 2012; Dick and Maxwell 2015; Stubbs and Benton 2016; Wintrich et al. 2017; Moon and

Stubbs 2020; Reeves et al. 2021). While the disparity of ichthyosaurian surviving lineages seems to be considerably reduced in comparison to their Triassic ancestors (Thorne et al. 2011; Dick and Maxwell 2015; Fischer et al. 2016; Stubbs and Benton 2016), post-Early Jurassic plesiosaurians have been characterized by an impressive ecomorphological diversity (O'Keefe 2002; Fischer et al. 2017, 2020b; O'Keefe et al. 2017; Soul and Benson 2017). Indeed, the evolutionary history of plesiosaurians has been marked by the iterative evolution of superficially similar phenotypes (e.g. 'plesiosauromorph' vs 'pliosauromorph', 'longirostrine' [long and slender snout] vs 'latirostrine' [short and robust snout] in short-necked plesiosaurians) over time (O'Keefe 2002; Fischer et al. 2017, 2018, 2020b), and by the ability to innovate in their swimming and feeding strategies in their late evolution (O'Keefe et al. 2017) .

This great ecomorphological diversification demonstrates that plesiosaurians were continuously capable of producing a large variety of forms and were therefore characterized by a high phenotypic plasticity which may have helped them to withstand or adapt to changes in the ecosystems over the Jurassic and the Cretaceous. The remarkable feeding specializations among Middle Triassic eosauropterygians coupled with their distinct regional patterns of diversification also highlight a such phenotypic plasticity in addition to their high developmental plasticity identified by the diversity of their life history traits (Klein and Griebeler 2018; Griebeler and Klein 2019). Our results would thus suggest that eosauropterygians have always displayed a wide range of craniodental architectures and that a high morphological plasticity has characterized their overall evolutionary history; the initial plesiosaurian radiation during the Early Jurassic being the exception with the lowest values of disparity recorded (Benson et al. 2012; Benson and Druckenmiller 2014; Stubbs and Benton 2016).

CONCLUSION

In this paper, we reinvestigate the ecomorphological diversification of Middle Triassic eosauropterygians. We found that this important diversification led to craniodental distinction and feeding specializations among pachypleurosauroids, nothosauroids and pistosauroids, suggesting low interspecific competition in the shallow intraplatform basins bordering the Tethys Ocean. On the other hand, our results indicate that their postcranial anatomy appear more m-homogeneous, mainly between

pachypleurosauroids and nothosauroids. This trend suggests a decoupling in the evolution of these two anatomical regions, similarly to what has been proposed for derived short-necked plesiosaurians. Our analyses also demonstrate that the disparity of pachypleurosauroids and nothosauroids differs along the Tethys margins, reflecting regional variations in their disparity. The eastern Tethys during the Pelsonian represented a unique 'hotspot' for the morphological diversification of pachypleurosauroids in which various craniodentally distinct taxa co-occurred. The western margin of the Tethys was dominated by nothosauroids, and their disparity has been mainly increased by the morphology of *Simosaurus*. This regional variation in disparity would suggests that Triassic eosauropterygians diversified in a different way depending on the biotic and abiotic features of the ecosystems. This high phenotypic plasticity also characterizes the evolution of post-Triassic plesiosaurians, casting the entire Eosauropterygia as a particularly plastic clade.

SUPPLEMENTS FOR CHAPTER 1

Data archiving statement

All 3D models used in this chapter are available on MorphoSource (https://www.morphosource.org/projects/000508432?locale=en). Supplementary data (Excel file containing measurements and ratios) and R script used to compute all analyses are available on https://peerj.com/articles/15776/#supplementary-material.

Definition of the ecomorphological traits

- **Longirostry: snout length/ skull length. Completeness: 97.1%**
  Characterizes the hydrodynamic potential of the snout such as the amount of drag during the locomotion (Busbey 1995), the resistance to lateral shaking (Holzman et al. 2012) or the water volume expelled on the closure of the mouth (Mccurry et al. 2017; Maclaren et al. 2022).
- **Snout shape ratio: snout width / skull length. Completeness: 94.3%**
  Proxy for the size of the potential ingested prey (MacLaren et al. 2022)and for the water volume that need to be expelled during the closure of the mouth (Mccurry et al. 2017).
- **Jaw robusticity: Jaw height at mid-dentigerous length / mandible length. Completeness: 54.3%**
  Characterizes the aspect ratio of the jaw and is a proxy of the robustness and the stiffness in the jaw under biting loads (Anderson et al. 2011; MacLaren et al. 2017, 2022a). The height of the jaw was measured at the mid-dentigerous zone.
- **Relative symphysial length: Symphyseal length / mandible length. Completeness: 57.1%**
  Characterizes the robustness of the anterior portion of the jaw and its resistance during the prey capture(Stubbs and Benton 2016; Fischer et al. 2017; MacLaren et al. 2017; Bennion et al. 2022).
- **Functional toothrow length: Dentigerous mandible length / mandible length. Completeness: 57.1%**
  Describe the proportion of the jaw which serves to the capture of the potential prey (MacLaren et al. 2017). Furthermore, differences in the length of the toothrow reflects different strategies in prey capture; a long dental row would indeed increase the variation in bites forces and speed which would result in more functional variability, as reflected by great differences between the anterior and posterior mechanical advantage (Stubbs and Benton, 2016).

- **Anterior mechanical advantage: Distance between the fulcrum and the mid-point of attachment for the adductor muscles on the dorsal surface of the mandible / distance between the fulcrum and the anterior tip of mandible. Completeness: 68.6%**
  The vertebrate mandible can be modelled as a third-order lever (Stubbs and Benton, 2016). The mechanical advantage (MA) is an estimation of the ability of a system to transfer the muscles force of the mandible to the prey and can be calculated as the ratio of the inlever and the outlever measurements (Stayton 2006; Stubbs and Benton 2016). The anterior mechanical advantage (AMA) can be defined as the lowest potential MA along the dental row (Stubbs and Benton 2016). Here, the inlever is the distance between the fulcrum (skull articulation with the mandible) to the mid-point of the adductor muscles area insertion while the outlever is represented by the distance from the fulcrum to the base of the anteriormost tooth. It has been demonstrated that animals with weak and rapid bites have low values for AMA while higher values are characteristics of powerful and slower bites (Anderson 2009).
- **Posterior mechanical advantage: Distance between the fulcrum and the mid-point of attachment for the adductor muscles on the dorsal surface of the mandible / distance between the fulcrum and the last mandible tooth. Completeness: 54.3%**
  The principle of the posterior mechanical advantage (PMA) is the same than the AMA except that the outlever is measured from the fulcrum to the base of the posteriormost tooth of the mandible. This morphological trait therefore estimates the highest force transfer along the mandibular dentition (Anderson et al. 2011; Stubbs and Benton 2016).
- **Opening mechanical advantage: Distance between the fulcrum and the retroarticular process / distance between the fulcrum and the mid-point of attachment for the adductor muscles on the dorsal surface of the mandible. Completeness: 82.9%**
  Characterizes the velocity during the opening of the jaw (MacLaren et al. 2017; Bennion et al. 2022). The inlever can be measured as the distance between the fulcrum and the posterior end of retroarticular process and the outlever, as the distance from the fulcrum to the base of the anteriormost tooth of the mandible.
- **Nares position: Distance between the anterior margin of the nares and the tip of the snout / skull length. Completeness: 100%**
  Proxy describing the ability to take a breath during a constant state swim (MacLaren et al. 2022).
- **Relative naris size: Length of the nares / skull length. Completeness: 100%**
  Amount of air that can be inhaled during a breath (MacLaren et al. 2022).
- **Relative orbit size: Mean diameter of the orbit / skull length. Completeness: 97.1%**

Characterizes the importance of the visual component in the multiple functions that skulls have to perform (MacLaren et al. 2022).

- **Occular offset: Distance from the centre of the orbit to the plane containing the upper tooth row / skull length. Completeness: 51.4%**
  Characterizes the position of the eyes in relation to the jaws.
- **Relative parietal foramen length: Length of the parietal foramen / skull length. Completeness: 100%**
  Characterizes the length of the parietal foramen and is a proxy for the relative size of the pineal gland (MacLaren et al. 2022).
- **Tooth crown shape: Tooth crown height / crown base width. Completeness: 97.1%**
  Characterizes the slenderness of the tooth and the resistance to bite forces (Massare 1987; Foffa et al. 2018b; Zverkov et al. 2018; Fischer et al. 2022a; MacLaren et al. 2022). Measurements have been taken on mid-dentigerous region and not on fangs.
- **Absolute crown height: Tooth crown height raw measurement. Completeness: 100%**
  This absolute trait has been shown to be a determinant of diet in modern cetaceans (Ridgway and Harrison 1999a) and have been recently used in marine reptile dataset (Fischer et al. 2020; Bennion et al. 2022).
- **Heterodonty index: Anterior tooth crown shape / posterior tooth crown shape. Completeness: 82.9%**
  Characterizes quantitatively the level of heterodonty in the dentition of taxa. A value close to 1 indicates no or very low level of heterodonty while a value which exceed 1 reflects a certain level of heterodonty. This quantitative trait however doesn't inform about the global morphology of the teeth should therefore be used in combination with discrete character as 18, 19, 20 which describe the morphology of the tooth crown.
- **Jaw or snout anterior constriction: Absent (0); Present (1). Completeness: 94.3%**
  Discrete character which represents a proxy for the preferential use of the anterior jaw for prey capture(MacLaren et al. 2022).
- **Pointed and recurved tooth crown: Absent (0); Present (1). Completeness: 94.3%**
  Discrete character which serves to differentiate the small-prey flesh piercers or cutters which have pointed recurved crowns than from the taxa which has straight or bulbous crowns with blunt or rounded apices and which could be referred in the durophage or generalist guilds in Massare (1987) and Fischer et al. (2022a).
- **Bulbous crushing dentition: Absent (0); Present (1). Completeness: 100%**
  Discrete character which serves to differentiate taxa with bulbous, blunt and rounded (globidont) dentition. This dental feature is characteristic of the durophage guild made up with taxa capable of crushing hard-shelled prey (Massare 1987; Fischer et al. 2022a). Please note that *Placodus* and cyamodontoid placodonts which are highly durophageous

taxa have a rather flat instead of bulbous dentition (Rieppel 2001b; Scheyer et al. 2012; Neenan et al. 2013; Crofts et al. 2016).

- **Enlarge procumbent dentition: Absent (0); Present (1)**. **Completeness: 100%**
  Discrete character which serves to differentiate taxa that possess fangs on lower and upper jaws. These fangs would have served to pierce pelagic preys (Massare 1987; Großmann 2007) or to create a fish-trap to prevent preys from escaping out of the buccal cavity (Chatterjee and Small 1989; Rieppel 2002).
- **Relative skull length: Skull length / trunk length. Completeness: 60%**
  Characterizes the proportion of the body used for prey capture and sensory capabilities.
- **Neck proportion: Neck length / trunk length. Completeness: 60%**
  Characterizes the general body plan but is also a proxy for potential feeding arch and reach of cranium away from the trunk (O'Keefe 2001a).
- **Trunk proportion: Trunk length / body length. Completeness: 40%**
  Characterizes the proportion of the body length available for lungs and digestive track.
- **Tail proportion: Tail length / body length. Completeness: 40%**
  Characterizes the proportion of the body used for the locomotion. Because Plesiosauria evolved to an undewater flight by using their four hydrofoil-like flippers (Krahl 2021), the role of the tail in the locomotion is greatly reduced as evidenced by the shortening of the tail (Krahl 2021). However, the stem groups Pachypleurosauroidea and Nothosauroidea are regarded as lateral undulatory swimmers even if the fore- and the hindflippers played an important role in the propulsion as there are morphologically derived (Carroll and Gaskill 1985; Sues 1987; Krahl 2021).
- **Propodial variation: Humerus proximo-distal length / femur proximodistal length: Completeness: 77.1%**
  Characterizes the appendicular body plan. The length of the humerus and the femur relative to each other can be considered as indicative of forelimb, hindlimb or equally driven underwater locomotion (Zeffer et al. 2003; Hinić-Frlog and Motani 2010).
- **Propodial size: Humerus proximo-distal length / skull length. Completeness: 77.1%**
  Characterizes the elongation of the limbs relative to the skull size. This trait is indicative of the ecology of taxa as species with long limbs and small head will swim and feed in a different way than taxa with a small limbs and large head (Taylor 1987; Massare 1988).
- **Humerus gracility: Humerus antero-posterior width / humerus proximo-distal length. Completeness: 85.7%**
  Characterizes the area of muscular insertion on the humerus and the mechanical efficiency of the pectoral girdle. This trait describes the implication of the forelimb in the locomotion.

- **Femur gracility: Femur antero-posterior width / femur proximo-distal length. Completeness: 80%**
  Characterizes the area of muscular insertion on the femur and the mechanical efficiency of the pelvic girdle. This trait describes the implication of the hindlimb in the locomotion.
- **Forelimb aspect ratio**: **Forelimb antero-posterior width / forelimb proximo-distal length. Completeness: 51.4%**
  Describes potential water displacement by the forelimbs or the pectoral paddles.
- **Hindlimb aspect ratio: Hindlimb antero-posterior width / forelimb proximo-distal length. Completeness: 62.9%**
  Describes potential water displacement by the hindlimbs or the pelvic paddles.

Table S1.1. List of taxa present in ecomorphological disparity analyses.

Taxon	Clade	Locality	Age range	Source of measurements
Anarosaurus heterodontus	Pachypleurosauroidea	Western Tethys	246.36 – 243.99	First-hand examination and photographs (Klein 2009, 2012)
Dawazisaurus brevis	Pachypleurosauroidea	Eastern Tethys	244.94 – 243.99	Photographs (Cheng et al. 2016)
Diandongosaurus acutidentatus	Pachypleurosauroidea	Eastern Tethys	244.94 – 243.99	Photographs (Sato et al. 2013, 2014a; Shang et al. 2017a)
Dianmeiosaurus gracilis	Pachypleurosauroidea	Eastern Tethys	244.94 – 243.99	Photographs (Shang & Li 2015)
Dianopachysaurus dingi	Pachypleurosauroidea	Eastern Tethys	244.94 – 243.99	Photographs (Liu et al. 2011)
Honghesaurus longicaudalis	Pachypleurosauroidea	Eastern Tethys	244.94 – 243.99	Photographs (Xu et al. 2022)
Luopingosaurus imparilis	Pachypleurosauroidea	Eastern Tethys	244.94 – 243.99	Photographs (Xu et al., 2023)
Keichousaurus hui	Pachypleurosauroidea	Eastern Tethys	239.1 – 237	First-hand examination and photographs (Holmes et al., 2008; Renesto et al., 2014)
Neusticosaurus edwardsii	Pachypleurosauroidea	Western Tethys	239.1 – 237	First-hand examination
Neusticosaurus peyeri	Pachypleurosauroidea	Western Tethys	241.5 – 239.1	First-hand examination
Neusticosaurus pusillus	Pachypleurosauroidea	Western Tethys	241.5 – 239.1	First-hand examination
Odoiporosaurus teruzzi	Pachypleurosauroidea	Western Tethys	243.99 – 241.5	Photographs (Renesto et al. 2014)
Panzhousaurus rotundirostris	Pachypleurosauroidea	Eastern Tethys	244.94 – 243.99	Photographs (Jiang et al. 2019)
Prosantosaurus scheffoldi	Pachypleurosauroidea	Western Tethys	241.5 – 239.1	First-hand examination
Qianxisaurus chajiangensis	Pachypleurosauroidea	Eastern Tethys	239.1 – 237	Photographs (Cheng et al. 2012)
Serpianosaurus mirigiolensis	Pachypleurosauroidea	Western Tethys	243.99 – 241.5	First-hand examination
Wumengosaurus delicatomandibularis	Pachypleurosauroidea	Eastern Tethys	244.94 – 243.99	Photographs (Jiang et al. 2008a; Wu et al. 2011)
Brevicaudosaurus jiyangshanensis	Nothosauroidea	Eastern Tethys	239.1 – 237	Photographs (Shang et al. 2020)
Lariosaurus calcagnii	Nothosauroidea	Western Tethys	241.5 – 239.1	First-hand examination
Lariosaurus balsami	Nothosauroidea	Western Tethys	239.1 – 237	First-hand examination
Lariosaurus buzzii	Nothosauroidea	Western Tethys	243.99 – 241.5	First-hand examination
Lariosaurus hongguoensis	Nothosauroidea	Eastern Tethys	244.94 – 243.99	Photographs (Jiang et al. 2006)
Lariosaurus xingyensis	Nothosauroidea	Eastern Tethys	239.1 – 237	Photographs (Lin et al. 2017; Rieppel et al. 2003)
Lariosaurus vosseveldensis	Nothosauroidea	Western Tethys	246.36 – 243.99	Photographs(Klein et al. 2016b)
Lariosaurus winkelhorsti	Nothosauroidea	Western Tethys	246.36 – 244.94	First-hand examination, photographs made by the authors
Lariosaurus youngi	Nothosauroidea	Eastern Tethys	239.1 – 237	Photographs (Ji et al. 2014)
Nothosaurus cristatus	Nothosauroidea	Western Tethys	239.1 – 237	First-hand examination
Nothosaurus luopingensis	Nothosauroidea	Eastern Tethys	244.94 – 243.99	Photographs (Shang et al. 2022)

Nothosaurus giganteus	Nothosauroidea	Western Tethys	243.99 – 233.5	First-hand examination and 3D models created by the authors
Nothosaurus jagisteus	Nothosauroidea	Western Tethys	241.5 – 239.1	First-hand examination
Nothosaurus marchicus	Nothosauroidea	Western Tethys	246.5 – 241.5	First-hand examination, photographs (Klein et al. 2015; Voeten et al. 2018)
Nothosaurus mirabilis	Nothosauroidea	Western Tethys	243.99 – 239.1	First-hand examination and 3D models created by the authors
Simosaurus gaillardoti	Nothosauroidea	Western Tethys	241.5 – 237	3D models created by the authors
Augustasaurus hagdorni	Pistosauroidea	Eastern Panthalassa	243.99 – 241.5	3D models created by the authors
Wangosaurus brevirostris	Pistosauroidea	Eastern Tethys	239.1 – 237	Photographs (Ma et al. 2015)
Yunguisaurus liae	Pistosauroidea	Eastern Tethys	239.1 – 237	Photographs (Cheng et al. 2006; Sato et al. 2014b)

Table S1.2. List of specimens and completeness for all morphological regions**.**

Taxon	Clade	Specimens	Craniodental completeness	Postcranial completeness	Whole body completeness
Anarosaurus heterodontus	Pachypleurosauroidea	NME 480000125, NME 480000130, NMNHL RGM 443855, NMNHL RGM 443856, SIPG R 594, SIPG R 595, SIPG R 596, NMNHL Wijk06-38, NMNHL Wij06-266, NMNHL Wijk09-582, NMNHL RGM.443858	95.24%	30%	75%
Dawazisaurus brevis	Pachypleurosauroidea	NMNS000933-F034397	90.48%	100%	93.75%
Diandongosaurus acutidentatus	Pachypleurosauroidea	IVPP V17760, NMNS-000933-F03498	95.24%	100%	96.88%
Dianmeiosaurus gracilis	Pachypleurosauroidea	IVPP V 17054, IVPP V 18630	90.48%	100%	93.75%
Dianopachysaurus dingi	Pachypleurosauroidea	LPV 31365	66.67%	60%	65.63%
Honghesaurus longicaudalis	Pachypleurosauroidea	IVPP V30380	95.24%	100%	96.88%
Luopingosaurus imparilis	Pachypleurosauroidea	IVPP V19049	80.95%	80%	81.25%
Keichousaurus hui	Pachypleurosauroidea	NMNS-cyn-2003-25, NMNS-cyn-2005-05, NMNS-cyn-2005-12, SMNS 81780, SMNS 59705	95.24%	100%	96.88%
Neusticosaurus edwardsii	Pachypleurosauroidea	PIMUZ T2810, PIMUZ T2811, PIMUZ T3430, PIMUZ T3439, PIMUZ T3453, PIMUZ T3452, PIMUZ T3460, PIMUZ T3708, PIMUZ T3758, PIMUZ T3759, PIMUZ T3776, PIMUZ T4761	100%	100%	100 %
Neusticosaurus peyeri	Pachypleurosauroidea	PIMUZ T3393, PIMUZ T3394, PIMUZ T3395, PIMUZ T3396, PIMUZ T3403, PIMUZ T3410, PIMUZ T3422,	100%	100%	100%

		PIMUZ T3423, PIMUZ T3431, PIMUZ T3445, PIMUZ T3461, PIMUZ T3464, PIMUZ T3467, PIMUZ T3474, PIMUZ T3476, PIMUZ T3479, PIMUZ T3497, PIMUZ T3511, PIMUZ T3542, PIMUZ T3546, PIMUZ T3607, PIMUZ T3710, PIMUZ T3728, PIMUZ T3744, PIMUZ T3902			
Neusticosaurus pusillus	Pachypleurosauroidea	PIMUZ T3902, PIMUZ T3400, PIMUZ T3421, PIMUZ T3426, PIMUZ T3429, PIMUZ T3442, PIMUZ T3468, PIMUZ T3509, PIMUZ T3530, PIMUZ T3536, PIMUZ T3538, PIMUZ T3547, PIMUZ T3556, PIMUZ T3574, PIMUZ T3598, PIMUZ T3601, PIMUZ T3604, PIMUZ T3605, PIMUZ T3612, PIMUZ T3614, PIMUZ T3625, PIMUZ T3627, PIMUZ T3639, PIMUZ T3649 A, PIMUZ T3649 B, PIMUZ T3649 C, PIMUZ T3653, PIMUZ T3654, PIMUZ T3658, PIMUZ T3658, PIMUZ T3671, PIMUZ T 3672, PIMUZ T3703, PIMUZ T3739, PIMUZ T3741 B, PIMUZ T3803 B, PIMUZ T3803 D, PIMUZ T3934, PIMUZ T4289, PIMUZ T5942	100%	100%	100%

Odoiporosaurus teruzzi	Pachypleurosauroidea	MSNM BES SC 1893	85.71%	40%	71.88%
Panzhousaurus rotundirostris	Pachypleurosauroidea	GMPKU-P- 1059	66.67%	80%	71.88%
Prosantosaurus scheffoldi	Pachypleurosauroidea	PIMUZ A/III 1197, PIMUZ A/III 1240, PIMUZ A/III 1273, PIMUZ A/III 1274, PIMUZ A/III 1275, PIMUZ A/III 4566	95.24%	80%	90.63%
Qianxisaurus chajiangensis	Pachypleurosauroidea	NMNS-KIKO-F044630	90.48%	60%	81.25%
Serpianosaurus mirigiolensis	Pachypleurosauroidea	PIMUZ T96, PIMUZ T951, PIMUZ T1071, PIMUZ T 3675, PIMUZ T3676, PIMUZ T3677, PIMUZ T3680, PIMUZ T3685, PIMUZ T3742, PIMUZ T3931, PIMUZ T3933	100%	100%	100%
Wumengosaurus delicatomandibularis	Pachypleurosauroidea	GMPKU-P-1210, IVPP V15314, NMNS-KIKO-F071129-Z, ZMNH M8758	90.48%	100%	93.75%
Brevicaudosaurus jiyangshanensis	Nothosauroidea	IVPP V 18625	76.19%	100%	84.38%
Lariosaurus balsami	Nothosauroidea	PIMUZ T4856	80.95%	80%	81.25%
Lariosaurus buzzii	Nothosauroidea	PIMUZ T2804	76.19%	40%	65.63%
Lariosaurus calcagnii	Nothosauroidea	PIMUZ T2460, PIMUZ T2461, PIMUZ T2462, PIMUZ T2464, PIMUZ T4836, PIMUZ T5151, PIMUZ T5559	95.24%	100%	96.88%
Lariosaurus hongguoensis	Nothosauroidea	GMPKU-P-1011	85.71%	50%	75%
Lariosaurus vosseveldensis	Nothosauroidea	TWE 480000504	66.67%	0%	46.88%
Lariosaurus youngi	Nothosauroidea	WS-30-R24	80.95%	80%	81.25%
Nothosaurus cristatus	Nothosauroidea	GPIT-PV-75067	66.67%	0%	46.88%
Nothosaurus luopingensis	Nothosauroidea	IVPP V 24895	66.67%	60%	65.63%
Nothosaurus giganteus	Nothosauroidea	PIMUZ T4829; SMNS 18058, SMNS 57047, SMNS 80217, SMNS 1598b ; SMNS 159157, SMNS 17822c, SMNS 81311	95.24%	80%	90.63%

Nothosaurus jagisteus	Nothosauroidea	SMNS 56618	66.67%	10%	50%
Nothosaurus marchicus	Nothosauroidea	JLW 300, NMNHL RGM 449995, TWE 480000375, TWE 4800000473, TWE 4800000474	85.71%	30%	68.75%
Nothosaurus mirabilis	Nothosauroidea	SMNS 13155, SMNS 15714, SMNS 16433, SMNS 56826, SMNS 59074, SMNS 84550	71.43%	10%	53.13%
Nothosaurus winkelhorsti	Nothosauroidea	TWE 4800000474	57.14%	0%	40.63%
Simosaurus gaillardoti	Nothosauroidea	GPIT-PV-60638, SMNS 10360, SMNS 16363, SMNS16638, SMNS 50714, SMNS 59366, SMNS 7861, SMNS 17223, SMNS 14733, SMNS 17590	100%	10%	71.88%
Augustasaurus hagdorni	Pistosauroidea	FMNH PR1974	85.71%	0%	59.38%
Wangosaurus brevirostris	Pistosauroidea	GMPKU-P-1529	80.95%	70%	78.13%
Yunguisaurus liae	Pistosauroidea	IVPP V14993, NMNS 004529/F003826, ZMNH M8738	95.24%	100%	96.88%

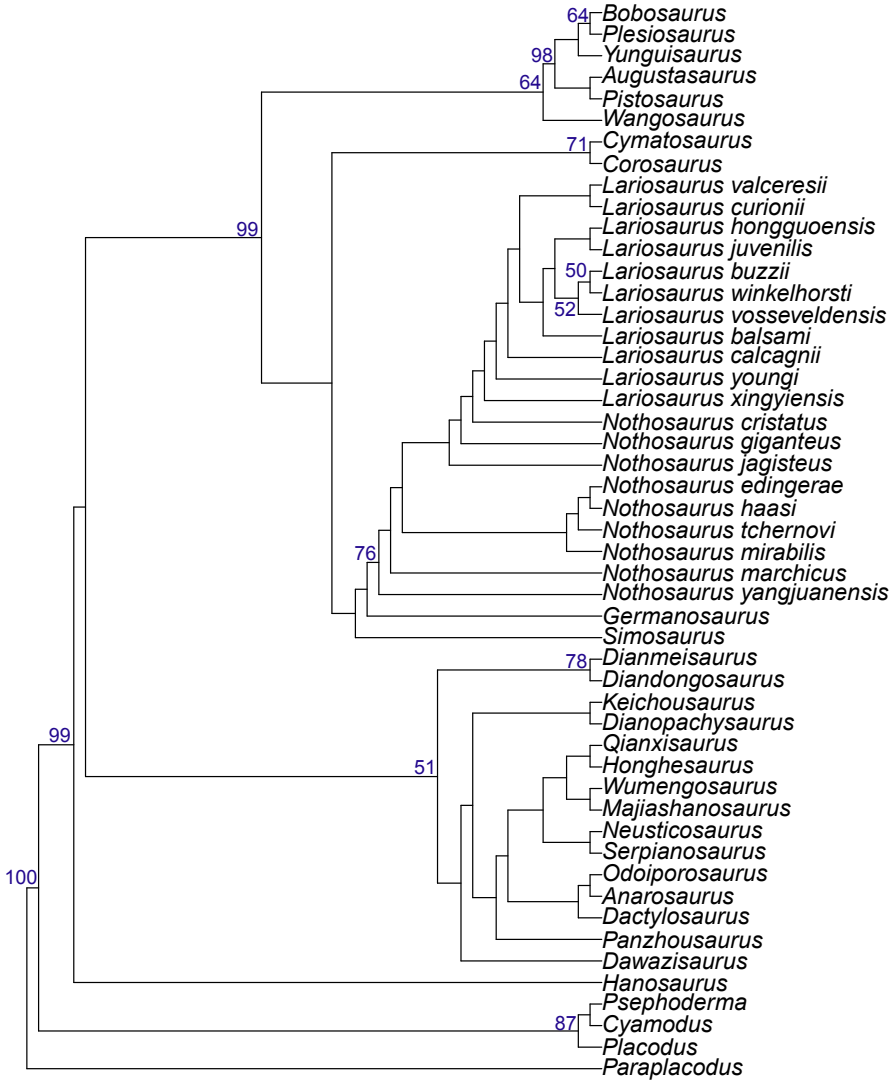

Figure S1.1. Most parsimonious tree arising from the implied weighting analysis (*k*=12). The Consistency Index is 0.310 and the Retention Index is 0.664. The dataset is the same than the original matrix of Xu et al. (2022) and no further taxa have been added. As we used the implied weighting algorithm, our topology shows slightly differences with the most parsimonious consensus tree of Xu et al. (2022). For example, in our analyse, *Honghesaurus* is no longer the sister taxon of *Wumengosaurus* as *Majiashanosaurus* occupies a more derived position. Values of the symmetric resampling ≥ 50 are indicated at their corresponding nodes.

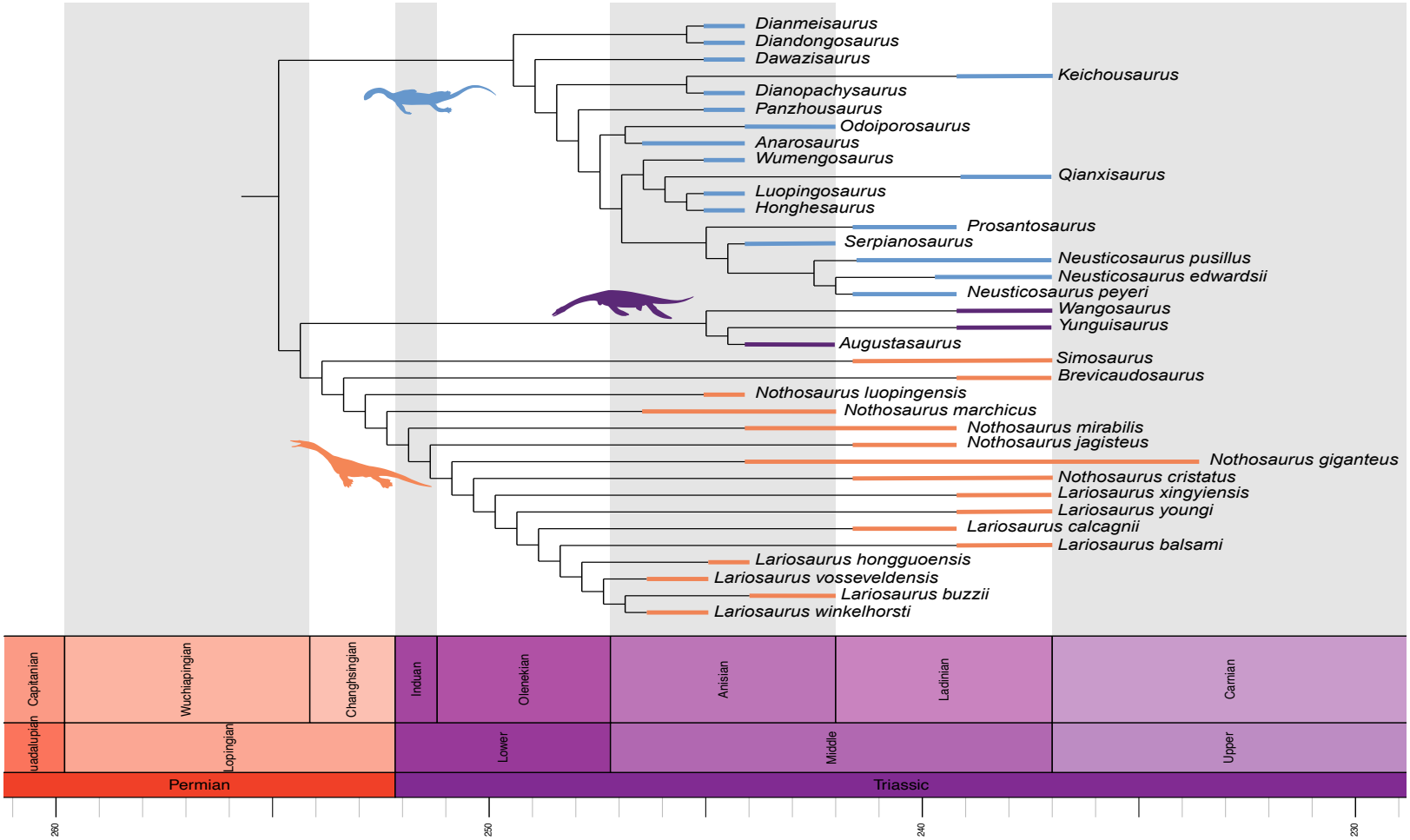

Figure S1.2:. Time-scaled phylogeny arising from implied weighting (*k*=12) maximum parsimony analysis using minimum branch length (MBL) algorithm, using a minimal value of 0.5 Myr. Only taxa present in our morphological dataset are shown. Ranges extensions of taxa have been coloured according to their respective clade

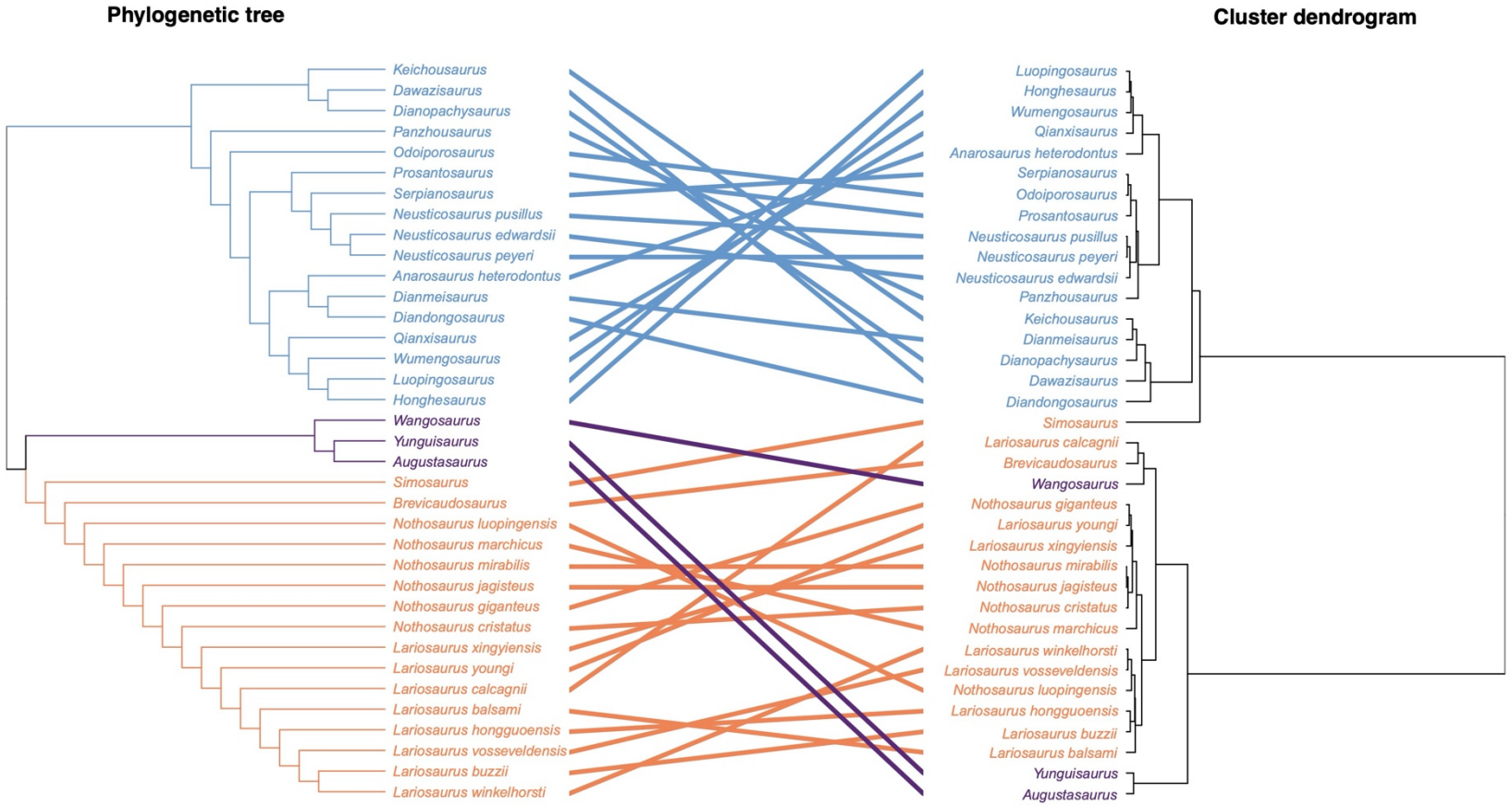

Figure S1.3. Tanglegram comparing the phylogeny with the hierarchy of a cluster dendrogram generated with the whole-body data. Each label has been coloured with respect to its relative clade. The phylogenetic tree has been generated in Maximum Parsimony framework under implied weighting (*k*=12). Mantel test result (r= 0.687 and p-value =0.001) indicates a significant correlation between the phylogenetic relationships and the hierarchy of the cluster dendrogram.

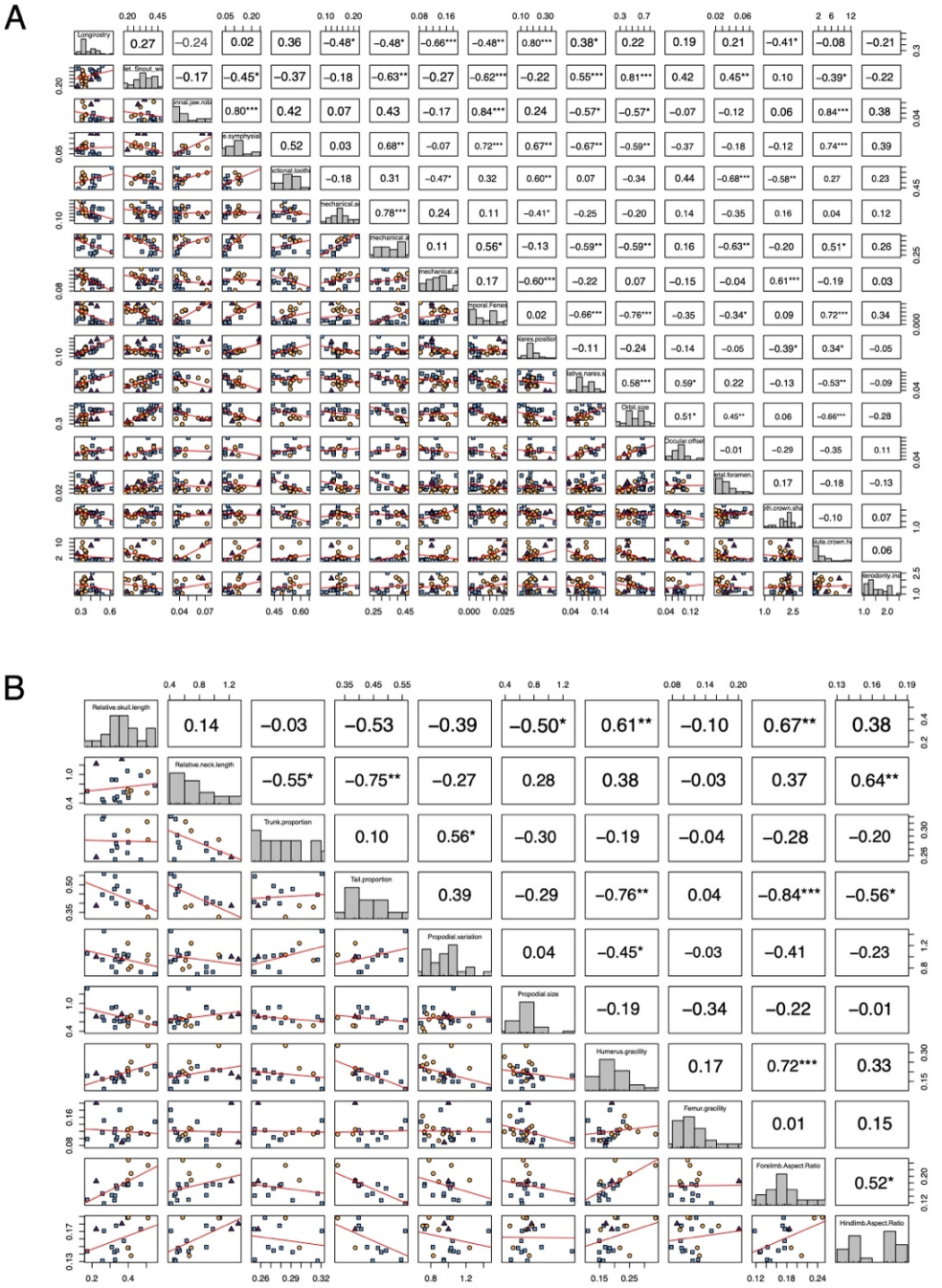

Figure S1.4: Eosauropterygian quantitative (A) craniodental and postcranial (B) trait histograms, pairwise distribution and correlation. Each dot is coloured with respect to their relative clade. The upper panel indicates the pairwise correlation (Pearson's correlation coefficient; * indicates significance at alpha = 0.05, ** at alpha 0.01).

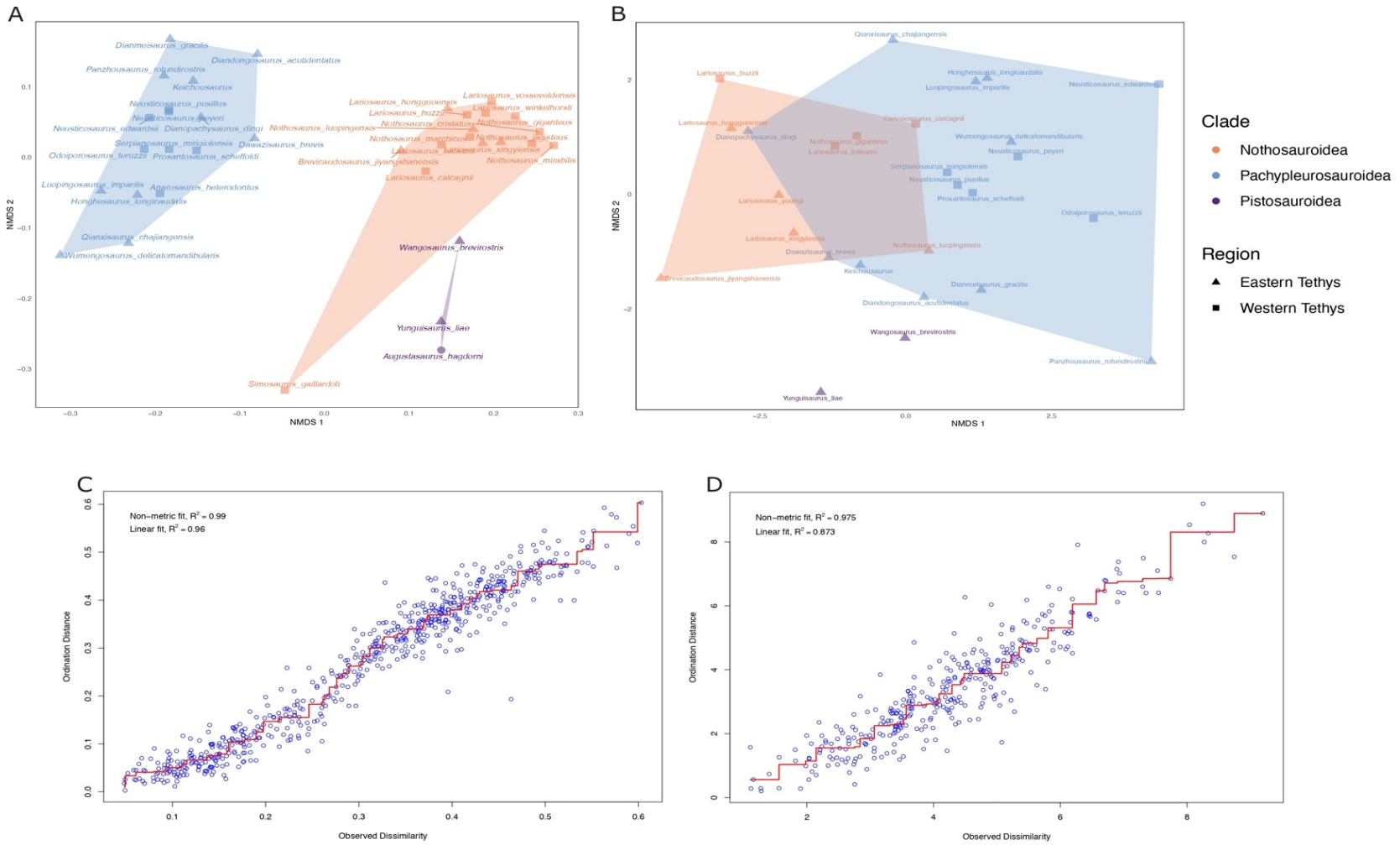

Figure S1.5. Eosauropterygian multivariate morphometric analyses. (A) craniodental and (B) postcranial NMDS (dimension =2). Non-metric fit of two-dimensional NMDS on the original dissimilarities for (C) craniodental and the (D) postcranial datasets respectively.

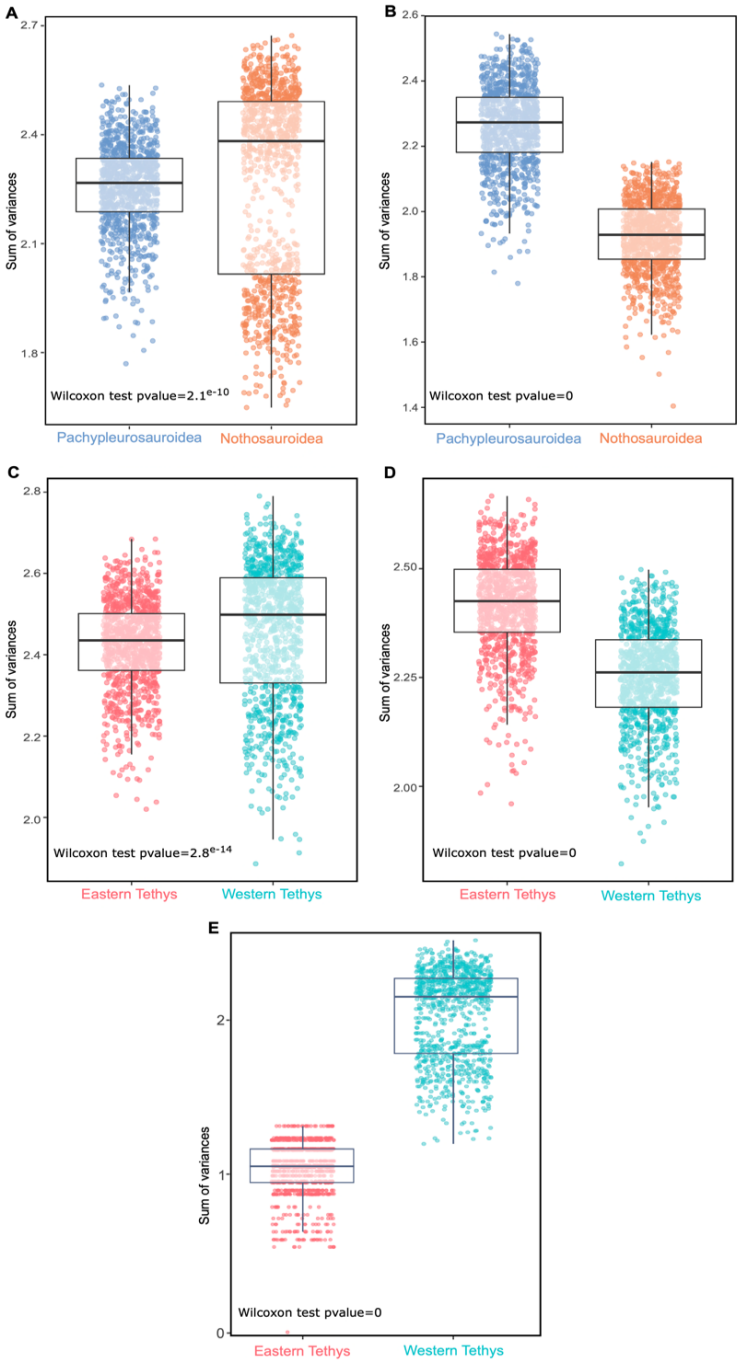

Figure S1.6. Whole body disparity distribution (sum of ranges) generated by using 1000 bootstrap replications. Comparison between (A) Pachypleurosauroidea and Nothosauroidea and (B) when *Simosaurus gaillardoti* is removed from Nothosauroidea. Regional comparison between (C) Eastern and Western Tethys and (D) when *S. gaillardoti* is removed. (E) Regional comparison among nothosaurdoids when *S. gaillardoti* is removed.

CHAPTER 2: IMPACT OF LATE TRIASSIC EVENTS ON THE MORPHOLOGICAL DIVERSIFICATION OF EOSAUROPTERYGIANS AND ICHTHYOSAURIANS

Laboury, A., T. L. Stubbs, A. S. Wolniewicz, J. Liu, T. M. Scheyer, M. E. H. Jones, and V. Fischer. 2024. Contrasting macroevolutionary patterns in pelagic tetrapods across the Triassic–Jurassic transition. Evolution DOI: 10.1093/evolut/qpae138

Abstract

The iconic marine raptorial predators Ichthyosauria and Eosauropterygia co-existed in the same ecosystems throughout most of the Mesozoic Era, facing similar evolutionary pressures and environmental upheavals. Both lineages seemingly went through a massive macroevolutionary bottleneck across the Triassic–Jurassic (T/J) transition that greatly reduced their morphological diversity, leaving pelagic lineages as the only survivors. However, analyses of marine reptile disparity across the T/J transition have usually employed phylogenetic or coarse morphological and temporal data. We comprehensively compare the evolution of ichthyosaurian and eosauropterygian morphology, as well as body size across the Middle Triassic to Early Jurassic interval and find contrasting macroevolutionary patterns. The ecomorphospace of eosauropterygians predominantly reflects a strong phylogenetic signal, resulting in the clustering of three clades with clearly distinct craniodental phenotypes, suggesting ‘leaps’ towards novel feeding ecologies. Ichthyosaurian diversification lacks a discernible evolutionary trend, as we find evidence for a wide overlap of craniodental morphologies between Triassic and Early Jurassic forms. The temporal evolution of ecomorphological disparity, fin shape and body size of eosauropterygians and ichthyosaurians during the Late Triassic does not support the hypothesis of an abrupt macroevolutionary bottleneck at or near the T/J transition. Rather, an important turnover event should be sought earlier, during times of rapid sea level falls.

Authors' contributions: AL, VF, TLS, and TMS conceived and designed the study. AL, ASW, JL, and MEHJ. collected the data. AL performed the analyses, wrote the code with inputs from VF and TLS, prepared all figures and tables and wrote the draft of the manuscript, with contributions of all authors.

INTRODUCTION

During the Mesozoic, reptiles notably occupied upper trophic levels in the marine realm for more than 180 million years(Motani 2009; Bardet et al. 2014). Several independent lineages rapidly invaded the seas in the aftermath of the catastrophic end-Permian mass extinction, experiencing an 'early-burst' radiation that led to the exploration of vacant or novel ecological guilds in shallow-marine environments (Benton et al. 2013; Stubbs and Benton 2016; Cheng et al. 2019; Huang et al. 2020; Moon and Stubbs 2020; Reeves et al. 2021; Qiao et al. 2022). These radiations resulted in a wide range of body sizes, swimming adaptations, and feeding specializations (Liu et al. 2014; Stubbs and Benton 2016; Sander et al. 2021; Gutarra et al. 2023; Laboury et al. 2023). Among these reptile lineages, Eosauropterygia (including the speciose post-Triassic plesiosaurians), and Ichthyosauria (the 'fish-shaped' reptiles) became the most successful and longest-lived clades of raptorial predators of the Mesozoic (Motani 2009; Bardet et al. 2014). These animals evolved into very distinctive body plans due to strong differences in their craniodental architecture and locomotion style. Indeed, eosauropterygians were paraxial swimmers (*e.g.*, the underwater flying plesiosaurians), characterized by repeated variations in neck length (O'Keefe 2002; Soul and Benson 2017), while the fusiform ichthyosaurians adopted a tail-propelled swimming mode (Motani 2009; Gutarra and Rahman 2021; Krahl 2021). Often sympatrically distributed (Motani 2009; Bardet et al. 2014), they were affected by the same environmental and ecological pressures, making them a meaningful example for evolutionary comparison. The morphological diversity of both clades peaked during the Middle and early Late Triassic due to the presence of many forms that were adapted to coastal environments. However, many of these coastal forms disappeared by the end of the Triassic and their niches were never re-occupied during the subsequent radiations of these two clades (Dick and Maxwell 2015; Stubbs and Benton 2016; Moon and Stubbs 2020; Reeves et al. 2021).

Indeed, the second half of the Triassic represents a key period in the history of the Mesozoic marine ecosystems, marked by rapid sea level changes that likely drove nearshore marine tetrapods to extinction (Bardet 1994; Benson and Butler 2011; Kelley et al. 2014). This ultimately left only pelagic lineages to survived and to diversify throughout the rest of the Mesozoic: Plesiosauria within eosauropterygians and Parvipelvia within ichthyosaurians (Benson et al. 2010, 2012; Thorne et al. 2011; Dick and Maxwell 2015). These extinctions are thought to represent a macroevolutionary bottleneck at the T/J transition (Thorne et al. 2011; Dick and Maxwell 2015), because the

disparity of speciose assemblages recorded at the start of the Jurassic is generally considered to be very small in comparison to their Triassic predecessors (Thorne et al. 2011; Benson et al. 2012; Stubbs and Benton 2016; Moon and Stubbs 2020; Reeves et al. 2021). Yet, most studies suggesting the existence of a bottleneck in marine reptile disparity were either based on phylogenetic characters (Thorne et al. 2011; Moon and Stubbs 2020) or investigated marine reptile diversification dynamics on a broad scale (Dick and Maxwell 2015; Stubbs and Benton 2016; Reeves et al. 2021; Gutarra et al. 2023), potentially confounding different temporally or phylogenetically isolated events. Here, we reinvestigate the end-Triassic macroevolutionary bottleneck hypothesis by comprehensively analysing the evolution of eosauropterygians and ichthyosaurians in terms of ecomorphospace occupation, fluctuation of disparity and evolution of fin shape, and body size.

MATERIAL AND METHODS

Taxonomic and morphological sampling

We gathered a series of functionally important continuous traits for a total of 326 specimens of ichthyosaurians and eosauropterygians, ranging from Middle Triassic to the end of the Early Jurassic (see supplements for chapter 2; **Figures S2.1 and S2.2**). Some functional traits are unique to one clade (*e.g.* the relative overbite length, which can greatly vary in ichthyosaurians, but not in eosauropterygians), difficult to measure depending on the state of preservation (*e.g.* crown curvature in ichthyosaurians, as most of their teeth are labio-lingually oriented and thus hardly measurable in teeth preserved *in situ*) or were not well preserved (*e.g.* sclerotic ring in eosauropterygians). As a result, we always analysed trends for both groups separately (214 eosauropterygian and 112 ichthyosaurian specimens, representing 51 and 32 species respectively). Morphological data were collected through first-hand observation of specimens, and measurements on high precision three-dimensional surface scans using MeshLab v2023.12 (Cignoni et al. 2008). When no other alternatives were available, we populated our datasets by taking measurements from first-hand photographs and figured specimens from the literature by using ImageJ (v.1.53) (Schneider et al. 2012), as well as by using published measurements (see supplements for chapter 2, **Tables S2.1–2.2** and **Tables S1.4–1.5**) for the full taxonomic sampling including all the studied specimens, the ages of taxa and the sources of the data). Measurements were used to generate 31 dimensionless ratios (with

only 29 applicable for eosauropterygians; see supplements for chapter 2), which have clear craniodental and postcranial morphofunctional implications (Stubbs and Benton 2016; Fischer et al. 2020; MacLaren et al. 2022; Laboury et al. 2023). The apicobasal height of the tooth crown, a proxy determining the range of possible prey items (Fischer et al. 2022a), represents the only absolute trait in both ichthyosaurian and eosauropterygian datasets. Finally, we also incorporated six binary discrete traits reflecting mandible and tooth morphologies. Therefore, in total we used 35 for eosauropterygians and 37 traits for ichthyosaurians. We applied a completeness threshold of 40% to each taxa by calculating the percentage of non-missing data for both the craniodental and postcranial regions as well as for the whole body architecture (craniodental and postcranial regions combined) for each group. This procedure serves to remove incomplete taxa (those with less than 40% of data for the corresponding morphological region) and thus minimizes the risk of distortions to our morphospace. However, it also leads to the removal of important but partially known Late Triassic taxa (*e.g. Paludidraco* or *Rhaeticosaurus* for eosauropterygians and *Californosaurus, Hudsonelpidia, Shonisaurus, Shastasaurus* for ichthyosaurians). Nevertheless, even if these taxa could not be integrated into our morphospace and disparity analyses, they are included within the body size and fin shape analyses (**Tables S2.1–2.6**). We also temper our interpretations of the results in the light of the absence of these taxa.

Phylogenetic data

We analysed the phylogenetic relationships of eosauropterygians and ichthyosaurians in order to generate phylomorphospaces and phenograms. To date, no cladistic matrices or analyses have thoroughly investigated the phylogenetic relationships of all eosauropterygians (both non-plesiosaurians and plesiosaurians) together. Therefore, we created a composite phylogenetic tree by combining topologies generated separately for Triassic eosauropterygians and for Early Jurassic plesiosaurians. Recent studies have recovered two main topologies for Triassic taxa: one where nothosauroids are either closely related to pachypleurosauroids (Hu et al. 2024) and another where they are more closely related to the pistosauroids (Xu et al. 2022). To test the influence of these conflicting topologies on our disparity and ordination analyses, we used datasets from both Hu et al. (2024) and Xu et al. (2022) and grafted their respective Triassic eosauropterygian topologies onto phylogenetic trees generated for the Early Jurassic with the dataset of Wintrich et al. (2017). Results from the composite tree using the Triassic dataset of Hu et al. (2024) are discussed in the main text, whereas results involving the Triassic dataset of Xu et al. (2022) are very similar and are available on the supplementary

information published on https://doi.org/10.1093/evolut/qpae138 (see supplements for chapter 2 for more information).

For ichthyosaurians, we used the character–taxon matrix of Laboury et al. (2022), deriving from the original dataset of Moon (2017), which appears to be most suitable for our analyses. The recent dataset of Bindellini et al. (2021), which comprehensively reinvestigated the phylogenetic relationships of Triassic ichthyosaurians appears to be an appropriate alternative but was not used as it does not incorporate most of the Early Jurassic taxa present in our ecomorphological dataset. We modified our cladistic matrix by incorporating revised scores for *Cymbospondylus nicholllsi* and *Cymbospondylus petrinus* from Klein et al. (2020) and adding *Cymbospondylus duelferi* as well as *Cymbospondylus youngorum* based on the scoring of Klein et al. (2020) and Sander et al. (2021).

All phylogenetic analyses were performed in TNT (v1.6) (Goloboff and Morales 2023) using an implied weighting maximum parsimony framework to reduce the impact of homoplasy and with a concavity constant *k* of 12. In each cladistic datasets, multi-states characters were unordered. The number of trees was set to 100,000 and we used the New Technology Search (ratchet activated: 200 iterations; drift activated: 10 cycles; 5 hits and 10 trees per replication) followed by a tree bisection-reconnection (TBR) algorithm (trees can be seen in supplements for chapter 2, **Figures S2.3–S2.6);** a single most parsimonious tree was then randomly selected for subsequent analyses. Since the cladistic datasets used do not include all eosauropterygian and ichthyosaurian specimens sampled in our ecomorphological datasets, we grafted missing taxa on trees using the *phytools* (v2.0-3) and *paleotree* (v3.4.5) packages (Bapst, 2012; Revell, 2012) in the R statistical environment (v4.2.3) (R Core Team, 2023). For eosauropterygians, we manually added Triassic taxa missing from the phylogenetic matrices of Hu et al. (2024) and Xu et al. (2022), as in Laboury et al. (2023) (**Chapter 1**) (see supplements for Chapter 2; Supplementary methods section). Furthermore, we also added *Microcleidus melusinae* to the phylogenetic tree generated for plesiosaurians, as the most basal member of *Microcleidus* (Vincent et al. 2017). For ichthyosaurians, the synonymy of *Temnodontosaurus platyodon* and the smaller *'Temnodontosaurus risor'* (McGowan 1994b) has been recently questioned due to numerous morphological differences (Bennion et al. 2024) and we therefore decided to separate these two taxa by adding *'T. risor'* as the sister taxon of *T. platyodon*.

To ensure consistent results, our composite eosauropterygian and ichthyosaurian trees were timescaled using the Hedman algorithm (**Figures S2.4 and S2.7**) — which constraints the age of a clade based on the ages of consecutive older groups that act as the clade outgroup (Hedman 2010; Lloyd et al. 2016) — and the minimum branch length (MBL) approach (**Figures S2.5 and S2.8**) (Bapst 2012). All analyses presented in the results section are based on trees timescaled with the Hedman method. Other results are presented in the https://doi.org/10.1093/evolut/qpae138.

Ordination methods and temporal disparity analyses.

All analyses were conducted in the R statistical environment (v4.2.3) (R Core Team 2023). We analysed eosauropterygians and ichthyosaurians separately, and we also separated skeletal regions (craniodental and postcranial). Continuous traits of all morphological datasets were z-transformed, and these datasets were used to generate a distance matrix by using Gower (for datasets containing continuous and discrete traits) (Gower 1971) or Euclidean (for datasets containing only continuous traits) distances. We generated morphospaces using non-multidimensional scaling (NMDS, dimension=2) with the *vegan* package (v.2.6-4) (Oksanen et al. 2022) and principal coordinate analysis (PCoA) with Caillez correction for negative eigenvalues, using the *ape* package (v.5.7-1) (Paradis et al. 2004). In order to test the influence of phylogeny on the clustering of taxa in our ordination analyses, we computed Mantel tests by using the *vegan* package (v.2.6-4) (Oksanen et al. 2022) based on tanglegrams (**Figures S2.11 and S2.12**) generated with our timescaled phylogenetic trees and cluster dendrograms (see detailed description of these analyses in supplements for chapter 2; Supplementary methods section). To compare the amount of disparity between different key time periods, we computed morphofunctional disparity for the following time bins: Anisian–Ladinian (Middle Triassic); Carnian–Norian (Late Triassic); Hettangian–Sinemurian (earliest Jurassic) and Pliensbachian–Toarcian (latest Early Jurassic). These bins have uneven temporal durations but were selected to ensure sufficient sampling. Because of the very limited amount of data available for the Rhaetian — no well-preserved and complete specimens have been found from this stage (Storrs 1994; Fischer et al. 2014b; Wintrich et al. 2017; Lomax et al. 2018a, 2024; Sander et al. 2022) — it was excluded from our analyses. Nevertheless, the scarcity of its fossil record was considered when discussing our results. The significance of both taxonomical group and temporal differences across morphospace axes was tested by using nonparametric multivariate analyses of variance (NPMANOVA). The p-values resulting from the pairwise comparisons (**Tables 3, S2.7 and S2.8**) were corrected using the Benjamini–Hochberg adjustment for controlling the false

discovery rate, which is the expected proportion of falsely rejected hypotheses (Benjamini and Hochberg 1995). We generated phylomorphospaces superimposed on the density of taxon occupation by using the modified *ggphylomorphospace* function provided in Fischer et al. (2020). We used all axes of the PCoAs to compute the bootstrapped disparity (1,000 replications for bootstraps iterations, sum of variances) for each time bin using the *dispRity* package (v.1.7.0) (Guillerme 2018). We primarily focus on presenting and discussing the craniodental results in the main text, but all other tables and morphospaces can be found in the supplements for chapter 2**.**

To address issues associated with under-sampled time intervals such as the late Norian and Rhaetian and the uneven length of time bins, we used a 'time-slicing' approach to sample ghost lineages, estimate ancestors values and compute disparity-through-time (Guillerme and Cooper 2018). For ichthyosaurians, we randomly selected a timescaled tree in which ancestral character states were estimated with a likelihood of ≥0.95 for each node by using the *claddis* package (v.0.6.6) (Lloyd 2016). This method uses cladistic data to compute disparity, which, although not ideal, allows for better sampling during the latest Triassic. This was our main goal in this analysis, as it incorporates partially known taxa that could not be added to our ecomorphological dataset (see the Taxonomic and morphological sampling section for ichthyosaurian examples). Reconstructed ancestral character states could not be estimated for eosauropterygians as we used a composite phylogenetic tree arising from different cladistic matrices. Therefore, we extracted morphospace coordinate positions of ancestral nodes and tips from the phylomorphospace generated with all ecomorphological data. For both eosauropterygians and ichthyosaurians, time-sliced sum of variance disparity was calculated through time at ten equidistant intervals and bootstrapped (1,000 iterations for replications). This procedure ensures sufficient taxon sample size for each interval and reliable comparisons, not biased by the unequal duration of the different stages. We adopted the gradual splits model of evolution, which selects, for a given branch, the ordination score from the ancestral node or the descendant with a probability function defined by the distance along the branch where the time slice samples this latter (Guillerme and Cooper 2018). Other models, such as proximity and equal splits, were also tested and are detailed in supplements for chapter 2 (**Figures S2.19 and S2.21**).

Limb architecture and body size

Brachial and crural indexes were determined by calculating the length of the zeugopodial bones (radius and tibia) relative to that of their corresponding propodial bones (humerus

and femur). They represent therefore the outlever/inlever ratio of the fore- and the hindlimb (Caldwell 2002; Gutarra et al. 2023). Lower values reflect a higher degree of adaptation to aquatic environments, as pelagic taxa are characterized by a relative shortening of the epipodial bones (Gutarra et al. 2023). We used our previously generated timescaled phylogenies (see above) to infer the ancestral node values in a maximum likelihood framework using the *phytools* (v.2.0-3) package (Revell, 2012) and to generate brachial and crural phenograms for eosauropterygians and ichthyosaurians.

Dimensions of dorsal vertebrae have often been used to estimate the overall body size of aquatic tetrapods when highly incomplete specimens or isolated centra are found in the fossil record (Romer and Price 1940; Currie 1978; Sennikov and Arkhangelsky 2010; Fischer et al. 2014b; Li and Liu 2020; Sander et al. 2022). To investigate the evolution of body size from the Late Triassic to the Early Jurassic, we gathered a dataset of dorsal vertebra height based on articulated specimens as well as numerous isolated vertebrae of ichthyosaurians and eosauropterygians mentioned in the literature (**Tables S2.3 and S2.6**).

RESULTS

Morphospace occupation and convergence

For the principal coordinate analysis (PCoA) of eosauropterygian and ichthyosaurian craniodental characters, the combination of the first two axes captures 28.71% and 32.65% of the total variance respectively. Eosauropterygians are placed in three distinct clusters (**Figure 16A** but see also **Table S2.7**) mainly reflecting phylogenetic affinities (Mantel test: p-value= 0.003) as in Laboury et al. (2023) (Chapter 1). The first cluster comprises all pachypleurosauroids, the second comprises the nothosauroids + *Wangosaurus* — the nothosauroid-like pistosauroid (Ma et al. 2015; Laboury et al. 2023) — and finally, the third consists of all pistosauroids (Triassic and post-Triassic taxa, with the exception of *Wangosaurus*). The pachypleurosauroids plot with negative axis 1 values whereas the two other clusters plot with positive values. Furthermore, nothosauroids plot with axis 2 negative values while most pistosauroids plot with positive values. Within these latter, rhomaleosaurids also occupy a distinct region and appear more diversified than the other plesiosaurians. The temporal distribution of taxa highlights a drastic change and significant reduction in the eosauropterygian ecomorphospace occupation

across the T/J transition (**Figure 16C** and **Table 3**), as both nothosauroids and pachypleurosauroids are solely found in the Triassic. A similar pattern is also observed when analysing postcranial data (**Figure S2.14B**). Nevertheless, the Triassic pistosauroids *Augustasaurus hagdorni* and *Yunguisaurus liae* are nested within a region of high occupational density, along with basal plesiosaurians (**Figure 16A and C**). This representation of morphological traits indicates that the 'typical' plesiosaurian cranial morphology, not just body shape, already appeared in Middle Triassic pistosauroids.

The pattern of ichthyosaurian ecomorphospace contrasts with that of eosauropterygians (**Figure 16B and D**, but see also supplementary material: **Table S2.8**). A clear distribution of the phylogenetic structure (Mantel test: p-value = 0.48) or temporal groups is not recovered, as species from different groups are widely spread across ecomorphospace. Most notably, Early Jurassic species occupy a broad area of the ecomorphospace, in contrast to the coeval plesiosaurians. Similarly, our statistical tests do not detect significant disparity shifts in ecomorphospace occupation between our time intervals (**Table 3**), including across the Triassic-Jurassic transition. Some phylogenetically and temporally distant ichthyosaurians occupy close positions in morphospace (**Figures 1B and 1D**), highlighting a recurrence of craniodental morphotypes throughout the Middle Triassic to Early Jurassic. Significant convergence is identified between the Triassic merriamosaurian *Qianichthyosaurus zhoui* and the small early Jurassic parvipelvian *Leptonectes moorei* no matter the number of axes or the methodology used (*i.e* Ct measures or method Castiglione et al. [2019] method) (**Tables S2.9 and 2.10**). The morphological resemblance between the large Triassic and Early Jurassic hypercarnivorous taxa (*Cymbospondylus youngorum* and *Temnodontosaurus eurycephalus*) is present but ambiguous, with only some metrics indicating convergence (**Tables S2.9 and 2.10**). Significant results between the Middle Triassic ichthyosaurian *Mixosaurus cornalianus* and the Early Jurassic thunnosaurian *Hauffiopteryx typicus* are recovered when considering the first two axes of variation but not when considering the first five and all axes of the PCoA or the Castiglione et al. (2019) method. Their proximity in the morphospace based on the first and second axes of the PCoA, along with the lack of significant statistical results when analysing convergence, rather reflects superficial similarities in their craniodental architecture than true morphological convergence. In ichthyosaurians, the pattern in postcranial morphological data contrast with that generated from the craniodental traits, and rather follow a similar trend to that of eosauropterygians, with a clear distinction visible between Triassic and Jurassic taxa and no evident overlap in ecomorphospace occupation (**Figure S2.16B**).

Temporal trends of disparity

Both eosauropterygians and ichthyosaurians peaked in ecomorphological disparity during the Middle Triassic (**Figures 17A and B**). Our more precise time-sliced analyses indicate that ichthyosaurians maintained a high level of disparity into the Carnian (early Late Triassic) (**Figure 17D**). During this period, Middle Triassic ichthyosaurian faunas experienced the replacement of mixosaurid– and cymbospondylid–dominated assemblages by the diversified early merriamosaurians (*i.e.* shastasaurids and early euichthyosaurians). Time-sliced analyses also suggest a significant decline in disparity in both clades during the first half of the Late Triassic, with this drop appearing even more severe in eosauropterygians (**Figures 17B and C**). This eosauropterygian reduction in disparity is mainly due to the disappearance of most non-plesiosaurian eosauropterygians; though this is likely exacerbated by the lack of well-articulated eosauropterygian specimens from Carnian and Norian strata. Indeed, morphologically disparate eosauropterygians, including pistosauroids (*e.g.* *Bobosaurus*), large nothosaurians ambush predators (*e.g.* *Nothosaurus giganteus*) but also durophagous and supposed filter-feeders (the simosaurid *Simosaurus* and *Paludidraco* respectively), are known from coastal environments of the early Carnian (Rieppel and Wild 1996; Dalla Vecchia 2006, 2008; Kear and Maxwell 2013; de Miguel Chaves et al. 2018b; García-Ávila et al. 2021). However, these taxa are not complete enough to be included in our ecomorphological analyses here. Their morphologies nevertheless suggest that the true disparity among the early Late Triassic eosauropterygians certainly is likely higher than what is recovered in our analyses (**Figure 17A**). As highlighted by Benson et al. (2012), even though subsequent eosauropterygian disparity gradually increases until the end of the Early Jurassic, early diverging plesiosaurians never achieved comparable levels of disparity to Middle Triassic eosauropterygians (**Figures 2A and C**). Ichthyosaurian disparity appears to progressively increase after the Norian, with the initial diversification of parvipelvians, and then reaches values comparable to those observed in the Carnian (**Figure 17D**). No dramatic disparity drop in disparity that could be identified as a macroevolutionary bottleneck at or close to the T/J transition is observed, neither for eosauropterygians nor for ichthyosaurians.

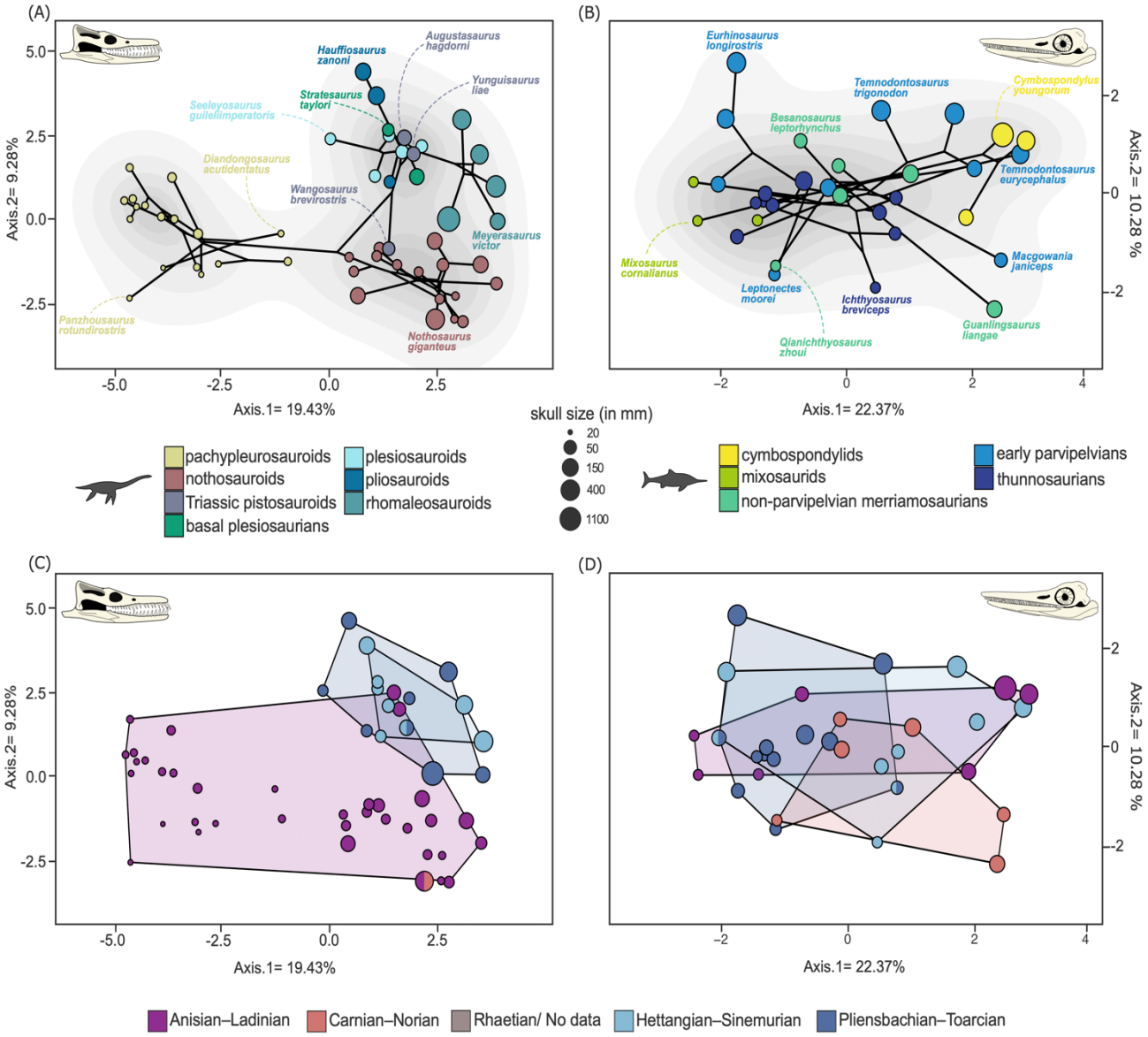

Figure 16. Eosauropterygian and ichthyosaurian phylo- and temporal craniodental ecomorphospace occupation based on the first two axes of PCoA analysis. Data points are coloured according to their taxonomic groups (A and B) or time bins (C and D) and their diameter is proportional to the skull size of the corresponding taxa. (A and B) Phylo-ecomorphospace occupation of (A) eosauropterygians and (B) ichthyosaurians, superimposed on the density of taxa visualized by the shades of grey (darker = higher density). (C and D) Temporal ecomorphospace occupation of (C) eosauropterygians and (D) ichthyosaurians. Polygons connect outlier taxa of each time bin.

Table 3. NPMANOVA results testing for the statistically significant temporal separation in the craniodental ecomorphospace occupation for ichthyosaurians and eosauropterygians. The four time bins chosen are Anisian–Ladinian; Carnian–Norian; Hettangian–Sinemurian and Pliensbachian–Toarcian. The NPMANOVA tests are based on the use of all axes of the PCoA generated with craniodental dataset. As the Carnian-Norian interval only contain one eosauropterygian taxon (*Nothosaurus giganteus*), NPMANOVA tests could not have been calculated for this time interval. P-values were corrected by using the Benjamini–Hochberg adjustment.

Time intervals	Clade	Group size	F test	R^2	p-value	Corrected p-value
Anisian–Ladinian VS Carnian–Norian	Ichthyosauria	7–6	1.00150	0.08345	0.34266	0.514
	Eosauropterygia	—	—	—	—	—
Anisian–Ladinian VS Hettangian–Sinemurian	Ichthyosauria	7–10	0.15422	0.01018	0.83417	0.834
	Eosauropterygia	36–7	2.96843	0.06751	0.00100	0.002
Anisian–Ladinian VS Pliensbachian–Toarcian	Ichthyosauria	7–11	1.11317	0.06505	0.32567	0.514
	Eosauropterygia	36–9	3.39705	0.07322	0.00100	0.0015
Carnian–Norian VS Hettangian–Sinemurian	Ichthyosauria	6–10	0.87294	0.05869	0.43057	0.517
	Eosauropterygia	—	—	—	—	—
Carnian–Norian VS Pliensbachian–Toarcian	Ichthyosauria	6–11	4.83311	0.24369	0.01299	0.0779
	Eosauropterygia	—	—	—	—	—
Hettangian–Sinemurian VS Pliensbachian–Toarcian	Ichthyosauria	11–10	2.86120	0.13088	0.07892	0.237
	Eosauropterygia	7–9	0.81948	0.05530	0.72228	0.722

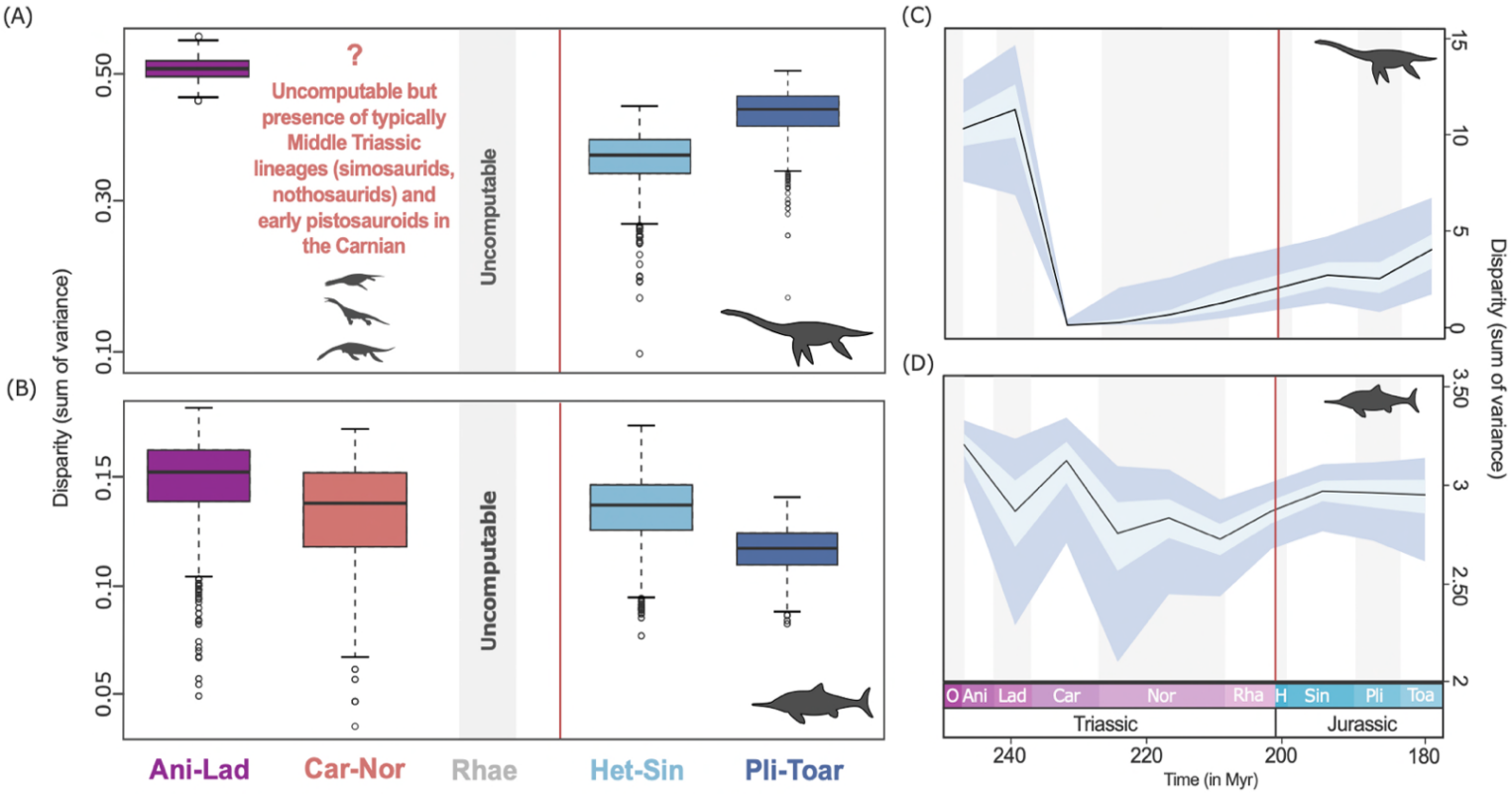

Figure 17. Temporal pattern of eosauropterygians and ichthyosaurians morphological disparity. (A and B) Disparity distributions (sum of variances metric and 1000 bootstraps replications) based on all axes of the PCoA calculated with all ecomorphological traits for our sampled time intervals for (A) eosauropterygians and (B) ichthyosaurians. The four temporal bins chosen are Ani–Lad (= Anisian–Ladinian); Car–Nor (= Carnian–Norian); Rhae (=Rhaetian); Het–Sin (= Hettangian–Sinemurian) and Pli–Toa (= Pliensbachian–Toarcian). (C and D) Evolution of time-sliced disparity (sum of variances metric and 1,000 bootstraps replications) through the Middle Triassic–Early Jurassic time interval based on (C) phylomorphospace occupation for eosauropterygians and on (D) our phylogenetic tree for ichthyosaurians (see Material and Methods, section Ordination methods and temporal disparity analyses, for more details). Light blue and blue envelopes represent respectively 95% and 50% confidence intervals. All phylogenetic trees used to calculate disparity or to compute the phylomorphospace were timescaled with the Hedman algorithm. In all graphs, red line indicates the Triassic-Jurassic transition.

Evolution of fin shape and body size

Rather than a stepwise evolutionary pattern, both the brachial and crural indexes (proxies for the degree of aquatic adaptation of the limbs) mapped across phylogeny reveal a drastic change in the relative size of zeugopods (radius/tibia) compared to stylopods (humerus/femur), during the first half of the Late Triassic, coinciding with the emergence of the 'underwater-flier' plesiosaurians and fusiform parvipelvians (**Figures 18 and 19**). Their much lower values on both indexes indicate a higher degree of adaptation to an open ocean lifestyle. Middle Triassic eosauropterygians are mostly clustered with high values for both the brachial and crural indexes (0.48–0.66 for the brachial index and 0.45–0.61 for the crural index), regardless of their phylogenetic affinities (**Figures 18A,C and 19A,C**). The pistosauroid *Yungisaurus liae,* considered to be a close relative of plesiosaurians, has the highest crural index value (0.61) and thus cannot be considered a morphological intermediate between Middle Triassic species and plesiosaurians in this context. Its relatively large tibia size seems to corroborate the inference of Gutarra et al. (2023) that the postcranial morphology of *Yungisaurus* is consistent with a more rowing locomotion, similar to nothosauroids. The lowest values among the sampled eosauropterygians we are those of the Rhaetian juvenile plesiosauroid *Rhaeticosaurus mertensi* highlighting a profound modification of limb shapes during the Late Triassic, at least in the preserved taxa.

A similar trend is also observed in ichthyosaurians. Large to gigantic ichthyosaurian taxa such as cymbospondylids and 'shastasaurids' (not monophyletic in our phylogenies), have brachial and crural index values within the same range as those of early ichthyosaurians, which were restricted to coastal environments (**Figures 18B,D and 19B,D**). However, these giant taxa are thought to have colonized the open ocean, considering their size and global distribution (Sander 1989a; Sander et al. 2011, 2021, 2022). Their index values likely indicate that these giants may have maintained an undulatory swimming mode, as suggested by their relatively high trunk proportions (Merriam 1908; Sander 1989a; Nicholls and Manabe 2004; Bindellini et al. 2021, 2024). Among the merriamosaurians that diversified during the Late Triassic, only euichthyosaurian *Callawayia neoscapularis* has a brachial index value and limb proportions comparable to that of parvipelvians (0.45) making it the only 'intermediate' between typically Triassic and Jurassic forms. Early Jurassic thunnosaurians such *Ichthyosaurus* and *Stenopterygius* have the lowest brachial and crural indexes of all in our sample. Their limb morphology thus reflects a substantial shift towards compact fins.

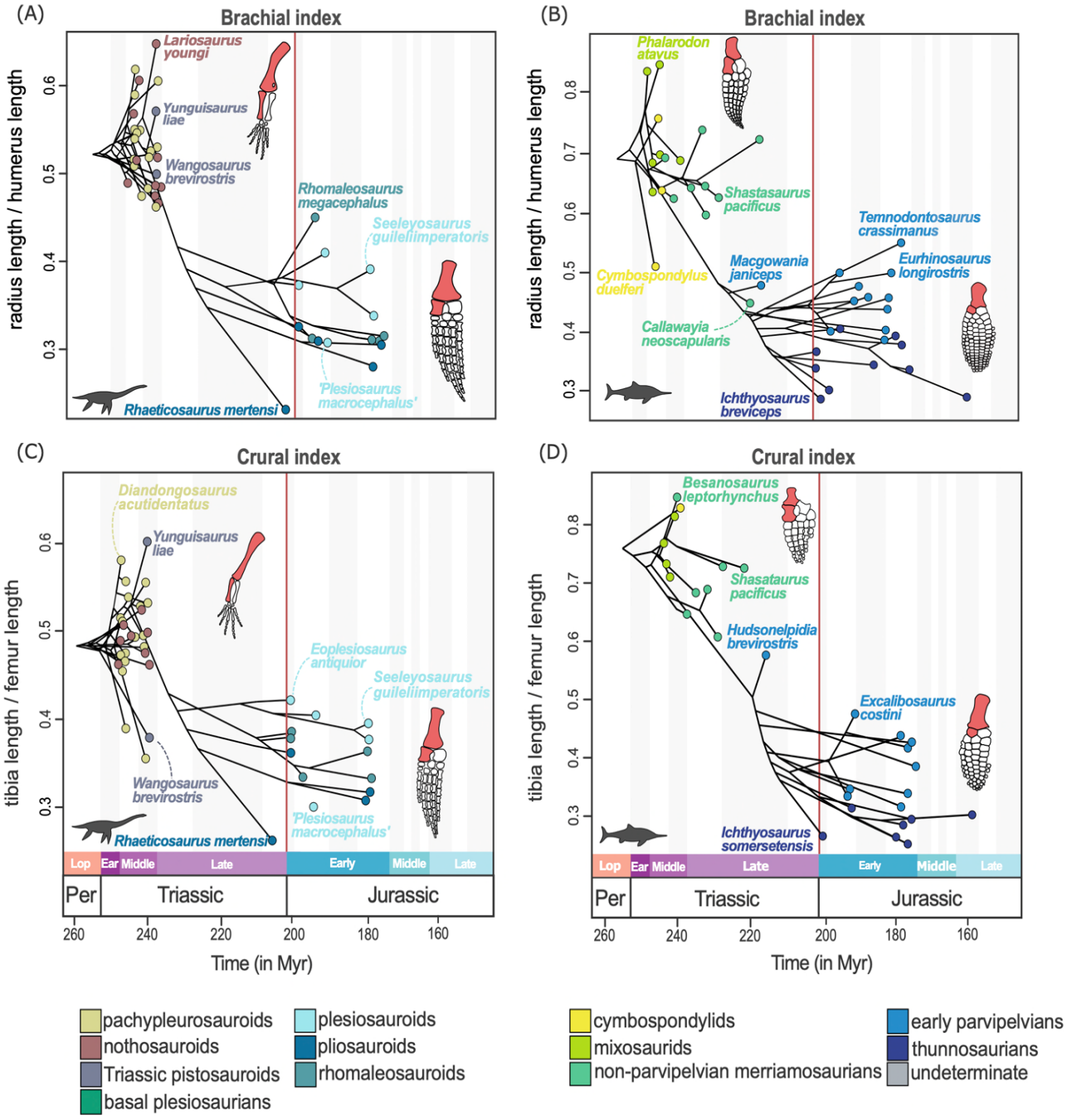

Figure 18. Pattern of fin shape evolution. Data points are coloured according to their taxonomic groups. (A and B) Brachial index phenograms for (A) eosauropterygians and (B) ichthyosaurians. (C and D) Crural index phenograms for (C) eosauropterygians and (D) ichthyosaurians. All phenograms were created with Hedman-dated corresponding phylogenetic trees. In all graphs, red line indicates the Triassic–Jurassic transition.

.

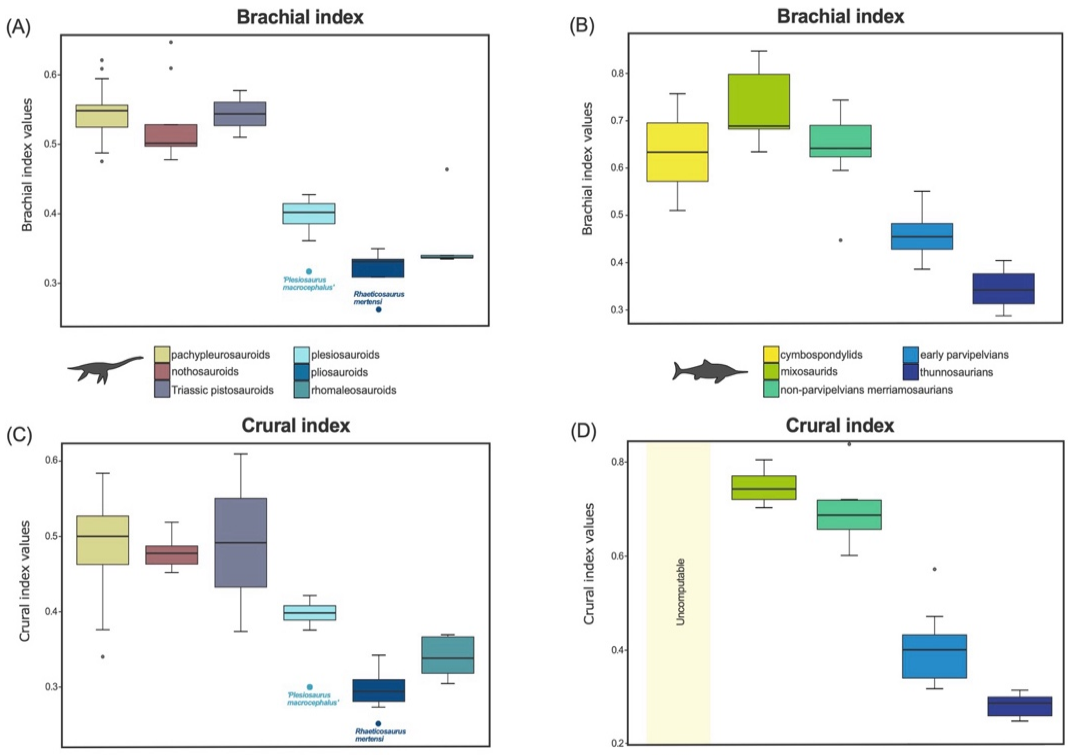

Figure 19. Distribution of brachial and crural index values. (A and B) Distribution of the brachial index values for (A) eosauropterygians and (B) ichthyosaurians. (C and D) Distribution of the crural index values for (C) eosauropterygians and (D) ichthyosaurians. In (D), as cymbospondylids contain only one taxon (*Xinminosaurus catactes*), distribution for this group could not have been computed.

Temporal fluctuations in dorsal centrum height, used here as a proxy for body size, also tend to reveal a different pattern in ichthyosaurians and eosauropterygians during the Late Triassic and Early Jurassic (**Figures 20A and B**). With the available material up to date, it seems that the T/J transition is associated with quite marked reduction in the size range for ichthyosaurians. This drop in maximal centrum size among ichthyosaurians is primarily due to the disappearance of the gigantic 'shastasaurids' during the end of the Triassic (Fischer et al. 2014b; Lomax et al. 2018a, 2024; Sander et al. 2022), while small and medium-sized forms persisted. The size range of the dorsal vertebrae of ichthyosaurians does not vary considerably during the Early Jurassic although some early parvipelvians such as *Temnodontosaurus* or *Eurhinosaurus* could have reached lengths greater than 5 m (McGowan and Motani 2003). Contrary to ichthyosaurians, centrum dimensions of eosauropterygians likely appear stable during the T/J transition even if more data in the latest Triassic would allow to better characterize their body size

evolution. In the Early Jurassic, the co-occurrence of large rhomaleosaurids with small early-diverging plesiosaurians results in a greater range of body sizes than in ichthyosaurians within the same time interval.

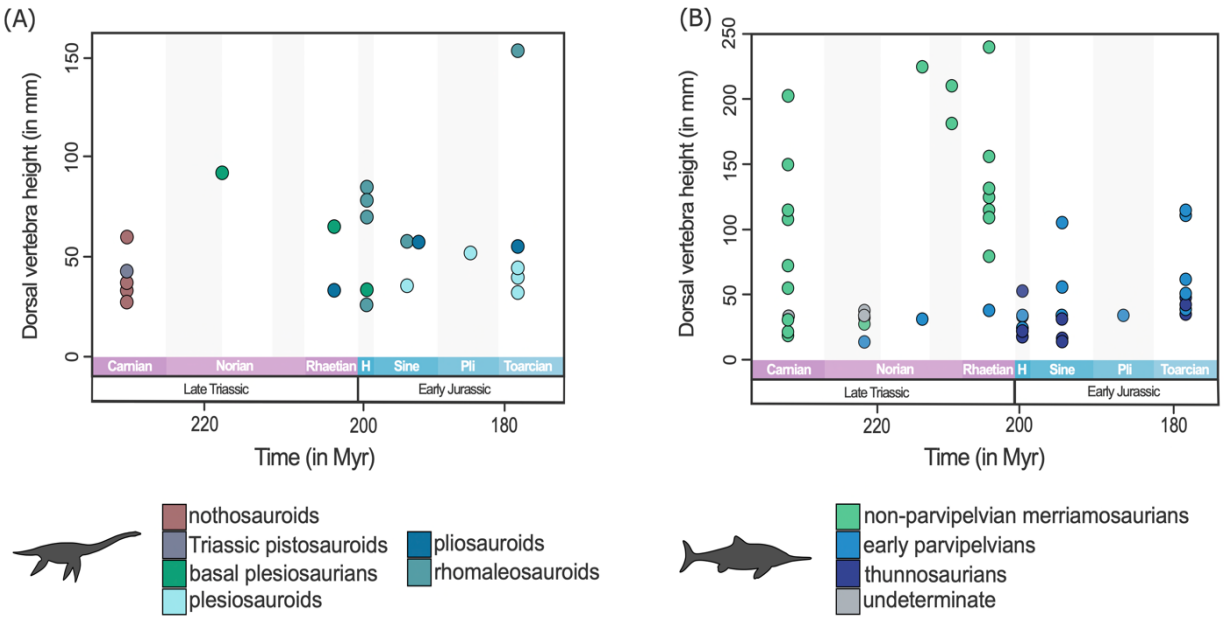

Figure 20. Pattern of the evolution of dorsal vertebrae dimensions. Data points are coloured according to their taxonomic groups. (A and B) Distribution of dorsal vertebrae height trough the Later Triassic–Early Jurassic time interval for (A) eosauropterygians and (B) ichthyosaurians.

DISCUSSION

Distinct evolutionary patterns in marine raptorial predators across the Triassic–Jurassic transition

Our analyses highlight contrasting patterns in the morphological diversification of ichthyosaurians and eosauropterygians during the Middle Triassic to Early Jurassic time interval. The craniodental diversification of eosauropterygians retains a significant underlying phylogenetic signal, as there is no overlap between the major clades (Pachypleurosauroidea, Nothosauroidea and Pistosauroidea). Indeed, each group retained distinct morphotypes, functional specializations, and exhibited niche conservatism relative to one another (Rieppel 2002; Laboury et al. 2023; Chapter 1). This pattern in eosauropterygians potentially indicates a stepwise colonization of novel

ecological niches — small suction feeders in Pachypleurosauroidea, moderate durophageous and taxa using their dentition as a fish trap in Nothosauroidea (*e.g.* see Rieppel 2002; Laboury et al. 2023; Chapter 1) — during the Triassic that were never re-explored after the extinction of Triassic taxa (Stubbs and Benton 2016; Reeves et al. 2021). Furthermore, our ecomorphospace analyses suggests that the development of the typical 'pistosaur/plesiosaur' cranial architecture would have remained relatively stable throughout the early evolutionary history of Pistosauria, with the exception of the peculiar rhomaleosaurids(Cruickshank 1994; Smith and Dyke 2008; Smith and Vincent 2010; Smith and Benson 2014).

Early Jurassic ichthyosaurians not only diversified into new morphotypes, notably hyperlongirostrine forms (McGowan 1986, 2003; Martin et al. 2012; Dick and Maxwell 2015), but also, in contrast to eosauropterygians, resembled and broadly overlapped with Middle to Late Triassic taxa. This overlap in morphospace reflects the iterative evolution of similar craniodental morphotypes repeatedly within Ichthyosauria over the Triassic–Jurassic transition, a pattern that is rarely detected (but see Stubbs and Benton 2016). This 'back-and-forth' pattern and the absence of a clear shift in craniodental anatomy between Triassic and Early Jurassic ichthyosaurians in our multivariate analyses markedly contrasts with the previous perception of a reduction in the range of skull phenotypes and a contraction in morphospace occupation after the Triassic (the 'bottleneck' hypothesis) (Thorne et al. 2011; Moon and Stubbs 2020; Reeves et al. 2021). However, this hypothesis stemmed from analyses based on cladistic characters or broad ecological categories in an ecospace modelling approach and may be oversimplified (Thorne et al. 2011; Moon and Stubbs 2020; Reeves et al. 2021). Our results also challenge the 'migration model' proposed by Dick and Maxwell (2015) which states that ichthyosaurians continuously abandoned previously occupied regions of ecospace or morphospace before colonizing new adaptative peaks. This model mainly arose through the use of a temporal character which essentially force a dissimilarity in the ecospace occupation between species from different time intervals and may be considered partially artificial. Dick and Maxwell (2015) argue that following the Middle/ Late Triassic transition, ichthyosaurians 'abandoned' circalittoral ecological niches in favour of open-ocean ones. However, while our analyses reveal major stepwise shifts in postcranial anatomy between coastal and pelagic taxa, these shifts are better explained by selective extinction of specific ecological niches due to sea regressions rather than the complete 'abandonment' of a morphospace region in place of another. Furthermore, because no clear migration in the craniodental ecomorphospace is evidenced over time, we believed

that this model should no longer be applicable to characterize the evolution of the cranium throughout T/J transition. Although some of the craniodental morphotypes re-appeared after the Triassic, ichthyosaurians never reached body sizes comparable to those of the colossal 'shastasaurids' after the Triassic (Moon and Stubbs 2020; Sander et al. 2021). Consequently, the Late Triassic extinction events still wiped out a unique aspect of Triassic disparity: whale-sized marine reptiles. Our different interpretation of the ichthyosaurian craniodental evolution from the 'bottleneck hypothesis' as well as the 'migration model' highlights that using of different type of data can produce contrasting macroevolutionary results (Anderson and Friedman 2012).

Did a macroevolutionary bottleneck in the latest Triassic influence the evolution of pelagic tetrapods?

The perception of a massive macroevolutionary bottleneck reshaping marine reptile assemblages at the end of the Triassic has been commonly accepted over the past decade (Thorne et al. 2011; Dick and Maxwell 2015; Moon and Stubbs 2020; Reeves et al. 2021). Several studies identifying this significant reduction in disparity relied on different data types, such as cladistic matrices (Thorne et al. 2011; Moon and Stubbs 2020), and general ecological characters designed for ecospace modelling (Dick and Maxwell 2015; Reeves et al. 2021). In these studies, data were binned at the Epoch-level (Thorne et al. 2011; Dick and Maxwell 2015; Moon and Stubbs 2020) despite marked differences in stage durations during the Late Triassic (Sander et al. 2022). Our findings suggest a different interpretation of the impacts of the end-Triassic extinction events, notably for the better sampled ichthyosaurians. Considering the data available for the latest Triassic, we propose here a two-phase extinction event for non-parvipelvians, rather than a single dramatic 'bottleneck' event at the end of the Triassic (Thorne et al. 2011). A similar scenario depicting two distinct extinction events affecting global marine diversity during the Late Triassic was previously proposed by Benton (1986). Based on the results of the present study and on previous work (Bardet 1994; Benson and Butler 2011; Kelley et al. 2014; Stubbs and Benton 2016), we clearly identify the first extinction phase that occurred in the early Late Triassic, leading to the disappearance of nearly all coastal forms (Bardet 1994; Benson and Butler 2011; Kelley et al. 2014). Extinctions in shallow water environments likely coincided with rapid sea-level fluctuations and a major regression event which greatly reshaped the structure of marine ecosystems and resulted in the loss of a large proportion of marine reptiles adapted to nearshore environments (Bardet 1994; Benson and Butler 2011; Kelley et al. 2014). This extinction event is indeed marked by both a reduction in disparity and slowing-down of rates of

morphological evolution among ichthyosaurians (Stubbs and Benton 2016; Moon and Stubbs 2020) (Moon & Stubbs, 2020; Stubbs & Benton, 2016), as only pelagic merriamosaurians are thought to have survived these events.

Carnian and Norian assemblages, also referred as ‘transitional ichthyosaur faunas’, exhibit significant similarities and are characterized by the dominance of colossal ‘shastasaurids’ alongside smaller merriamosaurians and early diverging parvipelvians (Merriam 1908; McGowan 1994a, 1995, 1996a, 1997; Nicholls and Manabe 2004; Kelley et al. 2022; Zverkov et al. 2022). The emergence of parvipelvians in the Norian is associated with appearance of significant modifications in fin shapes (McGowan 1995, 1996a). Although some remains of gigantic ‘shastasaurids’ have been found in the earliest Jurassic (Martin et al. 2015) — suggesting a more complex scenario — the disappearance of the vast majority of these giants by the end the Rhaetian (Fischer et al. 2014b; Lomax et al. 2018b, 2024; Sander et al. 2022) would represent the second phase in the extinction of Triassic ichthyosaurians. As mentioned by Fischer et al. (2014), it remains uncertain whether these shastasaurids suffered from diffuse extinctions since the Norian or restricted to the end of the Rhaetian. Nevertheless, these extinctions resulted in a profound turnover that led to the dominance of parvipelvians, mainly in Europe (Motani 2009; Benson et al. 2010; Bardet et al. 2014). Considering that the divergence of the major parvipelvians lineages likely occurred during the Late Triassic combined with their high diversity and disparity recorded at the base of the Jurassic (Fischer et al. 2013; Motani et al. 2017; Bindellini et al. 2021; Laboury et al. 2022), we speculate that pelagic parvipelvians diversified before (and therefore crossed) the T/J transition. This again contrasts with a macroevolutionary ‘bottleneck’ proposed at the very end of the Triassic. However, the poor sampling of marine reptile fossils from the latest Triassic (Bardet et al. 2014; Fischer et al. 2014b; Sander et al. 2022) obscures evidence of any substantial parvipelvian diversification before the Early Jurassic.

Despite the paucity of the Late Triassic eosauropterygians in the fossil record, evidence for a significant extinction event several million years before the latest Triassic is consistently emerging. Indeed, the end of the Middle Triassic and the early Carnian (~237–233.5 Ma; Julian substage) also correspond to the final extinction taxa more adapted to nearshore environments such as the last pachypleurosauroids, nothosauroids and early pistosauroids (Rieppel and Wild 1996; Dalla Vecchia 2006, 2008; de Miguel Chaves et al. 2018b; García-Ávila et al. 2021), likely leading to a drastic loss of both taxonomical and ecomorphological diversity. Subsequently, more advanced pistosauroids and/or plesiosaurians possibly emerged during the early to middle Norian

(Sennikov & Arkhangelsky, 2010) or at least during the Rhaetian (Wintrich et al. 2017). As observed in ichthyosaurians, the morphological resemblance of certain Late Triassic remains to Jurassic taxa (Storrs 1994; Fischer et al. 2014b) and the high diversity of plesiosaurians right at the start of the Jurassic also suggest an earlier diversification during the Late Triassic (Benson et al. 2012; Wintrich et al. 2017).

While it is clear that Carnian–Norian and earliest Jurassic marine reptile faunas are completely dissimilar (Rieppel and Wild 1996; McGowan and Motani 2003; Nicholls and Manabe 2004; Benson et al. 2012; Benton et al. 2013; de Miguel Chaves et al. 2018b; Zverkov et al. 2022; Reolid et al. 2024), the widespread narrative of a catastrophic loss of taxic and morphological diversity among marine reptiles at the end of the Triassic (Thorne et al. 2011; Dick and Maxwell 2015; Moon and Stubbs 2020) is difficult to reconcile with our results and those of other studies (Bardet 1994; Ketchum and Benson 2010; Benson and Butler 2011; Benson et al. 2012; Kelley et al. 2014; Wintrich et al. 2017). A shift in morphospace occupation and fin shape is observed earlier, during the first half of the Late Triassic and the limited fossil sampling from the Late Triassic–Early Jurassic interval rather suggests relative stability of ichthyosaurian and pistosauroid phenotypes.

Most extinction events appears to predate and are thus supposedly distinct from the Triassic–Jurassic transition volcanism and anoxia (Tanner et al. 2004; Whiteside et al. 2010; Blackburn et al. 2013; Ruhl et al. 2020; Bond et al. 2023). However, the end of the Triassic still unambiguously concentrates the final extinction of the last known placodont sauropterygians (Pinna and Mazin 1993; Neenan and Scheyer 2014), thalattosaurs (Renesto and Tintori 1995; Bastiaans 2024 and references therein) and potentially saurosphargids (Scheyer et al. 2022) as well. Our study highlights diverse, clade-specific responses to multiple, previously conflated Late Triassic events. Nevertheless, caution is still needed in our interpretations, as the scarcity of the latest Triassic fossil record oversimplifies what were likely more complex events. Significant shifts in sedimentary regimes and environmental conditions during the Late Triassic have resulted in a marine fossil record that is temporally uneven (Benson and Butler 2011; Dunhill et al. 2014; Kelley et al. 2014), obscuring our view of the precise tempo and magnitude of these events. As a result, interpreting signals from this period remains challenging, and the observed extinction patterns in the Late Triassic may therefore be somewhat influenced by the Signor-Lipps effect (Signor III and Lipps 1982). Nonetheless, our study sought to better characterize extinction events that affected pelagic tetrapods during the Late Triassic.

CONCLUSION

We comprehensively present the disparity, fin shape and body size evolution of the main raptorial marine predators across the Middle Triassic–Early Jurassic time interval in order to reinvestigate the hypothesis of a dramatic macroevolutionary bottleneck during the latest Triassic. We reveal for the first time contrasting macroevolutionary patterns in the craniodental diversification of both Eosauropterygia and Ichthyosauria during this crucial time interval. The ecomorphospace of eosauropterygians retain a deep phylogenetic structure characterized by a clear clustering of pachypleurosauroids, nothosauroids and pistosauroids. This pattern suggests the earliest members rapidly diverged from one another and did not subsequently radiate into each other craniodental morphospace and presumably ecological niche. In contrast, ichthyosaurians lack any discernible evolutionary trajectory in their craniodental disparity. They continued to radiate into different areas of morphospace, seemingly regardless of phylogenetic affinity. Alongside exploration of new ecomorphospace regions, ichthyosaurian evolution in the aftermath of the T/J transition is marked by the reappearance of phenotypes already present in the Triassic. Extinction events during the Late Triassic were previously conflated because of the coarser data, yielding the illusion of a single, abrupt ‘bottleneck’. While caution is needed to account for the various biases in the latest Triassic fossil record, our results support the existence of a major extinction event that likely decimated multiple coastal forms during the early Late Triassic, disconnected from the end-Triassic mass extinction.

SUPPLEMENTS FOR CHAPTER 2

Data archiving statement

All 3D models used in this chapter that are not related to the Chapter 1 are available on MorphoSource (https://www.morphosource.org/projects/000519988?locale=en and https://www.morphosource.org/projects/000614685?locale=en). Supplementary data (Excel file containing measurements, ratios and PCoAs scores for each analyses and R script used to compute all analyses) on Dryad at DOI: 10.5061/dryad.f4qrfj74j. The .docx file containing all the supplementary information for the article "Contrasting macroevolutionary patterns in pelagic tetrapods across the Triassic–Jurassic transition" is quite extensive, comprising over 100 pages. Therefore, only the figures essential for this Ph.D. manuscript have been included in this section. However, the complete set of information can be accessed here: https://doi.org/10.1093/evolut/qpae138

Supplementary methods

Phylogenetic analyses

Phylogenetic ichthyosaurian relationships were analysed by using the recently published dataset of Laboury et al. (2022), an updated version of the matrix of Maxwell and Cortés (2020). This latter derives from the dataset of Moon (2017), the largest available to date. The authors are aware of reserves expressed by some colleagues (*e.g.* Bindellini et al. [2021]) about using this cladistic matrix, considering the small numbers of specimens personally examined by Moon (2017). However, considering the progressive update by various subsequent works (Maxwell et al. 2019; Klein et al. 2020; Maxwell and Cortés 2020; Sander et al. 2021; Laboury et al. 2022) and the fact that a thorough re-evaluation of ichthyopterygian relationships is beyond the scope of this paper, we consider using the latest version of this original dataset appropriate to provide a global phylogenetic framework for analyses requiring a such context. As no cladistic matrices or analyses to date thoroughly investigated the phylogenetic relationships of all (non-plesiosaurian and plesiosaurian) eosauropterygians together, we created a composite phylogenetic tree combining topologies generated separately for Triassic eosauropterygians and for Early Jurassic plesiosaurians. Recent studies recovered two main overall topologies for Triassic taxa wherein nothosauroids are either closely related to pachypleurosauroids (Hu et al. 2024) or appeared more derived, being the sister lineage of pistosauroids (Xu et al. 2022; 2023). To test the influence of such diverging phylogenetic relationships on our disparity and ordination analyses, we used both datasets of Hu et al. (2024) and of Xu et

al. (2022) and grafted the respective topology on phylogenetic trees generated for the Early Jurassic taxa with the dataset of Wintrich et al. (2017). All phylogenetic analyses have been performed in TNT (v1.6) (Goloboff et al. 2023) within an implied weighting maximum parsimony framework to minimize the impact of homoplasy. We use different values of the concavity constant *k* (6, 9 and 12) to vary the weight on homoplastic characters on the estimation of phylogenetic relationships. The number of trees was set to 100,000 and we used the New Technology Search (ratchet activated: 200 iterations; drift activated: 10 cycles; 10 hits and 10 trees per replication). We applied a tree bisection-reconnection (TBR) algorithm on trees recovered by the ratchet to thoroughly explore most parsimonious tree islands. All of our most parsimonious trees were generated with a *k* value of 12 and one tree for each analysis was randomly selected.

As the three cladistic datasets used don't include all ichthyosaurian and eosauropterygian specimens sampled in our ecomorphological dataset we also grafted missing taxa on their corresponding phylogenies based on the literature, using the *phytools* (v2.0-3) and *paleotree* (v3.4.5) packages (Bapst 2012; Revell 2012) in the R statistical environment (v4.2.3) (R Core Team 2023). For ichthyosaurians, the synonymy of *Temnodontosaurus platyodon* and *'Temnodontosaurus risor*' (McGowan 1994b) has been recently questioned due to numerous morphological differences (Bennion et al. 2024). Considering the need of taxonomic revision for '*T. risor'* (Bennion et al. 2024), we decided to separate these two taxa and to add *'T. risor'* as the sister lineage of *T. platyodon* while waiting for an updated apomorphy-based definition of this taxon. Concerning the eosauropterygians, we added 6 Triassic taxa on the phylogenetic trees generated with the datasets of Hu et al. (2024) and Xu et al. (2022): as in Laboury et al. (2023), we split the OTU '*Neusticosaurus'* into its three species, *Neusticosaurus pusillus* as the sister taxa of the clade composed by *Neusticosaurus edwardsii* and *Neusticosaurus peyeri* (Klein et al. 2022b); and *Luopingosaurus imparilis* as the sister lineage of *Honghesaurus longicaudalis* (Xu et al. 2023) *Brevicaudosaurus jiyangshanensis* as the sister lineage of Nothosauridae (Shang et al. 2020); *Nothosaurus luopingensis* as the sister lineage of *Nothosaurus yangjuanensis* (Shang et al. 2022). Some additional modifications are exclusive to the dataset of Hu et al. (2024). Indeed, we manually added four supplementary taxa in the topology generated with this cladistic matrix: *Nothosaurus cristatus* as the sister lineage of *Nothosaurus mirabilis* (Hinz et al. 2019), *Lariosaurus winkelhorsti* as the sister lineage of *Lariosaurus buzzii* and *Lariosaurus vosseveldensis* as the sister lineage of the clade comprising *L. winkelhorsti* and *L. buzzii* (Laboury et al. 2023). Furthermore, we decided to remove the taxa 'Araeoscelidia', 'Archosauromorpha' and 'Younginiforme' they are beyond the scope of this paper. Finally, we renamed the taxa *Ceresiosaurus* as *Lariosaurus calcagnii* and

Paranothosaurus as *Nothosaurus giganteus* according to their taxonomic revision (Rieppel and Wild 1996; Rieppel 1998). We also grafted on the phylogenetic tree generated with the dataset of Wintrich et al. (2017), the taxon *Microcleidus melusinae* as the most primitive member of *Microcleidus* (Vincent et al. 2017). Our ichthyosaurian and composite eosauropterygian trees were timescaled by using the node dating Hedman algorithm, a method constraining the age of a clade based on the ages of consecutive older groups which thereby act as the clade's outgroup (Hedman 2010; Lloyd et al., 2016).

Ordination analyses: cluster dendrograms and tanglegrams

Our distance matrices were submitted to a cluster dendrogram analysis using the Ward clustering criterion to investigate ecomorphological similarities among each lineage. We applied a multiple bootstrapping procedure named the 'Approximatively Unbiased P-value' implemented in the *pvclust* package (v.2.2-0) (Suzuki et al. 2019) to determine the statistical support of the resulting clusters. This method, using the multiscaled bootstrapping by creating subsamples of different sizes from the original distance matrix, appears to be less biased than traditional bootstrapping (Suzuki et al. 2019) and the most suitable method when missing data are present in datasets (Kelley and Motani 2015; Fischer et al. 2020). We ran it from 0.5 to 10 times the size of our matrix with 0.5 increments and 1,000 bootstraps per replication. The phenotypic distances and the phylogenetic placement of taxa were compared by creating tanglegrams (**Figures S2.11 and S2.12**) using the dendextend (v.1.17.1) (Galili 2015) but also tested by computing Mantel test (1,000 permutations) using the *vegan* package (v.2.6-4) (Oksanen et al. 2022).

Convergences analyses

Our ordination analyses the ichthyosaurian morphological evolution tend to infer possible craniodental convergences (**Figure 16**) between phylogenetically and temporally well-separated taxa mentioned (*e.g.* see **Tables 3 and S2.8**).We thus statistically tested these patterns of morphological convergent evolution by applying to the selected pairs of taxa the novel Ct1, Ct2, Ct3 and Ct4 metrics (Grossnickle et al. 2024) updated from the widely used C1, C2, C3 and C4 metrics of Stayton (2015). In contrary to these latter (which successfully identify convergence and conservatism), the Ct measures differed by incorporating a time-based component and by differentiating divergent to convergent lineages. To briefly summarize, these distance-based measures test the extent to which the convergence process reduces the dissimilarity between two lineages, considering the morphology of their respective ancestors (Fischer et al. 2020). Ct1 and Ct2 (formerly C1 and C2) quantify the phenotypic distance, ideally in a phylomorphospace, between two taxa (tips) compared to their ancestors (nodes) that show the maximum of dissimilarity, whereas Ct3 and Ct4 (formerly C3 and C4) include

the overall amount of phenotypic evolution (reflected in the sum of all phenotypic distances) of clade defined by their last common ancestor (Stayton 2015; Fischer et al. 2020; Laboury et al. 2023). We randomly selected one of our most parsimonious phylogenetic trees and the significance of these measures was tested by simulating the evolution of the character under 1,000 Brownian simulations with the *convevol* package (v. 2.0.0) (Brightly and Stayton 2023) using respectively the first two, the first five and all axes of the PCoA.

In addition to the Ct metric to fully explore these patterns of morphological convergences, we also used the method developed by Castiglione et al. (2019) implemented in the *RRphylo* package (v.2.8.0) (Castiglione et al. 2018). This latter focuses on whether the observed morphological dissimilarity between supposedly convergent taxa — measured by the angle Ø between their phenotypic vector — is smaller than expected by their phylogenetic distance calculated under a Brownian Motion model of evolution (Castiglione et al. 2019). Indeed, the phenotypic distance between two non-convergent taxa is supposed to increase with the time spent since their cladogenesis event and the opposite phenomenon can be interpreted as evidence of morphological convergence (Fischer et al. 2020).

Definition of the ecomorphological quantitative traits

- **Longirostry: snout length/ skull length.**
  Characterizes the hydrodynamic potential of the snout such as the amount of drag during the locomotion (Busbey 1995),the resistance to lateral shaking (Holzman et al. 2012) or the water volume expelled on the closure of the mouth (Mccurry et al. 2017).
- **Snout shape ratio: snout width / skull length.**
  Proxy for the size of the potential ingested prey (MacLaren et al. 2022) and for the water volume that need to be expelled during the closure of the mouth (Mccurry et al. 2017).
- **Relative overbite length: overbite length / mandible length. Only applicable for ichthyosaurians.**
  The overbite is calculated as the length between the anterior tips of the snout and the mandible. The snout of some early parvipelvians is marked by a greater elongation than the mandible such as in *Excalibosaurus costini* and even more in *Eurhinosaurus longirostris*. The presence of a remarkable overbite can be seen on the extant swordfish (*Xiphias gladius*) and the comparison with this species has always been clear (McGowan 1979, 1986; Ellis 2013). The overbite would have served to slash and maim before ingesting them rather than be used as a spear (Stillwell and Kohler 1985; Ellis 2013). It is nevertheless noteworthy to notice that the snouts of *E. costini* and *E. longirostris* are dentigerous throughout their length whereas the snout of the swordfish is edentulous (McGowan 1979, 1986). Up to now, no overbite has been recorded in eosauropterygians.
- **Jaw robusticity: Jaw height at mid-dentigerous length / mandible length**
  Characterizes the aspect ratio of the jaw and is a proxy of the robustness and the stiffness in the jaw under biting loads (Anderson et al. 2011; Stubbs and Benton 2016; MacLaren et al. 2017, 2022). The height of the jaw was measured at the mid-dentigerous zone.
- **Relative symphysial length: Symphyseal length / mandible length.**
  Characterizes the robustness of the anterior portion of the jaw and its resistance during the prey capture (Stubbs and Benton 2016; Fischer et al. 2017; MacLaren et al. 2017; Bennion et al. 2022).

- **Functional toothrow length: Dentigerous mandible length / mandible length.**
  Describe the proportion of the jaw which serves to the capture of the potential prey (MacLaren et al. 2017) . Furthermore, differences in the length of the toothrow reflects different strategies in prey capture, a long dental row would indeed increase the

variation in bites forces and speed which would result in more functional variability, as reflected by great differences between the anterior and posterior mechanical advantage (Stubbs and Benton 2016).

- **Anterior mechanical advantage: Distance between the fulcrum and the mid-point of attachment for the adductor muscles on the dorsal surface of the mandible / distance between the fulcrum and the anterior tip of mandible.**
  The vertebrate mandible can be modelled as a third-order lever (Stubbs and Benton 2016). The mechanical advantage (MA) is an estimation of the ability of a system to transfer the muscles force of the mandible to the prey and can be calculated as the ratio of the inlever and the outlever measurements (Stayton 2006; Stubbs and Benton 2016). The anterior mechanical advantage (AMA) can be defined as the lowest potential MA along the dental row (Stubbs and Benton 2016). Here, the inlever is the distance between the fulcrum (skull articulation with the mandible) to the mid-point of the adductor muscles area insertion while the outlever is represented by the distance from the fulcrum to the base of the anterior-most tooth. It has been demonstrated that animals with weak and rapid bites have low values for AMA while higher values are characteristics of powerful and slower bites (Anderson 2009).
- **Posterior mechanical advantage: Distance between the fulcrum and the mid-point of attachment for the adductor muscles on the dorsal surface of the mandible/distance between the fulcrum and the last mandible tooth.**
  The principle of the posterior mechanical advantage (PMA) is the same than the AMA with the exception that the outlever is measured from the fulcrum to the base of the posterior-most tooth of the mandible. This morphological trait therefore estimates the highest force transfer along the mandibular dentition (Anderson et al. 2011; Stubbs and Benton 2016).
- **Opening mechanical advantage: Distance between the fulcrum and the retroarticular process / distance between the fulcrum and the mid-point of attachment for the adductor muscles on the dorsal surface of the mandible.**
  Characterizes the velocity during the opening of the jaw (MacLaren et al. 2017; Bennion et al. 2022). The inlever can be measured as the distance between the fulcrum and the posterior end of retroarticular process and the outlever, as the distance from the fulcrum to the base of the anterior most tooth of the mandible.
- **Nares position: Distance between the anterior margin of the nares and the tip of the snout / skull length.**

Proxy describing the ability to take a breath during a constant state swim (MacLaren et al. 2022).

- **Relative naris size: Length of the nares / skull length.**
  Amount of air that can be inhaled during a breath (MacLaren et al. 2022).
- **Relative orbit size: Mean diameter of the orbit / skull length.**
  Characterizes the importance of the visual component in the multiple functions that skulls have to perform (MacLaren et al. 2022).
- **Occular offset: Distance from the centre of the orbit to the plane containing the upper tooth row / skull length.**
  Characterizes the position of the eyes in relation to the jaws.
- **Sclerotic opening aperture: sclerotic opening diameter / skull length.**
  Only applicable for ichthyosaurians. Define relative space available between the sclerotic rings allowing light to enter in the pupil. The sclerotic ring is rarely preserved in eosauropterygians. For this reason, its diameter could not have been gathered.
- **Relative parietal foramen length: Length of the parietal foramen / skull length.**
  Characterizes the length of the parietal foramen and is a proxy for the relative size of the pineal gland (Maclaren et al. 2022).
- **Tooth crown shape: Tooth crown height / crown base width.**
  Characterizes the slenderness of the tooth and the resistance to bite forces (Massare 1987; Foffa et al. 2018b; Zverkov et al. 2018; Fischer et al. 2022a; MacLaren et al. 2022). Measurements have been taken on mid-dentigerous region and not on fangs for eosauropterygians.
- **Absolute crown height: Tooth crown height raw measurement.**
  This absolute trait has been shown to be a determinant of diet in modern cetaceans (Ridgway and Harrison 1999) and have been recently used in marine reptile dataset (Fischer et al. 2020; Bennion et al. 2022).
- **Heterodonty index: Anterior tooth crown shape / posterior tooth crown shape.**
  Quantitatively characterizes the level of heterodonty in the dentition of taxa. A value close to 1 indicates no or very low level of heterodonty while a value which exceed 1 reflects a certain level of heterodonty. This quantitative trait however doesn't inform about the global morphology of the teeth should therefore be used in combination with discrete characters which describe the morphology of the tooth crown.
- **Crown curvature: tooth crown tip offset at mid-base with / tooth crown height.**
  Only applicable for eosauropterygians in this study. Due to the labiol-lingual orientation of the ichthyosaurian crown curvature, the measurement of the crown tip

offset on teeth located in mandible or snout could not be gathered (this is the case for the majority of our specimens), leaving this trait too incomplete for inclusion. According to McLaren et al. (2022), this trait describes the dental curvature which represent a proxy for potential prey items.

- **Relative skull length: Skull length / trunk length.**
  Characterizes the proportion of the body used for prey capture and sensory capabilities.
- **Neck proportion: Neck length / trunk length.**
  Characterizes the general body plan but is also a proxy for potential feeding arch and reach of cranium away from the trunk (O'Keefe 2001).
- **Trunk proportion: Trunk length / body length.**
  Characterizes the proportion of the body length available for lungs and digestive track.
- **Tail proportion: Tail length / body length.**
  Characterizes the proportion of the body used for the locomotion. The evolution of Ichthyosauria and Eosauropterygia is marked by a shortening of the tail suggesting that a long one would represent a more primitive condition (Gutarra et al. 2023). Indeed, the eosauropterygian stem groups Pachypleurosauroidea and Nothosauroidea are regarded as lateral undulatory swimmers even if the fore- and the hindlimbs played an important role in the propulsion as there are morphologically derived (Carroll and Gaskill 1985; Sues 1987; Krahl 2021). By comparison to the propelled-tail locomotion of ichthyosaurians, plesiosaurians evolved to an underwater flight by using their four hydrofoil-like flippers (Krahl 2021). In this locomotion style, the tail would rather act as a rudder (Fish and Lauder 2017; Gutarra et al. 2023).
- **Propodial variation: Humerus proximo-distal length / femur proximodistal length.**
  Characterizes the appendicular body plan. The length of the humerus and the femur relative to each other can be considered as indicative of forelimb, hindlimb or equally driven underwater locomotion (Zeffer et al. 2003; Hinić-Frlog and Motani 2010).
- **Propodial size: Humerus proximo-distal length / skull length.**
  Characterizes the elongation of the limbs relative to the skull size. This trait is indicative of the ecology of taxa as species with long limbs and small head will swim and feed in a different way than taxa with a small limbs and large head (Taylor 1987; Massare 1988).
- **Humerus flare: Humerus distal width / humerus proximo-distal length**
  Characterizes the area of muscular insertion on the humerus and the mechanical efficiency of the pectoral girdle. This trait describes the implication of the forelimb in

swimming. A high value of this ratio indicates a relative wider distal extremity of the humerus and is indicative of the aquatic locomotion adaptation in various clades such as cetaceans (Cooper et al. 2007), or cheloniids (Rivera and Blob 2010) as clearly mentioned by (Gutarra et al. 2023).

- **Femur flare**: **Femur distal width / femur proximo-distal length**
  Characterizes the area of muscular insertion on the femur and the mechanical efficiency of the pelvic girdle. This trait describes the implication of the hindlimb in swimming and pelagic specialisation and is based on the same principle than the humerus flare (Gutarra et al. 2023).
- **Brachial index: Radius length / humerus length.**
  The forelimb can be considered as a third-order lever and the brachial index can be thus calculated as the ratio of the inlever and the outlever measurements. As Gutarra et al. (2023) and Caldwell (2002) stated, the brachial index may be indicative of the locomotion mode and thus of the degree of adaptation to oceanic environments. Indeed, low brachial index value indicates a shortening epipodial compared to the propodial and is a typical feature of pelagic animals (Caldwell 2002; Gutarra et al. 2023).
- **Crural index: Tibia length / femur length.**
  The functional implication of this ratio is the same as for the brachial index as the hindlimb can also be considered as a third-order lever.
- **Forelimb aspect ratio**: **Forelimb antero-posterior width / forelimb proximo-distal length.**
  Describes potential water displacement by the forelimbs or the pectoral paddles.
- **Hindlimb aspect ratio: Hindlimb antero-posterior width / forelimb proximo-distal length.**
  Describes potential water displacement by the hindlimbs or the pelvic paddles.

Definition of discrete traits

- **Jaw or snout anterior constriction: Absent (0), Present (1). Only applicable for eosauropterygians in this study.**
  Discrete character which represents a proxy for the preferential use of the anterior jaw for prey capture (Maclaren et al. 2022).
- **Bulbous crushing dentition: Absent (0), Present (1).**
  Discrete character which serves to differentiate taxa with bulbous, blunt and rounded (globidont) dentition. This dental feature is characteristic of the durophage guild made up with taxa capable of crushing hard-shelled prey (Massare 1987; Fischer et al. 2022a).
- **Enlarge procumbent fang dentition: Absent (0), Present (1). Only applicable for eosauropterygians.**
  Discrete character which serves to differentiate taxa that possess fangs on lower and upper jaws. These fangs would have served to pierce pelagic preys (Massare 1987; Großmann 2007) or to create a fish-trap to prevent preys from escaping out of the buccal cavity (Rieppel 2002).
- **Edentulous dentary: Absent (0), Present (1). Only applicable for ichthyosaurians in this study**.
  A remarkable reduction in dentition size or edentulous dentary is indicative of a suction feeding mechanism to catch preys (Heyning and Mead 1996; Sander et al. 2011). However, Motani et al. (2013) pointed out the absence of suction feeding in Ichthyosauria. Although explanation of the presence of edentulous mandibles in ichthyosaurians has yet to be found, this feature is nevertheless informative regarding a shift in prey capture mechanism. Up to date, the absence of dentition has never been recorded in Eosauropterygia.
- **Cutting edge dentition: Absent (0), Present (1).**
  Only applicable for ichthyosaurians in this study as the enamel of some post Early Jurassic pliosaurids are marked by the presence of carinae (Foffa et al. 2018b; Zverkov et al. 2018; Fischer et al. 2022a). These cutting edges serve to slice efficiently preys and is indicative of a megapredatory diet (Massare 1987; Fröbisch et al. 2013; Fischer et al. 2022a; Bennion et al. 2024).
- **Apicobasal crown ridges or marked serration: Absent (0), Present (1).**
  Dental ridges appeared independently in numerous aquatic-feeding tetrapods (Young et al. 2014; Zverkov et al. 2018; McCurry et al. 2019; Boessenecker et al. 2020; Street et al. 2021; Bennion et al. 2024). It has recently been proposed that even if this

ornamentation could secondarily strengthen the tooth (Young et al. 2014; McCurry et al. 2019), its main function would be to increase the cutting performance by maximizing, the grip, the puncture, and the removal efficiency(McCurry et al. 2019). This type of ornamentation is characteristic of generalized macrophagous diet for which crushing and slicing are essential (Young et al. 2014).

Table S2.1. List of eosauropterygian specimens present in ecomorphospace occupation and fin shape analyses. Species only integrated in phenogram analyses due to their overall incompleteness are indicated by an *****.

Taxon	Clade	Age range (in Myr)	Source of measurements
Anarosaurus heterodontus	Pachypleurosauroidea	247.2 – 242	First-hand measurements and photographs from Klein (2009, 2012)
Dawazisaurus brevis	Pachypleurosauroidea	247.2 – 242	Photographs from Cheng et al. (2016)
Diandongosaurus acutidentatus	Pachypleurosauroidea	247.2 – 242	Photographs from Shang et al. 2011 and Sato et al. (2014a)
Dianmeiosaurus gracilis	Pachypleurosauroidea	247.2 – 242	Photographs from (Shang and Li 2015)
Dianopachysaurus dingi	Pachypleurosauroidea	247.2 – 242	Photographs from Liu et al. (2011)
Honghesaurus longicaudalis	Pachypleurosauroidea	247.2 – 242	Photographs from Xu et al. (2022)
Luopingosaurus Imparilis	Pachypleurosauroidea	247.2 – 242	Photographs from Xu et al. (2023)
Keichousaurus hui	Pachypleurosauroidea	242 – 237	First-hand measurements and photographs from Holmes et al. (2008)
Neusticosaurus edwardsii	Pachypleurosauroidea	242 – 237	First-hand measurements
Neusticosaurus peyeri	Pachypleurosauroidea	242 – 237	First-hand measurements
Neusticosaurus pusillus	Pachypleurosauroidea	242 – 237	First-hand measurements
Odoiporosaurus teruzzi	Pachypleurosauroidea	247.2 – 242	Photographs from Renesto et al. (2014)
Panzhousaurus rotundirostris	Pachypleurosauroidea	247.2 – 242	Photographs from Jiang et al. (2019)
Prosantosaurus scheffoldi	Pachypleurosauroidea	242 – 237	First-hand measurements
Qianxisaurus chajiangensis	Pachypleurosauroidea	242 –237	Photographs from Cheng et al. (2012)
Serpianosaurus mirigiolensis	Pachypleurosauroidea	247.2 – 242	First-hand measurements
Wumengosaurus delicatomandibularis	Pachypleurosauroidea	247.2 – 242	Photographs provided by N. Klein and from Wu et al. (2011)
Brevicaudosaurus jiyangshanensis	Nothosauroidea	242 – 237	Photographs from Shang et al. (2020)
Lariosaurus calcagnii	Nothosauroidea	242 – 237	First-hand measurements
Lariosaurus balsami	Nothosauroidea	242 – 237	First-hand measurements
Lariosaurus buzzii	Nothosauroidea	247.2 – 242	First-hand measurements
Lariosaurus hongguoensis	Nothosauroidea	247.2 – 242	Photographs from Jiang et al. (2006)
Lariosaurus xingyensis	Nothosauroidea	242 – 237	Photographs Rieppel et al. (2003) and Lin et al. (2017)
Lariosaurus vosseveldensis	Nothosauroidea	247.2 – 242	Photographs from Klein et al. (2016b)
Lariosaurus winkelhorsti	Nothosauroidea	247.2 – 242	First-hand measurements, photographs
Lariosaurus youngi	Nothosauroidea	242 – 237	Photographs from Ji et al. (2014)
Nothosaurus cristatus	Nothosauroidea	242 – 237	First-hand measurements
Nothosaurus luopingensis	Nothosauroidea	247.2 – 242	Photographs from Shang et al. (2022)
Nothosaurus giganteus	Nothosauroidea	242 – 237	First-hand measurements and 3D models created by the authors
Nothosaurus jagisteus	Nothosauroidea	242 – 237	First-hand measurements
Nothosaurus marchicus	Nothosauroidea	247.2 – 242	First-hand measurements, photographs from Klein et al. (2015) and Voeten et al. (2018)
Nothosaurus mirabilis	Nothosauroidea	247.2 – 242	First-hand measurements and 3D models created by the authors
Simosaurus gaillardoti	Nothosauroidea	242 – 237	3D models created by the authors
Augustasaurus hagdorni	Pistosauroidea	247.2 – 242	3D models created by the authors

Wangosaurus brevirostris	Pistosauroidea	239.1 – 237	Photographs from Ma et al. (2015)
Yunguisaurus liae	Pistosauroidea	239.1 – 237	Photographs from Cheng et al. (2006), Sato et al. (2014b),Shang et al. (2017b)
Anningasaura lymense	Basal plesiosaurians	201.3 – 190.8	First-hand measurements
Stratesaurus taylori	Basal plesiosaurians	201.3 – 199.3	Photographs Benson et al. (2015a)
Plesiosaurus dolichodeirus	Plesiosauroidea	199.3 – 190.8	First-hand measurements, photographs and 3D models created by the authors
*'Plesiosaurus' macrocephalus**	Plesiosauroidea	199.3 – 190.8	3D model created by the authors
*Eoplesiosaurus antiquior**	Plesiosauroidea	201.3 – 199.3	Photographs from Benson et al. (2012)
Microcleidus brachypterygius	Plesiosauroidea	182.7 – 178.2	First-hand measurements
Microcleidus homaleospondylus	Plesiosauroidea	182.7 – 178.2	First-hand measurements
Microcleidus melusinae	Plesiosauroidea	182.7 – 178.2	First-hand measurements
Seeleyosaurus guilelimperatoris	Plesiosauroidea	182.7 – 178.2	First-hand measurements and photographs
Archaeonectrus rostratus	Rhomaleosauridae	199.6 – 190.3	First-hand measurements and 3D models created by the authors
Avalonnectes arturi	Rhomaleosauridae	201.3 – 199.3	3D model created by the authors
Meyerasaurus victor	Rhomaleosauridae	182.7 – 178.2	First-hand measurements and photographs from Smith and Vincent (2010)
Rhomaleosaurus cramptoni	Rhomaleosauridae	182 – 178.2	3D model created by the authors, photographs from Smith (2007) and Smith and Dyke (2008)
Rhomaleosaurus megacephalus	Rhomaleosauridae	201.3 – 199.3	Photographs Cruickshank (1994) and Smith (2007)
Rhomaleosaurus zetlandicus	Rhomaleosauridae	182 – 178.2	3D model created by the authors
Attenborosaurus conybeari	Pliosauridae	196.5 – 190.8	First-hand measurements, 3D model created by the authors
*Hauffiosaurus tomistomimus**	Pliosauridae	182 – 178.2	Photographs from Benson et al. (2011b)
Hauffiosaurus zanoni	Pliosauridae	182 – 178.2	Photographs and measurements from Vincent (2011)
*Rhaeticosaurus mertensi**	Pliosauridae	208.5 – 201.5	Photographs from Wintrich et al. (2017)
Thalassiodracon hawkinsii	Pliosauridae	201.3 – 199.3	First-hand measurements, 3D models, photographs from Storrs and Taylor (1996) and Benson et al. (2011a)

Table S2.2. List of eosauropterygian specimens and completeness for all morphological regions. Taxa only integrated in phenogram analyses due to their overall incompleteness, are indicated by an * and their completeness is inapplicable.

Taxon	Specimens	Craniodental completeness	Postcranial completeness	Whole body completeness
Anarosaurus heterodontus	NME 480000125, NME 480000130, NMNHL RGM 443855, NMNHL RGM 443856, SIPG R 594, SIPG R 595, SIPG R 596, NMNHL Wijk06-38, NMNHL Wij06-266, NMNHL Wijk09-582, NMNHL RGM.443858	91.30%	40%	74.29%
Dawazisaurus brevis	NMNS000933-F034397	86.96%	100%	88.57%
Diandongosaurus acutidentatus	IVPP V17760, NMNS-000933-F03498	86.96%	100%	91.43%
Dianmeiosaurus gracilis	IVPP V 17054, IVPP V 18630	86.96%	100%	91.43%
Dianopachysaurus dingi	LPV 31365	65.22%	80%	71.43%
Honghesaurus longicaudalis	IVPP V30380	91.30%	100%	88.57%
Luopingosaurus imparilis	IVPP V19049	78.26%	80%	80%
Keichousaurus hui	NMNS-cyn-2003-25, NMNS-cyn-2005-05, NMNS-cyn-2005-12, SMNS 81780, SMNS 59705	95.65%	100%	97.14%
Neusticosaurus edwardsii	PIMUZ T2810, PIMUZ T2811, PIMUZ T3430, PIMUZ T3439, PIMUZ T3453, PIMUZ T3452, PIMUZ T3460, PIMUZ T3708, PIMUZ T3758, PIMUZ T3759, PIMUZ T3776, PIMUZ T4761	100%	100%	100 %
Neusticosaurus peyeri	PIMUZ T3393, PIMUZ T3394, PIMUZ T3395, PIMUZ T3396, PIMUZ T3403, PIMUZ T3410, PIMUZ T3422, PIMUZ T3423, PIMUZ T3431, PIMUZ T3445, PIMUZ T3461, PIMUZ T3464, PIMUZ T3467, PIMUZ T3474, PIMUZ T3476,	100%	100%	100%

	PIMUZ T3479, PIMUZ T3497, PIMUZ T3511, PIMUZ T3542, PIMUZ T3546, PIMUZ T3607, PIMUZ T3710, PIMUZ T3728, PIMUZ T3744, PIMUZ T3902			
Neusticosaurus pusillus	PIMUZ T3902, PIMUZ T3400, PIMUZ T3421, PIMUZ T3426, PIMUZ T3429, PIMUZ T3442, PIMUZ T3468, PIMUZ T3509, PIMUZ T3530, PIMUZ T3536, PIMUZ T3538, PIMUZ T3547, PIMUZ T3556, PIMUZ T3574, PIMUZ T3598, PIMUZ T3601, PIMUZ T3604, PIMUZ T3605, PIMUZ T3612, PIMUZ T3614, PIMUZ T3625, PIMUZ T3627, PIMUZ T3639, PIMUZ T3649 A, PIMUZ T3649 B, PIMUZ T3649 C, PIMUZ T3653, PIMUZ T3654, PIMUZ T3658, PIMUZ T3658, PIMUZ T3671, PIMUZ T 3672, PIMUZ T3703, PIMUZ T3739, PIMUZ T3741 B, PIMUZ T3803 B, PIMUZ T3803 D, PIMUZ T3934, PIMUZ T4289, PIMUZ T5942	100%	100%	100%
Odoiporosaurus teruzzi	MSNM BES SC 1893	82.61%	5%	68.57%
Panzhousaurus rotundirostris	GMPKU-P- 1059	65.22%	80%	65.71%
Prosantosaurus scheffoldi	PIMUZ A/III 1197, PIMUZ A/III 1240, PIMUZ A/III 1273, PIMUZ A/III 1274, PIMUZ A/III 1275, PIMUZ A/III 4566	95.65%	80%	91.43%
Qianxisaurus chajiangensis	NMNS-KIKO-F044630	86.96%	80%	85.71%
Serpianosaurus mirigiolensis	PIMUZ T96, PIMUZ T951, PIMUZ T1071, PIMUZ T 3675,	100%	100%	100%

	PIMUZ T3676, PIMUZ T3677, PIMUZ T3680, PIMUZ T3685, PIMUZ T3742, PIMUZ T3931, PIMUZ T3933			
Wumengosaurus delicatomandibularis	GMPKU-P-1210, IVPP V15314, NMNS-KIKO-F071129-Z, ZMNH M8758	86.95%	100%	91.43%
Brevicaudosaurus jiyangshanensis	IVPP V 18625	73.91%	100%	82.86%
Lariosaurus balsami	PIMUZ T4856	82.61%	80%	82.86%
Lariosaurus buzzii	PIMUZ T2804	78.26%	20%	57.14%
Lariosaurus calcagnii	PIMUZ T2460, PIMUZ T2461, PIMUZ T2462, PIMUZ T2464, PIMUZ T4836, PIMUZ T5151, PIMUZ T5559	91.30%	100%	94.28%
Lariosaurus hongguoensis	GMPKU-P-1011	82.60%	50%	71.43%
Lariosaurus vosseveldensis	TWE 480000504	65.22%	0%	42.86%
Lariosauris xingyiensis	IVPP V 1886, XNGM WS-30-R19	95.65%	60%	82.86%
Lariosaurus winkelhorsti	TWE 4800000474	60.87%	0%	40%
Lariosaurus youngi	WS-30-R24	80.61%	80%	82.85%
Nothosaurus cristatus	GPIT-PV-75067	69.57%	0%	45.71%
Nothosaurus luopingensis	IVPP V 24895	69.57%	60%	68.57%
Nothosaurus giganteus	PIMUZ T4829, SMNS 18058, SMNS 57047, SMNS 80217, SMNS 1598b, SMNS 159157, SMNS 17822c, SMNS 81311	95.65%	100%	91.42%
Nothosaurus jagisteus	SMNS 56618	65.22%	0%	42.86%
Nothosaurus marchicus	JLW 300, NMNHL RGM 449995, TWE 480000375, TWE 4800000473, TWE 4800000474	86.96%	60%	74.29%
Nothosaurus mirabilis	SMNS 13155, SMNS 15714, SMNS 16433, SMNS 56826, SMNS 59074, SMNS 84550	69.56%	10%	48.57%
Simosaurus gaillardoti	GPIT-PV-60638, SMNS 10360, SMNS 16363, SMNS16638, SMNS 50714, SMNS 59366, SMNS 7861, SMNS 17223, SMNS 14733, SMNS 17590	100%	20%	71.43%
Augustasaurus hagdorni	FMNH PR1974	82.60%	0%	54.29%

Wangosaurus brevirostris	GMPKU-P-1529	73.91%	70%	71.42%
Yunguisaurus liae	IVPP V14993, NMNS 004529/F003826, ZMNH M8738	95.65%	100%	97.14%
Anningasaura lymense	NHMUK PV OR 49202	86.95%	0%	57.14%
Stratesaurus taylori	OUMNH J.10337, GSM 26035	78.26%	0%	51.42%
Plesiosaurus dolichodeirus	NHMUK PV OR 14113, NHMUK PV OR 22656, NHMUK PV OR 36183, NHMUK PV OR 39490, NHMUK PV R 255, NHMUK PV R 1756	95.65%	90%	94.29%
*'Plesiosaurus macrocephalus**	NHMUK PV OR 1336	—	—	—
*Eoplesiosaurus antiquior**	TTNCM 8348	—	—	—
Microcleidus brachypterygius	GPIT-RE-3185, SMNS 51143	69.57%	90%	77.14%
Microcleidus homaleosondylus	NHMUK PV OR 36184	52.17%	0%	34.29%
Microcleidus melusinae	MNHNL TV343	95.65%	10%	65.72%
Seeleyosaurus guilelimperatoris	MB.R.1992, SMNS 12039	65.22%	100%	74.28%
Archaeonectrus rostratus	NHMUK PV OR 38525, NHMUK PV R 37	65.22%	100%	77.14%
Avalonnectes_arturi	NHMUK PV OR 14550	0%	30%	8.57%
Meyerasaurus victor	SMNS 12478	60.87%	100%	74.28%
Rhomaleosaurus cramptoni	NHMUK PV R 34	69.57%	100%	80%
Rhomaleosaurus megacephalus	LEICS G22.1851, TCD.47762.a	52.17%	100%	62.85%
Rhomaleosaurus zetlandicus	WHITM 851S	56.52%	90%	65.71%
Attenborosaurus conybeari	NHMUK PV OR 40140, NHMUK PV R 1339	65,22%	70%	65.71%
*Hauffiosaurus tomistomimus**	MANCH LL 8004	—	—	—
Hauffiosaurus zanoni	HAUFF uncat	69.57%	100%	80%
*Rhaeticosaurus mertensi**	LWL-MFN P 64047	—	—	—
Thalassiodracon hawkinsii	CAMSM J46986; NHMUK PV OR 2018; NHMUK PV OR 2020; NHMUK PV OR 2022; NHMUK PV OR 2039	91.30%	100%	94.29%

Table S2.3. List of eosauropterygian taxa and their corresponding information used to compute the temporal evolution of dorsal centra height across the Triassic-Jurassic transition.

Taxon	Specimen	Data source	Group	Stage	Mid-Age	Dorsal centrum height (in mm)
Nothosaurus giganteus	SMNS 58453	Rieppel and Wild (1996)	Nothosauroidea	Carnian	234.5	34.7
Simosaurus gaillardoti	MFSN 31870	Dalla Vecchia (2008)	Nothosauroidea	Carnian	234.5	38.4
Paludidraco multidentatus	MUPA-ATZ0101	de Miguel Chaves et al. (2018b)	Nothosauroidea	Carnian	234.5	61.1
Bobosaurus forojuliensis	MFSN 27285	Dalla Vecchia (2006)	Pistosauroidea	Carnian	234.5	44.2
Alexeyisaurus karnoushenkoi	SGU 104a/36	Sennikov and Arkhangelsky (2010)	Basal plesiosaurians	early – middle Norian	219.2	92.9
Rhaeticosaurus mertensi	LWL-MFN P 64047	Wintrich et al. (2017)	Pliosauridae	Rhaetian	204.9	34.1
'Plesiosaurus bitractensis'	PLV 1936; PLV 1937	First-hand measurement	Basal plesiosaurians	Rhaetian	204.9	66.0
Eoplesiosaurus antiquor	TTNCM 8348	Benson et al. (2012)	Basal plesiosaurians	Hettangian	200.6	34.4
Macroplata tenuiceps	NHMUK PV R34588	First-hand photographs	Rhomaleosauridae	Hettangian	200.6	79.1
Eurycleidus arcuatus	NHMUK PV R 2027	First-hand photographs	Rhomaleosauridae	Hettangian	200.6	70.8
Rhomaleosaurus megacephalus	NMING F10194	Smith (2007)	Rhomaleosauridae	Hettangian	200.6	85.7
Avalonnectes arturi	NHMUK PV OR 14550	3D model	Rhomaleosauridae	Hettangian	200.6	28.8
Plesiosaurus dolichodeirus	MNHN A. C. 8592; NHMUK PV OR 22656	3D model and Vincent (2008)	Plesiosauroidea	Sinemurian	195.2	36.4
Archaeonectrus rostratus	NHMUK PV OR 38525; NHMUK PV OR 28318	First-hand measurement and 3D model	Rhomaleosauridae	Sinemurian	195.2	58.6
Attenborosaurus conybeari	NHMUK PV R 1339	First-hand measurement	Pliosauridae	Sinemurian	195.2	58.2

Westphaliasaurus simonsensii	LWL-MFN P 58091	Schwermann and Sander (2011)	Plesiosauroidea	Pliensbachian	186.8	52.8
Microcleidus brachypterygius	GPIT-RE-3185	First-hand photographs	Plesiosauroidea	Toarcian	180.5	40.6
Microcleidus tournemirensis	MMM J. T. 86-100	Bardet et al. (1999)	Plesiosauroidea	Toarcian	180.5	45.3
Seeleyosaurus guilelmiimperatoris	MB.R.1992	first-hand photographs	Plesiosauroidea	Toarcian	180.5	33.0
Hauffiosaurus tomistomimus	MANCH LL 8004	Benson et al. (2011b)	Pliosauridae	Toarcian	180.5	56.0
Rhomaleosaurus thorntoni	NHMUK PV R4853	Smith and Benson (2014)	Rhomaleosauridae	Torcian	180.5	153.9

Table S2.4. List and data sources of ichthyosaurian species present in ecomorphospace occupation and fin shape analyses. Species only integrated in the phenogram analyses due to their overall incompleteness, excepted *Ophthalmosaurus icenicus* which is younger that Early Jurassic, are indicated by an *. Previously considered as a junior synonym of *Temnodontosaurus platyodon,* the taxonomic attribution of '*Temnodontosaurus risor*' is controversial and in need of revision as stated by Bennion et al. (2024). We agree with the authors that this species should no longer be synonymized with *T. platyodon* as it shares lots of morphological similarities with *Ichthyosaurus* and/or *Protoichthyosaurus*. While waiting an apomorphy-based redescription of this species, we decide to consider *'T. risor'* as distinct of *T. platyodon* in our analyses.

Taxon	Group	Age range	Source of measurements
Mixosaurus cornalianus	Mixosaurids	247.2 – 242	First-hand measurements and photographs from Renesto S et al. (2020)
*Mixosaurus kuhnschnyderi**	Mixosaurids	247.2 – 242	Photographs from Brinkmann (1998)
Mixosaurus panxianensis	Mixosaurids	247.2 – 242	First-hand measurements
*Phalarodon atavus**	Mixosaurids	247.2 – 242	Measurements from Gutarra et al. (2023)
*Phalarodon callawayi**	Mixosaurids	247.2 – 242	Photographs from Schmitz et al. (2004)
Phalarodon fraasi	Mixosaurids	247.2 – 242	First-hand measurements
*Cymbospondylus buscheri**	Cymbospondylids	247.2 – 242	First-hand photographs
Cymbospondylus duelferi	Cymbospondylids	247.2 – 242	Photographs from Klein et al. (2020)
Cymbospondylus youngorum	Cymbospondylids	247.2 – 242	Photographs fromSander et al. (2021a)
Cymbospondylus petrinus	Cymbospondylids	247.2 – 242	First-hand photographs
*Xinminosaurus catactes**	Cymbospondylids	247.2 – 242	Photographs from Jiang et al. (2008)
Besanosaurus leptorhynchus	Non-parvipelvian merriamosaurians	247.2 – 242	First-hand measurements, photographs from Bindellini et al. (2021)
Callawayia neoscapularis	Non-parvipelvian merriamosaurians	227 – 216.4	First-hand measurements and photographs
Guanlingsaurus liangae	Non-parvipelvian merriamosaurians	237 – 227	First-hand photographs and from Yin et al. (2000) and Sander et al. (2011)
Guizhouichthyosaurus tangae	Non-parvipelvian merriamosaurians	237 – 227	First-hand photographs and from Shang and Li (2009) and Li and You (2002)
Guizhouichthyosaurus wollongangense	Non-parvipelvian merriamosaurians	237 – 227	Photographs from Chen et al. (2007)
*Shastasaurus pacificus**	Non-parvipelvian merriamosaurians	237 – 227	Schemes from Merriam (1908)

*Shastasaurus sikkanniensis**	Non-parvipelvian merriamosaurians	227 – 208.5	First-hand measurements and photographs
*Qianichthyosaurus xingyiensis**	Non-parvipelvian merriamosaurians	242 – 237	Photographs from Yang et al. (2013)
Qianichthyosaurus zhoui	Non-parvipelvian merriamosaurians	237 – 227	First-hand measurements, first-hand photographs and from Xiaofeng et al. (2008), measurement from the dataset of Gutarra et al. (2023)
*Californosaurus perrini**	Non-parvipelvian merriamosaurians	237 – 227	Schemes from Dal Sasso and Pinna (1996)
Macgowania janiceps	Early parvipelvians	216.4 – 211.4	First-hand measurements and photographs
Eurhinosaurus longirostris	Early parvipelvians	182.7 – 174.1	First-hand measurements and photographs, 3D models
Excalibosaurus costini	Early parvipelvians	199.3 – 190.8	First-hand measurements and photographs, 3D models
Leptonectes moorei	Early parvipelvians	190.8 – 182.7	First-hand measurements and photographs
*Leptonectes solei**	Early parvipelvians	199.3 – 190.8	3D model
Leptonectes tenuirostris	Early parvipelvians	201.3 – 199.3	First-hand measurements, first-hand photographs, 3D model and Maisch and Reisdorf (2006)
Hauffiopteryx typicus	Early parvipelvians	182.7 – 174.1	First-hand measurements, photographs from Maxwell and Cortés (2020), 3D model
Ichthyosaurus anningae	Thunnosaurians	190.8 – 182.7	First-hand photographs
Ichthyosaurus breviceps	Thunnosaurians	199.3 – 190.8	First-hand measurements,3D model created by the authors
Ichthyosaurus communis	Thunnosaurians	201.3 – 199.3	3D models created by the authors
Ichthyosaurus conybeari	Thunnosaurians	199.3 – 190.8	3D model, photographs from Bennett et al. (2012) and Massare and Lomax (2016)
Ichthyosaurus somersetensis	Thunnosaurians	201.3 – 199.3	3D model, photographs from Lomax and Sachs (2017)
Protoichthyosaurus appplebyi	Thunnosaurians	201.3 – 190.8	First-hand measurements, photographs from Srdic et al. (2019)
Stenopterygius quadriscissus	Thunnosaurians	182.7 – 174.1	First-hand measurements and photographs
Stenopterygius triscissus	Thunnosaurians	182.7 – 174.1	First-hand measurements and photographs, 3D model
Stenopterygius uniter	Thunnosaurians	182.7 – 174.1	First-hand measurements and photographs, 3D model
Suevoleviathan integer	Thunnosaurians	182.7 – 174.1	First-hand measurements and photographs, 3D model
*Temnodontosaurus azerguensis**	Early parvipelvians	182.7 – 178.2	First-hand photographs

*Temnodontosaurus crassimanus**	Early parvipelvians	182.7 – 174.1	Photographs from Swaby and Lomax (2020)
Temnodontosaurus eurycephalus	Early parvipelvians	199.3 – 190.8	First-hand photograph, 3D model
Temnodontosaurus platyodon	Early parvipelvians	199.3 – 190.8	First-hand measurements and 3D models
Temnodontosaurus 'risor'	Early parvipelvians	199.3 – 190.8	3D models
Temnodontosaurus trigonodon	Early parvipelvians	182.7 –174.1	First-hand measurements and photographs, 3D models. 3D model of SMNS 1950 has been provided by Pardo-Pérez et al. (2018)
*Ophthalmosaurus icenicus**	Thunnosaurians	166.1 – 152.1	Photographs fromMoon and Kirton (2016)

Table S2.5. List of ichthyosaurian specimens and completeness for all morphological regions. Taxa only integrated in phenogram analyses due to their overall incompleteness, excepted *Ophthalmosaurus icenicus* — which is younger that Early Jurassic — are indicated by an * and their completeness is inapplicable.

Taxon	Specimens	Craniodental completeness	Postcranial completeness	Whole body completeness
Mixosaurus cornalianus	BESC SC 1000, BESC SC 1001, NHMUK PV R 5702, PIMUZ T4848, PIMUZ T4858, PIMUZ T5925, PIMUZ T4923	95.83%	100%	97.22%
*Mixosaurus kuhnschnyderi**	PIMUZ T 1324	—	—	—
Mixosaurus panxianensis	GMPKU-P-1008, GMPKU-P-1033, GMPKU-P-1039, PIMUZ T2418	87.5%	75%	83.33%
*Phalarodon atavus**	LPV 30872	—	—	—
*Phalarodon callawayi**	CMC VP 7275	—	—	—
Phalarodon fraasi	PIMUZ T2417	79.17%	25%	61.11%
*Cymbospondylus buscheri**	PIMUZ T3451	—	—	—
Cymbospondylus duelferi	LACM DI 158109	66.67%	25%	52.78%
Cymbospondylus youngorum	LACM DI 157871	95.83%	16.67%	69.44%
Cymbospondylus petrinus	UCMP 9913, UCMP 9950	83.33%	8.33%	58.33%
*Xinminosaurus catactes**	GMPKU-P-1071	—	—	—
Besanosaurus leptorhynchus	BESC 999, PIMUZ T4376	95.83%	100%	97.22%
Callawayia neoscapularis	ROM 41993	79.17%	25%	61.11%
Guanlingsaurus liangae	GMR 014, YGMIR SPCV03107, YGMIR SPCV03108	83.33%	83.33%	83.33%
Guizhouichthyosaurus tangae	GNG dq-46, IVPP V11853, IVPPV11865, IVPPV11869, TR0001	91.66%	91.67%	91.66%
Guizhouichthyosaurus wollonggangense	SPCV10305	75%	0%	50%
*Shastasaurus sikanniensis**	TMP 94.378.2	—	—	—
*Shastasaurus pacificus**	UCMP 9076	—	—	—
*Qianichthyosaurus xingyiensis**	WS2011-46-R1	—	—	—
Qianichthyosaurus zhoui	CMNH V1412/C1120, GMPKU-P-1208, IVPP V11839, YIGMR TR00047, YGMIR XTw-Q3	83.33%	100%	88.88%
*Californosaurus perrini**	UCMP 9082	—	—	—
Macgowania janiceps	ROM 41992, RTMP 2009.121.0001	95.83%	0%	63.89%

Eurhinosaurus longirostris	GPIT 1491/4, GPIT_RE_9412, MNHN 1946_20, NHMUK PV R5465, ROM 47696, SMNS 14931, SMNS 18648, SMNS 81842	100%	100%	100%
Excalibosaurus costini	BRSMG Cc881, ROM 47697	87.5%	91.67%	88.89%
Leptonectes moorei	NHMUK PV R14370	83.33%	33.33%	66.67%
*Leptonectes solei**	MHN 96270	—	—	—
Leptonectes tenuirostris	NHMUK PV R 2160, NHMUK PV OR 36182, NHMUK PV R 498, NHMUK PV R 47436, NMO 26575, OUMNH J10305, ROM VP47698	91.67%	100%	94.44%
Hauffiopteryx typicus	GPIT RE 12905, GPIT 1491/4, SMNS 51552, SMNS 81962	91.67%	100%	94.44%
Ichthyosaurus anningae	NHMUK PV OR 120	83.33%	83.33%	83.33%
Ichthyosaurus breviceps	NHMUK PV R 216, NHMUK PV R 3367, NHMUK PV OR 39263, NHMUK PV OR 43006	91.67%	58.33%	80.56%
Ichthyosaurus communis	CAMSM J 35187, NHMUK PV R1162, NHMUK PV R 1163, NHMUK PV R 2013, NHMUK PV R 3372, NHMUK PV OR 39492, NHMUK PV OR 39845, NHMUK PV OR 41159	87.5%	100%	91.67%
Ichthyosaurus conybeari	BGS 956, NHMUK PV R 15907, NMW 93.5G.2	87.5%	91.67%	88.88%
Ichthyosaurus somersetensis	NHMUK PV OR 2013, NLMH106234	91.66%	100%	94.44%
Protoichthyosaurus applebyi	NHMUK PV R 1164, UNM.G.2017.1	75%	25%	58.33%
Stenopterygius quadriscissus	MNHN 1909_29, MNHNL TU664, MNHNL TU904, SMNS 15033, SMNS 50963, SMNS 51948, SMNS 54816, SMNS 55748, SMNS 80115, TMP 846601	100%	100%	100%
Stenopterygius triscissus	SMNS 14846, SMNS 54027, SMNS 80113, SMNS 96899	95.83%	100%	97.22%
Stenopterygius uniter	SMNS 17500, SMNS 57532, SMNS 97006	100%	100%	100%
Suevoleviathan integer	SMNS 15390, SMNS 4629,	100%	100%	100%

	Hauff uncat			
*Temnodontosaurus azerguensis**	MAMSPLP	—	—	—
*Temnodontosaurus crassimanus**	YORYM: 497	—	—	—
Temnodontosaurus eurycephalus	NHMUK PV R1157	79.17%	0%	52.77%
Temnodontosaurus platyodon	IRSNB R122, LYMPH 2013/20, NHMUK PV R 1158, NHMUK PV OR 2003	95.83%	100%	97.22%
'Temnodontosaurus' risor	CAMSM J68446, NHMUK PV OR 43971	83.33%	0%	55.56%
Temnodontosaurus trigonodon	GPIT RE9414, GPIT PV30026, SMNS 15950, SMNS 17560, SMNS 50000, SMNS 50004, SMNS 50006	69.56%	100%	100%
*Ophthalmosaurus icenicus**	NHMUK PV R 10031, NHMUK PV R 2134	—	—	—

Table S2.6. List of ichthyosaurian taxa and their corresponding information used to compute the temporal evolution of dorsal centra height across the Triassic-Jurassic transition. The symbol ***** indicates that the height has been measured on the last cervical vertebra, which in ichthyosaurians has a similar length to the dorsal centra.

Taxon	Specimen	Data source	Group	Stage	Mid-Age	Dorsal centrum height (in mm)
Euichthyosauria indet	ZIN PH 16/250	Zverkov et al. (2022)	Indeterminate	Carnian	234.5	32.5
Guanlingsaurus liangae	GMR 014	Yin et al. (2000)	Non-parvipelvian merriamosaurians	Carnian	232.0	72.5
Guizhouichthyosaurus_tangae	TR0001	First-hand photographs	Non-parvipelvian merriamosaurians	Carnian	232.0	55.2
Shastasaurus sp.	UCMP 9609	First-hand photographs	Non-parvipelvian merriamosaurians	Carnian	232.0	108.0
Shastasaurid like	ZIN PH 1/250	Zverkov et al. (2022)	Non-parvipelvian merriamosaurians	Carnian	232.0	115.0
Shonisaurus popularis	NSM-LV collections VM-2014- 057-FS-001 (according to Kelley et al. (2022))	Camp (1980)	Non-parvipelvian merriamosaurians	Carnian	232.0	202.9
Shonisaurus cf. *popularis*	MTSN 4896	Dalla Vecchia and Avanzini (2002)	Non-parvipelvian merriamosaurians	Carnian	232.0	150.0
Qianichthyosaurus xingyiensis	WS2011-46-R1	Yang et al. (2013)	Non-parvipelvian merriamosaurians	Carnian	232.0	18.9
Qianichthyosaurus zhoui	CMNH V1412/C1120; GMPKU-P_1208; IVPP V11839	First-hand photographs and et Haggart et al. (2003)	Non-parvipelvian merriamosaurians	Carnian	232.0	21.7
Toretocnemus californicus	ERNO-A3	Lucas (2002)	Non-parvipelvian merriamosaurians	Carnian	232.0	30.9
Auroroborealia incognita	ZIN PH 3/250; ZIN PH 23/250	Zverkov et al. (2022)	Indeterminate	Lower Norian	221.7	32.5
Callawayia neoscapularis	ROM 41993	First-hand measurements + 3D model	Non-parvipelvian merriamosaurians	Lower Norian	221.7	27.7
Euichthyosauria indet	ZIN PH 9/250	Zverkov et al. (2022)	Indeterminate	Lower Norian	221.7	38.0
Euichthyosauria indet	ZIN PH 11/250	Zverkov et al. (2022)	Indeterminate	Lower Norian	221.7	34.0

Hudsonelpidia brevirostris	ROM 41993	First-hand photographs	Early parvipelvians	Lower Norian	221.7	14.0
*Macgowania janiceps**	TMP 20091210001	First-hand measurements	Early parvipelvians	Middle Norian	213.9	31.5*
Shastasaurus sikkaniensis	TMP 94.378.002	First-hand photographs	Non-parvipelvian merriamosaurians	Middle Norian	213.9	225.0
Shastasaurid like	GZG.V.26007	Karl et al. (2014)	Non-parvipelvian merriamosaurians	Upper Norian	209.9	210.4
Shastasauridae sp.	PIMUZ A/III 1470 (a to g)	Sander et al. (2022)	Non-parvipelvian merriamosaurians	Upper Norian	209.9	181.5
Shastasaurid like	PLV 1932	First-hand measurements	Non-parvipelvian merriamosaurians	Rhaetian	204.9	115.2
Shastasaurid like	PLV 1950	First-hand measurements	Non-parvipelvian merriamosaurians	Rhaetian	204.9	124.9
Shastasaurid like	PLV 1948	Fischer et al. (2014)	Non-parvipelvian merriamosaurians	Rhaetian	204.9	131.8
'Ichthyosaurus_rhaeticus'	PLV 1961	Fischer et al. (2014)	Non-parvipelvian merriamosaurians	Rhaetian	204.9	79.7
Shastasaurid like	MHNTV PAL-1_10/2012	Fischer et al. (2014)	Non-parvipelvian merriamosaurians	Rhaetian	204.9	109.3
Shastasaurid sp. A	PIMUZ A/III 744a	Sander et al. (2022)	Non-parvipelvian merriamosaurians	Rhaetian	204.9	240.1
Euichthyosauria indet.	Specimen from Zapfe (1976)	Sander et al. (2022)	Non-parvipelvian merriamosaurians	Rhaetian	204.9	156.2
Parvipelvia indet.	BRSMG Csb85-48	Mears et al. (2016)	Early parvipelvians	Rhaetian	204.9	38.2
Ichthyosaurus larkini	BRSUG 25300	Lomax et al. (2017)	Thunnosaurians	Hettangian	200.4	33.4
Ichthyosaurus somersetensis	NHMUK PV OR 2013; NLMH106234	3D model and Lomax et al. (2017)	Thunnosaurians	Hettangian	200.4	53.0
Protoichthyosaurus applebyi	UNM.G.2017.1	Lomax et al. (2017)	Thunnosaurians	Hettangian	200.4	24.4
Protoichthyosaurus prostaxalis	BRLSI M3555	Lomax et al. (2017)	Thunnosaurians	Hettangian	200.4	28.4
Wahlisaurus massarae	LEICT G454.1951.5	Lomax	Early parvipelvians	Hettangian	200.4	30.0
Leptonectes tenuirostris	OUMNH J10305	First-hand photographs	Early parvipelvians	Hettangian–Pliensbachian	192,0	34.3
Ichthyosaurus communis	NHMUK PV R1162; NHMUK PV R 2013; NHMUK PV R 3372	3D model	Thunnosaurians	Hettangian–Pliensbachian	192,0	33.3
Ichthyosaurus breviceps	NHMUK PV R 216; NHMUK PV R 3367;	3D model	Thunnosaurians	Sinemurian	195.1	16.8

	NHMUK PV OR 43006					
Ichthyosaurus conybeari	NMW 93.5G.2; NHMUK PV R 15907	Massare and Lomax (2016) and Bennett et al. (2012)	Thunnosaurians	Sinemurian	195.1	14.2
Excalibosaurus costini	ROM 47697	First-hand measurements	Early parvipelvians	Sinemurian	195.1	56.1
Temnodontosaurus platyodon	IRSNB R123	First-hand measurements	Early parvipelvians	Sinemurian	195.1	105.5
Eurhinosaurus longirostris	GPIT RE 9412; ROM specimen; SMNS 14931; SMNS 81842	3D model and first-hand measurements	Early parvipelvians	Toarcian	178.4	62.0
Hauffiopteryx typicus	SMNS 51552; SMNS 81962	3D models	Thunnosaurians	Toarcian	178.4	39.0
Stenopterygius quadriscissus	SMNS 15033; SMNS 50963; SMNS 54816; SMNS 55748; TMP 846601	first-hand measurements and photographs	Thunnosaurians	Toarcian	178.4	48.0
Stenopterygius triscissus	SMNS 54027; SMNS 80113; SMNS 96899	first-hand measurements and photographs	Thunnosaurians	Toarcian	178.4	35.3
Stenopterygius uniter	SMNS 17500; SMNS 96899	first-hand measurements and photographs	Thunnosaurians	Toarcian	178.4	42.6
Suevoleviathan integer	SMNS 15390; Hauff uncat	3D models	Early parvipelvians	Toarcian	178.4	51.1
Temnodontosaurus azerguensis	MAMSPLP specimen	First-hand photographs	Early parvipelvians	Toarcian	178.4	111.11
Temnodontosaurus trigonodon	SMNS 15950; SMNS 50000	3D models	Early parvipelvians	Toarcian	178.4	115.0

Table S2.7. Significance of the different group separation in the craniodental ecomorphospace occupation of eosauropterygians assessed by using NPMANOVA tests based on the use of all axes of the PCoA generated with the craniodental dataset. P-values were corrected by using the Benjamini–Hochberg adjustment. As the 'basal plesiosaurians' group contains only two taxa in our dataset (*Anningasaura lymense* and *Stratesaurus taylori*) it was removed of our statistical comparison.

Groups tested	Group size	F test	R^2	p-value	Corrected p-value
Pachypleurosauroids VS nothosauroids	17–16	9.06335	0.22626	0.00010	0.0021
Pachypleurosauroids VS Triassic pistosauroids	17–3	3.13869	0.14848	0.00010	0.0021
Pachypleurosauroids VS rhomaleosaurids	17–5	6.69510	0.25080	0.00010	0.0021
Pachypleurosauroids VS pliosaurids	17–3	3.16587	0.14957	0.00010	0.0021
Pachypleurosauroids VS plesiosauroids	17–5	4.69345	0.19007	0.00010	0.0021
Nothosauroids VS Triassic pistosauroids	16–3	1.83533	0.09744	0.0040	0.0067
Nothosauroids VS rhomaleosaurids	16–5	2.94186	0.13408	0.00010	0.0021
Nothosauroids VS pliosaurids	16–3	2.87387	0.14461	0.0030	0.0056
Nothosauroids VS plesiosauroids	16–5	3.70292	0.16310	0.00010	0.0025
Triassic pistosauroids VS rhomaleosaurids	3–5	2.00989	0.25093	0.01499	0.0204
Triassic pistosauroids VS pliosaurids	3–3	1.08822	0.21387	0.3000	0.3000
Triassic pistosauroids VS plesiosauroids	3–5	1.31367	0.17961	0.05194	0.0599
Rhomaleosaurids VS pliosaurids	5–3	1.88706	0.23926	0.01798	0.0225
Rhomaleosaurids VS pleisosauroids	5–5	2.64018	0.24813	0.00500	0.0074
Pliosaurids VS Plesiosauroids	5–3	1.32652	0.18106	0.08691	0.0931

Table S2.8. Significance of the different group separation in the craniodental ecomorphospace occupation of ichthyosaurians assessed by using NPMANOVA tests based on the use of all axes of the PCoA generated with the craniodental dataset. P-values were corrected by using the Benjamini–Hochberg adjustment.

Group tested	Group size	F test	R^2	p-value	Corrected p-value
Cymbospondylids VS mixosaurids	3–3	5.41661	0.57522	0.1	0.125
Cymbospondylids VS non-parvipelvian merriamosaurians	3–6	2.30412	0.24765	0.01199	0.03
Cymbospondylids VS early parvipelvians	3–11	2.14990	0.15194	0.02298	0.0383
Cymbospondylids VS thunnosaurians	3–9	4.07754	0.28965	0.00300	0.02
Mixosaurids VS non-parvipelvian merriamosaurians	3–6	2.01563	0.22357	0.00599	0.02
Mixosaurids VS early parvipelvians	3–11	2.07174	0.14723	0.01898	0.038
Mixosaurids VS thunnosaurians	3–9	2.82601	0.22033	0.00500	0.02
Non-parvipelvian merriamosaurians VS early parvipelvians	6–11	0.93756	0.05882	0.47453	0.475
Non-parvipelvian merriamosaurians VS thunnosaurians	6–9	1.53899	0.10585	0.03497	0.05
Early parvipelvians VS thunnosaurians	11–9	1.35200	0.06986	0.14186	0.158

Table S2.9. Results of the ichthyosaurian convergence tests using the Ct metrics derived from the Stayton C-measures for selected pairs of taxa using the first two the first five and all the axes of PCoA analyses on the craniodental dataset. The phylogenetic tree used has been timescaled with the Hedman method. Abbreviations: *Cymb.y*, *Cymbospondylus youngorum*; *Guiz.t*, *Guizhouichthyosaurus tangae*; *Guiz.w*, *Guizhouichthyosaurus wolonggangense*, *Hauf.t*, *Hauffiopteryx typicus*; *Icht.c*, *Ichthyosaurus communis*; *Lept.m*, *Leptonectes moorei*; *Sten.q*, *Stenopterygius quadriscissus*; *Temn.e*, *Temnodontosaurus eurycephalus*.

Taxon pair	Ct1	p-value	Ct2	p-value	Ct3	p-value	Ct4	p-value
Qian.z – Lept.m – 2	0.17174	0	0.0035	0.0	0.0049	0.0	0.00087	0
Qian.z – Lept.m – 5	-1.75144	0	-0.03804	0	-0.04680	0	-0.00711	0
Qian.z – Lept.m – all	-6.97669	0.006	-0.29986	0.003	-0.24825	0.004	-0.03723	0
Cymb.y – Temn.e – 2	0.79757	0.003	0.18255	0.001	0.24492	0.004	0.03762	0.002
Cymb.y – Temn.e – 5	-0.54138	0.094	-0.14645	0.22	-0.14510	0.136	-0.02164	0.181
Cymb.y – Temn.e – all	-0.69788	0.025	-0.22483	0.113	-0.16735	0.042	-0.02167	0.043
Mixo.c – Hauf.t – 2	0.46305	0.01	0.06342	0.005	0.08423	0.009	0.01463	0.006
Mixo.c – Hauf.t – 5	-0.45716	0.02	-0.07292	0.027	-0.08239	0.025	-0.01235	0.024
Mixo.c – Hauf.t – all	-0.69788	0.025	-0.22483	0.113	-0.16735	0.042	-0.02167	0.043
Guiz.t – Icht.c – 2	-1.59030	0.822	-0.07895	0.47	-0.15941	0.526	-0.02019	0.422
Guiz.t – Icht.c – 5	-0.27856	0.302	-0.04910	0.233	-0.06562	0.25	-0.00932	0.217
Guiz.t – Icht.c – all	-0.405937	0.329	-0.11289	0.201	-0.09285	0.195	-0.01427	0.131
Guiz.w – Sten.q – 2	-1.27112	0.677	-0.06372	0.330	-0.12096	0.388	-0.01629	0.306
Guiz.w – Sten.q – 5	-0.97086	0.642	-0.0677	0.208	-0.09174	0.244	-0.01285	0.188
Guiz.w – Sten.q – all	-0.58362	0.329	-0.13428	0.143	-0.10176	0.15	-0.01698	0.092

Table S2.10. Results of ichthyosaurian convergence tests by using the Castiglione et al. (2019) method for selected pairs of taxa using the first two, the first five and all the axes of PCoA analyses based on the craniodental dataset. The phylogenetic tree used has been timescaled with the Hedman method. Abbreviations: *Cymb.y*, *Cymbospondylus youngorum*; *Guiz.t*, *Guizhouichthyosaurus tangae*; *Guiz.w*, *Guizhouichthyosaurus wolonggangense*, *Hauf.t*, *Hauffiopteryx typicus*; *Icht.c*, *Ichthyosaurus communis*; *Lept.m*, *Leptonectes moorei*; *Sten.q*, *Stenopterygius quadriscissus*; *Temn.e*, *Temnodontosaurus eurycephalus*.

Taxon pair	ang.state	p.ang.state	ang.state.time	p.ang.state.time
Qian.z – Lept.m – 2	2.69443	0.0165	0.03299	0.0095
Qian.z – Lept.m – 5	12.54163	0.002	0.15356	0.002
Qian.z – Lept.m – all	59.95517	0.012	0.73410	0.001
Cymb.y – Temn.e – 2	9.10430	0.0705	0.14711	0.0615
Cymb.y – Temn.e – 5	70.56040	0.3025	1.14011	0.2885
Cymb.y – Temn.e – all	79.24468	0.162	1.28043	0.297
Mixo.c – Hauf.t – 2	14.27239	0.093	0.17477	0.071
Mixo.c – Hauf.t – 5	55.40441	0.201	0.67844	0.073
Mixo.c – Hauf.t – all	68.42040	0.04	0.83783	0.004
Guiz.t – Icht.c – 2	69.09518	0.402	1.01704	0.339
Guiz.t – Icht.c – 5	65.40516	0.2635	0.96272	0.1835
Guiz.t – Icht.c – all	80.78400	0.195	1.18909	0.216
Guiz.w – Sten.q – 2	32.56706	0.2195	0.37508	0.1375
Guiz.w – Sten.q – 5	59.9909	0.222	0.69093	0.078
Guiz.w – Sten.q – all	88.53650	0.3805	1.01970	0.0685

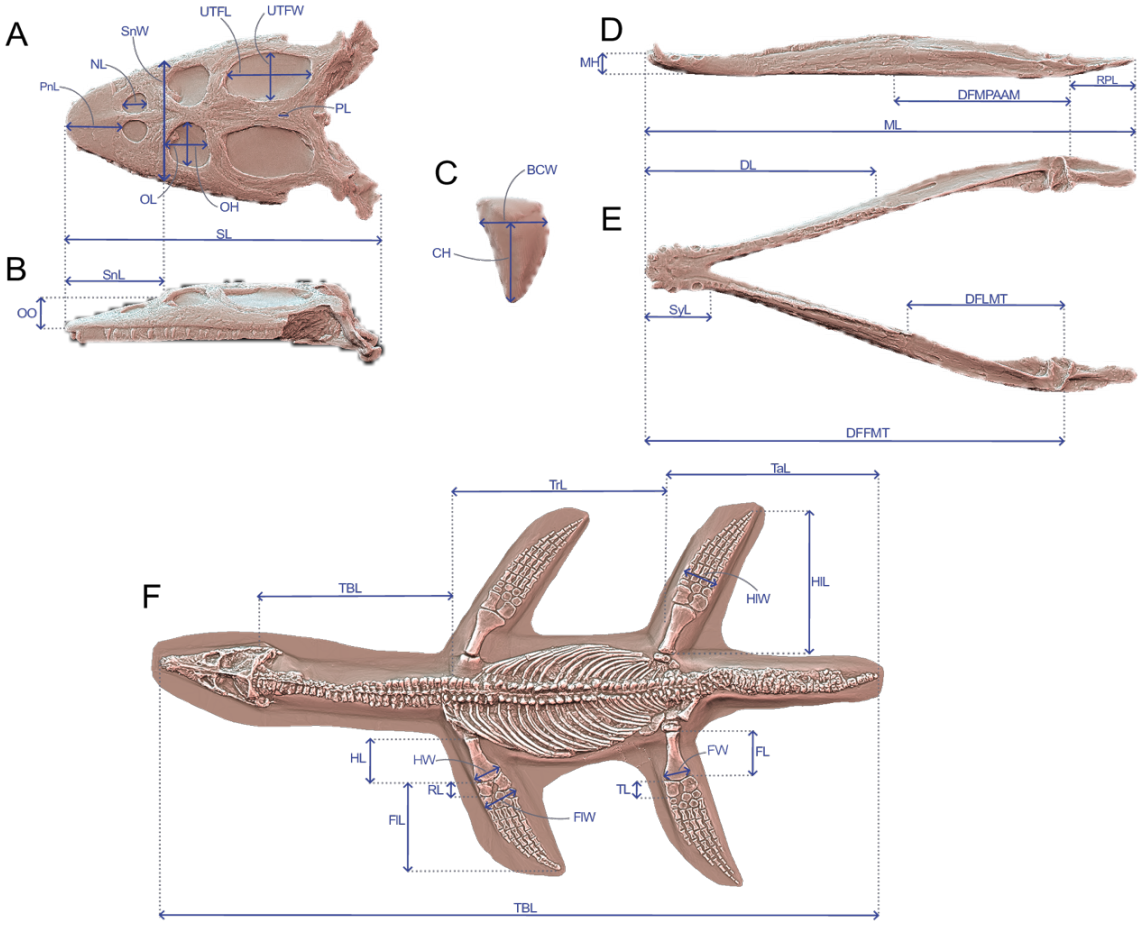

Figure S2.1. Linear measurements used to calculate ecomorphological traits used in our disparity analyses. (A and B) cranial measurements shown on the 3D model of *Simosaurus gaillardoti* (SMNS 16363) in (A) dorsal and in (B) lateral views; (C) tooth measurements shown on the 3D tooth model of *Simosaurus gaillardoti* (GPIT-PV-60638) in labial view; (D and E) mandibular measurements shown on the 3D model of *Nothosaurus giganteus* (SMNS 18058) in (D) dorsal and in (E) lateral views; (F) postcranial measurements shown on the specimen of *Rhomaleosaurus cramptoni* (NHMUK PV R 34). Abbreviations: BCW, basal crown width; CH; crown height; DFFMT, distance fulcrum — first mandible tooth; DFMLT, distance fulcrum — last mandible tooth; DFMPAAM, distance fulcrum — mid-point of attachment of the adductor muscles; DL, dentigerous length; FL, femur proximodistal length; FW, femur distal width; FlL, forelimb length; FlW, forelimb width; HL, humerus proximodistal length; HW, humerus distal width; HlL, hindlimb length; HlW, hindlimb width; MH, mandible height; ML, mandible length; NeL; neck length; NL, naris length; OL, orbit length; OH, orbit height; OO, ocular offset; PL, parietal foramen length; RL, Radius proximodistal length; RPL, retroarticular process length; PnL, prenarial length; SL, skull length; SW, skull width; SnL, snout length; SnW, snout width; SyL, symphysial length; TBL, total body length; TL, tibia proximodistal length, TaL, tail length; TrL, trunk length; UTFL, upper temporal fenestra length; UTFW, upper tempoal fenestra width

`

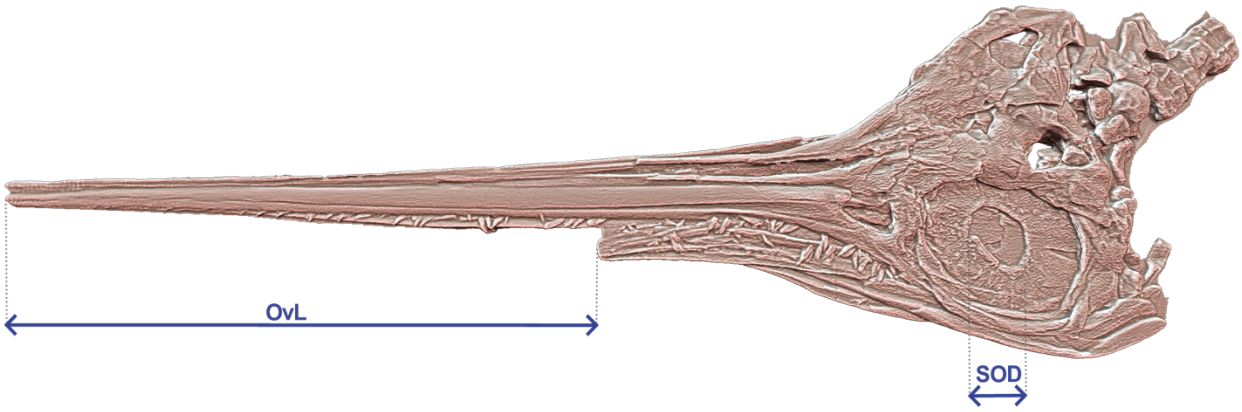

Figure S2.2. Craniodental linear measurements only applicable for ichthyosaurians used to calculate ecomorphological traits shown on the 3D model of Eurhinosaurus *longirostris* (NHMUK PV R 3938). Abbreviations: OvL, overbite length; SOD, sclerotic opening diameter.

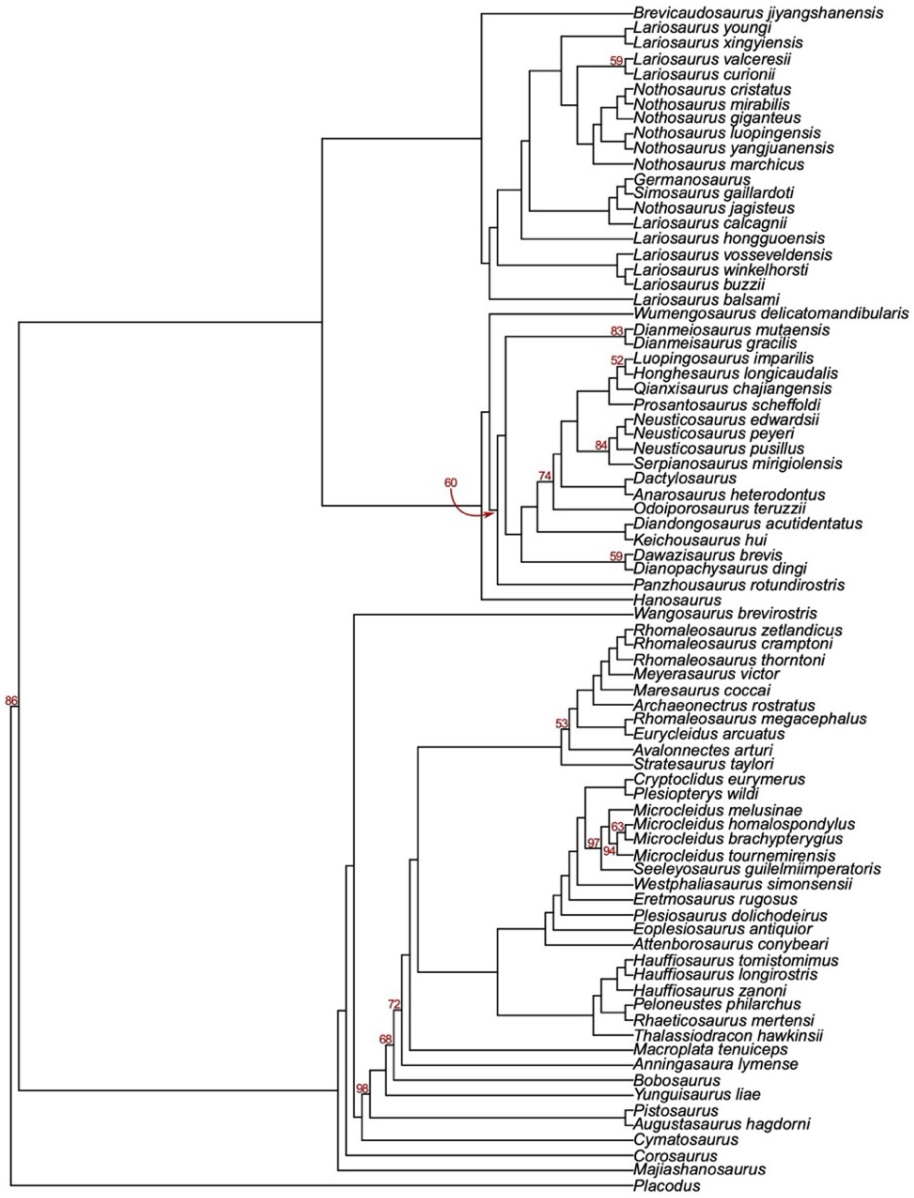

Figure S2.3. Eosauropterygian composite phylogenetic tree based on Hu et al. (2024) for Triassic eosauropterygians and Wintrich et al. (2017) for Jurassic plesiosaurians. Both phylogenetic matrices have been analysed within an implied weighting parsimony framework (*k*=12). Each tree has a length of 32.64 and 28.96 steps. Values of symmetric resampling have been generated for each phylogeny separately and values ≥ 50 are indicated at their corresponding nodes.

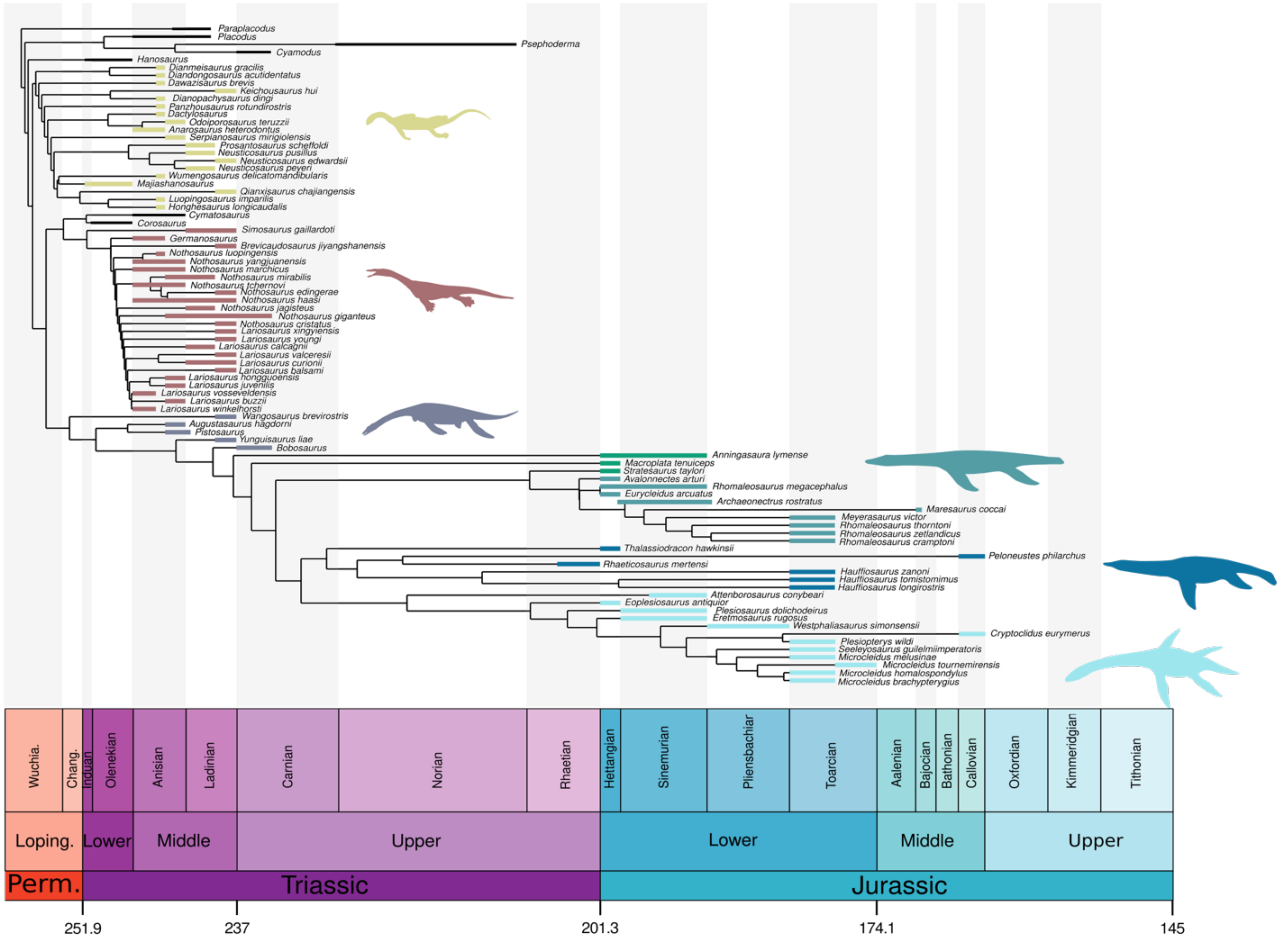

Figure S2.4. Eosauropterygian time-scaled composite phylogenetic tree based on the phylogenetic analyses of Hu et al. (2024) and Wintrich et al. (2017) with the **Hedman calibration method**. Taxa present in our ecomorphological datasets but absent in both phylogenetic matrices have been added according to the literature (see Supplementary methods section). This composite tree shows the main groups used in the ordination, convergence, limb architecture and body size analyses as well as their stratigraphical distributions. The stratigraphic range of each taxon is coloured with respect to its relative group (light yellow: pachypleurosauroids, dull red: nothosauroids, dull purple: pistosauroids, green: basal plesiosaurians, light blue: plesiosauroids, dark blue: pliosauroids, turquoise: rhomaleosaurids).

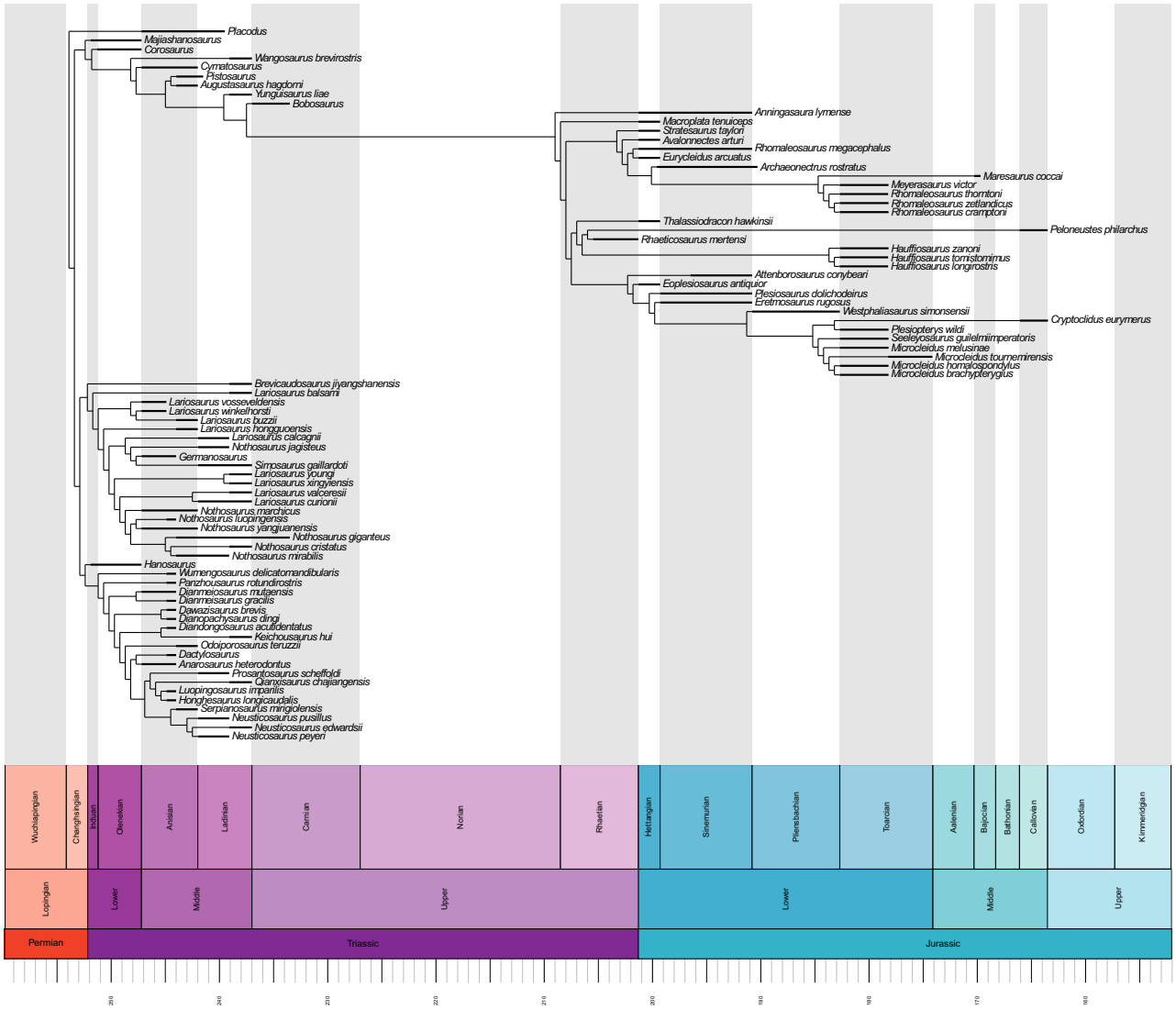

Figure S2.5. Eosauropterygian time-scaled composite phylogenetic tree based on the phylogenetic analyses of Hu et al. (2024) and Wintrich et al. (2017) with the **minimum branch length calibration method**. Taxa present in our ecomorphological datasets but absent in both phylogenetic matrices have been added according to the literature (sees Supplementary methods section).

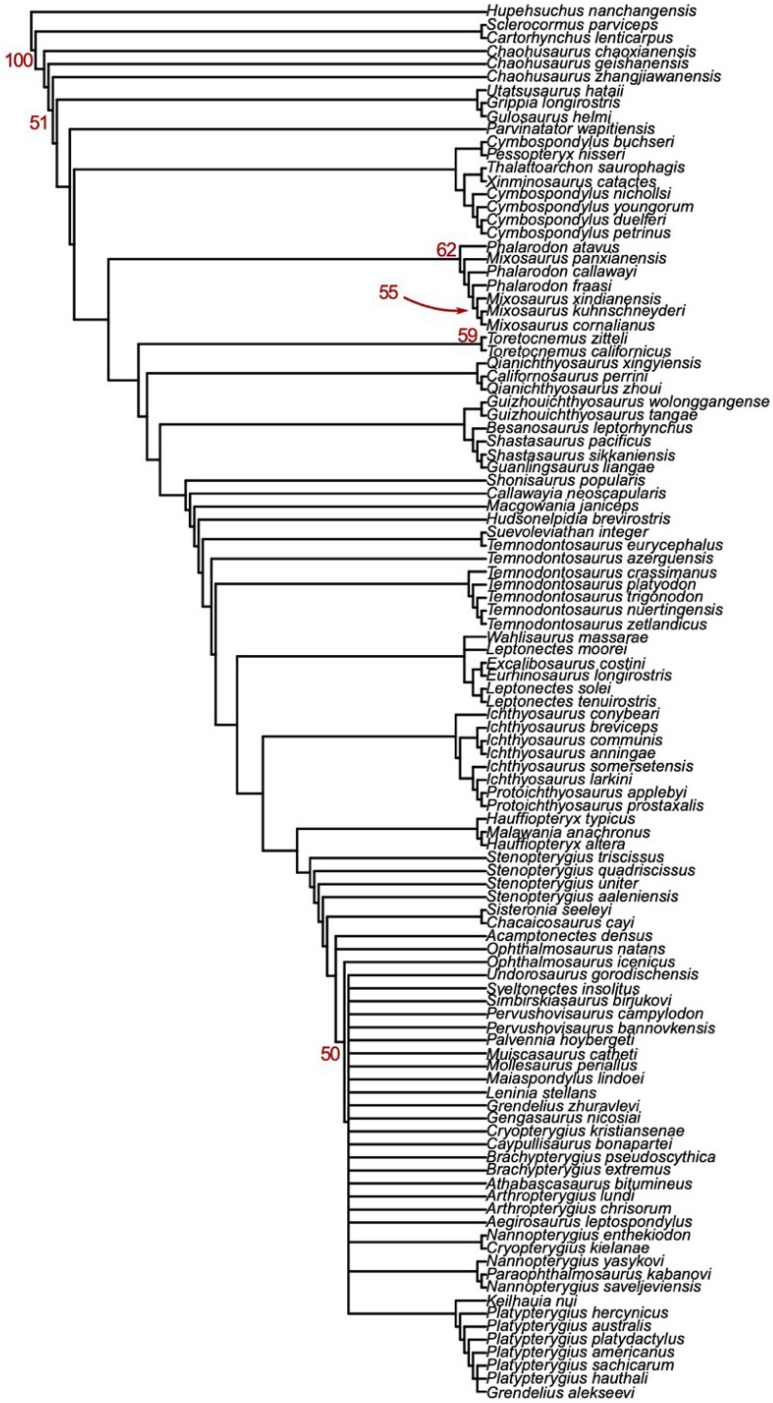

Figure S2.6. Ichthyosaurian strict consensus arising from implied weighting analysis (*k*=12). This analysis recovered 92 trees with a length of 69.88 steps. The dataset stems from the phylogenetic matrix of **Laboury et al. (2022)** with the addition of 2 taxa based on the literature (see Material and Methods): *Cymbospondylus duelferi*, *Cymbospondylus youngorum*. Values of symmetric resampling have been generated for each phylogeny separately and values ≥ 50 are indicated at their corresponding node

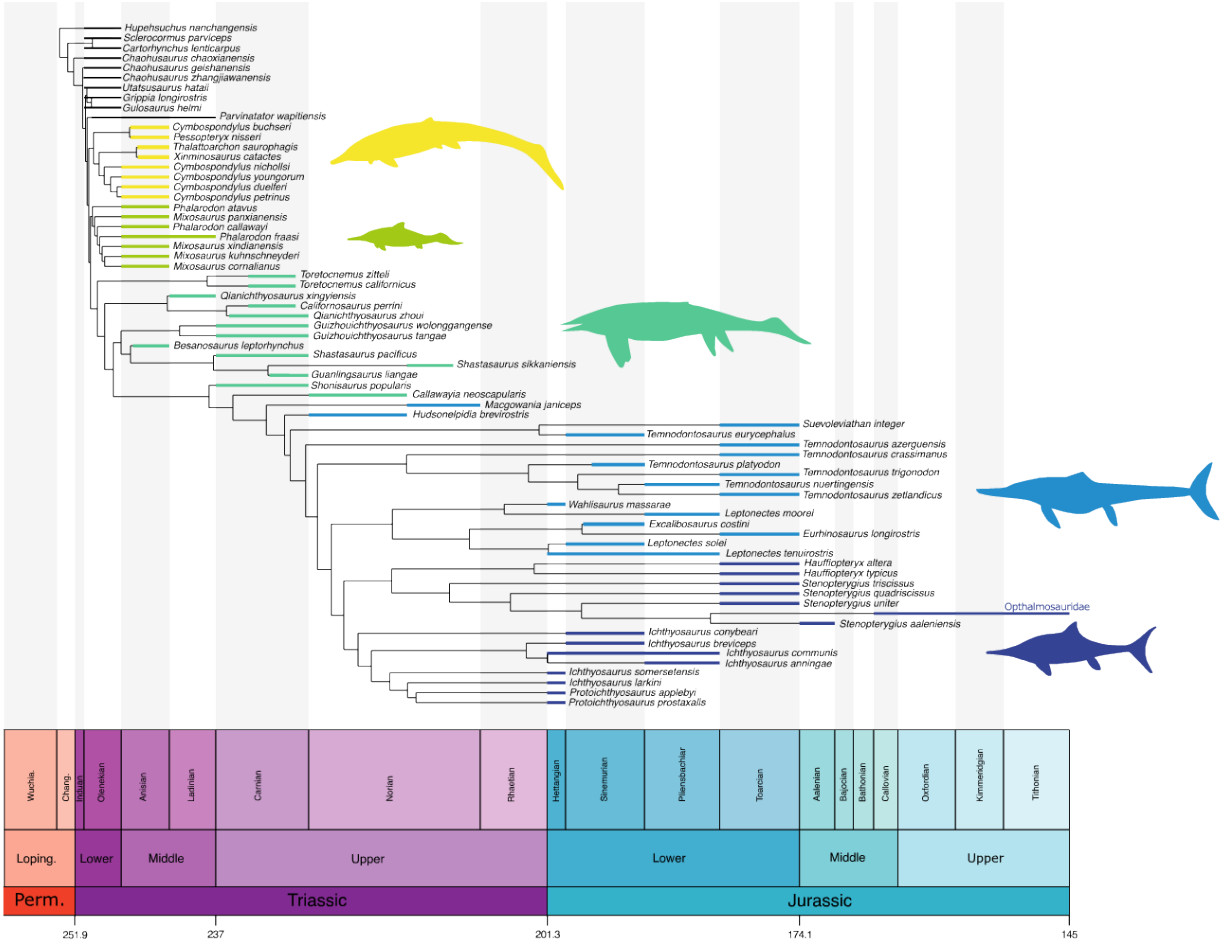

Figure S2.7. Simplified ichthyosaurian time-scaled phylogeny showing the main groups used in the ordination, convergence, limb architecture and body size analyses as well as their stratigraphical distributions. The tree topology arises from the implied weighting (*k*=12) Maximum Parsimony analysis using the **Hedman calibration method**. The dataset stems from the phylogenetic matrix of Laboury et al. (2022) with the addition of 3 taxa based on the literature (see Material and Methods): *Cymbospondylus duelferi*, *Cymbospondylus youngorum* and *a posteriori* '*Temnodontosaurus risor*'. The stratigraphic range of each taxon is coloured with respect to its relative group (yellow: cymbospondylids, light green: mixosaurids, green: non-parvipelvian merriamosaurians, blue: early parvipelvians, dark blue: thunnosaurians).

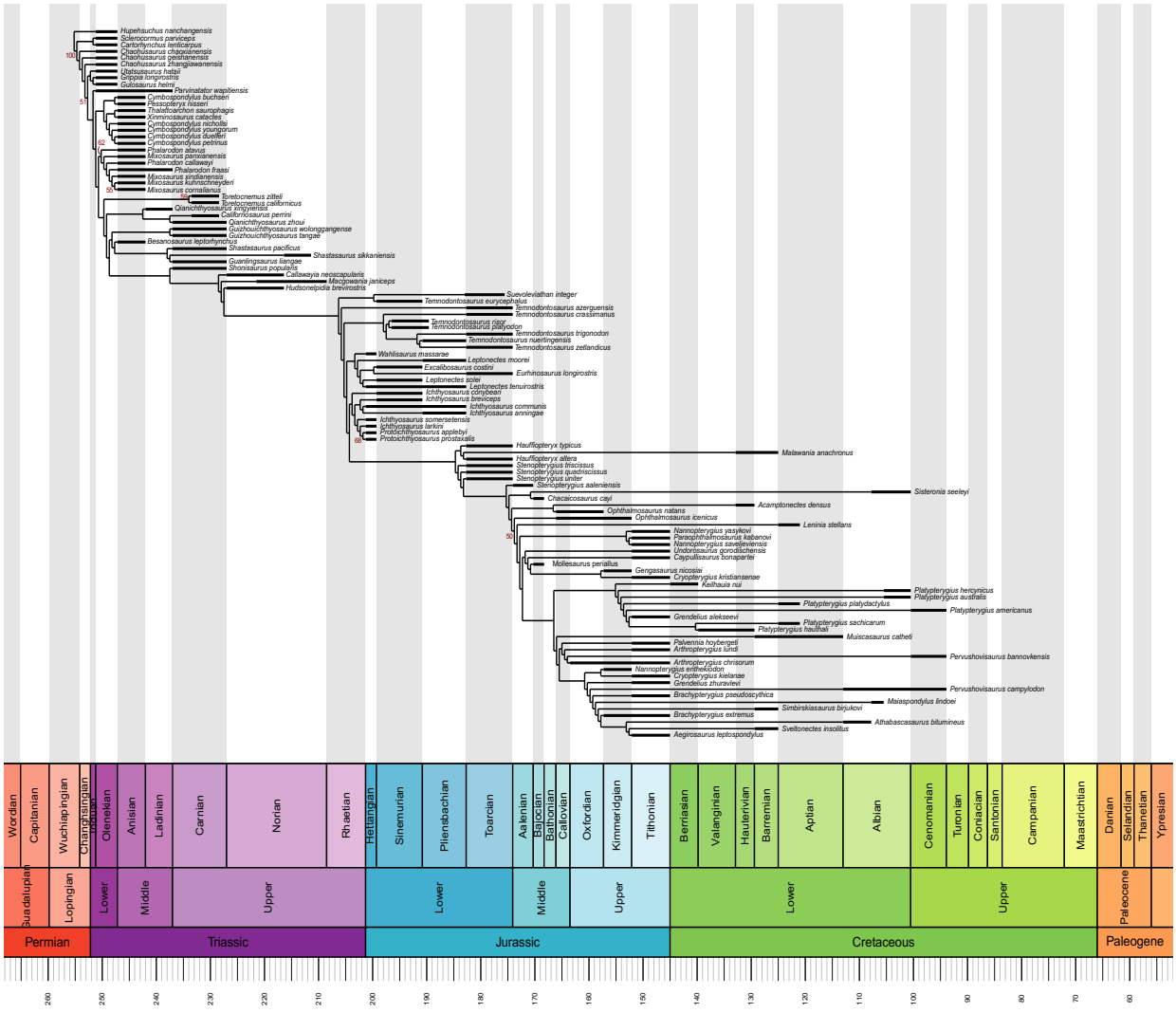

Figure S2.8. Ichthyosaurian time-scaled phylogeny arising from implied weighting (k=12) Maximum Parsimony analysis using **minimum branch length calibration method**. The tree has a length of 69.88 steps. The dataset stems from the phylogenetic matrix of Laboury et al. (2022) with the addition of 3 taxa based on the literature (see Material and Methods): *Cymbospondylus duelferi*, *Cymbospondylus youngorum* and '*Temnodontosaurus risor*'. Values of the symmetric resampling ≥ 50 are indicated at their corresponding nodes.

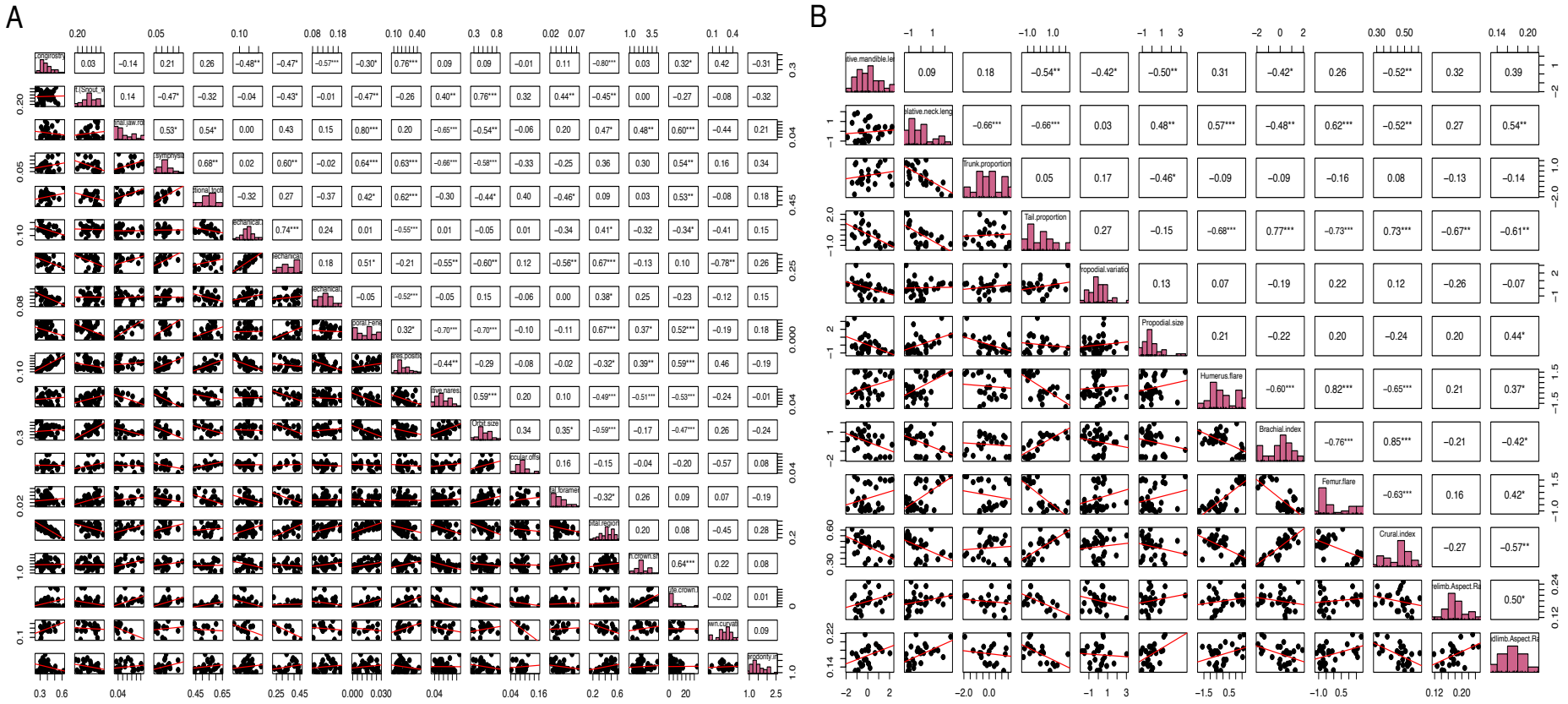

Figure S2.9. Eosauropterygian quantitative (A) craniodental and postcranial (B) trait histograms, pairwise distribution and correlation. The upper panel indicates the pairwise correlation (Pearson's correlation coefficient; * indicates significance at alpha = 0.05, ** at alpha 0.01)

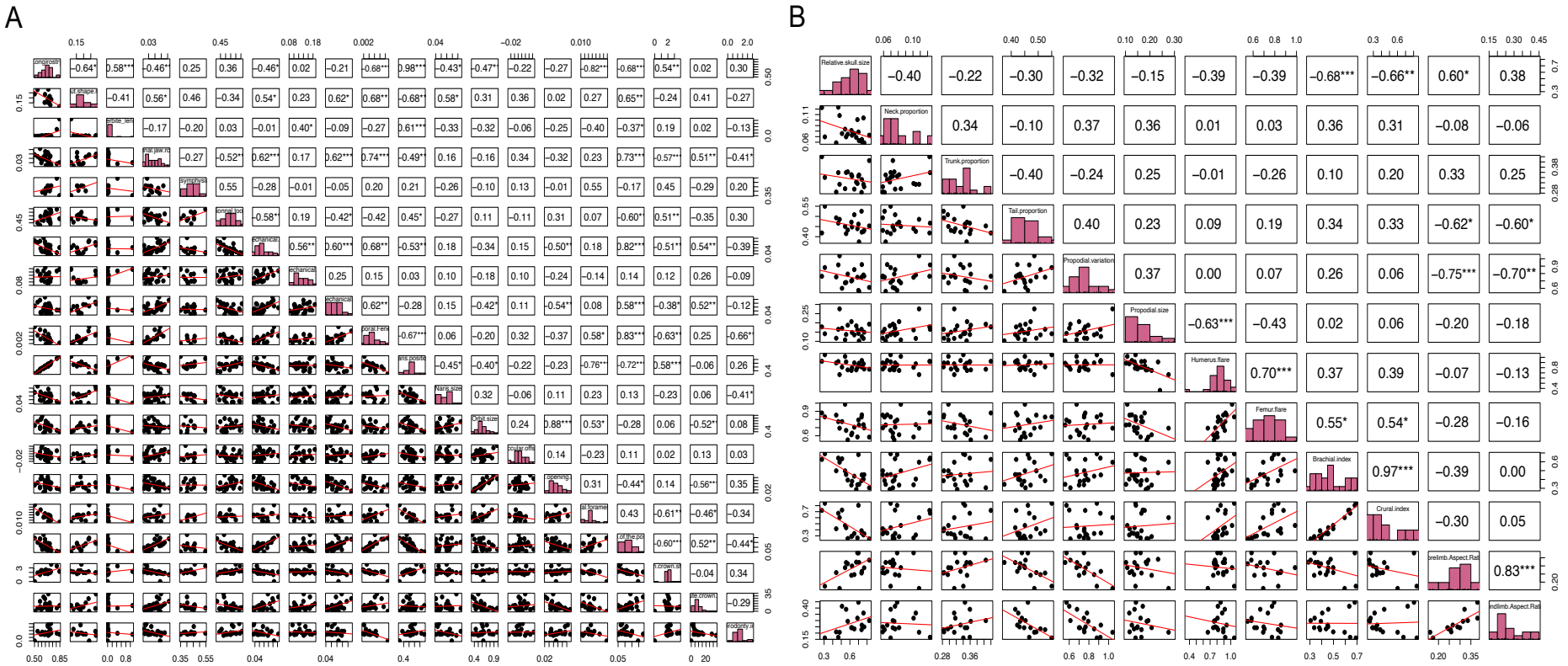

Figure S2.10. Ichthyosaurian quantitative (A) craniodental and postcranial (B) trait histograms, pairwise distribution and correlation. The upper panel indicates the pairwise correlation (Pearson's correlation coefficient; * indicates significance at alpha = 0.05, ** at alpha 0.01)

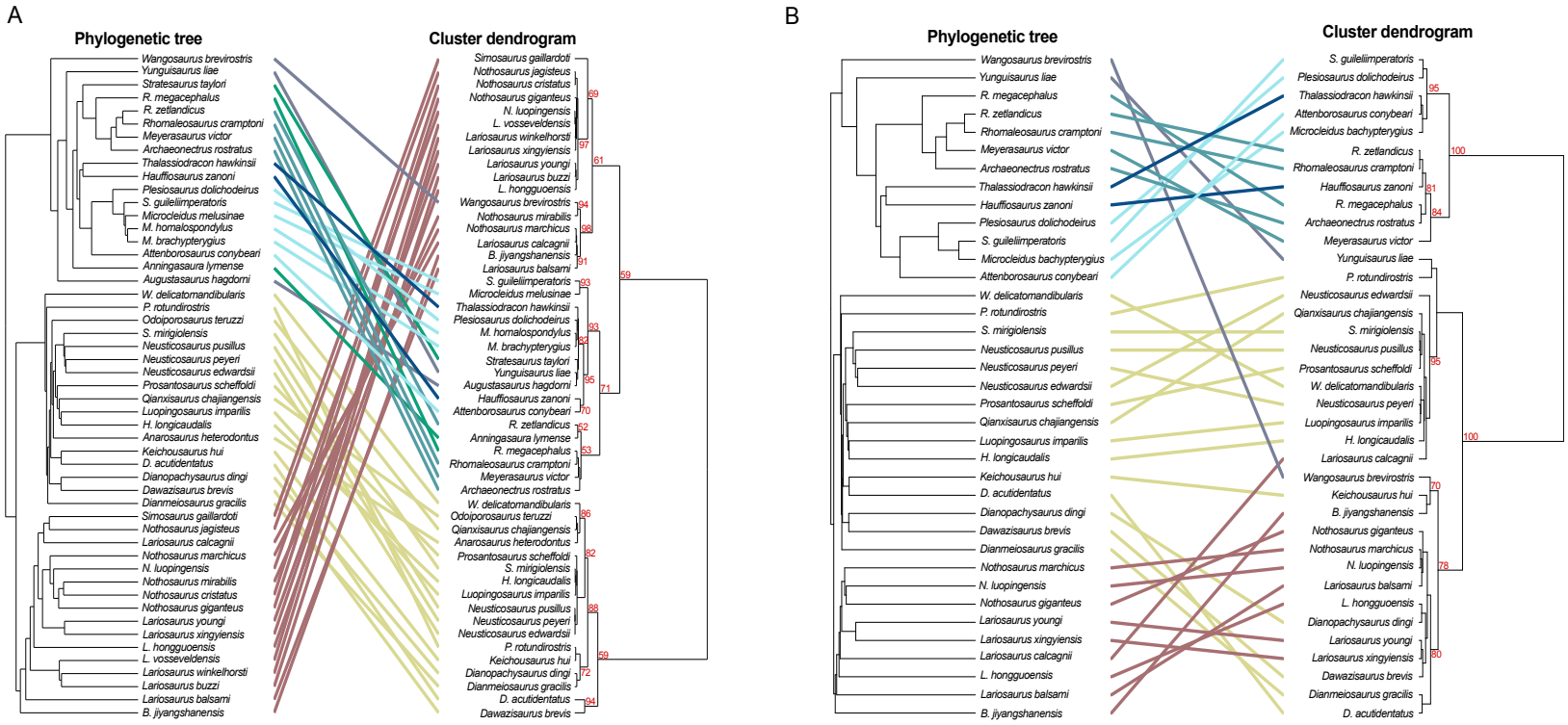

Figure S2.11. Eosauropterygian tanglegrams comparing the phylogeny with the hierarchy of a cluster dendrogram generated with (A) the craniodental and (B) the postcranial data. Each line is coloured with respect to its relative group (light yellow: pachypleurosauroids, dull red: nothosauroids, dull purple: pistosauroids, green: basal plesiosaurians, light blue: plesiosauroids, dark blue: pliosauroids, turquoise: rhomaleosaurids). The composite phylogenetic tree has been created by merging the phylogenetic analyses of Hu et al. (2024) and Wintrich et al. (2017) datasets generated in Maximum Parsimony framework under implied weighting (*k*=12). Only taxa present in the ecomorphological dataset were kept. Nodal support values (approximate unbiased p-value in percentage) under 50% are indicated at their corresponding nodes on the cluster dendrogram. Mantel test results (p-value=0.003 with the craniodental dataset and p-value=0.001 with the postcranial dataset) indicate a significant correlation between the phylogenetic relationships and the hierarchy of cluster dendrograms generated with both craniodental and postcranial dataset.

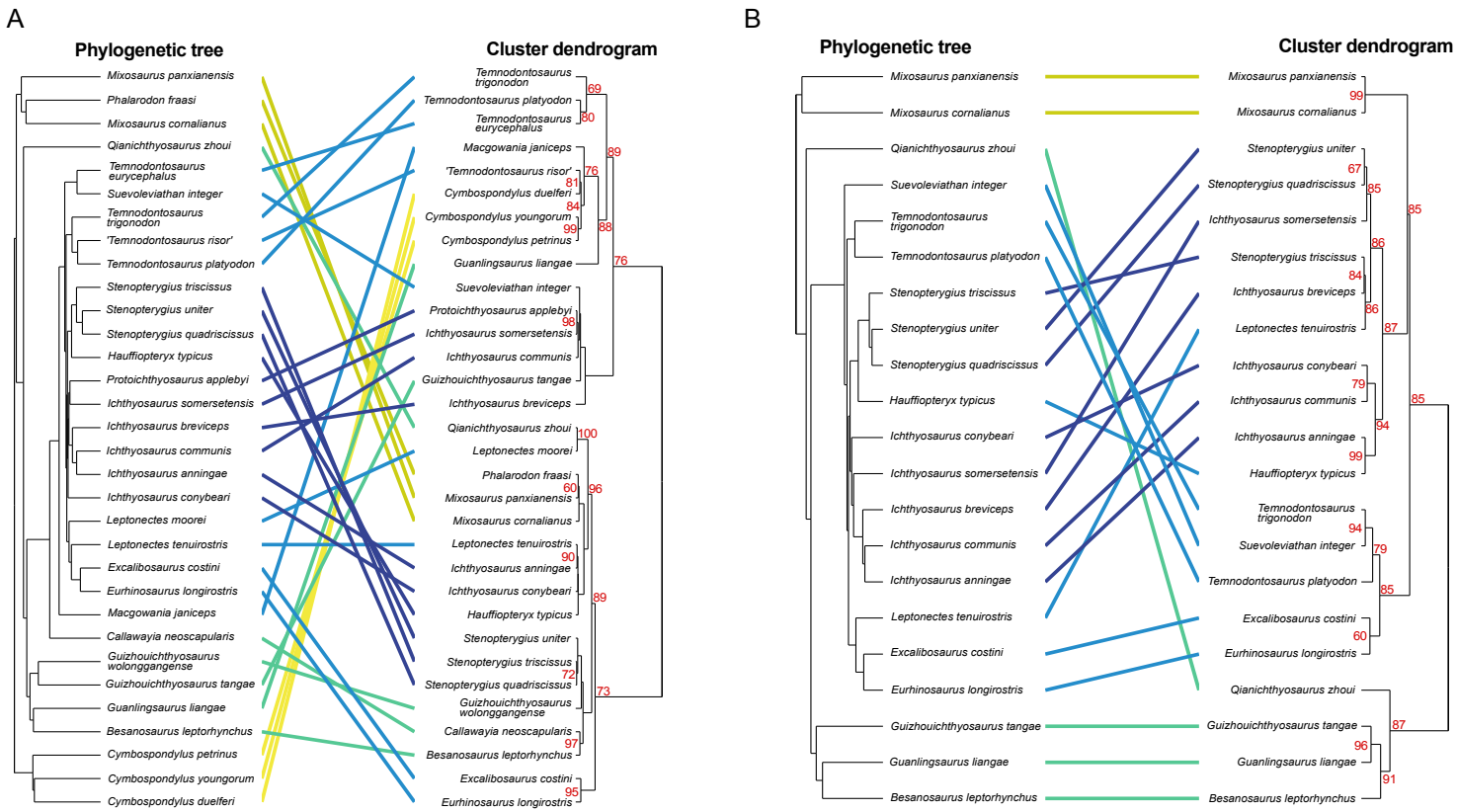

Figure S2.12. Ichthyosaurian tanglegram comparing the phylogeny with the hierarchy of a cluster dendrogram generated with with (A) the craniodental and (B) the postcranial data. Each line is coloured with respect to its relative group (yellow: cymbospondylids, light green: mixosaurids, green: non-parvipelvian merriamosaurians, blue: early parvipelvians, dark blue: thunnosaurians). The phylogenetic tree has been generated in Maximum Parsimony framework under implied weighting (*k*=12). Only taxa present in the ecomorphological dataset were kept. Nodal support values (approximate unbiased p-value in percentage) are indicated at their corresponding nodes on the cluster dendrogram. Mantel test result (p-value = 0.48) does not indicate a strong correlation between the phylogenetic relationships and the hierarchy of the cluster dendrogram.

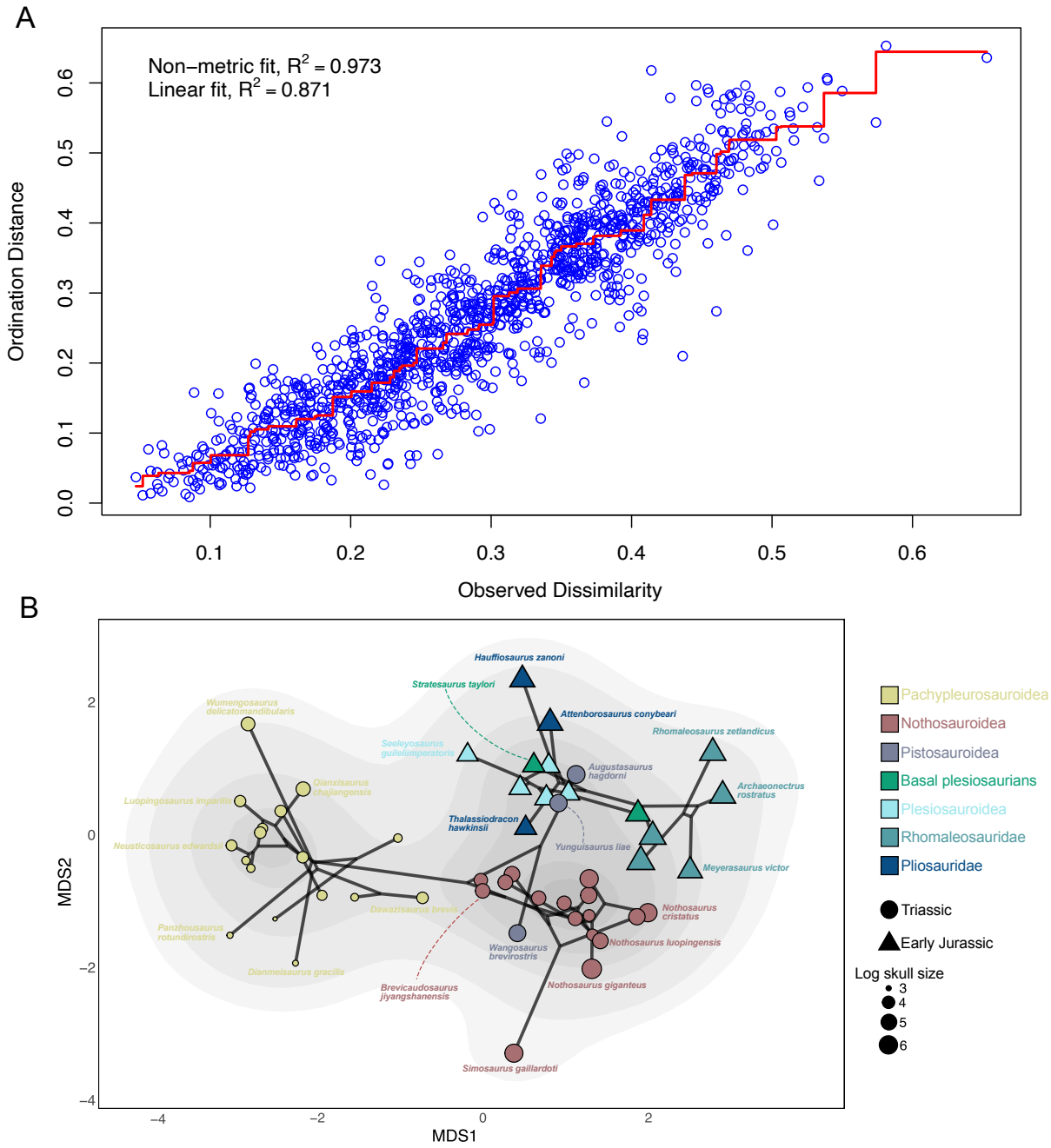

Figure S2.13. Eosauropterygian craniodental NMDS results. (A) stress plot , showing the relationship between the dissimilarities between taxa present in the craniodental dissimilarity matrix and the ordination on the NMDS morphospace (maximum number of random starts = 100). (B) phylo-ecomorphospace occupation computed by using NMDS (dimension=2) and composite phylogenetic tree based on the phylogenetic analyses of Hu et al. (2024) and Wintrich et al. (2017). The phylo-ecomorphospace is superimposed on the density of taxa. Point sizes are scaled to the skull size of taxa (log skull size).

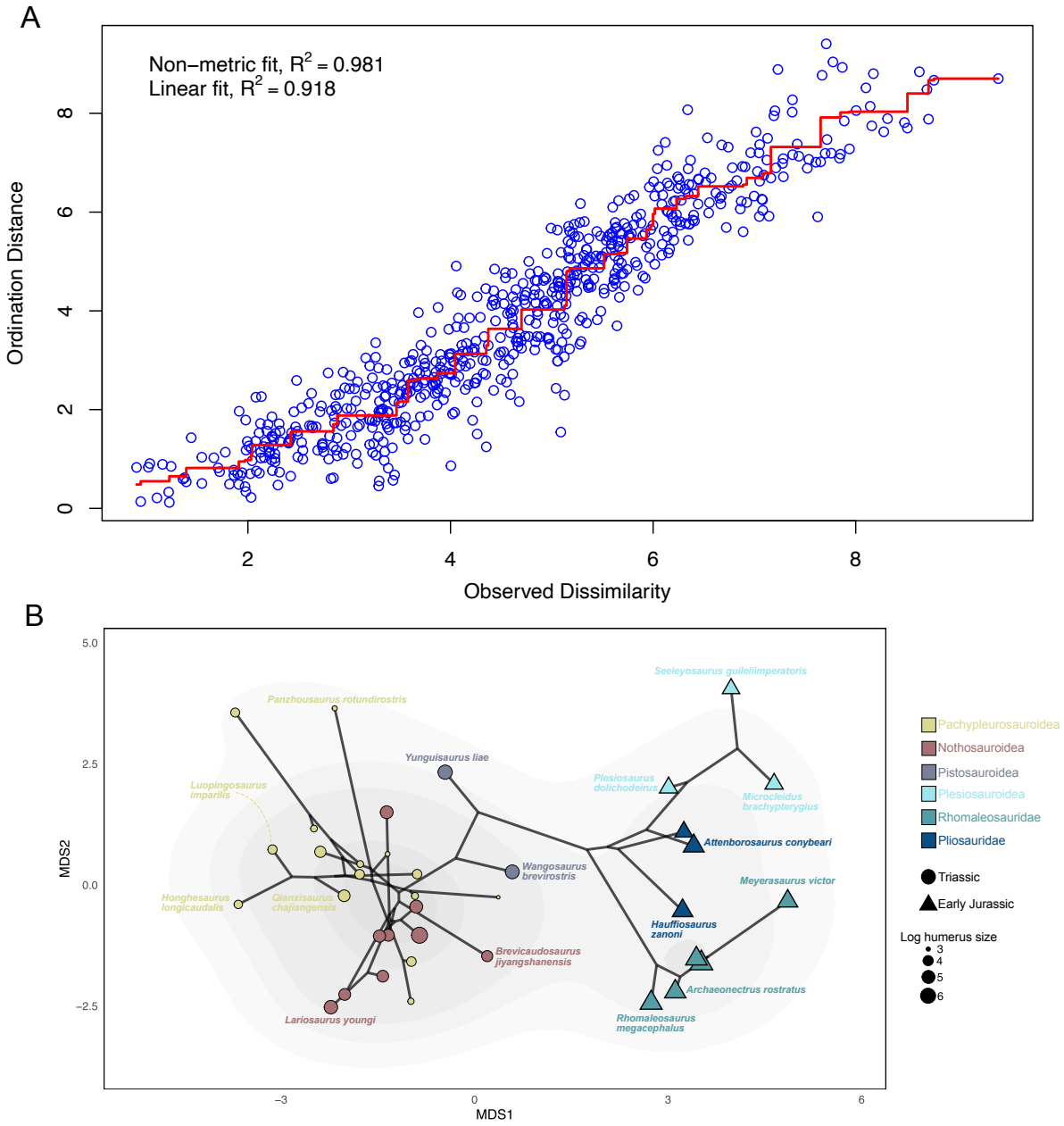

Figure S2.14. Eosauropterygian postcranial NMDS results. (A) stress plot, showing the relationship between the dissimilarities between taxa present in the postcranial dissimilarity matrix and the ordination on the NMDS morphospace (maximum number of random starts = 100). (B) phylo-ecomorphospace occupation computed by using NMDS (dimension=2) and composite phylogenetic tree based on the phylogenetic analyses of Hu et al. (2024) and Wintrich et al. (2017). The phylo-ecomorphospace is superimposed on the density of taxa. Point sizes are scaled to the skull size of taxa (log skull size).

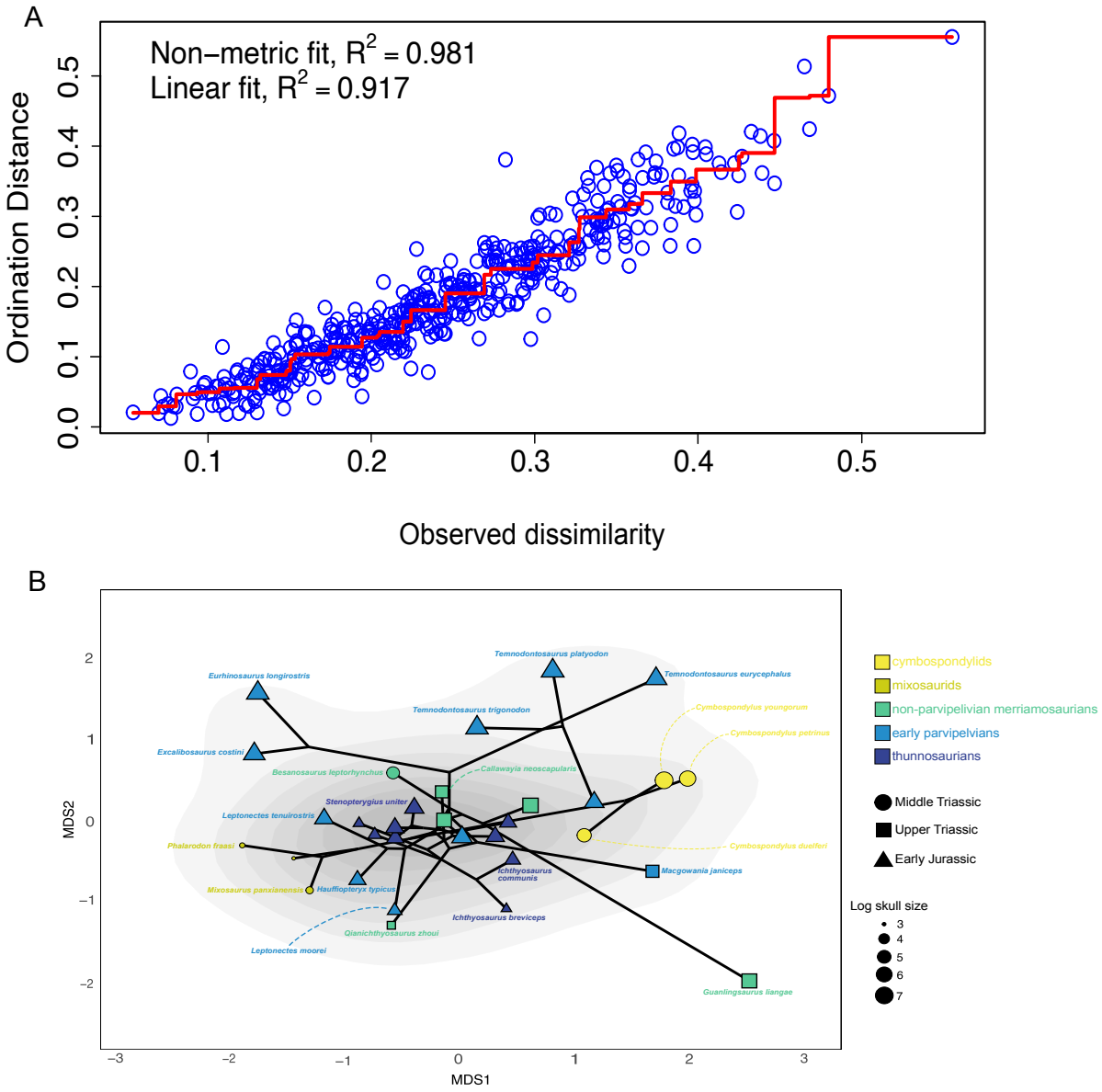

Figure S2.15. Ichthyosaurian craniodental NMDS results. (A) stress plot , showing the relationship between the dissimilarities between taxa present in the craniodental dissimilarity matrix and the ordination on the NMDS morphospace (maximum number of random starts = 100). (B) phylo-ecomorphospace occupation computed by using NMDS (dimension=2). The phylo-ecomorphospace is superimposed on the density of taxa. Point sizes are scaled to the skull size of taxa (log skull size).

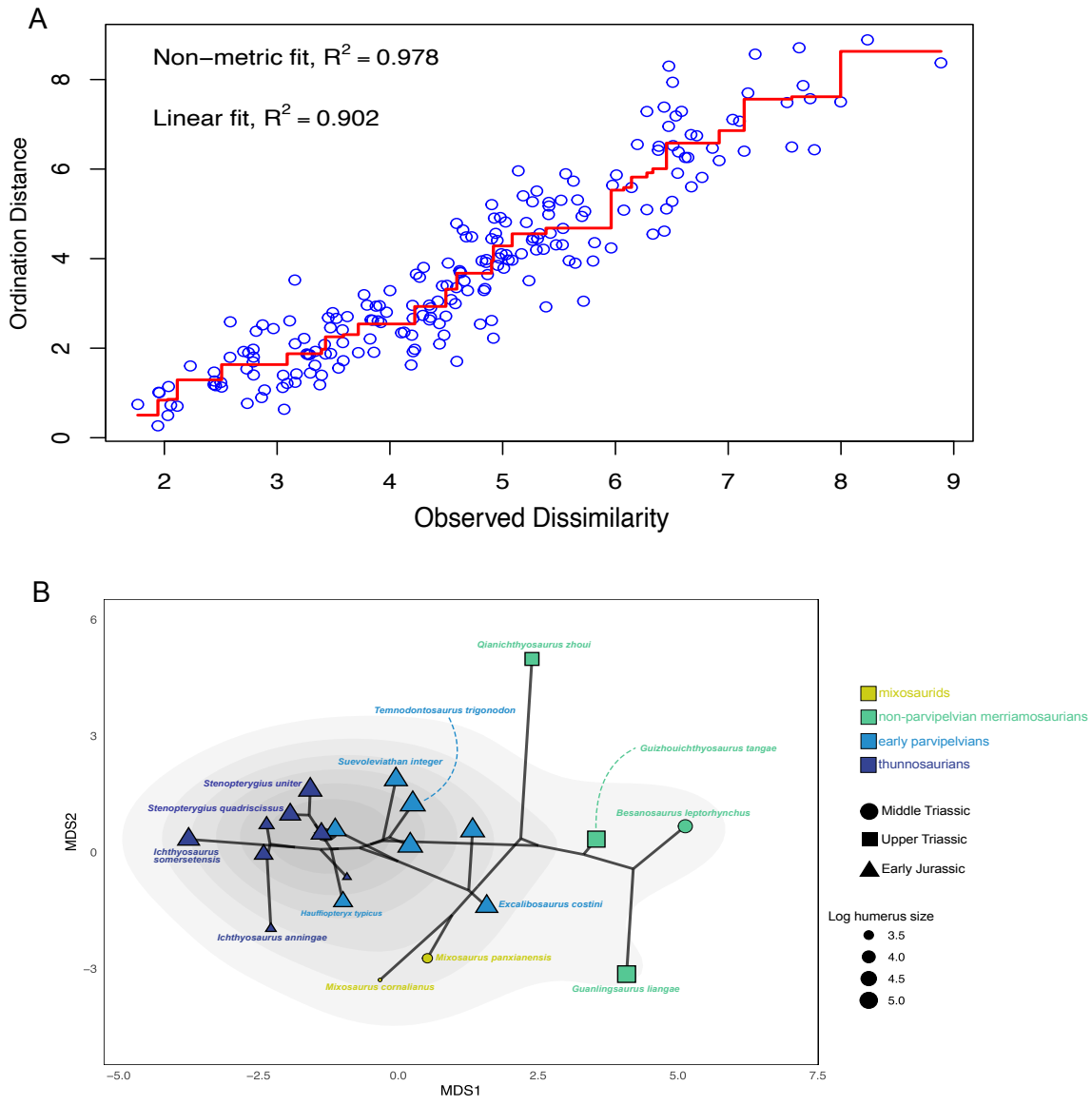

Figure S2.16. Ichthyosaurian postcranial NMDS results. (A) stress plot , showing the relationship between the dissimilarities between taxa present in the postcranial dissimilarity matrix and the ordination on the NMDS morphospace (maximum number of random starts = 100). (B) phylo-ecomorphospace occupation computed by using NMDS (dimension=2). The phylo-ecomorphospace is superimposed on the density of taxa. Point sizes are scaled to the skull size of taxa (log skull size).

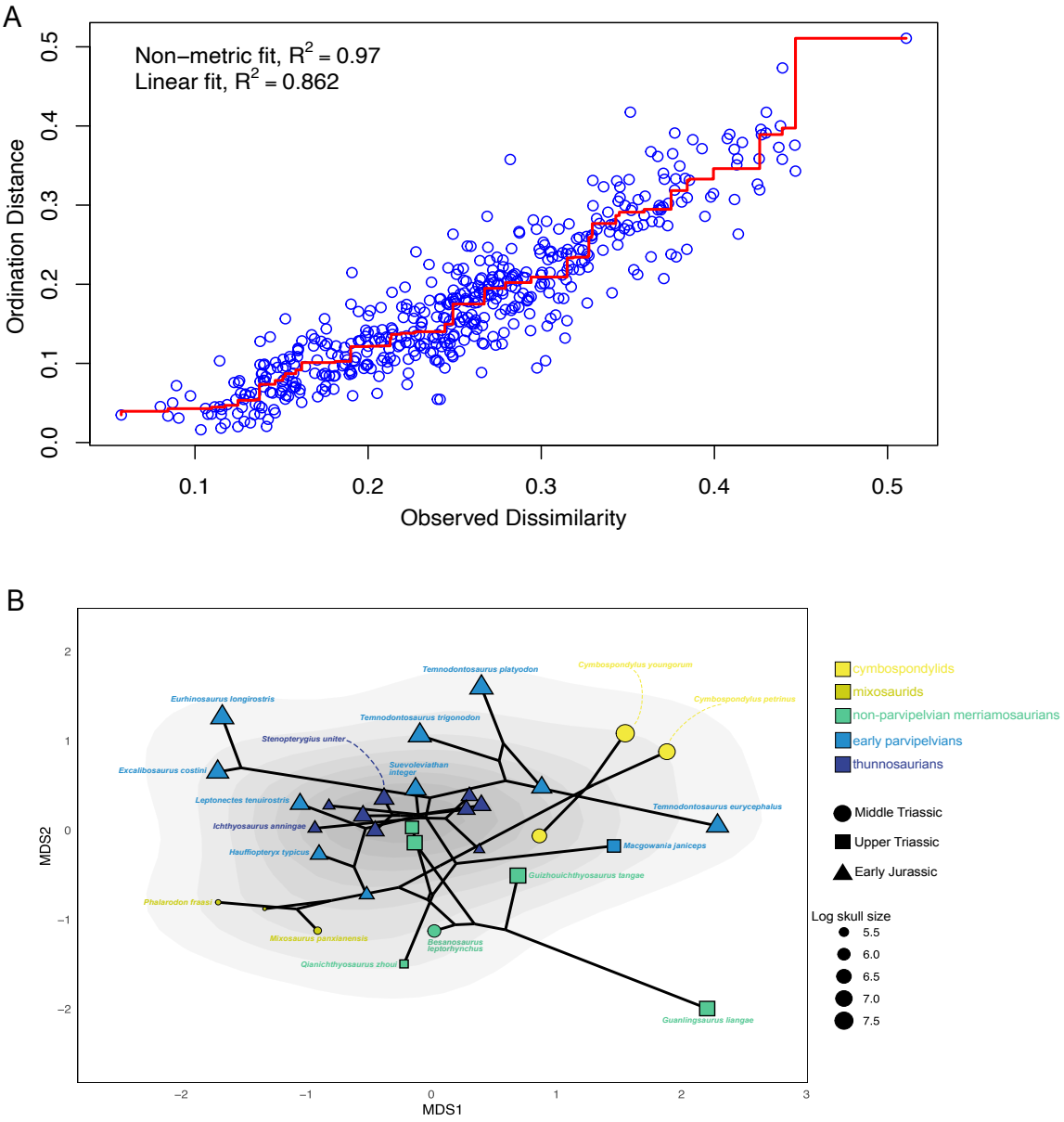

Figure S2.17. Ichthyosaurian whole-body NMDS results. (A) stress plot , showing the relationship between the dissimilarities between taxa present in the whole-body dissimilarity matrix and the ordination on the NMDS morphospace (maximum number of random starts = 100). (B) phylo-ecomorphospace occupation computed by using NMDS (dimension=2). The phylo-ecomorphospace is superimposed on the density of taxa. Point sizes are scaled to the skull size of taxa (log skull size).

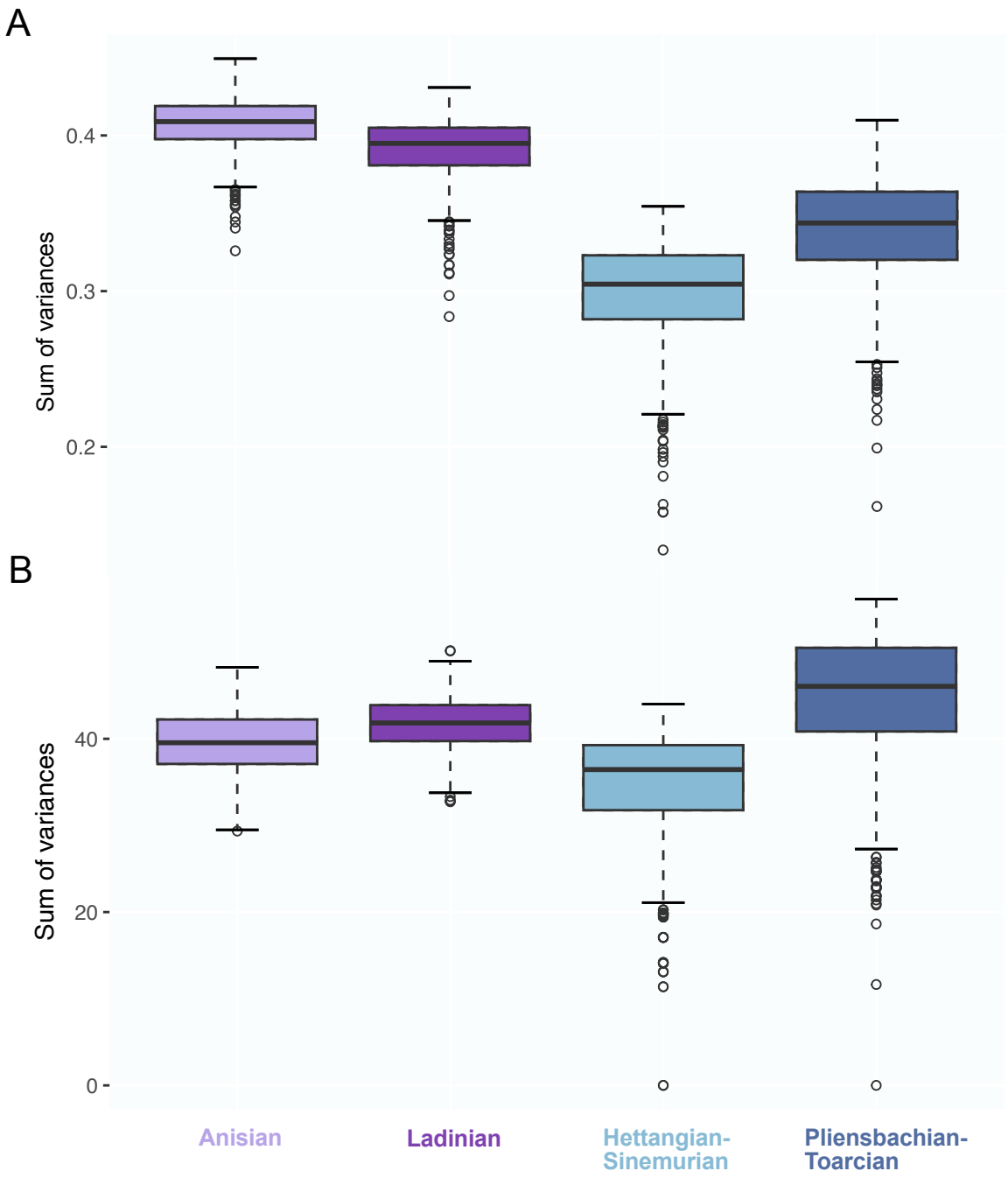

Figure S2.18. Comparison of eosauropterygian temporal disparity distribution generated with the (A) the craniodental and (B) the postcranial ecomorphological datasets. We used the sum of variances metric and 1000 bootstraps replications. As the occurrence of Middle Triassic taxa is well known and sufficiently precise, we treated Anisian and Ladinian as two distinctive time intervals. The disparity distribution of the interval Carnian-Norian can't be calculated as only one taxon is included (e.g., *Nothosaurus giganteus*).

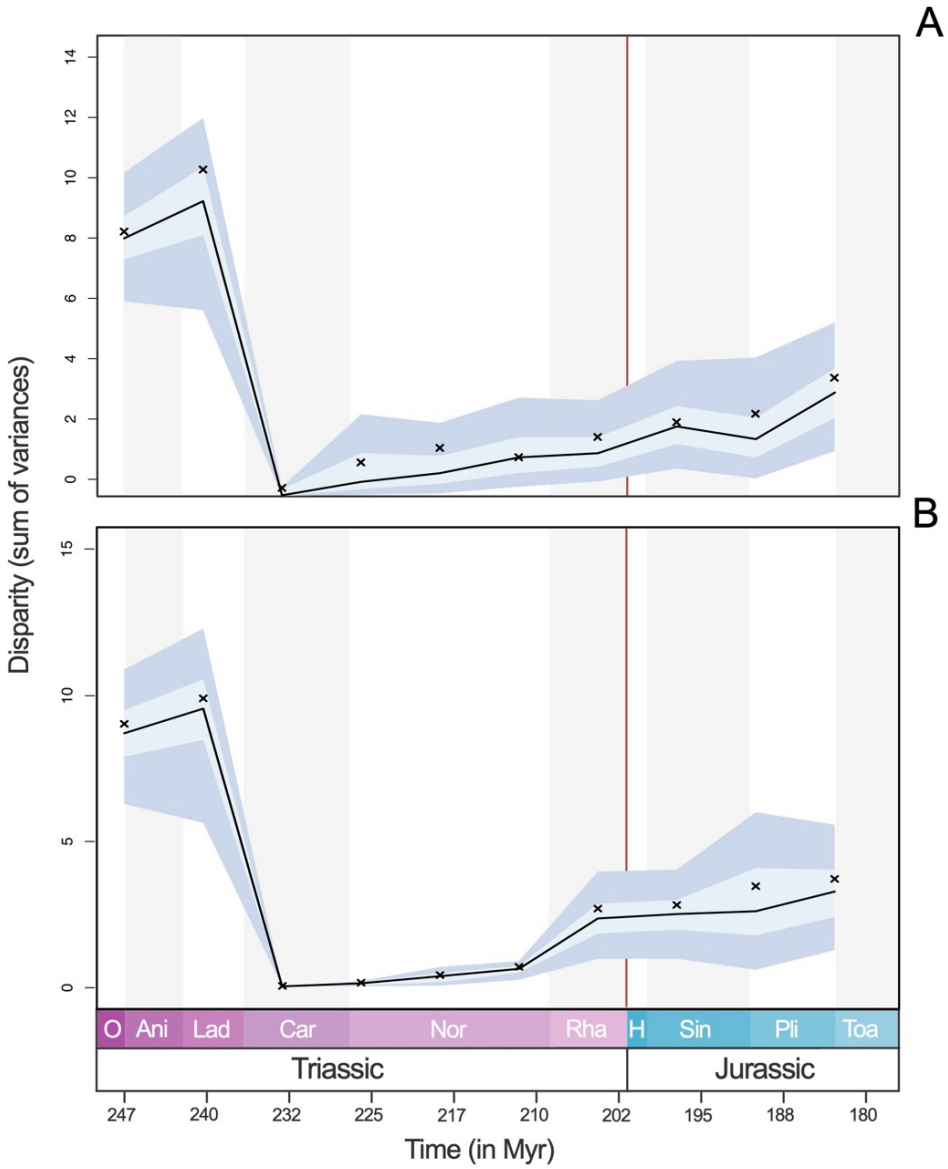

Figure S2.19. Eosauropterygian disparity through time during the Triassic–Lower Jurassic interval. Disparity has been calculated with the time-slicing approach (see Material and Methods) by using scores of tips and nodes present in the phylomorphospace computed with all morphological data and based on the phylogenetic analyses of Hu et al. (2024) and Wintrich et al. (2017). The phylogenetic tree is timescaled by using the Hedman method. Disparity have been calculated at 10 equidistant time under (A) 'equal splits' and (B) 'proximity' models of evolution. The 'equal splits' probabilistic model assigns the ordination score, with an equal probability, from both the ancestor and the descendant while the 'proximity' model selects the ordination of the ancestral node or the tips depending on which part of the branch the time-slice occurs. Light blue and blue envelopes represent respectively 95% and 50% confidence intervals based on 1000 bootstrap replicates. Red line indicates the Triassic-Jurassic transition and crosses indicate the observed disparity.

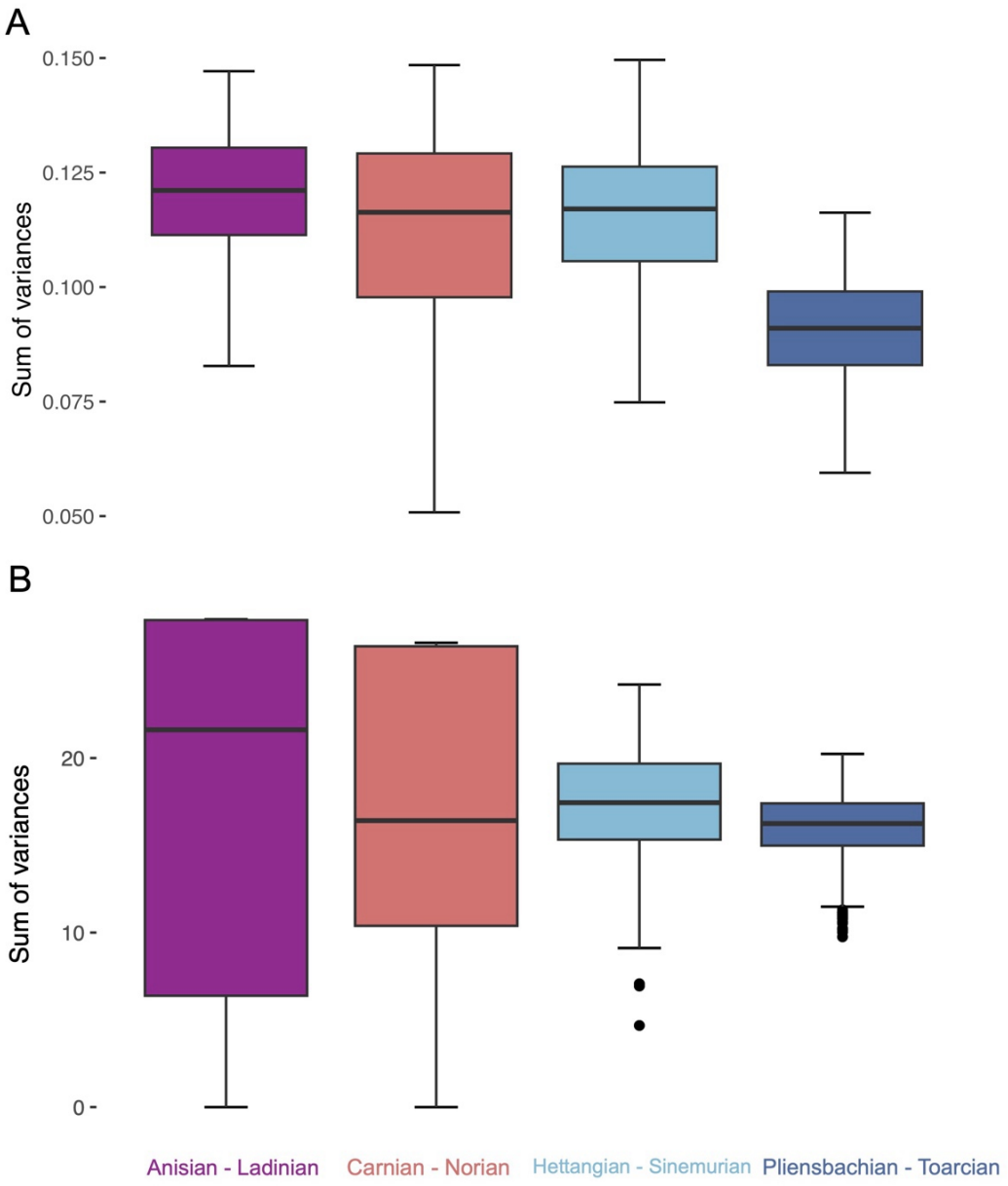

Figure S2.20. Comparison of ichthyosaurian temporal disparity distribution generated with the (A) the craniodental and (B) the postcranial ecomorphological datasets. We used the sum of variances metric and 1000 bootstraps replications. We used the sum of variances metric and 1000 bootstraps replications. The postcranial disparity distributions (B) of Triassic time intervals (Anisian–Ladinian and Carian–Norian) should be carefully interpreted due to a poor and incomplete sampling as they both only contain three taxa.

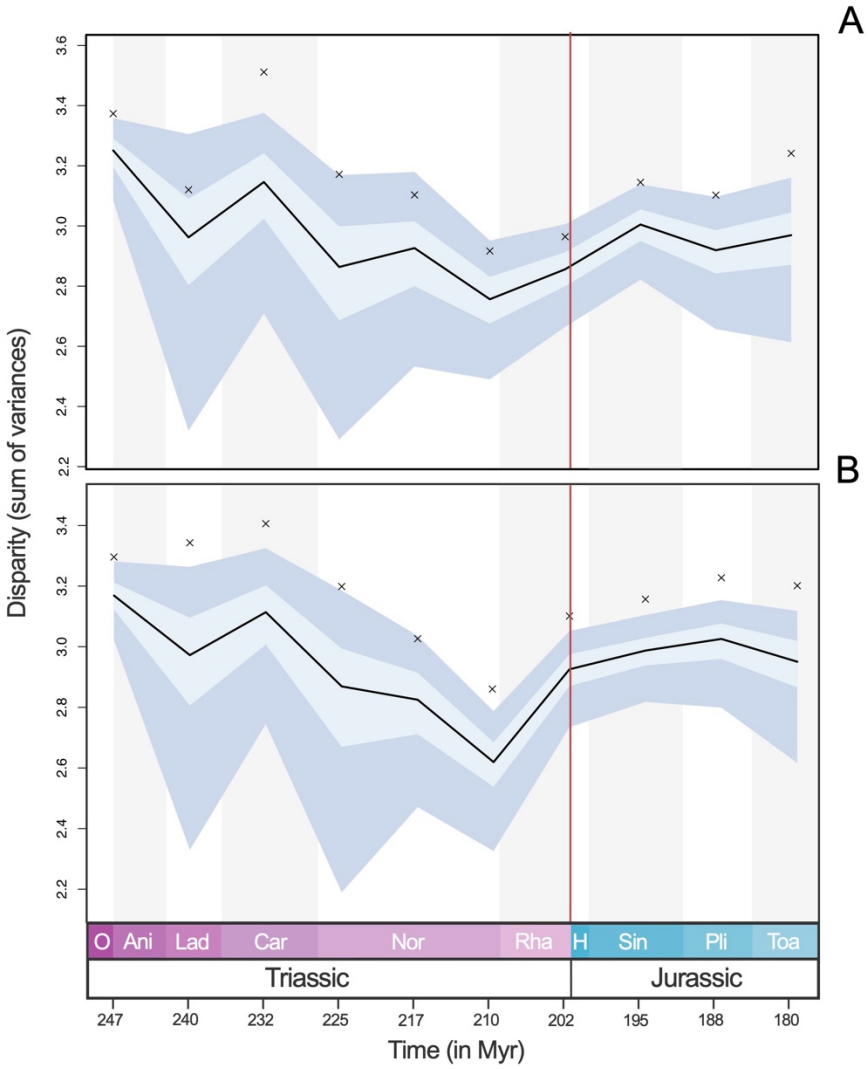

Figure S2.21. Ichthyosaurian disparity through time during the Triassic–Early Jurassic interval. Disparity has been computed by using the modified character-taxon matrix of Laboury et al. (2022) by using the Hedman-dated tree and the time-slicing approach (see Material and Methods). Disparity have been calculated at 10 equidistant time slices under (a) 'equal splits' and (b) 'proximity' models of evolution. The 'equal splits' probabilistic model assigns the ordination score, with an equal probability, from both the ancestor and the descendant while the 'proximity' model selects the ordination of the ancestral node or the tips depending on which part of the branch the time-slice occurs. Light blue and blue envelopes represent respectively 95% and 50% confidence intervals based on 1000 bootstrap replicates. Red line indicates the Triassic–Jurassic transition and crosses indicate the observed disparity.

CHAPTER 3: EXTINCTION SELECTIVITY OF TOP MARINE PREDATORS ACROSS THE TRIASSIC–JURASSIC TRANSITION

Laboury, A., T. L. Stubbs, T. M. Scheyer, V. Fischer. Formatted.

ABSTRACT

The harsh environmental conditions of the Late Triassic profoundly shaped the evolution of marine reptiles and, more globally, the structure of Mesozoic marine ecosystems. This period notably corresponds to the eradication of the 'typical' Triassic faunas along the following rise of pelagic parvipelvian ichthyosaurians and plesiosaurian eosauropterygians which subsequently populated the oceans for million years. Although our perception on diversification dynamics among ichthyosaurians and eosauropterygians has recently been improved, the role of phylogenetic signal and life traits in extinction risk during that period remains unexplored. We therefore evaluate the phylogenetic clustering and the intensity of extinctions affecting ichthyosaurians and eosauropterygians across the Middle Triassic–Early Jurassic time interval, while also investigating the correlation between extinction vulnerability. Our analyses employed as a framework a composite phylogenetic supertree regrouping Ichthyosauria and Eosauropterygia, calibrated with a variety of time-scaling methods. We reveal a phylogenetic signal in extinction across our time-dated phylogenies, with no significant influence of body size. Additionally, selectivity and severity of extinctions appear to be strongly correlated, indicating that greater extinction events predominantly affected more closely related species across the phylogeny during the investigated time interval. The Middle to Late Triassic transition is characterized by severe and highly selective extinctions, reflecting the substantial shift from coastal to pelagic marine reptile assemblages. While extinction pressures may not have favoured specific body sizes, the end-Triassic events still led to the eradication of whale-sized shastasaurids, suggesting greater vulnerability among larger-bodied taxa.

Authors' contributions: AL, VF, TLS,TMS conceived and designed the study. AL collected the data, performed the analyses, wrote the code with the inputs from VF and TLS, prepared all and wrote the draft of the manuscript, with contribution of all authors.

INTRODUCTION

Temporally bounded by the largest mass extinction of all times — the Permian–Triassic mass extinction (PTME: 251.9 Ma) — and a complex yet severe biological crisis culminating at the Triassic–Jurassic transition (ETME: ~201.3 Ma) (Raup and Sepkoski 1982; Bambach 2006; Alroy 2010), the Triassic saw the development of a unique biosphere, with a menagerie of unusual amniotes (Andres 2012; Benson 2013; Benton et al. 2013, 2014; Ruta et al. 2013; Neenan et al. 2015; Chun et al. 2016; Ezcurra and Butler 2018; Sulej and Niedźwiedzki 2019). In marine ecosystems, the recovery from the catastrophic PTME started during the Early Triassic and was largely achieved by the end of the Anisian (early Middle Triassic) (Song et al. 2011, 2018; Chen and Benton 2012; Benton et al. 2013; Scheyer et al. 2014). This recovery coincided with the onset of the first phase of the 'Mesozoic Marine Revolution' (Vermeij 1977; Salamon et al. 2012) but also with the set-up of complex trophic networks, mainly driven by the rapid phenotypic diversification of reptiles that had recently invaded marine habitats (Chen and Benton 2012; Liu et al. 2014; Scheyer et al. 2014; Huang et al. 2020; Moon and Stubbs 2020; Reeves et al. 2021; Sander et al. 2021; Wang et al. 2022; Laboury et al. 2023). In such a context, the Middle Triassic, and to a certain extent, the early Carnian (early Late Triassic), can be considered as a prolific period in terms of faunistic richness and biotic interactions in the seas (Benton et al. 2013). However, the Late Triassic was characterized by various drastic environmental changes, primarily caused by sea-levels fluctuations and volcanism activities, climaxing with the ETME (Ruhl et al. 2011; Kelley et al. 2014; Dunhill et al. 2018; Dal Corso et al. 2020; Schoepfer et al. 2022; Bond et al. 2023; Rigo et al. 2024). These abiotic disruptions greatly affected marine communities, although the ecological severity of the ETME may not have been as extreme and temporally constrained as once thought (Dunhill et al. 2018; Cribb et al. 2023). This period indeed also represents a time of significant faunal turnovers with radiations that were already initiated by the Mesozoic Marine Revolution (Dunhill et al. 2018; Dal Corso et al. 2020) (Dal Corso et al., 2020; Dunhill et al., 2018).

Marine reptiles, which have occupied upper levels of trophic webs during this period, likely suffered from the harsh environmental upheavals that took place during the Late Triassic. The emerging consensus is that major extinctions were not concentrated at the very end of the Triassic but rather occurred throughout the Late Triassic, notably during the Carnian, which was marked by rapid sea-level declines (Bardet 1994; Benson and Butler 2011; Kelley et al. 2014; Renesto and Dalla Vecchia 2018; Laboury et al. 2024;

Chapter 2). These extinctions events nearly eradicated all ‘typically Triassic’ forms adapted to nearshore environments, which had previously colonized numerous ecological niches: the mixosaurids, pachypleurosauroids, nothosauroids, most of placodonts (Stubbs and Benton 2016; Reeves et al. 2021; Sander et al. 2021; Gutarra et al. 2023; Laboury et al. 2023; Chapter 1), with the exception of thalattosaurs that persisted until the end of the Rhaetian (Bastiaans 2024 and references therein). Ichthyosauria and Eosauropterygia (*i.e*. Sauropterygia excluding the durophagous placodonts) were the only clades of marine reptiles that survived these events — not without extinctions — and crossed the Triassic–Jurassic (T/J) boundary (Motani 2009; Benson et al. 2010; Bardet et al. 2014; Laboury et al. 2024). Their survival is however coupled with an important turnover, leading to the diversification of taxa well-adapted to an open-ocean lifestyle: the fusiform parvipelvian ichthyosaurians and ‘underwater-flier’ plesiosaurian eosauropterygians (Motani 2009; Benson et al. 2010; Bardet et al. 2014). These fully pelagic animals appeared taxonomically and morphologically diverse by the earliest Jurassic, suggesting a pre-ETME radiation (Benson et al. 2012; Fischer et al. 2013; Motani et al. 2017; Wintrich et al. 2017; Laboury et al. 2022, 2024; Chapter 2).

The Late Triassic represents therefore a critical period in the evolutionary history of Ichthyosauria and Eosauropterygia, setting up the dominance of pelagic forms which became key predators during the rest of the Mesozoic (Motani 2009; Bardet et al. 2014). Despite recent research on their diversification dynamics across the T/J transition (Thorne et al. 2011; Dick and Maxwell 2015; Stubbs and Benton 2016; Moon and Stubbs 2020; Reeves et al. 2021; Laboury et al. 2024; Chapter 2), the role of phylogenetic signal in extinction selectivity during that period remains largely unexplored. This latter assumes that extinction events are not randomly distributed across phylogeny but are rather influenced by processes acting on phylogenetically conserved traits within clades (Bennett and Owens 1997; McKinney 1997; Purvis et al. 2005; Purvis 2008; Hardy et al. 2012; Allen et al. 2019). Studies on extinction selectivity using paleontological data have primarily investigated correlations between extinction risk and specific traits such as body or geographic range sizes (Friedman 2009; Hardy et al. 2012; Tomiya 2013; Harnik et al. 2014; Puttick et al. 2017; Allen et al. 2019). Body size is particularly relevant, as it encompasses wide-ranging ecological implications (Peters 1983). However, this trait has not shown strong correlation with extinction risk when analysing fossil data (Jablonski and Raup 1995; Friedman 2009; Tomiya 2013; Puttick et al. 2017; Allen et al. 2019). Body size significantly varied in early ichthyosaurians and eosauropterygians (Liu et al. 2014; Moon and Stubbs 2020; Sander et al. 2021), but Late Triassic events likely influenced this

trait, particularly in ichthyosaurians (*e.g.* see Chapter 2). Most notably, the gigantic shastasaurids, present in the fossil record since the Carnian (Merriam 1908; Camp 1980; Kelley et al. 2022; Zverkov et al. 2022), met their demise at or very close to the T/J transition (Fischer et al. 2014b; Lomax et al. 2018a, 2024; Sander et al. 2022) in favour of the smaller primitive parvipelvians (McGowan 1997) (McGowan 1997; Fischer et al. 2014b; Laboury et al. 2024; Lomax et al. 2024). Jurassic and Cretaceous ichthyosaurians never reached comparable extreme sizes again (Moon and Stubbs 2020; Sander et al. 2021; Gutarra et al. 2023), suggesting that these extinction events completely wiped out such body sizes (Fischer et al. 2014b; Lomax et al. 2018a, 2024; Laboury et al. 2024; Chapter 2). A similar trend is difficult to observe in eosauropterygians due to the scarcity of their fossil record in the Late Triassic (Laboury et al. 2024; Chapter 2). We nonetheless know that regression events in the Carnian likely led to the extinctions of large-sized nothosaurians (Rieppel and Wild 1996; Dalla Vecchia and Avanzini 2002) and that earliest Jurassic plesiosaurians were small-bodied (Benson et al. 2012).

In the present chapter, we assess the degree of phylogenetic clustering and body size selectivity in ichthyosaurians and eosauropterygians extinctions, from the Middle Triassic to the early Jurassic. Our findings thus aims to reveal an unexplored facet of the impact of Late Triassic events on the macroevolution of these two iconic marine reptiles clades.

MATERIAL AND METHODS

Phylogenetic framework

As our analyses require a phylogenetic framework, we created an informal composite tree grouping both ichthyosaurians and eosauropterygians (see **Figure 21**). The recently published matrix of Laboury et al. (2022), a revised version of the dataset of Moon (2017) which aims to reconstruct overall ichthyosaurian phylogeny, seems suitable for our analyses due to its extensive taxonomic sampling. Although relationships of parvipelvians have been extensively analysed with updated versions of Moon's (2017) matrix (*e.g.* see Maxwell and Cortés 2020; Laboury et al. 2022; Miedema et al. 2024), the relevance of this latter in analysing phylogenetic relationships of Triassic taxa has been questioned (*e.g.* see Bindellini et al. 2021). Indeed, Moon (2017) primarily scored post-Triassic species based on personal observation and only three Triassic taxa were examined. Additionally, the revised versions of Moon's (2017) matrix recovered differing relationships among Late Triassic taxa compared to those generated with the cladistic

dataset of Ji et al. (2016) or its updated versions (see Motani et al. 2017; Huang et al. 2019; Bindellini et al. 2021). These matrices specifically focus on Triassic ichthyosaurians, and the majority of taxa scores are based on first-hand examination (Bindellini et al. 2021). For these reasons, we re-analysed ichthyosaurian phylogenetic relationships by using the cladistic datasets of Bindellini et al. (2021) and Laboury et al. (2022) for Triassic and post-Triassic taxa respectively. The resulting topologies were then combined to create a composite ichthyosaurian phylogenetic tree. As already mentioned by Laboury et al. (2024), a comprehensive cladistic dataset combining Triassic and post-Triassic eosauropterygians (both non-plesiosaurians and plesiosaurians) has yet to be created. Then, we constructed a composite phylogenetic tree based on the topologies generated with the recent datasets of Hu et al. (2024) and Sachs et al. (2024) for Triassic and post-Triassic taxa respectively.

All cladistic datasets were re-analysed in TNT (v1.6) (Goloboff et al. 2023) in a maximum parsimony framework by using the implied weighting method which provides superior results in a maximum parsimony context (Goloboff et al. 2018; Smith 2019). This method reduces the influence of homoplasy, proportionally to the value of the concavity constant *k*; lowering its value implies increasing the penalty applied to homoplastic characters. All most parsimonious trees were generated with *k*=12, but we tested the influence of different character weighting strategies with *k*=6, and *k*=9. The maximum number of trees was set to 100,000 and we used the New Technology Search (ratchet activated: 200 iterations; drift activated: 10 cycles; 5 hits and 10 trees per replication) followed by a tree bisection-reconnection (TBR) algorithm applied on trees recovered by the ratchet to fully explore islands of most parsimonious topologies.

Several important Triassic ichthyosaurians and eosauropterygians were not incorporated in the phylogenetic matrices we used. We manually grafted these taxa on the informal composite tree within the R statistical environment (v.4.4.1) (R Core Team 2023), based on information from literature (the complete list of taxa and information can be found in supplements for chapter 3). Our analyses of extinction selectivity during the Norian and the Rhaetian may somewhat be biased by the poor fossil record of these period, marked by the absence of well-established species (Benson et al. 2010; Bardet et al. 2014; Sander et al. 2022). Most of the material described is fragmentary, making genus- or species-level identification and inclusion in phylogenetic analyses challenging. A certain diversity of large to gigantic shastasaurid ichthyosaurians from these two stages is presumed, as suggested by a series of incomplete and undiagnostic specimens exhibiting distinctive morphological features (*e.g.* estimated body-size, tooth-bearing or

edentulous mandibles)(Dong 1972; Nicholls and Manabe 2004; Druckenmiller et al. 2014; Fischer et al. 2014b; Lomax et al. 2018a, 2024; Sander et al. 2022). To incorporate this information and mitigate biases associated with the scarcity of the latest Triassic fossil record, we included two additional taxa from the Norian or the Rhaetian stages for which a shastasaurid affinity has been strongly suspected(Motani et al. 1999; Lomax et al. 2024) in our composite tree. The first taxon is the poorly known *Himalayasaurus*, found in the early Norian of Tibet and characterized by the presence large cutting-edge teeth (Dong 1972; Motani et al. 1999; Meng et al. 2019). Direct comparison with the only well-defined shastasaurid from the Norian, the gigantic, likely edentulous *Shonisaurus sikanniensis* (Nicholls and Manabe 2004), likely led the recognition of *H. tibetensis* as a distinct taxon. Numerous highly fragmented shastasaurid-like specimens have been found in the Rhaetian of Europe (Fischer et al. 2014b; Sander et al. 2022), but only *Ichthyotitan severnensis* has been erected as a new genus and species (Lomax et al. 2024). This taxon, represented by two fragmentary but remarkably massive surangulars, is estimated as one of the largest-bodied ichthyosaurians known to date (Lomax et al. 2024). We therefore decided to use *I. severnensis* as the second taxon to represent (even partially) the presence of giant shastasaurids in the Rhaetian. Due to the uncertain phylogenetic placement of *H. tibetensis* and *I. severnensis*, we performed 100 random resolutions of a polytomy that had been initially formulated to include nearly all shastasaurids minus the primitive species *Besanosaurus leptorhynchus* (*e.g.* see Bindellini et al. 2021, 2024; Laboury et al. 2022), as well as these two fragmentary Late Triassic shastasaurids. Poorly preserved plesiosaurian remains have also been reported in the Norian (Sennikov and Arkhangelsky 2010). However, due to taxonomic uncertain taxonomic affinity of this specimen, it was not included in our informal composite tree; the only Triassic plesiosaurian in our dataset is thus the Rhaetian species *Rhaeticosaurus mertensi* (Wintrich et al. 2017). 50% Majority rule consensus trees generated with each dataset can be viewed in supplements for chapter 3 (**Figures S3.1–S3.4**).

Tree time-scaling methods

Temporal ranges of each OTU were collected in the literature and in the Paleobiology Database (PBDB). The resulting dataset is resolved at geological stage level; the only exception being the Norian which was divided into ‘early–middle Norian’ and ‘late Norian’ due to its considerable length — 19.5 Myr in duration (Cohen et al. 2013). Phylogeny-based evolutionary analyses are sensitive to tree-scaling methods due to variations in estimating the timing of branching events (Bapst 2014; Lloyd 2016; Soul and Friedman 2017; Allen et al. 2019). To minimize biases related to the choice of a unique *post hoc*

time-scaling approach, branch lengths and node positions were estimated in our composite tree by using the well-known Equal (Brusatte et al. 2008) and Minimum Branch Length (MBL) (Bapst 2012) methods, but also likelihood-based Hedman (Hedman 2010) and Cal3 (Bapst 2013) algorithms. All time-scaling and subsequent analyses were performed in the R statistical environment (v.4.4.1) (R Core Team 2023). The Hedman method constraints the age of a specific node, using the ages of the consecutive older clades which therefore act as the node outgroup, in a Bayesian framework (Bapst 2013; Lloyd 2016). Hedman time-scaling analyses were performed by using the R script provided by Lloyd et al. (2016). The Cal3 approach constraints internal node positions based on fossil occurrences and branch lengths are estimated according to speciation, extinction and sampling distributions inferred from occurrence data (Bapst 2013).

We computed 100 replications of each time-scaling method, and a precise age was randomly assigned to all taxa, based on a uniform distribution within their corresponding age ranges. Only the age of *Corosaurus* was set as a fixpoint (249.2 Ma, mid-Olenekian) to allow the calculation of taxon absolute ages and thus the calibration of the replications. As in time-scaling analyses of Puttick et al. (2017) and Allen et al. (2019), our cal3-dated trees contain several zero-length branches and were removed from our further macroevolutionary analyses which were thus only performed with Equal, MBL and Hedman time-scaled trees. Examples of time-scaled composite supertrees using Equal, MBL and Hedman methods can be viewed in supplements for chapter 3 (**Figures S3.5–S3.7**).

Taxa collection of body size data

We gathered morphological data to evaluate the correlation between body sizes and extinction risk on 187 ichthyosaurians and eosauropterygians spanning from the Triassic to the Cretaceous (see supplements for chapter 3). Species from the post-Early Jurassic period were selected based on the criterion that the origin of their respective clades falls within the temporal range of our study (Middle Triassic to Early Jurassic). Total body size (length from the anterior tip of the snout to the posterior extremity of the last caudal centrum) was measured on completely preserved specimens. For species that are only represented by fragmentary fossils, their overall body sizes were estimated by using the linear regressions based on the length of the humerus for ichthyosaurians (see supplements for chapter 3, **figure S3.2**, equation provided by Scheyer et al. [2014]) and of the last four dorsal vertebrae for eosauropterygians (see supplements for chapter 3, **figure S3.3**, equation provided by Li and Liu [2020]). When the body size of a taxon was

measured or estimated from multiple specimens, the mean value was calculated. All values were log10 transformed before subsequent correlation analyses. Data were collected through first-hand observation of specimens and on high precision three-dimensional structured light models (digitized with an Artec Eva scanner, at a resolution of ≈0.5mm) using MeshLab v2023.12 (Cignoni et al. 2008). Furthermore, we also populated our morphological dataset by adding measurements from first-hand photographs and figured specimens from the literature by using ImageJ (v.1.53) (Schneider et al. 2012) or with measurements that were already published. The details of all measurement sources are provided in the supplements for chapter 3.

Additionally, in order to evaluate how proportions of body size categories evolved over time, we discretized body size into six different levels suggested by a univariate distribution of our continuous data (**Figure S3.11**) (0–0.5m (0); 0.5–1m (1); 1–2m (2); 2–6m (3); 6–12m (4); >12m (5)). For highly incomplete taxa, classification in categories was based on estimations mentioned in the literature or on comparisons of their preserved anatomical structures (*e.g.* skulls, limb bones) with close relatives for which body size could be collected or estimated (see supplements for chapter 3, Body size category assignment for ichthyosaurians and eosauropterygians sections).

Selectivity and severity of extinctions

To test whether extinction events through time are clustered or randomly spread across the phylogeny, we used the *D* statistic of Fritz and Purvis (2010). This metric estimates the phylogenetic clustering of a binary trait and is scaled to simulated distributions of evolution under both Brownian motion and random models (Fritz and Purvis 2010). The *D* statistic is calculated by scaling the observed sum of sister-clade differences (SSD) for tip and node values in a given time bin with the mean values of the SSD generated by random and Brownian motion distribution models, according to a certain number of iterations (Fritz and Purvis 2010; Puttick et al. 2017; Soul and Friedman 2017). A *D* value close to 1 indicates a random distribution of the trait while a value close to 0 signifies that this trait is distributed according to a Brownian motion model and therefore clustered (Fritz and Purvis 2010; Puttick et al. 2017; Soul and Friedman 2017). In the present study, the extinction and survival of a taxon or a lineage in a given time bin were treated as a binary trait (0: extinction and 1: survival). A taxon is considered extinct when its last occurrence falls within the time bin, while a taxon/lineage is regarded as having survived if its range extends to the end of the time bin, indicating its presence within that interval and in the subsequent one (Soul and Friedman 2017).

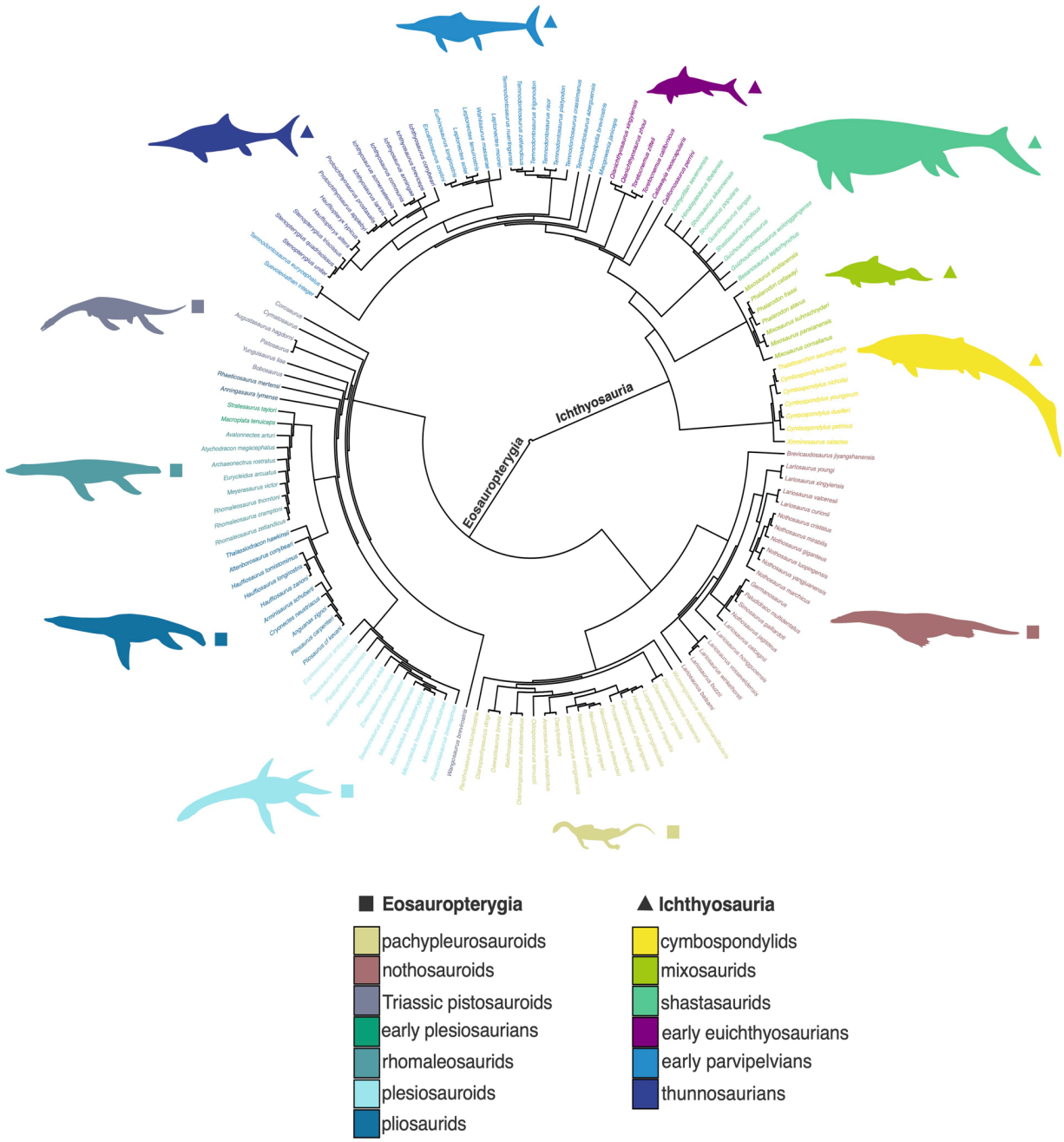

Figure 21. Informal composite supertree of ichthyosaurians and eosauropterygians. This tree illustrates all taxa spanning the Middle Triassic to the Early Jurassic for visualization purposes. All analyses were conducted using the complete dataset, which includes taxa from the Early Triassic to the end of the Cretaceous. Full supertrees incorporating all taxa are provided in supplements for chapter 3 (Figures S3.5–S3.7).

Duration of geological stages within the Middle Triassic–Early Jurassic time interval were chosen as the main time bins. Due to its extended duration, the Norian was divided into two bins (see Material & methods, tree time-scaling method section). Additionally, the 'late Norian' bin was merged with the 'Rhaetian' in order to attenuate the negative effects of the high scarcity of the latest Triassic fossil record on the selectivity analyses. The temporal resolution and the unevenness in length of time bins can have a significant influence on the intensity of the signal (Hardy et al. 2012; Soul and Friedman 2017). To avoid potential biases caused by irregular bins, selectivity analyses were also conducted by using nine equal time intervals (same number of bins than with the use of the geological stages) of 8.12Myr. All results generated with the equal time binning (selectivity and severity of extinction but selectivity of body size; see below) can be found in the supplements for chapter 3 (**Figures S3.8–S3.10;Tables S3.5 and S3.6**) and are mentioned in the Results section.

The *D* statistic was calculated for each time bin in R software with the *caper* package (v1.0.3) (Orme 2012) by using the 100 time-scaled trees generated with the Equal, MBL, and Hedman methods. We also extracted the number of taxa/lineages that survived and taxa that went extinct to compute the severity of extinctions for each time bin. The relation between the extinction selectivity and severity was determined by using a Pearson product–moment correlation test.

Selectivity of body size

Phylogenies could not provide statistically independent data because of the shared ancestry between OTUs. Closely related species are indeed expected to share more similar traits which, in turn, tend to produce more similar residuals from least square regression line (Felsenstein 1985; Symonds and Blomberg 2014). In order to consider the influence evolutionary history in our correlation between extinction and continuous body size data, we used the phylogenetic generalized least square regression (PGLS) by using the *caper* R package (v1.0.3) (Orme 2012). The Pagel's λ (Pagel 1999), a measure that evaluates the extent to which phylogenetic relationships among taxa account for trait variation, was also estimated simultaneously to the other parameters of the PGLS model. A λ value close to 0 signifies that the evolution of the trait is independent from phylogenetic relationships while a value close to 1 implies that this trait covaries in direct proportion to the shared evolutionary history of species (Pagel 1999; Freckleton et al. 2002; Puttick et al. 2017). Because PGLS tests require node values, we estimated ancestral body sizes (for nodes) by a likelihood method simulating a Brownian evolution

(100,000 iterations) with the function anc.ML function of the *phytools* package (v.2.3.0) (Revell 2012). This function allows missing data for some taxa and therefore appears to be the most appropriate as some species in our morphological dataset lack body size values. We computed the PGLS tests for the same time bins and using the same phylogenetic time-scaled trees than for the selectivity of extinction analyses.

RESULTS

Selectivity and severity of extinctions

Although results from extinction selectivity and severity analyses vary depending on the time-scaling methods used, the overall patterns remain consistent across each method (**Table 4; Figures 22 and 23**). Among the three time-scaling strategies we used, *D* values are the globally highest with MBL-dated trees — with the exception of the Anisian, Pliensbachian and Toarcian — intermediate with Equal-dated trees and lowest with Hedman phylogenies (**Table 4**), similar to what was recovered by Puttick et al. (2017) and Allen et al. (2019). Such a pattern implies that MBL trees seem more favourable to a random distribution, while the use of the Hedman phylogenies tends to greater support the clustering of extinction events. Middle and Late Triassic time bins exhibit low values of *D*, indicating that extinctions during these periods rather follow a Brownian motion than being randomly distributed phylogenetically. However, *D* values for the Carnian are associated with high standard deviations (0.195–0.319) and seem to significantly differ between time-scaling method (*e.g.* 0.844 and -0.101 with MBL– and Hedman–dated trees respectively). However, following the methodological recommendations of Soul and Friedman (2017), the Hedman time-scaling method is considered more reliable under conditions of low sampling rates — such as those observed for the Carnian in this study — by minimizing biases associated with poorly sampled intervals. Among all time bins, the 'late Norian–Rhaetian' exhibits the lowest *D* values but also the highest standard deviations, no matter the time-scaling methods (0.288–0.232). This pronounced extinction selectivity primarily stems from the predominance of inferred ghost lineages in time-scaled trees, relative to the limited proportion of taxa directly sampled within the time interval (**Table 4,** but also see **figures S3.5–S3.7**). Highly reduced sampling indeed extends branch lengths by shifting nodes backward in time, as calibration methods lack sufficient data to precisely estimate the timing of branching events. In contrast, the Anisian stage, which is better sampled, has the lowest standard deviations (0.066–

0.087). The distribution of the *D* statistic does not indicate a high clustering of extinctions across the Early Jurassic (**Table 4**; **Figure 22**). Although the Hettangian and Toarcian extinction events are considered selective, the *D* values for the Sinemurian and Pliensbachian approach or exceed 1 no matter the time-scaling method, suggesting random distributions of extinctions.

Great extinction severity is recorded during the Middle Triassic (Anisian and Ladinian) and the Carnian, with the highest rate occurring in the Ladinian (**Table 4**; **Figure 23**). Extinction intensity decreases in the 'early–middle Norian' time bin, reaching levels comparable to those observed in the Early Jurassic. The lowest percentage of extinct lineages occurs in the latest Triassic. Again, the high proportion of ghost lineages within the 'late Norian–Rhaetian' time bin implies artificially high surviving rates, which likely leads to underestimating the extinction severity. Starting from the Hettangian, the magnitude of extinctions gradually decreases until the end of the Pliensbachian, followed by a substantial increase to reach highest extinction rate of the Early Jurassic during the Toarcian. Our Pearson product–moment correlation tests do not evidence any strong relationship between the selectivity and the severity of extinctions when all time bins were used (**Figure 24A**). However, when under-sampled time bins (*e.g.* 'Early–Middle Norian' and 'Late Norian–Rhaetian') are excluded, a strong negative correlation emerges when using Equal and Hedman-dated trees (**Figure 24B**), suggesting that intense extinctions are highly clustered in our time-scaled supertrees.

Analyses of extinctions using equivalent time bins produce overly dispersed *D* statistic and extinction severity distributions for Late Triassic intervals, characterized by extremely high standard deviations, regardless the time-scaling method used (**Tables S3.4 and S3.5; Figures S3.8–S3.10**). Moreover, *D* values significantly differ within these intervals when comparing Hedman–dated trees with Equal and MBL phylogenies, leading to incompatible interpretations of extinction clustering, particularly in time bins 3 (230.96–222.84 Myr) and 4 (222.84–214.71 Myr). Indeed, trees scaled with both Equal and MBL methods suggest a random dispersion of extinctions events while those generated with the Hedman algorithm rather support a strong clustering. Such large variations in results can be mainly attributed to the significant difference in the number of surviving lineages generated by the time-scaling methods. Using geological stages as time bins for analysing selectivity and severity is therefore likely to yield more accurate results in our context because it is resolution at which the data presently exist.

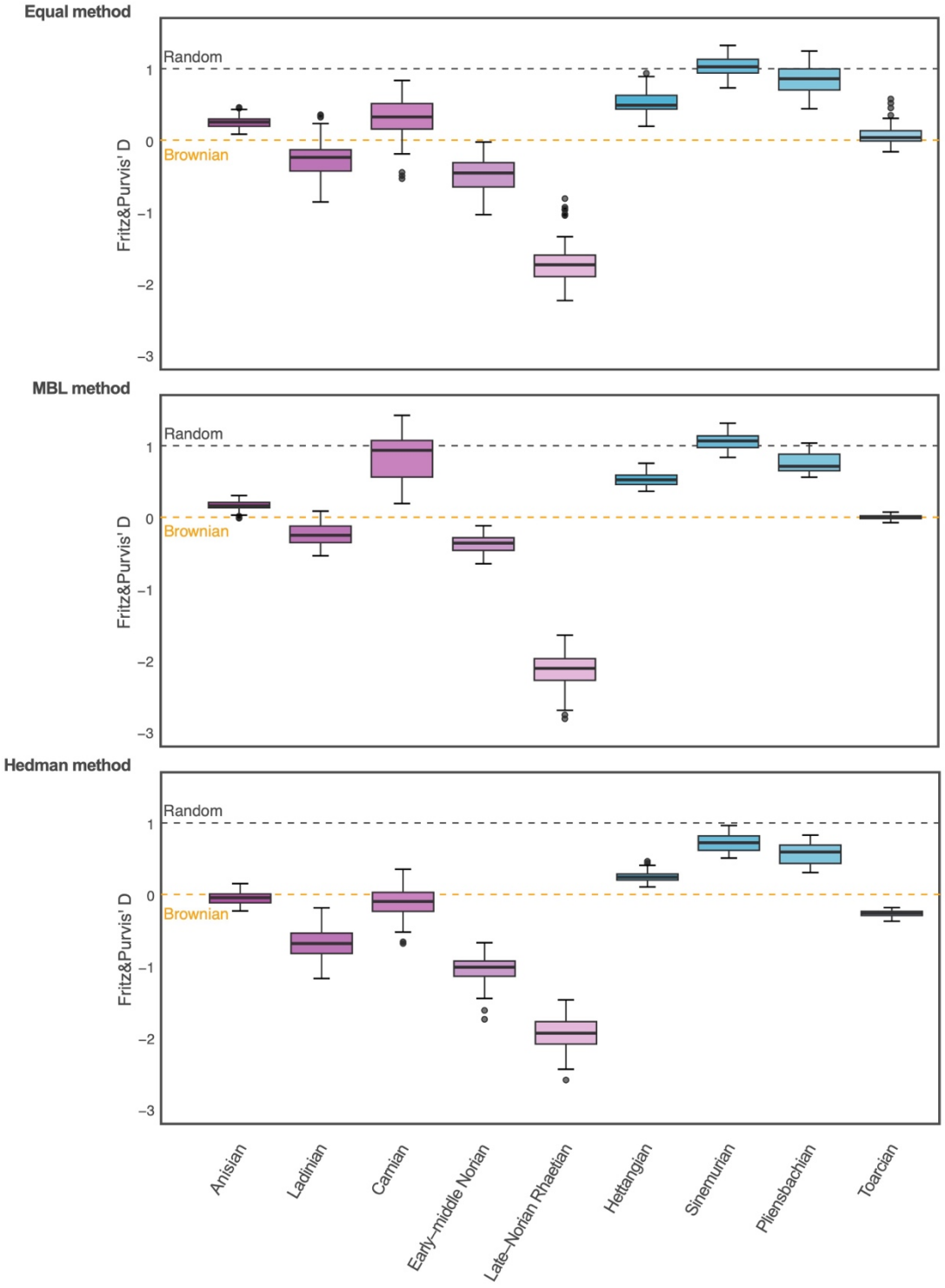

Figure 22. Distribution of the *D* statistic throughout the Middle Triassic to Early Jurassic time interval for 100 phylogenies dated using each method (Equal, MBL, and Hedman, respectively). A *D* value of 0 indicates a phylogenetically clustered pattern of extinctions within the time bin, consistent with a Brownian motion distribution, whereas a D value of 1 reflects a random extinction pattern.

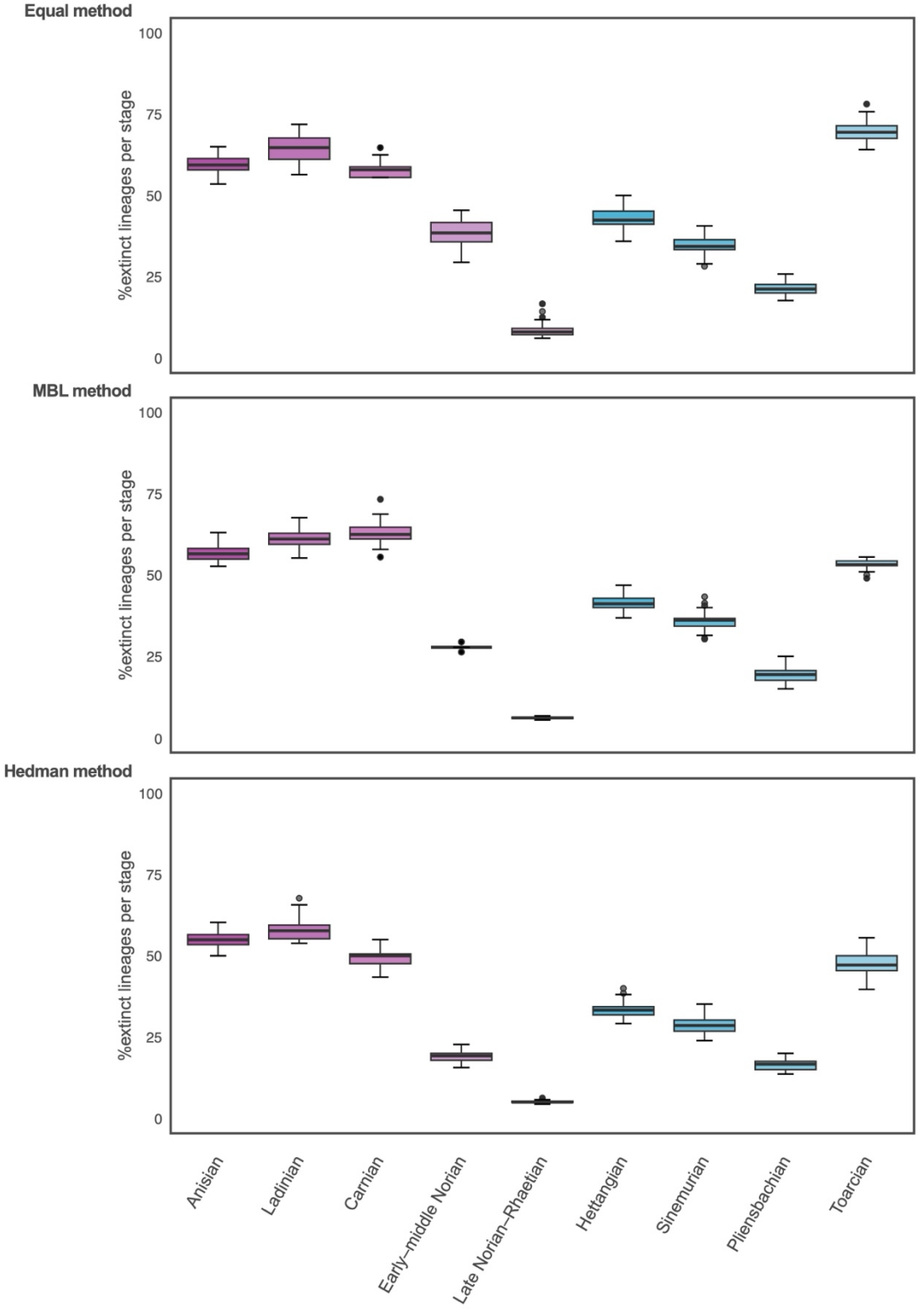

Figure 23. Distribution of extinction severity throughout the Middle Triassic to Early Jurassic time interval for 100 phylogenies dated using each method (Equal, MBL, and Hedman, respectively).

Table 4. Results of the selectivity test by using the *D* statistic for selected time bins**.** All values are the mean of 100 repetitions generated with trees time-scaled by using each method (Equal, MBL and Hedman respectively). Standard deviations are given in bracket for the *D* statistic.

Time bins	Time-scaling method	Survived	Extinct	Percentage of extinct lineages	*D* statistic (SD)	P-value (Brownian motion)	Proportion of p-value Brownian motion < 0.05	P-value (Random expectation)	Proportion of p-value Random expectation < 0.05
Anisian	Equal	27	39	59.1	0.24974 (0.07799)	0.00036	100	0.24107	0
	MBL	30	39	56.5	0.16198 (0.06609)	2E-05	100	0.32131	0
	Hedman	32	39	54.9	-0.05097 (0.08753)	1E-06	100	0.56972	0
Ladinian	Equal	12	22	64.7	-0.25356 (0.22846)	0.00355	99	0.68737	0
	MBL	14	22	61.1	-0.23505 (0.15348)	0.00021	100	0.70375	0
	Hedman	16	22	57.9	-0.69201 (0.18077)	4E-05	100	0.88174	0
Carnian	Equal	7	10	58.8	0.30568 (0.26747)	0.15235	6	0.3991	0
	MBL	6	10	62.5	0.84374 (0.31946)	0.38683	0	0.21624	0
	Hedman	11	10	47.6	-0.10807 (0.19532)	0.03409	78	0.56979	0
Early – Middle Norian	Equal	8	5	38.5	-0.49307 (0.24805)	0.03291	80	0.69925	0
	MBL	13	5	27.8	-0.36902 (0.11972)	0.00513	100	0.70128	0
	Hedman	22	5	18.5	-1.04309 (0.19012)	0.00078	100	0.88371	0
Late Norian – Rhaetian	Equal	23	2	8	-1.70987 (0.28692)	0.01166	100	0.86332	0
	MBL	31	2	6.1	-2.12483 (0.24242)	0.00474	100	0.93393	0
	Hedman	38	2	5	-1.95380 (0.23198)	0.00579	100	0.89258	0
Hettangian	Equal	19	14	42.4	0.50963 (0.14580)	0.03335	76	0.12268	24

	MBL	20	14	41.2	0.54031 (0.09991)	0.02629	91	0.10943	3
	Hedman	28	14	33.3	0.26402 (0.07700)	0.00329	100	0.27056	0
Sinemurian	Equal	23	12	34.3	1.02829 (0.12612)	0.52614	0	0.00574	100
	MBL	21	12	36.4	1.06149 (0.11424)	0.57344	0	0.00239	100
	Hedman	30	12	28.6	0.72714 (0.12079)	0.16143	13	0.04049	67
Pliensbachian	Equal	25	7	21.9	0.85244 (0.18317)	0.3293	1	0.05664	46
	MBL	30	7	18.9	0.76077 (0.13213)	0.20776	2	0.04539	59
	Hedman	35	7	16.7	0.55985 (0.14378)	0.10332	36	0.14608	1
Toarcian	Equal	11	25	69.4	0.06798 (0.12660)	0.00526	97	0.45619	0
	MBL	22	25	53.2	-0.00092 (0.02905)	0	100	0.50632	0
	Hedman	27	25	48.1	-0.26453 (0.04223)	0	100	0.77575	0

Selectivity and evolution of body size

Overall, results of Pagel's λ and PGLS are consistent across all time-scaling methods (**Table 5**). Body size almost consistently exhibits a strong phylogenetic signal through our sampled time periods (Pagel's λ >0.75). However, the magnitude of this signal varies depending on the sampling proportions within time bins and on the time-scaled trees. Notably, Pagel's λ values in the 'Early–middle Norian' time interval show the greatest variation between Equal- and Hedman-dated trees (0.398 and 0.989). As a result, the characterisation of the phylogenetic signal for this bin appears less clear, although the lowest value (0.398) is associated with a high standard deviation. Other Pagel's λ values < 0.75 are associated with Hedman time-scaled phylogenies, for the 'Carnian', 'Late Norian–Rhaetian' and 'Hettangian' time bins and are associated with the highest standard deviations within their respective bins. PGLS analyses are all characterized by very low positive or negative explanatory power (R^2) associated with low standard deviations and fail to provide evidence of significant correlation between body size and extinction susceptibility. With the exception of the 'Ladinian' and the 'Late Norian–Rhaetian' time bins, the distribution of body size does not reveal wide differences between extinct taxa and taxa/lineages that survived, no matter the time-scaling method used (**Figure 25**). During the Ladinian, surviving species tend to exhibit a larger body size, a trend likely attributable to the presumed presence of ancestors of the very large shastasaurids, whose fossils are restricted to the Late Triassic. Their demise prior to or at the T/J transition also explains the variation in median body length compared to surviving lineages in the 'Late Norian–Rhaetian' interval, partially represented by smaller parvipelvians (**Figure 25**). Although body size variance between extinct and surviving taxa/lineages remains largely similar over time, greater dispersion is observed among species that went extinct during the Anisian and 'Late Norian–Rhaetian interval, as well as among surviving taxa in the Hettangian.

The relative proportions of body size categories fluctuate over time, with significant differences observable between the Middle Triassic, Late Triassic and Early Jurassic (**Figure 26**). The Middle Triassic is characterized by the high proportion of smaller taxa (<1 m long) (*e.g.* mixosaurids, pachypleurosauroids and small nothosauroids) which co-existed alongside larger (1–6 m long) (*e.g.* large nothosauroids, early diverging pistosauroids and the smallest cymbospondylids) and very large to gigantic (>6 m long) species (*e.g.* giant cymbospondylids such as *C. youngorum* and *Thalattoarchon*). A notable shift towards larger body size likely occurs at the Middle–Late Triassic boundary,

coinciding with the complete disappearance of smaller forms, in both ichthyosaurians and eosauropterygians. Subsequently, the Late Triassic witnesses an increasing prevalence of gigantic ichthyosaurians, culminating in the Rhaetian, with the T/J transition likely eradicated these gigantic morphotypes. During Early Jurassic, large forms (2–6 m long) dominate over medium-sized ones (1–2 m long) in both clades, while the proportion of very large taxa (6–12 m long) gradually increases with ongoing diversification of temnodontosaurid ichthyosaurians and the emergence of large rhomaleosaurid plesiosaurians in the Toarcian.

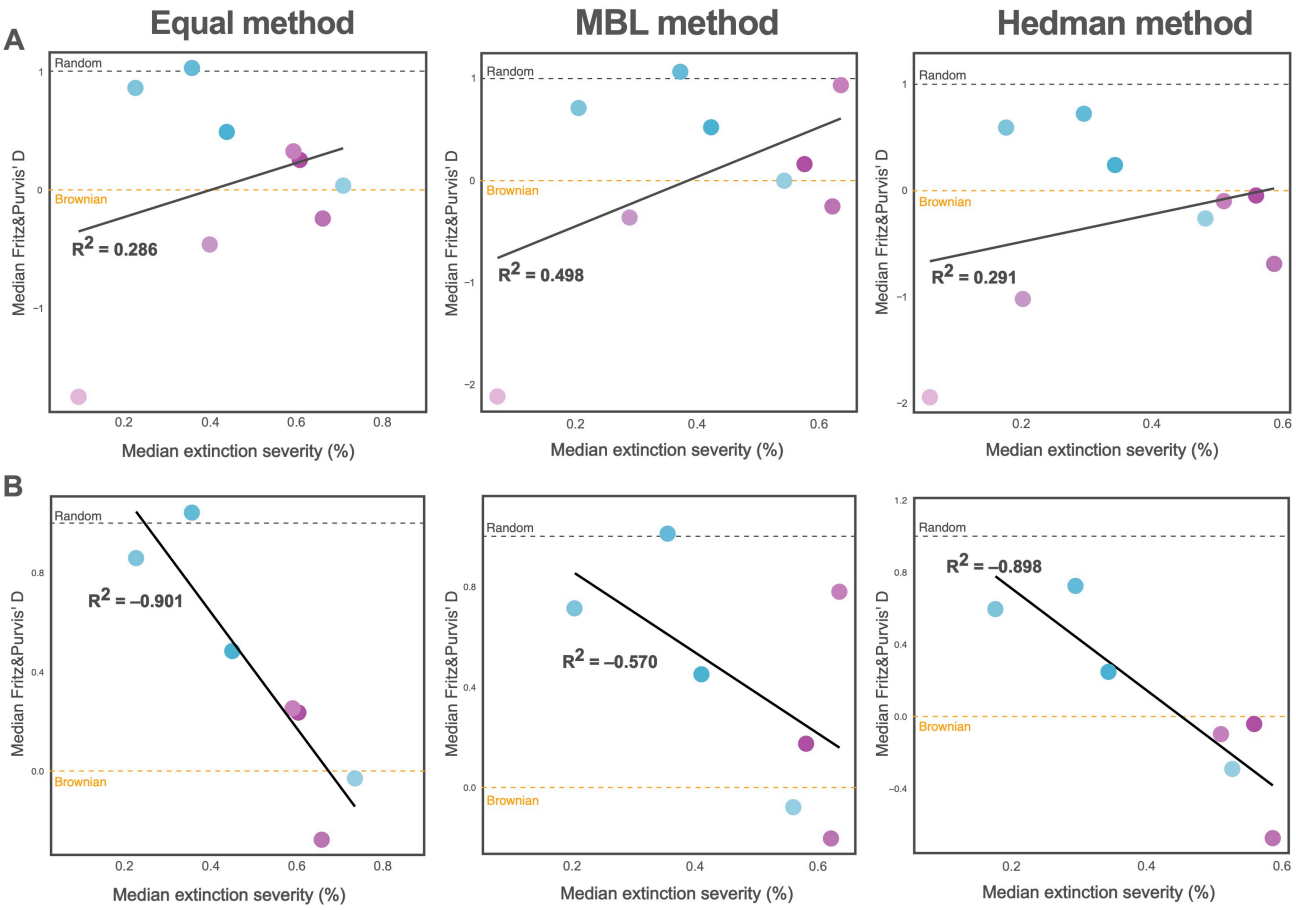

Figure 24. Correlation between the mean *D* statistic value and the mean extinction severity for time bins throughout the Middle Triassic to Early Jurassic time interval. (A) With all time bins and (B) with under-sampled time bins (*e.g.* 'Early–Middle Norian' and 'Late Norian–Rhaetian') removed.

Table 5. Results of PGLS analyses for selected time bins. All values are the mean of 100 repetitions generated with trees time-scaled by using each method (Equal, MBL and Hedman respectively). Standard deviations are given in bracket for phylogenetic signal (Pagel's λ) and the adjusted R^2.

Time bin	Time-scaling method	Survived	Extinct	Percentage of extinct lineages	Pagel's lambda (SD)	R^2 (SD)	P-value
Anisian	Equal	27	39	59.1	0.94589 (0.04277)	-0.01242 (0.00714)	0.66581
	MBL	28	39	58.2	0.97722 (0.01732)	-0.01194 (0.0056)	0.64172
	Hedman	32	39	54.9	0.96908 (0.04998)	-0.03244 (0.00864)	0.73018
Ladinian	Equal	12	22	64.7	0.9684 (0.04771)	-0.0116 (0.01835)	0.47113
	MBL	14	22	61.1	0.92637 (0.09581)	-0.0582 (0.03267)	0.64095
	Hedman	16	22	57.9	0.96614 (0.06123)	-0.0686 (0.01135)	0.77073
Carnian	Equal	7	10	58.8	0.9698 (0.06172)	-0.02773 (0.06295)	0.5607
	MBL	6	10	62.5	0.97746 (0.06258)	-0.02024 (0.06653)	0.5286
	Hedman	11	10	47.6	0.62588 (0.31986)	-0.04906 (0.02568)	0.77957
Early – middle Norian	Equal	8	5	38.5	0.39801 (0.43364)	-0.06873 (0.03697)	0.65956
	MBL	13	5	27.8	0.67357 (0.40834)	0.00865 (0.05238)	0.38572
	Hedman	21	5	18.5	0.98927 (0.02448)	-0.04179 (0.00418)	0.93452
Late Norian – Rhaetian	Equal	23	2	8	0.8014 (0.32678)	-0.04122 (0.01417)	0.77304
	MBL	31	2	6.1	0.80373 (0.38324)	-0.01424 (0.01827)	0.48875
	Hedman	38	2	5	0.62447 (0.26439)	-0.00203 (0.0078)	0.35115
Hettangian	Equal	19	14	42.4	0.88912 (0.25193)	0.05483 (0.10286)	0.33403
	MBL	20	14	41.2	0.94151 (0.19621)	0.0023 (0.023)	0.36004

	Hedman	28	14	33.3	0.67248 (0.21347)	0.02872 (0.02557)	0.19758
Sinemurian	Equal	23	12	34.3	0.91049 (0.11496)	-0.02488 (0.01635)	0.67891
	MBL	21	12	36.4	0.91484 (0.06142)	-0.01963 (0.01986)	0.55446
	Hedman	30	12	28.6	0.89409 (0.06122)	-0.00215 (0.02458)	0.44964
Pliensbachian	Equal	25	7	21.9	0.96362 (0.14033)	0.04006 (0.05168)	0.24841
	MBL	30	7	18.9	0.94806 (0.05033)	0.06916 (0.09907)	0.24682
	Hedman	35	7	16.7	0.91942 (0.10849)	-0.00771(0.02307)	0.48627
Toarcian	Equal	9	25	73.5	0.99321 (0.01422)	-0.02327 (0.01487)	0.66156
	MBL	22	25	53.2	0.89063 (0.05169)	0.01655 (0.01086)	0.21829
	Hedman	27	25	48.1	0.77953 (0.15157)	0.02983 (0.03174)	0.21544

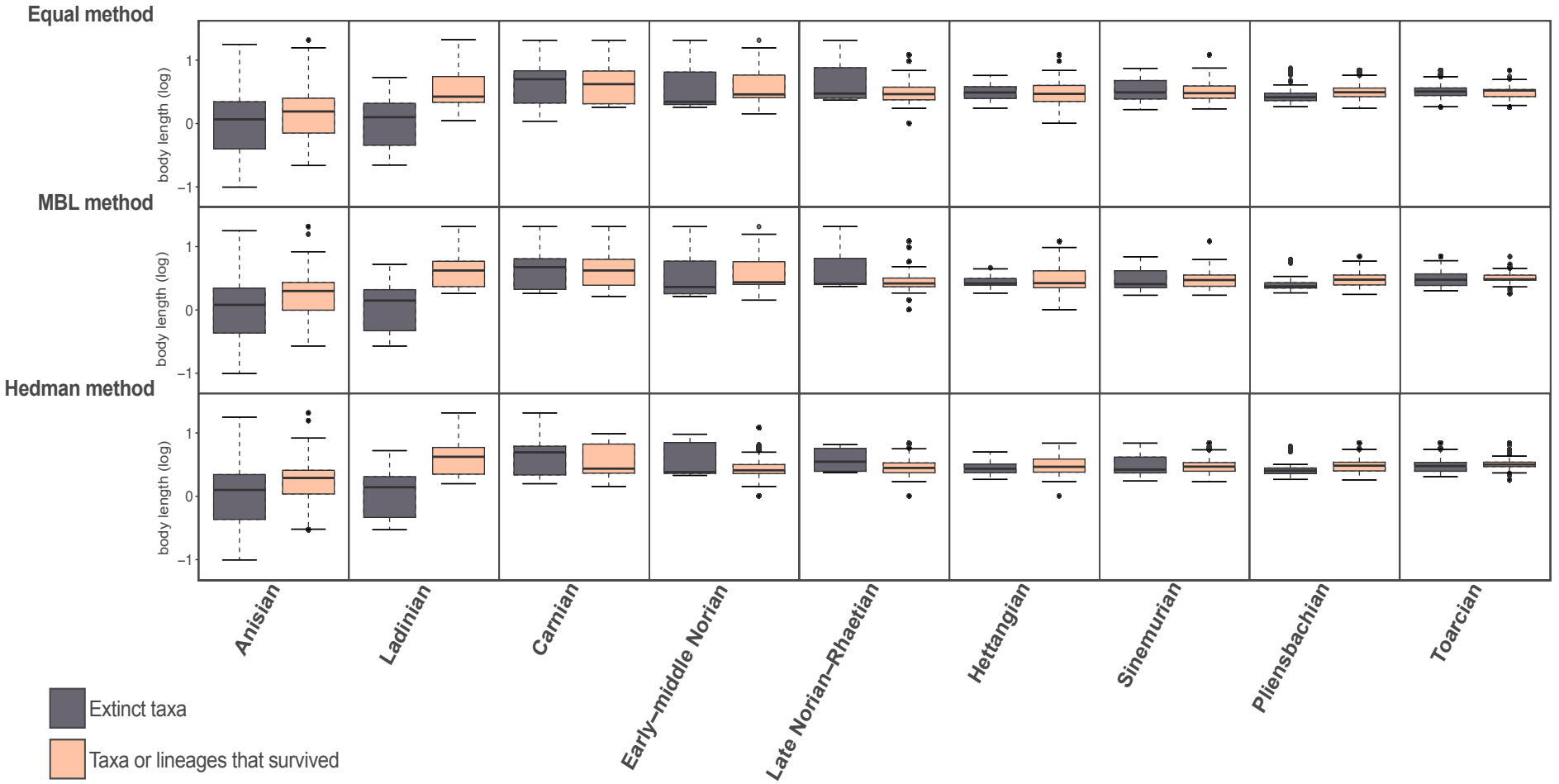

Figure 25. Body size distributions of extinct taxa (dark grey) versus surviving taxa/lineages (orange) across time bins (stages) from the Middle Triassic to the end of the Early Jurassic, based on three time-scaling methods (Equal, MBL, and Hedman). Taxa/lineages are classified as extinct if their last occurrence falls within a given time bin, and as surviving if their temporal range extend to the end of the bin, signifying their presence in both that interval and the subsequent one.

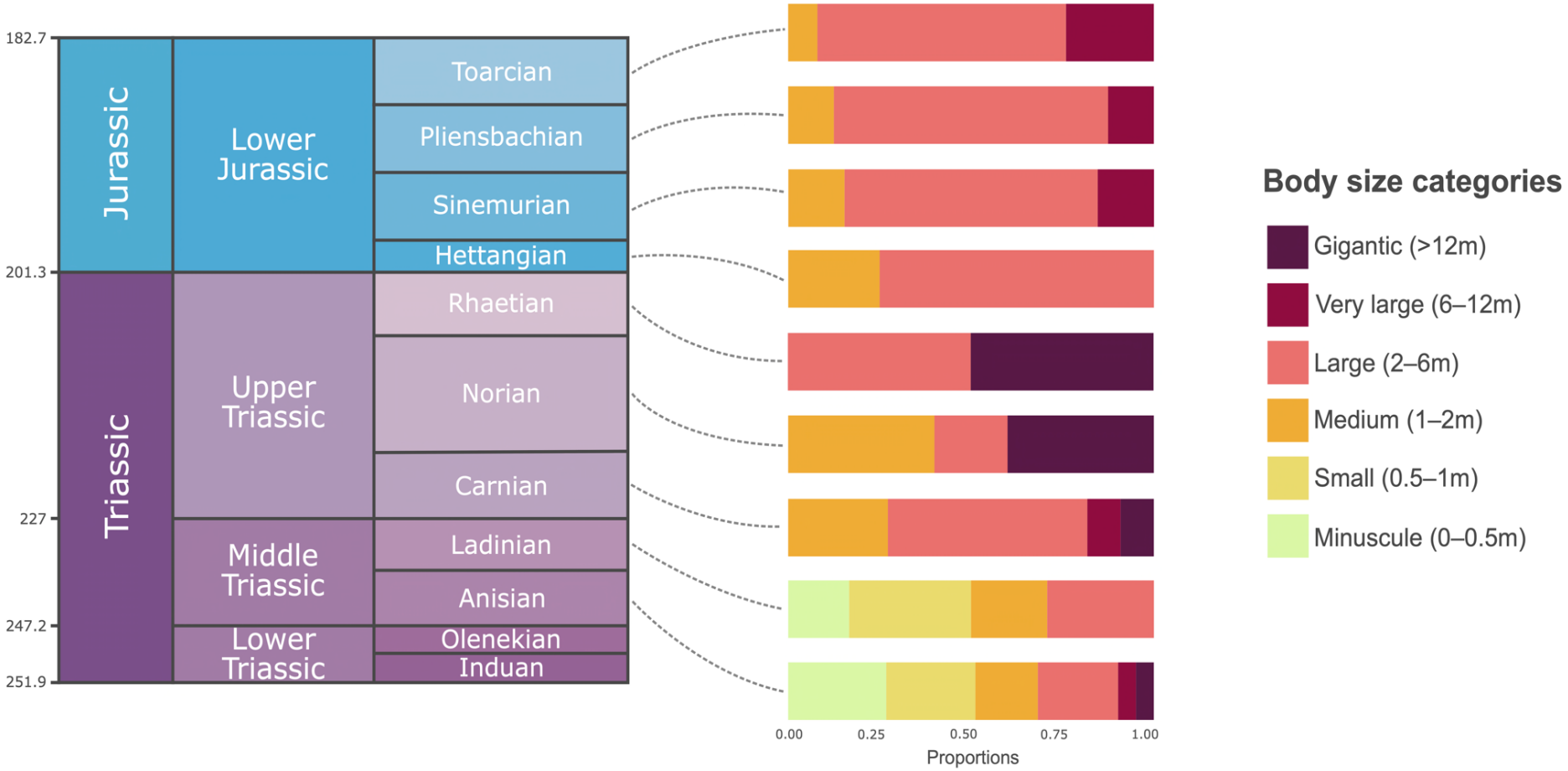

Figure 26. Relative proportions of each body size categories among ichthyosaurians and eosauropterygians in each stage of the Middle Triassic–Early Jurassic time interval.

DISCUSSION

Extinction selectivity from the Middle Triassic to the Early Jurassic and what to make of it

Throughout the Middle Triassic–Early Jurassic interval, extinction patterns among eosauropterygians and ichthyosaurians globally tend to be phylogenetically clustered. These findings are consistent with previous analyses on diverse taxonomic groups pointing out that extinctions over time are rarely the result of a random selection across the phylogeny, even during mass extinction events (McKinney 1997; Roy et al. 2009; Hardy et al. 2012; Puttick et al. 2017; Soul and Friedman 2017; Allen et al. 2019). Furthermore, the correlation between extinction selectivity and intensity has also been recovered in other fossil vertebrate clades (Soul and Friedman 2017; Allen et al. 2019), revealing that more severe extinctions tend to be associated with a greater pattern of phylogenetic clustering. Extinction events in best-sampled stages of Middle and Late Triassic (*i.e.* Carnian) appear more selective and severe than during the Early Jurassic, a pattern likely driven by significant turnovers in eosauropterygian and ichthyosaurian assemblages during the Triassic as lineages went extinct and new ones emerged (see the General Introduction: Evolution of marine reptiles assemblages from the Middle Triassic to the Early Jurassic section for a thorough review). The Anisian witnessed the extinction of most Middle Triassic ichthyosaurians including the cymbospondylids and nearly all mixosaurids, except *Phalarodon* (*e.g.* see the dataset of Kelley et al. 2014), as well as a significant portion of the pachypleurosauroids diversity among eosauropterygians (Benton et al. 2013; Laboury et al. 2023; Chapter 1). The highest selectivity and severity of extinctions recorded in the Ladinian reflect the overall restructuration marine reptiles communities, with the eradication of 'typical Middle Triassic fauna' (Bardet 1994; Benson et al. 2010; Benson and Butler 2011; Kelley et al. 2014; Laboury et al. 2024; Chapter 2). Indeed, the Ladinian–Carnian transition saw the final extinction of the last mixosaurids, pachypleurosauroids, almost all nothosauroids and early-diverging pistosauroids in favour of taxa adapted to open ocean (*e.g.* shastasaurids and euichthyosaurians among Ichthyosauria) for which our time-scaled phylogenies record their emergence prior to the Late Triassic (**Figures S3.5–S3.7**). In contrast to ichthyosaurians which are relatively well represented in the Carnian fossil record (Merriam 1908; Nicholls et al. 2002; Benton et al. 2013; Kelley et al. 2022; Zverkov et al. 2022), estimating the timing of the emergence of truly pelagic eosauropterygians remains challenging due to the lack of remains in the Late Triassic fossil record (Benson et al. 2012; Wintrich et al. 2017; Renesto and Dalla Vecchia

2018). Nevertheless, our results are in line with those of previous studies(Benson et al. 2010; Kelley et al. 2014; Laboury et al. 2024; Chapter) and tend to reinforce the idea that this turnover, resulting in a profound dissimilarity between Middle and Late Triassic assemblages, represents a pivotal event in the evolutionary history of ichthyosaurians and eosauropterygians. Marine reptile faunas throughout the Early Jurassic appear mor stable, notably during the Sinemurian and Pliensbachian, for which a more random pattern of extinction has been detected. Both stage are indeed characterized by similar assemblages, with the continued presence of the same genera among ichthyosaurians (*e.g. Ichthyosaurus*, *Leptonectes* and *Temnodontosaurus*) (Maisch and Hungerbühler 1997; McGowan and Milner 1999; McGowan and Motani 2003; Lomax and Massare 2015; Fischer et al. 2022b) and the predominance of rhomaleosaurids, alongside early plesiosauroids and pliosaurids (Owen 1840; Storrs and Taylor 1996; Hopley 2000; Benson et al. 2012; Vincent et al. 2013; Sachs and Kear 2018). Conversely, the highest Early Jurassic values observed in the Toarcian likely reflect the turnover occurring at the Early–Middle Jurassic transition, during which nearly almost early parvipelvians and plesiosaurians were replaced by lineages that diversified and populated marine ecosystems through the rest of the Mesozoic (*i.e.* ophthalmosaurid ichthyosaurians, cryptoclidid plesiosaurians and thalassophonean pliosaurids) (Maxwell et al. 2012; Fischer et al. 2013a, 2021; Vincent et al. 2013b; Benson and Druckenmiller 2014; Miedema et al. 2024; Reolid et al. 2024).

As already mentioned in the Results section (see above), the lack of information in the Late Triassic fossil record introduces biases in our analyses. Nonetheless, a close review of this latter helps to clarify extinction selectivity patterns during that period. Although Carnian and Norian ichthyosaurian faunas are often viewed as similar and described as ‘transitional’ — marked by presence of small- to medium-sized euichthyosaurians alongside large to giant shastasaurids (Merriam 1908; McGowan 1994a, 1995, 1996a, 1997; Nicholls and Manabe 2004; Zverkov et al. 2022) — the replacement of toretocnemids by early parvipelvians in the Norian, suggests a certain selectivity against the former lineage by the end of Carnian (Zverkov et al. 2022). Fossil remains, even highly fragmented, offer insights into the composition of Rhaetian marine assemblages, suggesting that open-water environments were still populated by gigantic shastasaurids, along a diverse range of parvipelvians and plesiosaurians as, inferred from branching events in time-scaled phylogenies (Storrs 1994; Fischer et al. 2013, 2014b; Motani et al. 2017; Wintrich et al. 2017; Lomax et al. 2018a, 2024; Laboury et al. 2022; Sander et al. 2022). Considering that these two lineages did not appear to be drastically

affected by major extinction events at the T/J transition (Benson et al. 2010, 2012; Wintrich et al. 2017; Renesto and Dalla Vecchia 2018; Laboury et al. 2024), and given the absence of shastasaurids in the Jurassic (but see Martin et al. 2015), we speculate a certain degree of selectivity in extinctions during the latest Triassic. However, last coastal marine reptiles such as placodonts (Pinna and Mazin 1993; Neenan and Scheyer 2014), thalattosaurs (Müller 2007; Bastiaans 2024 and references therein) and probably saurosphargids (Scheyer et al. 2022), met their demise at the very end of the Triassic, suggesting a more complex pattern of phylogenetic clustering in extinctions than previously inferred, affecting taxa of distinct habitats with different ecological niches. Assessing the magnitude and the impact of the biases related to the scarcity of the Late Triassic appear challenging. However, without new fossil data, our analyses and the remains present in the fossil record tend to indicates that extinctions during this period were selective similar to what has been observed in better sampled stages.

Pattern of body size evolution associated with extinction vulnerability

Body size in eosauropterygians and ichthyosaurians does not appear to have influenced extinction risk throughout the Middle Triassic–Early Jurassic interval. This lack of correlation tends to indicate that other biological and/or ecological factors, not considered here, are likely more relevant in explaining phylogenetic clustering in extinction. Our results support the growing consensus that body size is unlikely to be a selective factor in extinctions of both terrestrial and aquatic vertebrates (Friedman 2009; Sallan and Galimberti 2015; Puttick et al. 2017; Allen et al. 2019). The absence of relationship between the size of these marine reptiles and their extinction vulnerability is also reflected in the overall absence of strong difference in body length between surviving and extinct taxa over time. The lack of significant correlation between extinction risk and body size during the Ladinian is somewhat unexpected. The substantial turnover occurring at the Middle–Late Triassic transition seems to be associated with notable shifts in body size with a selection favouring larger pelagic animals over smaller forms more adapted to nearshore environments (Moon and Stubbs 2020; Gutarra et al. 2023). However, even though this transition corresponds to the rise of large to giant shastasaurids, it also witnessed the diversification of smaller pelagic forms such as the early euichthyosaurians, indicating that taxa with still a broad range of body size populated oceans during the early Late Triassic (Merriam 1908; Moon and Stubbs 2020; Gutarra et al. 2023; Laboury et al. 2024; Chapter 2). Similarly to the *D* statistic analyses, PGLS output values are also influenced by biases stemming from the scarcity of the latest Triassic record, limiting our interpretations in assessing the impact of body size in

extinction selectivity. Among ichthyosaurians, the 'early–middle Norian' period saw the extinction of small- to medium- basal euichthyosaurians and parvipelvians (McGowan 1994a, 1995, 1996a), alongside giant shastasaurids (Motani et al. 1999; Nicholls and Manabe 2004), suggesting that body size may not act as a reliable predictor in extinction during this period, similarly to what is observed through the rest of our investigated time interval (*i.e.* Middle Triassic–Early Jurassic). On the other hand, the end of the Triassic is characterized by a significant reduction in body size among ichthyosaurians, highlighted by the extinction of the last whale-sized shastasaurids and subsequent record of smaller parvipelvians in the earliest Jurassic (Fischer et al. 2014b; Lomax et al. 2018a, 2024; Sander et al. 2022; Gutarra et al. 2023; Laboury et al. 2024; Chapter 2). The correlation between body size and extinction vulnerability across the T/J transition still remains obscure, primarily due to the paucity of fossil data. Nevertheless, it appears evident that extinction events at the end of the Rhaetian played a key role in the evolutionary history of ichthyosaurians and more globally, of marine reptiles with the complete elimination of gigantism during the rest of the Mesozoic as no further lineages reached comparable sizes (Moon and Stubbs 2020; Gutarra et al. 2023; Laboury et al. 2024).

CONCLUSION

In this chapter, we assess the selectivity and severity of extinctions among eosauropterygians and ichthyosaurians from the Middle Triassic to the end of the Early Jurassic, while also evaluating body size as a predictor of extinction vulnerability. Our analyses, which applied various tree-scaling methods, consistently revealed that extinction were predominantly phylogenetically clustered, with body size playing no significant role in shaping these patterns. Furthermore, we find a strong negative correlation between extinction severity and selectivity, suggesting that more severe extinction events do not coincide with more a random pattern of phylogenetic clustering. Overall, Middle and early Late Triassic stages exhibited greater selectivity than those of the Early Jurassic, reflecting substantial turnovers in marine reptiles assemblages. The Ladinian–Carnian transition, exhibited pronounced extinction clustering, highlighting major changes in ecosystems and subsequently in marine reptile assemblages, including the loss of the vast majority of the smaller coastal dwellers and the diversification of pelagic taxa. During the Early Jurassic, extinctions appeared less phylogenetically clustered, particularly during the Sinemurian and the Pliensbachian, when marine

reptiles fauna remained relatively stable. However, the Toarcian stands out as an exception, showing the greatest selectivity due to the faunal turnover from the Early to Middle/Late Jurassic. Test for extinction selectivity and correlation between extinction risk and body size during the latest Triassic are likely biased by the paucity of the fossil record, potentially introducing statistical artefacts. Nonetheless, the extinction of the last whale-sized shastasaurid ichthyosaurians at the end of the Rhaetian and the survival of smaller taxa still suggest a degree of phylogenetic clustering and potentially a greater extinction susceptibility among large bodied-taxa during extinctions event occurring at the end of the Triassic.

SUPPLEMENTS FOR CHAPTER 3

List of taxa manually added in phylogenetic trees

Ichthyosaurians

- *Mixosaurus xindianensis*: placed as the sister taxon of the clade composed of *Mixosaurus kuhnschnyderi* and *Mixosaurus cornalianus*, according to Laboury et al. (2022).
- *Cymbospondylus duelferi*: placed as the sister taxon of *Cymbospondylus petrinus*, according to Klein et al. (2020).
- *Cymbospondylus youngorum*: placed as the sister taxon of *Cymbospondylus duelferi,* according to Sander et al. (2021).
- *Toretocnemus zitteli*: placed as the sister taxon of *Toretocnemus californicus*, according to Laboury et al. (2022).
- *Himalayasaurus tibetensis*: placed in a polytomy composed of nearly all shastasaurids — with the exception of the most primitive taxon, *Besanosaurus leptorhynchus* (*e.g* see Bindellini et al. 2021, 2024) — which has been randomly resolved 100 times.
- *Ichthyotitan severnensis*: placed in a polytomy composed of nearly all shastasaurids — with the exception of the most primitive taxon, *Besanosaurus leptorhynchus* (*e.g* see Bindellini et al. 2021, 2024) — which has been randomly resolved 100 times.
- *Temnodontosaurus risor*: Considering the need of taxonomic revision for 'T. risor' (Bennion et al. 2024), we decided to separate these two and add 'T. risor' as the sister lineage of T. platyodon while waiting for an updated apomorphy-based definition of this taxon.

Eosauropterygians

- *Wumengosaurus delicatomandibularis*: placed as the sister taxon of the clade Pachypleurosauridae, according to Shang et al. (2020).
- *Neusticosaurus peyeri*: placed as the sister taxon of *Neusticosaurus pusillus,* according to Klein et al. (2022b).
- *Neusticosaurus edwardsii*: placed as the sister taxon of *Neusticosaurus peyeri,* according to Klein et al. (2022b).
- *Luopingosaurus imparilis*: placed as the sister taxon of *Honghesaurus longicaudalis*, according to Xu et al. (2023).
- *Paludidraco multidentatus*: placed as the sister taxon of *Simosaurus* according to de Miguel Chaves et al. (2018b)
- *Brevicaudosaurus jiyangshanensis*: placed as the sister taxon of the clade Nothosauridae, according to Shang et al. (2020).
- *Nothosaurus luopingensis*: placed as the sister taxon of *Nothosaurus yangiuanensis*, according to Shang et al. (2022).
- *Nothosaurus cristatus*: placed as the sister taxon of *Nothosaurus mirabilis*, according to Hinz et al. (2019).
- *Lariosaurus winkelhorsti*: placed as the sister taxon of *Lariosaurus buzzi,* according to Xu et al. (2022).
- *Lariosaurus vosseveldensis*: placed as the sister taxon of the clade composed of *L. winkelhorsti* and *Lariosaurus buzzi*, according to Xu et al. (2022).
- *Microcleidus melusinae*: placed as the most primitive member of *Microcleidus*, according to Vincent et al. (2017).

Table 3.1. List of taxa present in our informal composite trees and used in PGLS and body proportions analyses.

Taxon	Clade	FAD	LAD	Stage	Total body length (in m)	Body size category	Total body length estimation sources
Chaohusaurus brevifemoralis	Ichthyopterygia	251.2	247.2	Olenekian	0.92	1	Estimation from AGM AGB 7401 (Huang et al. 2019)
Chaohusaurus chaoxianensis	Ichthyopterygia	251.2	247.2	Olenekian	0.60	1	Estimation from on IVPP VI1362 and IVPP VI13 (Motani and You 1998b)
Chaohusaurus geishanensis	Ichthyopterygia	251.2	247.2	Olenekian	0.90	1	Estimation from IVPP 4001 (Motani and You 1998a)
Chaohusaurus zhangjiawanensis	Ichthyopterygia	251.2	247.2	Olenekian	1.85	2	Estimation from WHGMR V26025 (Chen et al. 2013)
Gulosaurus helmi	Ichthyopterygia	251.2	247.2	Olenekian	0.79	1	Estimation from TMP 89.127.3 (Cuthbertson et al. 2013)
Grippia longirostris	Ichthyopterygia	251.2	247.2	Olenekian	NA	2	NA
Parvinatator wapitiensis	Ichthyopterygia	251.2	237	Olenekian–Ladinian	NA	2	NA
Utatsusaurus hataii	Ichthyopterygia	251.2	247.2	Olenekian	2.56	3	Measurements from Jiang et al. (2016) based on the specimen IGPS 95941
Mixosaurus cornalianus	Ichthyosauria	247.2	242.0	Anisian	0.90	1	Estimation based on first-hand measurements on NHMUK PV R5702; PIMUZ T4848; PIMUZ T4857; PIMUZ T4858; PIMUZ T5925; PIMUZ T4923 (first-hand measurements)
Mixosaurus kuhnschnyderi	Ichthyosauria	247.2	242.0	Anisian	0.81	1	Estimation from PIMUZ Tl324 (Brinkmann 1998)
Mixosaurus xindianensis	Ichthyosauria	247.2	242.0	Anisian	1.00	2	Measurement from Gutarra et al. (2023) based on YIGM SPC V-0732 (Chen and Chen 2010)

Mixosaurus panxianensis	Ichthyosauria	247.2	242.0	Anisian	1.49	2	Estimation from GMPKU-P-1033 and PIMUZ T2418 (first-hand measurements and pictures)
Phalarodon atavus	Ichthyosauria	247.2	242.0	Anisian	0.80	1	Measurement from Gutarra et al. (2023) based on the specimen LPV 30872 (Liu et al. 2013)
Phalarodon callawayi	Ichthyosauria	247.2	242.0	Anisian	1.71	2	Estimation from CMC VP 7276 (Schmitz et al. 2004)
Phalarodon fraasi	Ichthyosauria	247.2	237.0	Anisian–Ladinian	1.00	2	Estimation from PIMUZ T2417 (first-hand measurements)
Cymbospondylus buscheri	Ichthyosauria	247.2	242.0	Anisian	5.50	3	Estimation from PIMUZ T4351 (first-hand measurements)
Cymbospondylus duelferi	Ichthyosauria	247.2	242.0	Anisian	4.95	3	Estimation from LACM DI 158109 Klein et al. (2020)
Cymbospondylus nichollsi	Ichthyosauria	247.2	242.0	Anisian	7.60	4	Estimation provided by Sander et al. (2021) from the specimen FMNH PR2251
Cymbospondylus petrinus	Ichthyosauria	247.2	242.0	Anisian	12.56	5	Estimation provided by Sander et al. (2021) from UCMP 9950
Cymbospondylus youngorum	Ichthyosauria	247.2	242.0	Anisian	17.77	5	Estimation provided by Sander et al. (2021) from LACM DI 157871
Thalattoarchon saurophagis	Ichthyosauria	247.2	242.0	Anisian	8.50	4	Estimation provided by Fröbisch et al. (2013) and Sander et al. (2021) and from FMNH PR 3032
Xinminosaurus catactes	Ichthyosauria	247.2	242.0	Anisian	2.75	3	Estimation from GMPKU-P-1071 (Jiang et al. 2008a)
Besanosaurus leptorhynchus	Ichthyosauria	247.2	242.0	Anisian	5.42	3	Measured on the specimen BESC999 (Bindellini et al. 2021)
Guizhouichthyosaurus tangae	Ichthyosauria	237.0	227.0	Carnian	5.46	3	Estimation from IVPP V11853 (Shang et Li 2009) and YGMR TR0001 (first-hand pictures)

Guizhouichthyosaurus wolonggangense	Ichthyosauria	237.0	227.0	Carnian	4.57	3	Estimation from YIGMR SPCV 10306 (Chen et al. 2007)
Guanlingsaurus liangae	Ichthyosauria	237.0	227.0	Carnian	8.30	4	Estimation from YIGMR SPCV03109 (Sander et al. 2011)
Shastasaurus pacificus	Ichthyosauria	237.0	227.0	Carnian	5.83	3	Estimation from UCMP 9076 (Bindellini et al. 2021)
Himalayasaurus tibetensis	Ichthyosauria	227.0	211.4	Early–middle Norian	NA	5	NA
Shonisaurus sikanniensis	Ichthyosauria	227.0	211.4	Early–middle Norian	20.71	5	Estimation from TMP 94.378.2 (first-hand measurements)
Shonisaurus popularis	Ichthyosauria	237.0	227.0	Carnian	15.69	5	Estimation from the specimen FZVE-1 (Camp 1980)
Ichthyotitan severnensis	Ichthyosauria	208.5	201.3	Rhaetian	NA	5	NA
Qianichthyosaurus xingyiensis	Ichthyosauria	242.0	237.0	Ladinian	1.93	2	Estimation from WS2011-46-R1 (Yang et al. 2013)
Qianichthyosaurus zhoui	Ichthyosauria	237.0	227.0	Carnian	2.57	3	Estimation from IVPP V11839 (first-hand measurements), CMNH V1412/C1120 (Nicholls et al. 2002) and YGMIR XTw-Q3 (Xiaofeng et al. 2008)
Toretocnemus californicus	Ichthyosauria	237.0	227.0	Carnian	NA	2	NA
Toretocnemus zitteli	Ichthyosauria	237.0	227.0	Carnian	NA	2	NA
Callawayia neoscapularis	Ichthyosauria	227.0	211.4	Early–middle Norian	2.51	3	Estimation from ROM 41993 (first-hand measurements)
Californosaurus perrini	Ichthyosauria	237.0	227.0	Carnian	1.92	2	Estimation from UCMP 9082 (Bindellini et al. 2021)
Hudsonelpidia brevirostris	Ichthyosauria	227.0	211.4	Early–middle Norian	1.43	2	Estimation from ROM 41993 (first-hand measurements)
Macgowania janiceps	Ichthyosauria	227.0	211.4	Early–middle Norian	NA	2	NA

Temnodontosaurus platyodon	Ichthyosauria	199.3	190.8	Sinemurian	6.90	4	Estimation from NHMUK PV OR 2003 (first-hand measurements on 3D model)
'Temnodontosaurus risor'	Ichthyosauria	199.3	190.8	Sinemurian	NA	3	NA
Temnodontosaurus trigonodon	Ichthyosauria	182.7	174.1	Toarcian	8.48	4	Estimation from SMNS 15950; SMNS 17560 and SMNS 50000 (first-hand measurements on 3D model and photographs)
Temnodontosaurus zetlandicus	Ichthyosauria	182.7	174.1	Toarcian	NA	3	NA
Temnodontosaurus nuertingensis	Ichthyosauria	190.8	182.7	Pliensbachian	NA	4	NA
Temnodontosaurus crassimanus	Ichthyosauria	182.7	174.1	Toarcian	7.73	4	Estimation from WHIMS 2546S (3D model)
Temnodontosaurus eurycephalus	Ichthyosauria	199.3	190.8	Sinemurian	NA	3	NA
Temnodontosaurus azerguensis	Ichthyosauria	182.7	174.1	Toarcian	9.71	4	Estimation from MAMSPLP (measurements on first-hand photographs)
Suevoleviathan integer	Ichthyosauria	182.7	174.1	Toarcian	5.34	3	Estimation from SMNS 15390 and the Hauff specimen (measurements from 3D models)
Leptonectes tenuirostris	Ichthyosauria	201.3	182.7	Hettangian-Pliensbachian	4.16	3	Estimation from NHMUK PV R 47436; NHMUK PV OR 36182 and ROM VP47698 (first-hand measurements and photographs)
Leptonectes moorei	Ichthyosauria	190.8	182.7	Pliensbachian	2.85	3	Estimation from NHMUK PV R14370 (first-hand measurements)
Leptonectes solei	Ichthyosauria	199.3	190.8	Sinemurian	7.57	4	Estimation from on MHN 96270 (C. McGowan, 1993)
Eurhinosaurus longirostris	Ichthyosauria	182.7	174.1	Toarcian	6.72	4	Measured on SMNS 14931
Excalibosaurus costini	Ichthyosauria	199.3	190.8	Sinemurian	5.78	3	Estimation from ROM 47697 (First-hand measurement) and

							BRSMG Cc881 (first-hand photographs)
Wahlisaurus massarae	Ichthyosauria	182.7	174.1	Toarcian	NA	2	NA
Ichthyosaurus anningae	Ichthyosauria	190.8	182.7	Pliensbachian	1.85	2	Estimation from DONMG 1983.98 and NMW G.1597 (Lomax and Massare 2015)
Ichthyosaurus breviceps	Ichthyosauria	199.3	190.8	Sinemurian	1.59	2	Estimation from NHMUK PV R 216 and NHMUK PV OR 43006 (measurements on 3D models)
Ichthyosaurus communis	Ichthyosauria	201.3	182.7	Hettangian-Pliensbachian	2.38	3	Estimation from CAMSM J 35187; NHMUK PV R 2013 and NHMUK PV R 3372 (measurements on 3D models)
Ichthyosaurus conybeari	Ichthyosauria	199.3	190.8	Sinemurian	1.01	2	Estimation from BGS 956 and NMW 93.5G.2 (Massare & Lomax, 2016)
Ichthyosaurus larkini	Ichthyosauria	201.3	199.3	Hettangian	2.49	3	Estimation from BRSUG 25300 and AGC 11 (Lomax and Massare 2016)
Ichthyosaurus somersetensis	Ichthyosauria	201.3	199.3	Hettangian	2.67	3	Measured on NHMUK PV OR 2013 (on 3D model)
Protoichthyosaurus prostaxalis	Ichthyosauria	201.3	199.3	Hettangian	2.52	3	Estimation from BRLSI M3553 and AGC 12 (Lomax et al. 2017)
Protoichthyosaurus applebyi	Ichthyosauria	201.3	199.3	Hettangian	1.75	2	Estimation from UNM.G.2017.1 (Srdic et al. 2019) and UNM.G.2017.1 (Lomax et al. 2017)
Hauffiopteryx altera	Ichthyosauria	182.7	174.1	Toarcian	1.81	2	Estimation from the specimen FWD-129 (Maxwell and Cortes 2020)
Hauffiopteryx typicus	Ichthyosauria	182.7	174.1	Toarcian	2.91	3	Estimation from SMNS 51552 (first-hand measurement)
Stenopterygius quadriscissus	Ichthyosauria	182.7	174.1	Toarcian	3.38	3	Measured on SMNS 55748

Stenopterygius triscissus	Ichthyosauria	182.7	174.1	Toarcian	3.24	3	Measured on SMNS 14846
Stenopterygius uniter	Ichthyosauria	182.7	174.1	Toarcian	3.33	3	Measured on SMNS 17500
Stenopterygius aaleniensis	Ichthyosauria	174.1	170.3	Aalenian	3.97	3	Estimation from SMNS 90699 (Maxwell et al. 2012)
Chacaicosaurus cayi	Ichthyosauria	170.3	168.3	Bajocian	NA	3	NA
Malawania anachronus	Ichthyosauria	132.6	125.0	Hauterivian–Barremian	3.52	3	Estimation from NHMUK PV R6682 (first-hand photographs)
Sisteronia seeleyi	Ichthyosauria	107.8	100.5	Middle–Late Albian	3.53	3	Estimation from LE R004 (first-hand photographs)
Acamptonectes densus	Ichthyosauria	132.6	129.4	Hauterivian	4.89	3	Estimation from NBM 1284-R (first-hand photographs)
Ophthalmosaurus icenicus	Ichthyosauria	166.1	152.1	Callovian–Kimmeridgian	4.30	3	Measurement from GPIT RE 9410 (Gutarra et al. 2023)
Ophthalmosaurus natans	Ichthyosauria	166.1	157.3	Callovian–Oxfordian	NA	3	NA
Leninia stellans	Ichthyosauria	125.0	121.0	Early Aptian	NA	3	NA
Nannopterygius yasykovi	Ichthyosauria	152.1	145.0	Tithonian	3.04	3	Estimation from UPM EP-II-11 (Zverkov and Jacobs 2021)
Nannopterygius saveljeviensis	Ichthyosauria	152.1	145.0	Tithonian	3.00	3	Estimation from UPM EP-II-9 and UPM EP-II-16 (Zverkov and Jacobs 2021)
Undorosaurus gorodischensis	Ichthyosauria	152.1	145.0	Tithonian	6.32	4	Estimation from the specimen UPM EP-II-21(1075) (Zverkov and Efimov 2019)
Caypullisaurus bonapartei	Ichthyosauria	152.1	145.0	Tithonian	6.87	4	Estimation from MACN-N-32 (Fernández 2001)
Mollesaurus periallus	Ichthyosauria	170.3	168.3	Bajocian	NA	3	NA
Gengasaurus nicosiai	Ichthyosauria	157.3	152.1	Kimmeridgian	5.13	3	Estimation from MACN-N-32 (Fernández 2001)
Pervushovisaurus campylodon	Ichthyosauria	113.0	93.9	Albian–Cenomanian	NA	3	NA

Cryopterygius kristiansenae	Ichthyosauria	152.1	145.0	Tithonian	5.94	3	Estimation from PMO 214.578 (Druckenmiller et al. 2012)
Hanosaurus	Eosauropterygia	251.9	247.2	Olenekian	0.850	1	Estimation from IVPP V 15911 (Wang et al. 2022)
Majiashanosaurus	Eosauropterygia	251.9	247.2	Olenekian	0.850	1	Estimation from AGM-AGB5954 (Jiang et al. 2014)
Anarosaurus heterodontus	Eosauropterygia	247.2	242.0	Anisian	0.398	0	Estimation from specimen of Bleeker private collection (provided by N. Klein)
Dactylosaurus	Eosauropterygia	247.2	242.0	Anisian	0.266	0	Estimation provided by Li and Liu (2020) (from the specimen FMNH PR2660 (Sues and Carroll 1985)
Dawazisaurus brevis	Eosauropterygia	247.2	242.0	Anisian	0.460	0	Estimated from NMNS000933-F034397 (Cheng et al. 2016)
Diandongosaurus acutidentatus	Eosauropterygia	247.2	242.0	Anisian	0.292	0	Measured on the specimen VPP V17760 (Sato et al. 2014a)
Dianmeisaurus gracilis	Eosauropterygia	247.2	242.0	Anisian	0.288	0	Measured on IVPP V 17054 and IVPP V 18630 (Shang et al. 2017a)
Dianmeiosaurus mutaensis	Eosauropterygia	247.2	242.0	Anisian	0.099	0	Measured provided by (Hu et al. 2024) on HFUT MT-21-08-001
Dianopachysaurus dingi	Eosauropterygia	247.2	242.0	Anisian	0.169	0	Estimated from the specimen LPV 31365 (Liu et al. 2011)
Honghesaurus longicaudalis	Eosauropterygia	247.2	242.0	Anisian	0.471	0	Measured by (Xu et al. 2022) on IVPP V30380
Luopingosaurus imparilis	Eosauropterygia	247.2	242.0	Anisian	0.383	0	Estimated from the specimen IVPP V19049 (Xu et al. 2023)
Keichousaurus hui	Eosauropterygia	242.0	237.0	Ladinian	0.218	0	Measured on SMNS 81780 and SMNS 59705 (first-hand measurements)
Neusticosaurus edwardsii	Eosauropterygia	242.0	237.0	Ladinian	0.934	1	Measured on PIMUZ T2810 and PIMUZ T3460 (first-hand measurements)

Neusticosaurus peyeri	Eosauropterygia	242.0	237.0	Ladinian	0.298	0	Measurements on PIMUZ T3393; PIMUZ T3394 ; PIMUZ T3395; PIMUZ T3431 ; PIMUZ T3467 ; PIMUZ T3476 ; PIMUZ T3542 ; PIMUZ T3542 (first-hand measurements)
Neusticosaurus pusillus	Eosauropterygia	242.0	237.0	Ladinian	0.306	0	Measurements on PIMUZ T3902 ; PIMUZ T3400 ; PIMUZ T3421; PIMUZ T3530; PIMUZ T3536; PIMUZ T3556; PIMUZ T3574; PIMUZ T3605; PIMUZ T3612; PIMUZ T3639; PIMUZ T3653; PIMUZ T3658; PIMUZ T3658; PIMUZ T3671; PIMUZ T 3672; PIMUZ T3703; PIMUZ T3741 B; PIMUZ T4289 (first-hand measurements)
Odoiporosaurus teruzzii	Eosauropterygia	247.2	242.0	Anisian	NA	1	NA
Panzhousaurus rotundirostris	Eosauropterygia	247.2	242.0	Anisian	0.408	0	Estimation from GMPKU-P- 1059 (Jiang et al. 2019)
Prosantosaurus scheffoldi	Eosauropterygia	242.0	237.0	Ladinian	0.383	0	Estimation from PIMUZ A/III 1273 (first-hand measurements)
Qianxisaurus chajiangensis	Eosauropterygia	242.0	237.0	Ladinian	0.724	1	Estimation from NMNS-KIKO-F044630 (Cheng et al. 2012)
Serpianosaurus mirigiolensis	Eosauropterygia	247.2	242.0	Anisian	0.437	0	Measurements on PIMUZ T96 ; PIMUZ T1071 ; PIMUZ T3676 ; PIMUZ T3676 ; PIMUZ T3677 ; PIMUZ T3685 ; PIMUZ T3931 (cast) ; PIMUZ T3933 (first-hand measurements)
Wumengosaurus delicatomandibularis	Eosauropterygia	247.2	242.0	Anisian	0.952	1	Measurement on GMPKU-P-1210 (Jiang et al. 2008a)
Brevicaudosaurus jiyangshanensis	Eosauropterygia	242.0	237.0	Ladinian	0.588	1	Measurement on IVPP V 18625 (Shang et al. 2020)

Germanosaurus	Eosauropterygia	247.2	242.0	Anisian	NA	2	NA
Lariosaurus calcagnii	Eosauropterygia	242.0	237.0	Ladinian	2.332	2	Measurements on PIMUZ T2464 and PIMUZ T4836 (first-hand measurements)
Lariosaurus curionii	Eosauropterygia	242.0	237.0	Ladinian	NA	1	NA
Lariosaurus balsami	Eosauropterygia	242.0	237.0	Ladinian	0.832	1	Measurement on PIMUZ T4856 (cast) (first-hand measurement)
Lariosaurus buzzii	Eosauropterygia	247.2	242.0	Anisian	NA	1	NA
Lariosaurus vosseveldensis	Eosauropterygia	247.2	242.0	Anisian	NA	1	NA
Lariosaurus hongguoensis	Eosauropterygia	247.2	242.0	Anisian	0.5967	1	Estimated from GMPKU-P-1011 (Jiang et al. 2006a)
Lariosaurus xingyiensis	Eosauropterygia	242.0	237.0	Ladinian	0.708	1	Estimation from XNGM WS-30-R19 (Lin et al. 2017)
Lariosaurus valceresii	Eosauropterygia	242.0	237.0	Ladinian	0.900	1	Measurement on Museo Civicodi Scienze Naturali di Induno Olona P500 (Tintori and Renesto 1990)
Lariosaurus youngi	Eosauropterygia	242.0	237.0	Ladinian	NA	2	NA
Lariosaurus winkelhorsti	Eosauropterygia	247.2	242.0	Anisian	NA	1	NA
Nothosaurus cristatus	Eosauropterygia	242.0	237.0	Ladinian	NA	3	NA
Nothosaurus luopingensis	Eosauropterygia	247.2	242.0	Anisian	1.175	2	Estimation from IVPP V 24895 (Shang et al. 2022)
Nothosaurus giganteus	Eosauropterygia	247.2	227	Anisian-Carnian	4.010	3	Measurement on PIMUZ T4829 (first-hand measurement)
Nothosaurus jagisteus	Eosauropterygia	242.0	237.0	Ladinian	NA	2	NA
Nothosaurus marchicus	Eosauropterygia	242.0	237.0	Ladinian	0.726	1	Estimation from TWE 4800000474 (first-hand photographs)
Nothosaurus mirabilis	Eosauropterygia	247.2	237.0	Anisian-Ladinian	2.873	3	Estimation based on UMO 1000 (Klein et al. 2022a)

Nothosaurus yangjuanensis	Eosauropterygia	247.2	242.0	Anisian	2.203	3	Estimation provided by Li and Liu (2020) based on GMPKU-P-3014
Simosaurus gaillardoti	Eosauropterygia	242.0	237.0	Ladinian	NA	3	NA
Paludidraco multidentatus	Eosauropterygia	237.0	227.0	Carnian	NA	3	Estimation from MUPA-ATZ0101 (Cabezuelo-Hernández et al. 2024)
Corosaurus	Eosauropterygia	251.2	247.2	Olenekian	NA	2	NA
Cymatosaurus	Eosauropterygia	247.2	242.0	Anisian	0.933	1	Estimation from NMNHL RGM 449487A (Sander et al. 2014)
Augustasaurus hagdorni	Eosauropterygia	247.2	242.0	Anisian	NA	3	NA
Bobosaurus	Eosauropterygia	237.0	227.0	Carnian	2.893	3	Estimation from the specimen MFSN 27285 (Dalla Vecchia 2006)
Pistosaurus	Eosauropterygia	247.2	242.0	Anisian	NA	3	NA
Wangosaurus brevirostris	Eosauropterygia	242.0	237.0	Ladinian	2.467	3	Estimation provided by Li and Liu (2020) based on GMPKU-P-1529 (Ma et al. 2015)
Yunguisaurus liae	Eosauropterygia	242.0	237.0	Ladinian	4.200	3	Estimation from the specimen ZMNH M8738 (Sato et al. 2014b)
Rhaeticosaurus mertensi	Eosauropterygia	208.5	201.3	Rhaetian	2.128	3	Estimation based on LWL-MFN P 64047 (Wintrich et al. 2017)
Stratesaurus taylori	Eosauropterygia	201.3	199.3	Hettangian	NA	2	NA
Macroplata tenuiceps	Eosauropterygia	201.3	199.3	Hettangian	5.4181	3	Estimation from NHMUK PV R 5488 (Ketchum and Smith 2010)
Eoplesiosaurus antiquior	Eosauropterygia	201.3	199.3	Hettangian	NA	3	NA
Plesiopharos moelensis	Eosauropterygia	199.3	190.8	Sinemurian	NA	3	NA
Westphaliasaurus simonsensii	Eosauropterygia	190.8	182.7	Pliensbachian	4.736	3	Estimation from LWL-MFN P 58091(Schwermann and Sander 2011)
Eretmosaurus rugosus	Eosauropterygia	199.3	190.8	Sinemurian	NA	3	NA

Plesiosaurus dolichodeirus	Eosauropterygia	199.3	190.8	Sinemurian	2.852	3	Estimation from NHMUK PV R 22656 (measurement on 3D model)
Microcleidus brachypterygius	Eosauropterygia	182.7	174.1	Toarcian	3	3	Measured on GPIT-RE-3185 first-hand measurement)
Microcleidus homalospondylus	Eosauropterygia	182.7	174.1	Toarcian	NA	3	NA
Microcleidus melusinae	Eosauropterygia	182.7	174.1	Toarcian	NA	3	NA
Microcleidus tournemirensis	Eosauropterygia	182.7	174.1	Toarcian	NA	3	NA
Seeleyosaurus guilelmiimperatoris	Eosauropterygia	182.7	174.1	Toarcian	3.023	3	Measurement on MB.R.1992 (first-hand photographs)
Plesiopterys wildi	Eosauropterygia	182.7	174.1	Toarcian	1.707	2	Estimation from SMNS 16182 (first-hand measurements)
Franconiasaurus brevispinus	Eosauropterygia	182.7	174.1	Toarcian	4.628	3	Estimation from BT 011224.00 (Sachs et al. 2024)
Anningasaura lymense	Eosauropterygia	201.3	199.3	Hettangian	NA	3	NA
Archaeonectrus rostratus	Eosauropterygia	199.6	190.3	Sinemurian	3.554	3	Measurement on NHMUK PV OR 38525 (3D model)
Atychodracon megacephalus	Eosauropterygia	201.3	199.3	Hettangian	5.8	3	Estimation provided by Smith (2007) from LEICS G221.1851
Avalonnectes arturi	Eosauropterygia	201.3	199.3	Hettangian	2.244	3	Estimation from NHMUK PV OR 14550 (3D model)
Eurycleidus arcuatus	Eosauropterygia	201.3	199.3	Hettangian	NA	3	NA
Meyerasaurus victor	Eosauropterygia	182.7	174.1	Toarcian	3.447	4	Measurement on SMNS 12478 (first-hand measurement)
Rhomaleosaurus cramptoni	Eosauropterygia	182.7	174.1	Toarcian	6.679	3	Measurement on NHMUK PV 34 (cast) (3D model)
Rhomaleosaurus thorntoni	Eosauropterygia	182.7	174.1	Toarcian	6.650	4	Estimation provided by A. S. Smith & Benson (2014) from NHMUK PV R4853
Rhomaleosaurus zetlandicus	Eosauropterygia	182.7	174.1	Toarcian	4.544	3	Measurement on WHITM 851S (3D model)
Maresaurus coccai	Eosauropterygia	170.3	169.7	Bajocian	NA	4	NA

Borealonectes russelli	Eosauropterygia	166.1	163.5	Callovian	NA	3	NA
Hauffiosaurus tomistomimus	Eosauropterygia	182.7	174.1	Toarcian	4.21	3	Estimation from MANCH LL 8004 (Benson et al. 2011b)
Hauffiosaurus zanoni	Eosauropterygia	182.7	174.1	Toarcian	3.4	3	Measurement provided by Gutarra based on Hauff uncatalogued (Vincent 2011)
Hauffiosaurus longirostris	Eosauropterygia	182.7	174.1	Toarcian	NA	3	NA
Thalassiodracon hawkinsii	Eosauropterygia	201.3	199.3	Hettangian	1.959	2	Measurement from NHMUK PV OR 2020 (3D model)
Attenborosaurus conybeari	Eosauropterygia	201.3	199.3	Hettangian	4.112	3	Estimation from NHMUK PV OR 1339 (3D model)
Arminisaurus schuberti	Eosauropterygia	190.8	182.7	Pliensbachian	NA	3	NA
Cryonectes neustriacus	Eosauropterygia	190.8	182.7	Pliensbachian	NA	3	NA
Anguanax zignoi	Eosauropterygia	163.5	157.3	Oxfordian	NA	3	NA
Marmornectes candrewi	Eosauropterygia	166.1	163.5	Callovian	NA	3	NA
Peloneustes philarchus	Eosauropterygia	166.1	163.5	Callovian	4.2	3	Measurement provided by Gutarra et al. (2023) based on GPIT-RE-3182
Djupedalia engeri	Eosauropterygia	152.1	145.0	Tithonian	NA	3	NA
Ophthalmothule cryostea	Eosauropterygia	152.1	139.8	Tithonian–Berriasian	5.25	3	Estimation from PMO 224.248 (Roberts et al. 2020)
Pantosaurus striatus	Eosauropterygia	163.5	157.3	Oxfordian	5.1638	3	Estimation from USNM 53696 (Wilhelm and O'Keefe 2010)
Abyssosaurus nataliae	Eosauropterygia	132.6	129.4	Hauterivian	5.9515	3	Estimation from MChEIO, no. PM/1 (Berezin 2011)
Colymbosaurus svalbardensis	Eosauropterygia	152.1	145.0	Tithonian	NA	3	NA
Colymbosaurus megadeirus	Eosauropterygia	168.3	145	Bathonian–Tithonian	NA	3	NA
Cryptoclidus eurymerus	Eosauropterygia	166.1	163.5	Callovian	3.72	3	Measurement provided by Gutarra et al. (2023) based on GPIT RE 3183

Tatenectes laramiensis	Eosauropterygia	166.1	163.5	Callovian	4.0567	3	Estimation on USNM 536976 (O'Keefe et al. 2011)
Kimmerosaurus langhami	Eosauropterygia	152.1	145	Tithonian	NA	3	NA
Tricleidus seeleyi	Eosauropterygia	166.1	163.5	Callovian	NA	3	NA
Muraenosaurus leedsii	Eosauropterygia	166.1	163.5	Callovian	5.436	3	Measurement provided by Gutarra et al. (2023) based on NHMUK R 2678 (Andrews 1910)
Picrocleidus beloclis	Eosauropterygia	166.1	163.5	Callovian	NA	3	NA

Table S3.2. Humeral proximodistal length used in the body size estimation of incomplete ichthyopterygian species to estimate body size. The equation used in the estimation of size is: **Body_size_estimation**=0.0255***humerus_length**–0.2188, provided by Scheyer et al. (2014).

Taxon	Humerus length (in mm)	Body size estimation (in m)
Cartorhynchus lenticarpus	11.37	0.45
Chaohusaurus brevifemoralis	23.22	0.92
Chaohusaurus chaoxianensis	14.97	0.60
Chaohusaurus geishanensis	22.7	0.90
Chaohusaurus zhangjiawanensis	47.05	1.85
Utatsusaurus hataii	47.66	1.88
Mixosaurus cornalianus	22.76	0.90
Mixosaurus kuhnschnyderi	20.5	0.81
Phalarodon atavus	20.3	0.80
Phalarodon callawayi	43.26	1.71
Phalarodon fraasi	25.4	1.00
Mixosaurus panxianensis	37.9	1.49
Cymbospondylus buchseri	140	5.50
Cymbospondylus duelferi	126	4.95
Cymbospondylus youngorum	453.0	17.77
Xinminosaurus catactes	70	2.75
Qianichthyosaurus xingyiensis	49.02	1.93
Qianichthyosaurus zhoui	65.37	2.57
Guizhouichthyosaurus tangae	139	5.46
Guizhouichthyosaurus wolonggangense	116.25	4.57
Guanlingsaurus liangae	151.4	5.95
Shastasaurus pacificus	148.4	5.83
Callawayia neoscapularis	63.7	2.51
Shonisaurus popularis	400	15.69
Shonisaurus sikanniensis	528	20.71
Californosaurus perrini	48.8	1.92
Hudsonelpidia brevirostris	36.21	1.43
Temnodontosaurus crassimanus	196.81	7.73
Temnodontosaurus azerguensis	247.5	9.71
Leptonectes tenuirostris	105.75	4.16
Leptonectes moorei	72.4	2.85
Leptonectes solei	192.71	7.57
Excalibosaurus costini	139.4	5.48
Ichthyosaurus anningae	46.9	1.85
Ichthyosaurus breviceps	40.35	1.59
Ichthyosaurus communis	60.45	2.38

Ichthyosaurus conybeari	25.6	1.01
Ichthyosaurus larkini	63.26	2.49
Protoichthyosaurus prostaxalis	105.75	2.52
Protoichthyosaurus applebyi	64.0	1.75
Hauffiopteryx altera	46	1.81
Hauffiopteryx typicus	73.9	2.91
Stenopterygius aaleniensis	101	3.78
Malawania anachronus	89.45	3.24
Sisteronia seeleyi	89.83	5.27
Acamptonectes densus	124.42	3.97
Nannopterygius yasykovi	77.19	3.52
Nannopterygius saveljeviensis	76.22	3.53
Undorosaurus gorodischensis	160.86	4.89
Caypullisaurus bonapartei	175.03	3.04
Gengasaurus nicosiai	130.6	3.00
Cryopterygius kristiansenae	155	6.32

Table S3.3. Length of the last four dorsal vertebrae used in the body size estimation of incomplete eosauropterygian species to estimate body size. The equation used in the is: Log(Body_size_estimation)=0.0255*log(last_four_dorsal_vertebrae_length)–0.2188, provided by Li and Liu (2020).

Taxon	Length of the last four dorsal vertebrae (in mm)	Body size estimation (in m)
Hanosaurus hupehensis	41.446	0.8496
Majiashanosaurus discocoracoidis	22.945	0.4481
Anarosaurus heterodontus	20.552	0.3977
Dactylosaurus gracilis	14.161	0.2658
Dawazisaurus brevis	23.53	0.4605
Dianopachysaurus dingi	9.34	0.1694
Luopingosaurus imparilis	19.85	0.3831
Panzhousaurus rotundirostris	21.05	0.4082
Prosantosaurus scheffoldi	19.84	0.3829
Qianxisaurus_chajiangensis	35.76	0.7242
Lariosaurus balsami	40.66	0.8322
Lariosaurus hongguoensis	29.9	0.5967
Lariosaurus xingyiensis	35.02	0.7080
Nothosaurus luopingensis	55.94	1.1753
Nothosaurus marchicus	35.86	0.7264
Nothosaurus mirabilis	127.78	2.8728
Nothosaurus yangjuanensis	100	2.2035
Paludidraco multidentatus	152.36	3.4752
Cymatosaurus	45.183	0.9328
Bobosaurus forojuliensis	128.6	2.8927
Wangosaurus brevirostris	111	2.4669
Rhaeticosaurus mertensi	91.81	2.1275
Macroplata tenuiceps	229.68	5.4181
Westphaliasaurus simonsensii	202.83	4.7362
Plesiopterys wildi	78.97	1.7067
Franconiasaurus brevispinus	198.56	4.6284
Avalonnectes arturi	101.68	2.2436
Attenborosaurus conybeari	177.99	4.1119
Abyssosaurus nataliae	250.5	5.9515
Pantosaurus striatus	219.7	5.1638
Tatenectes laramiensis	175.78	4.0567

Body size category assignment for ichthyosaurians

- ***Himalaysaurus tibetensis*:** The holotype would have had a body length exceeding 15m (Dong 1972; Motani et al. 1999) .

- ***Ichthyotitan severnensis*:** According to the size of the two referred partial mandibles, the body length of this species is estimated between 2 and 2.5m (Lomax et al. 2024).

- ***Toretocnemus californicus*:** this taxon has a body size estimated between 1–1.5m (Merriam 1903; Li 1999; McGowan and Motani 2003; Zverkov et al. 2022).

- ***Toretocnemus zitelli*:** *T. zitelli* is thought to be very similar to *T. californicus* (Merriam 1903).

- ***Macgowania janiceps*:** Triassic parvipelvians are small-sized (McGowan 1995, 1996a). By personal observation of the holotype ROM 41992 and the specimen RTMP 2009.121.0001 and comparison with primitive parvipelvians, we estimate *M. janiceps* to measure between 1 and 2m.

- ***'Temnodontosaurus risor'* :** The species is only known from cranial material (McGowan 1994d). By comparison of skull dimensions with complete Early Jurassic parvipelvian specimens based on personal observation (A. Laboury, pers. obs.), we estimate *'T. risor'* to have a body length close to 3.5–4m.

- ***Temnodontosaurus zetlandicus*:** The species is only known from an almost complete skull which is estimated to be approximately 1 meter in total length (Laboury et al. 2022). By comparison with complete temnodontosaurids and based on personal observation (A. Laboury, pers. obs.), we estimate the size of *T. zetlandicus* to approximate or be slightly greater than 5m.

- ***Temnodontosaurus eurycephalus*:** The species is only known from a complete skull and mandible (McGowan 1974) which measures more than 1m. By comparison with complete temnodontosaurids, we estimate the size of *T. eurycephalus* between 5 and 6m long.

- ***Wahlisaurus massarae*:** The fragmentary holotype of species is considered as small-bodied (Lomax et al. 2018b). By comparison of mandible and element of girdles proportions with other Early Jurassic parvipelvian, we estimate the size of *W. massarae* between 1 and 2m long.

- ***Chacaicosaurus cayi*:** The cranium of the holotype approximates 1m (Fernández 1994) . By comparison with other Middle Jurassic ophthalmosaurids, we estimate the size of *C. cayi* between 5 and 6m long.

- ***Ophthalmosaurus natans*:** This species is considered similar in terms of body proportions to *Ophthalmosaurus icenicus* which is more than 4m long (Massare et al. 2006; Moon and Kirton 2016; Gutarra et al. 2023).

- ***Leninia stellans*:** The species is only known from a partially preserved cranium (Fischer et al. 2014a). By comparison of the orbit and the postorbital length with other ophthalmosaurids, we estimate the size of *L. stellans* between 3 and 5m long.

- ***Mollesaurus periallus*:** The species is only known from a partially preserved cranium and is considered as a large ichthyosaurian by (Fernández 1999). By comparison of the preserved structures with other ophthalmosaurids, we estimate the size of *M. periallus* between 3 and 5m long.

- ***Pervushovisaurus campylodon*:** The species is only known from teeth and partially preserved rostra (Carter 1846a,b; Fischer 2016). The specimen CAMSM B20671a consists of a partial rostrum of a large individual. By comparison with other ophthalmosaurid material, we estimate the size of *P. campylodon* between 4 and 6m long (V. Fischer, pers. obs.)

Body size category assignment for eosauropterygians

- ***Odoiporosaurus teruzzi*:** The species is known from a well preserved cranium and fragmented postcranial material (Renesto et al. 2014). By comparison with eosauropterygian specimens from the same age (Anisian) and locality (Monte San Giorgio), we estimate the size of *O. teruzzi* between 0 and 0.5m.

- ***Germanosaurus schafferi*:** The species is almost known from cranial material (Rieppel 1997). According to Rieppel (1997), dimensions the holotype (NHMW, uncatalogued), would approaches that of *Cymatosaurus*. Then, we estimate the size of *G. schafferi* between 1 and 2m long.

- ***Lariosaurus buzzi*:** The species is known from a partial specimen (Tschanz 1989). According to personal observation of the holotype (PIMUZ T2804) and by comparison with other Middle Triassic nothosaurians, we estimate the size *L. buzzi* between 0.5 and 1m long.

- ***Lariosaurus vosseveldensis*:** The species is known from a complete skull and very fragmented postcranial material (Klein et al. 2016b) (Klein, Voeten, et al., 2016). As the skull measures less than 0.05m (Klein et al. 2016b) and by comparison with other Middle Triassic nothosaurians, we estimate the size of *L. vosseveldensis* between 0.5 and 1m long.

- ***Lariosaurus youngi*:** The specimen described by Ji et al. (2014) (WS-30-R24) only lack the posterior portion of the tail and measures ~1.20m. Gastralia are preserved on the ventral side, making the estimation of the last four dorsal vertebrae not possible. Considering the size of the preserved part of WS-30-R24, we estimate the size *L. youngi* between 1.5 and 2m long.

- ***Lariosaurus winkelhorsti*:** The species is only known from a single complete cranium (Klein and Albers 2009). The skull size of the holotype (NMNHL RGM 443825) is similar in proportions to that of *L. vosseveldensis* (~0.05m) (A. Laboury, pers. obs.) suggesting that *L. winkelhorsti* would have had a body size between 0.5 and 1m long.

- ***Nothosaurus cristatus*:** The species is only known from a single complete cranium (Hinz et al. 2019). This skull has a similar in size than that of large *Lariosaurus calcagnii* specimens (*e.g.* PIMUZ T 4836) which measure more than 2m (A. Laboury, pers. obs.). By comparison, we estimate the size of *N. cristatus* between 2 and 4m long.

- ***Nothosaurus jagisteus*:** The species is only known from a complete cranium and partial postcranial material (Rieppel 2001a). The skull of the holotype (SMNS 56618) is similar in length to that of *L. youngi*. By comparison, we estimate the size of *N. jagisteus* between 1 an 2m long.

- ***Simosaurus gaillardoti*:** The total length of this species has been estimated between 3 and 4m long according to Rieppel (1994), de Miguel Chaves et al. (2018a) and personal observation of SMNS material referred as *S. gaillardoti* (A. Laboury, pers. obs.)

- ***Corosaurus alcovensis*:** According to Storrs (1991), the estimated length of the trunk is ~0.5m. Then, the total body size of *C. alcovensis* is evaluated at close to 2m long. Additionally, considering that the size of the cranium is ~0.13m (Storrs 1991), estimating the body size of *Corosaurus* between 1 and 2m appears more conservative.

- ***Augustasaurus hagdorni*:** Sander et al. (1997) by examination of the holotype (FMNH PR1974), estimated its body size between 2.5 and 3m long.

- ***Pistosaurus longaevus*:** According to Sander et al. (1997), *P. longaevus* and *A. hagdorni* would have the same body length.

- ***Stratesaurus taylori*:** According to Benson et al . (2015), *S. taylori* is a small body-size plesiosaurian, very similar to *Thalassiodracon hawkinsii* in terms of body proportions. Therefore, we estimate the size of *S. taylori* between 1.5 and 2m long.

- ***Eoplesiosaurus antiquior*:** The holotype (TTNCM 8348), measured ~3m long and is nearly complete as it lacks the cranium and the last caudal vertebrae (Benson et al. 2012). Therefore, we estimate the size of *E. antiquior* to approximate 3.5m.

- ***Plesiopharos moelensis*:** The species is known from a very fragmentary disarticulated specimen (Puértolas Pascual et al. 2021). The proximal length of the humerus is 0.15m. By comparison with other Early Jurassic plesiosaurians, we estimate the body size of *P. moelensis* between 2 and 3m long.

- ***Eretmosaurus rugosus*:** By personal observation of the nearly complete holotype (NHMUK PV OR 14435) (A. Laboury, pers. obs.), we estimate the body size of *E. rugosus* between 2 and 3m.

- ***Microcleidus homalospondylus*:** The species is only known from a nearly complete cranium (Owen 1865). By personal examination of the holotype (NHMUK PV OR 36184) and comparison with other microcleidids, we estimate the body size of *M. homalospondylus* between 2 and 3m long.

- ***Microcleidus melusinae*:** The species is only known from a nearly complete cranium and anterior part of the postcranial squeletton (Vincent et al. 2017). By personal examination of the holotype (MNHNL TV 434) and comparison with other microcleidids, we estimate the body size of *M. melusinae* between 2 and 3m long.

- ***Microcleidus tournemirensis*:** The species is only known from a nearly complete cranium and a disarticulated postcranial skeleton (Sciau et al. 1990). By comparison of the holotype with other microcleidids, we estimate the body size of *M. tournemirensis* between 2 and 3m long.

- ***Anningasaura lymense*:** The species is only known from a cranium preserved in three dimensions (Vincent and Benson 2012). By personal observation of the holotype (NHMUK PV OR 49202) (A. Laboury, pers. obs.), comparison with other

Early Jurassic plesiosaurian and considering that it is likely a juvenile (Vincent and Benson 2012), we estimate the body size of *A. lymense* between 3 and 5m long.

- ***Eurycleidus arcuatus*:** According to Smith (2007), the specimen NMING F8749 can be attributed to this species. The specimen is nearly complete and measure ~3.60m long.

- ***Maresaurus coccai*:** The species is known from a completely preserved cranium and by some anteriormost vertebrae (Gasparini 1997). By comparison with other rhomaleosaurids, the mandible length of *M. coccai* is similar to that of *Rhomaleosaurus cramptoni*. Therefore, we estimate the size of *M. coccai* to be more than 6m long.

- ***Borealonectes russeli*:** The species is known from a nearly complete cranium and some disarticulated postcranial elements (Sato and Wu 2008). By comparison of cranial and humerus dimensions with other rhomaleosaurids, *B. russeli* should have had a body size nearly similar or slightly bigger than *Meyerasaurus victor,* which measures ~3.35m (Smith and Vincent 2010; A. Laboury, pers. obs).

- ***Hauffiosaurus longirostris*:** The skull of *H. longirostris* (MCZ 1033) is larger than *H. zanoni* and *H. tomistomimus* which have an overall body length between 3.5 and 4.5m long (White 1940; Benson et al. 2011b; Vincent 2011). Then, we estimate the body size of *H. longirostris* between 4 and 6m long.

- ***Arminosaurus schuberti*:** The species is known from a fragment of the posterior part of the mandible and several postcranial isolated or fragmented elements (Sachs and Kear 2018). By comparison with other Early Jurassic pliosaurids, we estimated the body size of *A. schuberti* between 3 and 5m.

- ***Cryonectes neustriacus*:** The species is known from a complete mandible, a partial rostrum and some cervical centra (Vincent et al. 2013a). The size of the of the holotype mandible is 0.47m (Vincent et al. 2013a), a similar size to that of *Hauffiosaurus*. By comparison with the genus, we estimate the body size of *C. neustriacus* between 4 and 6m long.

- ***Anguanax zignoi*:** The species is known from a partial skull and mandible, teeth, and isolated postcranial material (Cau and Fanti 2015). By comparison of the cranial material with other pliosaurids, mostly with *H. zanoni*, we estimate the size of *A. zignoi* to be greater than 3.5m but not exceeding 5m long.

- ***Marmonectes candrewi*:** The species is known by a partial mandibles, isolated cranial bones and postcranial material (Ketchum and Benson 2011a). The size of

the complete mandible ramus is 0.89m. By comparison with other pliosaurids, especially *Peloneutes philarchicus* (Ketchum and Benson 2011b) , we estimate the size of *M. candrewi* between 4 and 6m long.

- ***Djupedalia engeri*:** The species is only known from partial postcranial material (Knutsen et al. 2012b). The humerus size of the holotype (PMO 216.839) is 0.3m. By comparison with close relatives, such as *Franconiasaurus*, we estimate the size of *D. engeri* between 4 and 5m long.

- ***Colymbosaurus svalbardensis*:** The species is known from partial and fragmentary postcranial material (Knutsen et al. 2012c) . The femora of the holotype PMO A 27745 are 0.42 and 0.44m long (Knutsen et al. 2012c) and are slightly longer than that of *Abyssosaurus nataliae* (Berezin 2011). By comparison, we estimate the body size of *C. svalbardensis* between 5 and 6m long.

- ***Colymbosaurus megadeirus*:** The species is only known from partial postcranial material (Benson and Bowdler 2014). Bones dimensions are similar to that of *C. svalbardensis* (Knutsen et al. 2012c). Then, we estimate the body size of *C. megadeirus* between 5 and 6m long.

- ***Kimmerosaurus langhami*:** The species is known from a partial cranium and isolated postcranial elements (Brown 1981). By comparison with other cryptocleidids, the skull size of *K. langhami* is comparable to that of *C. eurymerus* (Brown 1981). Therefore, we estimate the body size of *K. langhami* between 3.5 and 4.5m long.

- ***Tricleidus seeleyi*:** The species is known from a fragmented cranium and partial postcranial skeleton (Andrews 1910; Brown 1981). By comparison with other cryptocleidids, the skull size of *T. seeleyi* is comparable to that of *C. eurymerus* (Brown 1981). Therefore, we estimate the body size of *T. seeleyi* between 3.5 and 4.5m long.

- ***Picrocleidus beloclis*:** According to Brown (1981), the overall body length of this species is estimated at 2.5m.

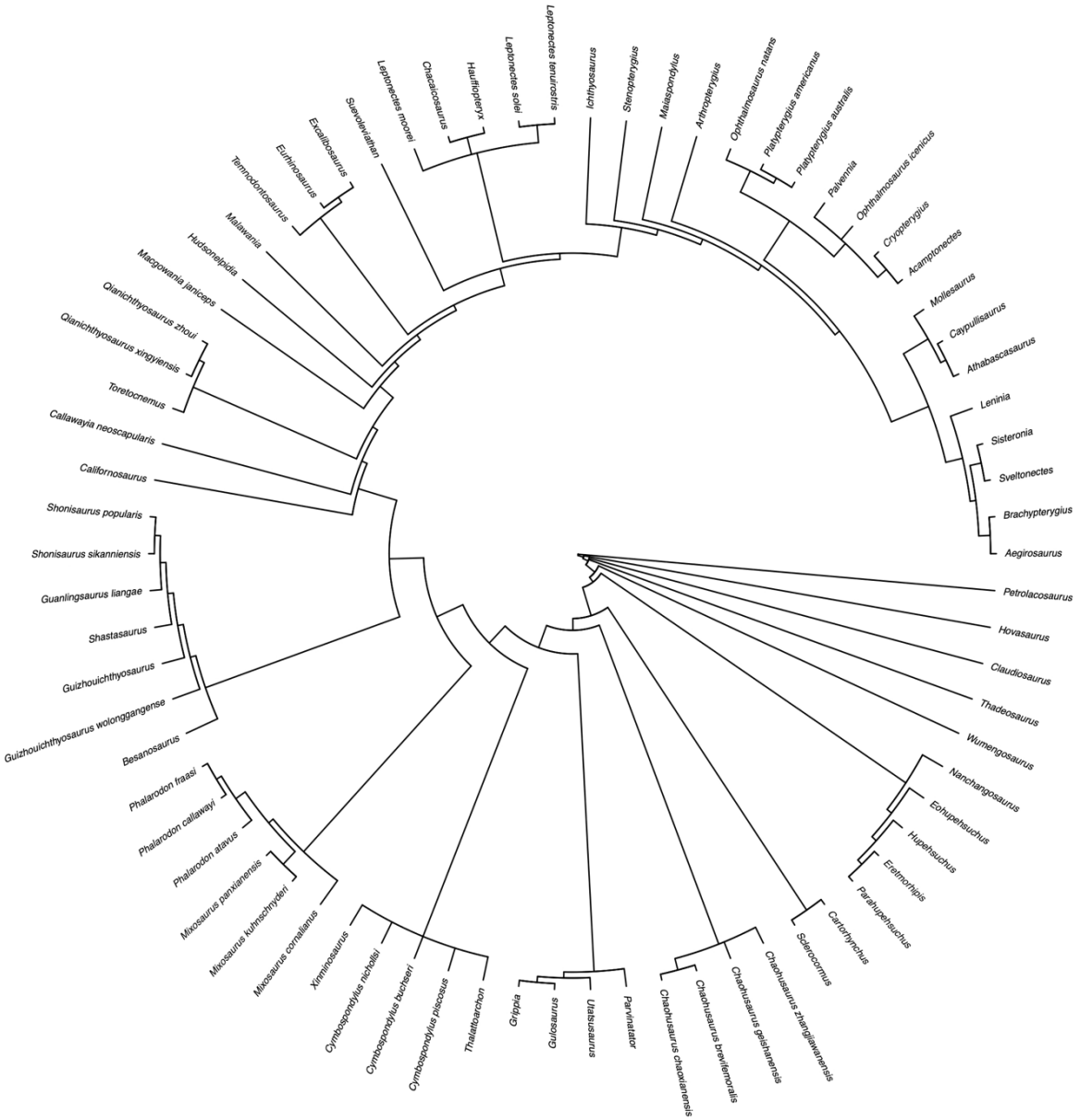

Figure S3.1. 50% majority rule consensus generated with the dataset of Bindellini et al. (2021) within a maximum parsimony framework by using the implied weighting method (*k*=12)

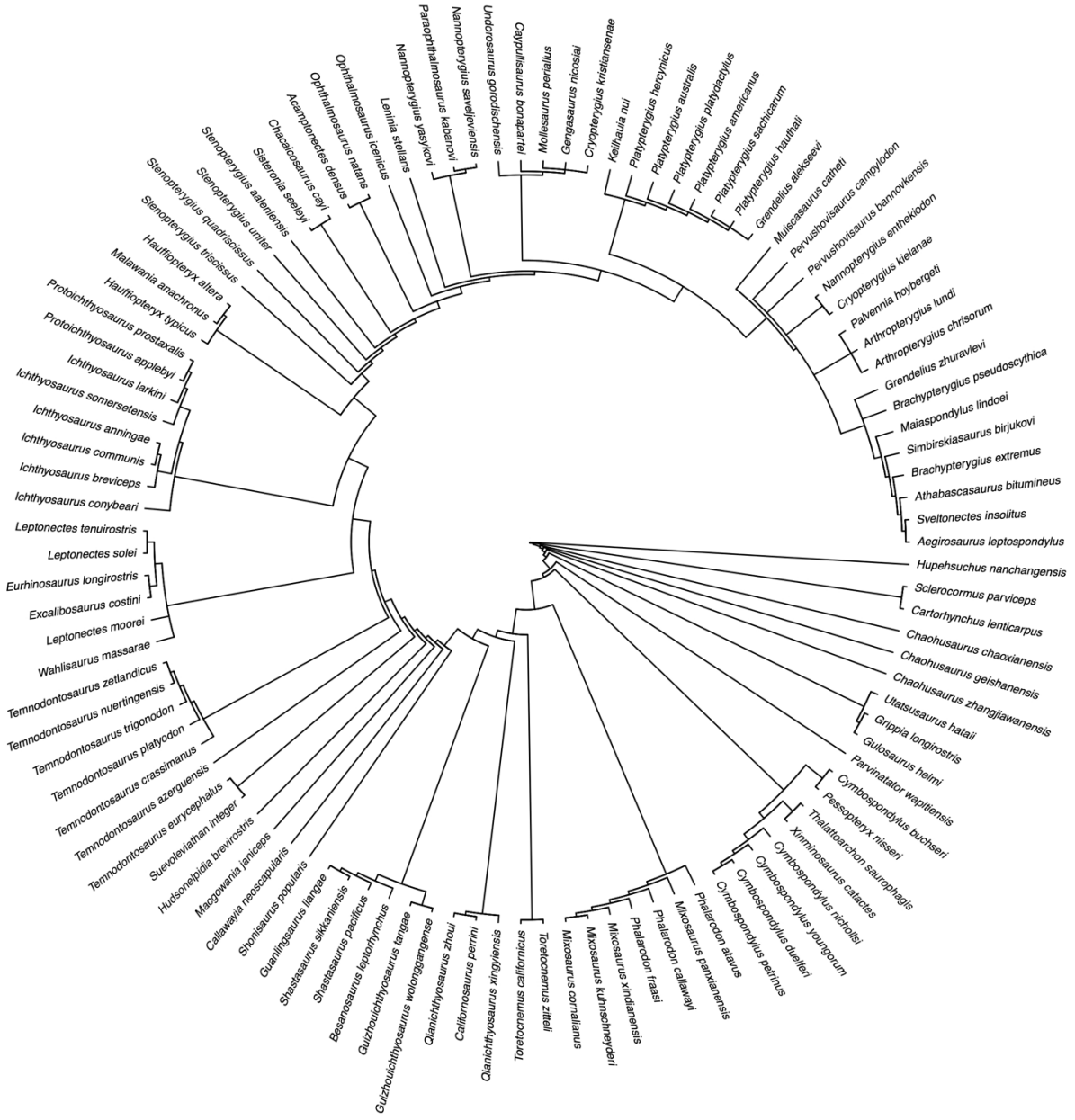

Figure S3.2. 50% majority rule consensus generated with the dataset of Laboury et al. (2022), within a maximum parsimony framework by using the implied weighting method (*k*=12)

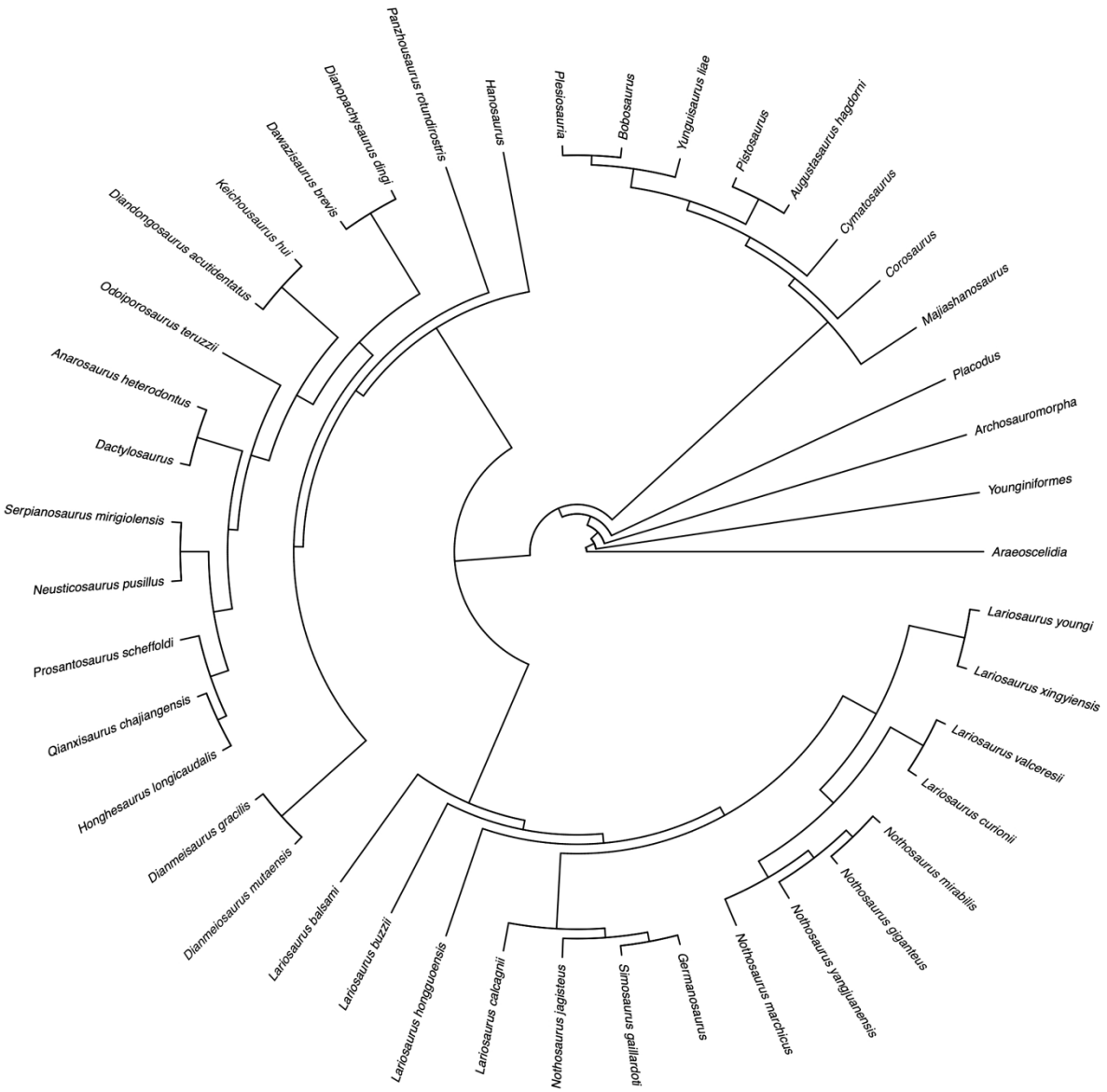

Figure S3.3. 50% majority rule consensus generated with the dataset of Hu et al. (2024), within a maximum parsimony framework by using the implied weighting method (*k*=12)

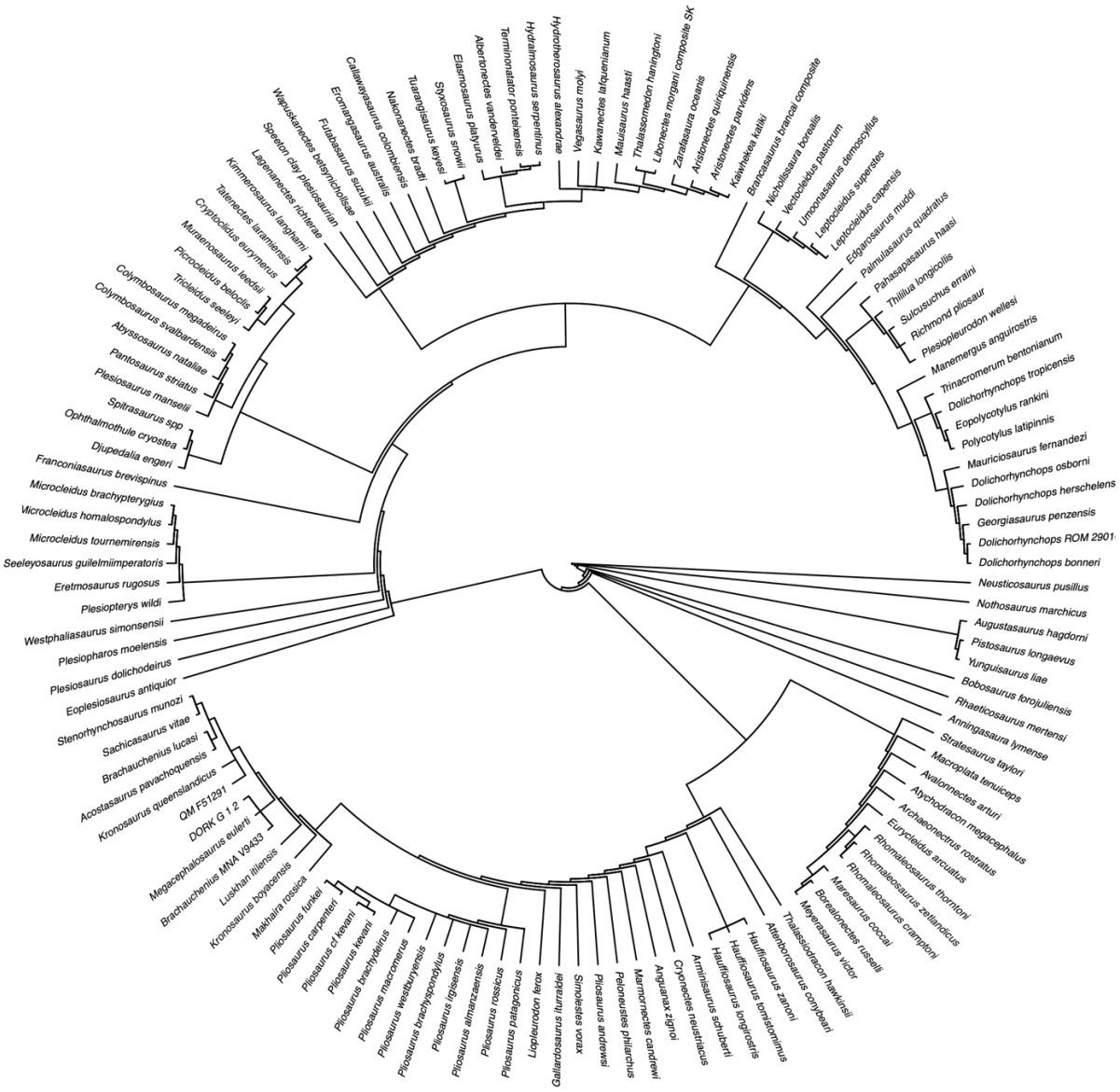

Figure S3.4. 50% majority rule consensus generated with the dataset of Sachs et al. (2024), within a maximum parsimony framework by using the implied weighting method (*k*=12)

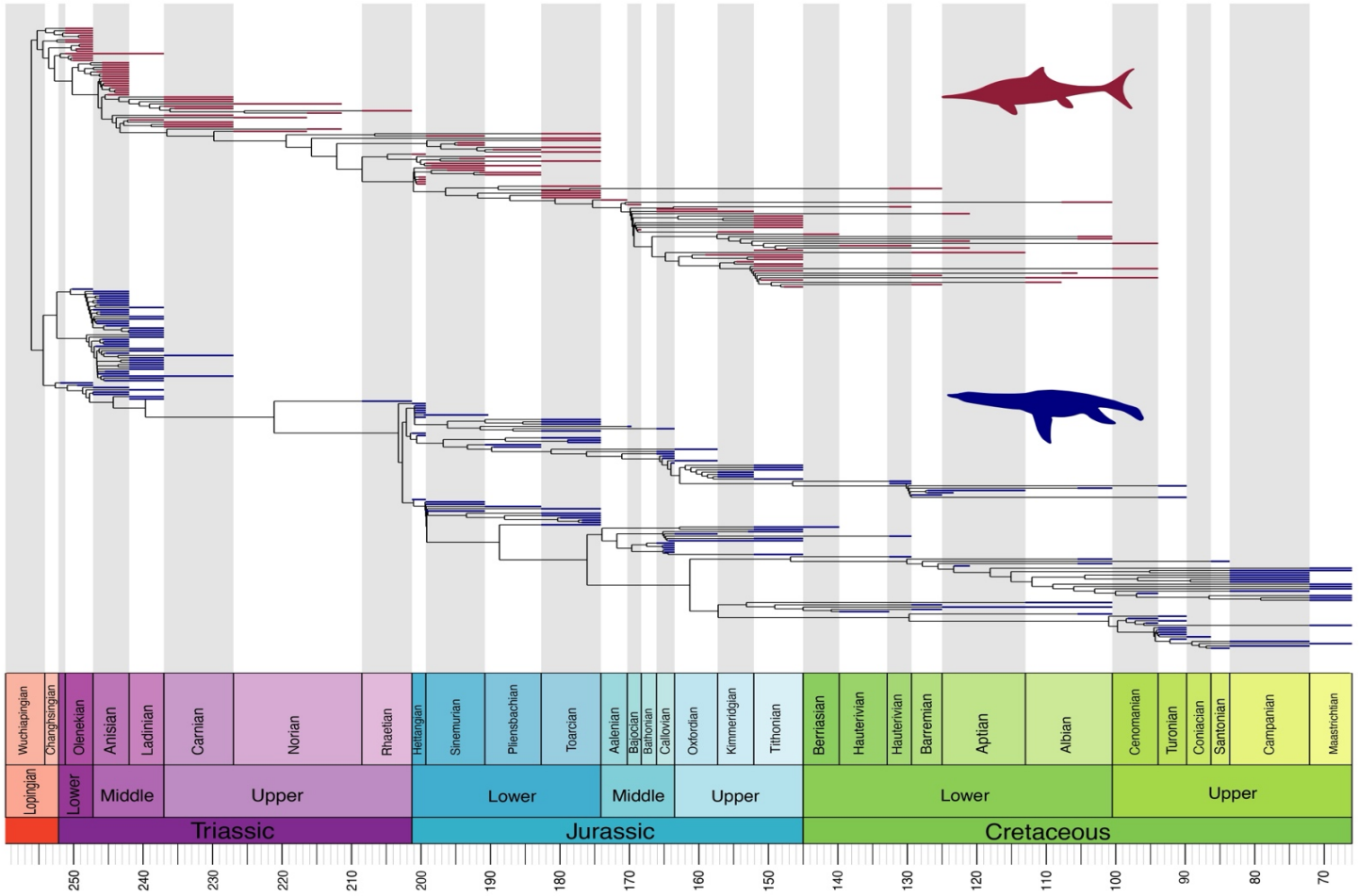

Figure S3.5. Randomly selected time-scaled informal composite tree from the Equal method including all taxa, from the Early Triassic to the Late Cretaceous. Occurrences of ichthyosauriformes and eosauropterygians taxa are coloured in burgundy and dark blue respectively.

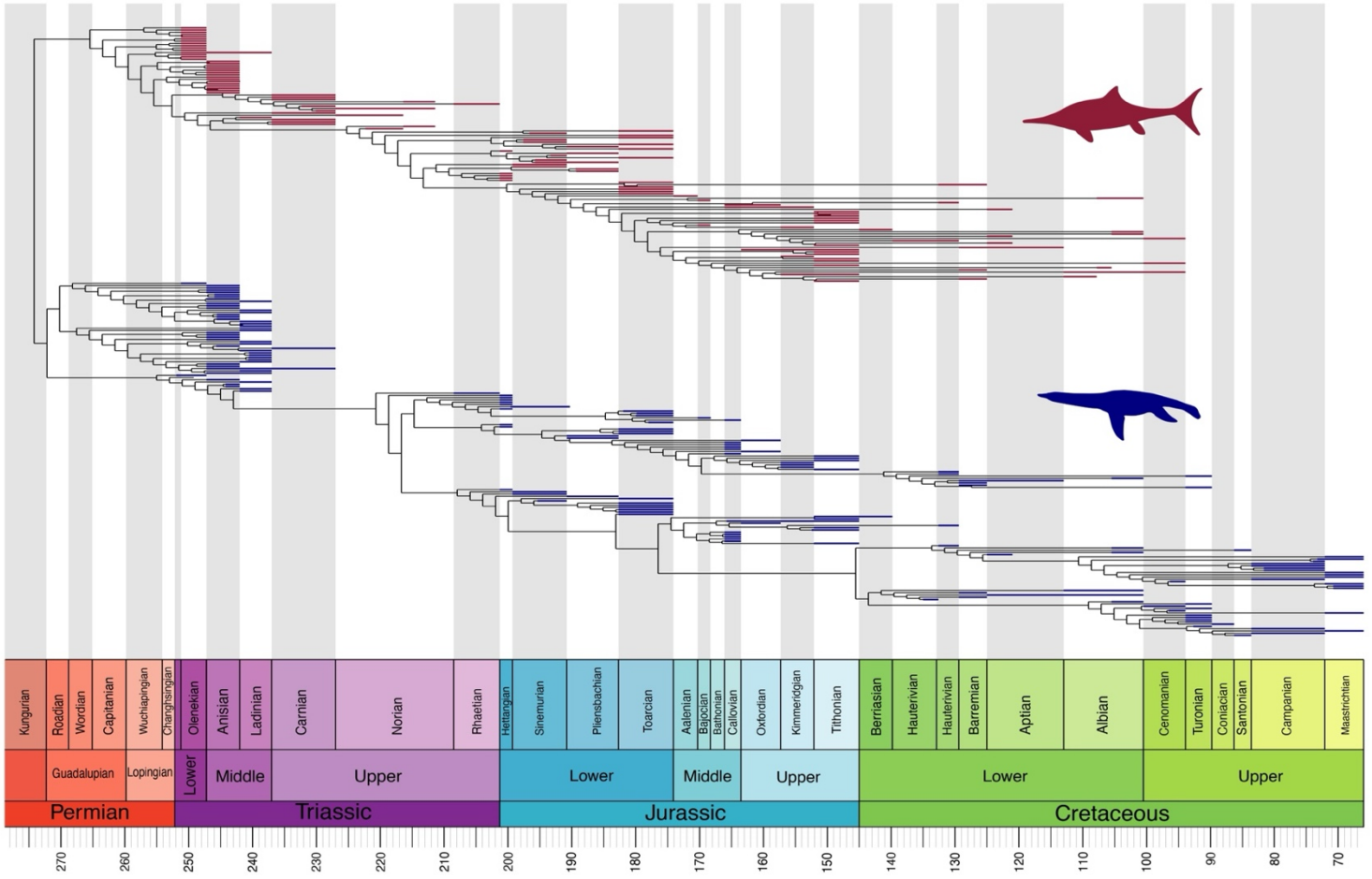

Figure S3.6. Randomly selected time-scaled informal composite tree from the MBL method including all taxa, from the Early Triassic to the Late Cretaceous. Occurrences of ichthyosauriformes and eosauropterygians taxa are coloured in burgundy and dark blue respectively.

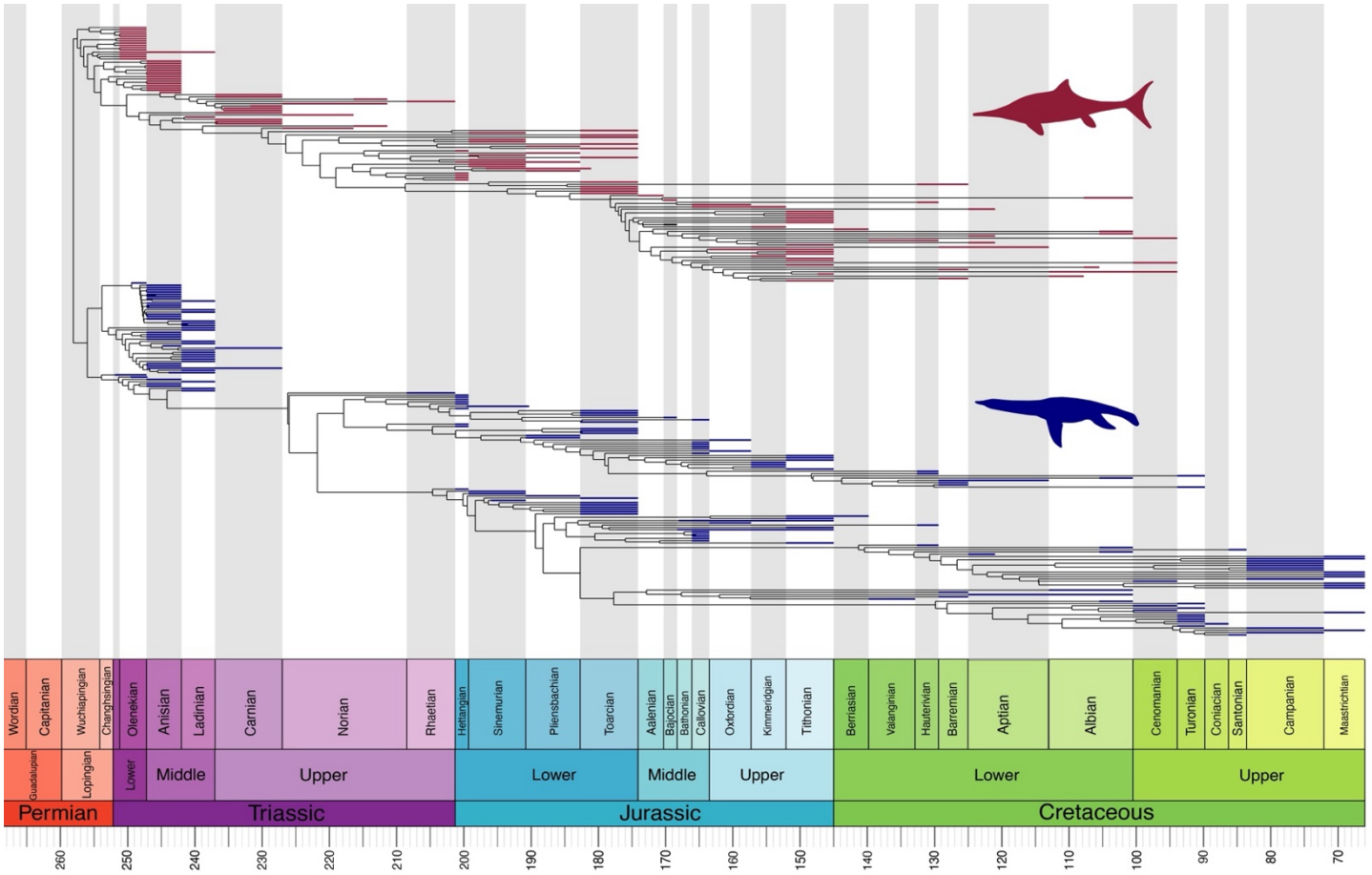

Figure S3.7. Randomly selected time-scaled informal composite tree from the Hedman method including all taxa, from the Early Triassic to the Late Cretaceous. Occurrences of ichthyosauriformes and eosauropterygians taxa are coloured in burgundy and dark blue respectively.

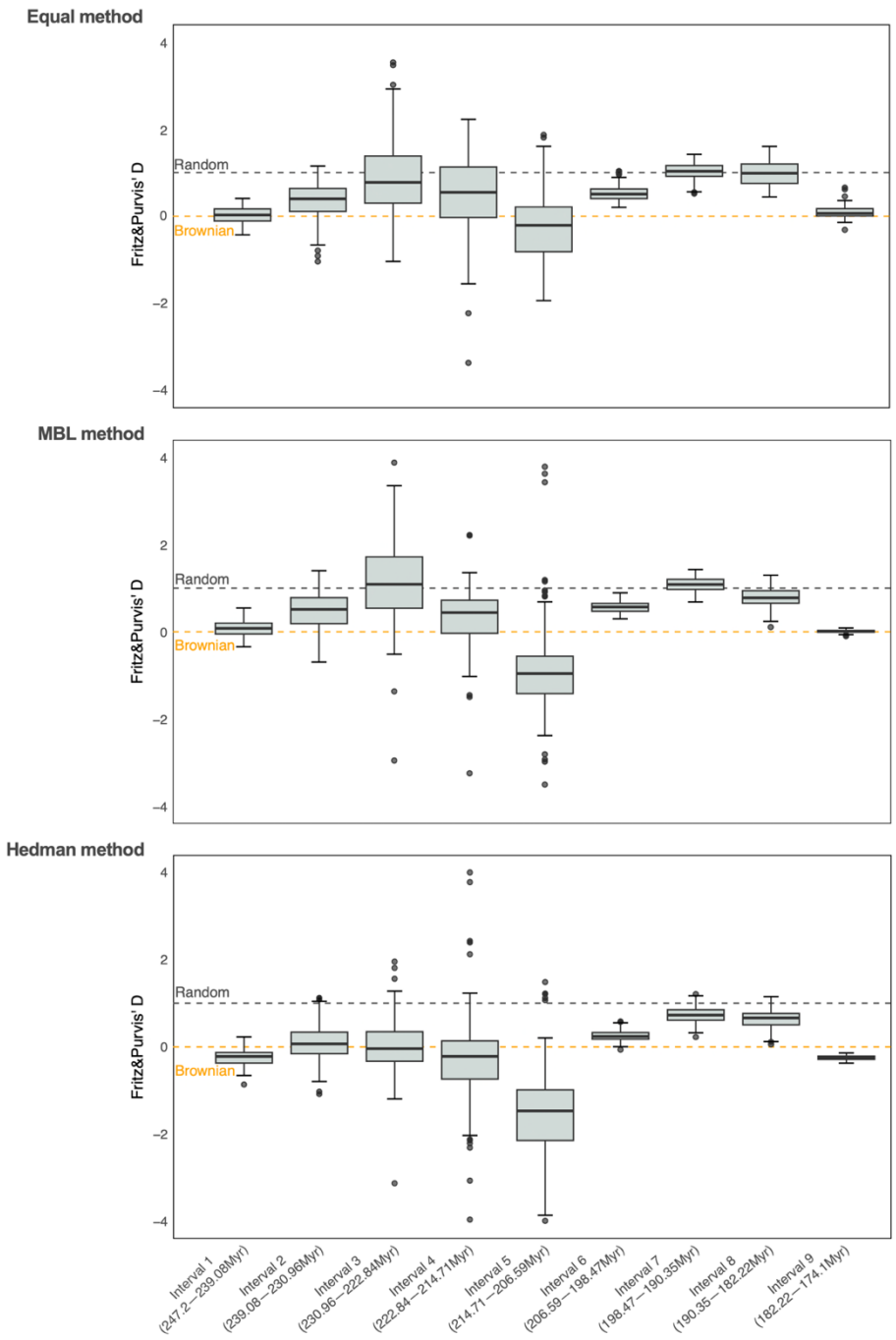

Figure S3.8. Distribution of the *D* statistic throughout the Middle Triassic to Early Jurassic across equivalent time bins for 100 phylogenies dated using each method (Equal, MBL, and Hedman, respectively). A *D* value of 0 indicates a phylogenetically clustered pattern of extinctions within the time bin, consistent with a Brownian motion distribution, whereas a D value of 1 reflects a random extinction pattern.

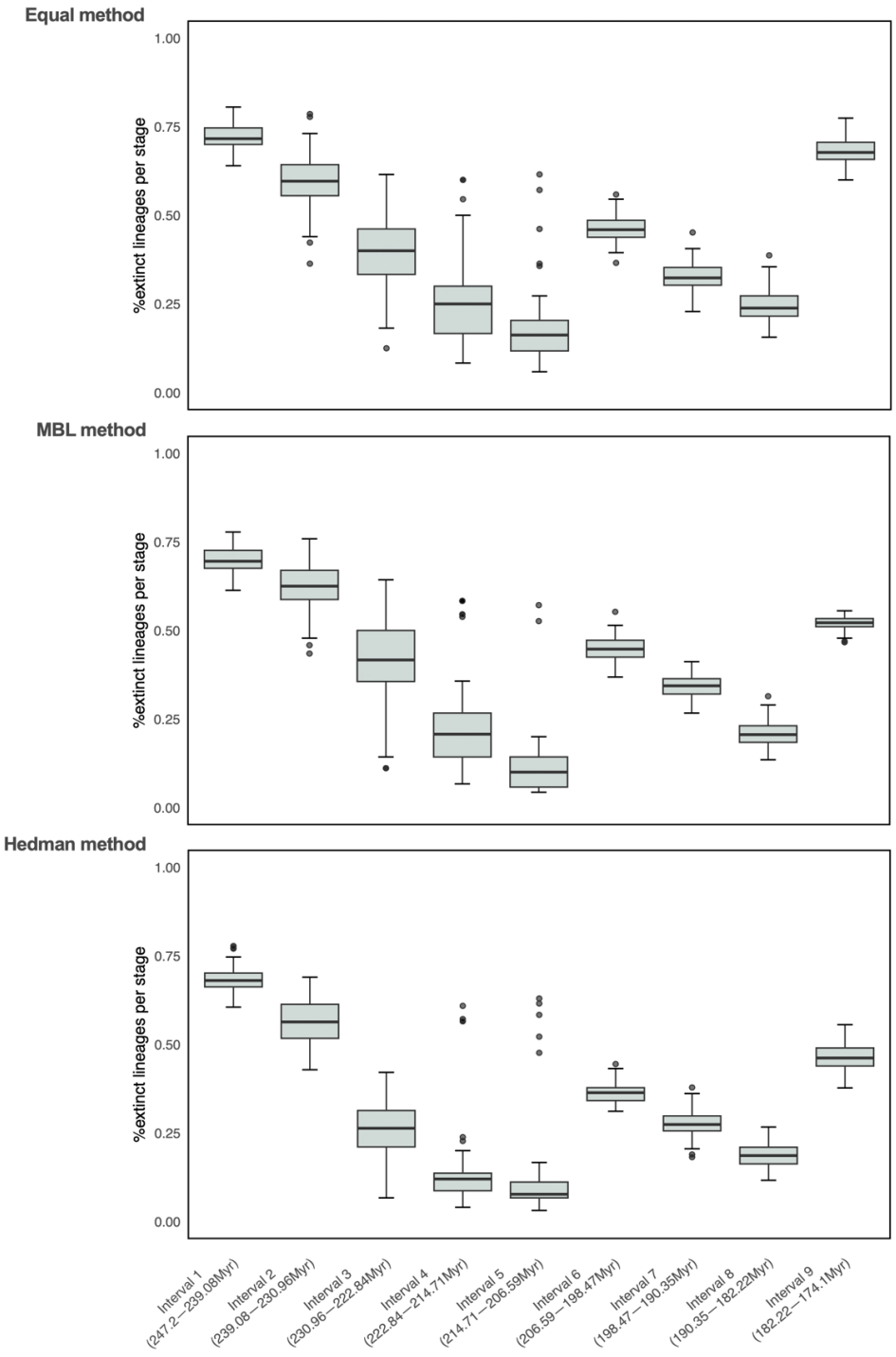

Figure S3.9. Distribution of extinction severity throughout the Middle Triassic to Early Jurassic across equivalent time bins for 100 phylogenies dated using each method (Equal, MBL, and Hedman, respectively).

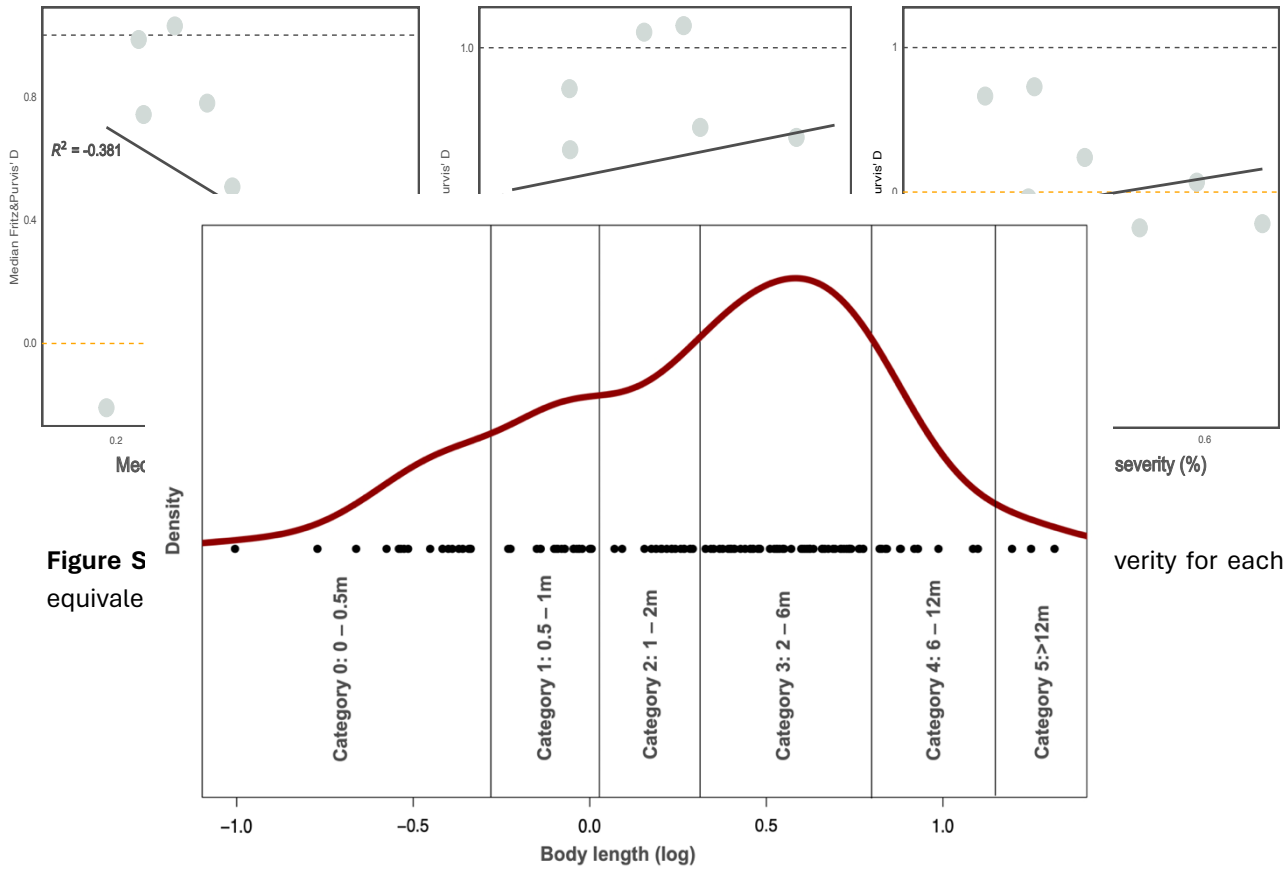

Figure S verity for each equivale

Figure S3.11. Univariate distribution of ichthyosaurian and eosauropterygian total body length (log-transformed) in order to discretize body size into discrete categories.

Table S3.4. Results of the selectivity tests by using the *D* statistic for equivalent time bins. All values are the mean of 100 repetitions generated with trees time-scaled by using each method (Equal, MBL and Hedman respectively). Standard deviations are given in bracket for the *D* statistic. Each time interval has a length of 8.12Myr.

Time bin	Time-scaling method	Survived	Extinct	percentage of extinct lineages	D statistic (SD)	P-value (Brownian expectation)	P-value (Random expectation)
Time bin 1 (247.2 — 239.08 Myr)	Equal	20	52	72.2	0.02207 (0.17580)	0.00039	0.49288
	MBL	22	52	70.3	0.08187 (0.17619)	0.00026	0.4272
	Hedman	24	52	68.4	0.25464 (0.19671)	1E-05	0.7277
Time bin 2 (239.08 — 230.96 Myr)	Equal	11	16	59.3	0.36004 (0.45325)	0.13948	0.31987
	MBL	10	16	61.5	0.48239 (0.42997)	0.18796	0.27205
	Hedman	12	16	57.1	0.09496 (0.43044)	0.07377	0.4791
Time bin 3 (230.96 — 222.84 Myr)	Equal	7	5	41.7	0.92760 (1.08127)	0.42893	0.29195
	MBL	7	5	41.7	1.14641 (1.11141)	0.51776	0.22793
	Hedman	14	5	26.3	0.02111 (0.66515)	0.12468	0.51648
Time bin 4 (222.84 — 214.72 Myr)	Equal	8	3	27.3	1.32936 (2.57406)	0.39302	0.32484
	MBL	11	3	21.4	0.50180 (1.64962)	0.23943	0.38354
	Hedman	20	3	13	0.26615 (1.11281)	0.11835	0.59718
Time bin 5 (214.72 — 206.60 Myr)	Equal	12	2	14.3	-0.20979 (0.86864)	0.13036	0.5885
	MBL	19	2	9.5	-0.80962 (1.17898)	0.11402	0.73711
	Hedman	25	3	10.7	-1.65807 (1.25925)	0.08466	0.79024
Time bin 6 (206.60 — 198.48 Myr)	Equal	20	17	45.9	0.53630 (0.18471)	0.04982	0.11592

	MBL	20	17	45.9	0.57037 (0.12704)	0.03124	0.10692
	Hedman	29	17	37	0.25268 (0.12220)	0.00201	0.27903
Time bin 7 (198.48 — 190.36 Myr)	Equal	23	11	32.4	1.02315 (0.20617)	0.52273	0.01341
	MBL	21	11	34.4	1.07855 (0.16265)	0.59377	0.00468
	Hedman	30	11	26.8	0.74381 (0.18177)	0.20077	0.04748
Time bin 8 (190.36 — 182.24 Myr)	Equal	24	8	25	0.97675 (0.28299)	0.46572	0.04477
	MBL	30	8	21.1	0.79218 (0.23351)	0.26891	0.05009
	Hedman	35	8	18.6	0.64279 (0.22093)	0.15892	0.11209
Time bin 9 (182.22 — 174.1 Myr)	Equal	11	24	68.6	0.09068 (0.14792)	0.007	0.43846
	MBL	22	24	52.2	0.00906 (0.03532)	0	0.49713
	Hedman	27	24	47.1	-0.24944 (0.05127)	0	0.75953

Table S3.5. Results of PGLS analyses for equivalent time bins. All values are the mean of 100 repetitions generated with trees time-scaled by using each method (Equal, MBL and Hedman respectively). Standard deviations are given in bracket for phylogenetic signal (Pagel's λ) and the adjusted R^2. Each time interval has a length of 8.12Myr.

Time bin	Timescaling method	Survived	Extinct	Percentage of extinct lineages	Pagel's λ (SD)	R^2 (SD)	P-value
Time bin 1 (247.2 — 239.1 Myr)	Equal	20	52	72.2	0.94745 (0.03958)	-0.00542 (0.01376)	0.56352
	MBL	22	52	70.3	0.97632 (0.03647)	-0.02933 (0.01284)	0.74212
	Hedman	24	52	68.4	0.95661 (0.05314)	-0.03098 (0.00548)	0.76332
Time bin 2 (239.1 — 230.96 Myr)	Equal	11	16	59.3	0.97991 (0.04123)	-0.00095 (0.07043)	0.50921
	MBL	10	16	61.5	0.96674 (0.06003)	-0.02394 (0.06956)	0.53985
	Hedman	12	16	57.1	0.95876 (0.05693)	-0.03006 (0.05226)	0.59144
Time bin 3 (230.96 — 222.84 Myr)	Equal	7	5	41.7	0.97203 (0.11128)	-0.041 (0.11029)	0.5936
	MBL	7	5	41.7	0.97469 (0.11064)	-0.04934 (0.10304)	0.61297
	Hedman	8	5	38.5	0.91767 (0.23764)	-0.04442 (0.10217)	0.60319
Time bin 4 (222.84 — 214.71 Myr)	Equal	8	3	27.3	0.47763 (0.44406)	-0.0492 (0.09972)	0.57624
	MBL	11	3	21.4	0.04912 (0.16523)	-0.03227 (0.05448)	0.51901
	Hedman	20	3	13	0.90697 (0.20962)	-0.03551 (0.01842)	0.69599
Time bin 5 (214.71 — 206.59 Myr)	Equal	12	2	14.3	0.34825 (0.41865)	0.01862 (0.17642)	0.50656
	MBL	15	2	11.8	0.25152 (0.38342)	0.02883 (0.16211)	0.45926
	Hedman	25	3	10.7	0.94218 (0.13119)	-0.01692 (0.03062)	0.57623
Time bin 6 (206.59 — 198.47 Myr)	Equal	20	17	45.9	0.92976 (0.12433)	0.02472 (0.07468)	0.41451
	MBL	20	17	45.9	0.96126 (0.10582)	0.00292 (0.02691)	0.38238
	Hedman	29	17	37	0.67345 (0.17570)	0.01399 (0.02401)	0.28463

Time bin 7 (198.47 — 190.35 Myr)	Equal	23	11	32.4	0.90904 (0.11955)	-0.02141 (0.01819)	0.6151
	MBL	21	11	34.4	0.90005 (0.06572)	-0.01857 (0.02635)	0.66145
	Hedman	30	11	26.8	0.89419 (0.06230)	0.00099 (0.03121)	0.44926
Time bin 8 (190.35 — 182.22 Myr)	Equal	24	8	25	0.9561 (0.17041)	0.0236 (0.059)	0.35701
	MBL	30	8	21.1	0.94283 (0.05768)	0.03732 (0.07548)	0.30608
	Hedman	35	8	18.6	0.90894 (0.11560)	-0.0068 (0.02951)	0.51568
Time bin 9 (182.22 — 174.1 Myr)	Equal	9	24	72.7	0.99224 (0.01561)	-0.02361 (0.01561)	0.65084
	MBL	16	24	60	0.88622 (0.05262)	0.01649 (0.01138)	0.22281
	Hedman	27	24	47.1	0.78405 (0.15382)	0.02849 (0.03232)	0.22594

GENERAL DISCUSSION

The Late Triassic, a transitional world after major extinction events

Results from both Chapter 2 and Chapter 3 strongly challenge the prevalence of a scenario in which ichthyosaurians and eosauropterygians were substantially affected by a dramatic bottleneck at or just prior the Triassic–Jurassic transition. Instead, they support a more gradual pattern of extinctions, likely starting near the limit between the Middle and the Late Triassic. As shown by other studies and this project, the reduction of shallow water habitats, caused by marine regressions, can be regarded as the primary driver in the restructuration of the marine reptile assemblages during the Late Triassic, triggering substantial extinctions among coastal faunas and a facilitating the diversification of pelagic ones (Bardet 1994; Benson and Butler 2011; Kelley et al. 2014; Renesto and Dalla Vecchia 2018; Druckenmiller et al. 2020; Laboury et al. 2024). It is relatively well established that strong regressions negatively affect the total of marine biodiversity due to the reduction of the total volume available for nearshore environments, which host the majority of marine productivity (Newell 1967; Hallam and Wignall 1999; Benson and Butler 2011; Kelley et al. 2014; Renesto and Dalla Vecchia 2018). While the relationship between eustasy and biodiversity is well-documented for marine invertebrates, the effect of sea-level fluctuations on diversification dynamics among predatory marine tetrapod has rarely been quantified (but see Benson and Butler 2011; Kelley et al. 2014). In addition to the effects of eustatic oscillations, the onset of a warm, humid climate, alongside regional probable volcanic activity — independent from the Central Atlantic Magmatic Province (CAMP) — may also have contributed to the ecological turnover experienced by marine reptiles within that period (Ruffel et al. 2016; Lu et al. 2018; Dal Corso et al. 2020; Zhang et al. 2021; Bastiaans 2024). The significant decline in disparity highlighted by broad macroevolutionary studies during the Late Triassic (Thorne et al. 2011; Dick and Maxwell 2015; Stubbs and Benton 2016; Gutarra et al. 2023), aligns with these environmental changes and appears to be the consequence of the extinction of nearly all ‘typical Middle Triassic’ coastal taxa (Benson and Butler 2011; Kelley et al. 2014; Stubbs and Benton 2016; Druckenmiller et al. 2020; Laboury et al. 2024). Even though Ichthyosauria and Eosauropterygia were both impacted by these regressions — particularly with the definitive extinction of small forms (Chapter 3) — eosauropterygians appear to have been more severely affected. The end of the Ladinian–early Carnian time interval likely coincide with the eradication of all pachypleurosauroids, nothosauroids and seemingly early diverging pistosauroids (Rieppel and Wild 1996; Dalla Vecchia 2006; Fabbri 2013; de Miguel Chaves et al. 2018b; García-Ávila et al. 2021), which had previously undergone remarkable taxonomical and morphological diversification (Laboury et al. 2023; Chapter 1). These animals displayed an impressive range of

morphologies, mainly in the craniodental region, reflecting a high degree of feeding specialization and suggesting the occupation of various ecological niches (Rieppel 2002; de Miguel Chaves et al. 2018; Laboury et al. 2023; Chapter 1). As evidenced in Chapter 2 (Laboury et al. 2024), most of non-pistosauroid eosauropterygian phenotypes were never reoccupied by plesiosaurians throughout the rest of the Mesozoic (Stubbs and Benton 2016; Reeves et al. 2021; Laboury et al. 2024), perhaps with the exception of the filter-feeding strategy that has been suggested for the Triassic simosaurid *Paludidraco* and Late Cretaceous aristonectine elasmosaurids, though their habitat preferences were notably different (O'Keefe et al. 2017; de Miguel Chaves et al. 2018). Although these extinction events do not indicate a reduction in disparity as dramatic in ichthyosaurians as that observed in eosauropterygians (Stubbs and Benton 2016; Laboury et al. 2024; Chapter 2), they still resulted in the definitive disappearance of the small durophagous mixosaurids (McGowan and Motani 2003; Kelley et al. 2014).

Because forms adapted to open-water habitats are supposedly more resilient to eustatic fluctuations (Kelley et al. 2014), pelagic ichthyosaurians and eosauropterygians were less impacted by the reduction of flooded continental shelves. Subsequent Late Triassic faunas, often described as 'transitional', mainly for ichthyosaurians (McGowan 1997), bridge the ecological and taxonomic changes between the Middle Triassic and Early Jurassic periods. However, information on marine reptile diversification in the Late Triassic is highly limited due to the scarcity of the fossil record, particularly during the Norian and the Rhaetian (Benson et al. 2010; Benson and Butler 2011; Fischer et al 2014b; Sander et al. 2022; Laboury et al. 2024; Chapters 2 and 3). Nonetheless, these ichthyosaurian assemblages were mainly characterized by the diversification of shastasaurids which evolved towards gigantism and adopted a variety of feeding strategies, including macropredation and ram-feeding (Camp 1980; Nicholls and Manabe 2004; Motani et al. 2013; Fischer et al. 2014b; Renesto and Dalla Vecchia 2018; Kelley et al. 2022; Sander et al. 2022; Zverkov et al. 2022; Lomax et al. 2024). Additionally, the Late Triassic also witnessed the gradual selective replacement of the smaller Carnian euichthyosaurians by the early diverging parvipelvians (Zverkov et al. 2022; Chapter 3). The pattern of eosauropterygian diversification during that period remains even more obscure, due to the extremely limited amount of informative material, resulting in a poorly documented interval spanning several million years. Nevertheless, some eosauropterygian remains, alongside incomplete specimens, suggest that more advanced pistosauroids and/or plesiosaurians diversified during the Late Triassic (Sennikov and Arkhangelsky 2010; Wintrich et al. 2017; Laboury et al. 2024; Chapter 2). The initial diversification of Parvipelvia and Plesiosauria during that period was marked by several morphological changes — including fin shapes — which may have contributed to the evolutionary success of these two clades, and at the very least, to clear differences between Triassic and post-Triassic assemblages (Chapter 2).

Consequence of the ETME on the evolutionary history of ichthyosaurians and eosauropterygians

While the alteration of taxonomic diversity in marine ecosystems caused by mass extinction events across the Phanerozoic remains uncontested (Raup and Sepkoski 1982; Bambach 2006; McGhee et al. 2013; Song et al. 2013; Benton and Newell 2014; Sallan and Galimberti 2015), emerging evidence indicates that their ecological severity may have been less dramatic than previously assumed, with no substantial loss in functional diversity (Foster and Twitchett 2014; Dunhill et al. 2018; Cribb et al. 2023). As previously mentioned, our results from disparity and extinction selectivity analyses do not support a catastrophic impact of the extinctions occurring at or close to the T/J transition on the evolution of marine reptiles, reinforcing the idea that these animals appear rather unaffected by these events (Benson et al. 2010; 2012; Wintrich et al. 2017; Renesto and Dalla Vechia 2018; Laboury et al. 2024; Chapters 2 and 3). Instead, the high diversity of lineages within both Parvipelvia and Plesiosauria recorded in the first 10 million years of the Early Jurassic, alongside the timing of cladogenesis events implied by multiple time-scaled topologies generated under both Maximum Parsimony and Bayesian Inference, indicate that major diversification events occurred during the Late Triassic (*e.g.* see Benson et al. 2012; Fischer 2013; Motani et al. 2017; Wintrich et al. 2017; Laboury et al. 2022; as well as time-scaled phylogenies in chapters 2 and 3). The high craniodental disparity among early parvipelvians, coupled with their ability to produce phenotypes similar to many of those from Triassic taxa (Laboury et al. 2024; Chapter 2), challenges the prevailing vision that the ETME massively affected ichthyosaurian morphology (Thorne et al. 2011; Moon Stubbs 2020). Even though early plesiosaurians exhibited low disparity in the aftermath of the T/J transition, especially by comparison to their Triassic predecessors (Benson et al. 2012; Stubbs and Benton 2016; Laboury et al. 2024; Chapter 2), the rarity of Late Triassic specimens hinders definitive conclusions regarding the impact of the end-Triassic events on their morphological diversification. Nevertheless, the clustering of earliest plesiosaurians with Triassic pistosauroids in the craniodental ecomorphospace suggests a permanent shift in skull morphology, occurring ~30 million years before the end of the Triassic (Laboury et al. 2024; Chapter 2). This pattern, along with the 'plesiosaurian' body plan of the first diagnostic plesiosaurian *Rhaeticosaurus mertensi* (Wintrich et al. 2017), hints a certain degree of phenotypic conservatism from the Late Triassic to the earliest Jurassic, though some differences in brachial and crural indexes are noticeable between Triassic pistosauroids and plesiosaurians (Laboury et al. 2024; Chapter 2).

Although parvipelvians and plesiosaurians appear to have been rather unaffected by end-Triassic events, this period still coincides with the extinction of the last 'typical' Triassic forms. The Rhaetian indeed witnessed the final demise of the last coastal lineages which may have found refuge in flooded continental shelves in the Alpine region that emerged during Norian

transgression event, including placodonts, thalattosaurs, and probably saurosphargids (Pinna and Mazin 1993; Renesto and Tintori 1995; Neenan and Scheyer 2014; Scheyer et al. 2022; Bastiaans 2024 and references therein). Furthermore, the extinction events at the T/J transition appeared selective against the whale-sized shastasaurids which disappeared by the end of the Rhaetian (Fischer et al. 2014b; Lomax et al. 2018a, 2024; Sander et al. 2022; Laboury et al. 2024; Chapters 2 and 3). The presence of a large isolated shastasaurid-like radius in the lowermost Jurassic of Wales, may suggest the survival of such giant species following the ETME (Martin et al. 2015), but no other remains of these taxa have been found in younger and well-sampled sediments. Additionally, Lomax et al. (2018a) raised doubts about the origin of this fossil, proposing that it may instead originate from the Rhaetian Westbury Mudstone Formation rather than from the lowermost Jurassic Blue Lias Formation (Martin et al. 2015). The T/J transition therefore likely marked the loss of unique morphologies among ichthyosaurians (Moon and Stubbs 2020; Sander et al. 2021; Chapter 3) but also among marine reptiles as a whole, since no subsequent Mesozoic clades reached comparable body size to that of the colossal shastasaurids, exceeding 20 m long (Nicholls and Manabe 2004; Gutarra et al. 2023; Lomax et al. 2024). The factors underlying the extinction of these giants have rarely been discussed and remain far from clear. Results from Chapter 3 tend to reveal that extinction vulnerability among raptorial marine predators appears to be independent of body size throughout the Middle Triassic–Early Jurassic time period, although additional data are required to comprehensively reconstruct this trend for the latest Triassic. Other studies on extinction selectivity also evidenced that body size was not a key factor in the extinction risk of both marine and terrestrial vertebrates during other mass extinction events (Friedman 2009; Sallan and Galimberti 2015; Puttick et al. 2017; Allen et al. 2019). It remains plausible that factors such as the high energy demand, low rate of population growth or other physiological and ecological traits associated with large body size (Pianka 1970; Peters 1983; Heim et al. 2015; Sallan and Galimberti 2015) may have contributed to extinction of the last shastasaurids, despite the absence of direct fossilisable evidence supporting such hypothesis.

Limitations and biases associated with the Late Triassic fossil record

Overall, macroevolutionary analyses are inherently subject to biases related to the spatiotemporally unevenness of the fossil record and ‘Lagerstätten effects’, by overrepresenting and inflating the perceived diversity and disparity of better-sampled periods or localities (Smith et al. 1994; Sepkoski 1996; Bottjer et al. 2002; Ketchum and Benson 2010; Benson and Butler 2011; Butler et al. 2011; Kelley et al. 2014; Flannery Sutherland et al. 2019; Woolley et al. 2024).

Given the high scarcity of the Late Triassic fossil record — particularly in the Norian and the Rhaetian — the magnitude and the timing of extinction events during this period remain blurry. As already outlined in Chapter 2, significant shifts in sedimentary regimes and environmental conditions during the Late Triassic resulted in a marine fossil record that is temporally unequal (Benson and Butler 2011; Dunhill et al. 2014b; Kelley et al. 2014). Indeed, the vast majority of taxa are known from the Carnian (Merriam 1908; Camp 1980; Sander et al. 1997; McGowan and Motani 2003; Dalla Vecchia 2006; Benton et al. 2013; de Miguel Chaves et al. 2018b; Kelley et al. 2022; Zverkov et al. 2022) leaving the Norian and the Rhaetian, representing approximatively 25 millions years — which is more than half of the Late Triassic (Cohen et al. 2013) — undersampled. Such uneven quality of the fossil record mainly biases macroevolutionary studies that rely on binning at the Epoch level. The sudden significant decline in ichthyosaurian disparity attributed to the end-Triassic extinction events reported by Thorne et al. (2011) is likely the consequence of a methodological decision caused by the use of coarse time bins (Benson et al. 2012; Sander et al. 2022; Laboury et al. 2024; Chapter 2), which tends to conflate multiple extinction phases into a single event. Additionally, the high morphological dissimilarity between Late Triassic and Early Jurassic ichthyosaurian faunas, evidenced by a complete shift in morphospace occupation across the T/J transition (Moon and Stubbs 2020) probably arises, in addition of broad time bins, from the use of phylogenetic characters, which are not recommended as a proxy of ecological disparity (Anderson and Friedman 2012).

Despite using more precise temporal resolution and ecologically-informative traits, our overall results remain affected by the limitations of the fossil record. It appears that extinction patterns observed throughout the Middle–Late Triassic transition are influenced by the presence of Lagerstätten. The majority of extinct coastal taxa during that period were collected in highly fossiliferous localities of nearshore habitats from China and Europe (*e.g.* Xingyi biota or site of Monte San Giorgio) and the loss of these species might be exaggerated by the subsequent predominance of open-water facies assemblages from North America, Arctic Russian and China (Merriam 1908; Furrer 2003; Xiaofeng et al. 2006; Stockar 2010; Benton et al. 2013; Lu et al. 2018; Zverkov et al. 2022; Klug et al. 2024). It could therefore be plausible that some diversity of non-pelagic ichthyosaurians and eosauropterygians persisted in shallow-marine refugia until the end of the Triassic, similarly to what have been observed for the last placodonts and thalattosaurs in the Alpine region (Pinna and Mazin 1993; Renesto Tintori; Neenan and Scheyer 2014; Bastiaans 2024 and references therein). However, none of these taxa have been discovered in lagoonal environments after the Julian substage (Early Carnian) (Renesto and Dalla Vecchia 2018), strengthening that their final demise may have occurred approximately 35 million years before the end of the Triassic. The limited understanding of marine reptile assemblages during the latest Triassic significantly restricts our ability to assess the impact of ETME on extinction and diversification dynamics. Indeed, pattern shastasaurid evolution during the latest Triassic remain poorly understood and may have been more gradual, rather than concentrated at or close the T/J transition (Fischer et al. 2014b; Laboury et al. 2024; N. Kelly pers. comm.). Uncertainty persists

as to whether gigantic taxa abruptly disappeared at the end of the Rhaetian or experienced diffuse and minor extinctions under the environmental upheavals that occurred throughout the Late Triassic (Tanner et al. 2004; Ruhl et al. 2011; Blackburn et al. 2013; Dal Corso et al. 2020; Schoepfer et al. 2022; Bond et al. 2023; Rigo et al. 2024). Concerning parvipelvians and plesiosaurians, the discovery of remains from the Norian and Rhaetian (Zapfe 1976; Storrs 1994; McGowan 1995, 1996a; Sennikov and Arkhangelsky 2010; Mears et al. 2016; Wintrich et al. 2017) combined with branching events inferred from time-scaled phylogenies, indicates that their initial diversification would have occurred during that time interval. However, the general lack of fossil data limits any precise assessment of its magnitude and consequently, the relative abundance of these pelagic taxa within latest Triassic assemblages, which negatively impacts the reliability of disparity and extinction selectivity analyses. The scarcity of Late Triassic marine reptile fossil record has a clear effect on our comprehension on the early plesiosaurian evolutionary history. the last basal pistosauroid *Bobosaurus* with the first diagnostic plesiosaurian *Rhaeticosaurus* are indeed separated by a gap of 30 million years (Wintrich et al. 2017), leaving a substantial part of their early history unknown.

Although affected by biases associated with the extreme scarcity of the fossil record, this project employed a comprehensive suite of quantitative analyses to better understand the nature and timing of Late Triassic extinction events among large marine tetrapods. The discovery of new fossil material — particularly from the Norian and the Rhaetian — is needed to shed light on this crucial period in the marine reptile, as well as aquatic ecosystems history expanding our comprehension of what may represent a more complex scenario. In the meantime, the narrative of a dramatic loss of taxonomical and morphological diversity among marine predators at the end of the Triassic is no longer tenable, with evidence pointing to significant earlier turnover events unrelated to the ETME (Bardet 1994; Benson et al. 2010, 2012; Benson and Butler 2011; Renesto and Dalla Vecchia 2018; Laboury et al. 2024; Chapters 2 and 3).

GENERAL CONCLUSION

How did ichthyosaurians and eosauropterygians morphologically diversify on both sides of the Triassic–Jurassic transition? Can we detect a permanent shift in their morphospace occupation, and if so, when?

The prevailing scenario of a macroevolutionary bottleneck dramatically affecting the disparity of pelagic raptorial predators at the Triassic–Jurassic transition is no longer tenable. In both ichthyosaurians and eosauropterygians, the end of the Triassic does not coincide with a sharp decline in morphological diversity, which is instead recorded during the early Late Triassic. In contrary to previous studies, no shift in ichthyosaurian morphospace occupation is detected across the T/J transition by our multivariate analyses, revealing important morphological overlap in cranial architecture between Triassic and Early Jurassic taxa. On the other hand, eosauropterygians likely experienced a permanent shift in their morphology ~30 million years before the end of the Rhaetian, associated with the disappearance of the disparate pachypleurosauroids and nothosauroids, and with the evolution — and relative stability — of the 'pistosauroid' body plan from the Middle Triassic to the Early Jurassic.

Were the extinctions concentrated at or close to the Triassic–Jurassic transition, compatible with a mass extinction scenario or were they the result of a more gradual and selective patterns throughout the Late Triassic?

The overall results of this Ph.D. project strongly challenge the vision of a single sudden and catastrophic extinction event that profoundly affected both ichthyosaurian and eosauropterygian macroevolution at the very end of the Rhaetian. Instead, they rather support a scenario of more gradual and selective extinctions throughout the Late Triassic. Notably, substantial eustatic fluctuations, leading to a major regression event during the Carnian, can be regarded as the main driver of the turnover in marine reptile assemblages occurring during the early Late Triassic, characterized by the loss of nearly all shallow marine forms and their replacement by pelagic-dominated faunas. Although taxa adapted to open ocean appeared globally unaffected by the ETME, the end of the Triassic still marks the final demise of the whale-sized shastasaurid which suggest a greater extinction susceptibility among colossal animals during that period.

.

REFERENCES

Allen, B. J., T. L. Stubbs, M. J. Benton, and M. N. Puttick. 2019. Archosauromorph extinction selectivity during the Triassic–Jurassic mass extinction. *Palaeontology* 62: 211–224.

Alroy, J. 2010. The shifting balance of diversity among major marine animal groups. *Science* 329: 1191–1194.

Anderson, P. 2009. Biomechanics, functional patterns, and disparity in Late Devonian arthrodires. *Paleobiology* 35: 321–342.

Anderson, P. S. L., and M. Friedman. 2012. Using cladistic characters to predict functional variety: experiments using early gnathostomes. *Journal of Vertebrate Paleontology* 32: 1254–1270.

Anderson, P. S. L., M. Friedman, M. D. Brazeau, and E. J. Rayfield. 2011. Initial radiation of jaws demonstrated stability despite faunal and environmental change. *Nature* 476: 206–209.

Andres, B. 2012. The Early Evolutionary History and Adaptive Radiation of the Pterosauria. *Acta Geologica Sinica* 86: 1356-1365.

Andrews, C. W. 1910. A descriptive catalogue of the marine reptiles of The Oxford Clay. Based on the Leeds Collection in the British Museum (Natural History), London. Part 1. 205.

Andrews, C. W. 1922. Notes on the skeleton of a large plesiosaur (Rhomaleosaurus thorntoni sp. n.) from the Upper Lias of Northamptonshire. *Annals and Magazine of Natural History* 9: 407–415.

Bambach, R. K. 2006. Phanerozoic biodiversity mass extinctions. *Annual review of Earth and Planetary Sciences* 34: 127–155.

Bambach, R. K., A. H. Knoll, and S. C. Wang. 2004. Origination, extinction, and mass depletions of marine diversity. *Paleobiology* 30: 522–542.

Bapst, D. W. 2013. A stochastic rate-calibrated method for time-scaling phylogenies of fossil taxa. *Methods in Ecology and Evolution* 4: 724–733.

Bapst, D. W. 2014. Assessing the effect of time-scaling methods on phylogeny-based analyses in the fossil record. *Paleobiology* 40: 331–351.

Bapst, D. W. 2012. paleotree: an R package for paleontological and phylogenetic analyses of evolution. *Methods in Ecology and Evolution* 3: 803–807.

Bardet, N. 1994. Extinction events among Mesozoic marine reptiles. *Historical Biology* 7: 313–324.

Bardet, N. 1992. Stratigraphic evidence for the extinction of the ichthyosaurs. *Terra Nova* 4: 649–656.

Bardet, N., J. Falconnet, V. Fischer, A. Houssaye, S. Jouve, X. Pereda Suberbiola, A. Pérez-García, J.-Claude. Rage, and P. Vincent. 2014. Mesozoic marine reptile palaeobiogeography in response to drifting plates. *Gondwana Research* 26: 869–887.

Bardet, N., P. Godefroit, and J. Sciau. 1999. A new elasmosaurid Plesiosaur from the Lower Jurassic of Southern France. *Palaeontology* 42: 927–952.

Bardet, N., X. P. Suberbiola, M. Iarochène, M. Amalik, and B. Bouya. 2005. Durophagous Mosasauridae (Squamata) from the Upper Cretaceous phosphates of Morocco, with description of a new species of Globidens. *Netherlands Journal of Geosciences* 84: 167–175.

Bastiaans, D. 2024. Thalattosauria in time and space: a review of thalattosaur spatiotemporal occurrences, presumed evolutionary relationships and current ecological hypotheses. *Swiss Journal of Palaeontology* 143: 36.

Beardmore, S., and H. Furrer. 2016. Preservation of Pachypleurosauridae (Reptilia; Sauropterygia) from the Middle Triassic of Monte San Giorgio, Switzerland. *Neues Jahrbuch für Geologie und Paläontologie - Abhandlungen* 280: 221–240.

Benjamini, Y., and Y. Hochberg. 1995. Controlling the False Discovery Rate: A Practical and Powerful Approach to Multiple Testing. *Journal of the Royal Statistical Society: Series B (Methodological)* 57: 289–300.

Bennett, P., and I. Owens. 1997. Variation in extinction risk among birds: Chance or evolutionary predisposition? *Proceedings of the Royal Society of London. Series B: Biological Sciences* 264: 401–408

Bennett, S. P., P. M. Barrett, M. E. Collinson, S. Moore-Fay, P. G. Davis, and C. P. Palmer. 2012. A new specimen of *Ichthyosaurus communis* from Dorset, UK, and its bearing on the stratigraphical range of the species. *Proceedings of the Geologists' Association* 123: 146–154.

Bennion, R. F., J. A. MacLaren, E. J. Coombs, F. G. Marx, O. Lambert, and V. Fischer. 2022. Convergence and constraint in the cranial evolution of mosasaurid reptiles and early cetaceans. *Paleobiology* 49: 215–231.

Bennion, R. F., E. E. Maxwell, O. Lambert, and V. Fischer. 2024. Craniodental ecomorphology of the large Jurassic ichthyosaurian *Temnodontosaurus*. *Journal of Anatomy* 244: 22–41.

Benson, R. B. J. 2013. Marine Reptiles. Pp. 267–279 eds. Grzimek's Animal Life Encyclopedia, Extinction.

Benson, R. B. J., K. T. Bates, M. R. Johnson, and P. J. Withers. 2011. Cranial anatomy of *Thalassiodracon hawkinsii* (Reptilia, Plesiosauria) from the Early Jurassic of Somerset, United Kingdom. *Journal of Vertebrate Paleontology* 31: 562–574.

Benson, R. B. J., and T. Bowdler. 2014. Anatomy of *Colymbosaurus megadeirus* (Reptilia, Plesiosauria) from the Kimmeridge Clay Formation of the U.K., and high diversity among Late Jurassic plesiosauroids. *Journal Vertebrate of Paleontology* 34: 1053–1071.

Benson, R. B. J., and R. J. Butler. 2011. Uncovering the diversification history of marine tetrapods: ecology influences the effect of geological sampling biases. *Geological Society of London Special Publications*. 358: 191–208

Benson, R. B. J., R. J. Butler, J. Lindgren, and A. S. Smith. 2010. Mesozoic marine tetrapod diversity: mass extinctions and temporal heterogeneity in geological megabiases affecting the vertebrates. *Proceedings of the Royal Society B: Biological Sciences* 277: 829–834.

Benson, R. B. J., and P. S. Druckenmiller. 2014. Faunal turnover of marine tetrapods during the Jurassic–Cretaceous transition. *Biological Reviews* 89:1–23.

Benson, R. B. J., M. Evans, and P. S. Druckenmiller. 2012. High diversity, low disparity and small body size in plesiosaurs (Reptilia, Sauropterygia) from the Triassic–Jurassic boundary. *PLoS ONE* 7: e31838.

Benson, R. B. J., M. Evans, and M. A. Taylor. 2015a. The anatomy of *Stratesaurus* (Reptilia, Plesiosauria) from the lowermost Jurassic of Somerset, United Kingdom. *Journal of Vertebrate Paleontology* 35.

Benson, R. B. J., H. F. Ketchum, D. Naish, and L. E. Turner. 2013. A new leptocleidid (Sauropterygia, Plesiosauria) from the Vectis Formation (early Barremian–early Aptian; Early Cretaceous) of the Isle of Wight and the evolution of Leptocleididae, a controversial clade. *Journal of Systematic Palaeontology* 11: 231–248.

Benson, R. B. J., H. F. Ketchum, L. F. Noè, and M. Gómez-Pérez. 2011b. New information on *Hauffiosaurus* (Reptilia, Plesiosauria) based on a new species from the Alum Shale member (Lower Toarcian: Lower Jurassic) of Yorkshire, UK. *Palaeontology* 54: 547–571.

Benson, R. B. J., N. G. Zverkov, and M. S. Arkhangelsky. 2015b. Youngest occurrences of rhomaleosaurid plesiosaurs indicate survival of an archaic marine reptile clade at high palaeolatitudes. *Acta Palaeontologica Polonica* 60: 769–780.

Benton, M. 1986. More than one event in the Late Triassic mass-extinction. *Nature* 321: 857–861.

Benton, M. J. 2014. Vertebrate palaeontology . 4th ed. Wiley-Blackwell.

Benton, M. J., J. Forth, and M. C. Langer. 2014. Models for the Rise of the Dinosaurs. *Current Biology* 24: R87–R95.

Benton, M. J., and A. J. Newell. 2014. Impacts of global warming on Permo-Triassic terrestrial ecosystems. *Gondwana Research* 25: 1308–1337.

Benton, M. J., and P. S. Spencer. 1995. Fossil reptiles of Great Britain.

Benton, M. J., Q. Zhang, S. Hu, Z.-Q. Chen, W. Wen, J. Liu, J. Huang, C. Zhou, T. Xie, J. Tong, and B. Choo. 2013. Exceptional vertebrate biotas from the Triassic of China, and the expansion of marine ecosystems after the Permo-Triassic mass extinction. *Earth-Science Reviews* 125: 199–243.

Berezin, A. Y. 2011. A new plesiosaur of the family Aristonectidae from the Early Cretaceous of the center of the Russian platform. *Paleontological Journal* 45: 648–660.

Bindellini, G., A. S. Wolniewicz, F. Miedema, C. Dal Sasso, and T. M. Scheyer. 2024. Postcranial anatomy of *Besanosaurus leptorhynchus* (Reptilia: Ichthyosauria) from the Middle Triassic Besano Formation of Monte San Giorgio (Italy/Switzerland), with implications for reconstructing the swimming styles of Triassic ichthyosaurs. *Swiss Journal of Palaeontology* 143: 32.

Bindellini, G., A. S. Wolniewicz, F. Miedema, T. M. Scheyer, and C. Dal Sasso. 2021. Cranial anatomy of *Besanosaurus leptorhynchus* Dal Sasso & Pinna, 1996 (Reptilia: Ichthyosauria) from the Middle Triassic Besano Formation of Monte San Giorgio, Italy/Switzerland: taxonomic and palaeobiological implications. *PeerJ* 9: e11179.

Blackburn, T., P. Olsen, S. Bowring, N. McLean, J. Puffer, G. McHone, T. Rasbury, and M. Et-Touhami. 2013. Zircon U-Pb Geochronology Links the End-Triassic Extinction with the Central Atlantic Magmatic Province. *Science* -340: 941–945.

Boessenecker, R. W., M. Churchill, E. A. Buchholtz, B. L. Beatty, and J. H. Geisler. 2020. Convergent Evolution of Swimming Adaptations in Modern Whales Revealed by a Large Macrophagous Dolphin from the Oligocene of South Carolina. *Current Biology* 30: 3267-3273.e2.

Bond, A. D., A. J. Dickson, M. Ruhl, R. Bos, and B. van de Schootbrugge. 2023. Globally limited but severe shallow-shelf euxinia during the end-Triassic extinction. *Nature Geosciences* 16: 1181–1187.

Bonnevier Wallstedt, I., P. Sjövall, B. Thuy, R. G. De La Garza, M. E. Eriksson, and J. Lindgren. 2024. Skin Anatomy, Bone Histology and Taphonomy of a Toarcian

(Lower Jurassic) Ichthyosaur (Reptilia: Ichthyopterygia) from Luxembourg, with Implications for Paleobiology. *Diversity* 16: 492.

Bos, R., R.-J. van Zonneveld, J. W. F. Reumer, G.-J. Vis, N. Janssen, T. Everwijn, A. Sluijs, and B. van de Schootbrugge. 2024. A high-resolution palynological and geochemical study of the end-Triassic mass-extinction based on a new cored succession at Winterswijk (the Netherlands). *Geological Magazine* 161: e17.

Böttcher, R. 1989. Über die Nahrung eines *Leptopterygius* (Ichthyosauria, Reptilia) aus dem süddeutschen Posidonienschiefer (Unterer Jura) mit Bemerkungen über den Magen der Ichthyosaurier.

Bottjer, D. J., W. Etter, J. W. Hagadorn, and C. M. Tang. 2002. Exceptional fossil preservation: a unique view on the evolution of marine life. Columbia University Press, NewYork.

Brayard, A., L. J. Krumenacker, J. P. Botting, J. F. Jenks, K. G. Bylund, E. Fara, E. Vennin, N. Olivier, N. Goudemand, T. Saucède, S. Charbonnier, C. Romano, L. Doguzhaeva, B. Thuy, M. Hautmann, D. A. Stephen, C. Thomazo, and G. Escarguel. 2017. Unexpected Early Triassic marine ecosystem and the rise of the Modern evolutionary fauna. *Sciences Advances* 3: e1602159.

Brayard, A., E. Vennin, N. Olivier, K. G. Bylund, J. Jenks, D. A. Stephen, H. Bucher, R. Hofmann, N. Goudemand, and G. Escarguel. 2011. Transient metazoan reefs in the aftermath of the end-Permian mass extinction. *Nature Geoscience* 4: 693–697.

Brightly, W. H., and T. C. Stayton. 2023. convevol: Analysis of Convergent Evolution.

Brinkman, D. D., Z. Xijin, and E. L. Nicholls. 1992. A primitive ichthyosaur from the Lower Triassic of British Columbia, Canada. *Palaeontology* 35: 465–474.

Brinkman, W. 1996. Ein Mixosaurier (Reptilia, Ichthyosauria) mit Embryonen aus der Grenzbitumenzone (Mitteltrias) des Monte San Giorgio (Schweiz, Kanton Tessin). *Eclogae geologiae Helvetiae* 89: 1321–1344.

Brinkmann, W. 1998. Die Ichthyosaurier (Reptilia) aus der Grenzbitumenzone (Mitteltrias) des Monte San Giorgio (Tessin, Schweiz) - neue Ergebnisse. *Vierteljahrsschrift der Naturforschenden Gesellschaft in Zürich* 143: 165–177.

Brown, D. 1981. The English Upper Jurassic Plesiosauroidea (Reptilia) and a review of the phylogeny and classification of the Plesiosauria. *Bulletin of the British Museum (Natural History) Geology* 35: 253–347.

Brown, D., P. Vincent, and N. Bardet. 2013. Osteological redescription of the skull of *Microcleidus homalospondylus* (Sauropterygia, Plesiosauria) from the Lower Jurassic of England. *Journal of Paleontology* 87: 537–549.

Brusatte, S. L., M. J. Benton, M. Ruta, and G. T. Lloyd. 2008. Superiority, competition, and opportunism in the evolutionary radiation of dinosaurs. *Science* 321: 1485–1488.

Brusatte, S. L., M. T. Young, T. J. Challands, N. D. L. Clark, V. Fischer, N. C. Fraser, J. J. Liston, C. C. J. MacFadyen, D. A. Ross, S. Walsh, and M. Wilkinson. 2015. Ichthyosaurs from the Jurassic of Skye, Scotland. *Scottish Journal of Geology* 51: 43–55.

Bucher, H. 1988. A new Middle Anisian (Middle Triassic) ammonoid zone from northwestern Nevada (USA). *Eclogae Geologicae Helvetiae* 81: 723–762.

Buchholtz, E. A. 2001. Swimming styles in Jurassic ichthyosaurs. *Journal of Vertebrate Paleontology* 21: 61–73.

Buchy, M.-C. 2005. An Elasmosaur (Reptilia: Sauropterygia) from the Turonian (Upper Cretaceous) of Morocco. *Carolinea* 63: 5–28.

Busbey, A. 1995. The structural consequences of skull flattening in crocodilians. Pp. 173–192 *in* J. Thomason, ed. Functional morphology in vertebrate paleontology. Cambridge University Press.

Butler, R. J., S. L. Brusatte, B. Andres, and R. B. J. Benson. 2011. How do geological sampling biases affect studies of morphological evolution in deep time? A case study of pterosaur (Reptilia: Archosauria) disparity. *Evolution* 66: 147–162.

Cabezuelo Hernández, A., C. De Miguel Chaves, F. Ortega, and A. Pérez García. 2024. Postcranial anatomy of the Spanish Upper Triassic sauropterygian *Paludidraco multidentatus* (Simosauridae). *Palaeontologia Electronica* 27.

Caldwell, M. 2002. From fins to limbs to fins: Limb evolution in fossil marine reptiles. *American Journal of Medical Genetics* 112: 236–249.

Callaway, J. M., and J. Massare. 1989. Geographic and stratigraphic distribution of the Triassic Ichthyosauria (Reptilia; Diapsida). *Neues Jahrbuch für Geologie und Paläontologie, Abhandlungen* 187: 37–58.

Camp, C. L. 1980. Large ichthyosaurs from the Upper Triassic of Nevada. *Paläontographica, Abteilung A* 170: 139–200.

Carpenter, K., F. Sanders, B. Reed, J. Reed, and P. Larson. 2010. Plesiosaur Swimming as Interpreted from Skeletal Analysis and Experimental Results. *Transactions of the Kansas Academy of Science* 113: 1–34.

Carroll, R. L., and Z.-M. Dong. 1991. *Hupehsuchus*, an enigmatic aquatic reptile from the Triassic of China, and the problem of establishing relationships. *Philosophical Transactions: Biological Sciences* 331: 131–153.

Carroll, R. L., and P. Gaskill. 1985. The nothosaur *Pachypleurosaurus* and the origin of plesiosaurs. *Philosophical Transactions of the Royal Society of London. B, Biological Sciences* 309:343–393.

Carte, A., and W. H. Bailey. 1863. Description of a new species of *Plesiosaurus*, from the Lias, near Whitby, Yorkshire. *Journal of the Royal Dublin Society* 4: 160–170.

Carter, J. 1846a. Notice of the jaws of an *Ichthyosaurus* from the chalk in the neighbourhood of Cambridge. *Reports of the British Association for the Advancement of Science* 1845: 60.

Carter, J. 1846b. On the occurrence of a new species of *Ichthyosaurus* in the Chalk. *London Geological Journal* 1: 7–9.

Case, E. C. 1936. A nothosaur from the Triassic of Wyoming. *University of Michigan Contributions from the Museum of Paleontology* 5: 1–36.

Castiglione, S., C. Serio, D. Tamagnini, M. Melchionna, A. Mondanaro, M. Di Febbraro, A. Profico, P. Piras, F. Barattolo, and P. Raia. 2019. A new, fast method to search for morphological convergence with shape data. *PLoS ONE* 14: e0226949

Castiglione, S., G. Tesone, M. Piccolo, M. Melchionna, A. Mondanaro, C. Serio, M. Di Febbraro, and P. Raia. 2018. A new method for testing evolutionary rate variation and shifts in phenotypic evolution. *Methods in Ecology and Evolution* 9: 974–983.

Cau, A., and F. Fanti. 2014. A pliosaurid plesiosaurian from the Rosso Ammonitico Veronese Formation of Italy. *Acta Palaeontologica Polonica* 59:643–650.

Cau, A., and F. Fanti. 2015. High evolutionary rates and the origin of the Rosso Ammonitico Veronese Formation (Middle-Upper Jurassic of Italy) reptiles. *Historical Biology* 1–11.

Cawthorne, M., D. I. Whiteside, and M. J. Benton. 2024. Latest Triassic terrestrial microvertebrate assemblages from caves on the Mendip palaeoisland, S.W. England, at Emborough, Batscombe and Highcroft Quarries. *Proceedings of the Geologists' Association* 135: 105–130.

Chatterjee, S., and B. J. Small. 1989. New plesiosaurs from the Upper Cretaceous of Antarctica. *Geological Society, London, Special Publications* 47: 197–215.

Chen, X., and L. Chen. 2010. A new species of *Mixosaurus* (Reptilia: Ichthyosauria) from the Middle Triassic of Pu'an, Guizhou, China. *Acta Palaeontologica Sinica* 2: 251–260.

Chen, X., L. Cheng, and P. M. Sander. 2007. A new species of *Callawayia* (Reptilia: Ichthyosauria) from the Late Triassic in Guanling, Guizhou. *Geology in China* 34: 974–982.

Chen, X., P. M. Sander, L. Cheng, and W. Xiaofeng. 2013. A New Triassic Primitive Ichthyosaur from Yuanan, South China. *Acta Geologica Sinica* 87: 672-677.

Chen, Z.-Q., and M. J. Benton. 2012. The timing and pattern of biotic recovery following the end-Permian mass extinction. *Nature Geoscience* 5: 375–383.

Cheng, L., B. C. Moon, C. Yan, R. Motani, D. Jiang, Z. An, and Z. Fang. 2022. The oldest record of Saurosphargiformes (Diapsida) from South China could fill an ecological gap in the Early Triassic biotic recovery. *PeerJ* 10: e13569.

Cheng, L., X.-H. Chen, Q. Shang, and X. Wu. 2014. A new marine reptile from the Triassic of China, with a highly specialized feeding adaptation. *Naturwissenschaften* 101: 251–259.

Cheng, L., X.-H. Chen, B.-M. Zhang, and X.-F. Wang. 2010. A new material of Thalattosauria (Reptilia: Diapsida) from the Middle Triassic of Luoping, Yunnan province. *Geosciences* 35: 507–511.

Cheng, L., R. Motani, D.-Y. Jiang, C.-B. Yan, A. Tintori, and O. Rieppel. 2019. Early Triassic marine reptile representing the oldest record of unusually small eyes in reptiles indicating non-visual prey detection. *Scientific Reports* 9: 1–11.

Cheng, Y., X. Wu, S. Tamaki, Shan, and H.-Y. Shan. 2016. *Dawazisaurus Brevis*, A New Eosauropterygian From the Middle Triassic of Yunnan, China. *Acta Geologica Sinica* 90: 401–424.

Cheng, Y.-N., R. Holmes, X.-C. Wu, and N. Alfonso. 2009. Sexual dimorphism and life history of *Keichousaurus hui* (Reptilia: Sauropterygia). *Journal of Vertebrate Paleontology* 29: 401–408.

Cheng, Y.-N., T. Sato, X.-C. Wu, and C. LI. 2006. First complete pistosaurid from the Triassic of China. *Journal of Vertebrate Paleontology* 26: 501–504.

Cheng, Y.-N., X.-C. Wu, and Q. Ji. 2004. Triassic marine reptiles gave birth to live young. *Nature* 432: 383–386.

Cheng, Y.-N., X.-C. Wu, T. Sato, and H.-Y. Shan. 2012. A new eosauropterygian (Diapsida, Sauropterygia) from the Triassic of China. *Journal of Vertebrate Paleontology* 32: 1335–1349.

Chun, L., O. Rieppel, C. Long, and N. C. Fraser. 2016. The earliest herbivorous marine reptile and its remarkable jaw apparatus. Science Advances 2: e1501659.

Cignoni, P., M. Callieri, M. Corsini, M. Dellepiane, F. Ganovelli, and G. Ranzuglia. 2008. MeshLab: an Open-Source Mesh Processing Tool.

Close, R. A., R. B. J. Benson, E. E. Saupe, M. E. Clapham, and R. J. Butler. 2020. The spatial structure of Phanerozoic marine animal diversity. *Science* 368: 420–424.

Cohen, K., S. Finney, P. Gibbard, and J. Fan. 2013. *The ICS International Chronostratigraphic Chart*. Episodes 36: 199-204.

Cooper, L. N., S. D. Dawson, J. S. Reidenberg, and A. Berta. 2007. Neuromuscular Anatomy and Evolution of the Cetacean Forelimb. *Anatomical Record* 290: 1121–1137.

Cribb, A. T., K. K. Formoso, C. H. Woolley, J. Beech, S. Brophy, P. Byrne, V. C. Cassady, A. L. Godbold, E. Larina, P. Maxeiner, Y.-H. Wu, F. A. Corsetti, and D. J. Bottjer. 2023. Contrasting terrestrial and marine ecospace dynamics after the end-Triassic mass extinction event. *Proceedings of the Royal Society B: Biological Sciences* 290: 20232232.

Crofts, S. B., J. M. Neenan, T. M. Scheyer, A. P. Summers. 2016. Tooth occlusal morphology in the durophagous marine reptiles, Placodontia (Reptilia: Sauropterygia). *Paleobiology* 43: 114-128.

Cruickshank, A. R. I. 1994. Cranial Anatomy of the Lower Jurassic Pliosaur *Rhomaleosaurus megacephalus* (Stutchbury) (Reptilia: Plesiosauria) *Philosophical Transactions of the Royal Society of London. Series B: Biological Sciences* 343: 247–260.

Currie, P. 1978. The orthometric linear unit. *Journal of Paleontology* 52: 964–971.

Cuthbertson, R. S., A. P. Russell, and J. S. Anderson. 2013. Cranial morphology and relationships of a new grippidian (Ichthyopterygia) from the Vega-Phroso Siltstone Member (Lower Triassic) of British Columbia, Canada. *Journal of Vertebrate Paleontology* 33: 831–847.

Dai, X., J. H. F. L. Davies, Z. Yuan, A. Brayard, M. Ovtcharova, G. Xu, X. Liu, C. P. A. Smith, C. E. Schweitzer, M. Li, M. G. Perrot, S. Jiang, L. Miao, Y. Cao, J. Yan, R. Bai, F. Wang, W. Guo, H. Song, L. Tian, J. Dal Corso, Y. Liu, D. Chu, and H.

Song. 2023. A Mesozoic fossil lagerstätte from 250.8 million years ago shows a modern-type marine ecosystem. *Science* 379: 567–572.

Dal Corso, J., M. Bernardi, Y. Sun, H. Song, L. Seyfullah, N. Preto, P. Gianolla, A. Ruffell, E. Kustatscher, G. Roghi, A. Merico, S. Hohn, A. Schmidt, A. Marzoli, R. Newton, P. B. Wignall, and M. Benton. 2020. Extinction and dawn of the modern world in the Carnian (Late Triassic). *Science Advances* 6: eaba0099.

Dal Corso, J., H. Song, S. Callegaro, D. Chu, Y. Sun, J. Hilton, S. E. Grasby, M. M. Joachimski, and P. B. Wignall. 2022. Environmental crises at the Permian–Triassic mass extinction. *Nature Reviews Earth & Environment* 3: 197–214.

Dal Sasso, C., and G. Pinna. 1996. *Besanosaurus leptorhynchus* n. gen. n. sp., a new Shastasaurid ichthyosaur from the Middle Triassic of Besano (Lombardy, N. Italy). *Paleontologia Lombarda nuova serie* Ed. Società Italiana di Scienze Naturali & Museo Civico di Storia Naturale, Milano 4

Dalla Vecchia, F. 2006. A new sauropterygian reptile with plesiosaurian affinity from the Late Triassic of Italy. *Rivista Italiana di Paleontologia e Stratigrafia* 112: 207–225.

Dalla Vecchia, F., and M. Avanzini. 2002. New findings of isolated remains of Triassic reptiles from Northeastern Italy. *Bollettino della Societa Paleontologica Italiana* 41: 215–235.

Dalla Vecchia, F. M. 2008. First record of *Simosaurus* (Sauropterygia, Nothosauroidea) from the Carnian (Late Triassic) of Italy. *Rivista Italiana di Paleontolgia e Stratigraphia* 114: 273–285.

de Miguel Chaves, C., F. Ortega, and A. Perez Garcia. 2018a. Cranial variability of the European Middle Triassic sauropterygian *Simosaurus gaillardoti*. Acta Palaeontologica Polonica 63: 315-326.

de Miguel Chaves, C., F. Ortega, and A. Pérez-García. 2018b. New highly pachyostotic nothosauroid interpreted as a filter-feeding Triassic marine reptile. *Biological Letters* 14: 20180130.

Dick, D. G., and E. E. Maxwell. 2015. The evolution and extinction of the ichthyosaurs from the perspective of quantitative ecospace modelling. *Biological Letters* 11: 20150339

Dick, D. G., G. Schweigert, and E. E. Maxwell. 2016. Trophic niche ontogeny and palaeoecology of early Toarcian *Stenopterygius* (Reptilia: Ichthyosauria). *Palaeontology* 59: 423-431.

Dong, Z.-M. 1972. An ichthyosaur fossil from the Qomolangma Feng region. *Academia Sinica, Institute of Vertebrate Paleontology and Palaeoanthropology, Memoir* 9:7–10.

Druckenmiller, P. S., J. Hurum, E. M. Knutsen, and H. A. Nakrem. 2012. Two new ophthalmosaurids (Reptilia: Ichthyosauria) from the Agardhfjellet Formation (Upper Jurassic: Volgian/Tithonian), Svalbard, Norway. *Norwegian Journal of Geology* 92: 311–339.

Druckenmiller, P. S., N. P. Kelley, E. T. Metz, and J. Baichtal. 2020. An articulated Late Triassic (Norian) thalattosauroid from Alaska and ecomorphology and extinction of Thalattosauria. *Scientific Reports* 10: 1746.

Druckenmiller, P. S., N. Kelley, M. T. Whalen, C. Mcroberts, and J. G. Carter. 2014. An Upper Triassic (Norian) ichthyosaur (Reptilia, Ichthyopterygia) from northern Alaska and dietary insight based on gut contents. *Journal of Vertebrate Paleontology* 34: 1460–1465.

Dunhill, A. M., W. J. Foster, J. Sciberras, and R. J. Twitchett. 2018. Impact of the Late Triassic mass extinction on functional diversity and composition of marine ecosystems. *Palaeontology* 61: 133–148.

Dunhill, A. M., B. Hannisdal, and M. J. Benton. 2014. Disentangling rock record bias and common-cause from redundancy in the British fossil record. *Nature Communication* 5: 4818.

Ellis, R. 2013. Swordfish: A Biography of the Ocean Gladiator. The University of Chicago Press.

Engelschiøn, V. S., A. J. Roberts, R. With, and Ø. Hammer. 2023. Exceptional X-Ray contrast: Radiography imaging of a Middle Triassic mixosaurid from Svalbard. *PLoS ONE* 18: e0285939.

Ezcurra, M. D., and R. J. Butler. 2018. The rise of the ruling reptiles and ecosystem recovery from the Permo-Triassic mass extinction. *Proceedings of the Royal Society B: Biological Sciences* 285: 20180361.

Fabbri, M. 2013. New information on *Bobosaurus forojuliensis* (Reptilia: Sauropterygia): implications for plesiosaurian evolution. *Historical Biology* 26: 661–669.

Fang, Y.-W., A. S. wolniewicz, and J. Liu. 2024. A new species of *Mixosaurus* (Ichthyosauria: Mixosauridae) from the Middle Triassic of Luxi County, Yunnan Province, South China. *Acta Palaeontologica Polonica* 69: 263–280.

Felsenstein, J. 1985. Phylogenies and the Comparative Method. *The American Naturalist* 125: 1–15.

Fernández, M. 1999. A new ichthyosaur from the Los Molles Formation (Early Bajocian), Neuquén basin, Argentina. *Journal of Paleontology* 73: 677–681.

Fernández, M. 1994. A new long-snouted ichthyosaur from the early Bajocian of Neuquén basin (Argentina). *Ameghiniana* 31: 291–297.

Fernández, M. 2001. Dorsal or ventral? Homologies of the forefin of *Caypullisaurus* (Ichthyosauria: Ophthalmosauria *Journal of Vertebrate Paleontology* 21: 515–520.

Fischer, V. 2013. Origin, biodiversity and extinction of Cretaceous ichthyosaurs. Université de Liège, Liège, Belgium.

Fischer, V. 2016. Taxonomy of *Platypterygius campylodon* and the diversity of the last ichthyosaurs. *PeerJ* 4: 1–21.

Fischer, V., R. M. Appleby, D. Naish, J. Liston, J. B. Riding, S. Brindley, and P. Godefroit. 2013. A basal thunnosaurian from Iraq reveals disparate phylogenetic origins for Cretaceous ichthyosaurs. Biological Letters 9: 20130021.

Fischer, V., M. S. Arkhangelsky, I. M. Stenshin, G. N. Uspensky, N. G. Zverkov, and R. B. J. Benson. 2015. Peculiar macrophagous adaptations in a new Cretaceous pliosaurid. *Royal Society Open Science* 2: 150552.

Fischer, V., M. S. Arkhangelsky, G. N. Uspensky, I. M. Stenshin, and P. Godefroit. 2014a. A new Lower Cretaceous ichthyosaur from Russia reveals skull shape conservatism within Ophthalmosaurinae. *Geological Magazine* 151: 60–70.

Fischer, V., N. Bardet, R. B. J. Benson, M. S. Arkhangelsky, and M. Friedman. 2016. Extinction of fish-shaped marine reptiles associated with reduced evolutionary rates and global environmental volatility. *Nature Communcation* 7: 10825.

Fischer, V., R. F. Bennion, D. Foffa, J. A. MacLaren, M. R. McCurry, K. M. Melstrom, and N. Bardet. 2022a. Ecological signal in the size and shape of marine amniote teeth. *Proceedings of the Royal Society B: Biological Sciences* 289: 20221214.

Fischer, V., R. B. J. Benson, P. S. Druckenmiller, H. F. Ketchum, and N. Bardet. 2018. The evolutionary history of polycotylid plesiosaurians. Royal Society Open Science 5: 172177.

Fischer, V., R. B. J. Benson, N. G. Zverkov, M. S. Arkhangelsky, I. M. Stenshin, G. N. Uspensky, and N. E. Prilepskaya. 2023. Anatomy and relationships of the bizarre Early Cretaceous pliosaurid *Luskhan itilensis*. *Zoological Journal of the Linnean Society* 198: 220–256.

Fischer, V., R. B. J. Benson, N. G. Zverkov, L. C. Soul, M. S. Arkhangelsky, O. Lambert, I. M. Stenshin, G. N. Uspensky, and P. S. Druckenmiller. 2017. Plasticity and convergence in the evolution of short-necked plesiosaurs. *Current Biology* 27: 1667–1676.

Fischer, V., H. Cappetta, P. Vincent, G. Garcia, S. Goolaerts, J. E. Martin, D. Roggero, and X. Valentin. 2014b. Ichthyosaurs from the French Rhaetian indicate a severe turnover across the Triassic–Jurassic boundary. *Naturwissenschaften* 101: 1027–1040.

Fischer, V., A. Laboury, K. Bernacki, L. Garbay, Y. Gillen, C. Rollinger, A. Thill, R. Weis, and B. Thuy. 2022b. A fragmentary leptonectid ichthyosaurian from the lower Pliensbachian of Luxembourg. *Palaeontologia Electronica* 25: a24.

Fischer, V., J. A. Maclaren, R. F. Bennion, P. S. Druckenmiller, and R. B. J. Benson. 2020a. The macroevolutionary landscape of short-necked plesiosaurians. *Scientific Reports* 10: 16434.

Fischer, V., R. Weis, and B. Thuy. 2021a. Refining the marine reptile turnover at the Early-Middle Jurassic transition. *PeerJ* 9:1–45.

Fischer, V., N. G. Zverkov, M. S. Arkhangelsky, I. M. Stenshin, I. V Blagovetshensky, and G. N. Uspensky. 2021b. A new elasmosaurid plesiosaurian from the Early Cretaceous of Russia marks an early attempt at neck elongation. *Zoological Journal of the Linnean Society* 192: 1167–1194.

Fish, F. E., and G. V Lauder. 2017. Control surfaces of aquatic vertebrates: active and passive design and function. *Journal of Experimental Biology* 220: 4351–4363.

Flannery Sutherland, J. T., B. C. Moon, T. L. Stubbs, and M. J. Benton. 2019. Does exceptional preservation distort our view of disparity in the fossil record? *Proceedings of the Royal Society B: Biological Sciences* 286: 20190091.

Foffa, D., A. R. Cuff, J. Sassoon, E. J. Rayfield, M. N. Mavrogordato, and M. J. Benton. 2014. Functional anatomy and feeding biomechanics of a giant Upper Jurassic pliosaur (Reptilia: Sauropterygia) from Weymouth Bay, Dorset, UK. *Journal of Anatomy* 225: 209–219.

Foffa, D., M. T. Young, and S. L. Brusatte. 2024. Comparative functional morphology indicates niche partitioning among sympatric marine reptiles. *Royal Society Open Science* 11: 231951.

Foffa, D., M. T. Young, and S. L. Brusatte. 2018a. Filling the Corallian gap: New information on Late Jurassic marine reptile faunas from England. *Acta Palaeontologica Polonica* 63: 287-313.

Foffa, D., M. T. Young, T. L. Stubbs, K. G. Dexter, and S. L. Brusatte. 2018b. The long-term ecology and evolution of marine reptiles in a Jurassic seaway. *Nature Ecology & Evolution* 2: 1548–1555.

Foster, W., and R. Twitchett. 2014. Functional Diversity of Marine Ecosystems after the Late Permian extinction event. *Nature Geoscience* 7: 233–238.

Fraas, E. E. 1891. Ichthyosaurier der Süddeutschen Trias und Jura-Ablagerungen. *Tübingen H. Laupp* 81.

Freckleton, R. P., P. H. Harvey, and M. Pagel. 2002. Phylogenetic Analysis and Comparative Data: A Test and Review of Evidence. *The American naturalist* 160: 712–726.

Friedman, M. 2009. Ecomorphological selectivity among marine teleost fishes during the end-Cretaceous extinction. *Proceedings of the National Academy of Sciences* 106: 5218–5223.

Fritsch, K. von. 1894. Beitrag zur der Saurier des Halle'schen unteren Muschelkalkes. *Abhandlungen der Naturforschenden Gesellschaft zu Halle* 20: s273–302.

Fritz, S. A., and A. Purvis. 2010. Selectivity in mammalian extinction risk and threat types: A new measure of phylogenetic signal strength in binary traits. *Conservation Biology* 24: 1042–1051.

Fröbisch, N. B., J. Fröbisch, P. M. Sander, L. Schmitz, and O. Rieppel. 2013. Macropredatory ichthyosaur from the Middle Triassic and the origin of modern trophic networks. *Proceedings of the National Academy of Sciences* 110: 1393–1397.

Fröbisch, N. B., P. M. Sander, and O. Rieppel. 2006. A new species of *Cymbospondylus* (Diapsida, Ichthyosauria) from the Middle Triassic of Nevada and a re-evaluation of the skull osteology of the genus. *Zoological Journal of the Linnean Society* 147: 515–538.

Fukuhara, A., M. Sato, H. Ogawa, T. Sato, W. Sellers, and A. Ishiguro. 2024. Rethinking the four-wing problem in plesiosaur swimming using bio-inspired decentralized control. *Scientific Reports* 14: 25333.

Furrer, H. 2003. Der Monte San Giorgio im Südtessin - vom Berg der Saurier zur Fossil-Lagerstätte internationaler Bedeutung.

Galili, T. 2015. dendextend: an R package for visualizing, adjusting and comparing trees of hierarchical clustering. *Bioinformatics* 31: 3718–3720.

García-Ávila, M., R. De la Horra, C. de Miguel Chaves, M. A. Juncal, A. Pérez-García, F. Ortega, and J. B. Diez. 2021. Palynological and sedimentological implications of the sauropterygian Upper Triassic site of El Atance (Central Iberian Peninsula). *Review of Palaeobotany and Palynology* 295: 104541.

Gasparini, Z. 1997. A new pliosaur from the Bajocian of the Neuquen Basin, Argentina. *Palaeontology* 40: 135–147.

Godefroit, P. 1993. The skull of *Stenopterygius longifrons* (Owen, 1881). *Revue de Paléobiologie de Genève volume spécial* 7: 67–84.

Goloboff, P. A., and S. A. Catalano. 2016. TNT version 1.5, including a full implementation of phylogenetic morphometrics. *Cladistics* 32: 221-238.

Goloboff, P. A., M., and E. Morales. 2023. TNT version 1.6, with a graphical interface for MacOS and Linux, including new routines in parallel *Cladistics* 39: 144-153.

Goloboff, P. A., and M. E. Morales. 2023. TNT version 1.6, with a graphical interface for MacOS and Linux, including new routines in parallel. *Cladistics* 39:144–153.

Goloboff, P. A., A. Torres, and J. S. Arias. 2018. Weighted parsimony outperforms other methods of phylogenetic inference under models appropriate for morphology. *Cladistics* 34: 407–437.

Gower, J. C. 1971. A General Coefficient of Similarity and Some of Its Properties. *Biometrics* 27: 857–871.

Greene, S. E., R. C. Martindale, K. A. Ritterbush, D. J. Bottjer, F. A. Corsetti, and W. M. Berelson. 2012. Recognising Ocean acidification in deep time: An evaluation of the evidence for acidification across the Triassic-Jurassic boundary. *Earth-Science Reviews* 113: 72–93.

Griebeler, E. M., and N. Klein. 2019. Life-history strategies indicate live-bearing in *Nothosaurus* (Sauropterygia). *Palaeontology* 62: 697–713.

Großmann, F. 2006. Taxonomy, phylogeny and palaeoecology of the plesiosauroids (Sauropterygia, Reptilia) from the Posidonia shale (Toarcian, Lower Jurassic) of Holzmaden, South West Germany.

Großmann, F. 2007. The taxonomic and phylogenetic position of the Plesiosauroidea from the Lower Jurassic Posidonia shale of south-west Germany. *Palaeontology* 50: 545–564.

Grossnickle, D. M., W. H. Brightly, L. N. Weaver, K. E. Stanchak, R. A. Roston, S. K. Pevsner, C. T. Stayton, P. D. Polly, and C. J. Law. 2024. Challenges and advances in measuring phenotypic convergence. *Evolution* 78: 1355–1371.

Guillerme, T. 2018. dispRity: A modular R package for measuring disparity. *Methods in Ecology and Evolution* 9: 1755–1763.

Guillerme, T., and N. Cooper. 2018. Time for a rethink: time sub-sampling methods in disparity-through-time analyses. *Palaeontology* 61: 481–493.

Gutarra, S., and I. A. Rahman. 2021. The locomotion of extinct secondarily aquatic tetrapods. *Biological Reviews* 97: 67–98.

Gutarra, S., T. L. Stubbs, B. C. Moon, B. H. Heighton, and M. J. Benton. 2023. The locomotor ecomorphology of Mesozoic marine reptiles. *Palaeontology* 66: e12645.

Gutarra, S., T. L. Stubbs, B. C. Moon, C. Palmer, and M. J. Benton. 2022. Large size in aquatic tetrapods compensates for high drag caused by extreme body proportions. Communications Biology 5: 380.

Hagdorn, H., and O. Rieppel. 1999. Stratigraphy of marine reptiles in the Triassic of Central Europe. *Zentralblatt Für Geologie Und Paläontologie Teil I* 7–8: 651–678.

Haggart, J. W., E. L. Nicholls, and R. Bartlett. 2003. The first record of a pliosaurid (Plesiosauria, Pliosauridae) from the Lower Cretaceous of North America. *Cretaceous Research* 24: 129–133.

Hallam, A. 2002. How catastrophic was the end-Triassic mass extinction? *Lethaia* 35: 147–157.

Hallam, A., and P. B. Wignall. 1999. Mass extinctions and sea-level changes. *Earth-Science Reviews* 48: 217–250.

Haq, B. U., J. Hardenbol, and P. R. Vail. 1987. Chronology of fluctuating sea levels since the Triassic. *Science* 235: 1156–1167.

Hardy, C., E. Fara, R. Laffont, J.-L. Dommergues, C. Meister, and P. Neige. 2012. Deep-Time Phylogenetic Clustering of Extinctions in an Evolutionarily Dynamic Clade (Early Jurassic Ammonites). *PLoS ONE* 7: e37977.

Harnik, P. G., P. C. Fitzgerald, J. L. Payne, and S. J. Carlson. 2014. Phylogenetic signal in extinction selectivity in Devonian terebratulide brachiopods. 40: 675–692.

He, T., J. Dal Corso, R. J. Newton, P. B. Wignall, B. J. W. Mills, S. Todaro, P. Di Stefano, E. C. Turner, R. A. Jamieson, V. Randazzo, M. Rigo, R. E. Jones, and A. M. Dunhill. 2020. An enormous sulfur isotope excursion indicates marine anoxia during the end-Triassic mass extinction. Science Advances 6: eabb6704.

He, T., P. B. Wignall, R. J. Newton, J. W. Atkinson, J. F. J. Keeling, Y. Xiong, and S. W. Poulton. 2022. Extensive marine anoxia in the European epicontinental sea during the end-Triassic mass extinction. *Global and Planetary Change* 210: 103771.

Hedman, M. M. 2010. Constraints on clade ages from fossil outgroups. *Paleobiology* 36: 16–31.

Heijne, J., N. Klein, and P. M. Sander. 2019. The uniquely diverse taphonomy of the marine reptile skeletons (Sauropterygia) from the Lower Muschelkalk (Anisian) of Winterswijk, The Netherlands. *PalZ* 93: 69–92.

Heim, N. A., M. L. Knope, E. K. Schaal, S. C. Wang, and J. L. Payne. 2015. Cope's rule in the evolution of marine animals. *Science* 347: 867–870.

Heyning, J. E., and J. G. Mead. 1996. Suction feeding in beaked whales: morphological and observational evidence. *Contributions in science* 464: 1–12.

Hinić-Frlog, S., and R. Motani. 2010. Relationship between osteology and aquatic locomotion in birds: determining modes of locomotion in extinct Ornithurae. *Journal of Evolutionary Biology* 23: 372–385.

Hinz, J. K., A. T. Matzke, and H.-U. Pfretzschner. 2019. A new nothosaur (Sauropterygia) from the Ladinian of Vellberg-Eschenau, southern Germany. *Journal of Vertebrate Paleontology* 39: e1585364.

Hodges, M., and G. Stanley Jr. 2015. North American coral recovery after the end-Triassic mass extinction, New York Canyon, Nevada, USA. *GSA Today* 25: 2–9.

Hodych, J. P., and G. R. Dunning. 1992. Did the Manicouagan impact trigger end-of-Triassic mass extinction? *Geology* 20: 51–54.

Holmes, R., Y.-N. Cheng, and X.-C. Wu. 2008. New information on the skull of *Keichousaurus hui* (Reptilia: Sauropterygia) with comments on sauropterygian interrelationships. *Journal of Vertebrate Paleontology* 28: 76–84.

Holzman, R., D. C. Collar, S. A. Price, C. D. Hulsey, R. C. Thomson, and P. C. Wainwright. 2012. Biomechanical trade-offs bias rates of evolution in the feeding apparatus of fishes. *Proceedings of the Royal Society B: Biological Sciences* 279: 1287–1292.

Home, E. 1814. Some Account of the Fossil Remains of an Animal More Nearly Allied to Fishes Than Any of the Other Classes of Animals. *Philosophical Transactions of the Royal Society of London* 104: 571–577.

Hopley, P. J. 2000. A new Plesiosaurid specimen from the Sinemurian, Lower Jurassic, of Southern England. *Proceedings of the Dorset Natural History and Archaeological Society* 122: 129–138.

Hu, S., Q. Zhang, Z.-Q. Chen, C. Zhou, T. Lü, T. Xie, W. Wen, J. Huang, and M. J. Benton. 2011. The Luoping biota: exceptional preservation, and new evidence on the Triassic recovery from end-Permian mass extinction. *Proceedings of the Royal Society B: Biological Sciences* 278: 2274–2282.

Hu, Y.-W., Q. Li, and J. Liu. 2024. A new pachypleurosaur (Reptilia: Sauropterygia) from the Middle Triassic of southwestern China and its phylogenetic and biogeographic implications. *Swiss Journal of Palaeontology* 143: 1.

Huang, J., R. Motani, D. Jiang, X. Ren, A. Tintori, O. Rieppel, M. Zhou, Y. Hu, and R. Zhang. 2020. Repeated evolution of durophagy during ichthyosaur radiation after mass extinction indicated by hidden dentition. *Scientific Reports* 10: 7798.

Huang, J., R. Motani, D. Jiang, A. Tintori, O. Rieppel, M. Zhou, X.-X. Ren, and R. Zhang. 2019. The new ichthyosauriform *Chaohusaurus brevifemoralis* (Reptilia, Ichthyosauromorpha) from Majiashan, Chaohu, Anhui Province, China. *PeerJ* 7: e7561.

Huene, F. von. 1923. Ein neuer Plesiosaurier aus dem oberen Lias Württembergs. *Jahreshefte des Vereins für Vaterländische Naturkunde in Württemberg* 79: 3–23.

Hurum, J. H., A. J. Roberts, H. A. Nakrem, J. A. Stenløkk, and A. Mørk. 2014. The first recovered ichthyosaur from the Middle Triassic of Edgeøya, Svalbard. *Norwegian Petroleum Directorate* 11: 97–110.

Jablonski, D., and D. M. Raup. 1995. Selectivity of End-Cretaceous Marine Bivalve Extinctions. *Science* 268: 389–391.

J.E Martin, P. Vincent, G. Suan, T. Sharpe, P. Hodges, M. Williams, C. Howells, V. F. 2015. A mysterious giant ichthyosaur from the lowermost Jurassic of Wales. *Acta Palaeontologica Polonica* 60: 837–842.

Jenkyns, H. 2010. Geochemistry of Oceanic Anoxic Events. Geochemistry Geophysics Geosystems - geochem geophys geosyst 11.

Jenkyns, H. 1985. The Early Toarcian and Cenomanian-Turonian anoxic events in Europe: Comparisons and contrasts. *Geologische Rundschau* 74: 505–518.

Ji, C., D.-Y. Jiang, R. Motani, O. Rieppel, W.-C. Hao, and Z.-Y. Sun. 2016. Phylogeny of the Ichthyopterygia Incorporating Recent Discoveries from South China. *Journal of Vertebrate Paleontology* 36: e1025956

Ji, C., D.-Y. Jiang, O. Rieppel, R. Motani, A. Tintori, and Z.-Y. Sun. 2014. A new specimen of Nothosaurus youngi from the Middle Triassic of Guizhou, China. *Journal of Vertebrate Paleontology* 34: 465–470.

Jiang, D., W.-B. Lin, O. Rieppel, R. Motani, and Z.-Y. Sun. 2019. A new Anisian (Middle Triassic) eosauropterygian (Reptilia, Sauropterygia) from Panxian, Guizhou Province, China. *Journal of Vertebrate Paleontology* 38: 1–9.

Jiang, D., M. Maisch, Z. Sun, Y. Sun, and W.-C. Hao. 2006a. A new species of Lariosaurus (Reptilia, Sauropterygia) from the Middle Anisian (Middle Triassic) of southwestern China. *Neues Jahrbuch für Geologie und Paläontologie - Abhandlungen* 242: 19–42.

Jiang, D., R. Motani, W. Hao, L. Schmitz, O. Rieppel, Y. Sun, and Z. Sun. 2008a. New primitive ichthyosaurian (Reptilia, Diapsida) from the Middle Triassic of Panxian, Guizhou, southwestern China and its position in the Triassic biotic recovery. *Progress in Natural Science* 18: 1315–1319.

Jiang, D., L. Schmitz, W.-C. HAO, and Y. Sun. 2009. A new mixosaurid ichthyosaur from the Middle Triassic of China. *Journal of Vertebrate Paleontology* 26: 60–69.

Jiang, D.-Y., R. Motani, W.-C. Hao, O. Rieppel, Y.-L. Sun, L. Schmitz, and Z.-Y. Sun. 2008b. First record of Placodontoidea (Reptilia, Sauropterygia, Placodontia) from the Eastern Tethys. *Journal of Vertebrate Paleontology* 28: 904–908.

Jiang, D.-Y., R. Motani, J.-D. Huang, A. Tintori, Y.-C. Hu, O. Rieppel, N. C. Fraser, C. Ji, N. P. Kelley, W.-L. Fu, and R. Zhang. 2016. A large aberrant stem ichthyosauriform indicating early rise and demise of ichthyosauromorphs in the wake of the end-Permian extinction. *Scientific Reports* 6: 26232.

Jiang, D.-Y., R. Motani, A. Tintori, O. Rieppel, G.-B. Chen, J.-D. Huang, R. Zhang, Z.-Y. Sun, and C. Ji. 2014. The Early Triassic eosauropterygian *Majiashanosaurus discocoracoidis*, gen. et sp. nov. (Reptilia, Sauropterygia), from Chaohu, Anhui Province, People's Republic of China. *Journal of Vertebrate Paleontology* 34: 1044–1052.

Jiang, D.-Y., R. Motani, A. Tintori, O. Rieppel, C. Ji, M. Zhou, X. Wang, H. Lu, and Z.-G. Li. 2020. Evidence Supporting Predation of 4-m Marine Reptile by Triassic Megapredator. *iScience* 23: 101347.

Jiang, D.-Y., L. Schmitz, W.-C. Hao, and Y.-L. Sun. 2006b. A New Mixosaurid Ichthyosaur from the Middle Triassic of China. *Journal of Vertebrate Paleontology* 26: 60–69.

Jost, A. B., A. Bachan, B. van de Schootbrugge, K. V Lau, K. L. Weaver, K. Maher, and J. L. Payne. 2017. Uranium isotope evidence for an expansion of marine anoxia during the end-Triassic extinction. Geochemistry, Geophysics, Geosystems 18: 3093–3108.

Karl, H.-V., G. Arp, E. Siedersbeck, and J. Reitner. 2014. A large ichthyosaur vertebra from the lower Kössen Formation (Upper Norian) of the Lahnewiesgraben near Garmisch-Partenkirchen, Germany. *Göttingen Contributions to Geosciences* 77: 191–197.

Kear, B. P., W. E. Boles, and E. T. Smith. 2003. Unusual gut contents in a Cretaceous ichthyosaur. *Proceedings of the Royal Society of London B Biological Sciences* 270: S206-S208.

Kear, B. P., V. S. Engelschiøn, Ø. Hammer, A. J. Roberts, and J. H. Hurum. 2023. Earliest Triassic ichthyosaur fossils push back oceanic reptile origins. *Current Biology* 33: R178–R179.

Kear, B. P., and E. E. Maxwell. 2013. Wiman's forgotten plesiosaurs: the earliest recorded sauropterygian fossils from the High Arctic. *GFF* 135:95–103.

Kear, B. P., A. J. Roberts, G. Young, M. Terezow, D. J. Mantle, I. S. Barros, and J. H. Hurum. 2024. Oldest southern sauropterygian reveals early marine reptile globalization. *Current Biology* 34: R562–R563.

Kelley, N. P. 2012. Trophic ecomorphology of Triassic marine reptiles. University of California, Davis.

Kelley, N. P., R. B. Irmis, P. E. dePolo, P. J. Noble, D. Montague-Judd, H. Little, J. Blundell, C. Rasmussen, L. M. E. Percival, T. A. Mather, and N. D. Pyenson. 2022. Grouping behavior in a Triassic marine apex predator. *Current Biology* 32: 5398-5405.e3.

Kelley, N. P., and R. Motani. 2015. Trophic convergence drives morphological convergence in marine tetrapods. *Biology Letters* 11: 1–5.

Kelley, N. P., R. Motani, D. Jiang, O. Rieppel, and L. Schmitz. 2014. Selective extinction of Triassic marine reptiles during long-term sea-level changes illuminated by seawater strontium isotopes. *Palaeogeography, Palaeoclimatology, Palaeoecology* 400: 9–16.

Kelley, N. P., and N. D. Pyenson. 2015. Evolutionary innovation and ecology in marine tetrapods from the Triassic to the Anthropocene. *Science* 348: aaa3716.

Ketchum, H. F., and R. B. J. Benson. 2011a. A new pliosaurid (Sauropterygia, Plesiosauria) from the Oxford Clay Formation (Middle Jurassic, Callovian) of England: evidence for a gracile, longirostrine grade of Early–Middle Jurassic pliosaurids. *Special Papers in Palaeontology* 86: 109–129.

Ketchum, H. F., and R. B. J. Benson. 2010. Global interrelationships of Plesiosauria (Reptilia, Sauropterygia) and the pivotal role of taxon sampling in determining the outcome of phylogenetic analyses. *Biological Reviews* 85: 361–392.

Ketchum, H. F., and R. B. J. Benson. 2011b. The cranial anatomy and taxonomy of *Peloneustes philarchus* (Sauropterygia, Pliosauridae) from the Peterborough Member (Callovian, Middle Jurassic) of the United Kingdom. *Palaeontology* 54: 639–665.

Ketchum, H. F., and A. S. Smith. 2010. The anatomy and taxonomy of Macroplata tenuiceps (Sauropterygia, Plesiosauria) from the Hettangian (Lower Jurassic) of Warwickshire, United Kingdom. *Journal of Vertebrate Paleontology* 30: 1069–1081.

Klein, N. 2012. Postcranial morphology and growth of the pachypleurosaur *Anarosaurus heterodontus* (Sauropterygia) from the Lower Muschelkalk of Winterswijk, The Netherlands. *Paläontologische Zeitschrift* 86: 389–408.

Klein, N. 2009. Skull morphology of *Anarosaurus heterodontus* (Reptilia: Sauropterygia: Pachypleurosauria) from the Lower Muschelkalk of the Germanic Basin (Winterswijk, The Netherlands). *Journal of Vertebrate Paleontology* 29: 665–676.

Klein, N., and P. Albers. 2009. A New Species of the Sauropsid Reptile Nothosaurus from the Lower Muschelkalk of the Western Germanic Basin, Winterswijk, the Netherlands. *Acta Palaeontologica Polonica* 54: 589–598.

Klein, N., S. Eggmaier, and H. Hagdorn. 2022a. The redescription of the holotype of *Nothosaurus mirabilis* (Diapsida, Eosauropterygia) — a historical skeleton from the Muschelkalk (Middle Triassic, Anisian) near Bayreuth (southern Germany). *PeerJ* 10: e13818.

Klein, N., H. Furrer, I. Ehrbar, M. Torres Ladeira, H. Richter, and T. M. Scheyer. 2022b. A new pachypleurosaur from the Early Ladinian Prosanto Formation in the Eastern Alps of Switzerland. *Swiss Journal of Palaeontology* 141: 12.

Klein, N., and E. M. Griebeler. 2016. Bone histology, microanatomy, and growth of the nothosauroid *Simosaurus gaillardoti* (Sauropterygia) from the Upper Muschelkalk of southern Germany/Baden-Württemberg. *Comptes Rendus Palevol* 15: 142–162.

Klein, N., and E. M. Griebeler. 2018. Growth patterns, sexual dimorphism, and maturation modeled in Pachypleurosauria from Middle Triassic of central Europe (Diapsida: Sauropterygia). *Fossil Record* 21: 137–157.

Klein, N., P. M. Sander, A. Krahl, T. M. Scheyer, and A. Houssaye. 2016a. Diverse Aquatic Adaptations in *Nothosaurus* spp. (Sauropterygia) — Inferences from Humeral Histology and Microanatomy. *PLoS ONE* 11: e0158448.

Klein, N., L. Schmitz, T. Wintrich, and P. M. Sander. 2020. A new cymbospondylid ichthyosaur (Ichthyosauria) from the Middle Triassic (Anisian) of the Augusta Mountains, Nevada, USA. *Journal of Systematic Palaeontology* 18: 1167–1191.

Klein, N., D. F. A. E. Voeten, A. Haarhuis, and R. Bleeker. 2016b. The earliest record of the genus Lariosaurus from the early middle Anisian (Middle Triassic) of the Germanic Basin. *Journal of Vertebrate Paleontology* 36: e1163712.

Klein, N., D. F. A. E. Voeten, J. Lankamp, R. Bleeker, O. J. Sichelschmidt, M. Liebrand, D. C. Nieweg, and P. Martin Sander. 2015. Postcranial material of *Nothosaurus marchicus* from the Lower Muschelkalk (Anisian) of Winterswijk, The Netherlands, with remarks on swimming styles and taphonomy. *Paläontologische Zeitschrift* 89: 961–981.

Klug, C., T. Scheyer, N. Klein, J. Liu, and R. Stockar. 2024. 100 years of scientific excavations at UNESCO World Heritage Site Monte San Giorgio and global research on Triassic marine Lagerstätten 143: 37

Knoll, A. H., R. K. Bambach, J. L. Payne, S. Pruss, and W. W. Fischer. 2007. Paleophysiology and end-Permian mass extinction. *Earth and Planetary Science Letters* 256: 295–313.

Knutsen, E. M., P. S. Druckenmiller, and J. Hurum. 2012a. A new species of *Pliosaurus* (Sauropterygia: Plesiosauria) from the Middle Volgian of central Spitsbergen, Norway. *Norwegian Journal of Geology* 92: 235–258.

Knutsen, E. M., P. S. Druckenmiller, and J. H. Hurum. 2012b. A new plesiosauroid (Reptilia: Sauropterygia) from the Agardhfjellet Formation (Middle Volgian) of central Spitsbergen, Norway. *Norwegian Journal of Geology* 92: 213–234.

Knutsen, E. M., P. S. Druckenmiller, and Jø. H. Hurum. 2012c. Redescription and taxonomic clarification of "*Tricleidus*" *svalbardensis* based on new material from the Agardhfjellet Formation (Middle Volgian). *Norwegian Journal of Geology* 92: 175–186.

Kolb, C., M. R. Sánchez-Villagra, and T. M. Scheyer. 2011. The palaeohistology of the basal ichthyosaur *Mixosaurus* Baur, 1887 (Ichthyopterygia, Mixosauridae) from the Middle Triassic: Palaeobiological implications. *Comptes rendus Palevol* 10: 403–411.

Krahl, A. 2021. The locomotory apparatus and paraxial swimming in fossil and living marine reptiles: comparing Nothosauroidea, Plesiosauria, and Chelonioidea. *PalZ* 95: 483–501.

Krahl, A., N. Klein, and P. M. Sander. 2013. Evolutionary implications of the divergent long bone histologies of *Nothosaurus* and *Pistosaurus* (Sauropterygia, Triassic). *BMC Evolutionary Biology* 13: 1–23.

Krahl, A., and I. Werneburg. 2023. Deep-time invention and hydrodynamic convergences through amniote flipper evolution. *Anatomical Record* 306: 1323–1355.

Kubo, T., M. T. Mitchell, and D. M. Henderson. 2012. Albertonectes vanderveldei, a new elasmosaur (Reptilia, Sauropterygia) from the Upper Cretaceous of Alberta. *Journal of Vertebrate Paleontology* 32: 557–572.

Laboury, A., R. F. Bennion, B. Thuy, R. Weis, and V. Fischer. 2022. Anatomy and phylogenetic relationships of *Temnodontosaurus zetlandicus* (Reptilia: Ichthyosauria). *Zoological Journal of the Linnean Society* 195: 172–194.

Laboury, A., T. M. Scheyer, N. Klein, T. L. Stubbs, and V. Fischer. 2023. High phenotypic plasticity at the dawn of the eosauropterygian radiation. *PeerJ* 11: e15776.

Laboury, A., T. L. Stubbs, A. S. Wolniewicz, J. Liu, T. M. Scheyer, M. E. H. Jones, and V. Fischer. 2024. Contrasting macroevolutionary patterns in pelagic tetrapods across the Triassic–Jurassic transition. *Evolution* qpae138.

Li, C. 1999. Ichthyosaur from Guizhou, China. *Chinese Science Bulletin* 44: 1329–1333.

Li, C., O. Rieppel, C. Long, and N. C. Fraser. 2016. The earliest herbivorous marine reptile and its remarkable jaw apparatus. Science Advances 2: e1501659.

Li, C., O. Rieppel, X.-C. Wu, L.-J. Zhao, and L.-T. Wang. 2011. A new Triassic marine reptile from southwestern China. *Journal of Vertebrate Paleontology* 31: 303–312.

Li, C., and H.-L. You. 2002. *Cymbospondylus* from the Upper Triassic of Guizhou, China. Vertebrata *PalAsiatica* 40: 9–16.

Li, Q., and J. Liu. 2020. An Early Triassic sauropterygian and associated fauna from South China provide insights into Triassic ecosystem health. *Communication Biology* 3: 63.

Lin, K., and O. Rieppel. 1998. Functional morphology and ontogeny of *Keichousaurus hui* (Reptilia, Sauropterygia). *Chicago Natural History Museum*.

Lin, W.-B., D.-Y. Jiang, O. Rieppel, R. Motani, C. Ji, A. Tintori, Z.-Y. Sun, and M. Zhou. 2017. A new specimen of *Lariosaurus xingyiensis* (Reptilia, Sauropterygia) from the Ladinian (Middle Triassic) Zhuganpo Member, Falang Formation, Guizhou, China. *Journal of Vertebrate Paleontology* 4634: e1278703.

Lin, W.-B., D.-Y. Jiang, O. Rieppel, R. Motani, A. Tintori, Z.-Y. Sun, and M. Zhou. 2021. *Panzhousaurus Rotundirostris* Jiang et al., 2019 (Diapsida: Sauropterygia)

and the Recovery of the Monophyly of Pachypleurosauridae. *Journal of Vertebrate Paleontology* 41: e1901730.

Lindgren, J., P. Sjövall, V. Thiel, W. Zheng, S. Ito, K. Wakamatsu, R. Hauff, B. P. Kear, A. Engdahl, C. Alwmark, M. E. Eriksson, M. Jarenmark, S. Sachs, P. E. Ahlberg, F. Marone, T. Kuriyama, O. Gustafsson, P. Malmberg, A. Thomen, I. Rodríguez-Meizoso, P. Uvdal, M. Ojika, and M. H. Schweitzer. 2018. Soft-tissue evidence for homeothermy and crypsis in a Jurassic ichthyosaur. *Nature* 564: 359–365.

Lingham-Soliar, T. 2016. Convergence in Thunniform Anatomy in Lamnid Sharks and Jurassic Ichthyosaurs. *Integrative and Comparative Biology* icw125.

Lingham-Soliar, T. 2003. Extinction of ichthyosaurs: a catastrophic or evolutionary paradigm? *Neues Jahrbuch für Geologie und Paläontologie, Abhandlungen* 228: 421–452.

Lingham-Soliar, T. 1999. Rare Soft Tissue Preservation Showing Fibrous Structures in a Ichthyosaur from the Lower Lias (Jurassic) of England. *Proceedings of the Royal Society B: Biological Sciences* 266: 2367–2373.

Lingham-Soliar, T. 2001. The ichthyosaur integument: skin fibers, a means for a strong, flexible and smooth skin. *Lethaia* 34: 287–302.

Lingham-Soliar, T., and G. Plodowski. 2007. Taphonomic evidence for high-speed adapted fins in thunniform ichthyosaurs. *Naturwissenschaften* 94: 65–70.

Liu, J., S. Hu, O. Rieppel, D. Jiang, M. J. Benton, N. P. Kelley, J. C. Aitchison, C. Zhou, W. Wen, J. Huang, T. Xie, and T. Lv. 2014. A gigantic nothosaur (Reptilia: Sauropterygia) from the Middle Triassic of SW China and its implication for the Triassic biotic recovery. *Scientific Reports* 4: 7142

Liu, J., R. Motani, D.-Y. Jiang, S.-X. Hu, J. C. Aitchison, O. Rieppel, M. J. Benton, Q.-Y. Zhang, and C.-Y. Zhou. 2013. The first specimen of the Middle Triassic *Phalarodon atavus* (Ichthyosauria: Mixosauridae) from South China, showing postcranial anatomy and peri-tethyan distribution. *Palaeontology* 56: 849–866.

Liu, J., O. Rieppel, D.-Y. Jiang, J. C. Aitchison, R. Motani, Q.-Y. Zhang, C.-Y. Zhou, and Y.-Y. Sun. 2011. A new pachypleurosaur (Reptilia: Sauropterygia) from the

lower Middle Triassic of southwestern China and the phylogenetic relationships of Chinese pachypleurosaurs. *Journal of Vertebrate Paleontology* 31: 292–302.

Liu, Q., T. Yang, L. Cheng, M. J. Benton, B. C. Moon, C. Yan, Z. An, and L. Tian. 2021. An injured pachypleurosaur (Diapsida: Sauropterygia) from the Middle Triassic Luoping Biota indicating predation pressure in the Mesozoic. *Scientific Reports* 11: 21818.

Liu, Q.-L., L. Cheng, T. L. Stubbs, B. C. Moon, M. J. Benton, C.-B. Yan, and L. Tian. 2023. Rapid neck elongation in Sauropterygia (Reptilia: Diapsida) revealed by a new basal pachypleurosaur from the Lower Triassic of China. BMC *Ecology and Evolution* 23: 44.

Liu, S., A. S. Smith, Y. Gu, J. Tan, C. K. Liu, and G. Turk. 2015. Computer Simulations Imply Forelimb-Dominated Underwater Flight in Plesiosaurs. *PLOS Computational Biology* 11: e1004605.

Lloyd, G. T. 2016. Estimating morphological diversity and tempo with discrete character-taxon matrices: implementation, challenges, progress, and future directions. *Biological Journal of the Linnean Society* 118: 131–151.

Lloyd, G. T., D. W. Bapst, M. Friedman, and K. E. Davis. 2016. Probabilistic divergence time estimation without branch lengths: dating the origins of dinosaurs, avian flight, and crown birds. *Biology Letters* **12:** 20160609.

Lomax, D. R. 2016. A new leptonectid ichthyosaur from the Lower Jurassic (Hettangian) of Nottinghamshire, England, UK, and the taxonomic usefulness of the ichthyosaurian coracoid. *Journal of Systematic Palaeontology* 15: 1–15.

Lomax, D. R. 2010. An ichthyosaurus (Reptilia, Ichthyosauria) with gastric contents from Charmouth, England: first report of the genus from the Pliensbachian. *Paludicola* 8: 22–36.

Lomax, D. R., P. De la Salle, J. A. Massare, and R. Gallois. 2018a. A giant Late Triassic ichthyosaur from the UK and a reinterpretation of the Aust Cliff 'dinosaurian'' bones.' *PLoS ONE* 13: 1–16.

Lomax, D. R., P. de la Salle, M. Perillo, J. Reynolds, R. Reynolds, and J. F. Waldron. 2024. The last giants: New evidence for giant Late Triassic (Rhaetian) ichthyosaurs from the UK. *PLoS ONE* 19: e0300289.

Lomax, D. R., M. Evans, and S. Carpenter. 2018b. An ichthyosaur from the UK Triassic – Jurassic boundary: A second specimen of the leptonectid ichthyosaur *Wahlisaurus massarae* Lomax 2016. *Geological Journal* 54: 83–90.

Lomax, D. R., and J. A. Massare. 2015. A new species of *Ichthyosaurus* from the Lower Jurassic of West Dorset, England, U.K. *Journal of Vertebrate Paleontology* 35.

Lomax, D. R., and J. A. Massare. 2016. Two new species of Ichthyosaurus from the lowermost Jurassic (Hettangian) of Somerset, England. *Papers in Palaeontology* 3: 1-20.

Lomax, D. R., J. A. Massare, and R. T. Mistry. 2017. The taxonomic utility of forefin morphology in Lower Jurassic ichthyosaurs: Protoichthyosaurus and Ichthyosaurus. *Journal of Vertebrate Paleontology* 37: e1361433.

Lomax, D. R., and S. Sachs. 2017. On the largest *Ichthyosaurus*: A new specimen of *Ichthyosaurus somersetensis* containing an embryo. *Acta Palaeontologica Polonica* 62 (3): 575–584

Lu, H., D.-Y. Jiang, R. Motani, P.-G. Ni, Z.-Y. Sun, A. Tintori, S.-Z. Xiao, M. Zhou, C. Ji, and W.-L. Fu. 2018. Middle Triassic Xingyi Fauna: Showing turnover of marine reptiles from coastal to oceanic environments. *Palaeoworld* 27: 107–116.

Lucas, S. G. 2002. *Toretocnemus*, a Late Triassic ichthyosaur from California, U.S.A. and Sonora, Mexico. *New Mexico Museum of Natural History and Science Bulletin* 21: 275–278.

Lucas, S., and L. Tanner. 2008. Ch. 9: Reexamination of end-Triassic Mass Extinction. P. *in* Mass Extinction.

Lucas, S., and L. Tanner. 2018. The Missing Mass Extinction at the Triassic-Jurassic Boundary. Pp. 721–785

Ma, L., D. Jiang, O. Rieppel, R. Motani, and A. Tintori. 2015. A new pistosauroid (Reptilia, Sauropterygia) from the late Ladinian Xingyi marine reptile level, southwestern China. *Journal of Vertebrate Paleontology* 35: 1–6.

MacLaren, J. A., P. S. L. Anderson, P. M. Barrett, and E. J. Rayfield. 2017. Herbivorous dinosaur jaw disparity and its relationship to extrinsic evolutionary drivers. *Paleobiology* 43: 15–33.

MacLaren, J. A., R. F. Bennion, N. Bardet, and V. Fischer. 2022. Global ecomorphological restructuring of dominant marine reptiles prior to the Cretaceous–Palaeogene mass extinction. *Proceedings of the Royal Society B: Biological Sciences* 289: 20220585.

Madzia, D., S. Sachs, and J. Lindgren. 2019. Morphological and phylogenetic aspects of the dentition of *Megacephalosaurus eulerti*, a pliosaurid from the Turonian of Kansas, USA, with remarks on the cranial anatomy of the taxon. *Geological Magazine*156: 1201–1216.

Maisch, M., and A. Matzke. 2000. The Ichthyosauria. *Stuttgarter Beiträge zur Naturkunde Serie B*. 298: 1-159.

Maisch, M. W. 2008. Revision der Gattung *Stenopterygius* Jaekel, 1904 emend. von Huene, 1922 (Reptilia: Ichthyosauria) aus dem unteren Jura Westeuropas. *Palaeodiversity* 1: 227–271.

Maisch, M. W., and A. Hungerbühler. 1997. Revision of *Temnodontosaurus nuertingensis* (v. Huene, 1931), a large ichthyosaur from the Lower Pliensbachian (Lower Jurassic) of Nürtingen, Southwestern Germany. *Stuttgarter Beiträge zur Naturkunde Serie B (Geologie und Paläontologie)* 248: 1–11.

Maisch, M. W., and A. T. Matzke. 1998. Observations on Triassic ichthyosaurs; Part III, A crested predatory mixosaurid from the Middle Triassic of the German Basin. *Neues Jahrbuch für Geologie und Paläontologie. Abhandlungen* 209: 105–134.

Maisch, M. W., A. T. Matzke, and W. Brinkmann. 2006. The otic capsule of the Middle Triassic ichthyosaur *Mixosaurus* from Monte San Giorgio (Switzerland):

new evidence on the braincase structure of basal ichthyosaurs. *Eclogae Geologiae Helvetiae* 99: 205–210.

Maisch, M. W., and A. G. Reisdorf. 2006. Evidence for the longest stratigraphic range of a post-Triassic Ichthyosaur: a *Leptonectes tenuirostris* from the Pliensbachian (Lower Jurassic) of Switzerland. *Geobios* 39: 491–505.

Martill, D. M., M. L. Jacobs, and R. E. Smith. 2023. A truly gigantic pliosaur (Reptilia, Sauropterygia) from the Kimmeridge Clay Formation (Upper Jurassic, Kimmeridgian) of England. *Proceedings of the Geologists' Association* 134: 361–373.

Martin, J. E., V. Fischer, P. Vincent, and G. Suan. 2012. A longirostrine *Temnodontosaurus* (Ichthyosauria) with comments on Early Jurassic ichthyosaur niche partitioning and disparity. *Palaeontology* 55: 995–1005.

Martin, J. E. J., P. Vincent, G. Suan, T. Sharpe, P. Hodges, M. Williams, C. Howells, and V. Fischer. 2015. A mysterious giant ichthyosaur from the lowermost Jurassic of Wales. *Acta Palaeontologica Polonica* 60: 837–842.

Martindale, R. C., W. M. Berelson, F. A. Corsetti, D. J. Bottjer, and A. J. West. 2012. Constraining carbonate chemistry at a potential ocean acidification event (the Triassic–Jurassic boundary) using the presence of corals and coral reefs in the fossil record. *Palaeogeography, Palaeoclimatology, Palaeoecology* 350–352: 114–123.

Massare, J. A. 1988. Swimming capabilities of Mesozoic marine reptiles: implications for the methods of predation. *Palaeobiology* 14: 187–205.

Massare, J. A. 1987. Tooth morphology and prey preference of Mesozoic marine reptiles. *Journal of Vertebrate Paleontology* 7: 121–137.

Massare, J. A., E. A. Buchholtz, J. Kenney, and A.-M. Chomat. 2006. Vertebral morphology of *Ophthalmosaurus natans* (Reptilia: Ichthyosauria) from the Jurassic Sundance Formation of Wyoming. *Paludicola* 5: 242–254.

Massare, J. A., and J. M. Callaway. 1990. The affinities and ecology of Triassic ichthyosaurs. *Geological Society of America Bulletin* 102: 409–416.

Massare, J. A., and D. R. Lomax. 2016. A new specimen of *Ichthyosaurus conybeari*(Reptilia, Ichthyosauria) from Watchet, Somerset, England, U.K., and a re-examination of the species. *Journal of Vertebrate Paleontology* e1163264.

Massare, J. A., and H. A. Young. 2005. Gastric contents of an ichthyosaur from the Sundance formation (Jurassic) of central Wyoming. *Paludicola* 5: 20–27.

Maxwell, E., and D. Cortés. 2020. A revision of the Early Jurassic ichthyosaur Hauffiopteryx (Reptilia: Ichthyosauria), and description of a new species from southwestern Germany. *Palaeontologia Electronica* 23: 1–43.

Maxwell, E. E. 2012. New metrics to differentiate species of *Stenopterygius* (Reptilia: Ichthyosauria) from the Lower Jurassic of southwestern Germany. Journal of Paleontology 86: 105–115.

Maxwell, E. E., D. Cortés, P. Patarroyo, and M. L. P. Ruge. 2019. A new specimen of *Platypterygius sachicarum* (Reptilia, Ichthyosauria) from the Early Cretaceous of Colombia and its phylogenetic implications. *Journal of Vertebrate Paleontology* 39: 1–12.

Maxwell, E. E., H. Diependaal, H. Winkelhorst, G. Goris, and N. Klein. 2016. A new species of *Saurichthys* (Actinopterygii: Saurichthyidae) from the Middle Triassic of Winterswijk, The Netherlands. *Neues Jahrbuch für Geologie und Paläontologie Abhandlungen* 280: 119–134.

Maxwell, E. E., M. S. Fernández, and R. R. Schoch. 2012. First diagnostic marine reptile remains from the Aalenian (Middle Jurassic): a new ichthyosaur from southwestern Germany. *PLoS ONE* 7: e41692.

Maxwell, E. E., and B. P. Kear. 2013. Triassic ichthyopterygian assemblages of the Svalbard archipelago: a reassessment of taxonomy and distribution. *GFF* 35: 85–94.

Maxwell, E. E., C. Romano, F. Wu, and H. Furrer. 2015. Two new species of *Saurichthys* (Actinopterygii: Saurichthyidae) from the Middle Triassic of Monte San Giorgio, Switzerland, with implications for character evolution in the genus. Zoological Journal of the Linnean Society 173: 887–912.

McCurry, M. R., A. R. Evans, E. M. G. Fitzgerald, C. R. McHenry, J. Bevitt, and N. D. Pyenson. 2019. The repeated evolution of dental apicobasal ridges in aquatic-feeding mammals and reptiles. *Biological Journal of the Linnean Society* 127: 245–259.

Mccurry, M. R., E. M. G. Fitzgerald, A. R. Evans, J. W. Adams, and C. R. Mchenry. 2017. Skull shape reflects prey size niche in toothed whales. *Biological Journal of the Linnean Society* 121: 936-946.

McGhee, G. R., M. E. Clapham, P. M. Sheehan, D. J. Bottjer, and M. L. Droser. 2013. A new ecological–severity ranking of major Phanerozoic biodiversity crises. Palaeogeography, Palaeoclimatology, *Palaeoecology* 370: 260–270.

McGowan, C. 1996a. A new and typically Jurassic ichthyosaur from the Upper Triassic of Birtish Columbia. *Canadian Journal of Earth Sciences* 33 24–32.

McGowan, C. 1993. A new species of a large, long-snouted ichthyosaur from the English lower Lias. Canadian Journal of Earth Sciences 30: 1197–1204.

McGowan, C. 1994a. A new species of *Shastasaurus* (Reptilia: Ichthyosauria) from the Triassic of British Columbia; the most complete exemplar of the genus. *Journal of Vertebrate of Paleontology* 14: 168–179.

McGowan, C. 2003. A new specimen of *Excalibosaurus* from the English Lower Jurassic. *Journal of Vertebrate of Paleontology* 23: 950–956.

McGowan, C. 1986. A putative ancestor for the swordfish-like ichthyosaur *Eurhinosaurus*. *Nature* 322: 454–456.

McGowan, C. 1995. A remarkable small ichthyosaur from the Upper Triassic of British Columbia, representing a new genus and species. *Canadian Journal of Earth Sciences* 32: 292–303.

McGowan, C. 1974. A revision of the longipinnate ichthyosaurs of the Lower Jurassic of England, with description of the new species (Reptilia, Ichthyosauria). *Life Science Contributions, Royal Ontario Museum* 97: 1–37.

McGowan, C. 1979. A revision of the Lower Jurassic ichthyosaurs of Germany with descriptions of two new species. *Palaeontographica. Abteilung A. Paläozoologie, Stratigraphie* 166: 93–135.

McGowan, C. 1997. A Transitional Ichthyosaur Fauna. Pp. 61–80 *in* eds. Ancient Marine Reptiles. Academic Press, San Diego, California.

McGowan, C. 1989a. Computed tomography reveals further details of *Excalibosaurus*, a putative ancestor for the swordfish-like ichthyosaur *Eurhinosaurus*. *Journal of Vertebrate Paleontology* 9: 269–281.

McGowan, C. 1996b. Giant ichthyosaurs of the Early Jurassic. *Canadian Journal of Earth Sciences* 33: 1011–1021.

McGowan, C. 1989b. *Leptopterygius tenuirostris* and other long-snouted ichthyosaurs from the English Lower Lias. *Palaeontology* 32: 409–427.

McGowan, C. 1994b. *Temnodontosaurus risor* is a juvenile of *T. platyodon* (Reptilia: Ichthyosauria). *Journal of Vertebrate Paleontology* 14: 472–479.

McGowan, C., and A. C. Milner. 1999. A new Pliensbachian ichthyosaur from Dorset, England. *Palaeontology* 42: 761–768.

McGowan, C., and R. Motani. 2003. Handbook of Paleoherpetology, Part 8 Ichthyopterygia.

McKinney, M. L. 1997. Extinction Vulnerability and Selectivity: Combining Ecological and Paleontological Views. *Annual Review of Ecology, Evolution, and Systematics* 28: 495–516.

McRoberts, C., L. Krystyn, and A. Shea. 2008. Rhaetian (Late Triassic) *Monotis* (Bivalvia: Pectinoida) from the Eastern Northern Calcareous Alps (Austria) and the End-Norian crisis in Pelagic faunas. *Palaeontology* 51: 721–735.

Mears, E. M., V. Rossi, E. MacDonald, G. Coleman, T. G. Davies, C. Arias-Riesgo, C. Hildebrandt, H. Thiel, C. J. Duffin, D. I. Whiteside, and M. J. Benton. 2016. The Rhaetian (Late Triassic) vertebrates of Hampstead Farm Quarry, Gloucestershire, UK. *Proceedings of the Geologists' Association* 127: 478–505.

Meng, Z., J. Wang, W. Ji, H. Zhang, F. Wu, and E. Garzanti. 2019. The Langjiexue Group is an in situ sedimentary sequence rather than an exotic block: Constraints from coeval Upper Triassic strata of the Tethys Himalaya (Qulonggongba Formation). *Science China Earth Sciences* 62: 783–797.

Merriam, J. C. 1904. A new marine reptile from the Triassic of California. *University of California Publications, Bulletin of the Department of Geology* 3: 419–421.

Merriam, J. C. 1903. New Ichthtyosauria from the Upper Triassic of California. *University of California Publications, Bulletin of the Department of Geology* 3: 249–263.

Merriam, J. C. 1906. Preliminary note on a new marine reptile from the Middle Triassic of Nevada. *University of California Publications: Bulletin of the department of Geology* 5: 77–79.

Merriam, J. C. 1902. Triassic Ichthyopterygia from California and Nevada. *University of California Publications: Bulletin of the department of Geology* 3: 63–108.

Merriam, J. C. 1908. Triassic Ichthyosauria with special reference to the American forms. *Memoirs of the University of California* 1: 1–154.

Meyer, von H. 1839. Mittheilung, a Professor Bronn gerichtet. *Neues Jahrbuch fur Mineralogie, Geognosie, Geologie und Petrefaktenkunde* 559–560.

Meyer, H. von. 1855. Die Saurier des Muschelkalkes mit Rücksicht auf die Saurier aus buntem Sandstein und Keuper. Heinrich Keller, Frankurt am Main.

Miedema, F., D. Bastiaans, T. M. Scheyer, C. Klug, and E. E. Maxwell. 2024. A large new Middle Jurassic ichthyosaur shows the importance of body size evolution in the origin of the Ophthalmosauria. *BMC Ecology and Evolution* 24:34.

Miedema, F., G. Bindellini, C. Dal Sasso, T. M. Scheyer, and E. E. Maxwell. 2023a. Ontogenetic variation in the cranium of *Mixosaurus cornalianus*, with implications for the evolution of ichthyosaurian cranial development. *Swiss Journal of Palaeontology* 142: 27.

Miedema, F., N. Klein, D. G. Blackburn, P. M. Sander, E. E. Maxwell, E. M. Griebeler, and T. M. Scheyer. 2023b. Heads or tails first? Evolution of fetal

orientation in ichthyosaurs, with a scrutiny of the prevailing hypothesis. *BMC Ecology and Evolution* 23: 12.

Miedema, F., and E. E. Maxwell. 2022. Ontogenetic variation in the skull of Stenopterygius quadriscissus with an emphasis on prenatal development. *Scientific Reports* 12: 1707.

Miedema, F., and E. E. Maxwell. 2019. Ontogeny of the Braincase in *Stenopterygius* (Reptilia, Ichthyosauria) from the Lower Jurassic of Germany. Journal of Vertebrate of Paleontology 39.

Monnet, C., and H. Bucher. 2005. New Middle and Late Anisian (Middle Triassic) ammonoid faunas from northwestern Nevada (USA): Taxonomy and biochronology. *Fossils and Strata* 1–121.

Moon, B. C. 2017. A new phylogeny of ichthyosaurs (Reptilia: Diapsida). Journal of Systematic of Palaeontology 17: 1–27.

Moon, B. C., and A. M. Kirton. 2016. Ichthyosaurs of the British Middle and Upper Jurassic Part 1, *Ophthalmosaurus*. *Monographs of the Palaeontographical Society* 170: 1–84.

Moon, B. C., and T. L. Stubbs. 2020. Early high rates and disparity in the evolution of ichthyosaurs. *Communication Biology* 3: 68.

Motani, R. 2008. Combining uniformitarian and historical data to interpret how Earth environment influenced the evolution of Ichthyopterygia. *Paleontological Society Papers* 14: 147–164.

Motani, R. 1996. Eel-like swimming in the earliest ichtyosaurs. *Nature* 382: 347–348.

Motani, R. 2005. Evolution of fish-shaped reptiles (Reptilia: Ichthyopterygia) in their physical environments and constraints. *Annual review of Earth and Planetary Sciences* 33: 395–420.

Motani, R. 1998a. First complete forefin of the Ichthyosaur *Grippia longirostris* from the Triassic of Spitsbergen. *Palaeontology* 41: 591–599.

Motani, R. 1998b. Ichthyosaurian swimming revisited: implications from the vertebral column and phylogeny. *Journal of Vertebrate Paleontology* 18: 65A.

Motani, R. 1997a. New information on the forefin of *Utatsusaurus hataii* (Ichthyosauria). *Journal of Paleontology* 71: 475–479.

Motani, R. 1999a. On the evolution and homologies of ichthyosaurian forefins. *Journal of the Vertebrate Paleontology* 19: 28–41.

Motani, R. 1999b. Phylogeny of the Ichthyopterygia. *Journal of the Vertebrate Paleontology* 19:473–496.

Motani, R. 2002a. Scaling effects in caudal fin propulsion and the speed of ichthyosaurs. *Nature* 415: 309–312.

Motani, R. 2002b. Swimming speed estimation of extinct marine reptiles: energetic approach revisited. *Paleobiology* 28: 251–262.

Motani, R. 1997b. Temporal and Spatial Distribution of Tooth Implantation in Ichthyosaurs. Pp. 81–103 eds. Ancient Marine Reptiles. Academic Press, San Diego, California.

Motani, R. 2009. The Evolution of Marine Reptiles. *Evolution: Education and Outreach* 2: 224–235.

Motani, R. 1999c. The Skull and Taxonomy of *Mixosaurus* (Ichthyopterygia). *Journal of Paleontology* 73: 924–935.

Motani, R., X. Chen, D. Jiang, L. Cheng, A. Tintori, and O. Rieppel. 2015a. Lunge feeding in early marine reptiles and fast evolution of marine tetrapod feeding guilds. *Scientific Reports* 5: 1–8.

Motani, R., C. Ji, T. Tomita, N. Kelley, E. Maxwell, D. Y. Jiang, and P. M. Sander. 2013. Absence of Suction Feeding Ichthyosaurs and Its Implications for Triassic Mesopelagic Paleoecology. *PLoS ONE* 8: e66075.

Motani, R., D. Jiang, A. Tintori, O. Rieppel, and G. Chen. 2014. Terrestrial Origin of Viviparity in Mesozoic Marine Reptiles Indicated by Early Triassic Embryonic Fossils. *PLoS ONE* 9: e88640.

Motani, R., D. Y. Jiang, A. Tintori, C. Ji, and J. D. Huang. 2017. Pre-versus post-mass extinction divergence of Mesozoic marine reptiles dictated by time-scale

dependence of evolutionary rates. *Proceedings of the Royal Society B: Biological Sciences* 284: 20170241.

Motani, R., D.-Y. Jiang, G.-B. Chen, A. Tintori, O. Rieppel, C. Ji, and J.-D. Huang. 2015b. A basal ichthyosauriform with a short snout from the Lower Triassic of China. *Nature* 517: 485–488.

Motani, R., D.-Y. Jiang, A. Tintori, Y.-L. Sun, HaoWei-Cheng, A. Boyd, S. Frlog-Hinic, L. Schmitz, J.-Y. Shin, and SunZuo-Yu. 2008. Horizons and assemblages of Middle Triassic marine reptiles from Panxian, Guizhou, China. *Journal of Vertebrate Paleontology* 28: 900–903.

Motani, R., M. Manabe, and Z.-M. Dong. 1999. The status of *Himalayasaurus tibetensis* (Ichthyopterygia). *Paludicola* 2: 174–181.

Motani, R., N. Minoura, and T. Ando. 1998. Ichthyosaurian relationships illuminated by new primitive skeletons from Japan. *Nature* 393: 255–257.

Motani, R., and H. You. 1998a. Taxonomy and limb ontogeny of *Chaohusaurus geishanensis* (Ichthyosauria) with a note on the allometric equation. *Journal of Vertebrate Paleontology* 18: 533–540.

Motani, R., and H. You. 1998b. The forefin of *Chensaurus chaoxianenesis* (Ichthyosauria) shows delayed mesopodial ossification. *Journal of Paleontology* 72: 133–136.

Motani, R., H. You, and C. McGowan. 1996. Eel-like swimming in the earliest ichthyosaurs. *Nature* 382: 347–348.

Müller, J. 2007. First record of a thalattosaur from the Upper Triassic of Austria. *Journal of Vertebrate Paleontology* 27: 236–240.

Müller, J. 2005. The anatomy of *Askeptosaurus italicus* from the Middle Triassic of Monte San Giorgio and the interrelationships of thalattosaurs (Reptilia, Diapsida). *Canadian Journal of Earth Sciences* 42: 1347–1367. NRC Research Press.

Müller, T., G. Price, D. Bajnai, A. Nyerges, D. Kesjár, B. Raucsik, A. Varga, K. Judik, J. Fekete, Z. May, and J. Pálfy. 2016. New multiproxy record of the Jenkyns

Event (also known as the Toarcian Oceanic Anoxic Event) from the Mecsek Mountains (Hungary): Differences, duration and drivers. *Sedimentology* 64.

Muscutt, L. E., G. Dyke, G. D. Weymouth, D. Naish, C. Palmer, and B. Ganapathisubramani. 2017. The four-flipper swimming method of plesiosaurs enabled efficient and effective locomotion. *Proceedings of the Royal Society B* 284: 6–11.

Nakajima, Y., Y. Shigeta, A. Houssaye, Y. D. Zakharov, A. M. Popov, and P. M. Sander. 2022. Early Triassic ichthyopterygian fossils from the Russian Far East. *Scientific Reports* 12: 5546.

Neenan, J. M., N. Klein, and T. M. Scheyer. 2013. European origin of placodont marine reptiles and the evolution of crushing dentition in Placodontia. *Nature Communication* 4: 1621.

Neenan, J. M., C. Li, O. Rieppel, F. Bernardini, C. Tuniz, G. Muscio, and T. M. Scheyer. 2014. Unique method of tooth replacement in durophagous placodont marine reptiles, with new data on the dentition of Chinese taxa. *Journal of Anatomy* 224.

Neenan, J. M., C. Li, O. Rieppel, and T. M. Scheyer. 2015. The cranial anatomy of Chinese placodonts and the phylogeny of Placodontia (Diapsida: Sauropterygia). Zoological Journal of the Linnean Society 175: 415-428.

Neenan, J. M., and T. M. Scheyer. 2014. New specimen of *Psephoderma alpinum* (Sauropterygia, Placodontia) from the Late Triassic of Schesaplana Mountain, Graubünden, Switzerland. *Swiss Journal of Geosciences* 107: 349–357.

Nesbitt, S. J., M. R. Stocker, B. J. Small, and A. Downs. 2009. The osteology and relationships of *Vancleavea campi* (Reptilia: Archosauriformes). Zoological Journal of the Linnean Society 157: 814–864.

Newell, N. D. 1967. Revolutions in the History of Life. P. 0 eds. Uniformity and Simplicity: A Symposium on the Principle of the Uniformity of Nature. Geological Society of America.

Nicholls, E. L., and D. B. Brinkman. 1995. A new ichthyosaur from the Triassic Sulphur Mountain formation of British Columbia. *Switzeland, Gordon and Breach Science Publishers*. 521–535.

Nicholls, E. L., and M. Manabe. 2004. Giant ichthyosaurs of the Triassic-A new species of *Shonisaurus* from the Pardonet Formation (Norian: Late Triassic) of British Columbia. *Journal of Vertebrate Paleontology* 24: 838–849.

Nicholls, E. L., C. Wei, and M. Manabe. 2002. New material of *Qianichthyosaurus* Li, 1999 (Reptilia, Ichthyosauria) from the Late Triassic of Southern China, and implications for the distribution of Triassic ichthyosaurs. *Journal of Vertebrate Paleontology* 22: 759–765.

O'Keefe, F. R. 2001a. A cladistic analysis and taxonomic revision of the Plesiosauria (Reptilia:Sauropterygia). *Acta Zoological Fennica* 213: 1–63.

O'Keefe, F. R. 2001b. Ecomorphology of plesiosaur flipper geometry. *Journal of Evolutionary Biology* 14: 987–991.

O'Keefe, F. R. 2002. The evolution of plesiosaur and pliosaur morphotypes in the Plesiosauria (Reptilia: Sauropterygia). *Palaeobiology* 28: 101–112.

O'Keefe, F. R., and M. T. Carrano. 2005. Correlated trends in the evolution of the plesiosaur locomotor system. *Palaeobiology* 31: 656–675.

O'Keefe, F. R., R. A. Otero, S. Soto-Acuña, J. P. O'gorman, S. J. Godfrey, and S. Chatterjee. 2017. Cranial anatomy of *Morturneria seymourensis* from Antarctica, and the evolution of filter feeding in plesiosaurs of the Austral Late Cretaceous. *Journal of Vertebrate Paleontology* 37: e1347570.

O'Keefe, F. R., H. P. Street, B. C. Wilhelm, C. D. Richards, and H. Zhu. 2011. A new skeleton of the cryptoclidid plesiosaur *Tatenectes laramiensis* reveals a novel body shape among plesiosaurs. *Journal of Vertebrate Paleontology* 31: 330–339.

Oksanen, J., G. Simpson, F. G. Blanchet, R. Kindt, P. Legendre, P. Minchin, R. B. O'Hara, P. Solymos, H. Stevens, E. Szöcs, H. Wagner, M. Barbour, M. Bedward, B. Bolker, D. Borcard, G. Carvalho, M. Chirico, M. De Cáceres, S. Durand, H. B. Evangelist, R. G. FitzJohn, M. Friendly, B. Furneaux, Hannigan

Geoffrey, O. O. Hill, L. Lahti, D. McGlinn, M.-H. Ouellette, E. R. Cunha, T. Smith, A. Stier, C. J. F. Ter Braak, and J. Weedon. 2022. vegan community ecology package version 2.6-2 April 2022.

Orchard, M. J. 2007. Conodont diversity and evolution through the latest Permian and Early Triassic upheavals. *Palaeogeography, Palaeoclimatology, Palaeoecology* 252: 93–117.

Orme, D. 2012. CAPER: Comparative Analyses of Phylogenetics and Evolution in R.

Owen, R. 1861. A monograph of the fossil Reptilia of the Liassic formations. Printed for the *Palæontographical society*, London.

Owen, R. 1865. A monograph of the Fossil Reptilia of the Liassic Formations, part third: *Plesiosaurus*, *Dimorphodon*, and *Ichthyosaurus*. *Monograph of the Palæontographical society* 12–130.

Owen, R. 1840. Report on British fossil reptiles. Part II. *Report of the British Association for the Advancement of Science* 11: 60–204.

Pagel, M. 1999. Inferring the historical patterns of biological evolution. *Nature* 401: 877–884.

Paradis, E., J. Claude, and K. Strimmer. 2004. APE: Analyses of phylogenetics and evolution in R language. *Bioinformatics* 20: 289–290.

Pardo-Pérez, J. M., B. P. Kear, H. Mallison, M. Gómez, M. Moroni, and E. E. Maxwell. 2018. Pathological survey on *Temnodontosaurus* from the Early Jurassic of southern Germany. PLoS ONE 13: e0204951.

Peters, R. H. 1983. The Ecological Implications of Body Size. Cambridge University Press, Cambridge.

Peyer, B. 1944. Die reptilien vom Monte San Giorgio. *Neujahrsblatt herausgegeben von der Naturforschenden Gesellschaft in Zürich* 88: 1–5.

Peyer, B. 1932. Triasfauna der Tessiner Kalkalpen V. *Pachypleurosaurus edwardsii* Corn. Spec. *Abhandlungen der schweizerischen Paläontologischen Gesellschaft*. 1–18.

Pianka, E. R. 1970. On r- and K-Selection. *The American Naturalist* 104: 592–597.

Pinna, G., and J.-M. Mazin. 1993. Stratigraphy and paleo-biogeography of the Placodontia. *Paleontologia Lombarda, New Series* 2: 125–130.

Pollard, J. E. 1968. The gastric contents of an ichthyosaur from the Lower Lias of Lyme Regis, Dorset. *Palaeontology* 11: 376–388.

Puértolas Pascual, E., M. Marx, O. Mateus, A. Saleiro, A. Fernandes, J. Marinheiro, C. Tomás, and S. Mateus. 2021. A new plesiosaur from the Lower Jurassic of Portugal and the early radiation of Plesiosauroidea. *Acta Palaeontologica Polonica* 66.

Purvis, A. 2008. Phylogenetic approaches to the study of extinction. *Annual Review of Ecology, Evolution, and Systematics* 39: 301–319.

Purvis, A., M. CarDillo, R. Grenyer, and B. Collen. 2005. Correlates of extinction risk: phylogeny, biology, threat and scale. Pp. 295–316 eds. Phylogeny and Conservation. Cambridge University Press, Cambridge.

Puttick, M. N., M. J. Benton, J. J. Kriwet, W. Wen, S.-X. S. Hu, G. H. Thomas, and M. J. Benton. 2017. Body length of bony fishes was not a selective factor during the biggest mass extinction of all time. *Palaeontology* 60: 1–15.

Pyenson, N. D., N. P. Kelley, and J. F. Parham. 2014. Marine tetrapod macroevolution: Physical and biological drivers on 250 Ma of invasions and evolution in ocean ecosystems. *Palaeogeography, Palaeoclimatology, Palaeoecology* 400: 1–8.

Qiao, Y., J. Liu, A. S. Wolniewicz, M. Iijima, Y. Shen, T. Wintrich, Q. Li, and P. M. Sander. 2022. A globally distributed durophagous marine reptile clade supports the rapid recovery of pelagic ecosystems after the Permo-Triassic mass extinction. Communication Biology 5: 1242.

R Core Team. 2023. R: a language and environment for statistical computing. R Foundation for Statistical Computing, Vienna.

Rasmussen, A. R., J. C. Murphy, M. Ompi, J. W. Gibbons, and P. Uetz. 2011. Marine Reptiles. *PLoS ONE* 6: e2737.

Raup, D. M., and J. J. Sepkoski. 1982. Mass Extinctions in the Marine Fossil Record. *Science* 215: 1501–1503.

Raup, D. M., and J. J. Sepkoski. 1984. Periodicity of extinctions in the geologic past. *Proceedings of the National Academy of Sciences of the United States of America* 81: 801–805.

Reeves, J. C., B. C. Moon, M. J. Benton, and T. L. Stubbs. 2021. Evolution of ecospace occupancy by Mesozoic marine tetrapods. *Palaeontology* 64: 31–49.

Renesto, S., G. Binelli, and H. Hagdorn. 2014. A new pachypleurosaur from the Middle Triassic Besano Formation of Northern Italy. *Neues Jahrbuch für Geologie und Paläontologie, Abhandlungen* 271: 151–168.

Renesto S, Dal Sasso C, Fogliazza F, and Ragni C. 2020. New findings reveal that the Middle Triassic ichthyosaur *Mixosaurus cornalianus* is the oldest amniote with a dorsal fin. *Acta Palaeontologica Polonica* 65: 511–522.

Renesto, S., and F. M. Dalla Vecchia. 2018. Late Triassic Marine Reptiles. Pp. 263–313 *in* L. H. Tanner, ed. The Late Triassic World: Earth in a Time of Transition.

Renesto, S., and A. Tintori. 1995. Functional morphology and mode of life of the late Triassic placodont *Psephoderma alpinum* Meyer from the Calcare di Zorzino (Lombardy, N Italy). *Rivista Italiana di Paleontologia e Stratigrafia* 101: 37–48.

Reolid, M., E. Mattioli, L. Duarte, and A. Marok. 2020. The Toarcian Oceanic Anoxic Event and the Jenkyns Event (IGCP-655 final report). Episodes 43.

Reolid, M., W. Ruebsam, J. Reolid, and M. Benton. 2024. Impact of early Toarcian climatic changes on marine reptiles: Extinction and recovery. *Earth Science Reviews*

Revell, L. J. 2012. phytools: an R package for phylogenetic comparative biology (and other things). *Methods in Ecology and Evolution* 3: 217–223.

Ridgway, S. H., and R. Harrison. 1999a. The Second Book of Dolphins and the Porpoise. Academic Press, San Diego. Academic Press, Cambridge.

Rieppel, O. 1989. A new pachypleurosaur (Reptilia: Sauropterygia) from the Middle Triassic of Monte San Giorgio, Switzerland. Philosophical *Transactions of the Royal Society of London. B, Biological Sciences* 323: 1–73.

Rieppel, O. 2001a. A new species of Nothosaurus (Reptilia: Sauropterygia) from the Upper Muschelkalk (Lower Ladinian) of southwestern Germany. *Palaeontographica, Abteilung A: Palaozoologie–Stratigraphie* 263: 137–161.

Rieppel, O. 2002. Feeding mechanics in Triassic stem-group sauropterygians: the anatomy of a successful invasion of Mesozoic seas. *Zoological Journal of the Linnean Society* 135: 33–63.

Rieppel, O. 1994. Osteology of *Simosaurus gaillardoti* and the relationships of stem-group Sauropterygia.

Rieppel, O. 1999. Phylogeny and paleobiogeography of Triassic Sauropterygia: problems solved and unresolved. *Palaeogeography, Palaeoclimatology, Palaeoecology* 153: 1–15.

Rieppel, O. 1997. Revision of the Sauropterygian Reptile Genus *Cymatosaurus* v. Fritsch, 1894, and the Relationships of *Germanosaurus* Nopcsa, 1928, from the Middle Triassic of Europe. *Fieldiana Geology, new series* 36: 1–38.

Rieppel, O. 2000. Sauropterygia I: Placodontia, Pachypleurosauria, Nothosauroidea, Pistosauroidea. *F. Pfeil*.

Rieppel, O. 2001b. The cranial anatomy of Placochelys placodonta Jaekel, 1902, and a review of the Cyamodontoidea (Reptilia, Placodonta). *Field Museum of Natural History, Chicago, Ill*.

Rieppel, O. 1998. The status of the sauropterygian reptile genera *Ceresiosaurus*, *Lariosaurus*, and *Silvestrosaurus* from the Middle Triassic of Europe.

Rieppel, O., L. Jinling, and J. Liu. 2003. *Lariosaurus xingyiensis* (Reptilia: Sauropterygia) from the Triassic of China. *Canadian Journal of Earth Sciences* 40: 621–634.

Rieppel, O., C. Li, and N. C. Fraser. 2008. The skeletal anatomy of the triassic protorosaur *Dinocephalosaurus orientalis* Li, from the Middle Triassic of

Guizhou Province, southern China. *Journal of Vertebrate Paleontology* 28: 95–110.

Rieppel, O., and K. Lin. 1995. Pachypleurosaurs (Reptilia: Sauropterygia) from the Lower Muschelkalk, and a review of the Pachypleurosauroidea. *Fieldiana Geology* 32: 1–44.

Rieppel, O., P. Sander, and G. Storrs. 2002. The skull of the Pistosaur *Augustasaurus* from the Middle Triassic of northwestern Nevada. *J Vertebr Paleontol* 22: 577–592.

Rieppel, O., and R. Werneburg. 1998. A new species of the sauropterygian *Cymatosaurus* from the Lower Muschelkalk of Thuringia, Germany. *Palaeontology* 41: 575–589.

Rieppel, O., and R. Wild. 1996. A revision of the genus *Nothosaurus* (Reptilia: Sauropterygia) from the Germanic Triassic, with comments on the status of *Conchiosaurus clavatus*. *Fieldana* (Geology) 34: 1–82.

Rigo, M., X. Jin, L. Godfrey, M. E. Katz, H. Sato, Y. Tomimatsu, M. Zaffani, M. Maron, S. Satolli, G. Concheri, A. Cardinali, Q. Wu, Y. Du, J. Z. X. Lei, C. S. van Wieren, L. S. Tackett, H. Campbell, A. Bertinelli, and T. Onoue. 2024. Unveiling a new oceanic anoxic event at the Norian/Rhaetian boundary (Late Triassic). *Scientific Reports* 14: 15574.

Rigo, M., T. Onoue, L. H. Tanner, S. G. Lucas, L. Godfrey, M. E. Katz, M. Zaffani, K. Grice, J. Cesar, D. Yamashita, M. Maron, L. S. Tackett, H. Campbell, F. Tateo, G. Concheri, C. Agnini, M. Chiari, and A. Bertinelli. 2020. The Late Triassic Extinction at the Norian/Rhaetian boundary: Biotic evidence and geochemical signature. *Earth-Science Reviews* 204: 103180.

Rivera, A. R. V, and R. W. Blob. 2010. Forelimb kinematics and motor patterns of the slider turtle (*Trachemys scripta*) during swimming and walking: shared and novel strategies for meeting locomotor demands of water and land. *Journal of Experimental Biology* 213: 3515–3526.

Roberts, A. J., P. S. Druckenmiller, B. Cordonnier, L. L. Delsett, and J. H. Hurum. 2020. A new plesiosaurian from the Jurassic–Cretaceous transitional interval of

the Slottsmøya Member (Volgian), with insights into the cranial anatomy of cryptoclidids using computed tomography. *PeerJ* 8: e8652.

Roberts, A. J., V. S. Engelschiøn, and J. H. Hurum. 2022. First three-dimensional skull of the Middle Triassic mixosaurid ichthyosaur *Phalarodon fraasi* from Svalbard, Norway. *Acta Palaeontologica Polonica* 67: 51–62.

Röhl, H.-J., A. Schmid-Röhl, H. Furrer, A. Frimmel, W. Oschmann, and L. Schwark. 2001. Microfacies, geochemistry and palaeoecology of the Middle Triassic Grenzbitumenzone from Monte San Giorgio (Canton Ticino, Switzerland). *Geologia Insubrica* 6: 1–13.

Romano, C., M. Koot, I. Kogan, A. Brayard, A. Minikh, W. Brinkmann, H. Bucher, and J. Kriwet. 2016. Permian-Triassic Osteichthyes (bony fishes): Diversity dynamics and body size evolution. *Biological Reviews* 91: 106–147.

Romer, A. S., and L. I. Price. 1940. Review of the Pelycosauria. The *Society*.

Roy, K., G. Hunt, and D. Jablonski. 2009. Phylogenetic Conservatism of Extinctions in Marine Bivalves. *Science* 325: 733–737.

Ruffel, A., M. J. Simms, and P. B. Wignall. 2016. The Carnian Humid Episode of the late Triassic: a review. *Geological Magazine* 153: 271–284.

Ruhl, M., N. R. Bonis, G.-J. Reichart, J. Sinninghe-Damste, and W. Kürschner. 2011. Atmospheric Carbon Injection Linked to End-Triassic Mass Extinction. *Science* 333: 430–434.

Ruhl, M., S. Hesselbo, A. Al Suwaidi, H. Jenkyns, S. Damborenea, M. Manceñido, M. Storm, T. A. Mather, and A. Riccardi. 2020. On the onset of Central Atlantic Magmatic Province (CAMP) volcanism and environmental and carbon-cycle change at the Triassic–Jurassic transition (Neuquén Basin, Argentina). *Earth-Science Reviews* 208: 103229.

Ruta, M., J. Botha-Brink, S. A. Mitchell, and M. J. Benton. 2013. The radiation of cynodonts and the ground plan of mammalian morphological diversity. *Proceedings of the Royal Society B: Biological Sciences* 280: 20131865.

Sachs, S., S. Eggmaier, and D. Madzia. 2024. Exquisite skeletons of a new transitional plesiosaur fill gap in the evolutionary history of plesiosauroids. *Frontiers in Earth Science* 12: 1341470.

Sachs, S., and B. P. Kear. 2018. A rare new Pliensbachian plesiosaurian from the Amaltheenton Formation of Bielefeld in northwestern Germany. Alcheringa: An *Australasian Journal of Palaeontology* 42: 487–500.

Sachs, S., J. Lindgren, D. Madzia, and B. P. Kear. 2021. Cranial osteology of the mid-Cretaceous elasmosaurid *Thalassomedon haningtoni* from the Western Interior Seaway of North America. *Cretaceous Research* 123: 104769.

Sachs, S., D. Madzia, B. Thuy, and B. P. Kear. 2023. The rise of macropredatory pliosaurids near the Early-Middle Jurassic transition. *Scientific Reports* 13: 17558.

Salamon, M. A., R. Niedźwiedzki, P. Gorzelak, R. Lach, and D. Surmik. 2012. Bromalites from the Middle Triassic of Poland and the rise of the Mesozoic Marine Revolution. *Palaeogeography, Palaeoclimatology, Palaeoecology* 321–322: 142–150.

Sallan, L., and A. K. Galimberti. 2015. Body-size reduction in vertebrates following the end-Devonian mass extinction. *Science* 350: 812–815.

Sander, P. 2000. Ichthyosauria: Their diversity, distribution, and phylogeny. *Paläontologische Zeitschrift* 74: 1–35.

Sander, P. M. 1988. A Fossil Reptile Embryo from the Middle Triassic of the Alps. *Science* 239: 780–783.

Sander, P. M. 1992. *Cymbospondylus* (Shastasauridae: Ichthyosauria) from the Middle Triassic of Spitsbergen: filling a paleobiogeographic gap. *Journal of Paleontology* 66: 332–337.

Sander, P. M. 1989a. The large ichthyosaur *Cymbospondylus buchseri*, sp. nov., from the Middle Triassic of Monte San Giorgio (Switzerland), with a survey of the genus in Europe. *Journal of Vertebrate Paleontology* 9: 163-173

Sander, P. M. 1989b. The pachypleurosaurids (Reptilia: Nothosauria) from the Middle Triassic of Monte San Giorgio (Switzerland) with the description of a new species. *Philosophical Transactions of the Royal Society of London. B, Biological Sciences* 325: 561–666.

Sander, P. M., and H. Bucher. 1990. On the presence of *Mixosaurus* (Ichthyopterygia: Reptilia) in the Middle Triassic of Nevada. *Journal of Paleontology* 64: 161–164.

Sander, P. M., X. Chen, L. Cheng, and X. Wang. 2011. Short-snouted toothless ichthyosaur from China suggests Late Triassic diversification of suction feeding ichthyosaurs. *PLoS ONE* 6: e19480.

Sander, P. M., E. M. Griebeler, N. Klein, J. V. Juarbe, T. Wintrich, L. J. Revell, and L. Schmitz. 2021. Early giant reveals faster evolution of large body size in ichthyosaurs than in cetaceans. *Science* 374: eabf5787.

Sander, P. M., N. Klein, P. C. H. Albers, C. Bickelmann, and H. Winkelhorst. 2014. Postcranial morphology of a basal Pistosauroidea (Sauropterygia) from the Lower Muschelkalk of Winterswijk, The Netherlands. *Paläontologische Zeitschrift* 88: 55–71.

Sander, P. M., O. C. Rieppel, and H. Bucher. 1997. A new pistosaurid (Reptilia: Sauropterygia) from the Middle Triassic of Nevada and its implications for the origin of the plesiosaurs. *Journal of Vertebrate Paleontolology* 17: 526–533.

Sander, P. Martin., P. R. Pérez de Villar, H. Furrer, and T. Wintrich. 2022. Giant Late Triassic ichthyosaurs from the Kössen Formation of the Swiss Alps and their paleobiological implications. *.Journal of Vertebrate Paleontolology* e2046017

Sato, T., Y.-N. Cheng, X.-C. Wu, and H.-Y. Shan. 2014a. *Diandongosaurus acutidentatus* Shang, Wu & Li, 2011 (Diapsida: Sauropterygia) and the relationships of Chinese eosauropterygians. *Geological Magazine* 151: 121–133.

Sato, T., and X. Wu. 2008. A new Jurassic pliosaur from Melville Island, Canadian Arctic Archipelago. *Canadian Journal of Earth Sciences* 45: 303–320.

Sato, T., L.-J. Zhao, X.-C. Wu, and C. Li. 2014b. A new specimen of the Triassic pistosauroid *Yunguisaurus*, with implications for the origin of Plesiosauria (Reptilia, Sauropterygia). *Palaeontology* 57: 55–76.

Sauvage, H. E. 1903. L'ichthyosaure du Lias inférieur de Curgy près d'Autun. *Bulletin de la Société d'Histoire naturelle d'Autun* 16: 319–320.

Sauvage, H. E. 1876. Note sur les débris d'ichthyosaure des couches rhétiennes de Saône-et-Loire. *Annales des Sciences Géologiques* 7: 1.

Scheyer, T. M., U. Oberli, N. Klein, and H. Furrer. 2022. A large osteoderm-bearing rib from the Upper Triassic Kössen Formation (Norian/Rhaetian) of eastern Switzerland. *Swiss Journal of Palaeontology* 141: 1.

Scheyer, T. M., C. Romano, J. Jenks, and H. Bucher. 2014. Early Triassic Marine Biotic Recovery: The Predators' Perspective. *PLoS ONE* 9: e88987.

Scheyer, T., J. Neenan, S. Renesto, F. Saller, H. Hagdorn, H. Furrer, O. Rieppel, and A. Tintori. 2012. Revised paleoecology of placodonts - with a comment on "The shallow marine placodont *Cyamodus* of the central European Germanic Basin: Its evolution, paleobiogeography and paleoecology" by C.G. Diedrich (Historical Biology, iFirst article, 2011: 1-19. *Historical Biology* 24: 257–267.

Scheyer, T., A. Neuman, and D. Brinkman. 2019. A large marine eosauropterygian reptile with affinities to nothosauroid diapsids from the Early Triassic of British Columbia, Canada. *Acta Palaeontologica Polonica* 64.

Schmitz, L. 2005. The taxonomic status of *Mixosaurus nordenskioeldii* (Ichthyosauria). *Journal of Vertebrate Paleontology* 25: 983–985.

Schmitz, L., P. M. Sander, G. W. Storrs, and O. Rieppel. 2004. New Mixosauridae (Ichthyosauria) from the Middle Triassic of the Augusta Mountains (Nevada, USA) and their implications for mixosaur taxonomy. *Palaeontographica Abteilung A (Paläozoologie, Stratigraphie)* 270: 133–162.

Schneider, C. A., W. S. Rasband, and K. W. Eliceiri. 2012. NIH Image to ImageJ: 25 years of image analysis. *Nature Methods* 9: 671–675.

Schoepfer, S. D., T. J. Algeo, B. van de Schootbrugge, and J. H. Whiteside. 2022a. The Triassic–Jurassic transition – A review of environmental change at the dawn of modern life. *Earth-Science Reviews* 232: 104099.

Schoepfer, S. D., J. Shen, H. Sano, and T. J. Algeo. 2022b. Onset of environmental disturbances in the Panthalassic Ocean over one million years prior to the Triassic-Jurassic boundary mass extinction. *Earth-Science Reviews* 224: 103870.

Schwermann, L., and P. M. Sander. 2011. Osteologie und Phylogenie von *Westphaliasaurus simonsensii*: Ein neuer Plesiosauride (Sauropterygia) aus dem Unteren Jura (Pliensbachium) von Sommersell (Kreis Höxter), Nordrhein-Westfalen, Deutschland. *Geologie und Paläontologie in Westfalen* 79: 5–56.

Sciau, J., J.-Y. Y. Crochet, and J. Mattei. 1990. Le premier squelette de plésiosaure de France sur le Causse du Larzac (Toarcien, Jurassique inférieur). *Geobios* 23: 111–116.

Sennikov, A. G., and M. S. Arkhangelsky. 2010. On a typical Jurassic sauropterygian from the Upper Triassic of Wilczek Land (Franz Josef Land, arctic Russia). *Paleontological Journal* 44: 567–572.

Sepkoski, J. J. 1984. A Kinetic Model of Phanerozoic Taxonomic Diversity. III. Post-Paleozoic Families and Mass Extinctions. *Paleobiology* 10: 246–267.

Sepkoski, J. J. 1996. Patterns of Phanerozoic extinction: a perspective from global data bases. Springer 31–35.

Shang, Q., and C. Li. 2015. A new small-sized eosauropterygian (Diapsida: Sauropterygia) from the Middle Triassic of Luoping, Yunnan, southwestern China. *Vertebrata PalAsiatica* 53: 265–280.

Shang, Q., C. Li, X.-C. Wu. 2017a. New information on *Dianmeisaurus gracilis* Shang & Li, 2015. *Vertebrata PalAsiatica* 55: 145–161.

Shang, Q.-H., and C. Li. 2009. On the occurence of the ichthyosaur *Shastasaurus* in the Guanling biota (Late Triassic), Guizhou, China. *Vertebrata PalAsiatica* 47: 178–193.

Shang, Q.-H., C. Li, and W. Wang. 2022. *Nothosaurus luopingensis* n. sp. (Sauropterygia) from the Anisian, Middle Triassic of Luoping, Yunnan Province, China. *Vertebrata PalAsiatica*

Shang, Q.-H., T. Sato, C. Li, and X.-C. Wu. 2017b. New osteological information from a 'juvenile' specimen of *Yunguisaurus* (Sauropterygia; Pistosauroidea). *Palaeoworld* 26: 500–509.

Shang, Q.-H., X.-C. Wu, and C. Li. 2020. A New Ladinian Nothosauroid (Sauropterygia) from Fuyuan, Yunnan Province, China. *Journal of Vertebrate Paleontology* 40: e1789651.

Signor III, P. W., and J. H. Lipps. 1982. Sampling bias, gradual extinction patterns and catastrophes in the fossil record. *Geological Society of America*.

Simões, T. R., O. Vernygora, M. W. Caldwell, and S. E. Pierce. 2020. Megaevolutionary dynamics and the timing of evolutionary innovation in reptiles. *Nature Communications* 11: 3322.

Smith, A. G., D. G. Smith, and B. M. Funnell. 1994. Systematics and the Fossil Record. Documenting Evolutionary Patterns. Blackwell Scientific Publications, London.

Smith, A. S. 2007. Anatomy and Systematics of the Rhomaleosauridae (Sauropterygia: Plesiosauria).

Smith, A. S., and R. Araújo. 2017. *Thaumatodracon wiedenrothi*, a morphometrically and stratigraphically intermediate new rhomaleosaurid plesiosaurian from the Lower Jurassic (Sinemurian) of Lyme Regis. *Palaeontographica Abteilung A* 308: 89–125.

Smith, A. S., and R. B. J. Benson. 2014. Osteology of *Rhomaleosaurus Thorntoni* (Sauropterygia: Rhomaleosauridae) from the Lower Jurassic (Toarcian) of Northamptonshire, England. *Monographs of the Palaeontographical Society* 168: 1–40.

Smith, A. S., and G. J. Dyke. 2008. The skull of the giant predatory pliosaur *Rhomaleosaurus cramptoni*: implications for plesiosaur phylogenetics. *Naturwissenschaften* 95: 975–980.

Smith, A. S., and P. Vincent. 2010. A new genus of pliosaur (Reptilia: Sauropterygia) from the Lower Jurassic of Holzmaden, Germany. *Palaeontology* 53: 1049–1063.

Smith, M. R. 2019. Bayesian and parsimony approaches reconstruct informative trees from simulated morphological datasets. *Biology Letters* 15: 20180632.

Song, H., P. B. Wignall, D. Chu, J. Tong, Y. Sun, H. Song, W. He, and L. Tian. 2014. Anoxia/high temperature double whammy during the Permian-Triassic marine crisis and its aftermath. *Scientific Reports* 4: 4132.

Song, H., P. B. Wignall, and A. M. Dunhill. 2018. Decoupled taxonomic and ecological recoveries from the Permo-Triassic extinction. *Science Advances* 4: eaat5091.

Song, H., P. B. Wignall, J. Tong, and H. Yin. 2013. Two pulses of extinction during the Permian–Triassic crisis. *Nature Geoscience* 6: 52–56.

Song, H., P. Wignall, Zh.-Q. Chen, J. Tong, D. Bond, X. Lai, X. Zhao, H. Jiang, C. Yan, Z. Niu, H. Yang, and Y. Wang. 2011. Recovery tempo and pattern of marine ecosystems after the end-Permian mass extinction. *Geology* 39: 739–742.

Soul, L. C., and R. B. J. Benson. **2017.** Developmental mechanisms of macroevolutionary change in the tetrapod axis: A case study of Sauropterygia. *Evolution* 71: 1164–1177.

Soul, L. C., and M. Friedman. 2017. Bias in phylogenetic measurements of extinction and a case study of end-Permian tetrapods. *Palaeontology* 60: 169–185.

Spiekman, S. N. F., M. D. Ezcurra, A. Rytel, W. Wang, E. Mujal, M. Buchwitz, and R. R. Schoch. 2024. A redescription of *Trachelosaurus fischeri* from the Buntsandstein (Middle Triassic) of Bernburg, Germany: the first European *Dinocephalosaurus*-like marine reptile and its systematic implications for long-necked early archosauromorphs. *Swiss Journal of Palaeontology* 143: 10.

Spiekman, S. N. F., J. M. Neenan, N. C. Fraser, V. Fernandez, O. Rieppel, S. Nosotti, and T. M. Scheyer. 2020. Aquatic Habits and Niche Partitioning in the

Extraordinarily Long-Necked Triassic Reptile *Tanystropheus*. *Current Biology* 30: 3889-3895.e2.

Spiekman, S. N. F., W. Wang, L. Zhao, O. Rieppel, N. C. Fraser, and C. Li. 2023. *Dinocephalosaurus orientalis* Li, 2003: a remarkable marine archosauromorph from the Middle Triassic of southwestern China. *Earth and Environmental Science Transactions of the Royal Society of Edinburgh* 114: 218–250.

Srdic, A., S. Beardmore, and D. R. Lomax. 2019. A rediscovered Lower Jurassic ichthyosaur skeleton possibly from the Strawberry Bank Lagerstätte, Somerset, UK. *Historical Biology* 33: 814–822.

Stanley, S. M. 2009. Evidence from ammonoids and conodonts for multiple Early Triassic mass extinctions. *Proceedings of the National Academy of Sciences* 106: 15264–15267.

Stayton, C. T. 2006. Testing hypotheses of convergence with multivariate data: Morphological and functional convergence among herbivorous lizards. *Evolution* 60: 824–841.

Stayton, C. T. 2015. The definition, recognition, and interpretation of convergent evolution, and two new measures for quantifying and assessing the significance of convergence. *Evolution* 69: 2140–2153.

Stockar, R. 2010. Facies, depositional environment, and palaeoecology of the Middle Triassic Cassina beds (Meride Limestone, Monte San Giorgio, Switzerland). *Swiss Journal of Geosciences* 103: 101–119.

Storrs, G. W. 1991. Anatomy and Relationships of *Corosaurus alcovensis* (Diapsida: Sauropterygia) and the Triassic Alcova Limestone of Wyoming. *Yale University Peabody Museum of Natural History Bulletin* 44: 1–150.

Storrs, G. W. 1994. Fossil vertebrate faunas of the British Rhaetian (latest Triassic). *Zoological Journal of the Linnean Society* 112: 217–259.

Storrs, G. W. 1993. Function and phylogeny in sauropterygian (Diapsida) evolution. *American Journal of Science* 293: 63–90.

Storrs, G. W., and M. A. Taylor. 1996. Cranial anatomy of a new plesiosaur genus from the lowermost Lias (Rhaetian/Hettangian) of Street, Somerset, England. *Journal of Vertebrate Paleontology* 16: 403–420.

Street, H., A. LeBlanc, and M. Caldwell. 2021. A histological investigation of dental crown characters used in mosasaur phylogenetic analyses. *Vertebrate Anatomy Morphology Palaeontology* 9: 83–94.

Stubbs, T. L., and M. J. Benton. 2016. Ecomorphological diversifications of Mesozoic marine reptiles: the roles of ecological opportunity and extinction. *Paleobiology* 42: 547–573.

Sues, H.-D. 1987. Postcranial skeleton of *Pistosaurus* and interrelationships of the Sauropterygia (Diapsida). *Zoological Journal of the Linnean Society* 90: 109–131.

Sues, H.-D., and R. L. Carroll. 1985. The pachypleurosaurid *Dactylosaurus schroederi* (Diapsida: Sauropterygia). *Canadian Journal of Earth Sciences* 22: 1602–1608.

Sulej, T., and G. Niedźwiedzki. 2019. An elephant-sized Late Triassic synapsid with erect limbs. *Science* 363: 78–80.

Suzuki, R., Y. Terada, and H. Shimodaira. 2019. pvclust: Hierarchical Clustering with P-Values via Multiscale Bootstrap Resampling.

Swaby, E. J., and D. R. Lomax. 2020. A revision of *Temnodontosaurus crassimanus* (Reptilia: Ichthyosauria) from the Lower Jurassic (Toarcian) of Whitby, Yorkshire, UK. *Historical Biology* 33: 2715–2731.

Symonds, M., and S. Blomberg. 2014. A Primer on Phylogenetic Generalised Least Squares. Pp. 105–130

Takahashi, Y., Y. Nakajima, and T. Sato. 2014. An Early Triassic Ichthyopterygian Fossil from the Osawa Formation in Minamisanriku Town, Miyagi Prefecture, Japan. *Paleontological Research* 18: 258–262.

Tanner, L. H., S. G. Lucas, and M. G. Chapman. 2004. Assessing the record and causes of Late Triassic extinctions. *Earth Science Reviews* 65: 103–139.

Taylor, M. A. 1987. How tetrapods feed in the water: a funtional analysis by paradigm. *Zoological Journal of the Linnean Society* 91: 171–195.

Taylor, M. A., and A. R. I. Cruickshank. 1993. A plesiosaur from the Linksfield erratic (Rhaetian, Upper Triassic) near Elgin, Morayshire. *Scottish Journal of Geology* 29: 191–196.

Thorne, P. M., M. Ruta, and M. J. Benton. 2011. Resetting the evolution of marine reptiles at the Triassic-Jurassic boundary. *PNAS* 108: 8339–8344.

Tintori, A., and S. Renesto. 1990. A new Lariosaurus from the Kalkschieferzone (Uppermost Ladinian) of Valceresio (Varese, N. Italy). *Bollettino Della Società Paleontologica Italiana* 29: 309–319.

Tomiya, S. 2013. Body Size and Extinction Risk in Terrestrial Mammals Above the Species Level. *The American Naturalist* 182: E196–E214.

Torrens, H. 1995. Mary Anning (1799–1847) of Lyme; 'the greatest fossilist the world ever knew.' *The British Journal for the History of Science* 28: 257–284.

Tschanz, K. 1989. *Lariosaurus buzzii* n. sp. from the Middle Triassic of Monte San Giorgio (Switzerland), with comments on the classification of nothosaurs. *Palaeontographica A* 208: 153–179.

Vermeij, G. J. 1977. The Mesozoic Marine Revolution: Evidence from Snails, Predators and Grazers. *Paleobiology* 3: 245–258.

Vermeij, G. J., and R. Dudley. 2000. Why are there so few evolutionary transitions between aquatic and terrestrial ecosystems? *Biological Journal of the Linnean Society* 70: 541–554.

Vermeij, G. J., and R. Motani. 2018. Land to sea transitions in vertebrates: the dynamics of colonization. *Paleobiology* 44: 237–250.

Vincent, P. 2011. A re-examination of *Hauffiosaurus zanoni*, a pliosauroid from the Toarcian (Early Jurassic) of Germany. *Journal of Vertebrate Paleontology* 31: 340–351.

Vincent, P. 2008. Les Plesiosauria (Reptilia, Sauropterygia) du Jurassique inférieur : systématique, anatomie, phylogénie et paléoécologie. Paris.

Vincent, P., N. Bardet, and E. Mattioli. 2013a. A new pliosaurid from the Pliensbachian (Early Jurassic) of Normandy (Northern France). *Acta Palaeontologica Polonica* 58: 471–485.

Vincent, P., and R. B. J. Benson. 2012. *Anningasaura*, a basal plesiosaurian (Reptilia, Plesiosauria) from the Lower Jurassic of Lyme Regis, United Kingdom. *Journal of Vertebrate Paleontology* 32: 1049–1063.

Vincent, P., J. E. Martin, V. Fischer, G. Suan, B. Khalloufi, B. Sucheras-Marx, A. Lena, K. Janneau, B. Rousselle, L. Rulleau, B. Suchéras-Marx, A. Léna, K. Janneau, B. Rousselle, and L. Rulleau. 2013b. A marine vertebrate fauna from the Toarcian-Aalenian succession of southern Beaujolais, Rhône, France. *Geological Magazine*150: 822–834.

Vincent, P., R. Weiss, G. Kronz, and D. Delsate. 2017. *Microcleidus melusinae*, a new plesiosaurian (Reptilia, Plesiosauria) from the Toarcian of Luxembourg. *Geological Magazine* 156: 99–116.

Voeten, D. F. A. E., T. Reich, R. Araújo, and T. M. Scheyer. 2018. Synchrotron microtomography of a *Nothosaurus marchicus* skull informs on nothosaurian physiology and neurosensory adaptations in early Sauropterygia. *PLoS ONE* 13: e0188509.

von Huene, F. 1922. Die Ichthyosaurier des Lias und ihre Zusammenhänge. *Verlag von Gebrüder Borntraeger*, Berlin.

Wang, W., C. Li, T. M. Scheyer, and L. Zhao. 2019. A new species of *Cyamodus* (Placodontia, Sauropterygia) from the early Late Triassic of south-west China. *Journal of Systematic Palaeontology* 17: 1237–1256.

Wang, W., Q. Shang, L. Cheng, X.-C. Wu, and C. Li. 2022. Ancestral body plan and adaptive radiation of sauropterygian marine reptiles. *iScience* 25: 105635.

Wang, W., S. N. F. Spiekman, L. Zhao, O. Rieppel, T. M. Scheyer, N. C. Fraser, and C. Li. 2023. A new long-necked archosauromorph from the Guanling Formation (Anisian, Middle Triassic) of southwestern China and its implications for neck evolution in tanystropheids. *The Anatomical Record* 1–15

White, T. E. 1940. Holotype of *Plesiosaurus longirostris* Blake and classification of the plesiosaurs. *Journal of Paleontology* 14: 451–467.

Whiteside, J. H., P. E. Olsen, T. Eglinton, M. E. Brookfield, and R. N. Sambrotto. 2010. Compound-specific carbon isotopes from Earth's largest flood basalt eruptions directly linked to the end-Triassic mass extinction. *Proceedings of the National Academy of Sciences* 107: 6721–6725.

Wignall, P. B. 2001. Large igneous provinces and mass extinctions *Earth-Science Reviews* 53: 1–33.

Wilhelm, B. C., and F. Robin. O'Keefe. 2010. A new partial skeleton of a cryptocleidoid plesiosaur from the Upper Jurassic Sundance Formation of Wyoming. *Journal of Vertebrate Paleontology* 30: 1736–1742.

Wintrich, T., S. Hayashi, A. Houssaye, Y. Nakajima, and P. M. Sander. 2017. A Triassic plesiosaurian skeleton and bone histology inform on evolution of a unique body plan. Science Advances 3: e1701144.

Wolniewicz, A. S., Y. Shen, Q. Li, Y. Sun, Y. Qiao, Y. Chen, Y.-W. Hu, and J. Liu. 2023. An armoured marine reptile from the Early Triassic of South China and its phylogenetic and evolutionary implications. *Elife* 12: e83163

Woolley, C. H., D. J. Bottjer, F. A. Corsetti, and N. D. Smith. 2024. Quantifying the effects of exceptional fossil preservation on the global availability of phylogenetic data in deep time. *PLoS ONE* 19: e0297637.

Wu, F., Y. Sun, and G. Fang. 2018. A new species of *Saurichthys* from the Middle Triassic (Anisian) of southwestern China. Vertebrata *PalAsiatica* 56: 273–294.

Wu, F., Y. Sun, W. Hao, D. Jiang, G. Xu, Z. Sun, and A. Tintori. 2009. New species of *Saurichthys* (Actinopterygii: Saurichthyidae) from Middle Triassic (Anisian) of Yunnan Province, China. *Acta Geologica Sinica* 83: 440–450.

Wu, X.-C., Y.-N. Cheng, C. Li, L.-J. Zhao, and T. Sato. 2011. New information on *Wumengosaurus delicatomandibularis* Jiang et al., 2008 (Diapsida: Sauropterygia), with a revision of the osteology and phylogeny of the taxon. *Journal of Vertebrate Paleontology* 31: 70–83.

Xiaofeng, W., G. H. Bachmann, H. Hagdorn, P. Sander, G. Cuny, C. Xiaohong, W. Chuanshang, C. Lide, L. Cheng, M. Fansong, and X. U. Guanghong. 2008. The Late Triassic Black Shales of the Guanling Area, Guizhou Province, South-West China: a unique marine Reptile and pelagic Crinoid fossil Lagerstätte. *Palaeontology* 51: 27-61.

Xiaofeng, W., G. H. Bachmann, H. Hagdorn, P. M. Sander, G. Cuny, C. Xiaohong, W. Chuanshang, C. Lide, C. Long, M. Fansong, and X. Guanghong. 2006. The Late Triassic black shales of the Guanling area, Guizhou Province, South-West China: a unique marine reptile and pelagic crinoid lagerstätte. *Palaeontology* 51: 27–61.

Xu, G.-H., Y. Ren, L.-J. Zhao, J.-L. Liao, and D.-H. Feng. 2022. A long-tailed marine reptile from China provides new insights into the Middle Triassic pachypleurosaur radiation. *Scientific Reports* 12: 7396.

Xu, G.-H., Q.-H. Shang, W. Wang, Y. Ren, H. Lei, J. Liao, L. Zhao, and C. Li. 2023. A new long-snouted marine reptile from the Middle Triassic of China illuminates pachypleurosauroid evolution. *Scientific Reports* 13: 16.

Yang, P., C. Ji, D.-Y. Jiang, R. Motani, A. Tintori, Y.-L. Sun, and Z.-Y. Sun. 2013. A new species of *Qianichthyosaurus* (Reptilia: Ichthyosauria) from Xingyi Fauna (Ladinian, Middle Triassic) of Guizhou. *Acta Scientiarum Naturalium Universitatis Pekinensis* 49: 1002–1008.

Yin, G., X.-G. Zhou, Z. T. Cao, Y.-Y. Yu, and Y.-M. Luo. 2000. A preliminary study on the Early Late Triassic marine reptiles from Guanling, Guizhou, China. *Geology, Geochemistry* 28: 1–23.

Young, M. T., L. Steel, S. L. Brusatte, D. Foffa, and Y. Lepage. 2014. Tooth serration morphologies in the genus *Machimosaurus* (Crocodylomorpha, Thalattosuchia) from the Late Jurassic of Europe. *Royal Society Open Science* 1:140269.

Zapfe, H. 1976. Ein großer Ichthyosaurier aus den Kössener Schichten der Nordalpen. *Annalen des Naturhistorischen Museums in Wien* 80: 239–250.

Zeffer, A., L. C. Johansson, and Å. Marmebro. 2003. Functional correlation between habitat use and leg morphology in birds (Aves). *Biological Journal of the Linnean Society* 79: 461–484.

Zhang, K., R. Liu, Z. Liu, and L. Li. 2021. Geochemical characteristics and geological significance of humid climate events in the Middle-Late Triassic (Ladinian-Carnian) of the Ordos Basin, central China. *Marine and Petroleum Geology* 131: 105179.

Zhang, Q., W. Wen, S. Hu, M. J. Benton, C. Zhou, T. Xie, T. Lü, J. Huang, B. Choo, Z.-Q. Chen, J. Liu, and Q. Zhang. 2014. Nothosaur foraging tracks from the Middle Triassic of southwestern China. *Nature communications* 5: 1–12.

Zverkov, N. G., and V. M. Efimov. 2019. Revision of *Undorosaurus*, a mysterious Late Jurassic ichthyosaur of the Boreal Realm. *Journal of Systematic Palaeontology* 17: 1183–1213.

Zverkov, N. G., V. Fischer, D. Madzia, and R. B. J. Benson. 2018. Increased Pliosaurid Dental Disparity Across the Jurassic – Cretaceous Transition. *Palaeontology* 61: 825-846.

Zverkov, N. G., D. V Grigoriev, A. S. Wolniewicz, A. G. Konstantinov, and E. S. Sobolev. 2022. Ichthyosaurs from the Upper Triassic (Carnian–Norian) of the New Siberian Islands, Russian Arctic, and their implications for the evolution of the ichthyosaurian basicranium and vertebral column. *Earth and Environmental Science Transactions of the Royal Society of Edinburgh* 113: 51–74.

Zverkov, N., and M. Jacobs. 2021. Revision of *Nannopterygius* (Ichthyosauria: Ophthalmosauridae): reappraisal of the “inaccessible” holotype resolves a taxonomic tangle and reveals an obscure ophthalmosaurid lineage with a wide distribution. *Zoological Journal of the Linnean Society* 191: 228–275.

Zverkov, N., and E. Pervushov. 2020. A gigantic pliosaurid from the Cenomanian (Upper Cretaceous) of the Volga Region, Russia. Cretaceous Research 110.

APPENDIX

Appendix I

Laboury, A., R. F. Bennion, B. Thuy, R. Weis, and V. Fischer. 2022. Anatomy and phylogenetic relationships of *Temnodontosaurus zetlandicus* (Reptilia: Ichthyosauria). *Zoological Journal of the Linnean Society* 195:172–194.

Zoological Journal of the Linnean Society, 2022, **XX**, 1–23. With 12 figures.

Anatomy and phylogenetic relationships of *Temnodontosaurus zetlandicus* (Reptilia: Ichthyosauria)

ANTOINE LABOURY[1,*], REBECCA F. BENNION[1,2], BEN THUY[3], ROBERT WEIS[3] and VALENTIN FISCHER[1]

[1]*Evolution & Diversity Dynamics Lab, University of Liège, 14 Allée du 6 Août, Liège 4000, Belgium*
[2]*Palaeontology Department, Royal Belgian Institute of Natural Sciences, 29, Rue Vautier, 1000 Brussels, Belgium*
[3]*Palaeontology Departement, Natural History Museum Luxembourg, 25 Rue Münster, L-2160 Luxembourg, Grand-Duchy of Luxembourg*

Received 25 October 2021; revised 30 November 2021; accepted for publication 4 December 2021

Parvipelvia is a major clade of ichthyosaurians that diversified during the Triassic-Jurassic transition. The interrelationships of early parvipelvians remain unclear and many genera are loosely diagnosed, such as *Temnodontosaurus*, an ecologically important genus from the Early Jurassic of Western Europe. One taxon concentrates many taxonomic issues: '*Ichthyosaurus*' *acutirostris* was previously assigned to *Temnodontosaurus* and for which '*Ichthyosaurus*' *zetlandicus* represents a junior synonym. We redescribe the holotype of '*Ichthyosaurus*' *zetlandicus* (CAMSM J35176) and a new specimen probably attributable to this taxon (MNHNL TU885) from the Toarcian of Luxembourg. We find that ***Temnodontosaurus zetlandicus* comb. nov.** is a valid species that should be referred to the genus *Temnodontosaurus*, sharing a number of traits with *Temnodontosaurus nuertingensis* and *Temnodontosaurus trigonodon*, despite having a distinct cranial architecture. Our phylogenetic analyses under both implied weighting maximum parsimony and Bayesian inference recover *T. zetlandicus* as closely related to several species currently assigned to *Temnodontosaurus*. Species included in *Temnodontosaurus* form a polyphyletic yet well-clustered group among basal neoichthyosaurians, demonstrating that the monophyly of this genus needs to be thoroughly investigated.

ADDITIONAL KEYWORDS: *Ichthyosaurus acutirostris* – Lower Jurassic – Luxembourg – Parvipelvia – phylogeny – taxonomy – Toarcian – Whitby – United-Kingdom.

INTRODUCTION

Ichthyosauria is a species-rich clade of marine reptiles that populated ancient oceans from the Early Triassic (Olenekian; e.g. Motani *et al.*, 2017) to the beginning of the Late Cretaceous (Cenomanian-Turonian boundary; Bardet, 1992; Fischer *et al.*, 2016). A single clade of ichthyosaurians, Parvipelvia, is thought to have survived the end-Triassic extinctions (McGowan, 1997; Motani, 2005; Thorne *et al.*, 2011; Fischer *et al.*, 2014; but see Martin *et al.*, 2015) and evolved into a disparate assemblage of forms, filling many roles in the marine ecosystems of the Early Jurassic (Böttcher, 1989; Godefroit, 1994; McGowan, 1996a; Massare, 1997; Martin *et al.*, 2012; Dick & Maxwell, 2015). However, the internal phylogenetic relationships of early parvipelvians appear poorly constrained (Moon, 2017).

Among early parvipelvians, *Temnodontosaurus* Lydekker, 1889 appears to be one of the most problematic genera, being polyphyletic (Moon, 2017) and in dire need of revision, as advocated by multiple authors in the past (McGowan, 1996a; Sander, 2000; Maisch, 2010; Swaby & Lomax, 2020). The current definition of *Temnodontosaurus* stems from phenetic analyses of skull and postcranial shapes in the 1970s (McGowan, 1974). Because skull shape in marine tetrapods is now known to be heavily influenced by ecomorphological convergence (e.g. Kelley & Pyenson, 2015; Fischer, 2016; Fischer

*Corresponding author. E-mail: A.Laboury@uliege.be
[Version of record, published online 18 February 2022; http://zoobank.org/urn:lsid:zoobank.org:pub:DACBA4A5-8D5F-479B-AFA5-E38B380F8962]

et al., 2017, 2020; McCurry *et al.*, 2017), these ratios are likely suboptimal to establish a stable taxonomy. Switching the taxonomy of Early Jurassic ichthyosaurians to apomorphy-based definitions is desirable and ongoing (Maisch & Matzke, 2000; Maisch, 2008, 2010; Martin *et al.*, 2012; Lomax, 2016; Maxwell & Cortés, 2020; Swaby & Lomax, 2020), but still far from complete. Several Early Jurassic ichthyosaurs have been included in *Temnodontosaurus* over the years (McGowan, 1974, 1996a, b; Godefroit, 1994; McGowan & Motani, 2003), but the monophyly of this genus has rarely been questioned (but see Maisch, 2010; Moon, 2017). The current taxonomic instability of *Temnodontosaurus* is notably illustrated by the species '*Ichthyosaurus*' *acutirostris* (Owen, 1840), whose systematic placement remains controversial due to a poorly described holotype (Maisch, 2010). This species has been assigned to *Leptonectes* McGowan, 1996, *Stenopterygius* Jaekel, 1904 and *Temnodontosaurus* in the past (McGowan, 1974; Maisch & Matzke, 2000; McGowan & Motani, 2003; Maisch, 2010) and according to Maisch (2010) it could represent a genus of its own. This is why '*I.*' *acutirostris* needs taxonomic revision. Furthermore, this species currently incorporates '*Ichthyosaurus*' *zetlandicus* (Seeley, 1880), even though the differences in cranial architecture between '*I.*' *zetlandicus* and '*I.*' *acutirostris* appear clear (compare Seeley, 1880; McGowan, 1974; Chapman & Doyle, 2002).

We provide a complete osteological redescription of the holotype of '*Ichthyosaurus*' *zetlandicus* and we report a new specimen probably attributable to this taxon from the Schistes Carton Formation of Luxembourg. This redescription and the assessment of its phylogenetic placement among Early Jurassic parvipelvians clarifies its systematic position and provides a much-needed step into re-evaluating the systematics of *Temnodontosaurus*.

Institutional abbreviations

CAMSM, Sedgwick Museum of Earth Sciences, Cambridge University, Cambridge, UK; MNHNL, Musée national d'Histoire naturelle de Luxembourg, Luxembourg; NHMUK, Natural History Museum, London, UK; PB, Petrefaktensammlung Banz, Germany; SMNS, Staatliches Museum für Naturkunde, Stuttgart, Germany.

MATERIAL AND METHODS

Spatiotemporal setting of the holotype of '*Ichthyosaurus*' *zetlandicus*

The holotype of '*Ichthyosaurus*' *zetlandicus*, CAMSM J35176, was discovered along the Whitby coastal section in North Yorkshire (UK) (Seeley, 1880; Supporting Information, Fig. S1) and presented to the Sedgwick Museum by the Earl of Zetland, who owned Loftus Alum Quarry (Benton & Taylor, 1984; Benton & Spencer, 1995). The outcrops in this area belong to the Whitby Mudstone Formation (WMF), which are laminated grey to dark grey mudstones (Powell, 2010). CAMSM J35176 is believed to have been found in the Main Alum Shales, a subdivision of the Alum Shale Member where many fossils of marine reptiles have been discovered (Benton & Taylor, 1984). These shales consist of a sequence of poorly laminated dark grey mudstones interbedded by bands of siderite and calcareous concretions and in the upper part by bands of phosphatic nodules (Powell, 2010; Swaby & Lomax, 2020). Biostratigraphically, it belongs to the Bifrons Zone, Middle Toarcian (Hodges *et al.*, 2004).

Spatiotemporal setting of MNHNL TU885

The specimen MNHNL TU885 was found at Schouweiler near Bascharage and Sanem, Grand Duchy of Luxembourg (Fig. 1B), a region well known for its marine reptile fossil richness (Streitz, 1983; Godefroit, 1994; Vincent *et al.*, 2017; Johnson *et al.*, 2019; Fischer *et al.*, 2021). Sediments of this region are Early Toarcian in age and belong to the Schistes Carton unit (Fig. 1A), roughly contemporaneous with the Posidonienschiefer (Germany) and the Whitby Mudstone Formation (England). The black shales that composed these outcrops contain nodular limestone in which many fossils are found preserved three-dimensionally and articulated (Hermoso *et al.*, 2014; Vincent *et al.*, 2017; Johnson *et al.*, 2019). Specimen MNHNL TU885 is likely to have come from one of these nodules (Fig. 1A). Biostratigraphically, the black shales of the Grand Duchy of Luxembourg can be assigned to the Serpentinum Zone, itself subdivided into two subzones: the Elegantum and Falciferum Subzones (Fig. 1A; Hermoso *et al.*, 2014; Vincent *et al.*, 2017; Johnson *et al.*, 2019).

Phylogenetic analyses

To assess the phylogenetic position of '*Ichthyosaurus*' *zetlandicus* among early parvipelvians, we scored this taxon based on personal observations on the holotype specimen (CAMSM J35176) in the cladistic data set of Maxwell & Cortés (2020). This cladistic data set derives from the matrix of Maxwell *et al.* (2019), which is itself a modified version of the matrix of Moon (2017). We merged scoring the two Operational Taxonomic Units (OTUs) *Hauffiopteryx typicus* (von Huene, 1931) 'UK' and *Hauffiopteryx typicus* 'German' to obtain a single OTU for this species. We revised the scoring of *Besanosaurus leptorhynchus* Dal Sasso & Pinna, 1996 based on new information provided by Bindellini *et al.* (2021) and we removed *Mikadocephalus gracilirostris*

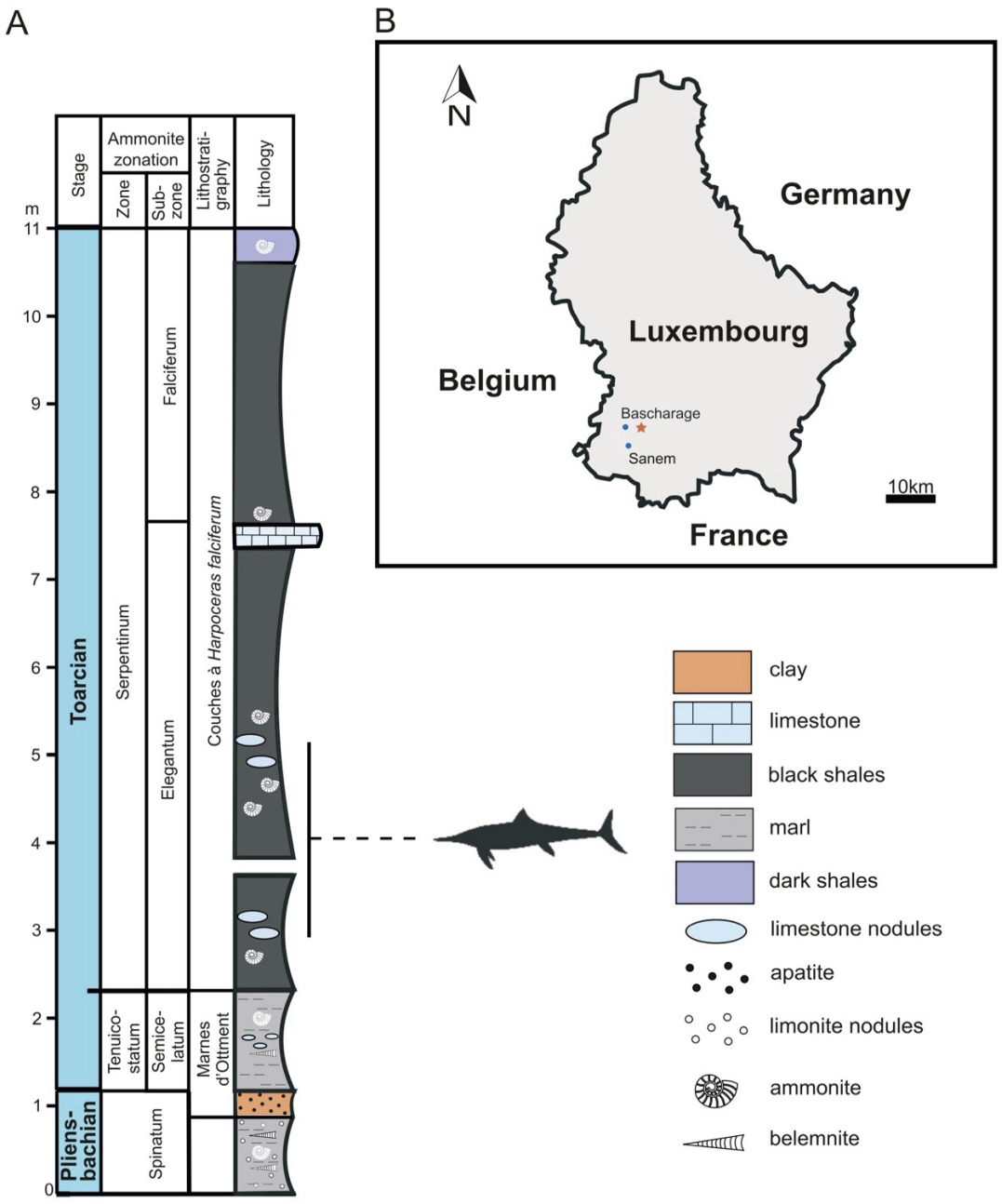

Figure 1. A, schematic log containing the lithology of the Lower Jurassic section of the Grand-Duchy of Luxembourg and the stratigraphic position of MNHNL TU885. B, map of the Grand-Duchy of Luxembourg. The star indicates the discovery site of MNHNL TU885.

Maisch & Matzke, 1997 because it has been demonstrated to be a synonym of *B. leptorhynchus* (Bindellini *et al.*, 2021). We also revised the scoring of all current species referred to as *Temnodontosaurus*, based on first-hand observations, high-precision 3D models (see below) and the literature (see Supporting Information Text S1). The final matrix is available in the Supporting Information (File S1). We have

realized 3D models of the holotype of '*I.*' *zetlandicus* CAMSM J35176, the Luxembourg specimen MNHNL TU885; and two specimens of *T. trigonodon* (Theodori, 1843) (SMNS 17650 and SMNS 50000). These 3D models are available on MorphoSource: https://www.morphosource.org/projects/000351961. We have also used the 3D models of *T. trigonodon* (SMNS 15950) and *T. nuertingensis* (von Huene, 1931) (SMNS 13488) published by Pardo-Pérez *et al.* (2018).

Phylogenetic analyses were carried out within a maximum parsimony and a Bayesian framework. Maximum parsimony analyses were carried out in TNT v.1.5 (Goloboff *et al.*, 2008; Goloboff & Catalano, 2016). In order to minimize the impact of homoplasy, we used the implied weighting method, which reduces the weight of each character proportionally to its homoplasy. We used different values of the concavity constant k (k = 6, k = 9 and k = 12); increasing the K value reduces the penalty applied to homoplastic characters. In a maximum parsimony framework, implied weighting appears to be the method of choice, providing accurate results (Goloboff *et al.*, 2018; Smith, 2019). In TNT, we raised the maximum number of trees to 100 000 and used the New Technology Search (ratchet activated: 200 ratchet iterations; drift activated: ten cycles; five hits; ten trees per replication), to identify islands of most parsimonious trees. We applied the tree bisection-reconnection (TBR) algorithm on the trees recovered by the ratchet analysis to fully explore these islands. In order to identify wildcard taxa, which may cause instability in our most parsimonious trees (MPTs), we used IterPCR (Pol & Escapa, 2009). Therefore, in our MPTs generated with k = 6, we pruned the taxa *Himalayasaurus tibetensis* Dong, 1972, *Palvennia hoybergeti* Druckenmiller *et al.*, 2012 and *Pervushovisaurus bannovkensis* Arkhangelsky, 1998, and with k = 9 and k = 12, we pruned *Palvennia hoybergeti* and *Pervushovisaurus bannovkensis*. We also used a symmetric resampling of 33% change probability, which gives the frequency differences for 10 000 replicates to analyse the nodal support of our trees in an implied weighting framework. This resampling method appears to be the most appropriate as it is not distorted by character weight variations (Goloboff *et al.*, 2003). Furthermore, we used the Templeton's parametric test (Templeton, 1983) in TNT to investigate the statistical difference of topology lengths between our trees and a tree within which there was a positive constraint, testifying the monophyly of *Temnodontosaurus*. Trees were plotted and time scaled *a posteriori* by using an 'equal' method of branch length reconstruction using the strap v.1.4 package (Bell & Lloyd, 2015) in R v.1.3.1093. The stratigraphic congruence was calculated by using the ape v.5.2 (Paradis *et al.*, 2004), geoscale v.2.0 (Bell, 2015) and paleotree v.3.3.25 (Bapst, 2012) packages.

Bayesian inference of topology was conducted in MrBayes (v.3.2.7a; Ronquist *et al.*, 2012) using the CIPRES Science Gateway v.3.3 (Miller *et al.*, 2010). Character states were unweighted and unordered, and state frequencies were defined using a symmetrical Dirchlet hyperprior fixed at infinity which makes all state transitions equally likely. The Mkv model was used for the analysis with a gamma distribution for site rate variation with an exp(1.0) as a hyperprior. We set four runs of four chains, 100 000 000 generations, sampling at every 1000. We also applied a burn-in which discarded the first 25%. Similar parameters have been used in previous Bayesian inferences of ichthyosaurian relationships (Fischer *et al.*, 2016; Moon, 2017). Our script for Bayesian analyses is available in the Supporting Information (File S2).

SYSTEMATIC DESCRIPTION

ICHTHYOSAURIA DE BLAINVILLE, 1835

PARVIPELVIA MOTANI, 1999B

NEOICHTHYOSAURIA SANDER, 2000

TEMNODONTOSAURIDAE MCGOWAN, 1974

TEMNODONTOSAURUS LYDEKKER, 1889

TEMNODONTOSAURUS ZETLANDICUS (SEELEY, 1880) **COMB. NOV.**

1880 *Ichthyosaurus zetlandicus* – Seeley
1881 *Ichthyosaurus longifrons* – Owen
1889b *Ichthyosaurus zetlandicus* – Lydekker
1890 *Ichthyosaurus zetlandicus* – Woodward & Sherborn
1891 *Ichthyosaurus zetlandicus* – Fraas
1922 *Stenopterygius zetlandicus* – Huene
1925 *Stenopterygius zetlandicus* – Hauff
1974 *Stenopterygius acutirostris* – McGowan
1997 *Temnodontosaurus acutirostris* – Maisch & Hungerbühler
2000 *Temnodontosaurus acutirostris* – Maisch & Matzke
2003 *Temnodontosaurus acutirostris* – McGowan
2010 '*Ichthyosaurus*' *acutirostris* – Maisch
2019 *?Temnodontosaurus acutirostris* – Lomax

Holotype, stratum typicum and locus typicus: CAMSM J35176, a three-dimensionally preserved skull missing the mandible and the anterior third of the rostrum, from the Whitby Mudstone Formation, Lower Toarcian, likely from the Loftus Alum Quarry close to Whitby, Yorkshire, UK.

Emended diagnosis: Temnodontosaurus zetlandicus is characterized by the following unique combination of unusual features among early neoichthyosaurians: a digitate anterior end of the jugal which covers the

maxilla, externally separates the maxilla and the lacrimal and slightly overlaps the subnarial process of the premaxilla (shared with *T. nuertingensis* and *T. trigonodon*); bifurcated posterior end of the jugal, resulting in the separation of the ascending process and a smaller anteroventrally oriented process (shared with *T. trigonodon*); presence of a prominent mediolaterally oriented ridge which forms the anterior margin of the supratemporal fenestra (shared with *T. trigonodon*); slender projection of the supratemporal which covers the postfrontal dorsally and does not reach the anterior margin of the supratemporal fenestra (shared with *T. trigonodon*); presence of a prominent sagittal crest on the parietal and a slender parietal fork that partially overlaps the frontal (shared with *T. trigonodon*); absence of a postnarial descending process; presence of two posterior processes of the nasal, the lateral ending by an interdigitated suture, overlapping the anterior edge of the postfrontal which thus is bifurcated and adopts a V-shape, resulting in the separation of a medial and an anterodorsal process; and dorsal region of the lacrimal less extended than in *T. trigonodon* and marked by a notch.

Comparative description of the holotype CAMSM J35176: First described by Seeley in 1880, this specimen (Figs 2–4) is a cranium measuring 720 mm long; the mandible is not preserved. The end of the rostrum appears to have been broken off and we estimate the cranium and the snout to be respectively 990 mm and 680 mm long *in vivo* by prolonging the lateral edges of the premaxilla. The rostrum is straight, unlike in '*Ichthyosaurus*' *acutirostris* (Owen, 1865–1881) even if this feature could be due to the taphonomic flattening. Some badly preserved teeth are located on the premaxilla and the maxilla (Fig. 2) and are marked by striations on the crown. The dorsal part of the basicranium is poorly preserved (Fig. 4); the posterior edge of the parietals, the supraoccipital, the exoccipitals and the dorsal part of the basioccipital are missing. Aside from these elements, the skull is well preserved in three dimensions. All elements of the braincase are made of finished bone and therefore do not have a rugose texture, especially the basioccipital for which the condyle is as smooth as the extracondylar area and for which the opisthotic facets are protruding. This suggests an adult or at least subadult ontogenetic stage for CAMSM J35176 (Miedema & Maxwell, 2019).

The **premaxilla** is markedly elongated and not fully preserved (Figs 2, 3). The medial suture is clearly visible. Laterally, the premaxilla is marked by the presence of the premaxillary fossa and forms the supranarial and subnarial processes, as in other early parvipelvians even if this character may be variable in *Hauffiopteryx* (Maxwell & Cortés, 2020). The supranarial process forms approximately half of the dorsal margin of the naris as in *Temnodontosaurus eurycephalus* (McGowan, 1974) and in *Temnodontosaurus trigonodon* (Maisch, 1998b). The suture of the supranarial process with the nasal is crenulated while the posterior extremity of subnarial process contacts the anterior end of the jugal as in *T. trigonodon* (Maisch, 1998b). The subnarial process also contacts the anterior edge of the lacrimal. Some badly preserved tooth roots are located on its ventral surface but cannot be precisely described.

The **maxilla** is dorsoventrally low, slender and extends anteriorly as far as the nasal (Fig. 2). This particular feature is typical of *Temnodontosaurus* (Maisch & Hungerbühler, 1997; Martin *et al.*, 2012; Swaby & Lomax, 2020) among early parvipelvians. The maxilla of *T. zetlandicus* seems to have a comparable size to that of '*I.*' *acutirostris* (Figs 2, 8) and lower than in *T. nuertingensis* which has a higher maxilla (Maisch & Hungerbühler, 1997). Moreover, the maxilla lacks a narial process and does not participate in the ventral margin of the external naris. The posterior part of the maxilla is covered by the jugal, thus excluding an external contact with the lacrimal as in *T. trigonodon* (Maisch, 1998b; Pardo-Pérez *et al.*, 2018).

The **external naris** has a typical droplet shape (Fig. 2) and is larger than in *Ichthyosaurus* De la Beche & Conybeare, 1821 (Lomax & Massare, 2016) and *Leptonectes* (Maisch & Matzke, 2003; McGowan, 1989). The anterior extremity is thinner than the posterior border which is exclusively formed by a shallow notch of the lacrimal.

The **nasal** is wide and robust, forming a fairly large portion of the dorsal region (Fig. 3A, B). The anterior part of the nasal cannot be precisely distinguished due to the reconstructed area but appears to end abruptly as in *Temnodontosaurus crassimanus* (Blake, 1876) (Swaby & Lomax, 2020), *T. nuertingensis* (Maisch & Hungerbühler, 1997) and *T. trigonodon* (Pardo-Pérez *et al.*, 2018). The posterior half of the two nasals form a well demarcated internasal cavity. Posteriorly, the nasal forms two processes (one medial and one lateral) overlapping the anterior part of the postfrontal (Fig. 3A, B). The medial process has no digitation and exclusively contacts the postfrontal medially. Therefore, there is no nasal-parietal contact, at least externally. The lateral process is located more laterally and marked by a three-finger digitation. Laterally, the nasal forms approximately half of the dorsal margin of the external naris and a lateral wing is absent, as is the case in all early parvipelvians with the exception of *Leptonectes tenuirostris* (Conybeare, 1822) (Maisch & Matzke, 2003; Massare *et al.*, 2021) and *Stenopterygius aaleniensis* Maxwell *et al.*, 2012 (Massare *et al.*, 2021). Furthermore, the nasal does

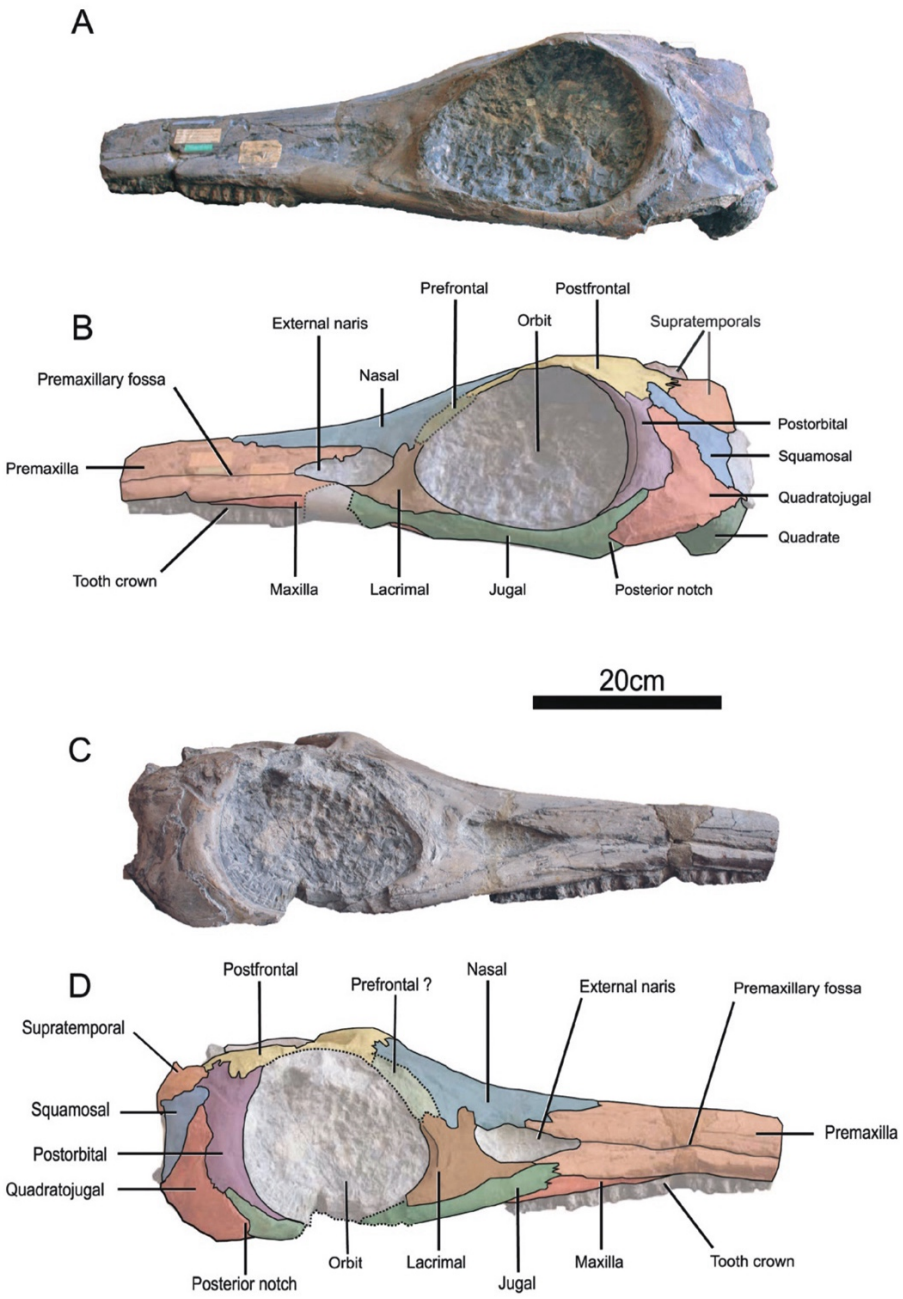

Figure 2. Photograph and interpretation of the holotype of *Temnodontosaurus zetlandicus* comb. nov. (CAMSM J35176). A, B, in left lateral view. C, D, in right lateral view.

not make a postnarial descending process, unlike *Temnodontosaurus platyodon* (Conybeare, 1822) (e.g. NHMUK R1158), *T. nuertingensis* (Maisch, 1997; Massare *et al.*, 2021) and *T. trigonodon* (Maisch, 1998b; Maisch & Hungerbühler, 2001).

The **lacrimal** has a broad hatchet shape, as is usual for ichthyosaurians (Fig. 2). The posterior margin participates to the anterior and anteroventral margins of the orbit while the anterior margin also forms the posterior margin of the external naris without forming a

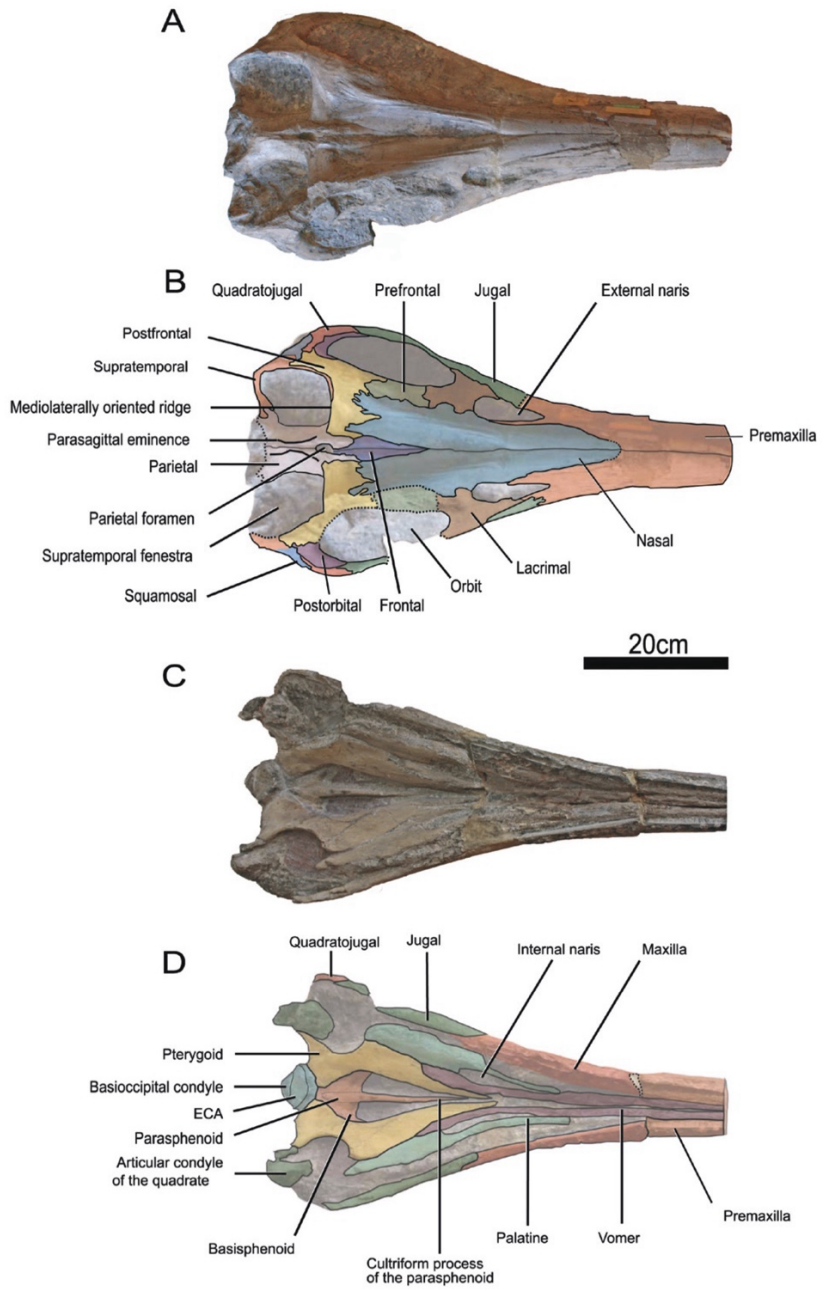

Figure 3. Photograph and interpretation of the holotype of *Temnodontosaurus zetlandicus* comb. nov. (CAMSM J35176). A, B, in dorsal view. C, D, in ventral view. Abbreviation: ECA, extracondylar area of the basioccipital.

rounded bulge or a prominent process within the naris, as can be seen in many specimens of *Temnodontosaurus* (Massare *et al.*, 2021). The lacrimal is marked by a notch on the dorsal edge unlike in *Temnodontosaurus platyodon* (Godefroit, 1993a), *Leptonectes* spp. (Maisch & Matzke, 2003), *Suevoleviathan* Maisch, 1998 spp. (Maisch, 2001), *Ichthyosaurus* spp. (Lomax & Massare, 2016), *Protoichthyosaurus* Appleby, 1979 (Lomax & Massare, 2018) and *Stenopterygius* spp. (Caine & Benton, 2011) and is not as extended dorsally as in

T. trigonodon where the dorsal notch is also absent (Maisch, 1998b; Maisch & Hungerbühler, 2001; Pardo-Pérez *et al.*, 2018). Moreover, the suture with the prefrontal is slightly crenulated. The ventral edge is more convex and entirely in contact with the jugal.

The **prefrontal** accounts for approximatively one third of the dorsal margin of the orbit (Figs 2, 3A, B). The anterior extremity contacts the lacrimal and this suture appears to be weakly crenulated. The prefrontal does not form a narial process, and hence does not participate to the rim of the external naris, a feature that is shared with most early parvipelvians with the exception of *Hauffiopteryx* Maisch, 2008 (Maxwell & Cortés, 2020). The prefrontal is not dorsomedially extended and does not contact the frontal or the parietal, unlike in *Leptonectes* (Maisch & Matzke, 2003), *Stenopterygius* (Maxwell *et al.*, 2012) and *Hauffiopteryx* (Maxwell & Cortés, 2020). The suture with the postfrontal seems to be slightly interdigitated.

Externally, the **frontal** is a small lanceolate bone that forms a narrow triangular process anteriorly (Fig. 3A, B). The posterior part is wider and is covered by the slender parietal fork, as in *T. trigonodon* (Maisch, 1998b) and therefore differs from *Hauffiopteryx* (Maxwell & Cortés, 2020), *Ichthyosaurus* (McGowan, 1973), *Leptonectes* (Maisch & Matzke, 2003; Vincent *et al.*, 2014), *Protoichthyosaurus* (Lomax *et al.*, 2020) and *Stenopterygius* (Maxwell *et al.*, 2012) in which the parietal anterior termination is broader. The frontal only participates in the formation of the anterior margin of the parietal foramen as in *T. trigonodon* (Maisch, 1998b), but unlike in *Hauffiopteryx* (Maxwell & Cortés, 2020), *Leptonectes* (Maisch & Matzke, 2003), *Protoichthyosaurus* (Lomax *et al.*, 2020), *Stenopterygius* (Maxwell *et al.*, 2012) or *Wahlisaurus* Lomax, 2016, in which frontals also form the lateral margin of the parietal foramen. Laterally, the frontal does not reach the supratemporal fenestra, as in all early parvipelvians (McGowan, 1973; Maisch & Matzke, 2003; Maxwell *et al.*, 2012; Marek *et al.*, 2015; Lomax, 2016; Maxwell & Cortés, 2020).

The **jugal** is slender and forms the ventral and posteroventral margins of the orbit (Fig. 2). The posterior extremity of the jugal contacts the postorbital and the quadratojugal, unlike in *Hauffiopteryx* (Maxwell & Cortés, 2020) and *Stenopterygius* (Maisch, 2008). This extremity appears bifurcated, resulting in the separation of the ascending process and a small anteroventrally oriented process (Fig. 2C, D). Such a bifurcation is also found in *T. trigonodon* and could be due to an anteroventral process of the quadratojugal (Maisch & Hungerbühler, 2001). However, the ascending process is broader in *T. trigonodon* (Maisch & Hungerbühler, 2001; Pardo-Pérez *et al.*, 2018). The anterior extremity of the jugal is digitated, contacting the subnarial process of the premaxilla and covering the posterior part of the maxilla (Fig. 2). This contact between the jugal and the premaxilla is also present in *T. trigonodon* (Maisch, 1998b; Fig. 12) and in *T. nuertingensis* (Maisch & Hungerbühler, 1997), but not in other early parvipelvians.

The **quadratojugal** appears to form the frame of the postorbital region and is well exposed (Fig. 2) as in *Ichthyosaurus* (Lomax & Massare, 2016) and *Temnodontosaurus* (McGowan, 1974; Godefroit, 1993a; Maisch & Hungerbühler, 2001) and unlike in *Hauffiopteryx* (Maxwell & Cortés, 2020) and *Stenopterygius* (Godefroit, 1993b; Maisch, 2008). The quadratojugal is wide, especially the ventral part where it extends to the level of the posterior digitation of the jugal (as in *T. trigonodon*; Maisch & Hungerbühler, 2001). The quadratojugal forms a large dorsal process, which nearly reaches the dorsal margin of the squamosal (Fig. 2). The articulation surface with the quadrate is strongly concave medioventrally. The anterior edge the quadratojugal seems to slightly cover the posterior margin of the postorbital. Posterodorsally, the quadratojugal contacts the squamosal along a relatively smooth suture. The postorbital region is large compared to the orbit but less than in *T. trigonodon* even if this ratio looks variable within the species (ratio length of the postorbital region to length of the orbit: ~0.5 for *T. zetlandicus* vs. ~0.6–1.0 for *T. trigonodon*; see Supporting Information, Table S1).

The **squamosal** is a relatively large triangular element within the postorbital region (Fig. 2) and has a morphology similar to that of *T. trigonodon* (Maisch & Hungerbühler, 2001). The posteroventral process of the squamosal is long and reaches the articulation between the quadratojugal and the condyle of the quadrate. Laterally, the suture with the quadratojugal is well extended and dorsally, the squamosal contacts the supratemporal and the postfrontal by an anterodorsal process (Fig. 2).

The crescent-shaped **postorbital** forms the posterior margin of the orbit (Fig. 2). Dorsally, the facet with the postfrontal is reduced in comparison to *Suevoleviathan* (Maisch, 2001) and ventrally, the postorbital contacts the jugal. The orbital crest is not prominent on postorbital, thus resulting in a lack of clear delimitation of the part involved in the formation of the orbit and the part forming the postorbital region. The postorbital thins dorsally and ventrally, buttressing the postfrontal and the dorsal margin of the jugal. Posteriorly, the postorbital contacts the quadratojugal and seems to be slightly overlapped by this element.

The **parietals** are relatively well preserved except at their posterior part and have a curved aspect

(Fig. 3A, B). The anterior extremity of the parietal is marked by a slender parietal fork that covers the posterior part of the frontal as in *T. trigonodon* (Fig. 12, B, C; Maisch, 1998b). As a result, the posterior and lateral margins of the parietal foramen are formed externally by this element and this foramen is nearly enclosed by the parietals except at its anterior edge (Fig. 3A, B, 7). This strongly contrasts with *Hauffiopteryx* (Marek *et al.*, 2015), *Stenopterygius* (Maxwell *et al.*, 2012) and *Wahlisaurus* (Lomax, 2016), where the parietal foramen is nearly completely enclosed by the frontals. The interparietal suture is surrounded by a prominent parasagittal ridge (Fig. 3A, B), which is present on both elements, thus forming a paired structure as in *T. trigonodon* (Fig. 12). This ridge becomes thinner and flatter posteriorly and ends anteriorly at the posterior edge of the parietal foramen. Dorsally, the suture between the parietal and the supratemporal adopts a sinusoidal configuration.

The **supratemporal** is a strongly curved bone (Fig. 3A, B). It forms the posterior and lateral margins of the supratemporal fenestra, forming an elongated anteromedial process that covers the postfrontal laterally and reaches the anterior ridge of the supratemporal fenestra (Fig. 3A, B) formed by the dorsal part of the postfrontal (see below) as in *T. trigonodon* (Fig. 12). The suture with the postfrontal is digitated and the contact with the squamosal is extensive (Fig. 2). The descending process of the supratemporal forms the lateral margin of the braincase, where it contacts the occipital lamella of the quadrate (Fig. 4).

The left postfrontal is completely preserved while the anterolateral portion of the right one is damaged (Figs 2, 3A, B). The **postfrontal** is an extensive structure participating in the dorsal and postorbital regions of the cranium. Anteriorly, this element is partially covered by the posterior processes of the nasal, giving it a V-shape dorsally, resulting in the bifurcation of a medial and a lateral process, which it is not seen in any early parvipelvians (Maisch, 1998b; Maisch & Matzke, 2003; Maxwell *et al.*, 2012; Vincent *et al.*, 2014; Marek *et al.*, 2015; Lomax, 2016; Lomax & Massare, 2016; Lomax *et al.*, 2020; Maxwell & Cortés, 2020). The suture with the prefrontal is not well preserved but appears undulated. The postfrontal forms the entire anterior margin of the supratemporal fenestra where this element forms an extensive mediolaterally oriented ridge (Fig. 3A, B, 7). This unusual structure is actually shared with *T. trigonodon* (Fig. 12). A short ridge is also present in *Protoichthyosaurus prostaxalis* Appleby, 1979 (Lomax & Massare, 2018). However, this postfrontal ridge appears shorter than in *T. zetlandicus* (medially vanished around mid-supratemporal fenestra width) and also appears to be oriented along the anteromedial-posterolateral axis whereas this ridge is mediolaterally oriented in *T. zetlandicus* (Figs 3A, B). Apart from these three species, the presence

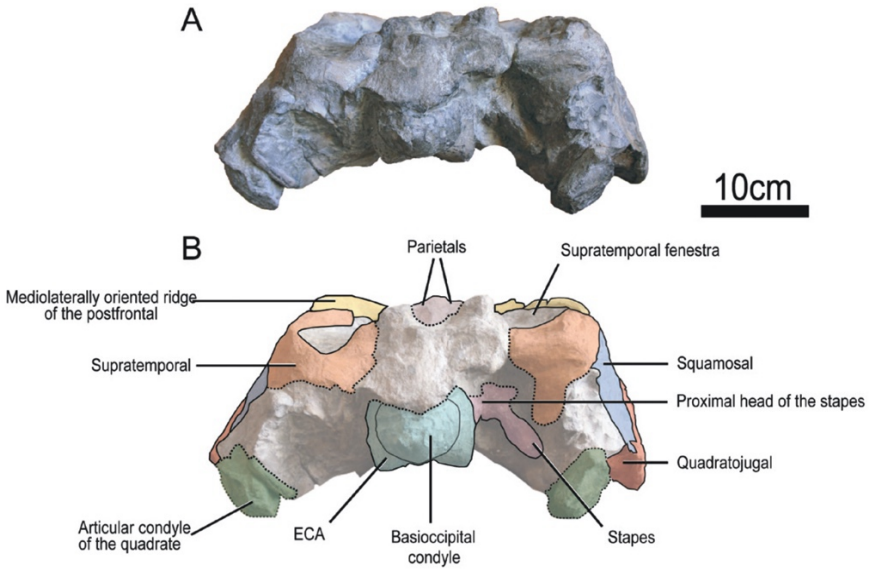

Figure 4. Photograph and interpretation of the holotype of *Temnodontosaurus zetlandicus* comb. nov. (CAMSM J35176). A, B, Basicranium in posterior view. Abbreviation: ECA, extracondylar area of the basioccipital.

of a postfrontal ridge which forms the anterior edge of the supratemporal fenestra is absent in all other early parvipelvians (McGowan, 1973; Maisch, 1998a; Maisch & Matzke, 2003; Maxwell *et al.*, 2012; Vincent *et al.*, 2014; Marek *et al.*, 2015; Lomax, 2016; Lomax & Massare, 2016; Lomax *et al.*, 2020; Maxwell & Cortés, 2020).

The **basioccipital** is partially preserved, having its dorsal part damaged (Fig. 4). Thus, its contribution to the foramen magnum cannot be characterized. The condyle is prominent and is clearly separated from the extracondylar area, a character shared by members of *Temnodontosaurus* (Swaby & Lomax, 2020) and more generally, non-ophthalmosaurid parvipelvians (Motani, 1999b; Fischer *et al.*, 2012) and the notochordal pit is located on the centre of the condyle. The extracondylar area is slightly expanded laterally and seems to be well developed ventrally and marked by the presence of a basal tubera, thus being saddle-shaped ventrally, unlike in *Stenopterygius quadriscissus* (Quenstedt, 1856) (Miedema & Maxwell, 2019) and *Chacaicosaurus* Fernández, 1994. The protrusion of the opisthotic and stapedial facets is discernible, resulting in concave and well-delimited facets.

The **stapes** possesses a robust shaft that is only slightly waisted (Fig. 4). The proximal head seems to be massive as in *T. trigonodon* (Maisch, 2002), *Eurhinosaurus longirostris* (Mantell, 1851) (e.g. SMNS 18648), *Hauffiopteryx* (Marek *et al.*, 2015) and *Stenopterygius quadriscissus* (Miedema & Maxwell, 2019) but unlike in *Ichthyosaurus* (McGowan, 1973), *Protoichthyosaurus* (Lomax *et al.*, 2019) and *Temnodontosaurus azerguensis* Martin *et al.*, 2012. The medial surface of the proximal head is concave, matching the slightly convex corresponding facet on the basioccipital. The distal facet for articulation with the quadrate is elliptic and weakly expanded with respect to the shaft.

Both **quadrates** are poorly preserved (Fig. 4). The dorsal suture with the supratemporal and the laterally to the right quadrate with the stapes is nevertheless visible. The condyle, located at the ventrolateral end of the posterior face, is better preserved and massive. With a reniform aspect, the dorsolateral edge adopts a shape complementary to the contact facet of the quadratojugal and is therefore largely convex. The ventral edge of the condyle is more concave and would serve to accommodate the surangular which is not preserved. The ventromedial edge contacts the quadrate wing of the pterygoid.

The **pterygoid** is a long robust element, markedly constricted at mid-length (Fig. 3C, D), as is usually the case in parvipelvians (McGowan, 1973). The markedly concave borders of the pterygoid delimit the suborbital fenestra laterally and the large interpterygoid vacuity. The narrow palatine ramus of the pterygoid sharply terminates medially of the internal naris. Laterally, the pterygoid contacts the palatine, and also the vomer more anteriorly by a long straight suture, and there is no postpalatine process. The pterygoid expands posteriorly, forming two horizontal lamellae in the region of the quadrate ramus. The larger lateral lamella contacts the condyle of the quadrate and the smaller medial one contacts the ventral extremity of the extracondylar area of the basioccipital.

The **palatine** is fairly elongated and forms posteriorly the anterior margin of the suborbital fenestra (Fig. 3C, D). Its concave medial edge forms the lateral margin of the internal naris. The anterior half of the palatine becomes considerably thinner and its extremity ends by a junction with the vomer.

The **vomer** is also elongated; its widest portion is set posteriorly, where it forms the medial margin of the internal naris (Fig. 3C, D). The vomer extends anteriorly as a slit-like process, contacting the premaxilla and the palatine. Posteriorly the vomer is not well extended as in *T. nuertingensis* and almost excludes a contact between the pterygoid and the palatine (Maisch & Hungerbühler, 1997).

The **basisphenoid** appears crescent shaped in ventral view as its anterior edge is concave (Fig. 3C, D). The posterior surface in contact with the basioccipital is hidden laterally by the pterygoids, as well as the basipterygoidal processes laterally. The basisphenoid is medially crossed throughout its entire length by the parasphenoid; even though the carotid foramina is not visible, this extension of the parasphenoid indicates that this foramen was paired like all members of *Temnodontosaurus* (Fraas, 1913; von Huene, 1931; Godefroit, 1993a; Maisch & Matzke, 2000; Maisch, 2002; Martin *et al.*, 2012).

The **parasphenoid** forms a relatively robust cultriform process (Fig. 3C, D). The parasphenoid extends from the posterior end of the basisphenoid to approximately half the length of the palate region but does not reach the interpterygoidal suture.

TEMNODONTOSAURUS CF. *ZETLANDICUS*

Referred specimen: MNHNL TU885, a partial skull from the Schistes Carton Formation, Lower Toarcian, Schouweiler, Grand Duchy of Luxembourg.

Comparative description of MNHNL TU885: The specimen MNHNL TU885 is, as preserved, 383 mm long and consists of a cranium lacking the snout

and a fragmentary surangular (Figs 5, 6). Due to its preservation state, the orbits and temporal fenestrae are not fully delimited and the right vomer and the left palatine have been slightly displaced (Fig. 6A, B). The sutures between the nasals, frontals, right prefrontal and postfrontals are often difficult to discern (Fig. 5C, D). The parietal foramen is entirely preserved and appears unusually large, with a markedly raised rim; it is presently unclear whether this condition is pathological or not, as the parietal foramen is not located on the cranial midline. The postorbital region is only preserved on the left side and is anteroposteriorly long (Fig. 5A, B), measuring 99 mm. The basicranium is completely preserved (Fig. 6C, D), only lacking the left opisthotic. Hereafter, we compare salient features of MNHNL TU885 with early neoichthyosaurians.

This specimen shares many features with early neoichthyosaurians such as a frontal without a temporal process, a supraoccipital with a shallow ventral notch, a robust stapes with a prominent proximal head, a stout opisthotic with a short paroccipital process, a basioccipital with a well-demarcated extracondylar area, which is ventrally saddle-shaped and marked by the presence of a basal tubera, and a paired carotid foramen as suggested by the morphology of the parasphenoid, even if the posterior part mostly seems to be broken (McGowan, 1973; Fischer *et al.*, 2011; Martin *et al.*, 2012; Marek *et al.*, 2015; Moon & Kirton, 2016; Lomax *et al.*, 2019; Miedema & Maxwell, 2019). In posterior view (Fig. 6C, D), the quadrate is a robust and large element that has a straight occipital lamella unlike *T. azerguensis* (Martin *et al.*, 2012) and *T. crassimanus* (Swaby & Lomax, 2020) and with a massive and well-developed condyle as in species currently referred to as *Temnodontosaurus* for which the quadrate is preserved, with the exception of *T. azerguensis* (Martin *et al.*, 2012). The postorbital region is well developed with a long,

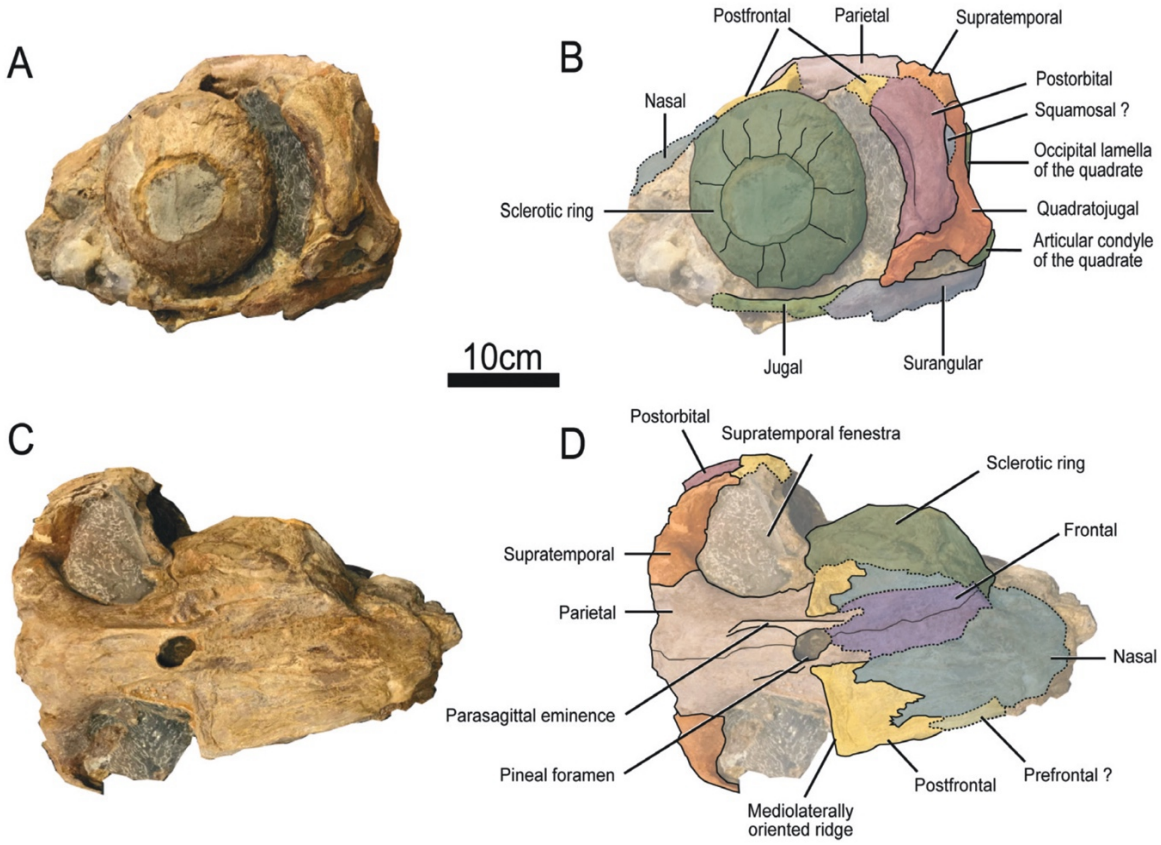

Figure 5. Photograph and interpretation of the specimen MNHNL TU885 *Temnodontosaurus* cf. *zetlandicus* A, B, in right lateral view. C, D, in dorsal view.

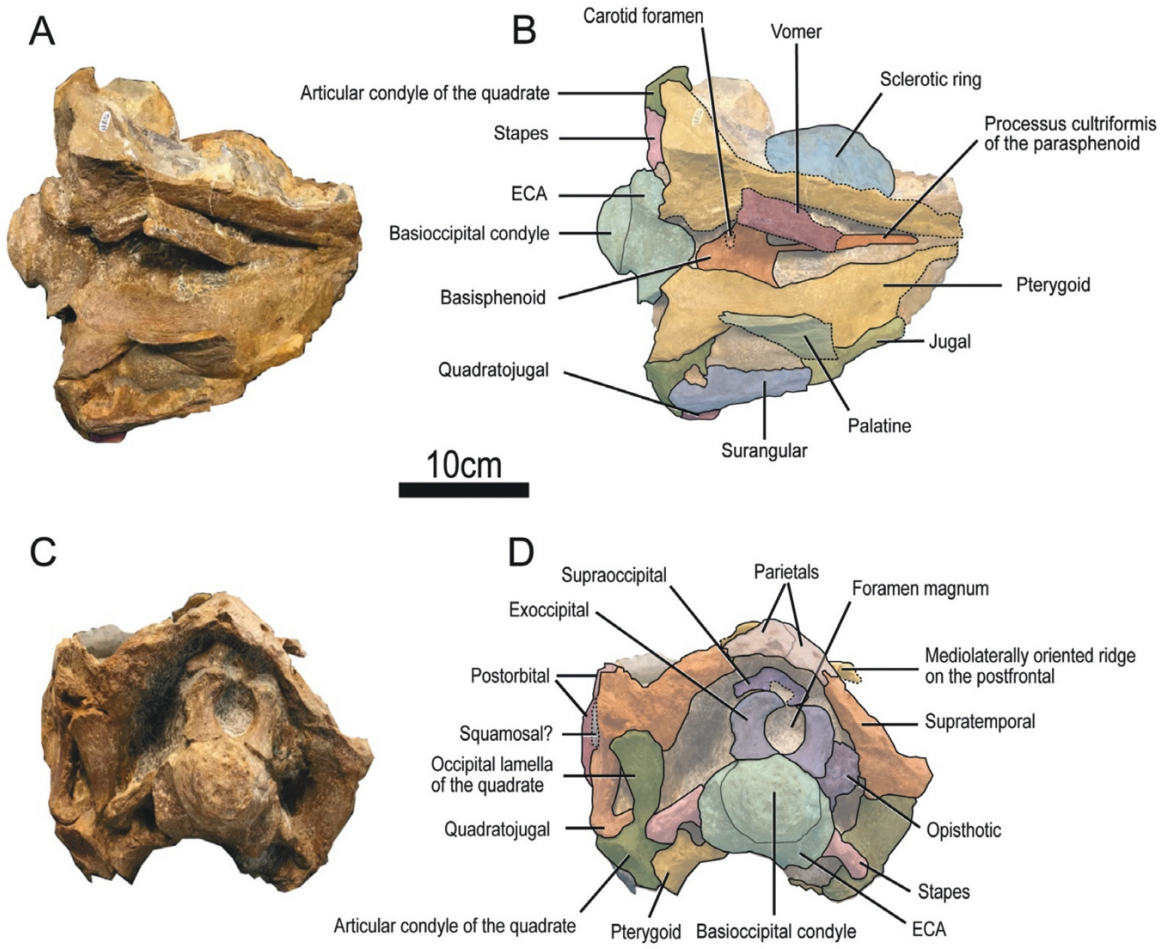

Figure 6. Photograph and interpretation of the specimen MNHNL TU885 *Temnodontosaurus* cf. *zetlandicus* A, B, palate in ventral view. C, D, Basicranium in posterior view. Abbreviation: ECA, extracondylar area of the basioccipital.

extensive quadratojugal, as in *Temnodontosaurus* spp. (McGowan, 1974, 1994; Maisch & Hungerbühler, 2001; Swaby & Lomax, 2020) but unlike in other Early Jurassic parvipelvians (Maisch, 2001, 2008; Maisch & Matzke, 2003; Lomax & Massare, 2016; Maxwell & Cortés, 2020). The contribution of the supraoccipital to the dorsal margin of the foramen magnum is limited and nearly absent, as in *Temnodontosaurus* (Maisch, 2002). The frontal has a reduced, lanceolate dorsal exposure and forms the anterior margin of the parietal foramen, as in *T. zetlandicus* and *T. trigonodon* (Maisch, 1998b).

For all of these reasons, MNHNL TU885 is clearly assignable to *Temnodontosaurus*. The skull roof of MNHNL TU885 shares many similarities with that of *T. zetlandicus* (Fig. 7), such as: (1) the bifurcated posterior processes of the nasal which partially covers the postfrontal which anteriorly appears in the medial and anterolateral processes; (2) the presence of a prominent mediolaterally oriented ridge on the postfrontal which forms the anterior margin of the supratemporal fenestra; and (3) a lanceolate frontal posteriorly covered by a slender forked process of the parietal. The skull roof of MNHNL TU885 also resembles that of *T. trigonodon*, but the presence of the bifurcated posterior processes of the nasal markedly differs from *T. trigonodon* (Maisch, 1998b). MNHNL TU885 is also similar in size and in cranial proportions to *T. zetlandicus* (see Table 1) and is here referred to as *T.* cf. *zetlandicus*.

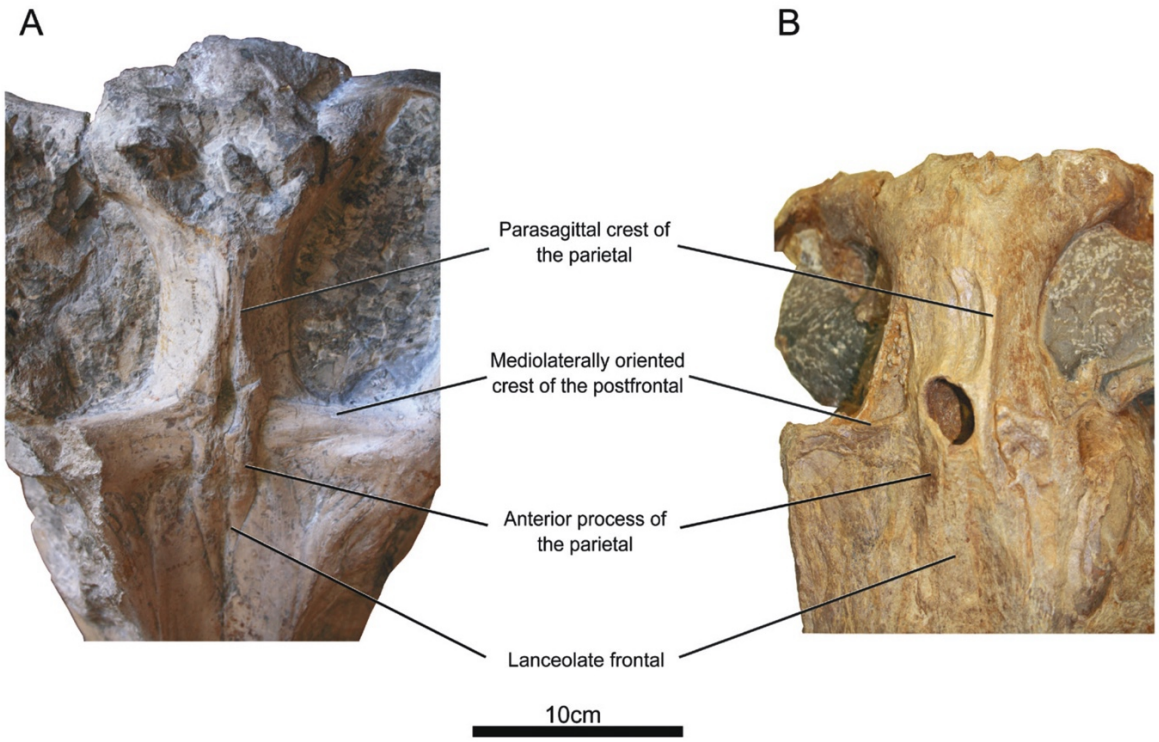

Figure 7. Braincase comparison of the holotype of *Temnodontosaurus zetlandicus* comb. nov. (CAMSM J35176) (A) and the referred specimen of *Temnodontosaurus* cf. *zetlandicus* (MNHNL TU885) (B).

SPECIES INQUIRENDA

ICHTHYOSAURUS ACUTIROSTRIS OWEN, 1840

In the past, *T. zetlandicus* has been regarded as a junior synonym of '*Ichthyosaurus*' *acutirostris* mainly because both came from the Lower Toarcian of Whitby (UK), without considering differences in cranial shape (McGowan, 1974; McGowan & Motani, 2003; Maisch, 2010). The current taxonomic placement of '*I.*' *acutirostris* is still controversial and has widely fluctuated overtime as this species has been classified in numerous genera (McGowan, 1974; Maisch & Matzke, 2000; McGowan & Motani, 2003; Maisch, 2010). According to Maisch (2010), this species might represent a novel genus of Early Jurassic ichthyosaurian. Considering that the referred material from Whitby requires a complete revision, possibly representing a variety of taxa (Maisch, 2010), focusing on the holotype seems adequate for the time being. However, this holotype (NHMUK PV OR 14553) (Fig. 8) was thought to be lost but finally relocated in the ichthyosaur collections about 20 years ago (Chapman & Doyle, 2002; Lomax, 2019), in a damaged state since the anterior part of the rostrum and the basal part of the right forefin are now missing. Even more problematic, the specimen is *de facto* unavailable for an undefined period of time (S. Chapman, pers. comm., August 2021) making the comparison even more challenging.

The right forefin of NHMUK PV OR 14553 is complete and composed of more than 25 elements on the longest digit (Fig. 8A); however, the authenticity of this trait has been questioned (Chapman & Doyle, 2002; Maisch, 2010; Lomax, 2019). If genuine, its length would represent an apomorphy since the number of elements in the longest digit in many early neoichthyosaurians does not exceed 20 (Motani, 1999a; Swaby & Lomax, 2020). Moreover, this condition looks more similar to *Stenopterygius uniter* (von Wurstemberger 1876), which has an elongated forefin (Maxwell, 2012). The left side of the skull is poorly preserved (Fig. 8), which restricts our comparisons with the holotype of *T. zetlandicus* (CAMSM J35176). Nevertheless, some remaining elements allow to differentiate the two specimens. Firstly, the most noticeable difference concerns the nasal. In *T. zetlandicus* this structure anteriorly ends as far as the maxilla and is not anterodorsally extended (Figs 2, 3A, B), whereas in '*I.*' *acutirostris*, the nasal, even if it is incomplete, seems to anteriorly

Table 1. Measurements (anteroposterior length, diameter, dorsoventral height, mediolateral width) of *Temnodontosaurus zetlandicus* comb. nov. (holotype CAMSM J35176) and *Temnodontosaurus* cf. *zetlandicus* (MNHNL TU885)

Measurements (in mm)	CAMSM J35176	MNHNL TU885
Length of the skull (estimation)	990	–
Length of the rostrum (estimation)	680	–
Length of the pre-naris rostrum (estimation)	544	–
Height of the left orbit	160	–
Length of the left orbit	195	–
Height of the right orbit	164	–
Length of the right orbit	201	–
Height of the left sclerotic ring	–	165
Length of the left sclerotic ring	–	159
Length of the left supratemporal fenestra	165	–
Length of the right supratemporal fenestra	~149	147
Length of the left naris	109	–
Length of the right naris	112	–
Length of the parietal foramen	30	28
Width of the parietal foramen	10	20
Length of the left postorbital region	106	89
Length of the right postorbital region	95	–
Length of the parietal	173	152
Length of the frontal	125	~120
Height of the basioccipital	–	102
Width of the basioccipital	90	103
Height of the basioccipital condyle	_	61
Width of the basioccipital condyle	66	78

end further than the maxilla (Fig. 8). This condition in '*I.*' *acutirostris* is more similar to the rest of the Early Jurassic parvipelvians (Maisch, 2008; Maxwell *et al.*, 2012; Lomax & Massare, 2016; Maxwell & Cortés, 2020) with the exception of *Suevoleviathan* (Maisch, 2001). The morphology of the jugal also seems to differ in that the posterior extremity would not be notched (Fig. 8B). In NHMUK PV OR 14553, the postfrontal does not bear a prominent ridge on the anterior margin of the supratemporal fenestra (Fig. 8B), which is a distinctive feature of *T. zetlandicus*. Concerning cranial dimensions, the length of the postorbital region is larger compared to the diameter of the orbit than in *T. zetlandicus* (~0.8 for '*I.*' *acutirostris* vs. ~0.5 for *T. zetlandicus*; see Supporting Information, Table S1) even if the skull appears to be smaller in '*I.*' *acutirostris*.

The taxonomic decisions in this paper require the assessment of the possible influence of ontogeny in driving the differences we observe between the holotype of '*I.*' *acutirostris*, which is small, and the holotype of *T. zetlandicus*. To do so, we assess the ontogenetic stage of the holotype of '*I.*' *acutirostris* by analysing the relative diameter of the sclerotic ring and the sclerotic aperture. This analysis has been used in the past to segregate juveniles (and supposed deep divers) from adults in neoichthyosaurians (Fernández *et al.*, 2005; Fischer *et al.*, 2013). Indeed, the orbit is nearly completely filled by the sclerotic ring in juveniles and deep divers, whereas in non-deep diving adult forms, the sclerotic rings tend to occupy a smaller area within the orbit. Our measurements (taking into account that the postorbital has been displaced in NHMUK PV OR 14553) place of the holotype of '*I.*' *acutirostris* well within the adult ontogenetic stage (Fig. 11). According to these results, the differences in size and morphology between the holotype of '*I.*' *acutirostris* and the holotype of *T. zetlandicus* cannot be regarded as driven by osteological immaturity.

Our morphological comparison, albeit limited, indicates that the incorporation of *T. zetlandicus* as a junior synonym of '*I.*' *acutirostris* is untenable. The other material referred to '*I.*' *acutirostris* needs a thorough reinvestigation once the material is accessible again (Maisch, 2010; Swaby & Lomax, 2020). Like Maisch (2010), we suggest removing '*I.*' *acutirostris* from *Temnodontosaurus* and placing it as *species inquirenda*, as *Ichthyosaurus acutirostris* according the initial assignment given by Owen (1840).

RESULTS

PHYLOGENETIC ANALYSES

Phylogenetic analyses under implied weighting maximum parsimony yielded 18 most-parsimonious trees (MPTs) with k = 12, each having a length of 68.312. The Consistency Index was 0.191 and the Retention Index was 0.644. Analyses conducted with k = 6 and k = 9 generated one MPT each with a length of 102.201 and 81.639, respectively (these topologies are presented in Supporting Information, Figs S2, S3). In all of our MPTs, *T. zetlandicus* is recovered as a member of *Temnodontosaurus*, being systematically grouped within a number of species currently referred to as *Temnodontosaurus*. Indeed, with k = 6 and 9, this species is considered to be the sister taxon of *T. trigonodon*, while *T. nuertingensis* is the sister taxon of *T. zetlandicus* with k = 12 and also closely related to *T. trigonodon*. Nevertheless, these relationships are not well supported by the symmetric resampling value [under 50%, as is the case for nearly all nodes of the phylogeny. Similar low values have been obtained on a previous version of the data set by Moon (2017)]. In MPTs generated with K = 12,

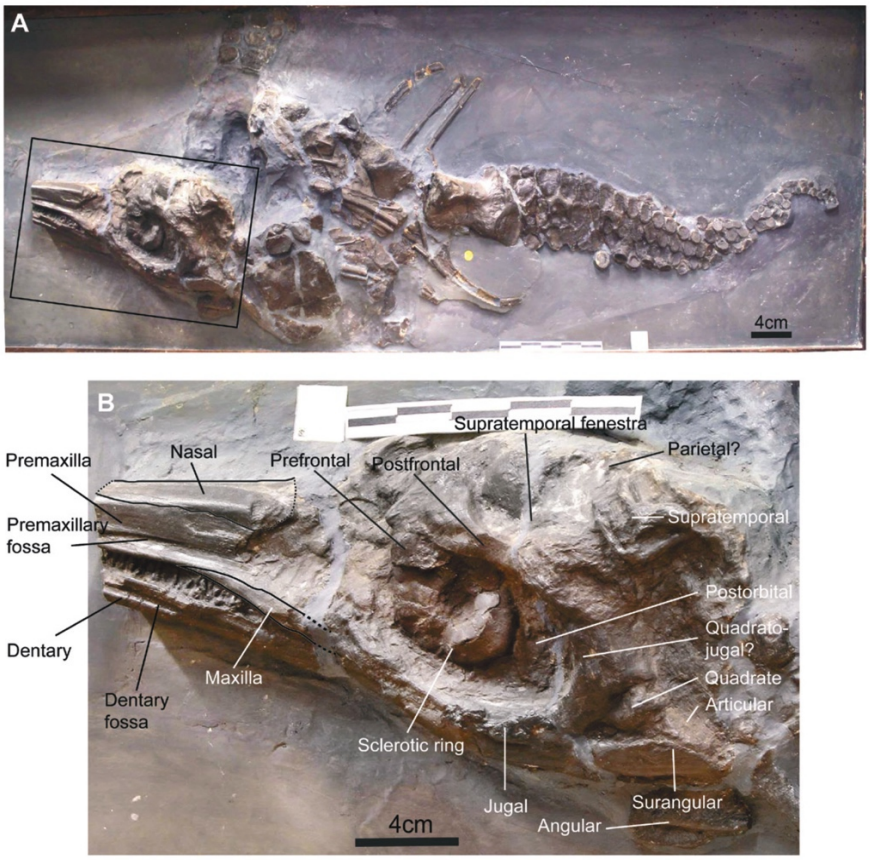

Figure 8. Photograph of the holotype of '*Ichthyosaurus*' *acutirostris* (NHMUK PV OR 14553). A, the whole specimen. B, interpretation of the skull.

the synapomorphies that unite these three species are the extension of the jugal that reaches the anterior end of the lachrymal (30.1) and the extensive participation of the splenial in the mandibular symphysis (122.0); the absence of a complexly lobate shape of its external naris (26.0) unites *T. zetlandicus* and *T. nuertingensis*. In all topologies, members of *Temnodontosaurus* appeared well clustered yet not monophyletic. This is essentially due to the fluctuating position of *T. azerguensis*, which is found to be more basal than the other species of *Temnodontosaurus* in k = 6 and more derived in k = 12, where it forms a clade with a diminutive version of Leptonectidae (*Leptonectes moorei* + *Leptonectes tenuirostris* (McGowan & Milner, 1999) + *Excalibosaurus costini* (McGowan, 1986)). As a whole, Leptonectidae is recovered more as a grade rather than a clade in k = 12 (Fig. 9), but not when homoplastic characters are more strongly penalized (k = 6 and k = 9; Supporting Information, Figs S2, S3). The polyphyletic status of *Temnodontosaurus* is also attributable to the inclusion of *Suevoleviathan* in k = 9 and in k = 12. In order to statistically test the monophyly of *Temnodontosaurus*, we computed a Templeton's parametric test with a tree in which the monophyly of the genus was forced (under k = 12). The result of the test indicated that this solution is statistically indistinguishable (*P*-value > 0.05) from our most parsimonious tree generated without monophyly constraints. A monophyletic *Temnodontosaurus* is thus a suboptimal yet fully probable topology with the data presently at hand (see Supporting Information, Fig. S4).

The position of *Temnodontosaurus*—or *Temnodontosaurus*-like forms [the temnodontosaurids or temnodontosauoids of some authors (McGowan, 1994; Maisch & Matzke, 2000; McGowan & Motani, 2003)]—fluctuates within neoichthyosaurians, depending on the penalty applied to homoplastic characters. Indeed, with k = 6, a clade comprising many species of *Temnodontosaurus* is found to be one of the most primitive clades of the Early Jurassic, as previously inferred (Sander, 2000; Maisch & Matzke, 2000; Maxwell *et al.*, 2012; Fischer *et al.*, 2016; Moon,

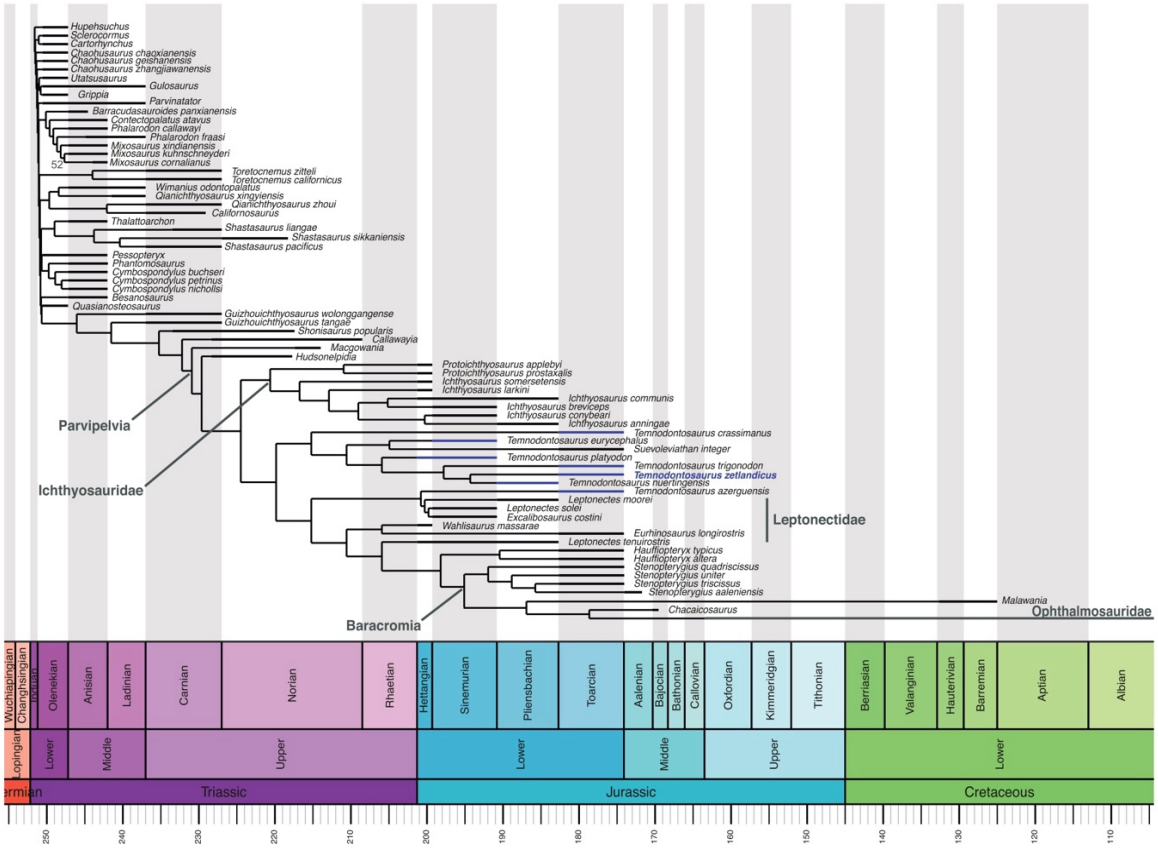

Figure 9. Time-scaled phylogeny of ichthyopterygians arising from implied weighting (k = 12) maximum parsimony analysis, in 'equal' reconstruction branches lengths. Branch values of resampling ≥ 50 are indicated on the branches leading their corresponding nodes.

2017; Zverkov & Jacobs, 2020). In k = 9 and 12, Ichthyosauridae appeared to be the basalmost family of neoichthyosaurians, as in Maxwell & Cortés (2020).

Bayesian inference (Fig. 10) provides a comparable topology to those generated in an implied weighting maximum parsimony framework with high values of k (9 and 12). *Temnodontosaurus zetlandicus* is also recovered within a clade grouping many other species currently referred to as *Temnodontosaurus*, as well as *Suevoleviathan*. Within this clade, *T. zetlandicus* forms a moderately well-supported (posterior probability of 65%) clade grouping *T. trigonodon* and *T. platyodon* and appears more derived than *T. nuertingensis*. Members of the genus appear well clustered and are not considered more primitive than Ichthyosauridae (*Ichthyosaurus*, *Protoichthyosaurus*) which is the most basal clade of Jurassic parvipelvians as shown in our maximum parsimony analyse, comparable to the results of Moon (2017) and Maxwell & Cortes (2020). Furthermore, *Temnodontosaurus* is still recovered as polyphyletic for the same reasons as in maximum parsimony analyses: *Suevoleviathan* is included within *Temnodontosaurus* and *T. azerguensis* clusters with leptonectids.

DISCUSSION

THE VALIDITY AND RELATIONSHIPS OF *TEMNODONTOSAURUS ZETLANDICUS*

Our osteological comparative study of *T. zetlandicus* and the comparison with the holotype of '*I.*' *acutirostris* indicates the validity of *T. zetlandicus* and provide new evidence for its placement in *Temnodontosaurus*. Indeed, this species shares with other temnodontosaurids a large skull, a low maxilla that anteriorly ends as far as the nasal (Figs 2, 3A,

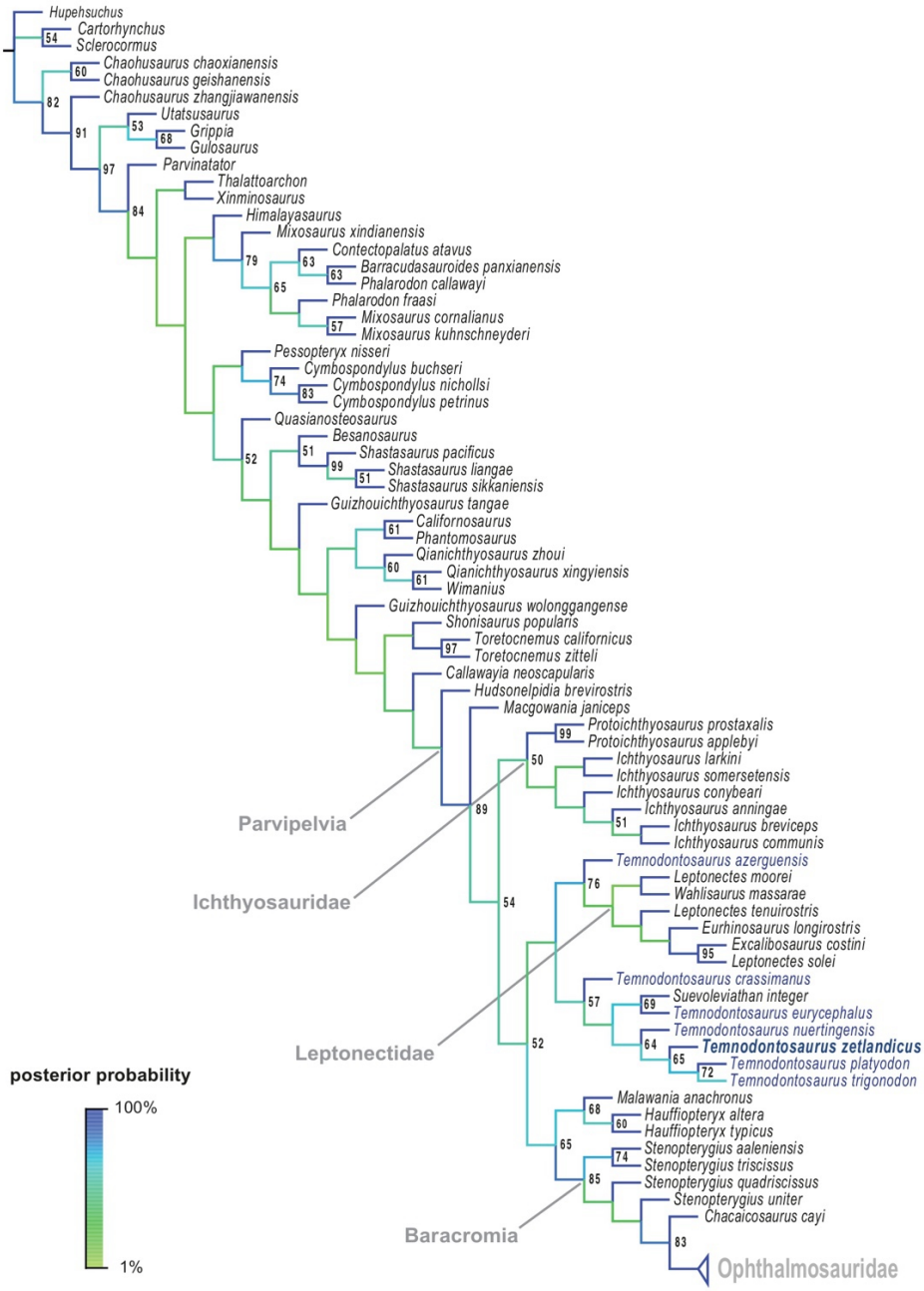

Figure 10. Phylogeny of ichthyopterygians arising from Bayesian inference. Colour coding indicates percentages of posterior probabilities for each branch. Percentages of posterior probabilities ≥ 50 are indicated in their corresponding nodes.

B; Martin *et al.*, 2012; Swaby & Lomax, 2020) and a parasphenoid that crosses the entire length of the basisphenoid (Fig. 3C, D) which forces a paired carotid foramina (Fraas, 1913; von Huene, 1931; Godefroit, 1993a; Maisch & Matzke, 2000; Maisch, 2002; Martin *et al.*, 2012).

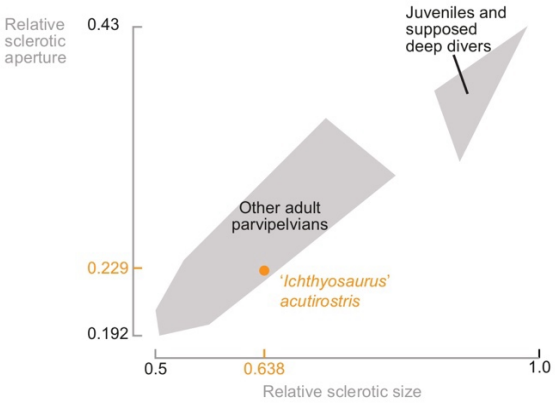

Figure 11. Sclerotic aperture and external sclerotic diameters of various parvipelvians relative to orbit diameter. The grey colour represents the repartition of the species included in the study of Fernández *et al.* (2005) and the orange colour is relative to the values and the position of '*Ichthyosaurus*' *acutirostris*. Modified from Fischer *et al.* (2013). Values for '*I. acutirostris*: sclerotic aperture diameter: 17.2 mm; external sclerotic diameter: 48.8 mm; orbit diameter: 76.5 mm.

These assumptions are also confirmed by our phylogenetic analyses as *T. zetlandicus* is recovered as closely related to *T. nuertingensis* and *T. trigonodon*, both in maximum parsimony (Fig. 9) and in Bayesian inference (Fig. 10). Morphologically, these three species possess a similar rostrum with a jugal that anteriorly contacts the subnarial process of the premaxilla and partially covers the maxilla (Maisch & Hungerbühler, 1997; Pardo-Pérez *et al.*, 2018). Nonetheless, some differences are noticeable. The maxilla of *T. nuertingensis* is dorsoventrally higher than in *T. zetlandicus* as it nearly reaches the external naris and on the palate region, the vomer is larger and almost excludes contact between the pterygoid and the palatine (Maisch & Hungerbühler, 1997). Furthermore, *T. nuertingensis* is older, currently only found in the Lower Pliensbachian strata of Germany (Maisch & Hungerbühler, 1997); yet the incompleteness of the holotype (SMNS 13488) severely limits our comparisons. For these reasons, further investigations are therefore required to better understand the relationship between *T. zetlandicus* and *T. nuertingensis*.

The cranial morphology of *T. trigonodon* is better known since many specimens have been found in western Europe (McGowan, 1996a). Our osteological comparison highlighted numerous common features between *T. zetlandicus* and *T. trigonodon* (Fig. 12), other than the anterior shape of the jugal, largely covering the maxilla. Indeed, in addition of a comparable configuration of the braincase and the palate, these two species share a similar architecture for the postorbital region, with an anteroposteriorly and dorsally well-extended quadratojugal, a triangular squamosal and a notched posterior extremity of the jugal. The architecture of the skull roof is also distinctive as it is marked by the presence of a prominent mediolaterally oriented ridge on the postfrontal, forming the anterior margin of the supratemporal fenestra and a prominent parasagittal crest on the parietal that anteriorly ends in a slender process slightly covering the slender frontal that only reaches the anterior margin of the parietal foramen. These common features on the skull roof only occur in *T. trigonodon*, *T. zetlandicus* and *T.* cf. *zetlandicus* (MNHNL TU885) (Figs 7, 12).

Despite these similarities, *T. zetlandicus* differs from *T. trigonodon* in a number of aspects (Fig. 12). The size of the skull is effectively smaller (~1 m in *T. zetlandicus* vs. > 1.5 m in *T. trigonodon*; see Supporting Information, Table S1), as is the relative size of the postorbital region (length of the postorbital region/length of the orbit ratio: ~0.5 for *T. zetlandicus* vs. ~0.8–0.9 for *T. trigonodon*; see Supplementary Information, Table S1). These differences could be due to variation in ontogenetic stages even if we are confident that CAMSM J35176 represents an adult specimen (see above). In addition to these variations in skull proportions, the lacrimal is notched and less extended dorsally in *T. zetlandicus* and the nasal, which does not possess a postnarial descending process, overlaps the postfrontal by two processes, the most lateral being digitated. Therefore, we consider these differences as sufficient to classify *T. zetlandicus* and *T. trigonodon* as two distinct but closely related species from the Early Toarcian of western Europe.

Taxonomic content and phylogenetic relationships of *Temnodontosaurus*

Despite recent progress (Swaby & Lomax, 2020) and our propositions (see above), *Temnodontosaurus* remains a loosely defined entity for which it is still complex to find compelling apomorphies (Swaby & Lomax, 2020; but see the emended diagnosis of the genus in Martin *et al.*, 2012). Whilst awaiting autapomorphy- and synapomorphy-based diagnoses, *Temnodontosaurus* as currently defined is possibly a wastebasket taxon containing large neoichthyosaurians from the Lower Jurassic (Swaby & Lomax, 2020). However, some species such as *T. crassimanus*, *T. platyodon*, *T. trigonodon* and *T. zetlandicus* appear sufficiently phylogenetically stable and well preserved, in contrary to *T. azerguensis*, *T. eurycephalus* McGowan, 1974 and *T. nuertingensis*, to form the core of *Temnodontosaurus*. Therefore, we

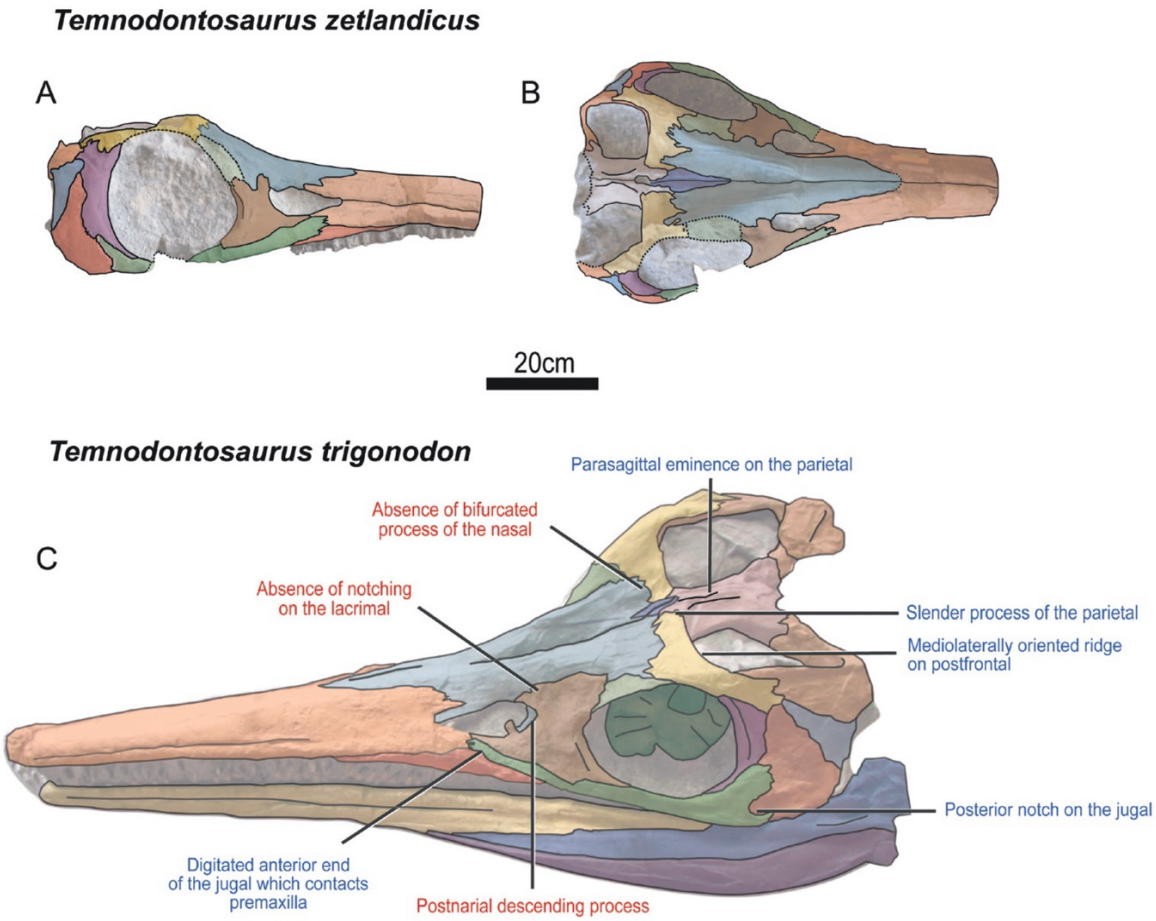

Figure 12. Anatomical comparison between the skulls of *Temnodontosaurus zetlandicus* comb. nov. and *Temnodontosaurus trigonodon*. A, B, interpretation of the lateral and the dorsal view of the holotype of *Temnodontosaurus zetlandicus* comb. nov. (CAMSM J35176), respectively. C, interpretation of *Temnodontosaurus trigonodon* (SMNS 15950), modified from Swaby & Lomax (2020). The blue-coloured labels indicate shared features whereas the red-coloured labels indicate morphological differences with *Temnodontosaurus zetlandicus* comb. nov.

suggest that diagnostic revisions of the genus be based on osteological examination of these species.

Members of *Temnodontosaurus* are still relatively well clustered among Jurassic parvipelvians in all of our phylogenetic analyses. This demonstrates that despite a diagnosis based on mainly phenetics, species currently included in the genus seem to be phylogenetically close even if they do not form a monophyletic entity. Nevertheless, the lack of statistical support demonstrates that interrelationships of *Temnodontosaurus* are far from being stable and are in need of new data. This phylogenetic instability can also be extended to the other clades of non-ophthalmosaurid parvipelvians as demonstrated by the low symmetric resampling values and the placement of Ichthyosauridae contrasting with previous topologies (Fischer *et al.*, 2016; Lomax, 2016; Lomax & Massare, 2016; Zverkov & Jacobs, 2020). For all of these reasons, our results combined with those of previous studies attest to the need to continue thorough osteological and phylogenetic re-evaluations that are ongoing (Martin *et al.*, 2012; Maxwell *et al.*, 2012; Fischer *et al.*, 2013; Marek *et al.*, 2015; Lomax, 2016; Maxwell, 2018; Lomax *et al.*, 2019; Swaby & Lomax, 2020) to find new and more suitable characters in order to clarify the tempo and the shape of the neoichthyosaurian radiation.

CONCLUSION

This paper provides an osteological redescription the holotype of '*Ichthyosaurus*' *zetlandicus*, which was previously synonymized under '*Ichthyosaurus*' *acutirostris*, which itself had been incorporated in various genera in the past. Anatomical evidence indicates that '*I.*' *zetlandicus* represents a valid taxon within *Temnodontosaurus* and is distinct from '*I.*' *acutirostris*. Instead, '*I.*' *zetlandicus* shares morphological traits with *Temnodontosaurus nuertingensis* and *T. trigonodon* and is phylogenetically close to these two species. We thus reassign '*Ichthyosaurus*' *zetlandicus* to *T. zetlandicus* and we also refer a new specimen from the Toarcian of Luxembourg to *Temnodontosaurus* cf. *zetlandicus*. Our phylogenetic analyses using multiple optimality criteria suggest that even if *Temnodontosaurus* as currently defined is not monophyletic, many of its members are relatively well clustered among Early Jurassic parvipelvians and could serve as a core to redefine the genus. Therefore, this study marks another step in revising the problematic taxonomy of *Temnodontosaurus* and provides new information about its interrelationships, despite the need for additional data to recover a stable phylogeny.

ACKNOWLEDGMENTS

We would like to thank Matt Riley (CAMSM), Erin Maxwell (SMNS) and Brigitte Eichner-Grünbeck (PB) for the opportunity to access to materials. AL would like to thank Emily Swaby for the authorisation to modify the figure which includes the specimen SMNS 15950. RFB would like to thank Eckhard Mönnig (Naturkunde-Museum Coburg) for his assistance facilitating the visit to PB. The work of AL and RFB was supported by the Fond de la Recherche Scientifique doctoral (F.R.S– FNRS) FRIA grant (AL grant number FC38761 and RFB grant number FC 23645) and the Yorkshire Geological Society Fearnsides Award (RFB). We would also like to thank Dean Lomax and Erin Maxwell again for their thorough reviews which have greatly contributed to the improvement of this paper.

REFERENCES

Bapst DW. 2012. Paleotree: an R package for paleontological and phylogenetic analyses of evolution. *Methods in Ecology and Evolution* **3:** 803–807.

Bardet N. 1992. Stratigraphic evidence for the extinction of the ichthyosaurs. *Terra Nova* **4:** 649–656.

Bell MA, Lloyd GT. 2015. strap: an R package for plotting phylogenies against stratigraphy and assessing their stratigraphic congruence. *Palaeontology* **58:** 379–389.

Benton MJ, Spencer PS. 1995. Fossil reptiles of Great Britain. Volume 10. London: Chapman & Hall, pp XII, 386. *Archives of Natural History* **23:** 150–151.

Benton MJ, Taylor MA. 1984. Marine reptiles from the Upper Lias (Lower Toarcian, Lower Jurassic) of the Yorkshire coast. *Proceedings of the Yorkshire Geological Society* **44:** 399–429.

Bindellini G, Wolniewicz AS, Miedema F, Scheyer TM, Dal Sasso C. 2021. Cranial anatomy of *Besanosaurus leptorhynchus* Dal Sasso & Pinna, 1996 (Reptilia: Ichthyosauria) from the Middle Triassic Besano Formation of Monte San Giorgio, Italy/Switzerland: taxonomic and palaeobiological implications. *PeerJ* **9:** e11179.

Blainville HMD. 1835. Description de quelques espèces de reptiles de la Californie: précédée de l'analyse d'un système général d'erpétologie et d'amphibiologie. *Nouvelles Annales du Muséum d'Histoire Naturelle, Paris* **4:** 233–296.

Böttcher R. 1989. Über die Nahrung eines *Leptopterygius* (Ichthyosauria, Reptilia) aus dem süddeutschen Posidonienschiefer (Unterer Jura) mit Bemerkungen über den Magen der Ichthyosaurier. *Stuttgarter Beiträge zur Naturkunde, Serie B (Geologie und Paläontologie)* **155:** 1–19.

Caine H, Benton MJ. 2011. Ichthyosauria from the Upper Lias of Strawberry Bank, England. *Palaeontology* **54:** 1069–1093.

Chapman SD, Doyle AM. 2002. *An initial investigation into the acquisition and conservation history of the fossil marine reptile* Stenopterygius acutirostris *(Owen) from the Upper Liassic near Whitby, Yorkshire, England*.

Dick DG, Maxwell EE. 2015. The evolution and extinction of the ichthyosaurs from the perspective of quantitative ecospace modelling. *Biology Letters* **11:** 20150339.

Fernández M. 1994. A new long-snouted ichthyosaur from the Early Bajocian of Neuquén basin (Argentina). *Ameghiniana* **31:** 291–297.

Fernández M, Archuby F, Talevi M, Ebner R. 2005. Ichthyosaurian eyes: paleobiological information content in the sclerotic ring of *Caypullisaurus* (Ichthyosauria, Ophthalmosauria). *Journal of Vertebrate Paleontology* **25:** 330–337.

Fischer V. 2016. Taxonomy of *Platypterygius campylodon* and the diversity of the last ichthyosaurs. *PeerJ* **4:** 1–21.

Fischer V, Appleby RM, Naish D, Liston J, Riding JB, Brindley S, Godefroit P. 2013. A basal thunnosaurian from Iraq reveals disparate phylogenetic origins for Cretaceous ichthyosaurs. *Biology Letters* **9:** 1–6.

Fischer V, Arkhangelsky MS, Uspensky GN, Stenshin IM, Godefroit P. 2013. A new Lower Cretaceous ichthyosaur from Russia reveals skull shape conservatism within Ophthalmosaurinae. *Geological Magazine* **151:** 60–70.

Fischer V, Bardet N, Benson RBJ, Arkhangelsky MS, Friedman M. 2016. Extinction of fish-shaped marine reptiles associated with reduced evolutionary rates and global environmental volatility. *Nature Communications* **7:** 10825.

Fischer V, Benson RBJ, Zverkov NG, Soul LC, Arkhangelsky MS, Lambert O, Stenshin IM, Uspensky GN, Druckenmiller PS. 2017. Plasticity and

convergence in the evolution of short-necked plesiosaurs. *Current Biology* **27:** 1667–1676.

Fischer V, Cappetta H, Vincent P, Garcia G, Goolaerts S, Martin JE, Roggero D, Valentin X. 2014. Ichthyosaurs from the French Rhaetian indicate a severe turnover across the Triassic–Jurassic boundary. *Naturwissenschaften* **101:** 1027–1040.

Fischer V, Maclaren JA, Bennion RF, Druckenmiller PS, Benson RBJ. 2020. The macroevolutionary landscape of short-necked plesiosaurians. *Scientific Reports* **10:** 16434.

Fischer V, Maisch MW, Naish D, Kosma R, Liston J, Joger U, Krüger FJ, Pardo Pérez J, Tainsh J, Appleby RM. 2012. New ophthalmosaurid ichthyosaurs from the European Lower Cretaceous demonstrate extensive ichthyosaur survival across the Jurassic-Cretaceous boundary. *PLoS One* **7:** e29234.

Fischer V, Masure E, Arkhangelsky MSMS, Godefroit P. 2011. A new Barremian (Early Cretaceous) ichthyosaur from western Russia. *Journal of Vertebrate Paleontology* **31:** 1010–1025.

Fischer V, Weis R, Thuy B. 2021. Refining the marine reptile turnover at the Early-Middle Jurassic transition. *PeerJ* **9:** e10647.

Fraas EE. 1913. Ein unverdrückter *Ichthyosaurus*-Schädel. *Jahreshefte des Vereins für Vaterländische Naturkunde in Württemberg* **69:** 1–12.

Godefroit P. 1993a. Les grands ichthyosaures sinémuriens d'Arlon. *Bulletin de l'Institut Royal des Sciences Naturelles de Belgique Sciences de la Terre* **63:** 25–71.

Godefroit P. 1993b. The skull of *Stenopterygius longifrons* (Owen, 1881). *Revue de Paléobiologie de Genève volume spécial* **7:** 67–84.

Godefroit P. 1994. Les reptiles marins du Toarcien (Jurassique inférieur) belgo-luxembourgeois. *Mémoires pour Servir à l'Explication des Cartes Géologiques et Minières de la Belgique* **39:** 98.

Goloboff PA, Catalano SA. 2016. TNT version 1.5, including a full implementation of phylogenetic morphometrics. *Cladistics* **32:** 221–238.

Goloboff PA, Farris JS, Källersjö M, Oxelman B, Ramìrez MJ, Szumik CA. 2003. Improvements to resampling measures of group support. *Cladistics* **19:** 324–332.

Goloboff PA, Farris JS, Nixon KC. 2008. TNT, a free program for phylogenetic analysis. *Cladistics* **24:** 774–786.

Goloboff PA, Torres A, Arias JS. 2018. Weighted parsimony outperforms other methods of phylogenetic inference under models appropriate for morphology. *Cladistics* **34:** 407–437.

Hermoso M, Delsate D, Baudin F, Le Callonnec L, Minoletti F, Renard M, Faber A. 2014. Record of Early Toarcian carbon cycle perturbations in a nearshore environment: the Bascharage section (easternmost Paris Basin). *Solid Earth* **5:** 793–804.

Hodges P, Simms M, Page K. 2004. 1. British Lower Jurassic stratigraphy: an introduction. *Geological Conservation Review Series* **30:** 28–37.

von Huene F. 1922. Die Ichthyosaurier des Lias und ihre Zusammenhänge. In: *Monographien zur Geologie und Paläontologie, 1*. Berlin: Borntraeger.

von Huene F. 1931. Neue Ichthyosaurier aus Württemberg. *Neues Jahrbuch für Mineralogie, Geologie und Paläontologie. Beilage. Abteilung B* **65:** 305–320.

Johnson MM, Young MT, Brusatte SL, Thuy B, Weis R. 2019. A catalogue of teleosauroids (Crocodylomorpha: Thalattosuchia) from the Toarcian and Bajocian (Jurassic) of southern Luxembourg. *Historical Biology* **31:** 1179–1194.

Kelley NP, Pyenson ND. 2015. Evolutionary innovation and ecology in marine tetrapods from the Triassic to the Anthropocene. *Science* **348:** aaa3716.

Lomax DR. 2016. A new leptonectid ichthyosaur from the Lower Jurassic (Hettangian) of Nottinghamshire, England, UK, and the taxonomic usefulness of the ichthyosaurian coracoid. *Journal of Systematic Palaeontology* **15:** 387–401.

Lomax DR. 2019. Ichthyopterygia. In: Lord AR, Munt M, eds. *Fossils from the Lias of the Yorkshire Coast*. London: The Palaeontological Association, 317–331.

Lomax DR, Massare JA. 2016. Two new species of *Ichthyosaurus* from the lowermost Jurassic (Hettangian) of Somerset, England. *Papers in Palaeontology* **3:** 1–20.

Lomax DR, Massare JA. 2018. A second specimen of *Protoichthyosaurus applebyi* (Reptila: Ichthyosauria) and additional information on the genus and species. *Paludicola* **11:** 164–178.

Lomax DR, Massare JA, Evans M. 2020. New information on the skull roof of *Protoichthyosaurus* (Reptilia: Ichthyosauria) and intraspecific variation in some dermal skull elements. *Geological Magazine* **157:** 640–650.

Lomax DR, Porro LB, Larkin NR. 2019. Descriptive anatomy of the largest known specimen of *Protoichthyosaurus prostaxalis* (Reptilia: Ichthyosauria) including computed tomography and digital reconstruction of a three-dimensional skull. *PeerJ* **7:** e6112.

Lydekker R. 1889. Palaeozoology: Vertebrata. In: *A manual of palaeontology for the use of students with a general introduction on the principles of palaeontology, 3rd edn*. Edinburgh: W. Blackwood, 889–1464.

Maisch MW. 1997. A case against a diapsid origin of the Ichthyosauria. *Neues Jahrbuch für Geologie und Paläontologie, Abhandlungen* **205:** 111–127.

Maisch MW. 1998a. A new ichthyosaur genus from the Posidonia Shale (Lower Toarcian, Jurassic) of Holzmaden, SW-Germany with comments on the phylogeny of post-Triassic ichthyosaurs. *Neues Jahrbuch für Geologie und Paläontologie, Abhandlungen* **209:** 47–78.

Maisch MW. 1998b. Short review of the ichthyosaurs of the Posidonienschiefer with remarks on the taxonomy of the Stenopterygiidae and Temnodontosauridae. *Neues Jahrbuch für Geologie und Paläontologie, Abhandlungen* **209:** 401–431.

Maisch MW. 2001. Neue Exemplare der seltenen Ichthyosaurier Gattung *Suevoleviathan* Maisch 1998 aus dem Unteren Jura von Südwestdeutschland. *Geologica et Palaeontologica* **35:** 145–160.

Maisch MW. 2002. A braincase of *Temnodontosaurus cf. trigonodon* (von Theodori, 1843) (Ichthyosauria) from the Lower Jurassic of Germany. *Geologica et Palaeontologica* **36:** 115–122.

Maisch MW. 2008. Revision der Gattung *Stenopterygius* Jaekel, 1904 emend. von Huene, 1922 (Reptilia: Ichthyosauria) aus dem unteren Jura Westeuropas. *Palaeodiversity* **1:** 227–271.

Maisch M. 2010. Phylogeny, systematics, and origin of the Ichthyosauria—the state of the art. *Palaeodiversity* **3:** 151–214.

Maisch MW, Hungerbühler A. 1997. Revision of *Temnodontosaurus nuertingensis* (v. Huene, 1931), a large ichthyosaur from the Lower Pliensbachian (Lower Jurassic) of Nürtingen, South Western Germany. *Stuttgarter Beiträge zur Naturkunde Serie B (Geologie und Paläontologie)* **248:** 1–11.

Maisch MW, Hungerbühler A. 2001. New evidence for a discrete supratemporal bone in the Jurassic Ichthyosaur *Temnodontosaurus*. *Historical Biology* **15:** 335–345.

Maisch MW, Mazke AT. 1997. *Mikadocephalus gracilirostris* n. gen., n. sp., a new ichthyosaur from the Grenzbitumenzone (Anisian-Ladinian) of Monte San Giorgio (Switzerland). *Paläontologische Zeitschrift* **71:** 267–289.

Maisch MW, Matzke AT. 2000. The Ichthyosauria. *Stuttgarter Beiträge zur Naturkude, Serie B (Geologie und Paläontologie)* **298:** 1–159.

Maisch MW, Matzke AT. 2003. The cranial osteology of the ichthyosaur *Leptonectes tenuirostris* from the Lower Jurassic of England. *Journal of Vertebrate Paleontology* **23:** 116–127.

Marek RD, Moon BC, Williams M, Benton MJ. 2015. The skull and endocranium of a Lower Jurassic ichthyosaur based on digital reconstructions. *Palaeontology* **58:** 723–742.

Martin JE, Fischer V, Vincent P, Suan G. 2012. A longirostrine *Temnodontosaurus* (Ichthyosauria) with comments on Early Jurassic ichthyosaur niche partitioning and disparity. *Palaeontology* **55:** 995–1005.

Martin JE, Vincent P, Suan G, Sharpe T, Hodges P, Williams M, Howells C, Fischer V. 2015. A mysterious giant ichthyosaur from the lowermost Jurassic of Wales. *Acta Palaeontologica Polonica* **60:** 837–842.

Massare JA. 1997. Faunas, behavior, and evolution. In: Callaway JM, Nicholls EL, eds. *Ancient marine reptiles*. San Diego: Academic Press, 401–421.

Massare JA, Lomax DR. 2016. A new specimen of *Ichthyosaurus conybeari* (Reptilia, Ichthyosauria) from Watchet, Somerset, England, U.K., and a re-examination of the species. *Journal of Vertebrate Paleontology* **36:** 5.

Massare JA, Wahl WR, Lomax DR. 2021. Narial structures in *Ichthyosaurus* and other Early Jurassic ichthyosaurs as precursors to a completely subdivided naris. *Paludicola* **13:** 128–139.

Maxwell EE. 2012. New metrics to differentiate species of *Stenopterygius* (Reptilia: Ichthyosauria) from the Lower Jurassic of southwestern Germany. *Journal of Paleontology* **86:** 105–115.

Maxwell EE. 2018. Redescription of the lost holotype of *Suevoleviathan integer* (Bronn, 1844) (Reptilia: Ichthyosauria). *Journal of Vertebrate Paleontology* e1439833: 1–6.

Maxwell EE, Cortés D. 2020. A revision of the Early Jurassic ichthyosaur *Hauffiopteryx* (Reptilia: Ichthyosauria), and description of a new species from southwestern Germany. *Palaeontologia Electronica* **23:** a31.

Maxwell EE, Cortés D, Patarroyo P, Ruge MLP. 2019. A new specimen of *Platypterygius sachicarum* (Reptilia, Ichthyosauria) from the Early Cretaceous of Colombia and its phylogenetic implications. *Journal of Vertebrate Paleontology* **39:** 1–12.

Maxwell EE, Fernández MS, Schoch RR. 2012. First diagnostic marine reptile remains from the Aalenian (Middle Jurassic): a new ichthyosaur from southwestern Germany. *PLoS One* **7:** e41692.

McCurry MR, Fitzgerald EMG, Evans AR, Adams JW, Mchenry CR. 2017. Skull shape reflects prey size niche in toothed whales. *Biological Journal of the Linnean Society* **121:** 936–946.

McGowan C. 1973. The cranial morphology of the Lower Liassic latipinnate ichthyosaurs of England. *Bulletin of the British Museum (Natural History) Geology* **24:** 1–109.

McGowan C. 1974. A revision of the longipinnate ichthyosaurs of the Lower Jurassic of England, with description of the new species (Reptilia, Ichthyosauria). *Life Science Contributions, Royal Ontario Museum* **97:** 1–37.

McGowan C. 1989. *Leptopterygius tenuirostris* and other long-snouted ichthyosaurs from the English Lower Lias. *Palaeontology* **32:** 409–427.

McGowan C. 1994. *Temnodontosaurus risor* is a juvenile of *T. platyodon* (Reptilia: Ichthyosauria). *Journal of Vertebrate Paleontology* **14:** 472–479.

McGowan C. 1996a. Giant ichthyosaurs of the Early Jurassic. *Canadian Journal of Earth Sciences* **33:** 1011–1021.

McGowan C. 1996b. The taxonomic status of *Leptopterygius* Huene, 1922 (Reptilia: Ichthyosauria). *Canadian Journal of Earth Sciences* **33:** 439–443.

McGowan C. 1997. A transitional ichthyosaur fauna. In: Callaway JM, Nicholls EL, eds. *Ancient marine reptiles*. San Diego: Academic Press, 61–80.

McGowan C, Motani R. 2003. *Ichthyopterygia. Handbook of paleoherpetology. Part 8*. Munich: Friedrich Pfeil.

Miedema F, Maxwell EE. 2019. Ontogeny of the braincase in *Stenopterygius* (Reptilia, Ichthyosauria) from the Lower Jurassic of Germany. *Journal of Vertebrate Paleontology* **39:** e1675164.

Miller MA, Pfeiffer W, Schwartz T. 2010. Creating the CIPRES Science Gateway for inference of large phylogenetic trees. In: *2010 Gateway Computing Environments Workshop (GCE)*. New Orleans, LA, USA: Institute of Electrical and Electronics Engineers, 1–8. doi:10.1109/GCE.2010.5676129

Moon BC. 2017. A new phylogeny of ichthyosaurs (Reptilia: Diapsida). *Journal of Systematic Palaeontology* **17:** 129–155.

Moon BC, Kirton AM. 2016. Ichthyosaurs of the British Middle and Upper Jurassic Part 1, *Ophthalmosaurus*. *Monographs of the Palaeontographical Society* **170:** 1–84.

Motani R. 1999a. On the evolution and homologies of ichthyosaurian forefins. *Journal of Vertebrate Paleontology* **19:** 28–41.

Motani R. 1999b. Phylogeny of the Ichthyopterygia. *Journal of Vertebrate Paleontology* **19:** 473–496.

Motani R. 2005. Evolution of fish-shaped reptiles (Reptilia: Ichtyopterygia) in their physical environments and constraints. *Annual Review of Earth and Planetary Sciences* **33:** 395–420.

Motani R, Jiang D, Tintori A, Ji C, Huang J. 2017. Pre-versus post-mass extinction divergence of Mesozoic marine reptiles dictated by time-scale dependence of evolutionary rates. *Proceedings of the Royal Society series B* **284:** 20170241.

Owen R. 1865–1881. *A monograph of the fossil Reptilia of the Liassic Formations, part third:* Plesiosaurus, Dimorphodon, *and* Ichthyosaurus. London: Monographs of the Palæontographical Society, 12–130.

Paradis E, Claude J, Strimmer K. 2004. APE: analyses of phylogenetics and evolution in R language. *Bioinformatics* **20:** 289–290.

Pardo-Pérez JM, Kear BP, Mallison H, Gómez M, Moroni M, Maxwell EE. 2018. Pathological survey on *Temnodontosaurus* from the Early Jurassic of southern Germany. *PLoS One* **13:** e0204951.

Pol D, Escapa IH. 2009. Unstable taxa in cladistic analysis: identification and the assessment of relevant characters. *Cladistics* **25:** 515–527.

Powell J. 2010. Jurassic sedimentation in the Cleveland Basin: a review. *Proceedings of the Yorkshire Geological Society* **58:** 21–72.

Ronquist F, Klopfstein S, Vilhelmsen L, Schulmeister S, Murray DL, Rasnitsyn AP. 2012. A total-evidence approach to dating with fossils, applied to the early radiation of the hymenoptera. *Systematic Biology* **61:** 973–999.

Sander PM. 2000. Ichthyosauria: their diversity, distribution, and phylogeny. *Paläontologische Zeitschrift* **7:** 1–35.

Seeley HG. 1880. On the skull of an *Ichthyosaurus* from the Lias of Whitby, apparently indicating a new species (*I. zetlandicus*, Seeley), preserved in the Woodwardian Museum of the University of Cambridge. *Quarterly Journal of the Geological Society* **36:** 635–647.

Smith MR. 2019. Bayesian and parsimony approaches reconstruct informative trees from simulated morphological datasets. *Biology Letters* **15:** 20180632.

Streitz JC. 1983. *Auf Fossiliensuche in Luxemburg. Entstehung und Beschreibung einer bemerkenswerten Privatsammlung*. Luxembourg: Imprimerie Saint-Paul.

Swaby EJ, Lomax DR. 2020. A revision of *Temnodontosaurus crassimanus* (Reptilia: Ichthyosauria) from the Lower Jurassic (Toarcian) of Whitby, Yorkshire, UK. *Historical Biology* **33:** 2715–2731.

Templeton AR. 1983. Phylogenetic inference from restriction endonuclease cleavage site maps with particular reference to the evolution of humans and the apes. *Evolution* **37:** 221–244.

Theodori C. 1843. Über einen kolossalen *Ichthyosaurus trigonodon*. *Gelehrte Anzeigen der Königlich Bayerischen Akademie der Wissenschaften, München* **16:** 906–911.

Thorne PM, Ruta M, Benton MJ. 2011. Resetting the evolution of marine reptiles at the Triassic-Jurassic boundary. *Proceedings of the National Academy of Sciences of the USA* **108:** 8339–8344.

Vincent P, Taquet P, Fischer V, Bardet N, Falconnet J, Godefroit P. 2014. Mary Anning's legacy to French vertebrate palaeontology. *Geological Magazine* **151:** 7–20.

Vincent P, Weiss R, Kronz G, Delsate D. 2017. *Microcleidus melusinae*, a new plesiosaurian (Reptilia, Plesiosauria) from the Toarcian of Luxembourg. *Geological Magazine* **156:** 99–116.

Zverkov N, Jacobs M. 2020. Revision of *Nannopterygius* (Ichthyosauria: Ophthalmosauridae): reappraisal of the 'inaccessible' holotype resolves a taxonomic tangle and reveals an obscure ophthalmosaurid lineage with a wide distribution. *Zoological Journal of the Linnean Society* **191:** 228–275.

SUPPORTING INFORMATION

Additional Supporting Information may be found in the online version of this article at the publisher's web-site:

File S1. Character-taxon matrix used for phylogenetic analyses.
File S2. Character-taxon matrix and parameters for Bayesian analysis. Character list copied from the study of Maxell & Cortés (2020) and character coding revision.
Figure S1. Schematic stratigraphic log of the Whitby coastal section in North Yorkshire (UK).
Figure S2. Time-scaled phylogenetic tree, arising from implied weighting (k = 6) maximum parsimony analysis, in 'equal' reconstruction branch lengths.
Figure S3. Time-scaled phylogenetic tree in which the monophyly of *Temnodontosaurus* is forced, arising from implied weighting (k = 9) maximum parsimony analysis, in 'equal' reconstruction branch lengths.
Figure S4. Time-scaled phylogenetic tree arising from implied weighting (k = 12) maximum parsimony analysis, in 'equal' reconstruction branch lengths.
Figure S5. Majority rule consensus cladogram generated with a Bayesian analysis.
Table S1. Selected measurements (mm) and notable cranial ratios between *T. zetlandicus*, *'I.' acutirostris* and *T. trigonodon*.

Appendix II

Fischer, V., **A. Laboury**, K. Bernacki, L. Garbay, Y. Gillen, C. Rollinger, A. Thill, R. Weis, and B. Thuy. 2022. A fragmentary leptonectid ichthyosaurian from the lower Pliensbachian of Luxembourg. *Palaeontologia Electronica* 25.

Palaeontologia Electronica
palaeo-electronica.org

A fragmentary leptonectid ichthyosaurian from the lower Pliensbachian of Luxembourg

Valentin Fischer, Antoine Laboury, Kamil Bernacki, Laurent Garbay, Yan Gillen, Charel Rollinger, Anjin Thill, Robert Weis, and Ben Thuy

ABSTRACT

Despite abundant fossils, the quality of the fossil record of Early Jurassic marine reptiles strongly fluctuates with time and space. Pliensbachian strata have yielded very few marine reptile remains, especially outside of England, obscuring the evolution of marine reptiles during the middle part of the Early Jurassic. We report a new Pliensbachian locality from Luxembourg that contains abundant marine fauna and ichthyosaurian remains likely representing a single individual, composed of a partial snout, a possible surangular, two centra, and several ribs and gastralia. Ammonites and belemnites place this locality within the Valdani-Luridum Ammonite subzones of the Ibex Ammonite Zone, lower Pliensbachian. We assign the new ichthyosaur specimen to the clade Leptonectidae, using a combination of features from the snout and teeth. This specimen indicates that large neoichthyosaurians were present in multiple places of the European archipelago in all stages of the Early Jurassic and suggests that the ichthyosaurian faunae of western Europe remained essentially similar across the Sinemurian–Pliensbachian interval.

Valentin Fischer. Evolution & Diversity Dynamics Lab, UR Geology, Université de Liège, Belgium (corresponding author). v.fischer@uliege.be
Antoine Laboury. Evolution & Diversity Dynamics Lab, UR Geology, Université de Liège, Belgium. a.laboury@uliege.be
Kamil Bernacki. Department of Palaeontology, Natural History Museum Luxembourg, Luxembourg, Grand-Duchy of Luxembourg. kamil_bernacki@yahoo.com
Laurent Garbay. Department of Palaeontology, Natural History Museum Luxembourg, Luxembourg, Grand-Duchy of Luxembourg. garblaur@gmail.com
Yan Gillen. Department of Palaeontology, Natural History Museum Luxembourg, Luxembourg, Grand-Duchy of Luxembourg. gillen.yan@gmail.com
Charel Rollinger. Department of Palaeontology, Natural History Museum Luxembourg, Luxembourg, Grand-Duchy of Luxembourg. Charel.ROLLINGER@mnhn.lu
Anjin Thill. Department of Palaeontology, Natural History Museum Luxembourg, Luxembourg, Grand-Duchy of Luxembourg. anjin@caspersclimbingshop.com

Final citation: Fischer, Valentin, Laboury, Antoine, Bernacki, Kamil, Garbay, Laurent, Gillen, Yan, Rollinger, Charel, Thill, Anjin, Weis, Robert, and Thuy, Ben. 2022. A fragmentary leptonectid ichthyosaurian from the lower Pliensbachian of Luxembourg. Palaeontologia Electronica, 25(2):a24. https://doi.org/10.26879/1205
palaeo-electronica.org/content/2022/3685-pliensbachian-leptonectid

Robert Weis. Department of Palaeontology, Natural History Museum Luxembourg, Luxembourg, Grand-Duchy of Luxembourg. RWEIS@mnhn.lu
Ben Thuy. Department of Palaeontology, Natural History Museum Luxembourg, Luxembourg, Grand-Duchy of Luxembourg. Ben.THUY@mnhn.lu.

Keywords: Neoichthyosauria; Leptonectidae; Early Jurassic; Luxembourg-Trier

Submission: 5 January 2022. Acceptance: 2 August 2022.

INTRODUCTION

Mesozoic marine reptiles have an abundant fossil record, documenting the beginning of their radiation during the earliest Triassic (Motani et al., 2015, 2017) to centimetres below the Cretaceous-Palaeogene boundary horizon (Jouve et al., 2008; Gallagher et al., 2012). However, the quality of their fossil record strongly fluctuates with time and space (Benson et al., 2010; Benson and Butler, 2011; Butler et al., 2011), and possibly less so with phylogeny (Tutin and Butler, 2017). This fluctuation appears fractal, being also present within Early Jurassic ichthyosaurians: the early Toarcian shales have provided thousands of fossils in western Europe, with most specimens from Germany and England (Hauff, 1953; Godefroit, 1994; Benson et al., 2010), while the Pliensbachian and late Toarcian assemblages are extremely poorly sampled (Bardet et al., 2008; Fernández et al., 2018; Lomax and Massare, 2018a; Fischer et al., 2021). Pliensbachian ichthyosaurian faunas generally resemble those from the Sinemurian, with the presence of *Leptonectes* (McGowan and Milner, 1999; Fernández et al., 2018; Lomax and Massare, 2018a), *Ichthyosaurus* (Lomax, 2010; Lomax and Massare, 2015; Massare and Lomax, 2016), and *Temnodontosaurus* (Huene, 1931a; Hungerbühler and Sachs, 1996; Maisch and Hungerbühler, 1997), but also *Hauffiopteryx* (Maisch and Reisdorf, 2006; Maxwell and Cortés, 2020). However, the vast majority of Pliensbachian ichthyosaurians come from England and Germany; one (Maisch and Reisdorf, 2006) is from Switzerland and another (Fernández et al., 2018) is from Spain. In this context, documenting new Pliensbachian occurrences of ichthyosaurians is important to better understand how marine predator faunas changed throughout the entire Early Jurassic. In this paper, we describe the likely associated remains of a large ichthyosaur showing leptonectid affinities from a new lower Pliensbachian locality in central Luxembourg.

MATERIAL AND METHODS

Institutional Abbreviations

BRSMG: Bristol City Museum and Art Gallery, Bristol, UK. MHNH: Muséum d'Histoire Naturelle du Havre, Le Havre, France. MNHN: Muséum National d'Histoire Naturelle, Paris, France. MNHNL: Muséum National d'Histoire Naturelle du Luxembourg, Luxembourg-ville, Luxembourg. NHMUK: Natural History Museum, London, UK. OUM: Oxford University Museum, Oxford, UK.

The Cloche d'Or Locality

The remains described herein consist of a series of articulated and disarticulated remains of a large ichthyosaurian, MNHNL LM266 from the Cloche d'Or locality, in the Gasperich quarter in southern Luxembourg City, central Luxembourg (Figure 1). The outcrop at Cloche d'Or is situated along the banks of a recently re-natured Weierbaach creek. The first fragments were found during preliminary prospections in April 2021, and most of the remains were collected during controlled excavations and prospections lead by several of us (B.T., R.W., K.B., L.G., C.R., A.T., and Y.G.) in July 2021 (Figure 2), complemented by subsequent finds cropping out after the millennial floods of summer 2021.

Lithostratigraphy of Cloche d'Or

Along the Weierbaach creek, two lithostratigraphic formations, as defined by the Geological map of Luxembourg, are exposed. The lower one, the Li4 ("Marnes pauvres en fossiles") unit, consists of blue-greyish marls with occasional micritic nodules, and yields ammonites, bivalves (mostly *Gryphaea macculocchi*, as well as cardiniids and pectinids), brachiopods (notably *Spiriferina, Zeilleria),* crinoids (*Pentacrinites* sp.), and small passaloteuthid belemnites *(Nannobelus oppeli).* The Li4 succession corresponds to our units I and II (Figure 3). The lithological transition towards the overlying formation Lm1 is not clearly visible, and approximately corresponds to unit III or the basal part of

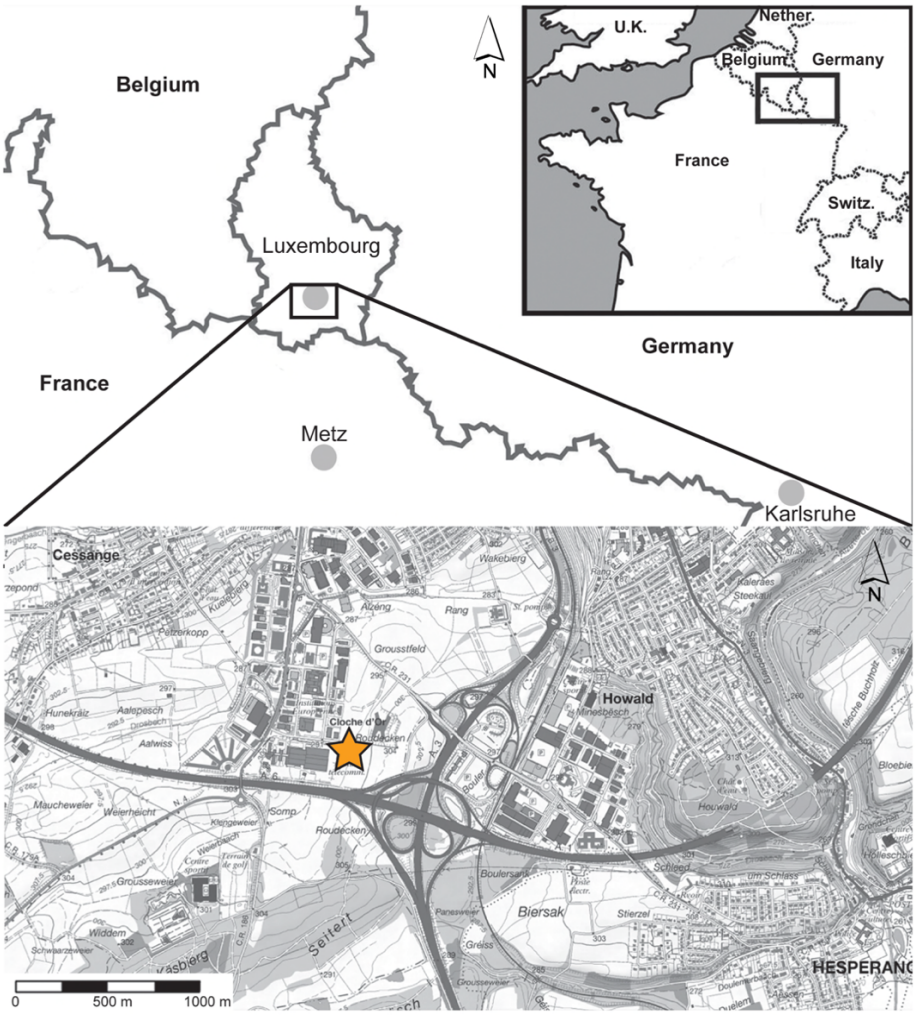

FIGURE 1. Map and location of the Cloche d'Or site, indicated by a star.

unit IV. The upper part of unit IV as well as the overlying units V-VII belong to the Lm1 ("Calcaire ocreux") formation, which consists here of sandy, yellow marls yielding numerous ammonites, echinoderm remains, and a more diversified belemnite fauna than the underlying Li4 formation. Usually, this formation consists of three members, a lower calcareous member ("Raricostaten-Schichten", roughly corresponding to the uppermost Sinemurian), a middle marly member ("Numismalis-Mergel", corresponding to the lower Pliensbachian) and an upper calcareous member ("Davoei-Kalk", also lower Pliensbachian) (Lucius, 1948; Maubeuge, 1950). The yellow marls at Cloche d'Or are interpreted here as an equivalent of the middle marly member of the Calcaire ocreux formation. This means that the lower calcareous member is missing at Cloche d'Or. A similar hiatus at the base of the formation had previously been observed for some localities in Luxembourg (Lucius, 1948; Maubeuge, 1950; Maubeuge and Antun, 1967). A more complete succession of the Li4 and Lm1 formations has been recorded in other localities, for instance Capellen (Guérin-Franiatte, 2003), to the west of Luxembourg-City. The ichthyosaur remains described in the present paper were found in unit V, corresponding to the middle marly member of the Lm1 formation.

FIGURE 2. Photograph of the Cloche d'Or locality taken on 17 June 2021 during the main excavation activities. Most of the bone fragments (MNHNL LM226) were found in the exposed layer between the two arrows.

Biostratigraphy of Cloche d'Or

The biostratigraphic interpretation of the exposed succession is based on ammonites (Figure 3). Two biozones are recognised: the Obtusum Zone of the upper Sinemurian and the Ibex Zone of the lower Pliensbachian. A characteristic association has been identified in unit VI: *Lytoceras fimbriatum* (Sowerby), *Acanthopleuroceras alisiense* (Reynès in Haug), and *Beaniceras luridum* (Simpson), an association corresponding to the upper part of the Ibex Zone (Valdani-Luridum subzones) (Christian Meister, personal communication). Belemnites retrieved from the succession corroborate and, in part, complement the ammonite-based zonation, although the biostratigraphic value of the belemnites is less precise compared to the ammonites (Riegraf, 1980; Combémorel, 1997; Schlegelmilch, 1998). Belemnites of the genus *Nannobelus*, in particular *Nannobelus oppeli*, found in units I and II, indicate an upper Sinemurian age. Belemnites of the genus *Passaloteuthis*, known from the lower Plienbachian onwards, were found in units IV to VII. Together with the ammonite association from unit VI, the belemnite evidence thus suggests that the ichthyosaur-bearing bed V is of lower Pliensbachian age. Multiple fragmentary specimens of the ammonite *Tragophylloceras* further corroborates the lower Pliensbachian age (Ibex Zone) of the ichthyosaurian specimen MNHNL LM266.

Taphonomy

The ichthyosaurian remains described in the present paper were either collected directly in bed V or picked from the weathered surface below and in the creek downstream. In some cases, fragments collected from the stream bed could be associated with fragments directly retrieved from bed V (in particular the two fragments of a possible surangular), corroborating that all the remains, in fact, originate from the same bed. Unit V consists of conspicuously bright-coloured clayey marl, readily distinguishable from the over- and underlying strata. Furthermore, unit V has yielded an extraordinary microfauna, including numerous minute spines of the echinoid *Cuspidentechinus* Smith, 2016 and cyrtocrinid remains that are absent from the under- and overlying strata. Thanks to the distinctive colour and microfauna of the adhering matrix, even bone fragments that were found downslope or in the creek could be unambiguously assigned to unit V.

The marls of unit V show no signs of re-sedimentation, reworking, or condensation, neither in macroscopic terms (e.g., reworked ammonites or belemnites, intraclasts, encrusted pebbles) nor in the microfaunal spectrum. Furthermore, the bones show no evidence of encrusting organisms or adhering matrix other than the marls from unit V. We therefore exclude the possibility of reworking or condensation to explain the co-occurrence of the

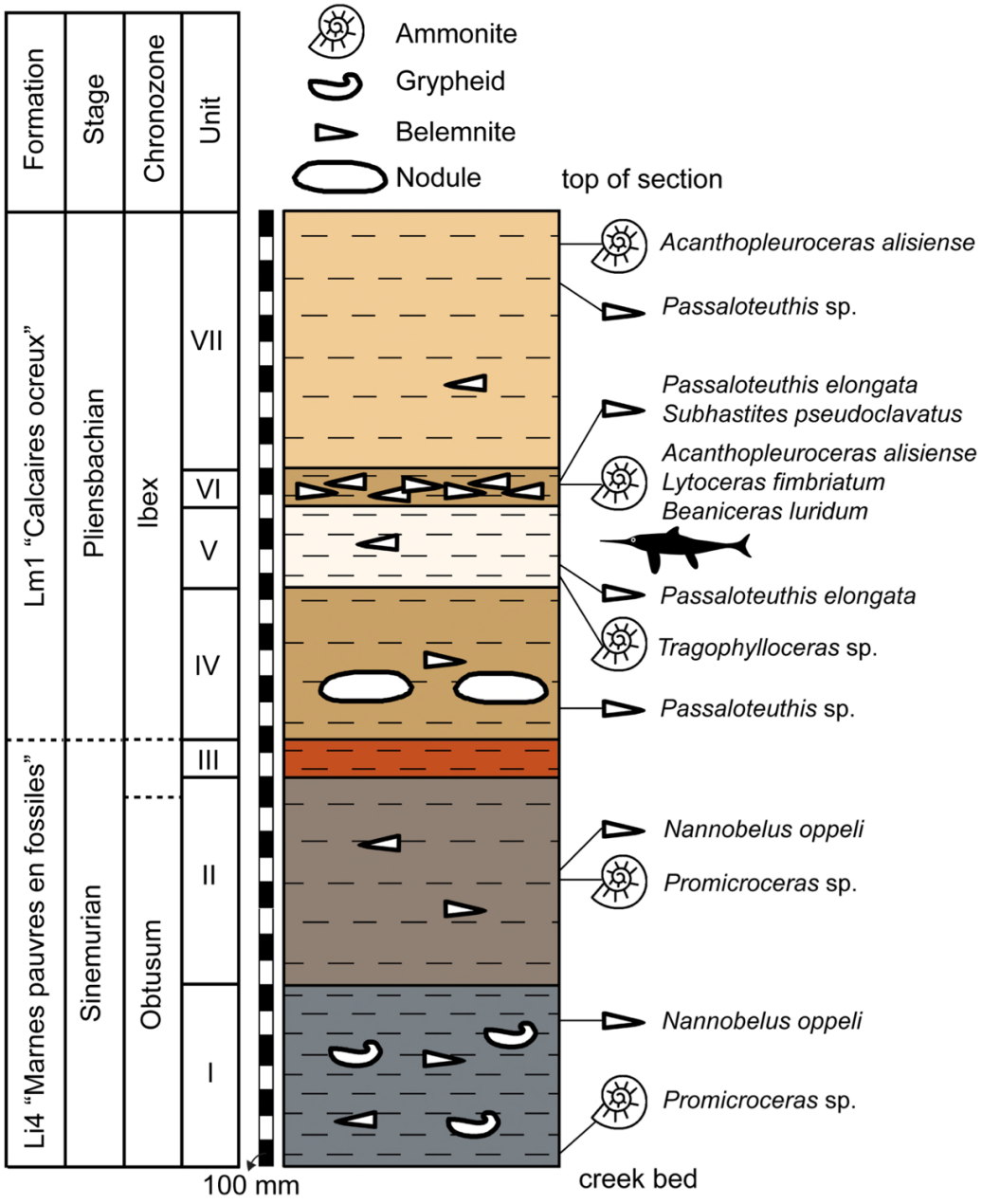

FIGURE 3. Stratigraphic log of the section at the Cloche d'Or locality.

bone fragments. While we cannot rule out that the bones belong to more than one individual, continuously controlled excavation allowed us to confirm the single origin of the bone fragments. All the remains can be traced down to a restricted area within bed V, approximately 5 m wide, on both sides of the creek.

The bone tissue is well preserved in most cases. Interestingly, some fragments, in particular the vertebra and the possible surangular, show millimetric, radially oriented scratch marks (Figure 4).

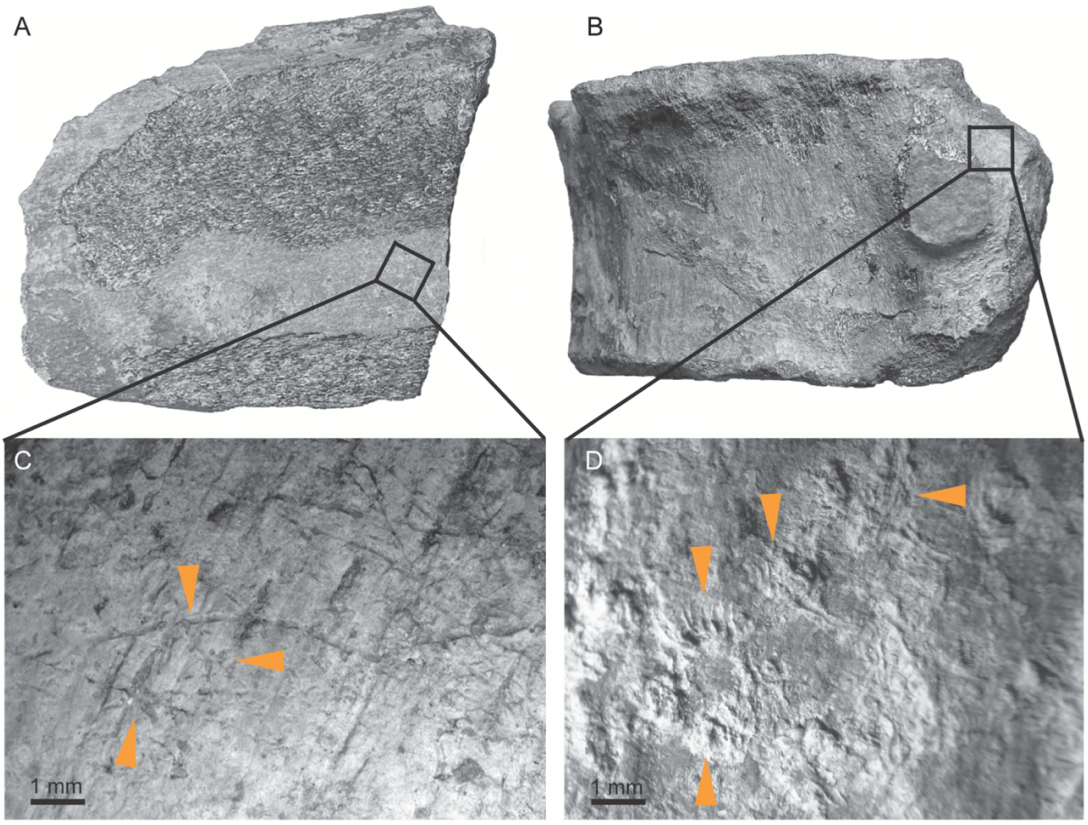

FIGURE 4. Post-mortem scratch marks. Details of the bone surface of the possible surangular (A) and a vertebral fragment (B) of MNHNL LM226. These scratch marks with their characteristic radial shape are assignable to the ichnogenus *Gnathichnus* sp. and attributed to the grazing activities of regular echinoids. The orange arrows indicate some of best-preserved marks.

The size, depth, orientation, and arrangement of the scratch marks are typical features of *Gnathichnus*, an ichnogenus attributed to the grazing activity of regular echinoids (Bromley, 1975). *Gnathichnus* is usually found on invertebrate shells or skeletal parts (e.g., Breton et al., 1992; Carrasco, 2003) but also on vertebrate bones (Meyer, 2011; Reolid et al., 2015), including on ichthyosaur remains (Danise et al., 2014). The sediment surrounding the bone fragments yields abundant spines, test plates, and masticatory apparatus components of a small regular echinoid with teeth of trapezoidal cross-section, reminiscent of the common and widespread Early Jurassic echinoid genus *Cunidentechinus*, which therefore qualifies as a possible producer of the grazing traces on the bones.

SYSTEMATIC PALAEONTOLOGY

Order ICHTHYOSAURIA De Blainville, 1835
Clade PARVIPELVIA Motani, 1999
Clade NEOICHTHYOSAURIA Sander, 2000
Family LEPTONECTIDAE Maisch, 1998
Leptonectidae indet.

Referred material. MNHNL LM266, from the lower Pliensbachian (Valdani to Luridum Ammonite subzones of the Ibex Ammonite Zone) of the Cloche d'Or locality, central Luxembourg.

Snout

Two contiguous fragments of a rostrum are preserved over 51 mm, containing articulated premaxillae, dentaries, splenials, and teeth (Figure 5). The premaxilla and the dentary are slender, being as dorsoventrally high as the apicobasal height of the corresponding tooth crowns. The premaxillary and dentary fossae are present, in the form of a

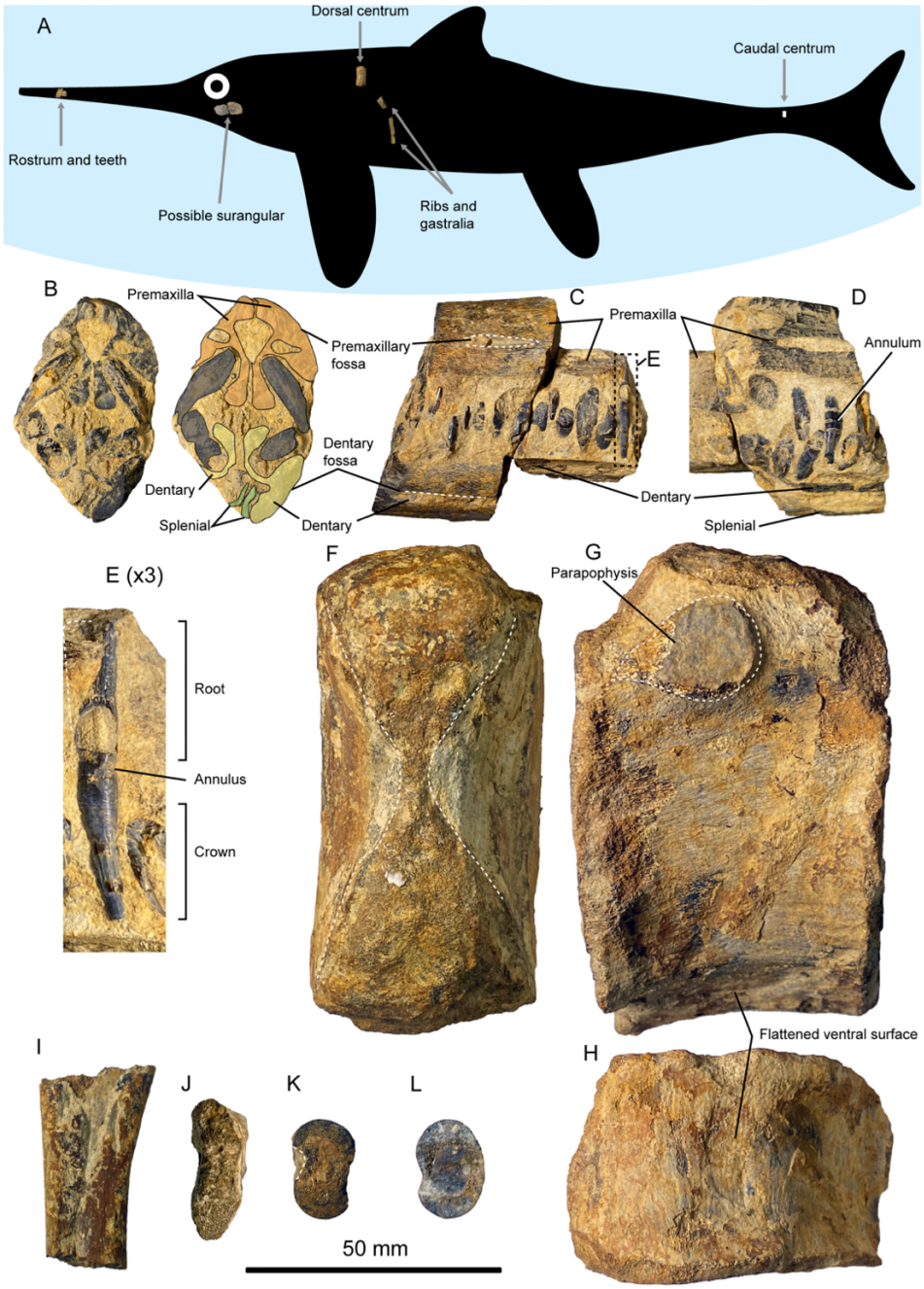

FIGURE 5. Location and anatomy of selected remains of the leptonectid ichthyosaurian MNHNL LM226. (A) silhouette with the location of selected remains; the total size of the animal is difficult to assess. (B) photograph and interpretation of the rostrum in ?anterior view. (C, D) rostrum in lateral views. (E) Detail of a tooth, magnified three times with respect to the other elements, showing the elongated crown and the near absence of striations on the root and acellular cementum ring. (F–H) fragmentary dorsal centrum in (F) medial, (G) lateroventral, (H) ventral views. (I) large rib fragment in internal view. (J) proximal cross-section of a rib, showing the 8-shaped cross-section. (K) cross-section of a rib, showing the 8-shaped cross-section. (L) distal cross-section of a rib showing the loss of one of the anterior/posterior grooves.

series of elongated foramina that are 13 mm long and 3 mm high for the premaxillary fossa and slightly longer for the dentary fossa. The anterior part of the splenial is preserved in articulation with the dentary and has a slit-like ventral exposure. The splenial thus possesses a long ventral exposure, which is similar to that of *Leptonectes moorei* (V.F. pers. obs. holotype specimen NHMUK PV R 14370) and differs from the condition seen in the rather short-snouted *Hauffiopteryx* spp., where the nasal rapidly protrude from the dorsal margin of the rostrum, extending anteriorly as far (or further) than the splenial (Marek et al., 2015; Maxwell and Cortés, 2020). In MNHNL LM266, the nasal is not even present internally, indicating its dorsal exposure is de facto set more posteriorly than that of the splenial.

The tooth crowns are slightly recurved and markedly elongated: the apicobasal height / basal diameter ratio is 11 mm / 4 mm = 2.75 (Figures 5, 6), very similar to some species of *Stenopterygius* (Maxwell, Fernández, et al., 2012), *Hauffiopteryx* (Maxwell and Cortés, 2020), and in leptonectids such as most species of *Leptonectes* (Fraas, 1892; Huene, 1922; McGowan, 1989, 1993) (with the exception of *Leptonectes moorei* [McGowan and Milner, 1999]), *Eurhinosaurus longirostris* (Reisdorf et al., 2011), and *Wahlisaurus massarae* (Lomax, 2016) (Figure 6). This condition is clearly distinct from the stouter teeth seen in *Temnodontosaurus* spp. (Fraas, 1891; McGowan, 1974; Godefroit, 1993), *Suevoleviathan* spp. (Maxwell, 2018), *Protoichthyosaurus* (Lomax and Massare, 2018b; Lomax et al., 2019), and some species of *Ichthyosaurus* (Fraas, 1891; Maisch, 1997; Maisch et al., 2008). Another similarity with *Stenopterygius, Hauffiopteryx,* and leptonectids is the reduction of longitudinal striations along the crown (Maisch, 1998; Maxwell, 2012; Lomax, 2016; Fernández et al., 2018) (Figures 5, 6). Yet, sparse striations are present in MNHNL LM266 but do not reach the apical quarter of the crown (as in *Leptonectes* spp.; Figure 6), and many crowns exhibit a single basal ring, as in *Wahlisaurus massarae* (Lomax, 2016), *Leptonectes* spp. (Figure 6), and *Eurhinosaurus longirostris* (in which more than one basal ring is usually present (e.g., Godefroit, 1994; Fischer et al., 2011)). The acellular cementum ring is not ridged, unlike in *Temnodontosaurus* (Godefroit, 1993; Maxwell, Caldwell, et al., 2012), *Ichthyosaurus* (McGowan, 1973; Vincent et al., 2014), and *Protoichthyosaurus* (Lomax et al., 2019). The root bears fine striations, but only in the basal half, as in some leptonectids (Fraas, 1892; Godefroit, 1994). This differs from the condition of *Leptonectes moorei* (Figure 6), *Leptonectes solei* (Figure 6), *Stenopterygius* (Godefroit, 1994), and *Hauffiopteryx* (Maxwell and Cortés, 2020), where the root ridges reach the base of the acellular cementum ring. The root is slightly expanded mesiodistally and slightly compressed labiolingually, another usual feature that is often present in leptonectids (Fraas, 1891; Reisdorf et al., 2011; Lomax, 2016).

The small size of these rostral fragments can be interpreted in two ways: (i) it belongs to a small individual, distinct from the other remains from the site or (ii) it represents the anterior extremity of a long snouted ichthyosaurian, where the tip of the rostrum can be extremely small compared to the size of the animal (McGowan, 1993, 2003). The presence of a discontinuous premaxillary fossa and, to a lesser extent, the absence of both a nasal and a maxilla (even internally) suggests that this fragment was located from the anterior quarter of the rostrum. The exposure of the splenial is less indicative of a position within the rostrum, because at least one leptonectid *(Leptonectes moorei)* possesses a very long ventral splenial exposure (V.F. pers. obs. holotype specimen NHMUK PV R 14370). In the absence of other evidence and given the taphonomy, stratigraphy, and the controlled excavations, we regard all the ichthyosaur fragments described here as likely belonging to a single individual. Even so, we detail the taxonomic information present in all fragments in isolation (Table 1), and the conclusions of the paper do not rely on this association.

Possible Surangular

Two contiguous fragments are interpreted here as the posterior part of a large right surangular (Figures 4, Supplementary Information Figure 1). The lateral surface is convex and forms a shallow anteroposterior ridge at mid-height. The medial surface is concave and forms a wide prominent ridge located within the ventral half of the medial surface. The ventral surface is rounded while the bone tapers dorsally to a thin, saddle-shaped ridge, as might be seen close to the coronoid process in neoichthyosaurians (Sollas, 1916; McGowan, 1973). The perfectly straight and parallel bone fibres on the concave side (Figures 4, Supplementary Information Figure 1) are features of ichthyosaurian surangulars (V.F. pers. obs. on material from MNHNL, MHNH). We do not derive taxonomic information from these fragments, because we consider their identification too tentative.

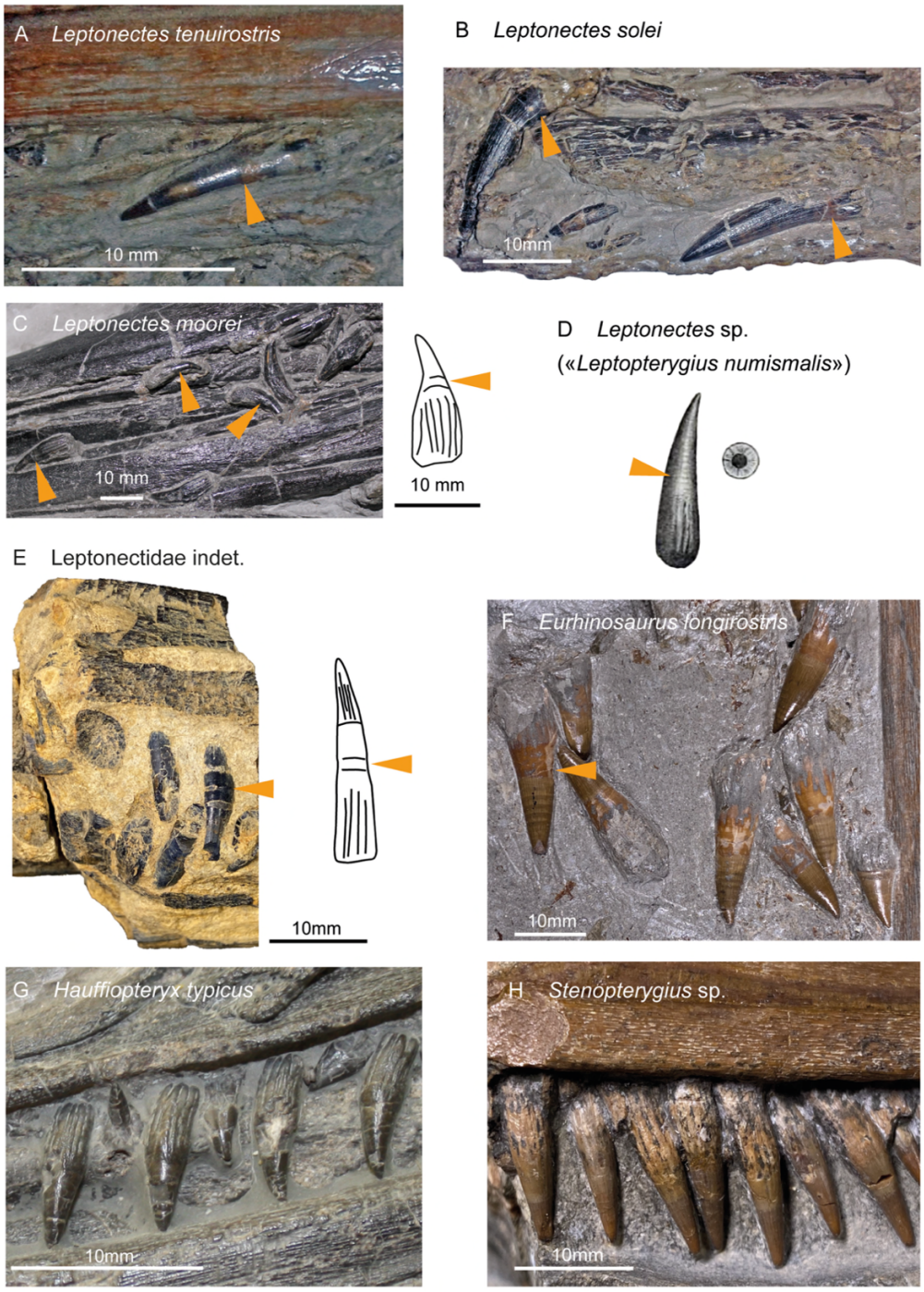

FIGURE 6. Diagnostic dental features of Early Jurassic ichthyosaurians with small and elongated tooth crowns. The distribution of concave ring at the level of the acellular cementum ring, which we term here "annulus" (indicated by orange arrows) appears restricted to leptonectids but are not fully expressed in all the teeth of an individual. (A) OUM J10305. (B) BRSMG Ce9856. (C) NHMUK R PV14370. (D) drawing extracted from Fraas (1892). (E) MNHNL LM226. (F) MNHNL TU112. (F) SMNS 81965. (H) MNHNL TV178.

Centra

Two centra fragments are present. One (Figures 4, 5) is a large dorsal centrum with an anteroposterior length of 52 mm and a diameter certainly above 100 mm (as the preserved portion is 100 mm wide), and probably between 120 and 130 mm. One apophysis is visible; the fact that the dorsal part of the centrum is missing suggests that this apophysis is the parapophysis. This apophysis is >20 mm long anteroposteriorly and 15 mm high dorsoventrally. It is teardrop-shaped, with anterior ridge connecting to the anterior margin of the centrum, as is typically of parvipelvians and clearly distinct from the dorsoventrally elongated diapophyses and often minuscule parapophyses seen in shastasaurids (Merriam, 1902; Sander, 1997; Fischer et al., 2014). Ventrally, the centrum forms a slightly concave surface. We interpret this as a parapophysis, present on the lateral surface of the centrum at mid-height. Accordingly, this centrum is regarded as an anterior dorsal centrum. The large size and the aspect ratio match with the morphology of *Temnodontosaurus* spp. (McGowan, 1974; Godefroit, 1993; Martin et al., 2012; Swaby and Lomax, 2021) and *Leptonectes solei* (McGowan, 1993). However, most other leptonectids have smaller centra, with diameters ranging from 25 to 65 mm (Huene, 1951; McGowan and Milner, 1999; McGowan, 2003; Lomax, 2016).

A second fragmentary bone solely consists of the margin of the articular surface of a small centrum. The lateral or ventral surface is concave and lacks chevron facets or apophyses. It is interpreted as a posterior caudal centrum, given the small size.

Ribs and Gastralia

Several tens of rib fragments are preserved (Figures 5, Supplementary Information Figure 1). Most have wide anterior and posterior grooves, giving the rib an “8” shape in cross-section, as is usually the case in neoichthyosaurians. However, the dorsal ribs of *Leptonectes tenuirostris, Temnodontosaurus azerguensis,* and some species of *Ichthyosaurus* seem to lack the grooves, giving their ribs a rounded cross-section (Martin et al., 2012; Lomax and Massare, 2016). In one fragment, one of the grooves can be observed vanishing medially; the largest fragments have a single groove, and the opposite side is gently convex (Figure 5). A series of other, small fragments are straight and exhibit a rugose texture; we interpret these as fragmentary gastralia.

DISCUSSION

The presence of long and slender teeth, with feint longitudinal striations, a ring/annulus at the base of the crown, and with a slightly rectangular root, combined with a slender rostrum suggest leptonectid affinities for the rostral fragments of MNHNL LM266 (Figure 6). Within leptonectids, the absence of an overbite and the slender teeth rule out *Eurhinosaurus longirostris, Excalibosaurus costini,* and *Leptonectes moorei* (Huene, 1931b; McGowan, 1986, 2003; McGowan and Milner, 1999). The large size of the associated centra – if they, as we think is the case, belong to the same individual – suggests an animal of large size, comparable to *Leptonectes solei*, and multiple species within *Temnodontosaurus*, notably *Temnodontosaurus platyodon* and *Temnodontosaurus trigonodon* (Godefroit, 1993; McGowan, 1993, 1996). *Leptonectes* is known to be present in the European Archipelago from the Hettangian to the Pliensbachian, including in nearby Belgium (Godefroit, 1992; McGowan and Milner, 1999; Lomax and Massare, 2018a) (if one regards the Pre-Planorbis beds as earliest Hettangian in age, as suggested by Hillebrandt and Kystyn (2009)) and is thus a solid candidate for the remains from the Cloche d’Or locality. However, we assign these remains to Leptonectidae indet., pending discovery of cranial and appendicular material that could clarify the taxonomic relationships of this specimen. It should be stressed here that the presence of leptonectids in the Luxembourg-Trier basin (see also Godefroit, 1992) during the early Pliensbachian does not require the skeletal elements we describe here to

TABLE 1. Diagnostic value of the elements of MNHNL LM266 if taken individually.

Anatomical element	Individual diagnostic value
Snout fragment (premaxillae, dentaries, splenials, teeth)	Leptonectidae
Possible surangular	Vertebrata
Centra (one dorsal and one posterior caudal)	Neoichthyosauria
Ribs (and possible gastralia)	Neoichthyosauria

origin from a single individual; only the presence of a large leptonectid does (Table 1).

Even if leptonectid neoichthyosaurians have been abundantly described (e.g., Fraas, 1891; Huene, 1922; McGowan, 1989, 1993; Godefroit, 1994; McGowan and Milner, 1999; Maisch and Matzke, 2003; Lomax, 2016), the details of the dental morphology of leptonectids are rarely documented, notably the concentric rings found towards the base of the tooth crown (but see Godefroit, 1994; Reisdorf et al., 2011; Lomax, 2016). These slightly concave rings, which we term here "annuli", clearly differ from the similarly positioned "enamel bands" of pliosaurids, which have a positive relief (Zverkov et al., 2018). Because it is not well distributed among neoichthyosaurians, this feature can be useful to segregate leptonectids from other taxa with smoothed and elongated tooth crowns, such as *Hauffiopteryx* and *Stenopterygius* (Figure 6). Indeed, even if *Hauffiopteryx* spp., *Stenopterygius* spp., and leptonectids all share a reduction of longitudinal ridges on tooth crown (Reisdorf et al., 2011; Maxwell, Fernández, et al., 2012; Fernández et al., 2018; Maxwell and Cortés, 2020), the presence of a such annuli has not been reported yet in *Hauffiopteryx* and *Stenopterygius.* A slightly labiolingually compressed root whose apicobasal ridges do not reach the acellular cementum ring, combined with the occurrence of one of more annuli close to the base of the crown can, therefore, at the current state of our knowledge, identify a tooth belonging to a leptonectid (Figure 6). Several of these rings have been reported on the crown of *Eurhinosaurus* (Godefroit, 1994; Fischer et al., 2011; Reisdorf et al., 2011) and might represent a diagnostic feature of this taxon.

The continued absence of baracromian ichthyosaurians in Pliensbachian strata suggests a sense of continuity in the ichthyosaurian assemblages during the Hettangian–Pliensbachian interval, which essentially (but not exclusively) contains leptonectids, *Ichthyosaurus*, and *Temnodontosaurus* (McGowan and Motani, 2003). A novelty of the Pliensbachian is to record the slightly more derived taxon *Hauffiopteryx* (Maxwell and Cortés, 2020). Thanks to the Cloche d'Or locality, all stages of the Early Jurassic are now known to contain large early neoichthyosaurians (with centra diameter > 10 cm) in many places of the European Archipelago (Godefroit, 1993; McGowan, 1996; Martin et al., 2012; Maxwell and Vincent, 2015; Fischer et al., 2021). By contrast, baracromians dominate ichthyosaurian assemblages in the European Archipelago by the early Toarcian with the ubiquitous presence of multiple species of *Stenopterygius* (Huene, 1931b; Hauff, 1953; Godefroit, 1994; Maisch, 2010; Maxwell, 2012; Dick et al., 2016) and are the only ichthyosaurians found after the Bajocian, with the exception of *Malawania anachronus* (Fernández, 1994; Fischer et al., 2013, 2021). The Pliensbachian gap in the fossil record of ichthyosaurians might contain this change of dominance; in any case, these remains further highlight the importance of the Luxembourg-Trier basin deposits in understanding the diversity dynamics of Jurassic marine reptiles.

CONCLUSIONS

Marine reptile remains are rare in Pliensbachian strata, worldwide. We describe remains of large ichthyosaurians from a new lower Pliensbachian locality in central Luxembourg (Ibex Ammonite zone). At least some of these remains belong to Leptonectidae, confirming the continuous presence of early neoichthyosaurians during the entire Hettangian–Pliensbachian interval in Western Europe.

ACKNOWLEDGEMENTS

We warmly thank Handling Editor Dr. M. Pole and our two reviewers, D. Cortés and an anonymous colleague, for making our paper better with thoughtful and constructive suggestions. The work of A.L. is supported by a FRIA grant of the F.R.S.–FNRS (FC38761).

REFERENCES

Bardet, N., Fernandez, M., Garcia-ramos, J.C., Pereda-Suberbiola, X., Pinuela, L., Ruiz-omenaca, J.I., and Vincent, P. 2008. A juvenile plesiosaur from the Pliensbachian (Lower Jurassic) of Asturias, Spain. Journal of Vertebrate Paleontology, 28:258–263. https://doi.org/10.1671/0272-4634(2008)28[258:AJPFTP]2.0.CO;2

Benson, R.B.J. and Butler, R.J. 2011. Uncovering the diversification history of marine tetrapods: ecology influences the effect of geological sampling biases, p. 191–208. In McGowan, A.J. and Smith, A.B. (eds.), Comparing the geological and fossil records: implications for biodiversity studies. Geological Society, Special Publications, 358. London.

Benson, R.B.J., Butler, R.J., Lindgren, J., and Smith, A.S. 2010. Mesozoic marine tetrapod diversity: mass extinctions and temporal heterogeneity in geological megabiases affecting the vertebrates. Proceedings of the Royal Society B: Biological Sciences, 277:829–834. https://doi.org/10.1098/rspb.2009.1845

Breton, G., Neraudeau, D., and Cuenca-Boulat, C. 1992. *Gnathichnus stellarum* ichnosp. nov., trace de broutage d'un echinide du Campanien des Charentes (France). Revue de Paléobiologie, 11:219–229.

Bromley, R.G. 1975. Comparative analysis of fossil and recent echinoid bioerosion. Palaeontology, 18:725–739.

Butler, R.J., Brusatte, S.L., Andres, B., and Benson, R.B.J. 2011. How do geological sampling biases affect studies of morphological evolution in deep time? A case study of pterosaur (Reptilia: Archosauria) disparity. Evolution, 66:147–162. https://doi.org/10.1111/j.1558-5646.2011.01415.x

Carrasco, J.F. 2003. Presencia de la icnoespecie *Gnathichnus pentax* sobre Dimya richei (Bivalvia) en el Eoceno inferior de La Puebla de Roda (Huesca). Batalleria, 11:37–40.

Combémorel, R. 1997. Bélemnites, p. 157–168. In Cariou, E. and Hantzpergue, P. (eds.), Biostratigraphie du Jurassique Ouest-Européen et Méditerranéen. Zonations parallèles et distribution des invertébrés et microfossiles. Bulletin du Centre de Recherches Elf Productions, Mémoire 17.

Danise, S., Twitchett, R.J., and Matts, K. 2014. Ecological succession of a Jurassic shallow-water ichthyosaur fall. Nature communications, 5:1–8. https://doi.org/10.1038/ncomms5789

de Blainville, H.M.D. 1835. Description de quelques espèces de reptiles de la Californie, précédée de l'analyse d'un système général d'Erpetologie et d'Amphibiologie. Nouvelles annales du Muséum d'Histoire naturelle, Paris, 4:233–296.

Dick, D.G., Schweigert, G., and Maxwell, E.E. 2016. Trophic niche ontogeny and palaeoecology of early Toarcian Stenopterygius (Reptilia: Ichthyosauria). Palaeontology, 59:423–431. https://doi.org/10.1111/pala.12232

Fernández, M. 1994. A new long-snouted ichthyosaur from the early Bajocian of Neuquén basin (Argentina). Ameghiniana, 31:291–297.

Fernández, M.S., Piñuela, L., and García-Ramos, J.C. 2018. First report of *Leptonectes* (Ichthyosauria: Leptonectidae) from the Lower Jurassic (Pliensbachian) of Asturias, northern Spain. Palaeontologia Electronica, 21.2.29A:1–15. https://doi.org/10.26879/802

Fischer, V., Guiomar, M., and Godefroit, P. 2011. New data on the palaeobiogeography of Early Jurassic marine reptiles: the Toarcian ichthyosaur fauna of the Vocontian Basin (SE France). Neues Jahrbuch für Geologie und Paläontologie, Abhandlungen, 261:111–127. https://doi.org/10.1127/0077-7749/2011/0155

Fischer, V., Appleby, R.M., Naish, D., Liston, J., Riding, J.B., Brindley, S., and Godefroit, P. 2013. A basal thunnosaurian from Iraq reveals disparate phylogenetic origins for Cretaceous ichthyosaurs. Biology Letters, 9:1–6. https://doi.org/10.1098/rsbl.2013.0021

Fischer, V., Cappetta, H., Vincent, P., Garcia, G., Goolaerts, S., Martin, J.E., Roggero, D., and Valentin, X. 2014. Ichthyosaurs from the French Rhaetian indicate a severe turnover across the Triassic–Jurassic boundary. Naturwissenschaften, 101:1027–1040. https://doi.org/10.1007/s00114-014-1242-7

Fischer, V., Weis, R., and Thuy, B. 2021. Refining the marine reptile turnover at the Early-Middle Jurassic transition. PeerJ, 9:1–45. https://doi.org/10.7717/peerj.10647

Fraas, E.E. 1891. Ichthyosaurier der Süddeutschen Trias und Jura-Ablagerungen. H. Laupp, Tübingen.

Fraas, E.E. 1892. *Ichthyosaurus numismalis*. Jahreshefte des Vereins für vaterländische Naturkunde in Württemberg, 48:22–31.

Gallagher, W.B., Miller, K.G., Sherrell, R.M., Browning, J.V., Field, M.P., Olsson, R.K., Sugarman, P.J., Tuorto, S., and Wahyudi, H. 2012. On the last mosasaurs: Late Maastrichtian mosasaurs and the Cretaceous-Paleogene boundary in New Jersey. Bulletin de la Société géologique de France, 183:145–150. https://doi.org/10.2113/gssgfbull.183.2.145

Godefroit, P. 1992. Présence de *Leptopterygius tenuirostris* (Reptilia, Ichthyosauria) dans le Lias moyen de Lorraine belge. Bulletin de l'Institut Royal des Sciences Naturelles de Belgique Sciences de la Terre, 62:163–170.
Godefroit, P. 1993. Les grands ichthyosaures sinémuriens d'Arlon. Bulletin de l'Institut Royal des Sciences Naturelles de Belgique Sciences de la Terre, 63:25–71.
Godefroit, P. 1994. Les reptiles marins du Toarcien (Jurassique inférieur) belgo-luxembourgeois. Mémoires pour servir à l'Explication des Cartes Géologiques et Minières de la Belgique, 39:98.
Guérin-Franiatte, S. 2003. Biostratigraphie dans le Lias du Grand-Duché de Luxembourg : le sondage de Capellen, p. 65–78. Paléontologie au Luxembourg. Ferrantia – Travaux scientifiques du Musée national d'histoire naturelle, Luxembourg, 36.
Hauff, B. 1953. Das Holzmadenbuch. Verlag der Hohenlohe'schen Buchhandlung, Öhringen.
Hungerbühler, A. and Sachs, S. 1996. Ein großer Ichthyosaurier aus dem Pliensbachium von Bielefeld. Neue Einblicke in die Ichthyosaurier des Mittleren Lias und das Gebiß von *Temnodontosaurus*. Bericht des Naturwissenschaftlichen Vereins Bielefeld und Umgegend, Bielefeld, 37:15–52.
Jouve, S., Bardet, N., Jalil, N.E., Suberbiola, X.P., Bouya, B., and Amaghzaz, M. 2008. The oldest African crocodylian: phylogeny, paleobiogeography, and differential survivorship of marine reptiles through the Cretaceous-Tertiary boundary. Journal of Vertebrate Paleontology, 28:409–421. https://doi.org/10.1671/0272-4634(2008)28[409:TOACPP]2.0.CO;2
Lomax, D. and Massare, J. 2018a. A forefin of *Leptonectes solei* from the Lower Jurassic (Pliensbachian) of Dorset, UK. Proceedings of the Geologists' Association, 129:770–773. https://doi.org/10.1016/j.pgeola.2018.07.005
Lomax, D. and Massare, J. 2018b. A second specimen of *Protoichthyosaurus applebyi* (Reptila: Ichthyosauria) and additional information on the genus and species. Paludicola, 11:164–178.
Lomax, D.R. 2010. An *Ichthyosaurus* (Reptilia, Ichthyosauria) with gastric contents from Charmouth, England: first report of the genus from the Pliensbachian. Paludicola, 8:22–36.
Lomax, D.R. 2016. A new leptonectid ichthyosaur from the Lower Jurassic (Hettangian) of Nottinghamshire, England, UK, and the taxonomic usefulness of the ichthyosaurian coracoid. Journal of Systematic Palaeontology, 15:387–401. https://doi.org/10.1080/14772019.2016.1183149
Lomax, D.R. and Massare, J.A. 2015. A new species of *Ichthyosaurus* from the Lower Jurassic of West Dorset, England, U.K. Journal of Vertebrate Paleontology, 35:e903260. https://doi.org/10.1080/02724634.2014.903260
Lomax, D.R. and Massare, J.A. 2016. Two new species of *Ichthyosaurus* from the lowermost Jurassic (Hettangian) of Somerset, England. Papers in Palaeontology, 3:1–20. https://doi.org/10.1002/SPP2.1065
Lomax, D.R., Porro, L.B., and Larkin, N.R. 2019. Descriptive anatomy of the largest known specimen of *Protoichthyosaurus prostaxalis* (Reptilia: Ichthyosauria) including computed tomography and digital reconstruction of a three-dimensional skull. PeerJ, 7:e6112. https://doi.org/10.7717/peerj.6112
Lucius, M. 1948. Geologie Luxemburgs. Das Gutland. Erläuterungen zu der geologischen Spezialkarte Luxemburgs, 5:1–397.
Maisch, M.W. 1997. The cranial osteology of *Ichthyosaurus intermedius* Conybeare, 1822 from the Lias of Great Britain. Stuttgarter Beiträge zur Naturkunde Serie B (Geologie und Paläontologie), 258:1-27.
Maisch, M.W. 1998. A new ichthyosaur genus from the Posidonia Shale (Lower Toarcian, Jurassic) of Holzmaden, SW-Germany with comments on the phylogeny of post-Triassic ichthyosaurs. Neues Jahrbuch für Geologie und Paläontologie, Abhandlungen, 209:47–78. https://doi.org/10.1127/njgpa/209/1998/47
Maisch, M.W. 2010. Phylogeny, systematics, and origin of the Ichthyosauria - the state of the art. Palaeodiversity, 3:151–214.
Maisch, M.W. and Hungerbühler, A. 1997. Revision of *Temnodontosaurus nuertingensis* (v. Huene, 1931), a large ichthyosaur from the Lower Pliensbachian (Lower Jurassic) of Nürtingen, South Western Germany. Stuttgarter Beiträge zur Naturkunde Serie B (Geologie und Paläontologie), 248:1–11.

Maisch, M.W. and Matzke, A.T. 2003. The cranial osteology of the ichthyosaur *Leptonectes* cf. *tenuirostris* from the Lower Jurassic of England. Journal of Vertebrate Paleontology, 23:116–127. https://doi.org/10.1671/0272-4634(2003)23[116:TCOOTI]2.0.CO;2

Maisch, M.W. and Reisdorf, A.G. 2006. Evidence for the longest stratigraphic range of a post-Triassic Ichthyosaur: a *Leptonectes tenuirostris* from the Pliensbachian (Lower Jurassic) of Switzerland. Geobios, 39:491–505. https://doi.org/10.1016/j.geobios.2005.04.005

Maisch, M.W., Reisdorf, A., Schlatter, R., and Wetzel, A. 2008. A large skull of *Ichthyosaurus* (Reptilia: Ichthyosauria) from the Lower Sinemurian (Lower Jurassic) of Frick (NW Switzerland). Swiss Journal of Geoscience, 101:617–627. https://doi.org/10.1007/s00015-008-1299-4

Marek, R.D., Moon, B.C., Williams, M., and Benton, M.J. 2015. The skull and endocranium of a Lower Jurassic ichthyosaur based on digital reconstructions. Palaeontology, 58:723–742. https://doi.org/10.1111/pala.12174

Martin, J.E., Fischer, V., Vincent, P., Suan, G., Martin, J.E., Fischer,V., Vincent, P., Suan, G., Martin, J.E., Fischer, V., Vincent, P., and Suan, G. 2012. A longirostrine *Temnodontosaurus* (Ichthyosauria) with comments on Early Jurassic ichthyosaur niche partitioning and disparity. Palaeontology, 55:995–1005. https://doi.org/10.1111/j.1475-4983.2012.01159.x

Massare, J.A. and Lomax, D.R. 2016. A new specimen of *Ichthyosaurus conybeari* (Reptilia, Ichthyosauria) from Watchet, Somerset, England, U.K., and a re-examination of the species. Journal of Vertebrate Paleontology, e1163264. https://doi.org/10.1080/02724634.2016.1163264

Maubeuge, P.L. 1950. Observations sur le Lotharingien et le Carixien du Grand-Duché de Luxembourg et comparaisons avec les régions voisines. Archives de l'Institut Grand-Ducal de Luxembourg, Section des Sciences naturelles, physiques et mathématiques, 19:357–364.

Maubeuge, P.L. and Antun, P. 1967. Observations sur le Lotharingien et le Carixien du Grand-Duché de Luxembourg. Bulletin de l'Académie royale de Belgique (Classe des Sciences) 5e série, 57:249–285.

Maxwell, E.E. 2012. New metrics to differentiate species of *Stenopterygius* (Reptilia: Ichthyosauria) from the Lower Jurassic of southwestern Germany. Journal of Paleontology, 86:105–115. https://doi.org/10.1666/11-038.1

Maxwell, E.E. 2018. Redescription of the lost holotype of *Suevoleviathan integer* (Bronn, 1844) (Reptilia: Ichthyosauria). Journal of Vertebrate Paleontology, 38:e1439833. https://doi.org/10.1080/02724634.2018.1439833

Maxwell, E.E. and Vincent, P. 2015. Effects of the early Toarcian Oceanic Anoxic Event on ichthyosaur body size and faunal composition in the Southwest German Basin. Paleobiology, 42:117–126. https://doi.org/10.1017/pab.2015.34

Maxwell, E.E. and Cortés, D. 2020. A revision of the Early Jurassic ichthyosaur *Hauffiopteryx* (Reptilia: Ichthyosauria), and description of a new species from Southwestern Germany. Palaeontologia Electronica, 23(2):a31. https://doi.org/10.26879/937

Maxwell, E.E., Caldwell, M.W., and Lamoureux, D.O. 2012. Tooth histology, attachment, and replacement in the Ichthyopterygia reviewed in an evolutionary context. Paläontologische Zeitschrift, 86:1–14. https://doi.org/10.1007/s12542-011-0115-z

Maxwell, E.E., Fernández, M.S., and Schoch, R.R. 2012. First diagnostic marine reptile remains from the Aalenian (Middle Jurassic): a new ichthyosaur from southwestern Germany. PLoS ONE, 7:e41692. https://doi.org/10.1371/journal.pone.0041692

McGowan, C. 1973. The cranial morphology of the Lower Liassic latipinnate ichthyosaurs of England. Bulletin of the British Museum (Natural History) Geology, 24:1–109.

McGowan, C. 1974. A revision of the longipinnate ichthyosaurs of the Lower Jurassic of England, with description of the new species (Reptilia, Ichthyosauria). Life Science Contributions, Royal Ontario Museum, 97:1–37.

McGowan, C. 1986. A putative ancestor for the swordfish-like ichthyosaur *Eurhinosaurus*. Nature, 322:454–456. https://doi.org/10.1038/322454a0

McGowan, C. 1989. *Leptopterygius tenuirostris* and other long-snouted ichthyosaurs from the English Lower Lias. Palaeontology, 32:409–427.

McGowan, C. 1993. A new species of a large, long-snouted ichthyosaur from the English lower Lias. Canadian Journal of Earth Sciences, 30:1197–1204.

McGowan, C. 1996. Giant ichthyosaurs of the Early Jurassic. Canadian Journal of Earth Sciences, 33:1011–1021.

McGowan, C. 2003. A new specimen of *Excalibosaurus* from the English Lower Jurassic. Journal of Vertebrate Paleontology, 23:950–956. https://www.jstor.org/stable/4524397
McGowan, C. and Milner, A.C. 1999. A new Pliensbachian ichthyosaur from Dorset, England. Palaeontology, 42:761–768. https://doi.org/10.1111/1475-4983.00096
McGowan, C. and Motani, R. 2003. Part 8. Ichthyopterygia. In Sues, H.-D. (ed.), Handbook of Paleoherpetology, 8. Verlag Dr. Friedrich Pfeil, München.
Merriam, J.C. 1902. Triassic Ichthyopterygia from California and Nevada. University of California Publications: Bulletin of the department of Geology, 3:63–108.
Meyer, C.A. 2011. Amazing graze – Grazing traces of sea urchins on turtles – An example from the Late Jurassic of Switzerland. Annalen des Naturhistorischen Museums in Wien, A113:555–565.
Motani, R. 1999. Phylogeny of the Ichthyopterygia. Journal of Vertebrate Paleontology, 19:473–496. https://www.jstor.org/stable/4524011
Motani, R., Jiang, D.-Y., Chen, G.-B., Tintori, A., Rieppel, O., Ji, C., and Huang, J.-D. 2015. A basal ichthyosauriform with a short snout from the Lower Triassic of China. Nature, 517:485–488. https://doi.org/10.1038/nature13866
Motani, R., Jiang, D.Y., Tintori, A., Ji, C., and Huang, J.D. 2017. Pre- versus post-mass extinction divergence of Mesozoic marine reptiles dictated by time-scale dependence of evolutionary rates. Proceedings of the Royal Society B: Biological Sciences, 284:e20170241. https://doi.org/10.1098/rspb.2017.0241
Reisdorf, A., Maisch, M.W., and Wetzel, A. 2011. First record of the leptonectid ichthyosaur *Eurhinosaurus longirostris* from the Early Jurassic of Switzerland and its stratigraphic framework. Swiss Journal of Geoscience, 104:211–224. https://doi.org/10.1007/s00015-011-0069-x
Reolid, M., Santos, A., and Mayoral, E. 2015. Grazing activity as taphonomic record of necrobiotic interaction: A case study of a sea turtle carapace from the Upper Jurassic of the Prebetic (south Spain). Revista mexicana de ciencias geológicas, 32:21–28.
Riegraf, W. 1980. Revision der Belemniten des Schwäbischen Jura. Palaeontographica Abteilung A, 169:128–206.
Sander, P.M. 1997. The paleobiogeography of *Shastasaurus*, p. 17–43. In Callaway, J.M. and Nicholls, E.L. (eds.), Ancient Marine Reptiles. Academic Press, San Diego, California.
Sander, P.M. 2000. Ichthyosauria: their diversity, distribution, and phylogeny. Paläontologische Zeitschrift, 74:1–35. https://doi.org/10.1007/BF02987949
Schlegelmilch, R. 1998. Die Belemniten des süddeutschen Jura: Ein Bestimmungsbuch für Geowissenschaftler und Fossiliensammler. Spektrum Akademischer Verlag, Heidelberg. https://doi.org/10.1007/978-3-8274-3083-0
Sollas, W.J. 1916. The skull of *Ichthyosaurus*, studied in serial sections. Philosophical transactions of the Royal Society of London, serie B, 208:63–126.
Swaby, E.J. and Lomax, D.R. 2021. A revision of *Temnodontosaurus crassimanus* (Reptilia: Ichthyosauria) from the Lower Jurassic (Toarcian) of Whitby, Yorkshire, UK. Historical Biology, 33:2715–2731. https://doi.org/10.1080/08912963.2020.1826469
Tutin, S.L. and Butler, R.J. 2017. The completeness of the fossil record of plesiosaurs, marine reptiles from the Mesozoic. Acta Palaeontologica Polonica, 62:563–573. https://doi.org/10.4202/APP.00355.2017
Vincent, P., Taquet, P., Fischer, V., Bardet, N., Falconnet, J., and Godefroit, P. 2014. Mary Anning's legacy to French vertebrate palaeontology. Geological Magazine, 151:7–20. https://doi.org/10.1017/S0016756813000861
von Hillebrandt, A. and Krystyn, L. 2009. On the oldest Jurassic ammonites of Europe (Northern Calcareous Alps, Austria) and their global significance. Neues Jahrbuch für Geologie und Paläontologie, Abhandlungen, 253:163–195. https://doi.org/10.1127/0077-7749/2009/0253-0163
von Huene, F. 1922. Die Ichthyosaurier des Lias und ihre Zusammenhänge. Monographien zur Geologie und Paläontologie,1. Verlag von Gebrüder Borntraeger, Berlin.
von Huene, F. 1931a. Neue Ichthyosaurier aus Württemberg. Neues Jahrbuch für Mineralogie, Geologie und Paläontologie. Beilage. Abteilung B, 65:305–320.
von Huene, F. 1931b. Neue Studien über Ichthyosaurier aus Holzmaden. Abhandlungen der Senckenbergischen Naturforschenden Gesellschaft, 42:345–382.
von Huene, F. 1951. Ein neuer Fund von *Eurhinosaurus longirostris*. Neues Jahrbuch für Geologie und Paläontologie, Abhandlungen, 93:277–283.